November 2005
Research Report: UCPRC-RR-2005-15

Investigation of Conditions for Moisture Damage in Asphalt Concrete and Appropriate Laboratory Test Methods

Authors:
Qing Lu and John T. Harvey

Work Conducted as part of Partnered Pavement Research Center Strategic Plan Element No. 4.9: "Investigation of Asphalt Concrete Moisture Damage"

PREPARED FOR:

California Department of Transportation
Division of Research and Innovation

PREPARED BY:

University of California
Pavement Research Center
UC Davis and Berkeley

DOCUMENT RETRIEVAL PAGE			Research Report No.: UCPRC-RR-2005-15
Title: Investigation of Conditions for Moisture Damage in Asphalt Concrete and Appropriate Laboratory Test Methods			
Authors: Q. Lu and J. T. Harvey			
Prepared for: Caltrans Division of Research and Innovation	**FHWA No.:** CA109999B	**Date Work Submitted:** April 1, 2008	**Date**: November 2005
Strategic Plan Element No: 4.9	**Status:** Stage 6, final		**Version No:** 1

Abstract:

Moisture damage in asphalt pavements is a complex phenomenon affected by a variety of factors, and has not been fully understood, with major knowledge gaps in three areas: major factors contributing to moisture damage in the field, appropriate laboratory test procedures, and the effectiveness of treatments. Both field and laboratory investigations were performed in this study to provide additional information in these three areas.

Statewide condition survey and field sampling were conducted to identify factors contributing to moisture damage, other than aggregate source. Statistical analysis revealed that air-void content, pavement structure, cumulative rainfall, mix type (DGAC vs RAC-G), use of anti-strip additive (lime or liquid), and pavement age significantly affect the extent of moisture damage. Laboratory experiments revealed that high air-void contents not only allow more moisture to enter mixes, but also significantly reduce the fatigue resistance of mixes in wet conditions. Less than optimum binder contents also reduce the moisture resistance of asphalt mixes under repeated loading.

The effectiveness of the Hamburg Wheel Tracking Device (HWTD) test to determine moisture sensitivity of asphalt mixes was evaluated by testing both laboratory-fabricated specimens and field cores. It was found that the test can correctly identify the effect of anti-strip additives; its results generally correlate with field performance except that the test may sometimes fail mixes that perform well in the field and, in a very few cases, provide false positive results.

A fatigue-based test procedure for evaluating moisture sensitivity was explored in this study. A test procedure was developed for comparative evaluation of different mixes. Application of the test procedure for use in pavement analysis/design is suggested for expensive projects.

The long-term effectiveness of both hydrated lime and liquid anti-strip agents was evaluated by both the tensile strength ratio (TSR) test and the fatigue beam test. Results showed that both types of treatment are effective in preventing moisture damage for up to one year's continuous moisture conditioning in the laboratory.

A database with all field and laboratory results has been prepared for Caltrans.

Keywords:

Moisture damage, Asphalt pavement, Hamburg wheel tracking device, Fatigue, Antistripping agent

Proposals for implementation:

Related documents:

Signatures:

Q. Lu **1st Author**	J. Harvey **Technical Review**	D. Spinner **Editor**	J. Harvey **Principal Investigator**	T. J. Holland **Caltrans Contract Manager**

DISCLAIMER

The contents of this report reflect the views of the authors who are responsible for the facts and accuracy of the data presented herein. The contents do not necessarily reflect the official views or policies of the State of California or the Federal Highway Administration. This report does not constitute a standard, specification, or regulation.

PROJECT OBJECTIVES

The goals of this project are to investigate the conditions for moisture damage in asphalt pavements in California and to recommend appropriate test and treatment methods.

These goals were achieved by completion of the following objectives:

1. Perform a statewide field investigation to estimate the effects of different variables on the occurrence and severity of moisture damage and to determine major factors associated with moisture damage in the field, other than aggregate source. To the extent possible with available data, analyze the extent of moisture damage in California.
2. Perform a laboratory investigation to determine the effects of some major factors (air-void content and binder content) on moisture damage. Recommend mitigation measures.
3. Evaluate the effectiveness of the Hamburg wheel tracking device test to determine the moisture sensitivity of asphalt mixes and to predict field performance. To the extent possible with available data, analyze the correlation between lab test results and field performance.
4. Develop and evaluate dynamic loading involved test procedures for determining moisture sensitivity of asphalt mixes. Recommend appropriate conditioning procedures for laboratory tests.
5. Evaluate the effectiveness, especially the long-term effectiveness, of hydrated lime and liquid anti-stripping agents in improving the moisture resistance of hot mix asphalt using both the current and new test procedures.

ACKNOWLEDGEMENTS

The work included in this report was funded by the California Department of Transportation, Division of Research and Innovation. The project manager for this work was Michael Samadian, assisted by Alfredo Rodriguez.

The authors would like to thank the staff of the UCPRC for their help with the field and laboratory work included in this report. They would also like to thank Terrie Bressette (METS Office of Flexible Pavements), the Pavement Standards Team technical advisor, for her help and advice throughout the project. The members of the Caltrans/Industry Moisture Sensitivity Task Group are also thanked for comments on the results and advice during the project. Caltrans District Maintenance crews across the state are thanked for supplying safe traffic closures.

Field data was provided by the Contra Costa County Materials Laboratory and Steve Buckman, and the Washington State Department of Transportation (WSDOT) and Jeff S. Uhlmeyer. Materials were contributed by Graniterock Company in Watsonville, J. F. Shea Co., Inc. in Redding, Syar Industries, Inc. in Solano, Shell Oil Products U.S. in Martinez, Valero Marketing and Supply Company in Pittsburg, Chemical Lime Company, and Akzo Nobel Company.

EXECUTIVE SUMMARY

Moisture damage is the progressive deterioration of asphalt mixes by loss of adhesion between asphalt binder and aggregate surface and/or loss of cohesion within the binder due to water. It is a complex phenomenon affected by a variety of factors, and has not been fully understood in the pavement community with major knowledge gaps in three areas: relative significance of factors affecting the damage process in the field, appropriate laboratory test procedures, and the effectiveness of treatments. Both field investigation and laboratory investigation were performed in this study to help fill these major gaps with the following objectives:

1. Perform a statewide field investigation to estimate the effects of different variables on the occurrence and severity of moisture damage and to determine major factors associated with moisture damage in the field, other than aggregate source. To the extent possible with available data analyze the extent of moisture damage in California.
2. Perform laboratory investigation to determine the effects of some major factors (air-void content and binder content) on moisture damage. Recommend mitigation measures.
3. Evaluate the effectiveness of the Hamburg wheel tracking device test to determine moisture sensitivity of asphalt mixes and to predict field performance. To the extent possible with available data analyze the correlation between lab test results and field performance.
4. Develop and evaluate dynamic loading involved test procedures for determining moisture sensitivity of asphalt mixes. Recommend appropriate conditioning procedures for laboratory tests.
5. Evaluate the effectiveness, especially the long-term effectiveness, of hydrated lime and liquid anti-stripping agents in improving the moisture resistance of hot mix asphalt using both the current and new test procedures.

The field investigation started with a general condition survey of nearly 200 California pavement sections, followed by project data collection. Caltrans recommended many of these sections, almost half coming from a list of QC/QA projects statewide and nearly one-fifth chosen by District Materials Engineers or industry professionals in different areas. Nearly one-third sections were randomly sampled in districts 2 and 6 where moisture damage historically has occurred. Most of the projects were four to eight years old at the time of the survey. Though not a random sample, the general survey represents pavements under a range of traffic and environmental conditions throughout California.

Based on the general condition survey results, a subset of 63 sections was selected for further intensive survey, in which both dry and wet cores were taken near locations of damage and then tested in the laboratory. About 80 percent of these sections were selected because they showed a range of distresses such as raveling and potholes, which might be related to moisture damage. The other 20 percent were "control" sections because they did not show any distress at the surface. Analysis and subsequent conclusions were based on the information obtained from both the general and the intensive survey.

Severe moisture damage was identified in several asphalt pavements. About ten percent of pavements with previously undocumented performance in the survey list showed medium or severe moisture damage. This finding can not be simply extrapolated because it is not based on a random sample. However, this suggests that moisture damage may be a factor to consider broadly in the performance of asphalt pavements.

Dry cores revealed that moisture exists in almost every pavement, with a content ranging from zero to three percent. In some cases, large amount of moisture was even discovered in pavements that had received little rain for several months.

Air-void content measured from cores was found to be significantly affected by the position in the lane (whether or not in the wheelpath), depth in the pavement, distance from the distressed areas, and construction specifications (whether or not QC/QA project). There is a strong correlation between moisture content and air-void content. High air-void content generally corresponds to high moisture content in the

asphalt mixes. In addition, it is also found that permeability measured on pavements is positively correlated with air-void content.

Statistical analysis, based on an ordered probit model, was performed on two different data sets: data from cores, and data from all sections in the general condition survey. The ordered probit model approach has been used to build discrete deterioration models in infrastructure management in civil engineering. Like all probability models, an ordered probit model enables calculation of predicted probabilities for each category of moisture damage as well as marginal effects. Marginal effects indicate how a change in an explanatory variable, such as age or traffic, affects the predicted probability that pavements will manifest each moisture damage level.

The ordered probit model results are generally consistent. Results based on core data showed that air-void content, cumulative rainfall, pavement age, and mix type are significant at the 90 percent confidence level in affecting moisture damage. The existence of repeated loading (whether or not in the wheelpath) has a marginally significant effect but cumulative truck traffic is not statistically significant. This indicates that repeated loading has a nonlinear effect on moisture damage: whether or not repeated loading exists has a marginally significant effect on the occurrence and extent of moisture damage, but the intensity of repeated loading, once it exists, makes no significant difference. Increasing in air-void content, rainfall and pavement age tends to increase the severity of moisture damage. Based on a limited number of samples, asphalt rubber mixes do not improve moisture resistance better than conventional dense graded mixes. In contrast, model results based on the generally surveyed sections showed that additives and pavement age are significant factors. Using additives (hydrated lime or liquid anti-stripping agents) tends to reduce the severity of moisture damage. One drawback of the model estimation is that aggregate type is not explicitly included as an independent variable due to the lack of an appropriate method to characterize aggregates. Instead aggregate is treated as a random effect in the model. The model estimation may be improved once aggregates can be properly characterized and included in the model, which remains to be future work.

Case studies on a few severely distressed pavements revealed that in specific cases, one factor or a few may dominate moisture-related damage in pavements. These factors include poor quality aggregate, high air-void content combined with ample source of water, poor pavement drainage design, inappropriate structural design, and others. In most cases, high air-void content was always found in the severely distressed pavements.

Laboratory investigation addressed two issues in detail: (1) characteristics of moisture ingress and retention processes in asphalt mixes and factors affecting these processes, and (2) effects of construction-induced variations on moisture damage.

A soaking-drying test was performed to study the moisture ingress and retention characteristics and influential factors. Results showed that the ingress or evaporation of moisture in the asphalt mixes is not as quick as expected, and takes time on a scale of weeks. The ultimate amount of moisture entering specimens is positively correlated with air-void content but saturation is insensitive to air-void contents for specimens with seven percent or higher air-void contents. Statistical analysis revealed that air-void content has the strongest influence on the amount of moisture entering asphalt mixes, but aggregate gradation and binder type also have significant influence.

The effect of variation in air-void content and binder content on the moisture sensitivity of asphalt mixes was studied by the flexural beam fatigue test. These two variables are important for pavement performance but are easily affected by construction quality. Results showed that a reduction in the binder content or an increase in the air-void content will significantly reduce the moisture resistance, in terms of fatigue life, of a good performance mix under repeated loading in an unfavorable, high temperature environment.

The effectiveness of Hamburg wheel tracking device (HWTD) test to determine moisture sensitivity of asphalt mixes was evaluated by both laboratory prepared specimens and field cores following a common test procedure. The test procedure used is similar to that used by most researchers/agencies, such as Aschenbrener et al at the Colorado DOT and Izzo et al at the Texas DOT, with the exception that the water temperature is fixed at 50°C for all mixes. This work was mostly completed prior to publication of AASHTO T 324 (2004), however the equipment is the same and the test procedure is similar. It was found that the test

procedure can correctly identify the effect of antistripping additives, but may underestimate the performance of mixes containing soft binders at the fixed test temperature 50°C. The correlation between test results and field performance seems acceptable except that the test procedure may fail mixes that perform well in the field and, in a very few cases, give false positive results. Further study is needed to improve the test procedure.

A fatigue-based test procedure for evaluating moisture sensitivity was evaluated. The procedure includes use of the AASHTO T 321 standard and moisture conditioning. The method consisted of evaluation of different mixes using a controlled-strain flexural beam fatigue test performed at 20°C, 10 Hz, and 200με on specimens presaturated using a 635 mm-Hg vacuum for 30 minutes and preconditioned at 60°C for one day. Use of the test procedure for pavement analysis/design was also discussed. The test procedure did distinguish mixes with different moisture sensitivities, and provided a ranking for these mixes consistent with prior field experience. However, variance of the fatigue test results was relatively large. *In the long term this may be a useful test since it has the potential to be incorporated in a mechanistic-empirical pavement design procedure, especially for expensive projects.*

Moisture effects on the rutting resistance of asphalt mixes was evaluated by the repeated shear test at constant height (RSST-CH) based on a limited number of samples. The preliminary evaluation did not produce expected results. In some cases, the existence of moisture reduced the permanent shear strain. It is possible that the preconditioning procedure used in this study is insufficient. A harsher conditioning procedure, such as use of high temperatures, is needed to better simulate the field conditions.

The long-term effectiveness of both hydrated lime and liquid antistripping agents in improving the moisture resistance of asphalt mixes was evaluated by both the tensile strength ratio (TSR) test and the flexural fatigue beam test. Results showed that both treatments are effective after one-year moisture conditioning in the laboratory. It is expected that the field performance of these additives would last longer than one year, but field data (or test sections) and analysis are needed to confirm this expectation.

TABLE OF CONTENTS

LIST OF FIGURES

LIST OF TABLES

1.0 INTRODUCTION AND OVERVIEW

The majority of asphalt concrete pavements are constructed with asphalt-aggregate mixtures compacted to a specified density at high temperatures. Due to repeated traffic loading and environmental influence, asphalt concrete pavements deteriorate gradually once they are open to traffic. The typical design life is 15–30 years for new asphalt concrete pavements, and 5–20 years for overlays.

1.1 General Characteristics of Moisture Damage

Environmental factors such as temperature, water, and air can have profound effects on the durability of asphalt concrete pavements. Water is a key element among these factors.

1.1.1 How Moisture Damage Is Defined

Moisture damage can be understood as the progressive deterioration of asphalt mixes by loss of adhesion between asphalt binder and aggregate surface and/or loss of cohesion within the binder primarily due to the action of water. Moisture damage often directly disrupts the integrity of the mix, thereby reducing pavement performance life by accelerating all the modes of distress of interest in pavement design, including fatigue cracking, permanent deformation (rutting) and thermal cracking in asphalt concrete, and rutting in the unbound soil layers due to the reduced load carrying capacity of distressed asphalt concrete layers. In some cases when pavement is not loaded, moisture may simply weaken the asphalt mix by softening or partially emulsifying the asphalt film without removing it from aggregate surfaces. The resulting loss of stiffness or strength is recovered when water is removed from the mix (Santucci 2002). However, when a pavement is loaded during this weakened condition damage is accelerated and may become irreversible.

1.1.2 Mechanisms of Moisture Damage

Moisture damage in asphalt concrete pavements is a complex phenomenon, affected by a variety of factors including material properties, mix composition, pavement drainage condition, traffic loading, and environment characteristics.

The first necessary condition for moisture damage is the ingress of moisture into asphalt concrete mixes. If asphalt pavements were impermeable, moisture damage would seldom happen, except for some surface raveling. In reality, an air-void system exists in all types of asphalt pavements, even those constructed with special mixes such as Gussasphalt (Huang and Qian 2001). Contemporary thinking is that voids are necessary or at least unavoidable for mixes to not have unacceptable permanent deformation under traffic at high temperatures and to not "bleed" asphalt to the surface, both of which cause traffic safety problems (Terrel et al. 1994). For conventional dense-graded mixes, excess rutting and bleeding typically occur if the air-void content is less than three percent.

In the laboratory, dense-graded mixes are typically designed at four percent air-void content, but the actual field air-void content typically ranges between 6 and 12 percent, which is in the pessimum void range suggested by Terrel et al. (1994). Terrel referred to this as the pessimum range because laboratory testing suggested that above this range the air voids become interconnected and moisture can flow out easily while below this range the air voids are disconnected and are relatively impermeable. In the pessimum range, water can enter the voids but cannot escape freely. These voids provide the major access for water, which may come from precipitation, irrigation, or groundwater, to get into asphalt concrete mixes. Voids in aggregates may also trap some moisture during construction because of incomplete drying, especially in plants using drum mixers. Furthermore, asphalt cements themselves are somewhat permeable to water (Nguyen et al. 1996), which provides extra access for moisture.

The presence of water in asphalt concrete mixes can lead to one or more of the following damage mechanisms: loss of cohesion, loss of adhesion, pore pressure, and hydraulic scouring.

1.1.2.1 Loss of Cohesion

In asphalt concrete, cohesion is described as the overall integrity of the material when subjected to load or stress. It is determined primarily by the attraction within the asphalt binder and influenced by factors such as the viscosity of the asphalt film.

Moisture can change the rheology of asphalt and reduce its cohesion through spontaneous emulsification, an inverted emulsion of water droplets in asphalt film. This has been observed by several researchers. Fromm (1974) submerged glass slides coated with a two-mil asphalt film in water and observed the formation of a brownish material at the asphalt surface in which he found an emulsion of water under microscopic examination. He also observed that once the emulsion formation penetrated to the substrate, the adhesive bond between the asphalt and the aggregate was broken. Williams (1998) soaked asphalt samples underwater at 60°C for 6 and 27 weeks and observed under an environmental scanning electron microscope (ESEM) that the depth to which the water penetrated increased from 183 μm to 278 μm over 21 weeks. Work done in SHRP Contract A-002A speculated that asphalt has the capability of incorporating and transporting water by virtue of the attraction of polar water molecules to polar asphalt components (Robertson 1991). Nguyen et al. (1996) claimed the same point and further pointed out that the highly polar components and the water-soluble impurities (e.g., ions and salts) in asphalt form the hydrophilic regions; thus the water transport through the asphalt to the aggregate-asphalt interface is not a uniform diffusion but rather a tortuous transport process mediated by pores.

The rate and extent of emulsification may be increased or decreased with the use of different additives or at different temperatures. Clay or other fines with surface ionic charges, and some antistripping additives can act as emulsifiers. Sodium naphthenate in the asphalt resulting from some refining processes can also work as a water-in-asphalt emulsifier (Dunning 1987). Iron naphthenate, however, is able to reduce both the rate and the severity of emulsification (Fromm 1974). At high temperatures, the rate and the amount of water penetration are also increased because asphalt becomes softer (Williams 1998).

Inverted emulsification is reversible. After evaporation of water from the emulsion, asphalt soon regains its original properties (Fromm 1974; Kiggundu 1987).

Water can also affect cohesion through saturation and expansion of the void system due to freeze-thaw cycles under temperature changes (Stuart 1990).

1.1.2.2 Loss of Adhesion

For asphalt concrete mixes, it is an objective of mix design to coat all aggregate surfaces with a film of asphalt to form a cemented composite material. The attraction between asphalt films and aggregate surfaces is defined as adhesion. Water can destroy adhesion by two mechanisms: detachment and displacement.

Detachment is the separation of asphalt from aggregate surfaces by a thin film of water without an obvious break in the asphalt film, while displacement is the removal of asphalt from aggregate surfaces by water. Detachment or displacement may be explained by the interfacial energy theory and/or chemical reaction theory. The theory of interfacial energy considers adhesion as a thermodynamic phenomenon related to the surface energies of the materials involved. Nature will always act so as to attain a condition of minimum total free energy. Most aggregates have electrically charged surfaces. Asphalt, which is a mixture of high molecular weight hydrocarbons and a small portion of heteratoms (e.g., nitrogen, oxygen, and sulfur) and metals (e.g., vanadium, nickel, and iron), has little polar activity. Water, on the other hand, has high polarity. Thus, in an aggregate-asphalt-water system, water can displace asphalt from most aggregate surfaces because it is better

able to reduce the interfacial free energy of the system to form a thermodynamically stable condition of minimum interfacial free energy (Stuart 1990). Surface free energy analysis has shown that the reversible work of adhesion between an asphalt film and an aggregate in the presence of water is negative for most, if not all, aggregates (Mathews 1958; Lytton 2002), implying that the asphalt-aggregate bond is not stable in water. Chemical reaction theory explains the detachment and displacement phenomena from another perspective. Research on the chemical composition of asphalt and aggregate has shown that these two materials may form chemical bonding, such as covalent bonds (Plancher et al. 1977). When water comes into contact with aggregate surfaces, a series of hydrolysis and slow decomposition processes commence, which can alter the pH of the surrounding water layer by several units (Scott 1978; Nguyen et al. 1996). The change in the pH of the water can alter the type of polar groups adsorbed by aggregates, as well as their state of ionization/dissociation, leading to the build-up of opposing, negatively-charged, electrical double layers on the aggregate and asphalt surfaces and the separation of the asphalt from the aggregate (Scott 1978; Tarrer 1986).

For either detachment or displacement to happen, moisture needs to exist at the interface of asphalt and aggregate. In addition to spontaneous emulsification, insufficient drying, and incomplete coating of aggregates during construction, water can also reach the aggregate surface by several other mechanisms: asphalt film rupture, pull-back, and osmosis.

Film rupture refers to water migration that begins through local inhomogeneities and pinholes in the asphalt film and then opens them wider. Inhomogeneities are inevitable because of the non-uniform nature of asphalt coating. Pinholes occur when the aggregate surface is contaminated by dust or clay. Washing the coarse aggregate can alleviate the pinhole problem (Fromm 1974; Balghunaim 1991). Pull-back was proposed by Fromm (1974). At typical in-service temperatures, the surface tension of asphalt is smaller than that of water. When asphalt is present at the air-water interface, the asphalt may be drawn up along that interface, which may make the film rupture or become thin to such extent that emulsion penetration is rapid. Parker et al. (1987) and Yoon (1987) also observed this phenomenon in performing the boiling water test on loose mixtures. No method has been found to prevent this phenomenon. Osmosis is the diffusion of water through the asphalt membrane (Mack 1964). It is assumed to occur due to the presence of salt solutions in the aggregate pores which apply an osmotic pressure. Incomplete drying of aggregates may lead to the existence of the pore solution.

One typical consequent phenomenon of loss of adhesion is the exposure of bare aggregates, which is named “stripping” in the pavement community.

1.1.2.3 Pore Pressure and Hydraulic Scouring

Dynamic loading can intensify the disrupting action of water on both cohesion and adhesion. Pore pressure of the water entrapped due to mix densification under traffic or vapor created by heat can lead to high internal stresses within a moist void, which may result in the rupture of the asphalt films, especially at aggregate edges where the stress may be high and asphalt film may be thin. Pore pressure may also accelerate the diffusion of water into asphalt films.

Hydraulic scouring usually happens in the surface layers and at the interface between lifts in asphalt concrete, where the saturation level is high and water may remain trapped for long periods of time. When the pavement surface is saturated, moving vehicle tires first apply a positive pressure then a negative pressure (suction) to the water in surface pores. This compression-tension cycle is likely to contribute to the stripping of the asphalt film from the aggregate surface. In addition, dust mixed with rainwater can enhance the abrasion of asphalt films.

1.1.2.4 Summary of Damage Mechanisms

The moisture damage mechanisms discussed above have been known for many years, but are only understood generally or at a conceptual level, and have only been demonstrated in the laboratory. Given the complexity of mixture composition and structure and the large number of influencing factors in the field, it is difficult to estimate the relative contribution of each mechanism in the field. Possibly they may vary significantly under different field conditions. One indication from the mechanisms is that some amount of moisture damage is inevitable for asphalt mixes if sufficient water is available in the mix for an extended period. The rate and severity of the damage, however, may be reduced by adjusting mix design or using antistripping agents.

Previous studies and tests of moisture damage emphasized the material properties of asphalt and aggregate, while the effect of repeated loading was not well explored. In recent years the latter is acquiring more and more attention in research. Triaxial tests performed on an asphalt-treated permeable base (ATPB) material by Harvey et al. (1999) showed that the ATPB mix softened somewhat under soaking without loading, while both softening and stripping occurred under soaking with repeated loading. Full-scale Heavy Vehicle Simulator (HVS) tests on a pavement containing the same material showed stripping in the wheelpath and no stripping 0.3 m outside the wheelpath, as shown in Figure 1-1 (Bejarano et al. 2003). It seems that traffic loading plays an important role in the development of moisture damage.

1.2 Why Moisture Damage Is Important

It has long been noticed that the failure rate of asphalt pavements may increase significantly when water can easily get into the pavements. In some cases the failure includes complete disintegration of the asphalt mixes within a few years after construction (Parr 1958; Sha 1999). In the early 1990s, a significant number of asphalt pavements in northern California experienced premature failures only two to five years after construction. Investigation revealed that stripping was the main cause (Shatnawi 1995).

1.2.1 Moisture Effect on Pavement Performance

The direct result of the "moisture effect" is a weakening or a loss of bond strength within asphalt mixes as well as a reduction in the composite stiffness of the mix (the basis of desirable pavement performance), leading to the appearance of many distresses, such as fatigue cracking, rutting, raveling, and bleeding.

Rutting contributed by asphalt concrete mainly occurs in the surface layer, where the shear stress due to wheel loading is high. Because the surface layer has a large chance of being saturated by water from precipitation, loss of cohesion in the binder due to water reduces the shear strength of the asphalt concrete and accelerates the development of rutting, especially when the mix is moisture sensitive and the rainfall and traffic are heavy. The loss of cohesion in the surface layer may also promote the onset of top down cracking.

The lower portion of the asphalt layer often retains moisture for a longer time because of the slow rate of evaporation through the surface layers. The in-tension stress state of this portion accelerates the degradation of the adhesion and cohesion within the asphalt-aggregate matrix and contributes to development of bottom up fatigue cracks.

Raveling occurs at the pavement surface, where the traffic induced stresses are a combination of the non-uniform vertical stresses and the radial horizontal forces and hence generate significant horizontal tensile stresses. Water progressively reduces the tensile strength of the surface mixture so that cracks and disintegration will occur under repeated traffic loading.

Sometimes the asphalt stripped from aggregate surfaces inside the asphalt concrete can migrate to the road surface due to traffic pumping. Excessive asphalt at the surface, known as "bleeding", reduces the surface friction and jeopardizes the traffic safety.

1.2.2 Field Observation of Moisture Damage

Moisture damage in the field is generally recognized by observing aggregates stripped of asphalt and water existing in the failure area. A condition survey of California pavements by the author revealed that severe rutting, raveling, cracking, bleeding, and potholes often develop in moisture damaged area. Moisture damage typically first occurs at the bottom of asphalt concrete layers or at the interface of two surface layers, gradually developed upward. Sometimes a core taken from the damaged pavement has the shape of an hourglass, with the middle portion disintegrated and aggregates essentially clean. It was also observed that moisture damage typically happens in the wheelpath, while at the same location there is much less damage between the wheelpaths or on the shoulder. Moreover, moisture damage often occurs randomly at isolated locations, more in some sections while less in other sections. This implies that the non-uniformity of the placed asphalt mixtures may affect moisture damage substantially.

Damage due to moisture has been identified as a major problem for asphalt concrete pavements in the United States (Hicks et al. 2003), as well as in other areas of the world. In the United States, it is thought to become more prevalent since 1970s because of the change in material sources, increased traffic volume and load, and changes in construction practice (Busching 1986; Kandhal 2001). Pavement failure due to moisture damage is difficult to repair. Placement of overlays over the moisture damaged pavement, which is the most cost-effective solution for many distresses, is usually ineffective. The common solution is to immediately mill away the old layer and resurface the pavement, which incurs a much higher cost.

1.3 What Are the Current Practice and Problems

The ultimate goal underlying all research on moisture damage is to find methods to minimize or eliminate it in pavements. Moisture damage occurring in the field is usually irreversible, so the development of reliable test procedures and cost-effective preventive measures becomes most important.

1.3.1 Moisture Damage in Current Pavement Practice

A recent survey conducted by the Colorado Department of Transportation revealed that moisture damage is not uniformly addressed in pavement design (Hicks et al. 2003):

> About ten percent of states do not consider this problem in their design because they believe their pavements do not experience moisture damage or because they do not know how to identify it, particularly if the damage is below the surface.
>
> About five percent of states deal with it empirically based on experience, i.e., if a mixture has no moisture damage history, it is continually used, otherwise an antistripping agent (lime or organic additives) is added.
>
> Other states evaluate the moisture damage potential in the mixture design by comparing the result from a moisture sensitivity test to a specified criterion. If the result is below the criterion, the mixture is identified as being sensitive to moisture and usually an antistripping agent is added.
>
> Moisture damage is usually not considered in the pavement structural design phase.

1.3.1.1 Test Methods in Current Research and Practice

Many test methods have been developed to determine the moisture sensitivity of asphalt concrete mixtures. The methods address the influencing factors at different levels of detail, as shown in Figure 1-2.

On Level 1 are fundamental surface interaction tests focused on the effects of material composition and the effects of surface properties of asphalt and aggregate on bonding and debonding potential. They include methods to measure free surface energy (e.g., Ring Method, Pendant Drop Method, and Wilhelmy Plate Method) and tests for chemical analysis (Majidzadeh et al. 1968; Peterson et al. 1982; Cheng et al. 2002). Results from these tests are useful in material selection and modification, but cannot be used to predict the performance of asphalt pavements because: (1) oversimplification and assumptions are often needed in the tests compared to pavement mixtures (e.g., using flat, smooth aggregate to measure the contact angle); (2) the composition of aggregate and asphalt and the surface properties of aggregates are complex and difficult to characterize or quantify (e.g., the mechanical interlock between asphalt and aggregate is hard to model); and (3) the bonding strength between aggregate and asphalt is not the only factor influencing the performance of asphalt concrete. These tests have only been used in research studies, but not applied in practice.

On Level 1-2 are qualitative tests concentrated on the stripping potential of neat asphalt from aggregate particles under some specific laboratory conditions, including the Boiling Water test, the Quick Bottle test, the Rolling Bottle Method, the Static Immersion test (ASTM D 1664) and many others (Stuart 1990). The Boiling Water test evaluates the percentage loss of asphalt coating of aggregate particles submerged in boiling water for 10 minutes. The Quick Bottle test is used to judge the coating ability of asphalt on sands; in this test the mixture is shaken vigorously under water then emptied onto a paper towel to observe the coating. The Rolling Bottle method is used in Europe, in which aggregates coated with asphalt are dropped in a bottle with distilled water and then the bottle is rolled for three days. The coating of asphalt on aggregates is evaluated at several time points and a mean degree of coverage is visually determined as the test result. Visual tests of this kind on loose mixtures do not provide in-service performance information. Rather their role is for screening purposes.

On Level 2 are the tests conducted on compacted asphalt mixtures, including different versions of the indirect tensile strength ratio (TSR) test (e.g., AASHTO T-283, ASTM D 4867, and CTM 371), the Tunnicliff-Root test (ASTM D 4875), the Immersion-Compression test (ASTM D 1075), and others. These tests are similar in procedures and result criteria. They compact asphalt mixture to a standard air-void content (6 percent to 8 percent), keep some specimens dry but submerge other specimens in hot and cold water for a certain period, then measure the tensile or compressive strengths of all specimens. The ratio of the average conditioned strength to the average dry strength is used to evaluate the moisture sensitivity of the mix. A single pass/fail criterion is typically used, which is determined from the correlation between laboratory test results and actual field performance.

Two other tests, the environmental conditioning system (ECS) developed under the Strategic Highway Research Program (Terrel et al. 1991) and the Hamburg wheel tracking device (HWTD) test introduced from Europe (Aschenbrener et al. 1994), also test the compacted specimens for their moisture sensitivity. ECS conditions a cylindrical specimen with flowing hot water (60°C) and repeated compressive loading for multiple cycles and evaluates the change in resilient modulus and permeability for its moisture sensitivity. Limited field validation of the ECS showed that it could discriminate among asphalt mixes that will perform well and those that will perform poorly with regard to water sensitivity (Allen et al. 1994). However, another study (Aschenbrener et al. 1994) showed that the ECS did not adequately identify mixes that were moisture susceptible. Additionally, the University of Texas at El Paso found that the ECS conditioning process was not severe enough and the precision of the resilient modulus test was poor (Tandon et al. 1997). The ECS was not adopted in Superpave™, a product of the SHRP asphalt research. Some effort was spent to improve this test system, but no conclusive results have been achieved yet (Tandon et al. 2004). The HWTD test was introduced into the U.S. from Germany in the early 1990s. It soaks a slab specimen in water at high temperature (45°C to 60°C) and runs a small steel wheel load back and forth on the slab. This test is still empirical, but it includes dynamic loading in the conditioning process. Aschenbrener et al. (1994) did a limited number of field validations of this method, using 20 sites in Colorado State, and it showed promise for use in discriminating

between mixes with different moisture sensitivities. Texas DOT is in favor of this method and claimed that it can tell whether or not a mix will show premature failure in the field (Rand 2002). There are other versions of the loaded wheel rut tests, such as PURWheel (Pan and White 1999) and the Asphalt Pavement Analyzer (APA) test (Collins et al. 1997). Their working mechanism is similar to that of the HWTD test.

Level 3 corresponds to experiments performed on field test sections or analysis performed on data collected from field pavements. This level of work provides the most complete information about what influencing factors are significant in the field and what factors should be included in the laboratory testing for better prediction. Experiments with test sections are expensive and time consuming. Only a limited number of test sections have been built in the U.S. to evaluate moisture damage (Lottman 1982; Tunnicliff et al. 1995), and systematic field data collection and analysis have not been well done. The South Carolina Department of Highways and Public Transportation did a statewide survey of stripping in selected highways in 1980s (Busching et al. 1986). Many data were obtained but no statistical analysis was performed.

In current practice in the U.S. and other countries, the most widely used tests are different versions of the TSR, primarily due to its simplicity and its inclusion in Superpave™. The HWTD test is also gaining more and more attention because it includes dynamic loading in the conditioning procedure and is believed to better simulate the actual field conditions.

1.3.1.2 Treatments in Current Practice

When an asphalt-aggregate mix is determined to be moisture sensitive based upon a certain test or criterion, the often applied remedial method is to select a "treatment" of some type to increase the moisture resistance of the mix. A variety of treatments have been used in practice, and they can be grouped into those that are added to the asphalt binder and those that are applied to the aggregate. The treatments added to the asphalt binder are a variety of chemicals, generally referred to as "liquid antistripping agents." The treatments applied to aggregates include hydrated lime, portland cement, fly ash, flue dust, polymers, and many others. Currently the most widely used treatments are liquid antistripping agents added to the asphalt binder and hydrated lime added to the aggregate.

1.3.1.2.1 Liquid Antistripping Agents

The majority of liquid antistripping agents are proprietary chemicals, being amines or chemical compounds containing amines, which are strongly basic compounds derived from ammonia. Most are cationic, designed to promote adhesion between acidic aggregate surfaces and acidic asphalt cement. Some contain both cationic compounds and anionic compounds and may improve adhesion with all aggregates and asphalt cements. A few are anionic and are designed to promote adhesion to basic aggregate surfaces (Tunicliff and Root 1982). These liquid additives are usually depicted as long chain molecules that form a bridge between the asphalt and the aggregate surface. Usually a charged functional group is shown attached to the aggregate surface and the long chain is shown extending into the asphalt.

The addition of liquid additives to asphalt may soften the asphalt (Anderson et al. 1982). Aging characteristics and temperature susceptibility of the binder can also be affected. Moreover, numerous studies have determined that a certain asphalt mixture will be affected differently by different chemical additives. The resistance to stripping may be significantly changed if either the asphalt binder, aggregate or additive is changed.

The total price increase in using a liquid antistripping agent is typically in the range of $0.50 to $0.81 per ton of hot-mix asphalt (Epps et al. 2003).

1.3.1.2.2 Hydrated Lime

Hydrated lime [$Ca(OH)_2$] has been used in asphalt mixes for a long time, both as mineral filler and as an antistripping agent. Researchers observed that when hydrated lime coats an aggregate particle, it induces polar components in asphalt cement to bond to the aggregate surface. This effect also inhibits hydrophilic polar groups in the asphalt from congregating on the aggregate surface (McGennis et al. 1984). In addition, lime can neutralize acidic aggregate surfaces by replacing or coating acidic compounds and water-soluble salts on the aggregates and can react pozzolanically to remove deleterious materials (Epps et al. 2003). Interestingly, lime can inhibit certain bacterial activity, which is also a source of stripping (Ramamurti and Jayaprakash 1987; Benefield and Parker 1988, 1989).

Hydrated lime can be introduced into asphalt mixes by several methods: lime slurry to dry or wet aggregate, dry lime to wet aggregate, dry lime to dry aggregate and dry lime to asphalt. Although little research has been done to quantify the difference in effects of these methods, it is sufficient to say that asphalt mixes benefit from the addition of hydrated lime, no matter how it is introduced into the mix (Epps et al. 2003).

Hydrated lime is typically added at a level of one to two percent by weight of aggregate. The total price increase due to adding hydrated lime to asphalt mixes varies with the method of addition. Typically it is between $1.00 and $4.00 per ton of mix (Epps et al. 2003).

The effectiveness of treatments is typically evaluated by laboratory tests in a short term. There is little, if any, information about the long-term effectiveness of the treatments in the field.

1.3.2 Problems and Questions in Current Practice

Although moisture damage in asphalt pavements has been known for many years and extensive research has been done, current practice still cannot handle this problem effectively and economically. In the states that do not consider moisture damage in their design, catastrophic damage may not be observed, but moisture may potentially accumulate inside the pavement slowly and affect mix performance subtly. The effect of moisture may then be erroneously attributed to factors other than moisture. For the states that deal with the problem empirically based on experience, without clear knowledge of the main causes of moisture damage, they often tend to become conservative and apply treatments to all pavements in certain areas. This leads to a significant increase in construction costs. For states that use a moisture sensitivity test, the indirect TSR test is the most widely used. However, it has been found that results of the test could not correctly indicate whether moisture damage would occur in the field. Inconsistency between predictions and actual field performance has been well noted (Lottman 1982; Kiggundu et al. 1988; Kennedy et al. 1991; Tunnicliff et al. 1995), which suggests that this test has significant deficiency in its procedure or criterion.

Major gaps in current knowledge exist in the following areas: (1) the major factors associated with moisture damage in the field, (2) appropriate testing and evaluation procedure, and (3) the long-term effectiveness of treatments.

1.3.2.1 Associated Factors

The effects of different factors on the moisture sensitivity of asphalt mixes have been studied by many researchers. However, correctly identifying the contributing factors — materials and construction — in the field still remains challenging. This is because most research only focused on laboratory testing and evaluation, and lacked sufficient consideration of the actual field conditions and performance. Actual field conditions are much more complex than the laboratory assumptions, and include variational weather and traffic conditions, different pavement structures, drainage design, and different construction qualities. Without a good representation of actual field conditions, laboratory testing may miss some key factors and arrive at irrelevant

conclusions and ineffective treatments. The main reason for the lack of field study is the difficulty in collecting relevant field data. Except for a few extreme failure cases, moisture damage is difficult to identify from pavement surface and is often mistaken for other distress causes. Taking cores is often necessary to identify it. Furthermore, moisture damage is not included in pavement management systems as a distress type, so there is no historical data available for analysis. Lack of well-documented field performance data has been identified as a particularly severe deficiency in the moisture sensitivity area (Berger et al. 2003).

1.3.2.2 Test Methods

Although different versions of the TSR test have been widely adopted, it has two limitations. First, its conditioning procedure does not include dynamic loading, which is different from actual field conditions. Field condition survey (Sha 1999, 2001) has revealed that moisture damage is more significant in the wheelpath than between the wheelpaths, indicating that dynamic loading is an important factor that needs to be included in the test. Second, this test uses strength, a parameter that is not directly used in pavement design, to determine whether unacceptable moisture damage will occur in the field, or to quantify the benefit of treatment methods in terms of pavement life extension. This second constraint is also common to many other tests, such as the boiling water test or the ECS. To calibrate the results of these tests, detailed field data covering the whole spectra of possible field conditions are needed, but currently they are insufficiently available. A literature review showed that only a limited number of field pavement sections (less than 30) had been used to determine the currently specified passing/fail criteria for the TSR test and the sections were typically two to five years old (Lottman 1982; Aschenbrener et al. 1994; Allen et al. 1994; Tunnicliff et al. 1995). This further limits evaluation of the effect of moisture to the early ages of the pavement, i.e., catastrophic early failure. There is a need to develop a test procedure that can better simulate field conditions (e.g., including dynamic loading) and can be integrated into pavement design procedures to predict pavement performance life. Pavement performance-based tests, such as fatigue test and simple shear test, hold such promise.

A positive feature of the Hamburg wheel tracking device (HWTD) test is that dynamic loading is included. Currently, limited research has been done to calibrate the test procedure and to correlate test results with field performance. Aschenbrener et al. (1994) first performed field validation of the test in the U.S., using 20 sites in Colorado, and showed its promising use to discriminate mixes with different moisture sensitivities. The scope of the research, however, is limited and specific mix compositions such as binder type have not been considered in the analysis. The Texas Department of Transportation (TxDOT) ran the HWTD test on mixes consisting of a variety of asphalts and aggregates and claimed that it can tell whether or not a mix will show premature failure in the field (Rand 2002), but limited direct comparison with field performance data was shown. At the 2003 national seminar in San Diego on the moisture sensitivity of asphalt pavements, it was agreed that the HWTD test might be useful in the near term but that standardized procedures for specimen preparation and testing are still needed. It was also agreed that it is necessary to establish test conditions and criteria for different environments and mix characteristics. Although the HWTD test is a potential near-term substitute for the TSR test, research is needed to further investigate the effectiveness of HWTD test, as well as a correlation of its results with field performance on a broader range of material types and field conditions—particularly in areas where this test has never been applied.

1.3.2.3 Long-Term Effectiveness of Treatments

The effectiveness of both hydrated lime and liquid antistripping agents has been verified by laboratory tests that condition specimens in moisture for a short period (up to a few days). Whether or not the effectiveness of these additives will deteriorate with time in the pavement is unknown. This information is important to justify the use of additives because they increase the construction cost.

1.4 Research Objectives

This research is aimed at filling up some of the major gaps in current knowledge by completing the following objectives:

1. Perform a statewide field investigation to estimate the effect of different variables on the occurrence and severity of moisture damage, and to determine major factors associated with moisture damage in the field, other than aggregate source. To the extent possible with available data, analyze the extent of moisture damage in the state of California.
2. Perform laboratory investigation to determine the effect of some major factors (air-void content and binder content) on moisture damage. Recommend mitigation measures.
3. Evaluate the effectiveness of the HWTD test procedure to determine the moisture sensitivity of asphalt mixes and to predict field performance. To the extent possible with available data, analyze the correlation between lab test results and field performance.
4. Develop and evaluate testing procedures involving dynamic loading to determine the moisture sensitivity of asphalt mixes. Recommend appropriate conditioning procedures for laboratory tests.
5. Evaluate the effectiveness, especially the long-term effectiveness, of hydrated lime and liquid antistripping agents in improving the moisture resistance of hot-mix asphalt (HMA) using both current and new test procedures.

1.5 Project Overview

This research involves both field investigation and laboratory investigation. In the field investigation, both statewide condition survey and field sampling were conducted to collect data for the first and second objectives. In the laboratory investigation, different experiments were designed and performed for different research objectives. Laboratory test results were compared with field performance to the extent possible with the available data.

The detailed work and findings are described in the remaining chapters of this report. Chapter 2 describes the selection and acquisition of materials used in the experiments, mix design, and specimen preparation procedures. Chapter 3 and Chapter 4 detail the methodologies and the results of the investigation of contributing factors to moisture damage, including both field and laboratory investigations. In the field investigation, a cross-sectional data set was obtained and analyzed statistically. The laboratory investigation mainly studies the factors affecting moisture ingress and retention in asphalt concrete and the effect of construction-related variations on moisture damage. In Chapter 5 the HWTD test was evaluated with both laboratory-compacted specimens and in-service field cores. In Chapter 6 a fatigue-based test procedure for evaluating moisture damage was developed. Emphasis was put on determination of the appropriate conditioning procedure. Results from the new test procedure were compared with results from both the TSR and the HWTD tests. Moreover, a rutting-based test was also developed and evaluated preliminarily. In Chapter 7 the long-term effectiveness of both hydrated lime and liquid antistripping agents were evaluated by both the fatigue based test and the TSR test. The time effect of moisture on mix properties was also studied. Chapter 8 summarizes the major findings, recommendations, and future research. Supplementary experiments and test data are included in the appendices.

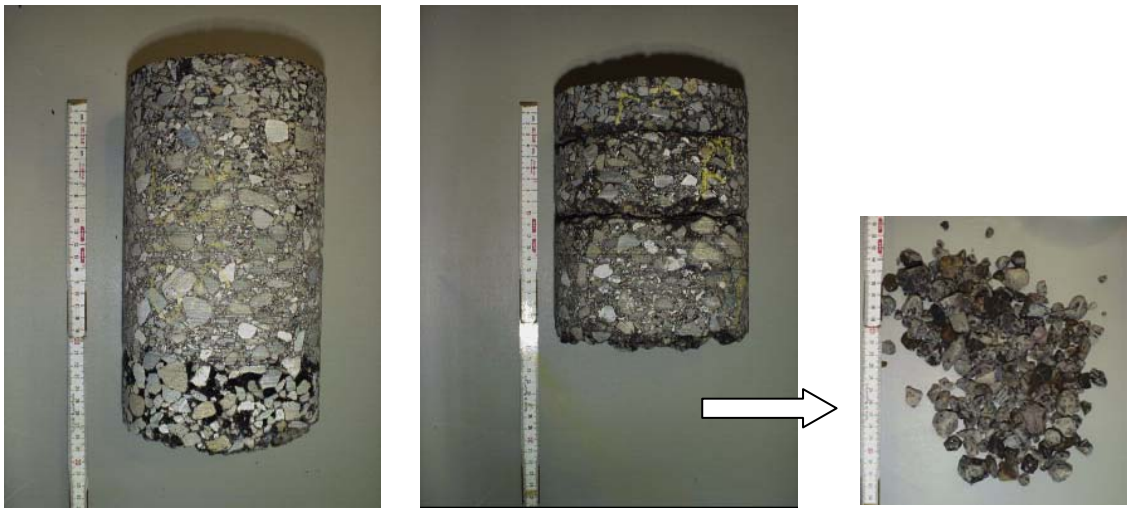

(a) (b)

Figure 1-1. Cores taken from an HVS test section of ATPB materials that were tested in wet condition: (a) taken from a location outside the wheelpath; (b) taken from a location in the wheelpath (Bejarano et al. 2003).

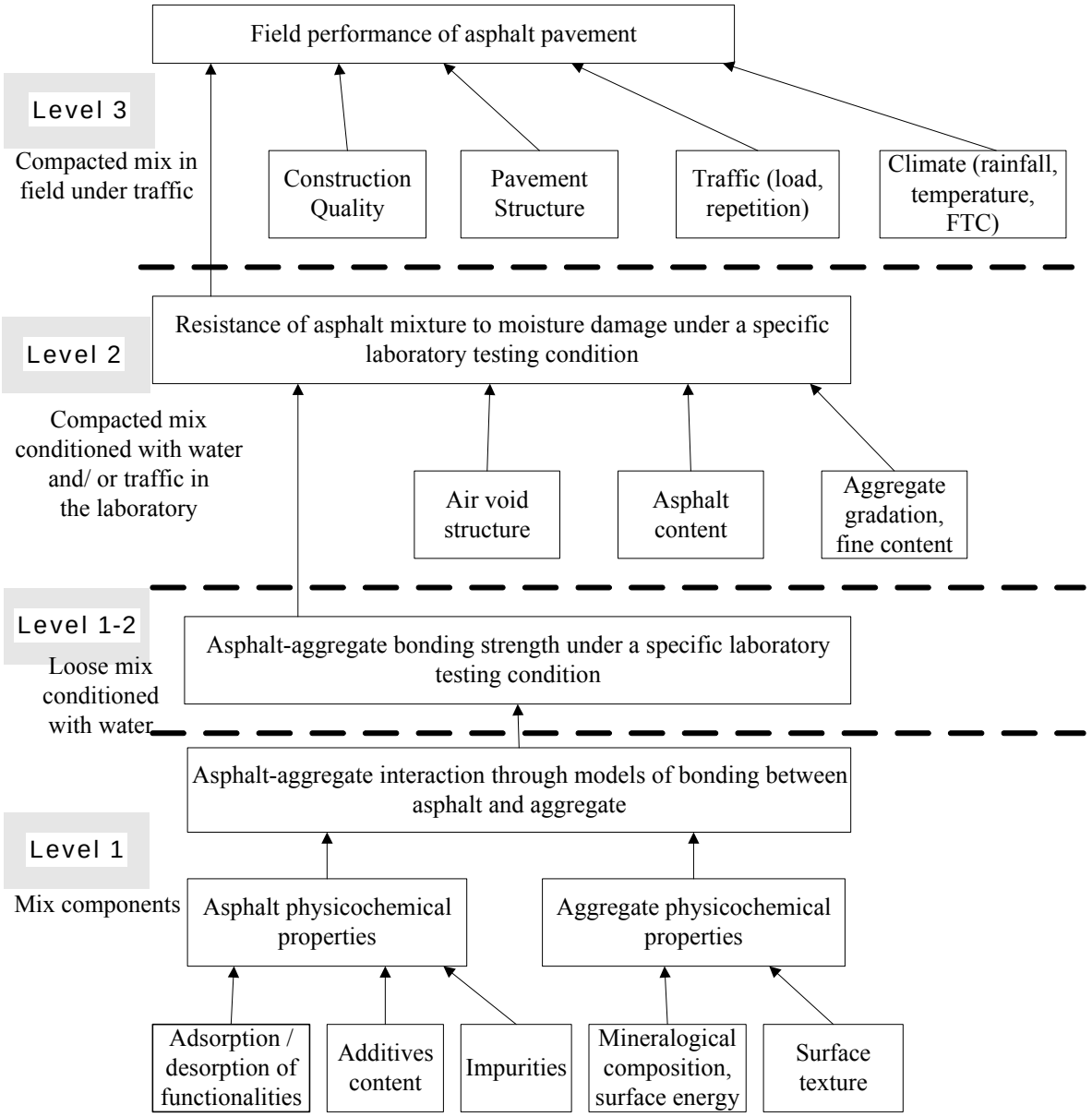

Figure 1-2. Factors influencing moisture damage of asphalt pavements.

2.0 MATERIAL SELECTION, MIX DESIGN AND SPECIMEN PREPARATION FOR LABORATORY EXPERIMENTS

This chapter describes the material selection, mix design, and specimen preparation procedures that are common to all the laboratory experiments in this research.

2.1 Material Selection

Two aggregates, two asphalts, and three treatments were incorporated in this project to form a variety of asphalt mixtures with different moisture sensitivity.

2.1.1 Aggregates

It is generally believed that aggregate properties (mineral composition, porosity, surface texture, etc.) affect the moisture resistance of asphalt concrete mixtures. To account for this factor in the laboratory experiments, two contrasting aggregates were used: one with good compatibility with asphalt and the other with poor compatibility.

2.1.1.1 Aggregate Selection

Initially five aggregates were selected as candidates based on their field or laboratory performance: B, CC, M, L, and A. Aggregates B and CC are from two adjacent gravel pits south of Redding, California. Aggregate B was considered to have good compatibility with asphalt because most of the pavement sections containing this aggregate had not shown moisture damage (Shatnawi et al. 1995), while Aggregate CC was recommended by Caltrans District pavement engineers to be a poor performance representative. Aggregate M comes from a gravel pit in the Eastern Region of Washington State and has a poor performance history. Aggregate L comes from a quarry north of Solano County, California. It is of a basaltic-volcanic nature, which is commonly thought to be more compatible with asphalt than granite, but pavements containing this aggregate have shown poor performance. Aggregate A is obtained from a quarry in central California. No severe moisture damage has been observed on pavements containing this aggregate, but a laboratory indirect tensile strength ratio (TSR) test suggested it has poor compatibility with asphalt.

Originally, aggregates B and CC were selected for the experiments based upon recommendations from District pavement engineers. However, doubts were raised as to whether they were really different from each other given the short distance between their pits. Therefore, aggregates M, L, and A were considered to replace Aggregate CC as the "poor" performance representative although Aggregate A had only showed poor performance in the laboratory but not the field. Two tests were performed to provide further information for comparison of the five aggregates: the X-Ray Fluorescence Spectrometry (XRF) test and the Boiling Water test (ASTM D 3625-96).

2.1.1.1.1 XRF Test

The XRF test is used to analyze the chemical and mineral compositions of the aggregates. The way it works is briefly introduced in the following (Shackley 2002):

> *High-energy primary X-ray photons are used to irradiate the atoms in a sample material, whose electrons are ejected in the form of photoelectrons. This creates electron "holes" in one or more of the orbitals, converting the atoms into ions - which are unstable. To restore the atoms to a more stable state, the holes in inner orbitals are filled by electrons from outer*

orbitals. Such transitions may be accompanied by an energy emission in the form of a secondary x-ray photon - a phenomenon known as "fluorescence". The characteristic X-ray emissions result in an energy spectrum that is a "fingerprint" of the specimen. Based on the intensities of the peaks in the spectrum, the concentrations of the constituent elements can be calculated.

The XRF analysis of the five aggregates was performed at the Department of Earth and Planetary Science at the University of California, Berkeley (EPS-UCB). The element composition for each of the five aggregates in terms of their oxides is shown in Table 2.1 and Figure 2-1. For comparison, the typical chemical compositions of granite and basalt are also included in the table (Stuart 1990). Figure 2-1 shows that the chemical composition of Aggregate L is very similar to that of basalt. The chemical composition of Aggregate CC is similar to that of Aggregate B, except that the Aggregate CC contains a higher percentage of SiO_2, and a lower percentage of CaO. Aggregate M contains the highest percentage of SiO_2, while Aggregate A has a SiO_2 percentage lower than that of granite, but higher than that of basalt.

The mineral composition of each aggregate was calculated using the software *MINPET* available at EPS-UCB, and is shown in Table 2.2. One can see that the mineral compositions of Aggregate B and Aggregate CC are similar. Aggregate A has a lower percentage of quartz, but a higher percentage of albite and anorthite than aggregates C, CC, and M. Aggregate A is on the border of being granite or granodiorite. Based on the feldspar content, it appears that this aggregate is quartz monzodiorite (Shomglin 2003).

2.1.1.1.2 Boiling Water Test

The Boiling Water test (ASTM D 3625-96) is used to determine the relative compatibility of the five aggregates with asphalt in the presence of water. In this test loose mixtures are immersed in boiling water for 10 minutes and the percentage of asphalt film retained on aggregates is visually estimated. The more the asphalt retains, the better the compatibility between them. In this study, a dense gradation with 12.5-mm nominal maximum aggregate size (Figure 2-2) was used for all aggregates, mixed with 6.3 percent (by dry weight of aggregate) Valero AR-4000 asphalt.

The results (Table 2.3) indicate that the ranking of the five aggregates from high compatibility to low compatibility is: L > B > CC > M > A. The compatibility of Aggregate CC is not significantly lower than that of Aggregate B. The compatibility of Aggregate A is significantly lower than that of the others.

2.1.1.1.3 Selection of Aggregates for Tests

Results of the two tests showed that there is no significant difference between aggregates B and CC. The poor performance of pavements containing Aggregate CC may result from reasons other than the aggregate type, such as poor mix design and construction deficiencies. Therefore, aggregates B and CC were not selected simultaneously in the experiments. Other aggregates are different from each other in terms of mineral composition, and the Boiling Water test showed that both Aggregates M and W have poor compatibility with asphalt. Aggregate M was not selected because of the high cost of hauling it from Washington State. Aggregate L was not selected because of the lack of highway pavement sections with performance data. Finally, both aggregates B and A were chosen as the representatives of good and poor compatibility with asphalt.

2.1.1.2 Aggregate Data

Aggregate B was produced from a gravel pit in the drainage basin west of the Sacramento River in Northern California. The aggregate samples were obtained from four stockpiles: 19.5-mm, 9.5-mm, natural sand, and crushed dust, and were stored in 208-L plastic barrels. The large particles of this material are generally semispherical, with some crushed faces and some round faces, have a semismooth surface texture, and are generally dusty. The Sand Equivalent test result (Table 2.4) indicated that this aggregate has relatively high clay content, but it does not exceed the allowable value specified in the Standard Specifications of California Department of Transportation. The Los Angeles Abrasion Test results (Table 2.4) indicate that this aggregate is resistant to mechanical degradation.

Aggregate A was obtained from hard rock mining from a large batholith. It is generally white, with black and grey inclusions, and completely crushed. The aggregate samples were obtained from five stockpiles: 19.5−12.5-mm, 12.5−4.75-mm, 6.3−2-mm, N4−N8, and sand, and stored in 208-L plastic barrels. The Los Angeles Abrasion test results (Table 2.4) indicate that this aggregate is less resistant to mechanical degradation. Dust tends to be produced during laboratory sieving. The Sand Equivalent test result (Table 2.4) shows that this aggregate has low clay content.

The amount of potential harmful materials (including clay and organic material) in the fines passing the 0.075-mm (No. 200) sieve was checked for both aggregates by the Methylene Blue test. Previous studies have shown that the Methylene Blue test results can give a good indication of the stripping potential of asphalt from aggregates tested (Kandhal et al. 1998; Aschenbrener et al. 1994). The test was performed following a procedure used by the Ohio Department of Transportation, which is included in the appendices. The results (Table 2.4) show that both aggregates have a methylene blue value less than 9 mg/g. Generally a methylene blue value less than 10 mg/g corresponds to little harmful material and good pavement performance (Aschenbrener et al. 1994), so the potential confounding effect of the harmful materials in aggregates can be excluded.

2.1.2 Asphalts

Two asphalts were selected for this project: AR-4000 and PBA-6a. The AR-4000 asphalt is processed from California Valley crude sources, and was obtained from Shell Oil Products US Company in Martinez, California. The PBA-6a is a polymer modified binder obtained from Valero Marketing and Supply Company in Pittsburg, California. Both asphalts are commonly used in California highways, and the PBA-6a binder has been used as one of the countermeasures to reduce moisture damage in some regions of California. The basic binder properties were provided by the material suppliers, and are shown in Table 2.5.

2.1.3 Treatments

Three treatments were used in this project: hydrated lime and two liquid antistripping agents. Hydrated lime is a dry white powder resulting from the controlled slaking of quicklime with water. It was received in 50-lb sealed bags from Chemical Lime Company. The liquid antistripping agents were two anonymous proprietary products coded “A” and “B.” According to the supplier, liquid antistripping Agent A was expected to perform better than Agent B.

2.2 Mix Design

2.2.1 Aggregate Gradation

Two aggregate gradations (Figure 2-3) were included in this project: 19-mm nominal maximum medium gradation and 19-mm nominal maximum coarse gradation. Both gradations are proposed in California Department of Transportation (Caltrans) Standard Specifications and are commonly used in California pavements.

2.2.2 Optimum Binder Contents

The optimum binder contents were determined in accordance with California Test Method 367, using the air void, flushing, and stability requirements of the standard Hveem method, which requires a minimum "Hveem stability" value of 37, a minimum air-void content of 4 percent, and no flushing on the specimen surface. The optimum binder content was determined separately for mixes containing different aggregate types, but assumed the same value for mixes containing the same aggregate but different binders. The mix design data are listed in Table 2.6 and graphically shown in Figure 2-4. From these data the optimum binder content was determined to be 5 percent for mixes containing Aggregate A and 6 percent for mixes containing Aggregate B (mass of aggregate basis).

2.2.3 Treatment Contents

The amount of treatment added into mixtures was determined based upon the range recommended by material suppliers.

2.2.3.1 Hydrated Lime

Hydrated lime was added at a rate of 1.4 percent by weight of dry aggregates. To exclude the confounding effect of the extra fines due to the added lime, the same mass of fines passing the 0.075-mm sieve was removed from the original aggregates so that the aggregate gradation in the mix remained nearly unchanged.

2.2.3.2 Liquid Antistripping Agents

Both liquid antistripping agents were added at a rate of 0.75 percent by weight of asphalt, based on the recommendations from the supplier. This rate is higher than the common addition rate (0.25 to 0.50 percent) of liquid antistripping agents. Engineering practice and laboratory experiments have shown that the binder properties are not significantly affected by the liquid antistripping agents at the ratio in the common range (Epps et al. 2003). However, concerns had been raised in this study that higher amounts of liquid antistripping agents might change the rheological properties of the binders and potentially cause unexpected degradation of pavement performance. To resolve these concerns, several binder tests were performed on the AR-4000 asphalt with and without the liquid antistripping Agent A, including: (1) the dynamic shear rheometer (DSR) test (AASHTO TP5), (2) the Penetration test (ASTM D 5), and (3) the absolute viscosity by vacuum capillary viscometer test at 60°C (ASTM D 2171). All three tests were performed on both the original binder and the short-term aged binder. Short-term aging was realized by following the Rolling Thin Film Oven (RTFO) procedure specified in ASTM D 2872.

2.2.3.2.1 Dynamic Shear Rheometer Test

The dynamic shear rheometer (DSR) test is used to characterize both viscous and elastic behavior by measuring the complex shear modulus (G^*) and phase angle (δ) of asphalt binders at medium to high temperatures. G^* is a measure of the total resistance of a material to deformation when exposed to repeated pulses of shear stress. δ is an indicator of the relative amounts of recoverable and non-recoverable deformation. This test was performed at 60°C and 1.59Hz frequency, at the Valero Refining Company at Benicia, California.

The test results are summarized in Table 2.7. As it can be seen, for the un-aged binder, the addition of liquid antistripping Agent A reduces the complex shear modulus (G^*) by about 17 percent and slightly increases the phase angle (δ). On the other hand, for the aged binder, the addition of liquid antistripping Agent A increases the complex shear modulus (G^*) by about four percent and causes no change to the phase angle (δ).

2.2.3.2.2 Penetration Test

Penetration is defined as the distance that a standard needle vertically penetrates a sample under known conditions of loading, time, and temperature. It reflects the consistency of a bituminous material. This test was performed at 25°C with a load of 0.1 kg and 5-second duration.

The test results are shown in Table 2.8. As can be seen, the addition of 0.75 percent liquid antistripping Agent A has little effect on the penetration of the AR-4000 binder both before and after the RTFO aging. A two-sample t test for mean shows that the null hypothesis that liquid antistripping agent has no effect is accepted at the 95 percent confidence level.

2.2.3.2.3 Absolute Viscosity Test

Absolute viscosity is defined as the ratio between the applied shear stress and rate of shear. It is a measure of the resistance to flow of the binder. This test was performed at 60°C by vacuum capillary viscometers.

The test results are shown in Table 2.9. As can be seen, the addition of 0.75 percent liquid antistripping Agent A reduces the viscosity of the un-aged AR-4000 binder by about four percent, while it has little effect on the viscosity of the aged binder. A two-sample t test for mean shows that the null hypothesis that liquid antistripping agent has no effect is accepted for both un-aged and aged asphalt.

2.2.3.2.4 Summary

Results from the three tests show that the addition of 0.75 percent liquid antistripping Agent A slightly changes the rheological properties of the un-aged AR-4000 binder in the DSR test, but not in the penetration and viscosity tests. The general trend is that the liquid antistripping agent reduces the resistance to deformation of the binder. This reduction can facilitate the mixing of asphalt and aggregates. On the other hand, the liquid antistripping agent does not affect the rheological properties of the short-term aged asphalt. Because short-term aging occurs in construction during the mixing and placement phases, the addition of 0.75 percent liquid antistripping agent may not adversely affect the actual field performance of the hot-mix asphalt pavement. The short-term aging is also simulated in laboratory testing by placing loose mix in a 135°C forced-draft oven for

four hours before compaction. Therefore, the effects, other than improving moisture resistance, of the liquid antistripping agent on the binder properties can also be excluded from the laboratory data analysis.

2.2.4 Mix Designation

Several mixes were included in this project. For clarity and brevity in the presentation of test results, a coding system is used in this study to designate different mixes. A mix is generally represented by the following code:

$$P_1P_2P_3(P_4)-(P_5P_6)$$

where,

P_1 = aggregate type: A (Aggregate A) or B (Aggregate B);

P_2 = binder type: A (AR-4000) or P (PBA-6a);

P_3 = treatment type: N (no treatment), M (hydrated lime), LA (liquid antistripping agent A), or LB (liquid antistripping Agent B);

P_4 = aggregate gradation: this code is omitted if the gradation is 19-mm nominal maximum medium gradation. If the gradation is 19-mm nominal maximum coarse gradation, letter C is placed;

P_5 = binder content: OM (optimum binder content), LM (optimum binder content minus 0.5 percent), or EM (optimum binder content minus 1.0 percent);

P_6 = nominal air-void content: 4 (4 percent), 5 (5 percent), 7 (7 percent), 8 (8 percent), 10 (10 percent), 11 (11 percent), or 13 (13 percent).

If P_5P_6 is omitted, the mix has optimum binder content and 7 percent air-void content. As an example, AANC represents a mix consisting of Aggregate A and AR-4000 binder without treatment, having coarse gradation, optimum binder content, and 7 percent air-void content.

2.3 Specimen Preparation Methods

This section describes the specimen preparation methods for both laboratory compacted specimens and field compacted specimens. The laboratory compacted specimens include beams (50.8 mm × 63.5 mm × 381.0 mm), cylindrical specimens (152.4 mm ϕ × 50.8 mm), TSR specimens (101.6 mm ϕ × 63.5 mm), and HWTD specimens (241.3 mm × 330.2 mm ×76.2 mm). The field compacted specimens are cylindrical specimens cut for the HWTD test.

2.3.1 Aggregate Preparation

Aggregates A and B were obtained from five and four stockpiles respectively at the source pit or quarry. Plenty of moisture was observed in most aggregates, so they were spread out on trays and dried in a forced-draft oven at 110°C to a constant mass (usually for three days). After being removed from the oven, they were allowed to cool and then placed in 208-L plastic barrels with lids to prevent contamination of water and other elements.

Each stockpile had has a unique distribution of aggregate sizes. The gradation of each stockpile material was provided by the material suppliers, but was re-analyzed in the laboratory by dry and wet sieve tests. The proportion of each stockpile material was determined based upon solutions of the following constraint minimization problem:

$$\begin{aligned} &\min: \sum_i (\sum_j P_j A_{ji} - T_i)^2 \\ &s.t.: 0 \le P_j \le 1 \\ &\quad \sum_j P_j = 1 \end{aligned} \qquad \textbf{(2-1)}$$

where P_j = proportion of stockpile j; A_{ji} = percent of aggregate passing sieve size i in stockpile j; T_i = target percent of aggregate passing sieve size i.

The gradation of each stockpile material and its proportion to form the 19-mm nominal maximum medium gradation are shown in Table 2.10. For Aggregate A, two additional components, 19-mm and dust (fines passing 0.075-mm sieve), were added to reduce the squared error to an acceptable level. Problem (2-1) was solved in Microsoft® *Excel* by the "Solver" tool.

The aggregate for all specimens was assembled in 1.2-kg or 7-kg batches in plastic containers, and placed in aluminum pans prior to mixing.

2.3.2 Binder Preparation

The two binders (AR-4000 and PBA-6a) were received from the suppliers in 18.9-L (5-gal) sealed buckets. Each bucket was heated and stirred at 135°C for four to five hours until the fluid was of a uniform consistency, then it was poured into small liter-sized tin cans with lids and stored in a 20°C room for future use.

2.3.3 Addition of Hydrated Lime

In this project, dry hydrated lime was added to dampened aggregates by the following procedure:

1. Weigh out the quantity of aggregate to be treated and put in a sieve stack consisting of 4.75-, 2.36-, 0.6-, 0.3-, and 0.075-mm sieves. Sieve for three minutes and subtract an amount of fines passing the 0.075-mm sieve equivalent to the amount of hydrated lime to be added, then recombine the remaining aggregates into a mixing bowl.
2. Weigh out individual lime batches in small round tins.
3. Add 3 percent water by dry weight of aggregate, using a graduated cylinder, to thoroughly dampen the sample.
4. Mix aggregates with water for two minutes.
5. Add the desired amount of lime and continue mixing for additional three minutes.
6. Put the aggregates in aluminum pans and dry to a constant mass in an oven at 110°C.

After drying, the aggregates were usually immediately heated to the mixing temperature and mixed with asphalt. In a few cases, the aggregates were cooled to the room temperature for future use, but the storage time was no more than 48 hours.

2.3.4 Addition of Liquid Antistripping Agents

The liquid antistripping agents were added into asphalt prior to mixing the aggregates with asphalt, following these steps:

1. Heat asphalt in liter-sized tins to the required mixing temperature.
2. Heat the liquid antistripping agent at a temperature between 21°C and 60°C to fluid status.
3. Weigh the liquid antistripping agent needed with a dropper and pour into the asphalt
4. Mix the asphalt and the liquid antistripping agent thoroughly.

The mixing of aggregates with asphalt usually followed immediately after the above steps. Occasionally, the blended asphalt and antistripping agent were cooled for future use, but the storage time was no more than 96 hours.

2.3.5 Mixing of Asphalt and Aggregate

Both aggregate and asphalt were heated at the mixing temperature for two hours prior mixing. For mixtures containing the AR-4000 binder, the mixing temperature was derived from the binder grade analysis data supplied by the binder suppliers, including viscosity (135°C, 60°C) and penetration (25°C) test results. By plotting these test results on a Bitumen Test Data Chart, the mixing temperature was chosen as the temperature at which the binder viscosity was 0.17 Pa·s, a value based on mixing experience with 16 different asphalts used in the SHRP A-003A project (Harvey 1991). The selected mixing temperature for the AR-4000 binder was 144°C. For mixtures containing the PBA-6a binder the mixing temperature was 149°C, which the supplier recommended.

For the beam specimens, cylindrical specimens, and HWTD specimens, aggregate was heated in aluminum pans in about 7-kg batches, while for the TSR specimens it was heated in aluminum pans in about 1.2-kg batches. Asphalt was heated in liter-sized tins with lids. Mixing spoons and a mixing bowl were also heated to the same temperature prior mixing. The mixing blades and base of the batch mixer were heated with a heating lamp during the preheating and mixing process.

Each batch of aggregate was combined with the appropriate amount of asphalt in the mixing bowl and mixed for five minutes in the mixer. For aggregates treated with hydrated lime, the mixing time was extended to seven minutes to ensure complete coating by asphalt. Spoons were used to turn over any unmixed aggregate at the bottom and edges of the mixing bowl during mixing. After mixing, the accumulated fines and binder were scraped off the blade into the mix.

2.3.6 Aging and Storage

After mixing, the loose mixture was poured back into the pans and aged in ovens for a short term. The mixture was aged at 135°C for 4 hours for the beam specimens, cylindrical specimens, and HWTD specimens, and at 60°C for 16 hours for the TSR specimens. This process was used to simulate the mixture aging that occurs during plant mixing and construction. After aging, two 2-kg samples were extracted from each mixture for measuring the theoretical maximum specific gravity (Rice) according to ASTM D 2041. The resulting Rice value was used throughout the project to determine the air-void content of specimens.

Following aging, the oven temperature was immediately changed to the temperature for compaction. In a few cases, the mixture was cooled to room temperature and then a few days later it was reheated to the compaction temperature and compacted. The time interval between mixing and compaction was usually less than seven days. The reheating resulted in some additional aging compared to the specimens that were not reheated.

2.3.7 Compaction

Two compaction methods were used in this project: kneading compaction for the TSR specimens and rolling wheel compaction for the other specimens.

2.3.7.1 Kneading Compaction

The TSR specimens were compacted by a kneading compactor at a temperature between 110°C and 115°C, following the procedure specified in the California test method CTM 371. After compaction, a leveling-off load of 56 kN was applied at a head speed of 6.4 mm/min until a specimen height of 63.5 ± 3.0 mm was achieved.

2.3.7.2 Rolling Wheel Compaction

The beams, cylindrical specimens, and HWTD specimens were all compacted by a UCB rolling wheel compactor (Harvey 1991). This equipment is a tandem steel wheel roller, self-propelled with forward and reverse control in a static (nonvibratory) mode. Three different molds were used for the three types of specimens: a two-ingot short mold, a three-ingot long mold, and a slab mold. All molds have a height of 76 mm. The two-ingot short mold is 167 mm wide and 502 mm long at the bottom of each ingot, and can produce four beams. The three-ingot long mold is 155 mm wide and 595 mm long at the bottom of each ingot, and can produce nine cylindrical specimens. The slab mold is 426 mm wide and 498 mm long at the bottom of the ingot, and can provide two HWTD specimens. The sides of these molds have a 4:1 slope to prevent insufficient compaction along the edges of the molds.

For mixtures containing the AR-4000 binder, the compaction temperature, also derived from the Bitumen Test Data Chart, was 122°C, corresponding to a 0.6 Pa·s binder viscosity (Harvey 1991). For mixtures containing the PBA-6a binder, the compaction temperature was 138°C, recommended by the supplier.

The mass of loose mixture needed to reach the target air-void content was calculated by the following formula:

$$M = G_m \cdot V \cdot (1 - AV) + L \qquad \textbf{(2-2)}$$

where M = the mass of loose mixture used for compaction; G_m = theoretical maximum specific gravity (Rice) of the mixture; V = volume of the mold; AV = adjusted air-void content; and L = material loss during compaction (0.11 kg).

Past compaction experience reveals that the target air-void content usually cannot be used directly in Equation (2-2). Instead, it should be adjusted based upon the correlation between the air-void content used for calculation (adjusted air-void content) and the obtained air-void content (target air-void content). The relationship obtained in this project is shown in Figure 2-5.

After the required mass of loose mixture was heated to the compaction temperature, which usually took two hours in the oven, it was poured into the preheated compaction mold in two lifts. A spatula was used to distribute the material uniformly in the mold after each lift was poured. The compactor was then repeatedly passed over the mixture back and forward for a total of 50 passes in the following order: 10 passes on the center of the mold, 10 passes on the left half of the mold, 10 passes on the center again, 10 passes on the right half of the mold, and 10 passes on the center again. This sequence aimed to create a shearing force along the edge of the rolling wheel to achieve a compaction similar to that in field construction. After compaction, the mix was allowed to cool overnight.

2.3.8 Coring and Cutting

After overnight cooling, the ingots were extracted from the molds and cored and/or cut into the required specimens. The cylindrical specimens were first cored from the ingots with a Concore Model A-5 coring machine, and then cut with a double-bladed saw to the required dimensions. Both the beams and the HWTD specimens were cut from the ingots with a single-bladed stone saw.

2.3.9 Air-Void Measurement

Air-void content was determined for all specimens. It was calculated from the bulk specific gravity (G_b) and the theoretical maximum specific gravity (Rice) (G_m) by the following equation:

$$AV = 100 \times (1 - G_b / G_m)\% \quad \textbf{(2-3)}$$

The Rice was predetermined for each mix in accordance with ASTM D 2041 and used throughout the project. The bulk specific gravity was measured on each specimen. Three methods were used to measure the bulk specific gravity: the UCB Parafilm method, the Water Displacement method, and the Corelok® method.

2.3.9.1 UCB Parafilm Method

The UCB Parafilm method was used to measure the bulk specific gravity of beams and cylindrical specimens whose surfaces were all cut faces. The procedure is outlined as follows (Harvey, 1991):

1. After cutting or coring, specimens were placed on perforated shelves for overnight drying.
2. The specimen was dried with compressed air at a pressure of approximate 724 MPa. The tip of the air gun was kept about one inch from the specimen surface and the specimen was dried until no trace of moisture was visible beneath the compressed air. The mass of the specimen was measured in air. This mass was coded as WANP.
3. The specimen was completely wrapped with Parafilm M®, a moisture-resistant, thermoplastic flexible plastic sheet, and weighed in air. This mass was coded as WAWP.
4. The sealed specimen was weighed under water, and coded as WWWP.
5. After removing the parafilm, the specimen was weighed under water again, and was coded as WWNP.

Two bulk specific gravities were calculated, the specific gravity with parafilm (G_{wwp}) and the specific gravity without parafilm (G_{wnp}), by the following two equations:

$$G_{wwp} = \frac{WANP}{(WANP - WAWP)/0.9 + WAWP - WWWP} \quad \textbf{(2-4)}$$

$$G_{wnp} = \frac{WANP}{WANP - WWNP} \quad \textbf{(2-5)}$$

The air-void content calculated from G_{wwp} is more close to the real value and was used in the data analysis and reporting. The air-void content calculated from G_{wnp} is always lower than the real value and was only used as a reference to check if mistakes occurred during the measurement.

2.3.9.2 Water Displacement Method

The Water Displacement method was used to measure the bulk specific gravity of TSR specimens and HWTD specimens which had as-compacted surfaces. The procedure specified in AASHTO T 166 Method A was followed and is outlined below:

1. Specimen was immersed in water at 25°C for four minutes.
2. The mass of specimen was weighed in water and recorded as C.
3. The specimen was removed from water and quickly damp dried by blotting with a damp towel. The surface dry mass was measured and recorded as B.
4. The specimen was dried to a constant mass at 52°C, and weighed for its dry mass A.

The bulk specific gravity of the specimens (G_B) was calculated by the following equation:

$$G_B = \frac{A}{B - C} \qquad \textbf{(2-6)}$$

2.3.9.3 Corelok® Method

The Corelok® method was used to measure the bulk specific gravity of certain specimens that had as-compacted surface and was used in an experiment in which no water was allowed to contact the specimens. Corelok® is a vacuum-sealing device utilizing an automatic vacuum chamber with a specially designed, puncture-resistant, resilient plastic bag, which tightly conforms to the sides of the sample and prevents water from infiltrating into the sample (Cooley et al. 2002). The test procedure specified by the manufacturer was followed, which is outlined below:

1. Measure the specimen mass and the bag mass in air.
2. Place the specimen into the bag and place the bag inside the vacuum chamber.
3. Close the vacuum chamber door. The vacuum pump will start automatically and evacuate the chamber to 760 mm-Hg.
4. In approximately two minutes, the chamber door will automatically open with the sample completely sealed within the plastic bag and ready for water displacement testing.
5. Measure the mass of the sealed bag in water.

The bulk specific gravity of the specimen was calculated with a formula similar to Equation (2-4).

In all three methods, the temperature of the water used for mass measurement was kept at 25°C.

2.3.10 Preparation of Field Compacted Specimens

Field compacted specimens were 152-mm diameter cores taken from different pavement sections on California highways. Some of the cores were tested in the Hamburg wheel tracking device. After being brought back to the laboratory, they were cut into a height of 76 mm or a height equivalent to the layer thickness, whichever was smaller, by a single-bladed stone saw. The surface was trimmed if it was rough. Bulk specific gravity was measured using the UCB Parafilm method.

Table 2.1. Chemical Composition of Aggregates by the XRF Analysis

	Weight Percent (%)									
Aggregate	**Na_2O**	**MgO**	**Al_2O_3**	**SiO_2**	**P_2O_5**	**K_2O**	**CaO**	**TiO_2**	**MnO**	**Fe_2O_3**
B	1.59	3.28	10.96	68.61	0.10	0.47	6.54	0.48	0.08	5.64
CC	2.19	2.10	9.99	73.19	0.12	0.75	3.43	0.53	0.22	5.67
M	1.68	0.57	7.21	85.72	0.06	1.39	0.71	0.27	0.02	1.63
L	4.44	4.30	15.20	49.23	0.15	0.50	9.22	1.42	0.15	10.97
A	2.96	3.48	17.14	57.36	0.07	0.42	7.47	0.70	0.13	7.91
Granite	2.70	0.80	14.80	68.30	NA	5.00	2.30	NA	NA	1.30
Basalt	2.41	6.73	15.85	51.6	0.13	0.44	11.67	0.76	0.17	10.47

Table 2.2. Mineral Composition of Aggregates (%)

Mineral	**Aggregate**				
	M	**L**	**CC**	**B**	**A**
Quartz	68.9	1.1	48.5	42.1	18.9
Orthoclase	8.3	3.1	4.5	2.8	2.5
Albite	14.3	39.3	18.9	13.8	25.6
Anorthite	3.2	21.0	15.5	21.9	33.0
Others	5.3	35.6	12.6	19.4	19.9
Total	100.0	100.0	100.0	100.0	100.0

Table 2.3. Boiling Water Test Results

Aggregate Type		**Asphalt Retained on Aggregate Surface (%)**
B	Coarse	90
	Fine	95
CC	Coarse	90
	Fine	90
M	Coarse	85
	Fine	90
L	Coarse	98
	Fine	98
A	Coarse	70
	Fine	70

Table 2.4. Aggregate Properties (Harvey 1991; Shatnawi 1995)

Aggregate Property		Test Method	Aggregate A	Aggregate B
Specific Gravity	Coarse	CTM 206	2.86	2.63
	Fine	CTM 208	2.74	2.71
Los Angeles Abrasion Tests (% Loss)	100 R	CTM 211	8	4
	500 R	CTM 211	30	18
Crushed Particles (%)	Coarse	CTM 205	100	100
	Fine	CTM 205	100	100
	Combined	CTM 205	100	100
Sand Equivalent	Combined	CTM 217	76	58
Water Absorption (%)	Coarse	CTM 206	0.94	1.32
Methylene Blue Test (mg/g)	Fine	Ohio DOT Supplement 1052	8.0	4.8
			7.5	4.1
			7.3	4.0

Table 2.5. Physical and Chemical Properties of Binders (Provided by Material Suppliers)

	Test Method (AASHTO)	AR-4000	PBA-6a
Refinery	-	Shell Oil Products US in Martinez, California	Valero Marketing and Supply Company in Pittsburg, California
Appearance & Odor	-	Black viscous semi-solid. Asphalt or rotten egg odor.	Black viscous semi-solid. Asphalt or rotten egg odor.
Chemical Family of Substance	-	Petroleum Hydrocarbon	Petroleum Hydrocarbon
On original asphalt			
Flash Point (°C) (Chevland Open Cup)	T 48	290.6	232+
Specific Gravity @ 25°C	T 228	1.016	1.001
Absolute Viscosity at 60°C (Pa·s)	T 202	233	200+
Penetration (25°C, 100g, 5s) (0.1mm)	T 49	50	NA
Solubility in Trichloroethylene (%)	T 44	99.9	99.9
On residue from RTFC (AASHTO T 240)			
Absolute Viscosity @ 60°C (Pa·s)	T 202	437	513
Penetration (25°C, 100g, 5s) (0.1mm)	T 49	32	NA
Kinematic Viscosity at 135°C (cSt)	T 201	356	456
Ductility at 25°C (cm)	T 51	150+	70+

Table 2.6. Hveem Mix Design Data

Aggregate	**A**	**Percent of Fines**	**49.5**
Asphalt	**AR-4000**	**Asphalt Specific Gravity**	**1.016**
Additive	**None**	**Fine Specific Gravity**	**2.74**
Binder Content (%)	**4.5**	**Coarse Specific Gravity**	**2.86**
Date Tested	**6/2/2003**	**Maximum Specific Gravity**	**2.603**

Items	**Sample 1**	**Sample 2**	**Sample 3**	**Average**
Diameter, mm	102.0	102.0	102.0	102.0
Thickness, mm	63.5	64.0	64.5	64.0
Mass in Air (AASHTO T-166, "A"),g	1200.6	1201.3	1203.0	1201.6
Saturated Surface Dry Mass (T-166),g	1207.4	1209.5	1210.8	1209.2
Mass in water after 4 mins' soaking (T-166),g	714.1	714.6	713.0	713.9
Air-void Content (AASHTO T-166, "A"), %	6.5	6.7	7.1	6.8
Flush	no	no	no	
Hori. Pressure @2.22 kN vertical load (psi)				
Hori. Pressure @4.45 kN vertical load (psi)	11.8	9.7	14.0	11.8
Hori. Pressure @8.90 kN vertical load (psi)	16.0	12.0	22.0	16.7
Hori. Pressure @13.3 kN vertical load (psi)	20.0	14.0	28.0	20.7
Hori. Pressure @17.8 kN vertical load (psi)	26.0	17.9	32.0	25.3
Hori. Pressure @22.2 kN vertical load (psi)	32.0	23.0	38.0	31.0
Hori. Pressure @26.7 kN vertical load (psi)	40.0	30.0	45.0	38.3
Number of turns to reach 689.5 kPa	3.1	3.4	3.1	3.2
Stabilometer Value	45	51	41	45

Table 2.6. Hveem Mix Design Data (cont'd.)

Aggregate	**A**	**Percent of Fines**	**49.5**
Asphalt	**AR-4000**	**Asphalt Specific Gravity**	**1.016**
Additive	**None**	**Fine Specific Gravity**	**2.74**
Binder Content (%)	**5.0**	**Coarse Specific Gravity**	**2.86**
Date Tested	**6/2/2003**	**Maximum Specific Gravity**	**2.583**

Items	**Sample 1**	**Sample 2**	**Sample 3**	**Average**
Diameter, mm	102.0	102.0	102.0	102.0
Thickness, mm	63.5	63.5	64.0	63.7
Mass in Air (AASHTO T-166, "A"),g	1200.6	1201.0	1201.3	1201.0
Saturated Surface Dry Mass (T-166),g	1207.2	1206.7	1209.1	1207.7
Mass in water after 4 mins' soaking (T-166),g	714.9	709.7	713.5	712.7
Air-void Content (AASHTO T-166, "A"), %	5.6	6.5	6.2	6.1
Flush	no	no	no	
Hori. Pressure @2.22 kN vertical load (psi)				
Hori. Pressure @4.45 kN vertical load (psi)	17.5	11.0	16.0	14.8
Hori. Pressure @8.90 kN vertical load (psi)	20.0	17.0	23.0	20.0
Hori. Pressure @13.3 kN vertical load (psi)	27.5	23.0	28.0	26.2
Hori. Pressure @17.8 kN vertical load (psi)	30.0	30.0	34.0	31.3
Hori. Pressure @22.2 kN vertical load (psi)	40.0	38.0	40.0	39.3
Hori. Pressure @26.7 kN vertical load (psi)	47.5	48.0	47.0	47.5
Number of turns to reach 689.5 kPa	3.3	3.0	3.1	3.1
Stabilometer Value	38	42	39	40

Table 2.6. Hveem Mix Design Data (cont'd.)

Aggregate	**A**	**Percent of Fines**		**49.5**	
Asphalt	**AR-4000**	**Asphalt Specific Gravity**		**1.016**	
Additive	**None**	**Fine Specific Gravity**		**2.74**	
Binder Content (%)	**5.5**	**Coarse Specific Gravity**		**2.86**	
Date Tested	**6/2/2003**	**Maximum Specific Gravity**		**2.565**	
Items		**Sample 1**	**Sample 2**	**Sample 3**	**Average**
Diameter, mm		102.0	102.0	102.0	102.0
Thickness, mm		63.5	63.5	63.5	63.5
Mass in Air (AASHTO T-166, "A"),g		1199.3	1199.5	1198.8	1199.2
Saturated Surface Dry Mass (T-166),g		1202.1	1203.6	1202.5	1202.7
Mass in water after 4 mins' soaking (T-166),g		718.0	720.5	716.3	718.3
Air-void Content (AASHTO T-166, "A"), %		3.4	3.2	3.9	3.5
Flush		no	no	no	
Hori. Pressure @2.22 kN vertical load (psi)					
Hori. Pressure @4.45 kN vertical load (psi)		16.0	16.0	17.0	16.3
Hori. Pressure @8.90 kN vertical load (psi)		24.0	27.0	29.0	26.7
Hori. Pressure @13.3 kN vertical load (psi)		33.0	35.0	40.0	36.0
Hori. Pressure @17.8 kN vertical load (psi)		43.0	45.0	52.0	46.7
Hori. Pressure @22.2 kN vertical load (psi)		54.0	56.0	65.0	58.3
Hori. Pressure @26.7 kN vertical load (psi)		66.0	69.0	78.0	71.0
Number of turns to reach 689.5 kPa		2.95	3.05	2.90	3.0
Stabilometer Value		33	31	28	31

Table 2.6. Hveem Mix Design Data (cont'd.)

Aggregate	**A**	**Percent of Fines**	**49.5**
Asphalt	**AR-4000**	**Asphalt Specific Gravity**	**1.016**
Additive	**None**	**Fine Specific Gravity**	**2.74**
Binder Content (%)	**6.0**	**Coarse Specific Gravity**	**2.86**
Date Tested	**6/2/2003**	**Maximum Specific Gravity**	**2.546**

Items	**Sample 1**	**Sample 2**	**Sample 3**	**Average**
Diameter, mm	102.0	102.0	102.0	102.0
Thickness, mm	64.0	63.5	63.5	63.7
Mass in Air (AASHTO T-166, "A"),g	1197.3	1195.0	1196.3	1196.2
Saturated Surface Dry Mass (T-166),g	1199.3	1197.0	1198.8	1198.4
Mass in water after 4 mins' soaking (T-166),g	722.9	719.4	722.0	721.4
Air-void Content (AASHTO T-166, "A"), %	1.3	1.7	1.5	1.5
Flush	flush	flush	flush	
Hori. Pressure @2.22 kN vertical load (psi)				
Hori. Pressure @4.45 kN vertical load (psi)	31.0	36.0	26.0	31.0
Hori. Pressure @8.90 kN vertical load (psi)	52.0	78.0	47.0	59.0
Hori. Pressure @13.3 kN vertical load (psi)	73.0	121.0	68.0	87.3
Hori. Pressure @17.8 kN vertical load (psi)	96.0	170.0	93.0	119.7
Hori. Pressure @22.2 kN vertical load (psi)	124.0	200.0	118.0	147.3
Hori. Pressure @26.7 kN vertical load (psi)	150.0	-	146.0	148.0
Number of turns to reach 689.5 kPa	2.7	2.7	3.1	2.8
Stabilometer Value	16	-	15	15

Table 2.6. Hveem Mix Design Data (cont'd.)

Aggregate	**B**	**Percent of Fines**	**49.5**
Asphalt	**AR-4000**	**Asphalt Specific Gravity**	**1.016**
Additive	**None**	**Fine Specific Gravity**	**2.705**
Binder Content (%)	**5.0**	**Coarse Specific Gravity**	**2.634**
Date Tested	**6/2/2003**	**Maximum Specific Gravity**	**2.477**

Items	**Sample 1**	**Sample 2**	**Sample 3**	**Average**
Diameter, mm	102.0	102.0	102.0	102.0
Thickness, mm	64.0	64.0	64.0	64.0
Mass in Air (AASHTO T-166, "A"),g	1200.2	1199.1	1197.2	1198.8
Saturated Surface Dry Mass (T-166),g	1206.5	1205.8	1205.4	1204.8
Mass in water after 4 mins' soaking (T-166),g	689.6	687.3	689.1	687.6
Air-void Content (AASHTO T-166, "A"), %	6.3	6.6	6.4	6.4
Flush	no	no	no	
Hori. Pressure @2.22 kN vertical load (psi)	8.4	8.2	9.0	8.5
Hori. Pressure @4.45 kN vertical load (psi)	11.8	10.6	11.8	11.4
Hori. Pressure @8.90 kN vertical load (psi)	16.0	16.0	15.8	15.9
Hori. Pressure @13.3 kN vertical load (psi)	20.8	21.8	20.2	20.9
Hori. Pressure @17.8 kN vertical load (psi)	25.6	26.4	25.8	25.9
Hori. Pressure @22.2 kN vertical load (psi)	31.2	32.0	31.6	31.6
Hori. Pressure @26.7 kN vertical load (psi)	36.6	38.6	38.8	38.0
Number of turns to reach 689.5 kPa	2.7	2.9	2.3	2.6
Stabilometer Value	50	47	53	50

Table 2.6. Hveem Mix Design Data (cont'd.)

Aggregate	**B**	**Percent of Fines**	**49.5**
Asphalt	**AR-4000**	**Asphalt Specific Gravity**	**1.016**
Additive	**None**	**Fine Specific Gravity**	**2.705**
Binder Content (%)	**5.5**	**Coarse Specific Gravity**	**2.634**
Date Tested	**6/2/2003**	**Maximum Specific Gravity**	**2.460**

Items	**Sample 1**	**Sample 2**	**Sample 3**	**Average**
Diameter, mm	102.0	102.0	102.0	102.0
Thickness, mm	64.0	64.0	63.5	63.8
Mass in Air (AASHTO T-166, "A"),g	1197.3	1198.3	1197.8	1197.8
Saturated Surface Dry Mass (T-166),g	1204.6	1205.3	1206.1	1205.9
Mass in water after 4 mins' soaking (T-166),g	688.9	686.9	689.0	688.8
Air-void Content (AASHTO T-166, "A"), %	5.6	6.0	5.8	5.8
Flush	no	no	no	
Hori. Pressure @2.22 kN vertical load (psi)	7.8	7.8	7.8	7.8
Hori. Pressure @4.45 kN vertical load (psi)	10.0	10.2	10.0	10.1
Hori. Pressure @8.90 kN vertical load (psi)	14.0	14.4	14.0	14.1
Hori. Pressure @13.3 kN vertical load (psi)	18.2	19.0	18.0	18.4
Hori. Pressure @17.8 kN vertical load (psi)	23.0	23.8	22.8	23.2
Hori. Pressure @22.2 kN vertical load (psi)	28.0	28.6	28.0	28.2
Hori. Pressure @26.7 kN vertical load (psi)	34.0	35.8	34.0	34.6
Number of turns to reach 689.5 kPa	2.5	2.2	2.8	2.5
Stabilometer Value	54	56	51	54

Table 2.6. Hveem Mix Design Data (cont'd.)

Aggregate	**B**	**Percent of Fines**	**49.5**
Asphalt	**AR-4000**	**Asphalt Specific Gravity**	**1.016**
Additive	**None**	**Fine Specific Gravity**	**2.705**
Binder Content (%)	**6.0**	**Coarse Specific Gravity**	**2.634**
Date Tested	**6/2/2003**	**Maximum Specific Gravity**	**2.444**

Items	**Sample 1**	**Sample 2**	**Sample 3**	**Average**
Diameter, mm	102.0	102.0	102.0	102.0
Thickness, mm	63.5	63.5	63.5	63.5
Mass in Air (AASHTO T-166, "A"),g	1198.0	1196.5	1193.9	1196.1
Saturated Surface Dry Mass (T-166),g	1204.9	1203.6	1201.0	1202.6
Mass in water after 4 mins' soaking (T-166),g	692.2	692.6	692.4	691.8
Air-void Content (AASHTO T-166, "A"), %	4.4	4.2	3.9	4.2
Flush	no	no	no	
Hori. Pressure @2.22 kN vertical load (psi)	7.6	9.6	8.4	8.5
Hori. Pressure @4.45 kN vertical load (psi)	10.0	12.0	11.4	11.1
Hori. Pressure @8.90 kN vertical load (psi)	15.6	16.2	15.8	15.9
Hori. Pressure @13.3 kN vertical load (psi)	21.6	21.0	20.4	21.0
Hori. Pressure @17.8 kN vertical load (psi)	28.0	26.0	26.0	26.7
Hori. Pressure @22.2 kN vertical load (psi)	36.0	31.2	32.0	33.1
Hori. Pressure @26.7 kN vertical load (psi)	46.0	38.0	40.0	41.3
Number of turns to reach 689.5 kPa	2.3	2.5	2.7	2.5
Stabilometer Value	49	51	48	49

Table 2.6. Hveem Mix Design Data (cont'd.)

Aggregate	**B**	**Percent of Fines**	**49.5**
Asphalt	**AR-4000**	**Asphalt Specific Gravity**	**1.016**
Additive	**None**	**Fine Specific Gravity**	**2.705**
Binder Content (%)	**6.5**	**Coarse Specific Gravity**	**2.634**
Date Tested	**6/2/2003**	**Maximum Specific Gravity**	**2.428**

Items	**Sample 1**	**Sample 2**	**Sample 3**	**Average**
Diameter, mm	102.0	102.0	102.0	102.0
Thickness, mm	63.5	64.0	63.5	63.7
Mass in Air (AASHTO T-166, "A"),g	1198.0	1192.1	1193.1	1194.4
Saturated Surface Dry Mass (T-166),g	1204.5	1199.8	1200.4	1201.3
Mass in water after 4 mins' soaking (T-166),g	693.0	690.0	693.0	691.7
Air-void Content (AASHTO T-166, "A"), %	3.5	3.7	3.1	3.4
Flush	flush	flush	flush	
Hori. Pressure @2.22 kN vertical load (psi)	9.4	9.4	13.2	10.7
Hori. Pressure @4.45 kN vertical load (psi)	12.2	12.8	18.4	14.5
Hori. Pressure @8.90 kN vertical load (psi)	17.0	17.6	30.0	21.5
Hori. Pressure @13.3 kN vertical load (psi)	22.0	23.4	44.0	29.8
Hori. Pressure @17.8 kN vertical load (psi)	27.4	29.6	60.0	39.0
Hori. Pressure @22.2 kN vertical load (psi)	33.4	36.6	76.0	48.7
Hori. Pressure @26.7 kN vertical load (psi)	41.6	44.4	96.0	60.7
Number of turns to reach 689.5 kPa	3.1	3.2	2.2	2.8
Stabilometer Value	44	41	30	38

Table 2.7. Dynamic Shear Rheometer Test Results

	Unaged AR-4000		Unaged AR-4000 + Liquid		Aged AR-4000		Aged AR-4000 + Liquid	
No.	G^* **(kPa)**	δ **(°)**	G^* **(kPa)**	δ **(°)**	G^* **(kPa)**	δ **(°)**	G^* **(kPa)**	δ **(°)**
1	1.26	89.7	1.04	90.0	2.92	88.6	3.03	88.6
2	1.26	89.7	1.04	90.0	2.92	88.6	3.03	88.6
3	1.26	89.7	1.04	90.0	2.92	88.6	3.03	88.6
4	1.26	89.7	1.03	90.0	2.92	88.6	3.03	88.6
5	1.26	89.7	1.04	90.0	2.92	88.6	3.03	88.6
6	1.26	89.7	1.03	90.0	2.92	88.6	3.03	88.6
7	1.26	89.7	1.03	90.0	2.92	88.6	3.03	88.6
8	1.26	89.7	1.03	90.0	2.92	88.6	3.03	88.6
9	1.26	89.7	1.03	90.0	2.92	88.6	3.03	88.6
10	1.26	89.7	1.03	90.0	2.92	88.6	3.03	88.6
Mean	1.26	89.7	1.03	90.0	2.92	88.6	3.03	88.6
Standard Deviation	0.00	0.0	0.01	0.0	0.00	0.0	0.00	0.0

Table 2.8. Penetration Test Results (0.1 mm)

No.	AR-4000	AR-4000+Liquid	Aged AR-4000	Aged AR-4000+Liquid
1	39.7	39.2	27.3	27.8
2	39.5	38.4	26.5	27.6
3	37.0	38.3	25.5	25.4
4	43.0	40.2	26.1	24.4
5	43.5	40.2		
6	41.9	40.2		
Mean	40.77	39.42	26.35	26.30
Standard Deviation	2.48	0.91	0.75	1.67
p-value from t-test	0.2388		0.9582	

Table 2.9. Viscosity Test Results (Pa·s)

No.	AR-4000	AR-4000+Liquid	Aged AR-4000	Aged AR-4000+Liquid
1	247.5	233.2	498.6	493.7
2	238.6	234.7	474.8	491.9
3	234.1	224.6		495.4
4	233.8	227.3		488.5
5				485.7
6				485.9
Mean	238.49	229.94	486.71	490.18
Standard Deviation	6.39	4.77	16.80	4.08
p-value from t-test	0.0760		0.6051	

Table 2.10. Proportion and Gradation of Stockpile Aggregates for 19-mm Medium Dense Gradation (a – Aggregate A; b – Aggregate B).

Sieve Size (mm)	Target Gradation (%)	Stockpile Gradation (%)							Combined (%)
		19	19–12.5	12.5–4.75	6.3–2	N4–N8	sand	dust	
0.075	5	0.0	0.4	1.3	0.9	3.1	6.8	100.0	5.01
0.15	7	0.0	0.5	1.9	1.1	3.5	12.5	100.0	7.56
0.30	12	0.0	0.5	1.9	1.1	3.9	25.4	100.0	12.95
0.60	19	0.0	0.5	1.9	1.1	4.1	42.6	100.0	20.08
1.18	27	0.0	0.5	2.0	1.2	4.5	62.6	100.0	28.41
2.36	38	0.0	0.5	2.0	1.2	7.2	84.2	100.0	37.64
4.75	51	0.0	0.6	2.5	1.6	67.2	99.9	100.0	51.57
9.50	72	0.0	2.7	60.8	91.9	100.0	100.0	100.0	72.55
12.50	83	0.0	16.9	95.3	100.0	100.0	100.0	100.0	83.53
19.00	98	0.0	100.0	100.0	100.0	100.0	100.0	100.0	98.54
25.40	100	100	100	100	100.0	100.0	100.0	100.0	100.00
Proportion		0.015	0.167	0.244	0.026	0.121	0.413	0.014	

(a)

Sieve Size (mm)	Target Gradation (%)	Stockpile Gradation (%)				Combined (%)
		19-mm	9.5-mm	Natural Sand	Dust	
0.075	5	0.7	2.2	3.2	12.6	4.9
0.15	7	1.0	3.5	7.2	16.5	7.1
0.30	12	1.0	4.8	17.3	22.0	10.8
0.60	19	1.1	6.2	34.6	30.3	16.5
1.18	27	1.1	7.9	58.2	45.7	25.4
2.36	38	1.1	11.2	83.7	71.5	38.1
4.75	51	1.2	34.5	99.8	99.7	54.4
9.50	72	9.3	97.9	100.0	100.0	71.6
12.50	83	42.9	100	100.0	100.0	82.4
19.00	98	95.5	100	100.0	100.0	98.6
25.40	100	100	100	100.0	100.0	100.0
Proportion		0.308	0.230	0.175	0.287	

(b)

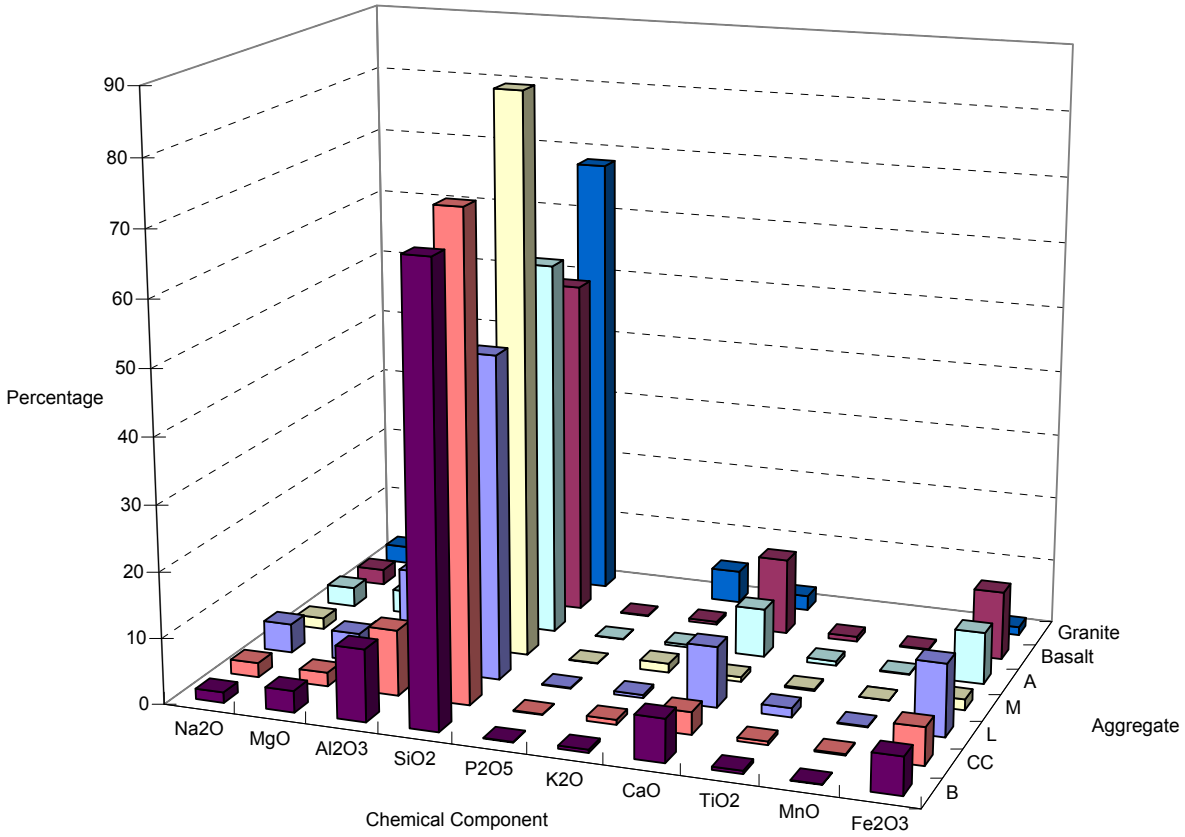

Figure 2-1. Chemical composition of aggregates by the XRF analysis.

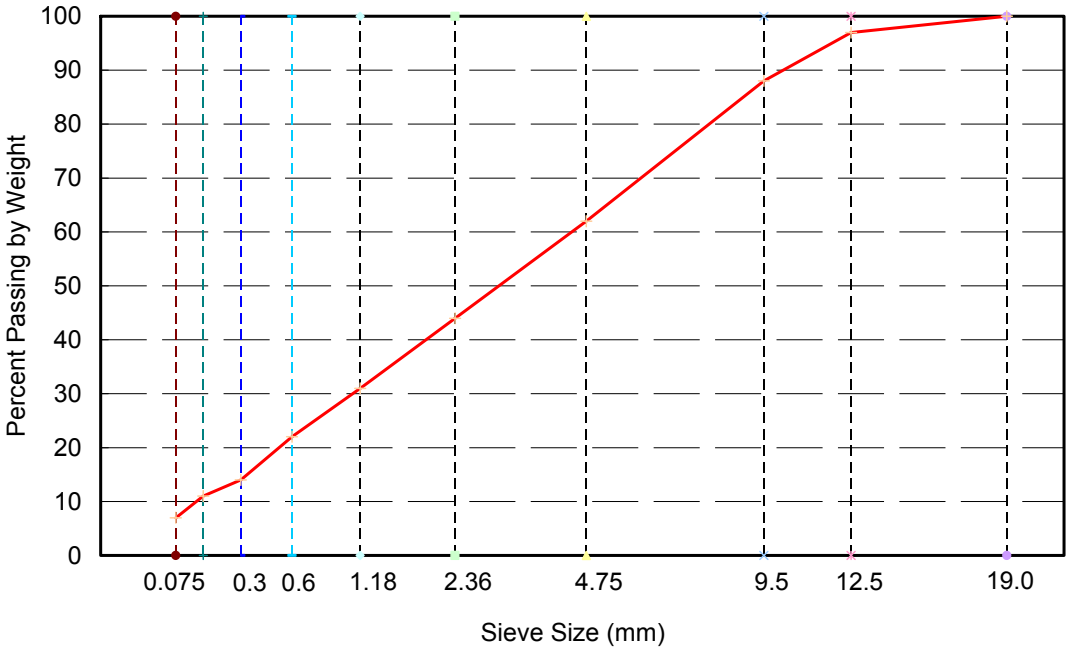

Figure 2-2. Aggregate gradation used in the Boiling Water test (sieve sizes raised to 0.45 power).

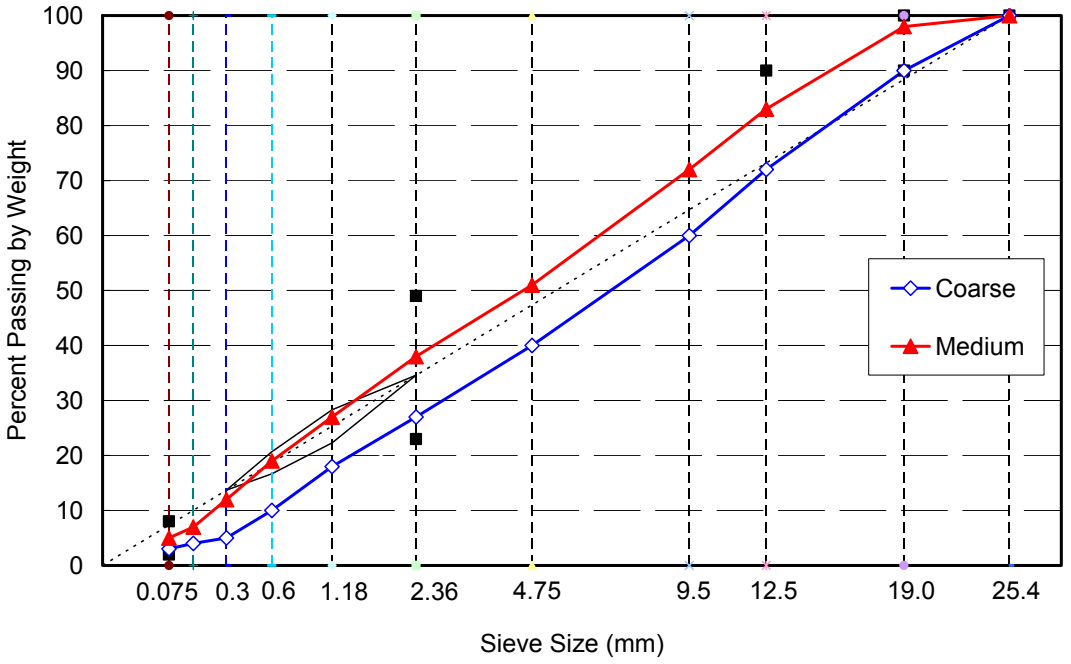

Figure 2-3. Two aggregate gradations used in the experiments (sieve sizes raised to 0.45 power).

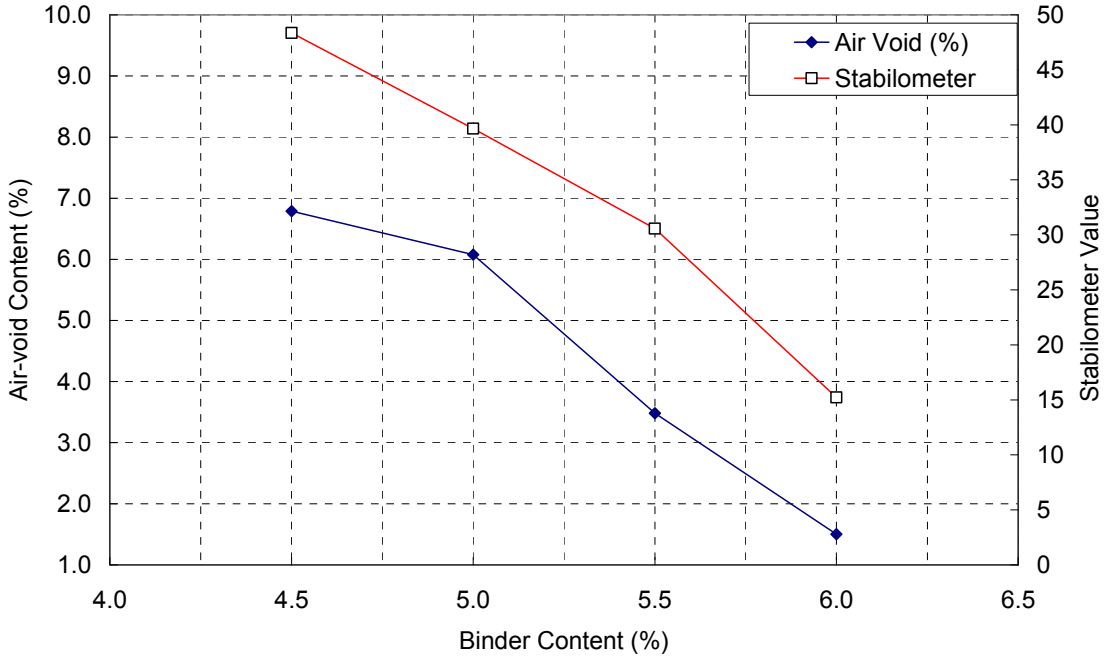

(a)

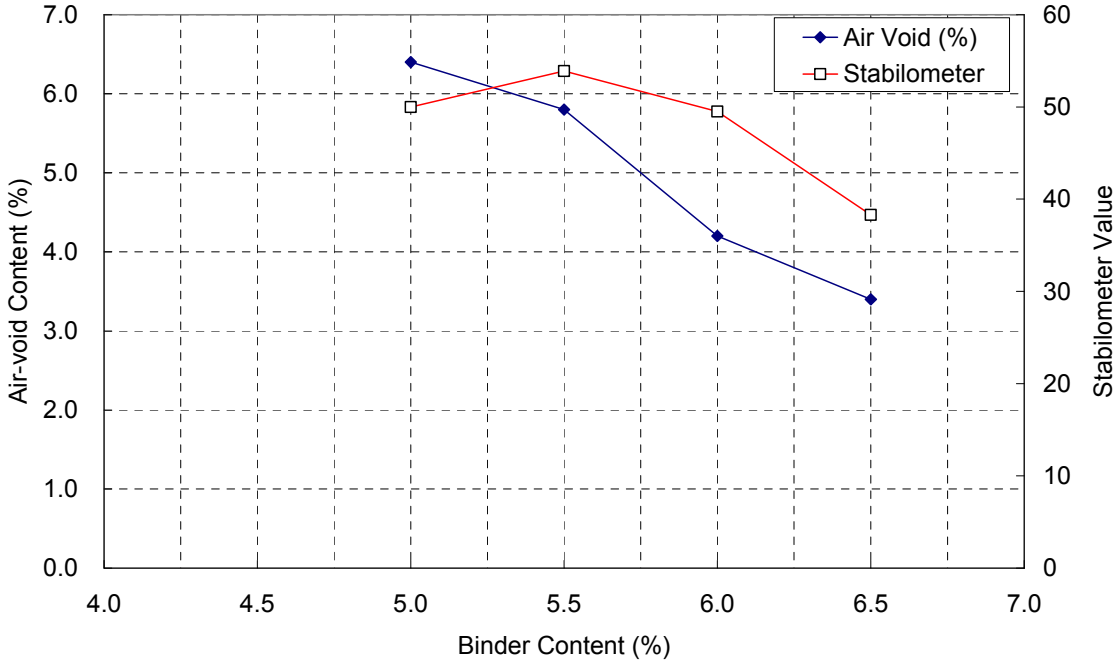

(b)

Figure 2-4. Hveem mix design curves (a – Aggregate A/AR-4000 Binder; b – Aggregate B/AR-4000 Asphalt).

Figure 2-5. Relationship between target air-void content and adjusted air-void content for compaction.

3.0 FIELD INVESTIGATION OF FACTORS ASSOCIATED WITH MOISTURE DAMAGE

Although the root cause of moisture damage is the existence of moisture in asphalt concrete, a variety of factors may affect the damage process. These factors include those that affect (a) the amount of water in the asphalt mixture (rainfall, drainage design, air-void content, etc.), (b) a material's resistance to moisture (material type, mix composition, pavement structure, etc.), and (c) other exogenous factors (traffic loading level and frequency, temperature, freeze-thaw cycles, etc.). The relative significance of these factors is not fully understood. In this chapter the effects of different factors on the occurrence and severity of moisture damage are investigated based on the first-hand data collected from in-service pavements.

3.1 Introduction

Although the main objective of the field investigation is to estimate the relative contributions of different factors to moisture damage in the field, the investigation also serves other research objectives, including providing in-situ moisture content information for the development of laboratory test procedures, and providing pavement performance data for validation of the HWTD test.

The field investigation started with a general condition survey of a large number of California pavement sections, and then the project data for each section were collected. Based on the general condition survey results, a sample set of pavements was selected for a further, more intensive survey in which cores were taken from the pavements and tested in the laboratory. Analysis and inference were based on the information obtained from both surveys. This chapter describes the field investigation plan, general observations, methodologies for data analysis, estimation results, and case studies, and concludes with a summary of the knowledge obtained.

3.2 Field Investigation Plan

The field investigation, performed on California highways, consists of a general condition survey, project data collection, field sampling, and laboratory testing.

3.2.1 General Condition Survey

The general condition survey was conducted to provide pavement condition data and to learn the extent of possible moisture damage in the pavements so that the sections to be studied in an intensive survey could be determined. About 194 pavement sections (Figure 3-1) on California highways, selected from different sources, were visited for the general condition survey. Forty-three percent of sections, which were distributed across the state, were on a list of Quality Control/Quality Assurance (QC/QA) projects provided by Caltrans. These QC/QA projects were primarily constructed by one construction company between the years 1996 and 2000. These sites were chosen because QC/QA data (primarily relative compaction and binder content data) for them were available. Approximately 11 percent and 21 percent of the sections were randomly selected from Caltrans District Materials Engineers Offices in District 2 (Northern California) and District 6 (Central California), respectively, because these two regions had a history of moisture damage in their asphalt pavements. The selected sections in these two regions were generally placed or overlaid during the years 1995 and 2000. Another 19 percent of the 194 sections were provided by construction companies, Caltrans Material Engineers in other districts, and Caltrans Materials Engineering and Testing Services (METS). These sites were either QC/QA projects or showed some premature failure. The remaining six percent of the sections were

discovered during the general condition survey and were included due to signs of possible moisture damage. A summary of the number of pavement sections from the different sources is shown in Table 3.1, along with a subdivision into their different mix types and compaction specifications. As a whole, such a sample is not a random sampling of pavements in California, but it covers all the areas in the state with different traffic and environmental characteristics, as can be seen from Figure 3-1. The condition survey was conducted from December 2003 to December 2004, with the result that the large majority of the sections evaluated were four to eight years old at the time of the survey.

Each pavement section was visually surveyed following a field condition survey form, as shown in Appendix B. The extent and severity of all observable pavement distresses such as cracking, rutting, potholes, segregation, raveling, bleeding, and patching, were carefully recorded and photographed. The geometries and drainage condition of each pavement section were also recorded.

3.2.2 Project Data Collection

The historical project data including mix design, pavement structure, and construction records, were primarily pulled from Caltrans District Materials Engineers Offices and other pavement design and maintenance offices. Although great effort had been spent, the project data collection was not completed because of many cases of missing data. The quality of project data documentation (especially mix design data) changes significantly from district to district. This partly limited the number of sections used for analysis.

Traffic information, primarily the annual average daily truck traffic (AADTT), was extracted from a single database table in the Caltrans Pavement Management System (PMS), containing traffic information from 1980 to 1997. Concerns were raised about the quality of the traffic data (Lea and Harvey 2004), so it was first checked by comparing the AADTT from Weigh-In-Motion (WIM) stations in the state with the AADTT extracted from the PMS at the same sites. A good correlation was found between the AADTT from two sources, and the truck traffic count data in the PMS were regarded as acceptable. The AADTT from the PMS was then further converted to the AADTT on the design lane, using the truck lane distribution factors developed from the Caltrans Weigh-in-Motion (WIM) data (Lu et al. 2002). A uniform three percent compound growth rate was assumed for all sections to calculate the cumulative truck traffic.

The climate data, including annual rainfall, freeze-thaw cycles, and degree-days greater than 30°C, were estimated from weather stations in California, Nevada, Oregon, and Arizona contained in the *Climate Database for Integrated Model (CDIM)* software (version 1.0) (PaveSys, 2004). An interpolation of the weather station data was necessary to estimate the climate data at any point in the state. This interpolation was performed in the software *ArcView GIS* using data from twelve closest stations (Breslin 1999). For illustration, the distributions of AADTT and annual rainfall are shown in Figure 3-2.

3.2.3 Field Sampling and Laboratory Testing

After the general condition survey, a total of 63 sections were selected for intensive survey, with the locations shown in Figure 3-3 and Table 3.2. About 80 percent of the sections were selected because they had shown different types of distress, such as potholes, raveling, cracking, rutting, and bleeding, some of which might be related to moisture damage. Pavements showing strong indications of moisture damage (such as frequent potholes and irregular rutting) had all been included in the coring list. The other 20 percent of sections were “control” sections that did not show any distress on the surface. The coring was generally done near locations where damage was more advanced.

Such sampling was biased toward the distressed pavements instead of being completely random. This is because the purpose of the study was to estimate the relative contributions of different factors to moisture damage instead of making inferences about the overall extent of moisture in the state.

Most sections were cored between June and September (the dry season in California) and between March and April (the rainy season in California), as shown in Table 3.2. At each section, four dry cores were taken in the truck lane by a laser-welded coring bit without using water as the cooling agent (see Figure 3-5): two in the wheelpath and two between the wheelpaths, and generally spaced at 10 to 20 meters from the most advanced surface manifestation of the distress. Compressed air was connected into the coring bit to blow away loose materials that might get cores stuck in the hole. Once a core was extracted from the pavement it was quickly labeled, photographed, and sealed in a heavy-duty plastic bag to retain the in-situ moisture content.

Close to the coring positions, pavement permeability was measured with a falling-head Gilson AP-1B permeameter (Figure 3-6) to provide an extra explanatory variable. Three measurements were taken at each site along a longitudinal straight line in areas without cracks. If the pavement was not overlaid with an open-graded layer or chip seal, or any other thin maintenance layer, the measurement positions were along the center of the truck lane, roughly three meters apart. Otherwise, the measurements were either not done or were taken on the shoulder if the original mixture existed on the shoulder. The coefficient of permeability was calculated by the following equation:

$$K = (aL / At)\ln(h_1 / h_2) \quad \textbf{(3-1)}$$

where K = coefficient of permeability; a = inside cross-sectional area of standpipe (varies depending on tier used for testing); L = thickness of the asphalt pavement layer; A = cross-sectional area of permeameter through which water can penetrate the pavement; t = elapsed time between h_1 and h_2; h_1 = initial head; and h_2 = final head.

Eight wet cores were also taken at each section by a conventional coring bit using water as the coolant: four in the wheelpath and four between the wheelpaths if the pavement had no severe distress, one in the wheelpath and seven between the wheelpaths if the pavement had severe distress in the wheelpath. These wet cores were primarily used for the validation of the HWTD test, which is discussed in Chapter 5.

Once the cores were transported back to the laboratory, they were photographed and their condition was examined carefully for the class of moisture damage on a scale as described in Table 3.6. The dry cores were then weighed and placed in an oven at 50°C for two weeks. Their mass was measured periodically and fitted with an exponential function to estimate the original moisture content in each core. Substantial amounts of moisture were commonly found in the dry cores, even those collected during the summer (dry) season.

After being taken out of the oven, the dry cores were cut into different mix layers and measured for their bulk specific gravities by the UCB Parafilm method. Then they were broken down at high temperatures and used for Rice measurement.

3.3 General Observation

The percentage of section length showing any type of distress has been estimated for each project section, as an indication of the extent of damage. Table 3.3 lists these values for the cored sections. At many sections the distresses were continuous and distributed across most of the project length, but at other sections, the distresses were generally localized in a few short ranges, as illustrated in Figure 3-4. Localized distresses are more likely related to moisture due to localized pavement deficiencies such as high air-void contents and poor drainage. However, it is difficult to determine the extent to which moisture contributes to the surface distresses. Some distresses may not be caused by moisture damage at all.

Some factors that are closely related to moisture damage are investigated, including the air-void content and the moisture content in pavements.

3.3.1 Air-Void Content

The air-void contents of both dry and wet cores were measured in the laboratory using the UCB Parafilm method for dense-graded asphalt concrete (DGAC) and the Corelok® method for gap- or open-graded mixes. For cores consisting of multilayer mixes, the air-void content of each layer was measured.

Factors affecting the in-situ air-void contents may include the mix type, construction specification, location in the pavement (horizontal and vertical positions), and distance from distressed areas. The measured values may also be influenced by the conditions of the core, such as the amount of moisture residing in the cores. Figure 3-7 shows box plots of the air-void contents at different levels of each factor. It can be seen that the average air-void content of DGAC cores is about two percent smaller than that of non-DGAC cores (primarily rubberized asphalt concrete, RAC-G, in this study). This is also obvious in the estimated distribution curves of the air-void contents of the two mixes (Figure 3-8).

Since the majority of cores were taken from DGAC pavements, an analysis of variance was performed on air-void contents measured from these DGAC cores using Type 3 sum of squares, with the results shown in Table 3.4. It can be seen that at the 95 percent confidence level, air-void content is significantly affected by the position in the lane (whether or not in the wheelpath), depth in the pavement, distance from the distress areas, and construction specifications (whether or not a QC/QA project). The coring method also has a significant effect on the measured air-void contents. Based on the box plots in Figure 3-7, the following conclusions can be drawn:

1. Air-void content in the wheelpath is smaller than that in the unloaded areas (between the wheelpaths, shoulder, or median).
2. Air-void content generally increases with depth of the mix in the pavement. Mixes closer to the surface have smaller air-void contents.
3. Air-void content in pavement sections showing distresses is generally larger than that in sections without distresses.
4. Pavement sections constructed under the QC/QA specification generally have smaller air-void contents than non-QC/QA pavements.
5. Air-void contents measured from dry cores are generally larger than those measured from wet cores, with an average difference of 0.5 percent. This difference resulted primarily from the different conditioning procedures for dry and wet cores before air-void measurement. Dry cores were left in an oven at 50°C for two weeks before air-void measurement, while wet cores were left in air for a couple of days and dried with compressed air before air-void measurement. A certain amount of moisture might still exist in the wet cores when the air-void content was measured, which reduced the volume of air in the cores.

3.3.2 Moisture Content

Moisture was found in almost every pavement, ranging between zero and three percent. In some cases, a large amount of moisture was even discovered in pavements that had received little rain for several months. The factors affecting the amount of moisture in pavements were analyzed statistically based upon the data measured on dry cores, with the linear regression results shown in Table 3.4. It can be seen that at the 90 percent confidence level, the location of the core (whether or not in the wheelpath), air-void content, days since last rain, distance from distressed areas, and degree days greater than 30°C all significantly affect the in-situ moisture content. The signs of the estimated parameters indicate that under similar conditions mixes in the wheelpath or those with higher air-void contents contain more moisture than mixes between the wheelpaths or with lower air-void contents. In addition, mixes closer to the distressed areas contain more moisture, suggesting that there is a positive correlation between moisture content and the extent of distress. The

environmental effects are as expected, that is, the longer the dry season or high temperature duration, the less moisture in the pavement.

The relation between moisture content and air-void content is further illustrated in Figure 3-9. As can be seen, there is a good linear correlation between the two variables. Higher air-void contents generally correspond to higher moisture contents.

3.3.3 Field Pavement Permeability

In the field pavement permeability has an important influence on the amount and rate of moisture infiltration into the mixes. However, the in-situ measurement of permeability was not easy. The original design of Gilson AP-1B permeameter could not ensure a good seal between the permeameter and the pavement surface. In most cases, water would leak out during measurement. Therefore, extra weight (about 80 kg) was applied to the base of the permeameter achieves a satisfactory seal. Another problem was that many pavement sections had been overlaid with a thin open-graded friction course or a chip seal layer, on which the permeability is either too large or virtually zero. Due to the short time window of traffic closure, it was not possible to remove the overlay and take measurements, so permeability on these pavements was mostly unmeasured. For the pavements measured, determination of layer thickness for use in the calculation was another issue. Many pavements have underlying old AC layers. Whether or not to include the thickness of these old AC layers in the calculation posed a challenge. In this study, it was decided to include them if the bonding between the surface layer and underlying layers was good, otherwise only the thickness of the surface layer was used in the calculation.

About 60 percent of the cored sections were measured for permeability. The values generally ranged between 0 and 600×10^{-5} cm/s, which is in the normal range measured in other states on DGAC pavements (Choubane et al. 1998).

There is a roughly positive correlation between the measured permeability and the in-situ air-void content, as shown in Figure 3-10. As can be seen, high air-void content is related to high pavement permeability.

3.4 Analysis of Factors Associated with Moisture Damage

As introduced in Chapter 1, moisture damage can be understood as the progressive deterioration of a pavement mixture by loss of the adhesive bond between the asphalt binder and the aggregate surface and/or loss of cohesion within the binder primarily due to the action of water. Because moisture damage directly disrupts the integrity of the mixture, it can reduce the performance life by accelerating all the distress modes of interest in pavement design. The most common phenomenon of moisture damage is stripping. The reduction in pavement life—in terms of fatigue cracking, rutting, or thermal cracking—is difficult if not impossible to measure and to use as an index of the severity of moisture damage in the field survey. In the field, moisture damage is often recognized due to the existence of stripping. Therefore, the extent of stripping, which is observable, can be used as a reflection of the severity of moisture damage in most cases. Due to the ambiguity in visual inspection, it is more appropriate to quantify the extent of stripping on a discrete ordered scale rather than a continuous variable. In this context, the scale value of a mix is a function of its inherent moisture damage, which itself is a function of mix composition, mix component properties, moisture conditions and dynamics, etc. The inherent moisture damage function is composed of a deterministic component and a random component. The deterministic component reflects observable factors that influence the level of moisture damage, while the random component represents unobservable factors, random individual behavior, and measurement error.

3.4.1 Methodology for Data Analysis

Moisture damage takes the form of a multivalued response variable that has intrinsic order. If we let 0 represent "no or slight damage," 1 represent "medium damage," and 2 represent "severe damage" (Table 3.6), damage is a discrete variable with three values inherently ordered. In this case, an ordered probit model can be used as a framework for analysis.

The ordered probit model was introduced in the social sciences to model characteristics that are not observable in the population. It has been applied to build discrete deterioration models in infrastructure management in civil engineering (Madanat et al. 1995). The model assumes the existence of an underlying continuous unobservable random variable so that it can capture the latent nature of infrastructure performance. In this model, the dependant variable, y, is a discrete value greater than or equal to zero, which indicates the extent of the latent moisture damage at the time of inspection. This latent moisture damage, y^*, is a function of exogenous variables, **x**, such as age, cumulative traffic, mix type, pavement structure, and environmental factors. Although some moisture damage (e.g., loss of stiffness) has been seen to be reversible (Schmidt et al. 1972), the damage in this model is assumed to be irreversible for two reasons:

1. The primary concern is the permanent damage to the mix rather than the temporary reversible loss of stiffness caused solely by the presence of the water.
2. The dependant variable is measured as the visually observable loss of bonding between the asphalt and aggregates because, as previously mentioned, it is nearly impossible to measure stiffness in the field and separate the effects of temperature and underlying support from those of moisture damage.

Therefore, y^* can be defined as the latent continuous deterioration and is represented by a random variable. The relationship between y and y^* is governed by several thresholds, μ_i. If the random variable y^* falls between two thresholds μ_i and μ_{i+1}, then the condition rating, y, is equal to *i*. Therefore, the probability of observing moisture damage in condition i, is equal to the probability of y^* falling between μ_i and μ_{i+1}. This probability is given by the area under the probability density function of the random variable y^* bounded by μ_i and μ_{i+1}. Specifically, we specify a latent deterioration model by a linear-in-the-parameter relationship between the latent moisture damage y^* and a set of observable exogenous variables as follows:

$$\log(y^*) = \boldsymbol{\beta}'\mathbf{x} + \varepsilon \qquad \textbf{(3-2)}$$

In the above equation, **x** is a vector of observable exogenous variables, including mix properties, pavement structure variables, cumulative traffic and weather factors; $\boldsymbol{\beta}$ is a vector of parameters to be estimated; ε is a random error term including unobserved factors, measurement error, and inherent variation in pavement response; and y^* represents the unobserved deterioration due to moisture. The use of the logarithm of y^* as the dependent variable guarantees that the latent deterioration y^* is positive, that is, pavement damage due to moisture will not recover in the field. This relationship cannot be directly estimated since y^* is unobservable. What is observed are the visual ratings of moisture damage, y, which is related to y^* through

$$\begin{aligned} y &= 0 \text{ if } \log(y^*) \le 0, \\ &= 1 \text{ if } 0 < \log(y^*) \le \mu_1 \\ &= 2 \text{ if } \mu_1 < \log(y^*) \end{aligned} \qquad \text{(3-3)}$$

where μ_1 is an unknown threshold to be estimated with β.

Note the first threshold has been normalized to zero. This relationship can be rewritten as follows:

$$
\begin{aligned}
y &= 0 \text{ if } \varepsilon \le -\boldsymbol{\beta}'\mathbf{x}, \\
&= 1 \text{ if } -\boldsymbol{\beta}'\mathbf{x} \le \varepsilon \le \mu_1 - \boldsymbol{\beta}'\mathbf{x} \\
&= 2 \text{ if } \mu_1 - \boldsymbol{\beta}'\mathbf{x} \le \varepsilon
\end{aligned}
\qquad \textbf{(3-4)}
$$

It is assumed that ε is normally distributed across observations, and normalize its mean and variance to 0 and 1. This model can also be estimated with a logistically distributed disturbance, but this trivial modification appears to make virtually no difference in practice (Greene 2000). With the normal distribution, we have the following probabilities:

$$
\begin{aligned}
&\text{Prob}(y = 0) = \Phi(-\boldsymbol{\beta}'\mathbf{x}) \\
&\text{Prob}(y = 1) = \Phi(\mu_1 - \boldsymbol{\beta}'\mathbf{x}) - \Phi(-\boldsymbol{\beta}'\mathbf{x}) \\
&\text{Prob}(y = 2) = 1 - \Phi(\mu_1 - \boldsymbol{\beta}'\mathbf{x})
\end{aligned}
\qquad \textbf{(3-5)}
$$

where $\Phi(\cdot)$ is the standard normal cumulative distribution function.

For the three probabilities, the marginal effects of changes in the continuous regressors are calculated as:

$$
\begin{aligned}
&\frac{\partial \text{Prob}(y = 0)}{\partial \mathbf{x}} = -\phi(\boldsymbol{\beta}'\mathbf{x})\boldsymbol{\beta} \\
&\frac{\partial \text{Prob}(y = 1)}{\partial \mathbf{x}} = [\phi(-\boldsymbol{\beta}'\mathbf{x}) - \phi(\mu_1 - \boldsymbol{\beta}'\mathbf{x})]\boldsymbol{\beta} \\
&\frac{\partial \text{Prob}(y = 2)}{\partial \mathbf{x}} = \phi(\mu_1 - \boldsymbol{\beta}'\mathbf{x})\boldsymbol{\beta}
\end{aligned}
\qquad \textbf{(3-6)}
$$

where $\phi(\cdot)$ is the standard normal probability density function.

Note that the marginal effects sum to zero, which follows from the requirement that the probabilities add to 1. For binary (dummy) explanatory variables, marginal effects are discretely approximated using the difference in predicted probabilities when the dummy variable under question is set to one and zero with the other variables held at their sample means:

$$
\frac{\Delta \text{Prob}(y = i)}{\Delta x_k} = \text{Prob}(y = i \mid x_k = 1) - \text{Prob}(y = i \mid x_k = 0), \quad i = 0, 1, 2 \qquad \textbf{(3-7)}
$$

The maximum likelihood estimation (MLE) procedure was used to estimate the value of parameter vector $\boldsymbol{\beta}$ and of the threshold μ_1 simultaneously. The likelihood function of the ordered probit model is

$$
L = \prod_i \text{Prob}(y_i) \qquad \textbf{(3-8)}
$$

Like all probability models, an ordered probit model allows for calculation of predicted probabilities for each moisture damage category and marginal effects. When calculated at the means of the explanatory variable data, predicted probabilities indicate the chance of the average pavement under average traffic and climate conditions falling within each of the categorical moisture damage levels. Marginal effects indicate how a change in an explanatory variable affects the predicted probability that pavements experience each of the moisture damage levels.

3.4.2 Estimation Results

The model estimation was performed repeatedly on two different data sets: data from cores and data from all sections in the general condition survey. The cores provided more information than the general condition survey. Some key variables, such as the extent of stripping, moisture content, and in-situ air-void content were only available from cores. However, the coring data set has a small sample size and includes fewer mix types, aggregate types, pavement structures, etc. On the other hand, sections in the general condition survey span wider ranges of mix types, traffic and environment variation, and other factors, but the extent of moisture damage has to be estimated and some variables have to be omitted in the analysis. Analysis on both data sets would provide better understanding of the factors that contribute to moisture damage.

3.4.2.1 Analysis Based on Cored Sections

In this section, the ordered probit model was estimated based on observations from cores. A description of the explanatory variables included in the empirical model is provided in Table 3.7, along with their mean, minimum, and maximum values. Binder type, additive, pavement structure, core location, interlayer, and mix type are dummy variables, with the omitted reference value (zero) selected arbitrarily. The pavement permeability measured in the field was not included because about 50 percent of the pavement sections had been treated with chip seal or overlaid with an open-graded layer on which the permeability could not be measured. On the other hand, it has been shown that field permeability is positively correlated with air-void content (Figure 3-10), so the inclusion of air-void content in the model can sufficiently characterize the moisture ingress potential of pavements. Aggregate type was not included in the model because this information is absent for most pavement sections. Although it is generally believed that the mineral composition of particular aggregates affects the moisture resistance of asphalt concrete, there is no clear relationship between characteristic parameters for aggregate type, such as mineral composition, and moisture damage. Given the great diversity of aggregates used in the pavements, it is viable to include the aggregate effect in the random error term. Table 3.8 shows the distribution of the dependant variable (moisture damage) in the sample. The empirical model was estimated using the ORDPROB command in a statistical software *TSP* (Pindyck et al. 1997).

Parameter estimates and summary statistics of the ordered probit model are presented in Table 3.9. Since the ordered probit model is nonlinear, the estimated coefficients are not marginal effects. As such, coefficient estimates and marginal effects are discussed separately. For the model, a likelihood ratio test was used to test the null hypothesis that the estimated coefficients were jointly equal to zero. This joint null hypothesis was rejected at the 99 percent confidence level. Estrella's scaled R-squared[a] has a value of 0.219, indicating a reasonably good fit. Among the fourteen estimated coefficients, six are significant at the 95 percent confidence level, including the coefficients for the constant term, air-void content, structure, cumulative rainfall, mix type, and the threshold parameter μ_1. Moreover, the effect of pavement age is significant at the 90 percent confidence level.

Table 3.10 shows the predicted probabilities and marginal effects from the estimated model. Predicted probabilities for the three moisture damage categories were evaluated at the sample means of the explanatory variable data. Since the sample used for model estimation was not random, these probabilities could not be generalized to the entire pavement system in California. The useful information from these results is that the close match between them and the observed proportions of moisture damage (Table 3.8) indicates a good fit with the model.

The marginal effects, shown in the lower panel of Table 3.10, reflect the relative importance of the explanatory variables. Interpretation of the marginal effects for continuous variables is straightforward: all

[a] The scaled R-squared is a measure of goodness of fit relative to a model with only a constant term, computed as a nonlinear transformation of the likelihood ratio test for zero slopes (Estrella 1998).

other things being equal, a one unit change in the explanatory variable will result in an increase or decrease in the predicted probability equal to the size of the marginal effect. In the case of a dummy variable, the marginal effect is the change in predicted probability based on whether the explanatory variable falls into that category or not. Because all remaining variables assume their respective average values when the marginal effects are calculated, the marginal effects show the change in the predicted probability for each moisture damage category for an average pavement under average traffic and environmental conditions, according to the variable being considered.

Beginning with the air-void content, we see that a rise in the air-void content will increase the probabilities of both medium and severe moisture damage in asphalt pavements. This is rational since higher air-void contents will allow more moisture entering the pavements with all other things being equal.

Pavements with cement-treated base (CTB) or old portland cement concrete (PCC) slabs underneath have less probability of experiencing moderate or severe moisture damage. One possible reason might be that the underlying CTB or PCC layer acts as a moisture barrier reducing the amount of moisture vapor getting into the upper asphalt concrete layers from underneath. This phenomenon needs further investigation.

An increase in the cumulative rainfall leads to worse moisture damage. This is reasonable because more rainfall generally corresponds to a greater chance for water to get into asphalt pavements.

Pavement age is significant at the 90 percent confidence level. As pavement age increases, the probability of showing moisture damage rises. Note that in the model both truck traffic and environmental factors are represented in the cumulative form so their confounding effects on pavement age have been largely removed. Other factors related to age, such as oxidative aging, loss of lightweight components in the binder, and some long-term chemical reaction inside the mix, may contribute to this result.

Mix type also tends to influence the extent of moisture damage. The marginal probabilities indicate that conventional dense-graded asphalt mixes (DGAC) experience less moisture damage than gap-graded asphalt rubber mixes (RAC-G) under the same conditions. This result is consistent with observations in an earlier study of premature distress in asphalt concrete in California (Shatnawi 1995). Indirect tensile strength tests performed on specimens prepared in the laboratory, however, suggested that RAC-G has better moisture resistance than DGAC (Ntekim 2001). The high air-void contents of the RAC mix in the field may be one of the reasons leading to moisture damage. Because the number of RAC projects in the data set is limited, further analysis on more field sections using the RAC mix is needed. As far as the results here reveal, asphalt rubber mixes do not seem to improve moisture resistance any more than conventional dense-graded mixes do.

Other explanatory variables in the probit model are insignificant at the 90 percent confidence level; they include binder type, use of additive, wheelpath, cumulative truck traffic, cumulative degree-days greater than 30°C, cumulative freeze-thaw cycle, and interlayer. Among them, wheelpath (whether or not cores were taken in the wheelpath) is marginally significant at the 80 percent confidence level, and its marginal probabilities suggests that repeated truck loading may contribute to the development of moisture damage in the pavements.

3.4.2.2 Analysis Based on Sections in the General Condition Survey

Before applying the ordered probit model to the sections in the general condition survey, the extent of moisture damage of each section had to be determined. The direct and reliable way to determine moisture damage is to take cores, but this information was unavailable for many sections. What was available was the extent and severity of all observable pavement distresses, such as cracking, rutting, potholes, segregation, raveling, bleeding, and patching. Therefore, the extent of moisture damage had to be determined from these observable distresses, which could possibly be done by establishing a mapping between them based on the information from the cored sections.

The relationship between moisture damage and surface distresses is complex. It is unlikely that a clear functional form can be determined. In this study, an attempt was made to model the relationship with an

artificial neural network (ANN), trained by the data from the 63 sections selected for intensive survey. The extent of moisture damage of the uncored sections was then estimated by the trained ANN, using the surface conditions as inputs.

ANNs are models that attempt to parallel and simulate the functionality and decision-making processes of the human brain. They are good at recognizing patterns, generalizing, and predicting trends. ANNs have been broadly used in different disciplines for classification, clustering, function approximation, and trend prediction (Aria et al. 2003).

Before performing the ANN modeling, two assumptions were made to reduce the computational complexity: (1) a pavement has no moisture damage if it does not show any distress on its surface; (2) there is no severe moisture damage in the uncored pavements. Both assumptions are reasonable. The first assumption is supported by the data from the cored sections. Generally little moisture damage has been observed in the control sections selected for intensive survey. For the second assumption, its reasonability resides in the fact that pavements showing strong indication of moisture damage (e.g., frequent potholes, irregular rutting) have all been cored. It is unlikely that a pavement with severe moisture damage would show little sign of it at the surface.

Based on the two assumptions, the task of the ANN became to classify the remaining uncored pavements into two categories: those with slight moisture damage and those with medium moisture damage. Correspondingly, the cored sections with slight or medium moisture damage were used for training and testing the ANN (40 sections for training and 9 sections for testing).

The NeuroSolutions package was used in this study to perform neural network calculations. It is available for evaluation free of cost via the Internet. The commonly used multilayer feed-forward neural network with back-propagation algorithm was used for calculation. The ANN consists of three layers: an input layer, a hidden layer, and an output layer. The input layer contains 11 neurons, corresponding to 11 surface condition indices: segregation, patching, potholes, pumping, raveling, rutting, shoving, stripping, stage A alligator cracking, stage B alligator cracking, and stage C alligator cracking. The hidden layer and the output layer have three neurons and one neuron respectively.

The ANN was trained with the 40 cored sections. Its accuracy of prediction was about 80 percent based on the nine testing sections. Different numbers of neurons in the input or hidden layers were also tried, but no improvement in the prediction accuracy resulted. Therefore, the above ANN was used to estimate the extent of moisture damage of those uncored sections. The estimated moisture damage was subsequently used in the ordered probit model as the dependent variable.

As mentioned previously, it is impossible to find the complete project information for each section. In many cases, some data have been lost forever. The records (pavement sections) with missing key data were then deleted from the analysis. Therefore, only 139 pavement sections were included in the model estimation.

The explanatory variables included in the ordered probit model, as shown in Table 3.12, are similar to those used in the model estimation on core data (Table 3.7), except that the air-void content (AIRVOID) and the variable indicating whether or not in the wheelpath (WHEELPATH) were removed because they were either unavailable or inapplicable for the generally surveyed sections. As a rough approximator, a dummy variable indicating whether or not the section is a QC/QA project was used to represent the level of air-void contents, based on the assumption that QC/QA projects generally result in lower air-void contents than non-QC/QA projects. To reduce the number of parameters to be estimated, two environmental factors, freeze-thaw cycles and degree-days greater than 30°C, were also removed from the model due to their insignificance in the preliminary analysis.

Parameter estimates and summary statistics are presented in Table 3.14. The null hypothesis that the estimated coefficients were jointly equal to zero was rejected at the 99 percent confidence level. Estrella's scaled R-squared has a value of 0.186, indicating a reasonably good fit. Among the 11 estimated parameters, three are significant at the 95 percent confidence level, including the coefficients for additive, pavement age, and the threshold parameter μ_1.

The marginal effects, shown in the lower panel of Table 3.15, reveal that the use of antistripping additives (liquids or hydrated lime) can significantly reduce the probabilities of moisture damage in asphalt pavements. Moreover, moisture damage also increases with pavement age, which is consistent with the findings from the analysis of core data.

Other variables are insignificant at the 95 percent confidence level. The marginal effects of the indicator variable QCQA suggest that QC/QA pavements may suffer less moisture damage than non-QC/QA pavement, but the corresponding p-value is 0.43, which makes the conclusion weak.

3.4.3 Discussion

The two model estimates produced different but generally consistent results. The estimate based on core data revealed that air-void content, pavement structure, cumulative rainfall, pavement age, and mix type are significant at the 90 percent confident level, while the estimation based on the generally surveyed sections revealed that additive and pavement age are significant at the 95 percent confident level. Although significant in only one model estimate, the estimated parameters have the same signs for additive, air-void content (QCQA), cumulative rainfall, and mix type. This consistency indicates that these variables are very likely to have a significant influence on moisture. On the other hand, the estimated parameter for structure has opposite signs in the two model estimates, which adds uncertainty to the effect of underlying layers to moisture damage.

The two model estimates provide insights from different perspectives. The effectiveness of their conclusions largely relies on the size and quality of the data set. For the first estimate, the core data provide a precise description of the extent of moisture damage and actual measurements of air-void content and moisture content, and include reasonable proportions of samples with and without noticeable moisture damage. For the second estimate, the generally surveyed sections include more mix types, pavement structures, and traffic and environmental variations, but the determination of moisture damage is ambiguous and less reliable. Furthermore, this data set contains a high proportion of pavement sections with no moisture damage or very little (around 75 percent, as shown in Table 3.16), which may reduce the power[a] of statistical testing and turn significant factors into insignificant ones. For a comparison, the conclusions from the first model estimate should be more reliable.

It should be mentioned that in both model estimates, aggregate effect was not included as an explanatory variable due to the lack of appropriate information and method to characterize aggregate type. Instead it was included implicitly in the random error term, which essentially inflated the variance of the error term and reduced the power of hypothesis testing. If aggregate characteristics can be clearly identified and included in the model, some of the insignificant factors may become significant, but the significant factors in current model will remain significant in the improved model.

As a reference for later laboratory test results, the field performance of pavement sections containing aggregates A and B are briefly discussed here. The performance and main project data of these sections are shown in Table 3.17. Three sections containing Aggregate A have an average age of six years. Two of them (Sections 1 and 3) do not have noticeable stripping in the mix while the third (Section 2) shows signs of moisture damage (slight stripping and loss of fines). The two sections containing Aggregate B are eight years old and all show stripping in the mix (Shatnawi 1995). Although laboratory tests have revealed that mixes containing Aggregate B have better moisture resistance than mixes containing Aggregate A, the field performance seems to be contrary. This indicates that the extent to which moisture damage associated with aggregate type can be overcome by other factors. Table 3.17 shows that the two nonstripped sections containing Aggregate A have low in-situ air-void contents (5.7 percent and 4.9 percent), and are in areas where annual rainfall is low (382 mm and 399 mm respectively), while the stripped section containing Aggregate A

[a] The power of a statistical hypothesis test measures the test's ability to reject the null hypothesis when it is actually false.

has a high in-situ air-void content (averaged at 13.4 percent) and is in an area where annual rainfall is relatively high (868 mm). As a result, the two nonstripped sections have much lower moisture contents than the stripped one (0.64 percent, 0.65 percent versus 2.31 percent), which is very possibly the reason why stripping has not occurred in them. On the other hand, the two sections containing Aggregate B both show higher air-void contents (7.6 percent and 8.7 percent) and were in areas where annual rainfall (1,484 mm and 1,391 mm) is high, which leads to high moisture contents in the mixes. Moreover, both the high temperature duration (degree-days greater than 30°C) and freeze-thaw cycles are much larger for these two sections than for the sections containing Aggregate A. These adverse conditions may have accounted for the greater moisture damage in mixes containing Aggregate B than mixes containing Aggregate A. The above discussion reveals that although aggregate type affects moisture sensitivity, other factors such as construction compaction and environmental conditions, may well overcome the aggregate effect and complicate pavement performance.

3.5 Case Study

The statistical analysis in the previous section investigated factors affecting moisture damage from a general point of view. For a particular pavement, damage may be caused mainly by one or some of these factors, or even by some special variables that were not or could not be included in the statistical analysis. This section details a few sections that showed severe damage, and tries to analyze the main reason(s) for damage in each case. A total of five sections are analyzed.

3.5.1 2N2_1

This section is on Interstate Highway 5 in Siskiyou County. The section was rehabilitated in 2002 with 90-mm Type A dense-graded asphalt concrete. Based on the statements of Caltrans engineers, the pavement showed distresses so severe that the surface mix in the truck lane was completely removed and replaced with a new mix in the next year. Cores were taken on August 4, 2004, on the shoulder, where the original mix still exists. Old asphalt concrete (AC) and aggregate base (AB) were found under the surface layer.

Observed Distress Conditions

The field survey was performed on June 7, 2004, when the distressed truck lane had already been repaved. No severe distress was observed in the passenger-car lane or on the shoulder except for surface aggregates that were friable and worn off. The cores taken on the shoulder were all in good condition, and dry cores contained little moisture inside. The average moisture content and saturation level in the pavement were 0.48 percent and 19.5 percent, respectively.

Mix Design and Construction Records

The mix used for rehabilitation was Type A asphalt concrete using 19-mm nominal maximum size, medium dense graded aggregates from Hart quarry (CMID# 91-47-0001) and Timber Hitch Quarry (CMID# 91-47-0055), and PBA-6a binder from Sheldon Telfer at Pittsburg, CA. The aggregate was 99.5 percent crushed, with a sand equivalent (SE) 67 and Los Angeles Abrasion 20 percent at 500 revolutions. The optimum binder content (OBC) was 5.8 percent. Hydrated lime was added to the aggregates at a rate of 1.5 percent (by dry mass of aggregate) to improve the moisture resistance of the mix.

Field and Laboratory Test Findings

This section is on a slope and the edge drainage system is in good condition. It is unlikely that water would pond on the pavement during rain. The average permeability measured on the shoulder is 55.7×10^{-5} cm/s, and the in-place air voids are 6.6 percent and 5.8 percent for the overlay and the underlying AC layer respectively, suggesting that water infiltration during rain would also be slow. However, when the cores were broken down by heating, many coarse aggregates were found broken in the mix. Since there was little traffic on the shoulder, these aggregates must have been crushed during construction.

Some field mix retained during construction was obtained from the District Office and compacted in the laboratory for both the indirect tensile strength ratio (TSR) test and the Hamburg wheel tracking device (HWTD) test. The TSR test was conducted following Caltrans test method CTM 371-03. The average TSR value is 70 percent, while the rut depth in the HWTD test is over 20 mm after 20,000 wheel passes. Many coarse aggregates were crushed in the HWTD test and tended to release clay-like fines.

Traffic and Climate

The annual average daily traffic (AADT) and the annual average daily truck traffic (AADTT) in 2002 were 19,851 and 6,321 respectively, and the 10-year Traffic Index (TI) was 10.5. The annual average rainfall is 1,200 mm and the degree-days over 30°C is 215. The average yearly snow is 948 mm and the number of freeze-thaw cycles is 91.

Comments

The AC layer has relatively small air-void contents and permeability, and the edge drainage system is in good condition. It is unlikely that an excess amount of moisture would exist in the mix. This judgment is also supported by the fact that little moisture was measured in the dry cores. The failure of this mix in both the TSR test and the HWTD test indicates that it is susceptible to moisture damage, even with lime treatment. Observations both in the field and laboratory show that the coarse aggregates are friable and prone to weathering, and may be easily degraded under multiple freeze-thaw cycles. It is very possible that the poor quality of the coarse aggregate is the main reason for the premature failure of the pavement. In addition, the high rainfall and heavy truck traffic may have further accelerated the degradation of the aggregates and damage of the pavement.

3.5.2 2D18, 2D19, 2D20, 2D21

This project is on Highway 139 in Modoc County. It was placed in 1991 as multistructure test sections for relieving reflective cracking. Section 2D18 was overlaid with 122-mm Type A DGAC with a stress absorption membrane interlayer (SAMI) over a 113-mm old AC layer. Section 2D19 was overlaid with 183-mm Type A DGAC over the old AC layer. Section 2D20 was overlaid with 76-mm rubberized asphalt concrete (RAC) and a layer of SAMI. Section 2D21 was overlaid with 183-mm polymer modified asphalt concrete (PMAC) and a layer of pavement reinforcement fabric (PRF). Cores taken in March 2001 and August 2004 revealed a 61-mm OGAC layer underlying the old AC layer.

Observed Distress Conditions

The field survey was performed in both March 2001 and June 2004. In March 2001, slight raveling, medium rutting, Stage A alligator cracking, and a few potholes were observed on sections 2D18, 2D19, and 2D20, but Section 2D21 showed no signs of distress. In June 2004, the surface layer in the wheelpath had been mostly dug out and replaced with new mixes on sections 2D18, 2D19, and 2D20. The mix remaining in the lane center and on the shoulder showed Stage C alligator cracking, many bare aggregates, medium pumping, closely spaced transverse cracking, and potholes. On the other hand, Section 2D21 was overlaid with a chip seal and showed no obvious distress.

Cores taken from sections 2D18 and 2D19 showed that there was abundant moisture in the DGAC mix. Delamination occurred at the interface of two lifts of surface layer and at the interface of the surface layer and the old AC layer. The DGAC mix was weak and severely stripped, especially at the delamination interfaces.

Cores taken from Section 2D20 showed that there was also abundant moisture in the RAC mix. Four out of twelve cores showed delamination between the overlay and the SAMI. The mix was weak and stripped at the delamination interfaces. The underlying old AC layer was crumbled, cracked, and delaminated.

Cores taken from Section 2D21 showed that there was a moderate amount of moisture in the PMAC. Most cores were in good condition, except that two of them showed delamination between the PMAC mix and the PRF and there was slight stripping at the delamination interface.

Mix Design and Construction Records

The mix used in sections 2D18 and 2D19 was Type A DGAC using the AR4000 binder from the Witco Asphalt Plant in Oregon (currently Golden Bear Inc.), at 4.85 percent optimum binder content (OBC). No antistripping additives were used. The aggregate was 100 percent crushed basalt.

The mix used in Section 2D20 was RAC-G, using the PBA-2 binder from the Witco Asphalt Plant in Oregon (currently Golden Bear Inc.) at 6.1 percent optimum binder content (OBC). The binder contained 15 percent crumbled rubber. No antistripping additives were used.

The mix used for overlay was DGAC, using the PBA-6 binder from the Witco Asphalt Plant in Oregon (currently Golden Bear Inc.) at 4.9 percent optimum binder content (OBC).

All mixes used the same aggregate, obtained from one quarry, which is basalt in nature and 100 percent crushed. No antistripping additives were used.

Construction records were not available for this project.

Field and Laboratory Test Findings

This project is on a slope and the drainage ditches seemed to work. It is unlikely that water would pond on the pavement during rain. However, this highway section is in a large agricultural field with a ditch along with the road. The high water level in the ditch indicated that the underground water table below the pavement might be high.

The average permeability measured in the lane center is nearly 0×10^{-5} cm/s for all sections, due to the existence of chip seal or fog seal. The in-place air-void content in the lane center is 10.0, 12.5, 11.2, and 9.1 percent for 2D18, 2D19, 2D20, and 2D21 respectively. The average moisture content is around 1.4, 1.2, 1.6, and 1.2 percent (by the dry mass of mix) for the four sections respectively, with a corresponding saturation level ranging between 21 percent and 30 percent.

Previous TSR testing on a similar DGAC mix (EA 02-258904) showed a value of 73 percent. The HWTD test showed good results for all mixes, with little stripping observed in the specimens after the test.

Traffic and Climate

The AADT and AADTT in 1991 were 2,288 and 297 respectively, and the 10-year Traffic Index (TI) was 7.0. The annual average rainfall was 300 mm and the degree-days over 30°C was 85. The average yearly snow was 809 mm and the number of freeze-thaw cycles was 158.

Comments

Cores were taken from the lane center on Section 2D18, which had experienced little traffic loading, but stripping in the mix was still very severe. Several factors may have contributed to the distress:

1. The volcanic basalt aggregate is incompatible with asphalt and easily stripped off by moisture. According to the district material engineers, volcanic origin aggregates are believed to be the most moisture-sensitive aggregates in District 2.
2. Although both the rainfall and the surface permeability are low, the high air-void contents in mixes and the possible high water table allowed water to get into the pavement and stay there for an extended period.
3. Multiple freeze thaw cycles might degrade the moisture-rich mix.

The mix used in Section 2D19 is the same as that used in Section 2D18. The only difference is that Section 2D19 used a thicker layer and without SAMI. The distresses observed on both sections were similar. In this scenario, the pavement structure seemed to have an insignificant influence on distress.

Section 2D20 used a rubberized asphalt concrete (RAC) mix, but it showed similar distresses as sections 2D18 and 2D19. In this scenario, both the RAC and DGAC tended to have similar moisture resistance.

On the other hand, Section 2D21 showed much better performance, which indicates that under similar traffic and environmental conditions, polymer modified asphalt mixes have much better resistance to moisture damage than conventional DGAC and RAC mixes.

3.5.3 4U1

This section is on Interstate Highway 80 in the Solano County. The section was rehabilitated in 1997 with 60-mm RAC-G mix. Cores taken in the truck lane on June 30, 2004, revealed a 160-mm old DGAC layer and a 300-mm cement-treated base (CTB) layer underneath the surface layer. The mix for the shoulder was a Type B 19-mm dense-graded asphalt concrete.

Observed Distress Conditions

The condition survey was performed on February 18, 2004, one day after a heavy rain. The whole section was generally severely distressed in the truck lane. Large potholes, pumping, cracking, raveling, and rutting were observed. Potholes also showed bare aggregates raveling inside. At the time of survey, a large amount of water seemed to exist in the truck lane. Some water flowed out of potholes and ran across the shoulder surface.

Most cores taken in the right wheelpath showed delamination between the RAC layer and the underlying DGAC layer. Both mixes were severely stripped around the interface. In some cores, the DGAC was mostly disintegrated and coarse aggregates were totally stripped of asphalt.

Most cores taken in the lane center were generally well integrated except a weak layer interface. Some mixes around the interface were crumbled.

One core taken on the shoulder was in good condition without showing any weak material or stripped aggregates.

Mix Design and Construction Records

The mix used in this section is RAC-G, using 7.1 percent AR4000 binder and aggregates from the Teichert-Esparto Quarry (SMARA #91-57-0011). No antistripping additives were used. Construction information is unavailable.

Field and Laboratory Test Findings

The average permeability measured at the lane center is close to zero, possibly due to the densification of surface mix and clog of voids by dust and excess asphalt. Core measurement showed that the in-situ air-void content was 11.8 percent and 8.7 percent in the lane center and right wheelpath respectively for the RAC mix, and 11.7 percent and 10.2 percent in the lane center and right wheelpath respectively for the underlying DGAC mix. The average moisture content in the RAC layer was 1.1 percent and 1.4 percent (by the dry mass of mix) in the lane center and right wheelpath respectively. The average moisture content in the underlying DGAC was 2.3 percent and 1.8 percent in the lane center and in the right wheelpath respectively. The corresponding saturation level in the RAC was 20 percent in the lane center and 37 percent in the right wheelpath, and those in the DGAC were 44 percent and 40 percent in the lane center and in the right wheelpath respectively. The HWTD test performed on the RAC mix showed good results with small rut depth and little stripping.

Traffic and Climate

The AADTT in 1997 was 10,165, and the 10-year TI was 13. The annual average rainfall was 580 mm. There was no snow at this site and only a few freeze-thaw cycles in each year.

Comments

Two reasons may be responsible for the severe distress at this section: improper structure design and heavy traffic.

Both the surface RAC layer and the underlying DGAC layer had high air-void contents at this section. During rain, water might easily get into the pavement, especially on the passenger-car lanes where the surface mix was less densified. The high air-void contents allowed water to flow horizontally towards the shoulder. The intact DGAC mix on the shoulder, however, might have worked as a dike preventing water flowing through, leading to large amount of water accumulating in the truck lane. This point is supported by the field observation that water flowed out of potholes and ran across the shoulder after the rain.

The truck traffic on this site is very heavy. The repeated loading promoted stripping in mixes in the wheelpath. This is supported by the fact that the cores taken in the right wheelpath showed severe stripping, while the cores taken in the lane center showed much less and the core taken on the shoulder showed none at all. Mixes in the passenger-car lanes were also generally in good condition.

3.5.4 R12

This section is on State Highway 395 in the Mono County. The section was overlaid in 1997 with 19-mm medium dense-graded asphalt concrete, using the PBA-6a binder. Cores were taken on September 14, 2004, at post mile 93.0 northbound; six cores in the lane center, and five in the right wheelpath. The structure revealed by the cores is: Chip seal/119-mm DGAC/86-mm old AC.

Observed Distress Conditions

This section, surveyed on March 16, 2004, was covered with a chip seal. At post mile 93, a 100-m stretch showed many irregular shallow potholes in the right wheelpath without alligator cracking. Potholes were not observed in the other portion of the section. Moreover, transverse thermal cracks had developed to medium sizes with small spacing.

Cores taken in the lane center were generally debonded between the two lifts of the surface layer and showed some moisture. On the other hand, cores taken in the right wheelpath showed severe stripping and total disintegration in the surface layer. The underlying old AC layer was in much better condition and had little moisture damage.

Mix Design and Construction Records

The surface mix was DGAC containing 4.5 percent PBA-6a binder. The QC/QA data showed that the aggregate gradation during construction was generally within the specification limits. The binder content was averaged at 4.48 percent with a standard deviation 0.14 percent. The air void during construction averaged 5.9 percent with a standard deviation 0.6 percent.

Field and Laboratory Test Findings

The average permeability measured in the lane center was 0.3×10^{-5} cm/s. The average in-situ air voids were 13.0 and 6.3 percent for the surface DGAC layer and the underlying old AC layer respectively. The average moisture contents were 0.42 and 0.12 percent (by the dry mass of mix) for the cores taken in the lane center and right wheelpath respectively, and the corresponding saturation levels were 11.6 and 5.5 percent respectively.

Traffic and Climate

The AADT and AADTT in 1997 were 3,150 and 158 respectively, and the 10-year TI was 7.0. The annual average rainfall was 454 mm and the degree-days over 30°C was 83. The average yearly snow was 2,261 mm and the number of freeze-thaw cycles was 170.

Comments

This site showed very severe moisture damage, especially in the surface layer. There was little moisture in the surface layer of the dry core, possibly because most of it had evaporated due to the high air-void content. Truck traffic at this section is not heavy and the annual rainfall is not high, but the amount of

annual snow is very high and there are many freeze-thaw cycles. The causes of the moisture damage may be a combination of high air-void content, heavy snow, and multiple freeze-thaw cycles.

3.5.5 8N6

This section is on Interstate Highway 15 in San Bernardino County, close to the Nevada border. The section was not included in the list for condition survey. It was recommended later by the material engineer in District 8, so project data was not collected. However, due to the severe moisture damage at this site, it is worth including in this report.

This section showed premature failure quickly and digout repair was needed only two years after construction. Removal of the stripped asphalt mixes and their replacement with PCC pavement were scheduled at the time of the original research. The cores taken from the truck lane contained severe stripping and crumbled mixes, while those taken from the passenger-car lanes showed much less distress and little stripping.

The pavement structure revealed by the cores was 64-mm DGAC with 19-mm nominal maximum aggregate size (NMAS) over a 76-mm large stone mix with 38-mm NMAS, which itself is over 178-mm DGAC with 19-mm NMAS. Underlying the asphalt layers was cement-treated base (CTB). Large stone mix was used with the expectation that it would provide a stable structural section. However, it actually resulted in a high air-void mix between two normal air-void layers. Water from summer thunderstorms gets into the pavement and may stay in the large stone mix for an extended period. Whenever the sun comes out, it can quickly bring the pavement temperature up to 70°C. High moisture content and high temperature, combined with the heavy truck traffic, may easily lead to severe moisture damage in the mixes. This is verified by the fact that the cores showed that the large stone layer had experienced the worst damage and in some areas had turned into a layer of gravel in the middle of the structural section.

3.6 Summary

This section sought to determine moisture damage in asphalt concrete pavements and to estimate the relative effects of different factors. The severity of moisture damage was observed directly from dry cores taken from 63 pavement sections in California, and the data about the severity was fed to an artificial neural network. Of the 166 pavement sections with previously unknown performance, cores showed that 14 had appreciable moisture damage, and the artificial neural network estimate revealed another 8 sections potentially had significant moisture damage. In other words, about 8 to 13 percent of the randomly selected pavement sections in this study suffered moisture-related problems. Although this does not necessarily reflect the statewide extent of moisture damage due to the incompletely random sampling used in this study, it does suggest that moisture damage should not be neglected in asphalt pavements in California.

An ordered probit model was estimated using both the core data and generally surveyed sections. The model parameters and the marginal effects of independent variables were used to examine the influence of material characteristics, pavement structure, and traffic and climate factors on the severity of moisture damage.

The model's estimates based on sections that were cored showed that air-void content, pavement structure (whether or not underlying PCC or CTB exists), cumulative rainfall (since time of construction), pavement age, and mix type (DGAC or RAC-G) are significant at the 90 percent confidence level in affecting moisture damage. The existence of repeated loading (based on whether or not the core was taken in the wheelpath) has a marginally significant effect but cumulative truck traffic is insignificant. This indicates that repeated loading from trucks has a nonlinear effect on moisture damage: whether or not repeated loading exists has a marginally significant effect on the extent of moisture damage, but the intensity of repeated loading, once it exists, makes no significant difference. An increase in air-void content, rainfall, and pavement age tends to increase the severity of moisture damage, while the presence of PCC or CTB instead of granular underlying layers and use of DGAC mixes instead of RAC-G are associated with decreased damage severity. Limited data showed that use of asphalt rubber mixes does not improve moisture resistance any more than use of

conventional dense-graded mixes. Other factors, including binder type, use of additives, high temperature duration, freeze-thaw cycles, and existence of interlayer, are insignificant in the estimate. The model estimate based on the generally surveyed sections showed that additive and pavement age are significant factors. Using additives (hydrated lime or liquid antistripping agents) tends to reduce the severity of moisture damage. Both model estimates may be improved by explicitly including the aggregate effect. Unfortunately, an appropriate method to characterize aggregate type was not available during this investigation. Raw aggregate samples were also not available. SMARA (Surface Mining and Reclamation Act of 1975) numbers for aggregate sources were recorded in the database for this project where they were available.

Case studies on a few severely distressed sections revealed that in a specific case, one or a few factors may dominate moisture-related damage in pavements. These factors, as is evident in the case studies, include poor quality aggregate, high air-void content combined with an ample source of water, poor pavement drainage design, and inappropriate structural design. High air-void content was found in the severely distressed pavements in most cases.

Based on the above findings, the following countermeasures are recommended to mitigate moisture damage in asphalt pavements:

1. Air-void content should be controlled more strictly during construction to reduce both the average value and the standard deviation. For the samples tested in the study, the average air-void content in mixes showing little or no moisture damage was about 7 percent; the air-void content in the mixes showing medium or severe damage was 1 to 1.5 percent higher, as shown in Table 3.11. The standard deviation of air-void content was also greater in sections showing medium or severe damage, indicating greater variability of compaction in sections with problems. It is therefore desirable to reduce the air-void content of dense-graded mixes to less than 7 percent during construction.
2. Additives (hydrated lime or liquids) or polymer-modified binders can be used to increase the resistance of asphalt mixes to moisture damage.
3. The pavement drainage system should be well designed and maintained to ensure quick removal of water both on top of and inside the pavement during rain. Since the amount of rainfall has a significant effect on moisture damage and rainfall cannot be controlled by design, it is necessary to have an efficient drainage system to reduce the chance of water getting into and residing in pavements.
4. For RAC-G mixes, further research on their moisture sensitivity should be conducted. At the current stage, the compaction effect duration construction may need to be increased to reduce air-void content.
5. From a pavement structure perspective, designs that include a layer with a high air-void content between two layers with low air-void contents should be avoided, especially in areas where high temperatures and heavy traffic exist.

In this study the probit model was estimated based on 235 core samples or 139 pavement sections, which is relatively small in size. In addition, the lack of complete information of the explanatory variables (e.g., aggregate properties) also limited the applicability of the estimated model. The proposed methodology, however, is appropriate for modeling moisture damage in asphalt pavements, and so has the potential to be used in pavement management to predict the moisture damage probability in asphalt pavements at any age and to establish possible correlation between laboratory test results and field performance. If moisture sensitivity test results (e.g., tensile strength ratio) are available for the field mixes and included in the model, the model can provide guidelines to determine the acceptance criterion for test results for pavements in different traffic and environmental conditions.

Table 3.1. Subdivision of Pavement Sections

			Mix Type		
			RAC	**DGAC**	**Others**
All 194 projects	Potentially problematic projects 28/26/20*	Recommended by Caltrans, Industry 18/16/12	4/4/4	11/11/8	3/1/0
		Discovered by UCPRC 10/10/8	1/1/1	9/9/7	0/0/0
	Prior performance unknown projects 166/37/14	With visually observed distress 84/24/12	7/3/2	75/21/10	2/0/0
		Without visually observed distress 82/13/2	0/0/0	80/13/2	2/0/0
Total			12/8/7	175/54/27	7/1/0

* Note: The first number represents the number of projects in each category; the second number represents the number of projects that were cored; the third number represents the number of projects that showed moisture damage.

			Construction Specification		
			QC/QA	**Non-QC/QA**	**Unknown**
All 194 projects	Potentially problematic projects 28/26/20*	Recommended by Caltrans, Industry 18/16/12	3/3/2	4/4/3	11/9/7
		Discovered by UCPRC 10/10/8	6/6/5	3/3/3	1/1/0
	Prior performance unknown projects 166/37/14	With visually observed distress 84/24/12	16/1/0	57/20/9	11/3/3
		Without visually observed distress 82/13/2	65/13/2	6/0/0	11/0/0
Total			12/8/7	175/54/27	90/23/9

* Note: The first number represents the number of projects in each category; the second number represents the number of projects that were cored; the third number represents the number of projects that showed moisture damage.

Table 3.2. Locations of Coring Sites

Section Code	District	County	Route	Coring Date
1U1	1	Mendocino	101	08/17/04
1U2	1	Mendocino	101	08/17/04
1U2_1	1	Mendocino	101	08/18/04
1U3	1	Humbolt	101	08/19/04
1U4	1	Mendocino	20	05/26/05
1U6	1	Del Norte	101	05/25/05
Q2	1	Humbolt	101	08/17/04
Q3	1	Humbolt	299	08/19/04
2D18	2	Modoc	139	08/05/04
2D19	2	Modoc	139	08/05/04
2D20	2	Modoc	139	08/05/04
2D21	2	Modoc	139	08/05/04
2D6_3	2	Siskyou	97	08/04/04
2N2_1	2	Siskyou	5	08/04/04
2N3	2	Modoc	139	08/06/04
2N5	2	Lassen	395	08/11/04
Q10	2	Lassen	395	08/11/04
Q8	2	Modoc	299	08/10/04
4U1	4	Solano	80	06/30/04
Q27	4	Sonoma	12	06/21/04
Q29	4	Alameda	680	06/24/04
Q32	4	Alameda	880	07/06/04
5N1	5	San Luis Obispo	101	02/16/05
5N10	5	San Luis Obispo	33	02/16/05
Q35	5	San Benito	156	05/12/05
Q36	5	Santa Barbara	101	02/17/05
Q38	5	San Luis Obispo	166	02/16/05
W5	5	San Benito	156	05/12/05
W7	5	Santa Cruz	1	05/12/05
6D11	6	Tulare	65	09/29/04
6D24	6	Kern	58	10/01/04
6D5	6	Kern	14	09/30/04
6N12/13	6	Kings	5	09/28/04
6N19	6	Madera	49	09/22/04
6N20	6	Kern	155	09/20/04
Q41	6	Kern	223	10/01/04
R7	6	Madera	99	09/22/04

Table 3.2. Locations of Coring Sites (cont'd).

Section Code	District	County	Route	Coring Date
7N1	7	Los Angeles	Hawthorne Blvd (107)	03/22/05
7N2	7	Los Angeles	60	03/24/05
7N3	7	Los Angeles	Rosemead	03/21/05
7N3_2	7	Los Angeles	Rosemead	03/21/05
7N4	7	Los Angeles	138	03/25/05
8N4	8	San Bernardino	40	03/01/05
8N5	8	San Bernardino	40	03/01/05
Q54	8	San Bernardino	18	03/02/05
Q62	8	San Bernardino	58	03/02/05
Q70	9	Mono	395	09/14/04
Q71	9	Kern	395	09/15/04
Q76	9	Inyo	395	09/15/04
Q77	9	Inyo	395	09/16/04
R11	9	Inyo	395	09/16/04
R12	9	Mono	395	09/14/04
10N1	10	Alpine	88	05/04/05
10U1	10	Merced	99	03/30/05
10U2	10	San Joaquin	99	03/28/05
10U3	10	Stanislaus	5	03/30/05
Q78	10	San Joaquin	4	04/01/05
Q80	10	Calaveras	4	04/01/05
Q81	10	Alpine	88	05/04/05
Q82	11	Imperial	86	03/09/05
Q83	11	San Diego	79	03/08/05
R15	11	San Diego	76	03/08/05
Q84	12	Orange	91	03/25/05

Table 3.3. Extent of Surface Distress at Each Section

Section Code	Percentage of Length Showing Distress	Section Code	Percentage of Length Showing Distress
1U1	60	6N12/13	40
1U2	60	6N19	100
1U2_1	30	6N20	20
1U3	70	Q41	0
1U4	30	R7	10
1U6	60	7N1	20
Q2	80	7N2	100
Q3	30	7N3	100
2D18	100	7N3_2	10
2D19	100	7N4	60
2D20	80	8N4	40
2D21	0	8N5	0
2D6_3	50	Q54	80
2N2_1	100	Q62	0
2N3	70	Q70	20
2N5	50	Q71	0
Q10	40	Q76	40
Q8	10	Q77	0
4U1	40	R11	10
Q27	20	R12	10
Q29	20	10N1	30
Q32	0	10U1	0
5N1	70	10U2	30
5N10	40	10U3	20
Q35	20	Q78	20
Q36	30	Q80	70
Q38	60	Q81	60
W5	0	Q82	100
W7	10	Q83	20
6D11	10	R15	30
6D24	40	Q84	0
6D5	20		

Table 3.4. ANOVA for Air-Void Content in the Field (Type 3 Sum of Squares)

Factors	Degrees of Freedom	Sum of Squares	Mean Sum of Squares	F-value	p-value
In Wheelpath or Not	1	126.60	126.60	21.29	<0.0001
Layer	3	192.92	64.30	10.81	<0.0001
Dry or Wet Core	1	62.84	62.83	10.57	0.0012
Distance from Distresses	1	29.37	29.36	4.94	0.0260
QC/QA or Not	2	347.52	173.76	29.23	<0.0001
Control Section or Not	1	0.13	0.13	0.02	0.8811
Residuals	787	4678.81	5.94		

Table 3.5. Linear Regression Results for In-Situ Moisture Content

Coefficients for Factors	Estimated Value	Standard Error	t statistics	p-value
(Intercept)	-0.0093	0.2429	-0.0384	0.9694
In the wheelpath	0.1195	0.0729	1.6387	0.1029
Air-void content	0.1613	0.0187	8.6357	<0.0001
Days since last rain	-0.0042	0.0009	-4.6985	<0.0001
Distance from distress	-0.1725	0.0806	-2.1412	0.0335
QCQA	0.0630	0.1236	0.5093	0.6111
QCQA unknown	-0.0157	0.1446	-0.1089	0.9134
Annual rainfall	0.0001	0.0001	0.7414	0.4593
Degree days >30°C	-0.0003	0.0001	-1.8994	0.0590

R^2=0.483

Table 3.6. Classification of Moisture Damage in Cores

Moisture Damage Category	Value	Description
Slight stripping or none	0	Core is intact, integrated without any fines missing
Medium stripping	1	Core is debonded between two layers. Noticeable quantity of coarse aggregates or fines is missing along the interface or sides or the core. Approximately 10 to 30% bare aggregates exist in cores.
Severe stripping	2	Core is cracked, or mix is tender or crumbles. Severe loss of materials on sides or interfaces. Over 30% bare aggregates shown in the core.

Table 3.7. Description and Summary Statistics of Explanatory Variables

Variable	Mean	Minimum	Maximum
Air-void content (AIRVOID)			
Continuous variable, %	7.73	3.34	15.49
Binder type (BINDER)			
1 = Polymer modified binder, 0 = Conventional binder	0.34	0	1
Is additive (liquid or lime) used? (ADDITIVE)			
1 = Yes, 0 = No	0.34	0	1
Is there CTB or PCC underneath? (STRUCTURE)			
1 = Yes, 0 = No	0.20	0	1
Core was taken in the wheelpath? (WHEELPATH)			
1 = Yes, 0 = No	0.48	0	1
Cumulative truck traffic on truck lane (CULANEAADTT)			
Continuous variable (×365,000)	8.07	0.34	41.46
Cumulative rainfall (CURAINFALL)			
Continuous variable (×100 mm)	39.17	5.46	255.25
Cumulative degree-days greater than 30°C (CUDD30)			
Continuous variable (×100)	20.07	0.40	108.01
Cumulative freeze-thaw cycles (CUFT)			
Continuous variable (×100)	4.36	0.00	21.06
Years in service of the pavement (AGE)			
Continuous variable	6.92	2	25
Is interlayer used? (INTERLAYER)			
1 = Yes, 0 = No	0.34	0	1
Mix type? (MIXTYPE)			
1 = DGAC, 0 = RAC-G	0.82	0	1

Table 3.8. Distribution of Dependent Variables

Moisture Damage Category	Frequency	Proportion
Slight stripping or none	108	46.0%
Medium stripping	122	51.9%
Severe stripping	5	2.1%

Table 3.9. Maximum Likelihood Estimates of the Ordered Probit Model

Variable	Parameter Estimate	Standard Error	t-statistic (asymptotic)	p-value
Constant	-1.394	0.705	-1.977	0.048
AIRVOID	0.142	0.043	3.302	0.001
BINDER	-0.209	0.186	-1.129	0.259
ADDITIVE	-0.134	0.240	-0.557	0.578
STRUCTURE	-0.885	0.274	-3.225	0.001
WHEELPATH	0.234	0.171	1.366	0.172
CULANEAADTT	-0.002	0.011	-0.155	0.877
CURAINFALL	0.008	0.004	1.984	0.047
CUDD30	0.003	0.006	0.458	0.647
CUFT	-0.024	0.028	-0.882	0.378
YEAR	0.136	0.078	1.748	0.080
INTERLAYER	-0.188	0.222	-0.847	0.397
MIXTYPE	-0.580	0.269	-2.153	0.031
Threshold value μ_1	2.463	0.219	11.230	.000

Log likelihood =-156.316, Scaled R-squared = 0.219
Likelihood ratio test of joint zero coefficients =53.758, with a p-value =3.02e-7

Table 3.10. Predicted Probabilities and Marginal Effects from the Estimated Ordered Probit Model

	Moisture Damage=0	Moisture Damage=1	Moisture Damage=2
Predicted probabilities	0.45071	0.53964	0.00965
		Marginal Effects	
Air-void content	-0.05596	0.05231	0.00365
Change conventional binder to modified binder	0.08266	-0.07704	-0.00561
Use antistripping additives	0.05296	-0.04964	-0.00331
CTB or PCC underneath	0.33854	-0.32454	-0.01401
Cores taken in the wheelpath	-0.09228	0.08611	0.00617
Cumulative truck traffic	0.00083	-0.00078	-0.00005
Cumulative rainfall	-0.02075	0.01939	0.00135
Cumulative degree-days greater than 30ºC	-0.00963	0.00900	0.00063
Cumulative freeze-thaw cycles	0.01064	-0.00994	-0.00069
Pavement age	-0.07131	0.06666	0.00466
Interlayer (SAMI or PRF) in the pavement	0.07466	-0.07011	-0.00456
Mix of dense-graded asphalt concrete	0.21644	-0.19165	-0.02479

Table 3.11. Average Value of Each Variable for Each Damage Category (Ratios are used for dummy variables.)

	Moisture Damage=0	Moisture Damage=1	Moisture Damage=2
Sample size	108	122	5
Air-void content (%)	6.95 (1.83)[a]	8.46 (2.35)	7.78 (3.28)
Ratio of sections with polymer modified binders to sections with conventional binders	1.51	1.03	4.00
Ratio of treated sections to untreated sections	0.93	0.31	1.50
Ratio of sections with PCC or CTB underneath to sections without PCC or CTB underneath	0.38	0.14	0.25
Ratio of samples in the wheelpath to samples between the wheelpaths	0.89	0.91	4.00
Cumulative truck traffic on truck lane (×365,000)	7.72 (8.80)	8.44 (11.49)	1.82 (1.56)
Cumulative rainfall (×100 mm)	34.60 (31.21)	43.50 (30.62)	49.11 (27.16)
Cumulative degree-days greater than 30°C (×100)	22.45 (22.57)	20.07 (14.31)	9.53 (5.77)
Cumulative freeze-thaw cycles (×100)	3.89 (4.63)	4.74 (6.40)	9.94 (7.70)
Pavement age (year)	6.57 (1.64)	7.32 (2.13)	8.20 (2.68)
Ratio of sections with interlayers to sections without interlayers	0.48	0.56	0.00
Ratio of DGAC sections to RAC-G sections	17.00	3.21	∞

[a] The number in parenthesis is standard deviation.

Table 3.12. Description and Summary Statistics of Explanatory Variables for the Second Model Estimate

Variable	Mean	Minimum	Maximum
Binder type (BINDER)			
1 = Polymer modified binder, 0 = Conventional binder	0.17	0	1
Is additive (liquid or lime) used? (ADDITIVE)			
1 = Yes, 0 = No	0.36	0	1
Is there CTB or PCC underneath? (STRUCTURE)			
1 = Yes, 0 = No	0.26	0	1
Cumulative truck traffic on truck lane (CULANEAADTT)			
Continuous variable (×365,000)	8.44	0.05	49.90
Cumulative rainfall (CURAINFALL)			
Continuous variable (×100 mm)	38.08	3.58	255.25
Is QCQA project? (QCQA)			
1 = Yes, 0 = No	0.66	0	1
Years in service of the pavement (AGE)			
Continuous variable	6.27	1	25
Is interlayer used? (INTERLAYER)			
1 = Yes, 0 = No	0.19	0	1
Mix type? (MIXTYPE)			
1 = DGAC, 0 = RAC-G	0.93	0	1

Table 3.13. Distribution of Dependent Variables for the Second Model Estimate

Moisture Damage Category	Frequency	Proportion
Slight stripping or none	105	75.5%
Medium stripping	29	20.9%
Severe stripping	5	3.6%

Table 3.14. Maximum Likelihood Estimates from the Second Model Estimate

Variable	Parameter Estimate	Standard Error	t-statistic (asymptotic)	p-value
Constant	-1.000	0.650	-1.540	0.124
BINDER	0.218	0.397	0.550	0.583
ADDITIVE	-0.731	0.346	-2.110	0.035
STRUCTURE	0.398	0.325	1.226	0.220
CULANEAADTT	-0.012	0.013	-0.969	0.333
CURAINFALL	0.000	0.004	-0.063	0.950
AGE (YEAR)	0.106	0.052	2.030	0.042
QCQA	-0.066	0.437	-0.150	0.881
INTERLAYER	0.057	0.329	0.173	0.863
MIXTYPE	-0.260	0.331	-0.787	0.431
Threshold value μ_1	1.202	0.209	5.753	0.000

Log likelihood =-79.881, Scaled R-squared = 0.186.
Likelihood ratio test of joint zero coefficients =26.586, with a p-value =1.64e-3.

Table 3.15. Predicted Probabilities and Marginal Effects from the Second Model Estimate

	Moisture Damage=0	Moisture Damage=1	Moisture Damage=2
Predicted probabilities	0.78946	0.18811	0.02242
		Marginal Effects	
Change conventional binder to modified binder	-0.06653	0.05305	0.01348
Use antistripping additives	0.19323	-0.15891	-0.03432
CTB or PCC underneath	-0.12336	0.09716	0.02620
Cumulative truck traffic	0.00360	-0.00293	-0.00066
Cumulative rainfall	0.00007	-0.00006	-0.00001
Pavement age	-0.03060	0.02494	0.00565
QCQA project	0.01940	-0.01569	-0.00371
There is interlayer (SAMI or PRF) in the pavement	-0.01666	0.01352	0.00315
Mix is dense-graded asphalt concrete	0.07743	-0.06227	-0.01516

Table 3.16. Average Value of Each Variable for Each Damage Category in the Second Model Estimate (Ratios are used for dummy variables.)

	Moisture Damage=0	Moisture Damage=1	Moisture Damage=2
Sample size	105	29	5
Ratio of sections with polymer modified binders to sections with conventional binders	0.25	0.04	0.25
Ratio of treated sections to untreated sections	0.82	0.07	0.25
Ratio of sections with PCC or CTB underneath to sections without PCC or CTB underneath	0.30	0.53	0.25
Cumulative truck traffic on truck lane (×365,000)	8.43 (9.40) [a]	8.96 (12.49)	6.31 (4.38)
Cumulative rainfall (×100 mm)	33.55 (34.77)	45.43 (32.14)	96.06 (97.35)
Pavement age (year)	5.68 (2.72)	7.69 (3.51)	12.40 (8.35)
Ratio of QCQA projects to non-QCQA projects	2.42	1.07	0.25
Ratio of sections with interlayers to sections without interlayers	0.19	0.45	0.25
Ratio of DGAC sections to RAC-G sections	20.00	4.80	∞

[a]The number in parenthesis is standard deviation.

Table 3.17. Performance and Project Data of Sections Containing Aggregates A and B

Number	1	2	3	1	2
Aggregate	A	A	A	B	B
Performance	No obvious distress. Cores were generally in good condition. No stripping.	10% of section showed alligator B cracking. Cores showed slight stripping and loss of fines.	20% of section showed alligator B fatigue cracking. Cores were generally in good condition.	Slight rutting. Cores revealed stripping in the mix, especially the portion between PRF and PCC.	Continuous longitudinal cracking in wheelpaths and alligator cracking in some locations Cores revealed some stripping in the mix, especially between PRF and PCC.
Age (year)	6	5	7	8	8
Air-void Content measured from QC/QA (%)	4.8(0.7)[a]	5.0(0.7)	6.4(0.6)	N/A	N/A
Air-void Content measured from cores (%)	5.7 (0.8)	13.4 (2.2)	4.9 (1.9)	7.6 (0.4)	8.7 (2.3)
Binder Type	AR4000	AR4000	AR8000	AR4000	AR4000
Use of Additive	no	no	no	no	No
Underlying Layer Type	AC	AC	AC	PCC	PCC
AADTT	2136	295	2060	3720	3860
Annual Rainfall (mm)	382	868	399	1484	1391
Degree-days greater than 30°C	157	127	193	243	244
Freeze-thaw cycles	18	15	18	84	91
Existence of interlayer	no	PRF	PRF	PRF	PRF
Aggregate Gradation	19mm DG	19mm DG	19mm DG	19mm DG	19mm DG
Average Moisture Content (%)	0.64	2.31	0.65	high	moderate
Drainage Condition	Fair	Fair. Water may pond on surface during raining.	Fair	Poor	Fair

[a]The value in parenthesis is standard deviation.

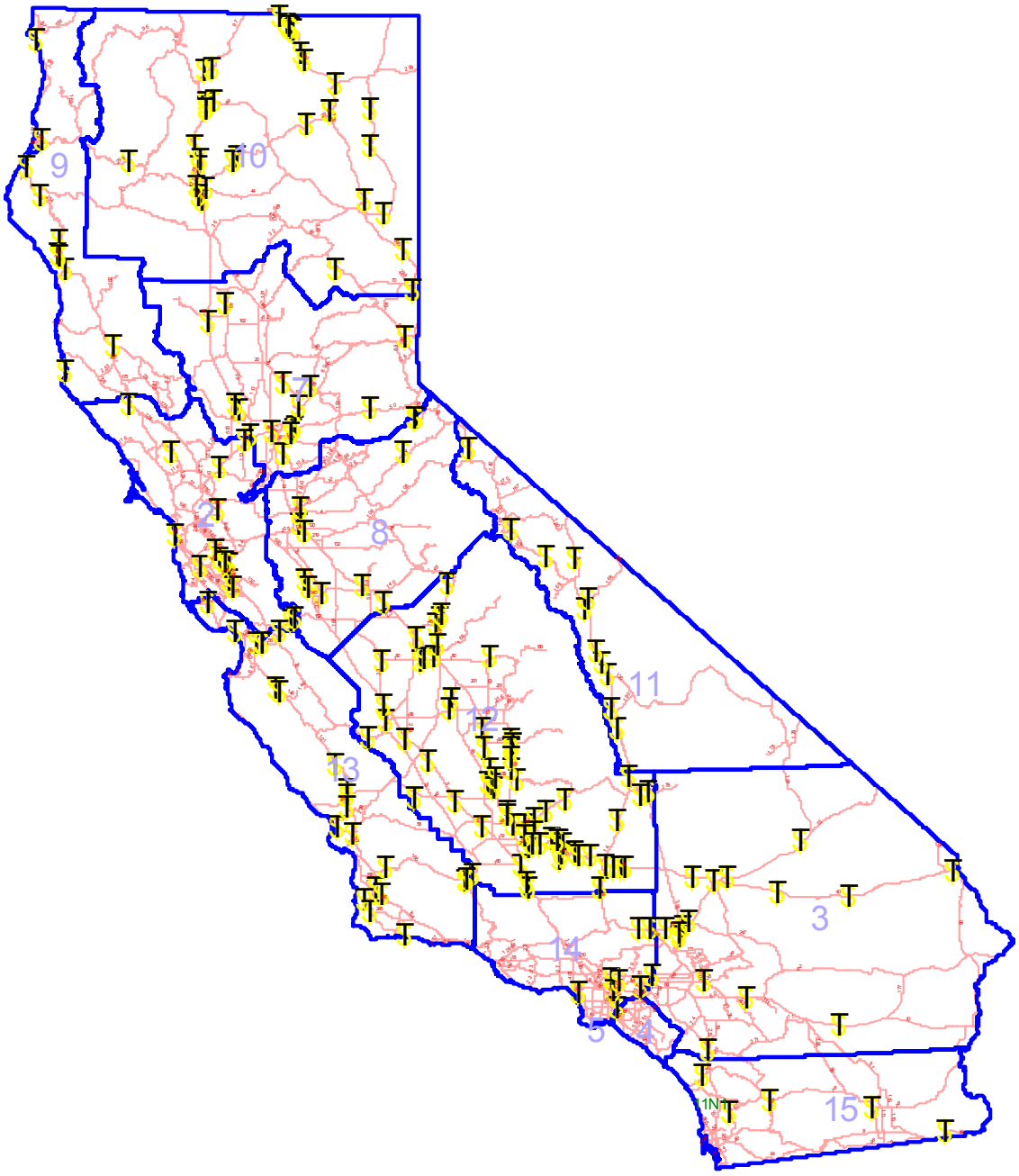

Figure 3-1. Distribution of general condition survey sites.

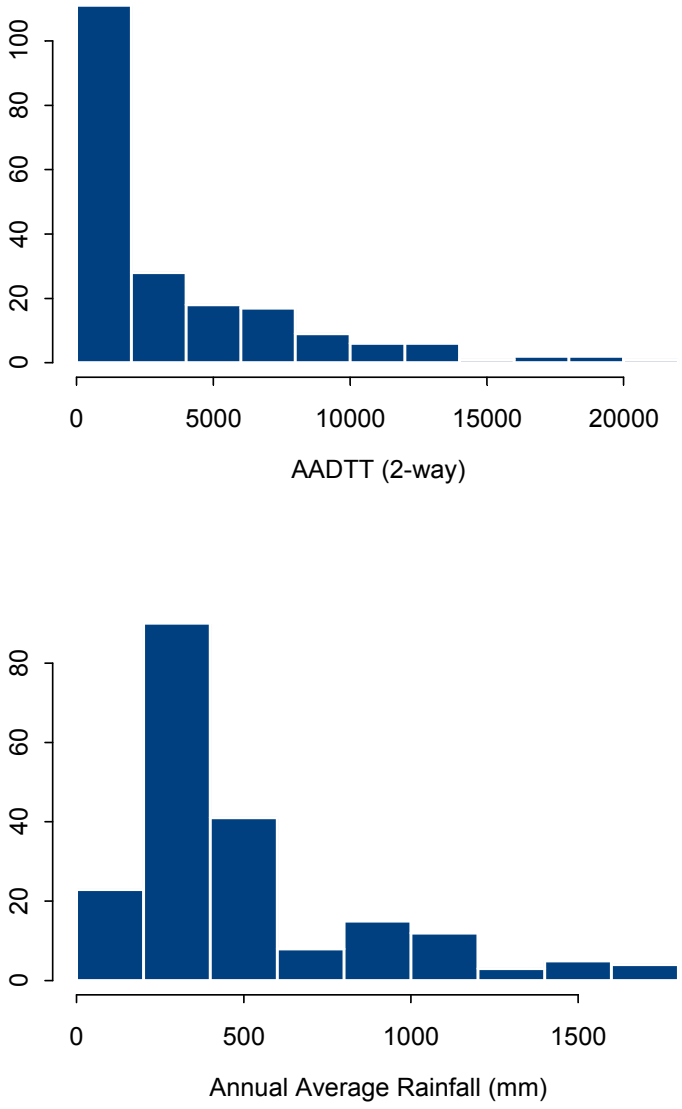

Figure 3-2. Distributions of AADTT and annual average rainfall.

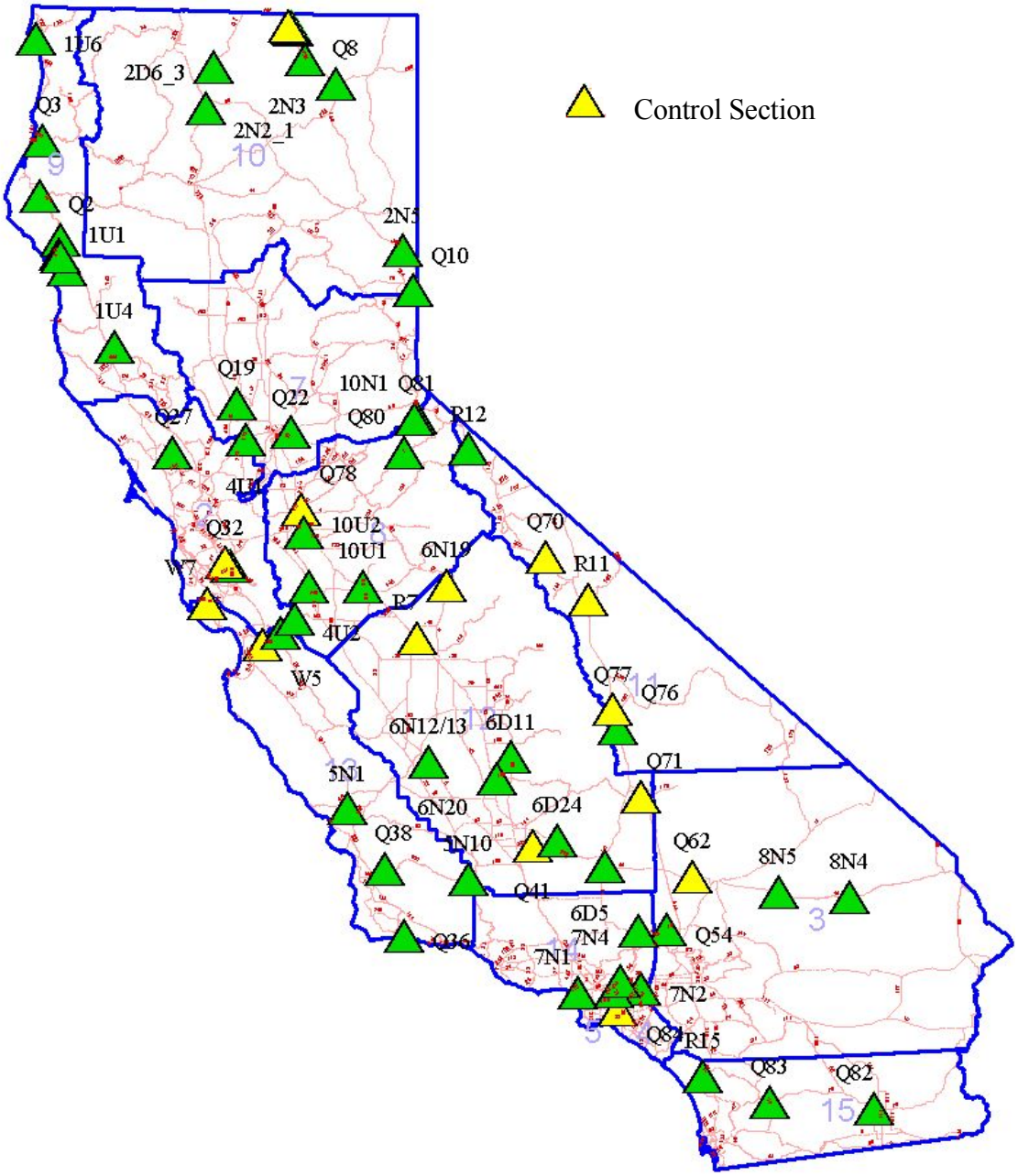

Figure 3-3. Distribution of coring sites.

(a)

(b)

Figure 3-4. Isolated distresses possibly related to moisture damage (a – R12, b – 8N4).

Figure 3-5. Equipment for taking dry cores in the field.

Figure 3-6. Gilson AP-1B Falling-head Permeameter.

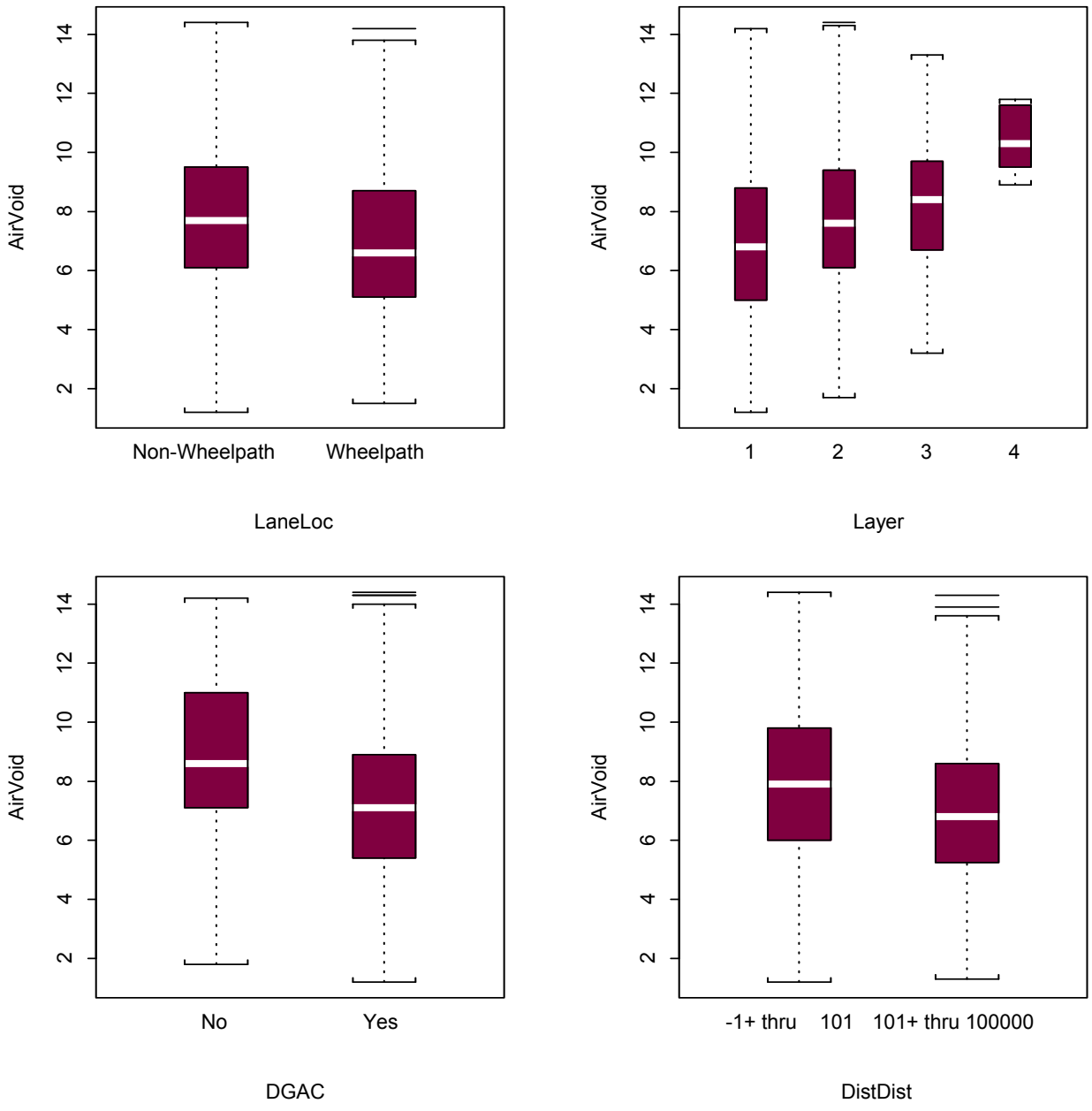

Figure 3-7. Box plots of factors affecting air-void content.

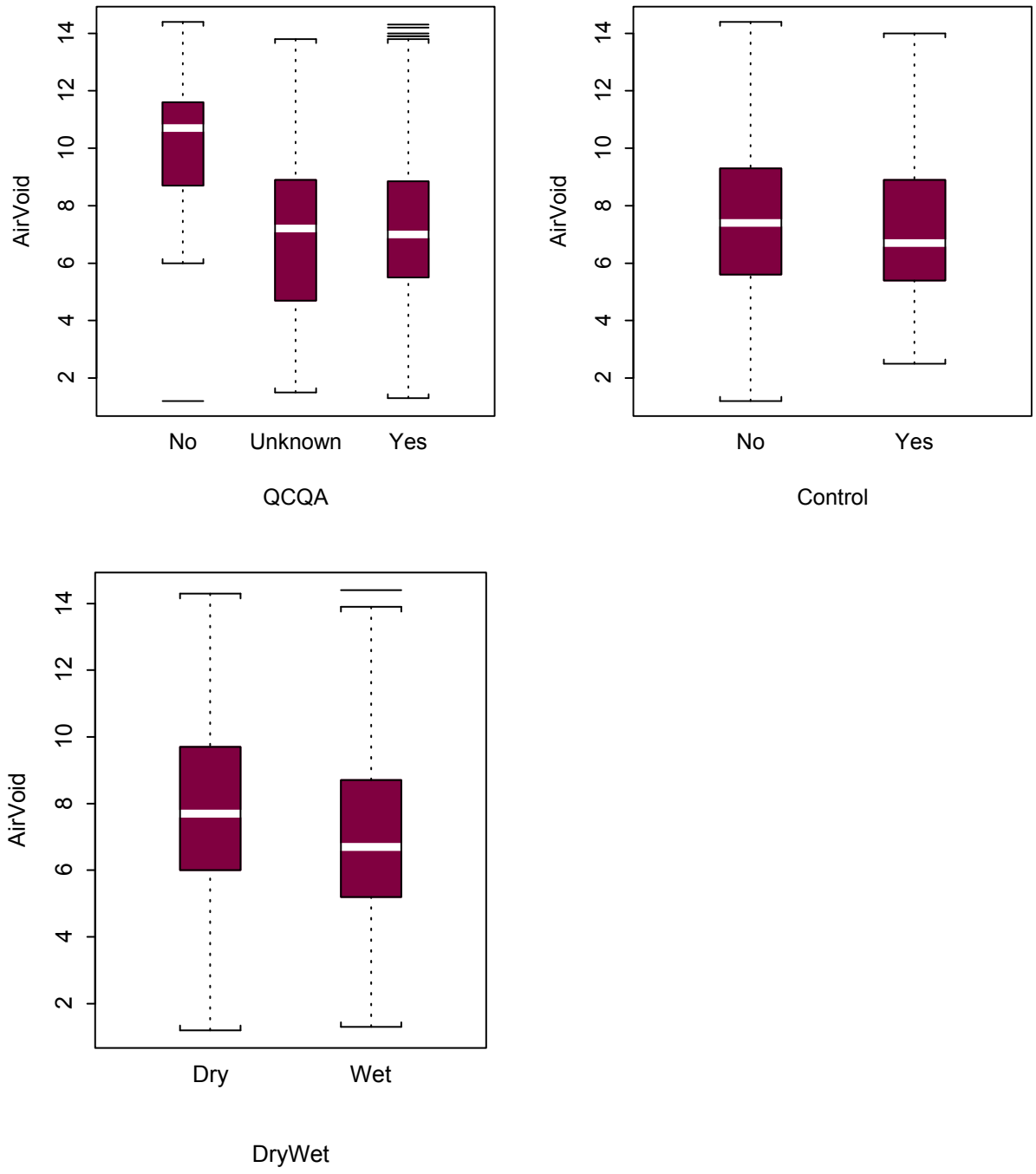

Figure 3-7. Box plots of factors affecting air-void content. (cont'd).

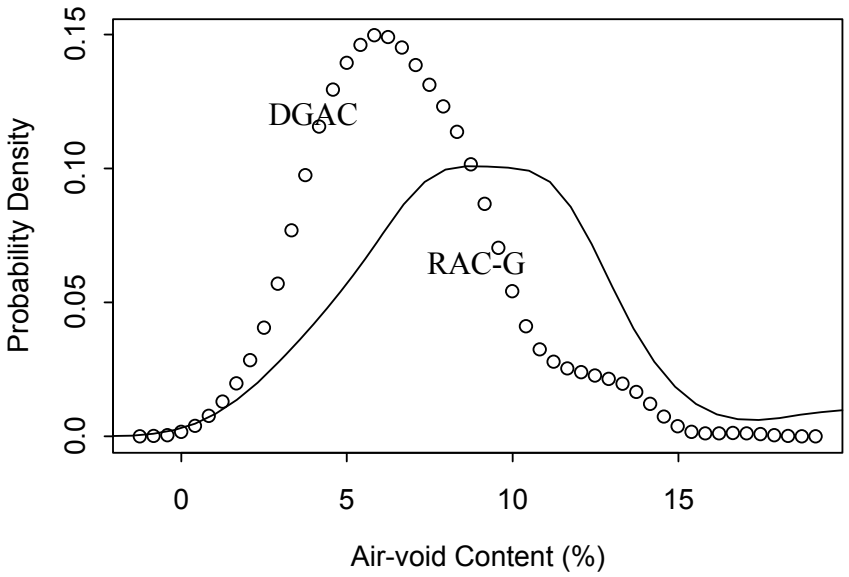

Figure 3-8. Distribution of air-void contents in DGAC and RAC-G from kernel density estimate.

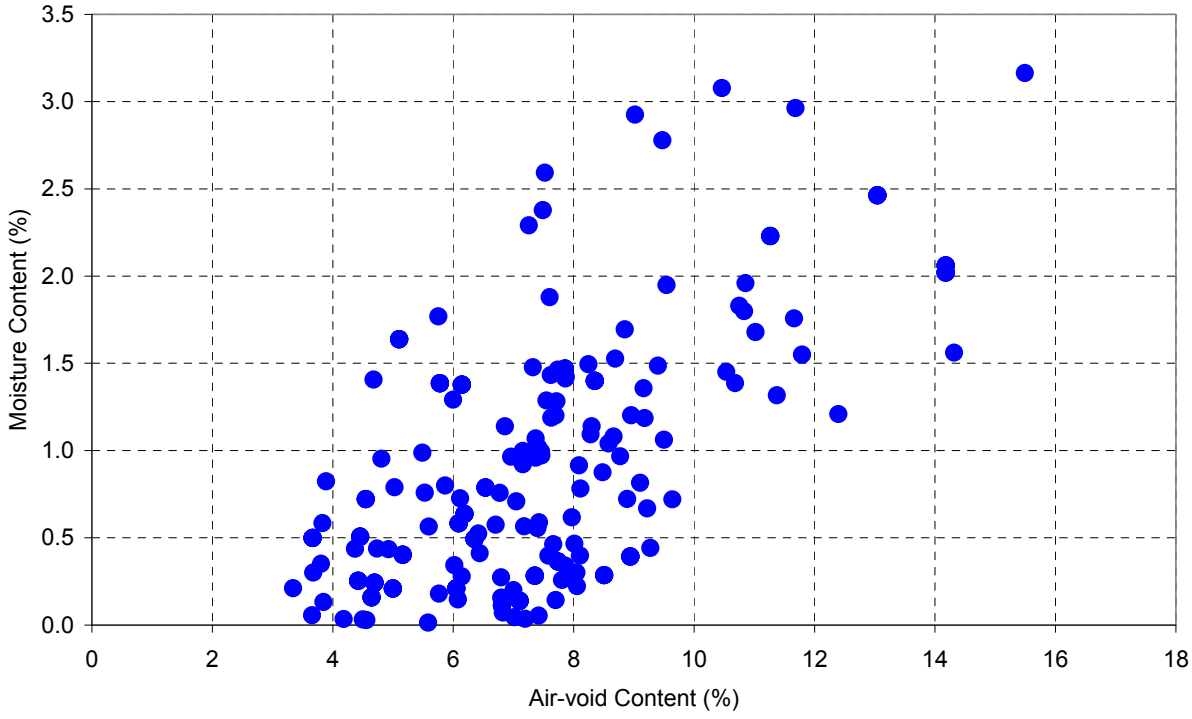

Figure 3-9. In-situ moisture content versus air-void content.

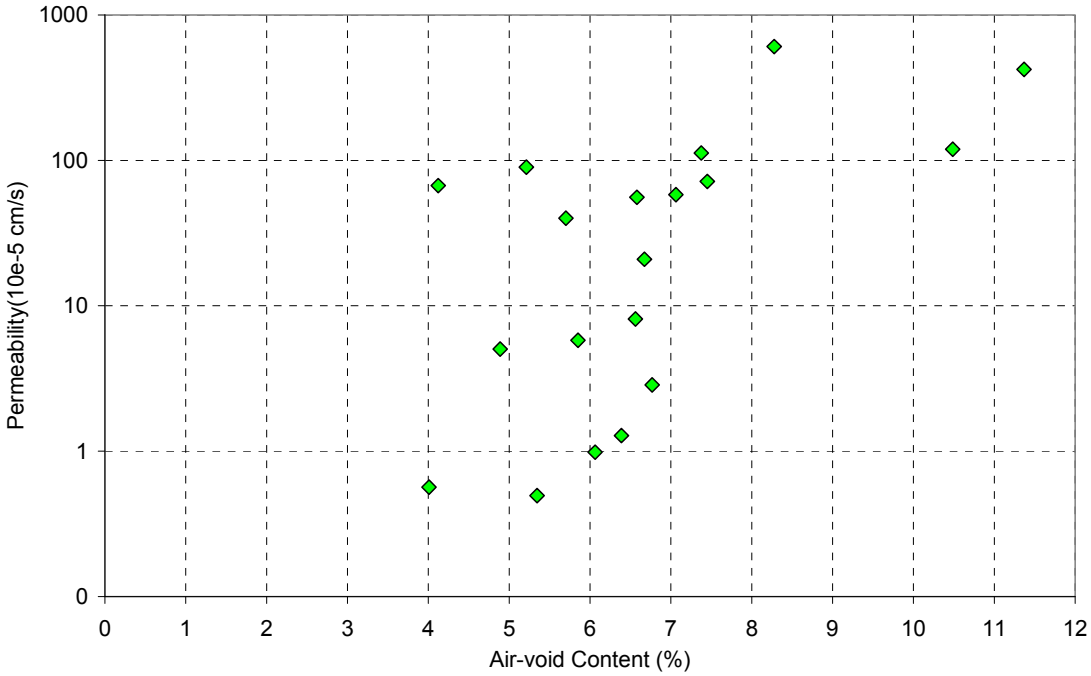

Figure 3-10. Field permeability versus air-void content.

4.0 LABORATORY INVESTIGATION OF FACTORS AFFECTING MOISTURE DAMAGE

The laboratory investigation examines two aspects of moisture damage in detail: (1) the characteristics of moisture ingress and retention processes in asphalt concrete, and the factors affecting these processes, and (2) the effect of construction-induced variations on moisture damage. An understanding of the first aspect can help in the design of less water-absorbent mixtures, and knowledge of the second aspect can shed light on the importance of construction quality control.

4.1 Moisture Ingress and Retention Experiment

The prerequisite condition for moisture damage is the existence of moisture in an asphalt concrete pavement, so reducing the chance and amount of moisture ingress can fundamentally reduce moisture damage. To do this, we need to know the characteristics of moisture ingress and retention in asphalt concrete and the factors affecting these processes. This knowledge can also help us choose an appropriate range of moisture content for laboratory testing and provide supporting evidence for choosing appropriate measures in mix design and construction practice.

4.1.1 Experimental Design

Moisture mainly gets into asphalt concrete pavements in two forms: liquid water and moisture vapor. Liquid water, coming from precipitation, irrigation, or underground, may enter asphalt mixes by capillary action or hydraulic pressure, or the action of gravity. Moisture vapor, mainly coming from underground, moves upward due to heat and may be trapped in asphalt mixes that have small air permeability. An experiment was designed to simulate the movements of both water forms to some extent in the laboratory. The experiment procedure is summarized below:

1. Dry specimens in an oven at 50°C until their mass is constant (this needs about seven days).
2. Place specimens on perforated shelves in a conditioning room at 25°C and 100 percent relative humidity (RH). This process is named “vapor conditioning.”
3. Measure the specimen mass periodically until it stabilizes, which takes about four months.
4. Place specimens on perforated shelves in another conditioning room at 20°C and 20 to 60 percent RH for drying. This process is named “drying after vapor conditioning.”
5. Measure the specimen mass periodically until it stabilizes, which takes about three months.
6. Submerge specimens in water at 25°C under a head of about 0.1 m. This process is named “soaking.”
7. Measure the specimen mass periodically until it stabilizes, which takes about three months.
8. Place specimens on perforated shelves in another conditioning room at 20°C and 20 to 60 percent RH for drying. This process is named “drying after soaking.”
9. Measure the specimen mass periodically until it stabilizes, which takes about three months.

Steps 2 and 6 were designed to study the ingress of moisture vapor and liquid water respectively. This experiment procedure can be summarized into four consecutive steps: vapor conditioning, drying, soaking, and drying. The moisture mass profiles obtained in each step are named respectively: moisture adsorption curve, moisture evaporation curve, moisture absorption curve, and moisture evaporation curve. Vapor conditioning is used to simulate field conditions where there is little rainfall but abundant underground water capable of

reaching the asphalt pavement in the form of vapor or capillary water. Soaking is used to simulate field conditions where there is a frequent and ample source of water on the surface or sides of asphalt pavements.

Cylindrical specimens (152.4 mm ϕ × 50.8 mm) containing Aggregate A were used in the experiment and were fabricated following the procedure described in Chapter 2. Factors and their levels are described below:

1. Air-void Content. Four air-void content levels that cover the range common in field pavements were included: four, 3 to 5 percent; seven, 6 to 8 percent; ten, 9 to 11 percent; and thirteen, 12 to 14 percent.
2. Binder Type. Two binder types were included: Type A, AR-4000; Type P, PBA-6a.
3. Aggregate Gradation. Two gradations were used in the experiment: Aggregate M, 19-mm nominal maximum medium gradation; Aggregate C, 19-mm nominal maximum coarse gradation.

A full factorial design for all three factors was used and two replicates were tested at each combination of factor levels, so a total of 32 specimens were required.

The mass of moisture in the specimen was calculated differently during the four steps, by the following two equations:

$$W_t = W_{at} - W_d \quad \textbf{(4-1)}$$

$$W_t = W_{wt} - W_{w4} + W_{ao} - W_d \quad \textbf{(4-2)}$$

where,

W_t = mass of moisture in the specimen at time t,

W_{at} = mass of surface dry specimen in air at time t since vapor conditioning or drying begins,

W_d = mass of dry specimen in air,

W_{wt} = mass of specimen in water at time t since soaking begins,

W_{w4} = mass of specimen in water after four minutes soaking,

W_{ao} = mass of surface dry specimen in accordance to Method A of AASHTO T 166-93.

Equation (4-1) was used for the vapor conditioning and drying steps, while Equation (4-2) was used for the soaking step.

Saturation, defined as the percentage of air-void content filled with water, was calculated by the following formula:

$$S = \frac{W_t}{AV \times (W_{ao} - W_{w4})} \times 10000 \quad \textbf{(4-3)}$$

where,

S = saturation (percent),

AV = air-void content (percent).

4.1.2 Results and Analysis

Moisture mass in each specimen in the entire test process is summarized in Table 4.1 through Table 4.4, and the average moisture mass profile for each factor level combination is shown in Figure 4-1.

4.1.2.1 General Observation

The average moisture mass profiles (Figure 4-1) show that during the vapor conditioning process moisture mass increased continuously over time for all mixes. Air-void content affected the amount of moisture ingress. A general trend is that higher air-void contents led to more moisture adsorption. This trend is clear in the mixes containing the AR-4000 binder, but vague in the mixes containing the PBA-6a binder. One possible reason is that specimens containing the PBA-6a binder had similar sizes and distributions of open air voids at surfaces at different air-void contents, while specimens containing the AR-4000 binder had larger open air voids at surfaces when their air-void content was higher. As for aggregate gradation, mixes with coarse gradation tended to adsorb more moisture than mixes with medium gradation, possibly because specimens with coarse gradation had more open air voids on their surfaces.

During the soaking process, the moisture ingress rate was much higher in the first two weeks than in the subsequent period, although the amount of moisture that entered the voids after the first two weeks (about 80 days) was comparable to the ingress during the first two weeks. The reason for the different ingress rates might be that in the first two weeks moisture mainly entered the surface aggregates with cut faces and the inner connected air-void system of the specimen. In the late stage, moisture mainly filled the small air-void system of the binder-fines mastic through capillary or osmosis action. The effect of air-void content on the amount of moisture ingress was very significant in the soaking process. Specimens with higher air-void contents absorbed much more moisture than specimens with lower air-void contents, but in terms of normalized moisture contents (i.e., saturation), air-void content seemed to be much less significant. Moreover, aggregate gradation seemed to be insignificant in affecting moisture absorption, while specimens containing the AR-4000 binder tended to absorb more water than specimens containing the PBA-6a binder.

The two drying processes after vapor conditioning and after soaking are similar. Moisture evaporated quickly in the first few days, then followed a much slower rate in the late stage. Specimens with 4 percent air-void content retained more moisture than specimens with higher air-void contents. In the first three days, around 30 to 40 percent of the moisture was lost from specimens with 4 percent air voids, and around 50 to 60 percent of the moisture was lost from specimens with 7 percent to 13 percent air voids. However, the moisture did not completely evaporate from specimens, even after a period as long as four months. The effects of aggregate gradation and binder type did not seem to be significant in affecting both drying processes.

As a summary, the following important observations are obtained from the experiment:

1. Moisture ingress takes time. Although the initial ingress rate is high, the saturation level reached after the first two weeks of soaking or vapor conditioning is generally less than 50 percent. Therefore, a good surface drainage system that can quickly remove water from the pavement surface and some internal barrier layer that can intercept rising moisture vapor or capillary water from underneath can significantly reduce the amount of water entering asphalt pavements, even in a region with heavy rainfall.
2. Complete drying is very difficult. It is very possible that some amount of moisture exists in pavement year around.
3. Air-void content has a significant effect on the amount of moisture ingress.
4. Aggregate gradation and binder type tend to have different effects in different processes.

The above conclusions about the effects of different factors on moisture ingress and retention processes are essentially rough. Instead, rigorous inferences should be obtained from statistical analysis. To facilitate the statistical analysis, the series of response values (i.e., repeated measures of moisture content) need to be reduced to a few parameters by curve fitting. With curve fitting, the ultimate amount of moisture in specimens during each conditioning process can also be estimated by the asymptotic value of the fitting functions.

4.1.2.2 Curve Fitting and Analysis

After a preliminary search, different exponential function forms were chosen for curve fitting for different processes:

During vapor conditioning: $y = \beta_1[1 - \exp(\beta_2 t)]$ **(4-4)**

During soaking and drying: $y = \beta_1 + \beta_2 \exp(\beta_3 t)$ **(4-5)**

where,

y = mass of water in a specimen, g

t = conditioning time, days

$\beta_1, \beta_2, \beta_3$ = parameters to be estimated.

Theoretically, for the soaking process the parameter β_2 in Equation (4-4) should be equal to $-\beta_1$ because at the beginning of each process there should be no moisture in the specimen and for the drying process $\beta_1 + \beta_2$ should be equal to the mass of moisture in the specimen before drying. However, when either constraint was applied, the least squares fitting generally gave a poor result, while a much better fitting could be obtained when the constraint was relaxed. The pseudo R-squares for the fitting after constraint relaxation were all larger than 0.90. In this case, the moisture absorption process and drying process were modeled by a combination of two curves, as illustrated in Figure 4-2. The first curve is a straight vertical line, representing an amount of moisture absorbed/evaporated instantaneously at the beginning of soaking/drying ($t = 0$). The second segment is an exponential curve, representing the moisture ingress/retention process since $t > 0$.

Parameters β all have physical meanings. β_1 represents the asymptotic mass of water in a specimen. In Equation (4-4), $-\beta_2$ represents the normalized initial ingress rate of moisture, $-\beta_2 = \frac{1}{\beta_1}\frac{dy}{dt}\Big|_{t=0}$. In Equation (4-5), $\beta_1 + \beta_2$ represents the amount of moisture absorbed instantaneously at the beginning of soaking for the soaking process, and represents the amount of moisture residing in specimens at the start of drying for the drying process. $-\beta_3$ represents the normalized ingress rate of moisture at time greater than zero for the soaking process, and represents the normalized evaporation rate for the drying process, $\beta_3 = \frac{1}{\beta_2}\frac{dy}{dt}\Big|_{t=0}$.

Based on the two-segment curve modeling, a certain amount of moisture is absorbed instantaneously at the start of soaking or evaporated instantaneously at the start of drying. This amount, m_i, can be calculated by the following two equations respectively:

Instantaneous absorption: $m_i = \beta_1 + \beta_2$ **(4-6)**

Instantaneous evaporation: $m_i = m_0 - \beta_1 - \beta_2$ **(4-7)**

where m_0 = mass of moisture in the specimen before drying.

The ratio of the instantaneous absorption to the total absorption, $\frac{m_i}{\beta_1} \times 100\%$, increases with the air-void content, while the ratio of the instantaneous evaporation to the total evaporation, $\frac{m_i}{m_0 - \beta_1} \times 100\%$ is quite stable for specimens with different air-void contents, generally between 20 percent and 40 percent, as shown in Figure 4-3.

The asymptotic mass of water in each specimen in each conditioning process, β_1, and its corresponding saturation are plotted in Figure 4-4 and Figure 4-5 respectively, along with the second-order polynomial regression curves. It can be seen from Figure 4-4 that during the vapor conditioning or soaking the ultimate amount of moisture ingress was correlated to the air-void content. Generally larger air-void contents led to more moisture ingress. This correlation was more significant during the soaking process than in the

vapor conditioning. The residual moisture after drying, however, was not very sensitive to the air-void content, except that specimens with 4 percent air voids retained slightly more moisture than specimens with higher air-void contents. From the saturation perspective, Figure 4-5 shows that the ultimate saturation in each conditioning process was generally insensitive to the air-void content except for specimens with 4 percent air voids, which achieved and retained higher saturation than specimens with higher air-void contents. Such high saturation is primarily a result of small air-void contents in calculation with Equation (4-3). It does not necessarily indicate worse moisture damage.

The ultimate (maximum) moisture content (or saturation) during the soaking conditioning is useful to help choose the moisture content (or saturation) used in the laboratory moisture sensitivity tests. From Figure 4-5 it can be seen that the maximum saturation, generally between 50 percent and 80 percent, is similar for specimens with air-void contents higher than 7 percent. This similarity can be deduced mathematically from the good correlation between the ultimate moisture content and the air-void content shown in Figure 4-4. Suppose the ultimate moisture content can be calculated by the following formula:

$$y = b_0 + b_1 \cdot A \qquad \textbf{(4-8)}$$

where,

y = ultimate absorbed moisture (g),

A = air-void content (percent),

b_0, b_1 = parameters.

The saturation level can be calculated by

$$S = \frac{10000y}{A \cdot V} = \left(\frac{b_0}{A} + b_1 \right) \times \frac{10000}{V} \qquad \textbf{(4-9)}$$

where V = specimen volume (cm^3).

Using the first-order Taylor series expansion and assuming the parameters b_0 and b_1 are fixed, the variance of saturation can be estimated by

$$\text{var}(S) \approx \frac{10^8 b_0^2}{V^2 A^4} \text{var}(A) \qquad \textbf{(4-10)}$$

With parameters b_0 and b_1 estimated from linear regression and assuming one as the variance of air-void content, formulae (4-9) and (4-10) are plotted in Figure 4-6. Figure 4-6(a) shows that when the air-void content is greater than 5 percent, the ultimate saturation level of specimens soaked in water barely changes with the air-void content. Therefore, it is reasonable to specify the same saturation range in a moisture sensitivity test for specimens with different air-void contents (greater than 5 percent). Figure 4-6(b) shows that when the air-void content is less than 5 percent, the contribution of error in air-void measurement to the error in the calculated saturation level will become large, which makes the saturation level calculated for specimens with small air-void contents unreliable. In this case, it is more appropriate to directly specify the moisture contents for specimens with air-void contents less than 5 percent.

4.1.2.3 Statistical Analysis

The response variable in this experiment is repeated measures on the same experimental unit for a certain period. This type of data is typically analyzed by a two-stage procedure, in which the repeated measures from one experiment unit are fitted by a regression function and represented by a few estimated parameters of the function, then the estimated parameters are treated as the response variables and a conventional analysis of variance (ANOVA) is performed. Although this two-stage analysis is conceptually and computationally simple, it has two problems:

1. Possible useful information is lost in summarizing the sequence of observations for one specimen by parameters of the regression function.

2. Random variability is introduced by replacing the response variables in the analysis of variance with their estimates from the regression.

Nonlinear mixed models are a powerful tool for the analysis of experiments where some response variable is nonlinear and observed on multiple occasions. Each parameter in the model can be represented by a fixed effect that stands for the mean value of the parameter as well as a random effect that expresses the difference between the value of the parameter fitted for each specific subject and the mean value of the parameter. With mixed models heteroscedasticity and correlation among observations may be modeled. In addition, experimental designs of unbalanced and unequally replicated repeated measures can be accommodated. Nonlinear mixed effect models have been widely used in pharmacokinetic research for many years (Peek et al. 2002; Davidian and Giltinam 2003), but not in pavement engineering research.

4.1.2.3.1 Model Specifications

Consider that p_i measures for the i subject are available, and let y_{ij} be the response variable at time t_{ij}, $i = 1, \cdots, n$, $j = 1, \cdots, p_i$. The nonlinear model for the data of subject i can be expressed as:

$$y_{ij} = f(\boldsymbol{\beta}_i, t_{ij}, x_{ij}) + \varepsilon_{ij} \quad \textbf{(4-11)}$$

where f is a nonlinear function relating the response variable to time and to other possible covariates x_{ij} varying with individual and time, and $\boldsymbol{\beta}_i$ ($p \times 1$) is a vector of parameters of the nonlinear function; ε_{ij} is a random error term incorporating measurement error and assumed to have independent normal distribution with zero mean.

The $\boldsymbol{\beta}_i$ vector may be modeled as:

$$\boldsymbol{\beta}_i = \mathbf{d}(\mathbf{a}_i, \boldsymbol{\beta}, \mathbf{b}_i), \quad i = 1, \cdots, n \quad \textbf{(4-12)}$$

where $\mathbf{d}$ is a p-dimensional function depending on an vector of fixed parameters $\boldsymbol{\beta}$ and a vector of random effects $\mathbf{b}_i$ associated with individual i. The distribution of $\mathbf{b}_i$ can take any form. A standard assumption is $\mathbf{b}_i \sim N(\mathbf{0}, \boldsymbol{\Sigma})$, i.e., multivariate normal distribution with zero expectation (Davidian and Giltinam 2003).

In this study, the model (4-11) assumes different forms for different processes:

During vapor conditioning: $y_{ij} = \beta_{1i}[1 - \exp(\beta_{2i} t_{ij})] + \varepsilon_{ij}$ **(4-13)**

During soaking or drying: $y_{ij} = \beta_{1i} + \beta_{2i} \exp(\beta_{3i} t_{ij}) + \varepsilon_{ij}$ **(4-14)**

where the meaning of each term is the same as in equations (4-4) and (4-5).

The parameter vector $\boldsymbol{\beta}_i$ is modeled as a linear function of the covariates and random effects:

$$\begin{aligned} \beta_{1i} &= C_1 + (Binder_{1i} + Gradation_{1i} + AirVoids_{1i})^2 + b_{1i} \\ \beta_{2i} &= C_2 + (Binder_{2i} + Gradation_{2i} + AirVoids_{2i})^2 + b_{2i} \\ \beta_{3i} &= C_3 + (Binder_{3i} + Gradation_{3i} + AirVoids_{3i})^2 + b_{3i} \end{aligned} \quad \textbf{(4-15)}$$

where $C_j, j = 1,2,3$, is the intercept term, $Binder_{ji}, j = 1,2,3$, is the main effect of binder type of specimen i, $Gradation_{ji}, j = 1,2,3$, is the main effect of aggregate gradation of specimen i, and $AirVoids_{ji}, j = 1,2,3$, is the main effect of air-void content of specimen i; the square represents that the second order interaction terms are all included; $\mathbf{b}_i = (b_{1i}, b_{2i}, b_{3i})^T$ are assumed to be independent and identically distributed.

4.1.2.3.2 Results

Each of the four moisture conditioning processes was analyzed separately. Parameters were estimated by the maximum likelihood method (MLE) using the *nlme* routine in S-Plus®. As iterative algorithms are used for the fit of nonlinear model, initial values for the parameters must be set. In this study, the initial values were estimated by the conventional two-stage procedure mentioned previously. Hypotheses concerning the effects of different factors were tested by the Wald F-test. Part of the S-Plus® code for the analysis is shown in Figure 4-7 and the results are summarized in Table 4.5. A discussion of the results for each conditioning process is given below.

During the vapor conditioning, aggregate gradation, binder type, and air-void content and their interactions are all significant in affecting the asymptotic amount of ingress moisture (β_1). Specimens containing the AR-4000 binder, coarse gradation, or higher air-void content absorb more moisture than specimens containing the PBA-6a binder, medium gradation, or lower air-void content. Aggregate gradation, air-void content, and their interaction significantly affect the normalized initial ingress rate of moisture ($-\beta_2$), while binder type is insignificant. The F-values for different factors are comparable with each other, indicating there is no dominant factor in the vapor conditioning process.

During the drying process after vapor conditioning, aggregate gradation, binder type, and air-void content are all significant in affecting the normalized initial evaporation rate ($-\beta_3$) and the asymptotic residual moisture (β_1). Specimens containing the AR-4000 binder, low air-void contents, or coarse gradation retain more moisture than specimens containing the PBA-6a binder, high binder contents, or medium gradation. The F-values suggest that the air-void content has the strongest influence on β_1 while binder type has the weakest influence.

During the soaking process, aggregate gradation, binder type, and air-void content are all significant in affecting both the normalized initial ingress rate ($-\beta_3$) and the asymptotic amount of ingress moisture (β_1). Specimens containing the AR-4000 binder, medium gradation, or high air-void contents absorb more moisture than specimens containing the PBA-6a binder, coarse gradation, or low air-void contents. Based on the F-values, air-void content is by far most significant among the three factors in affecting the asymptotic amount of ingress moisture, while the influence of aggregate gradation and binder type is comparable.

During the drying process after soaking, only binder type is significant in affecting the normalized initial evaporation rate ($-\beta_3$), but all three factors are significant in affecting the asymptotic residual moisture (β_1). Specimens containing the AR-4000 binder, medium gradation, or low air-void contents retain more moisture than specimens containing the PBA-6a binder, coarse gradation, or high binder contents. This is consistent with the results from the drying process after vapor conditioning. Among the three factors, air-void content has the strongest influence.

As a summary of the statistical analysis, air-void content has the strongest influence on the amount of moisture entering asphalt mixes, but aggregate gradation and binder type also have significant effects on the moisture ingress and evaporation process under different conditions. In general, mixes containing the AR-4000 binder absorb and retain more moisture in both vapor conditioning and soaking than mixes containing the

PBA-6a binder. The effect of aggregate gradation is more complicated. Mixes with coarse gradation adsorb more moisture during the vapor conditioning but absorb less moisture during the soaking than mixes with medium gradation. The reason for the inconsistency is unclear and needs further investigation.

4.1.3 Summary and Discussion

In this experiment, moisture ingress and retention characteristics and influential factors were studied by the vapor conditioning, soaking, and drying tests. The moisture ingress process in vapor conditioning was characterized by the Mitscherlich model, while the moisture ingress in the soaking process and moisture evaporation was fitted by a two-segment curve. A nonlinear mixed effect model was applied for statistical analysis of the relative influence of binder type, aggregate gradation, and air-void content.

The ingress and evaporation of moisture in the asphalt mixes take time. Although the ingress rate is higher during the first two weeks than later period, the amount of moisture ingress or evaporation during the time after the first two weeks is generally comparable to the amount in the first two weeks. This indicates that a good drainage system that can quickly remove water from the pavement surface and intercept rising moisture vapor or capillary water from underneath can significantly reduce the amount of water entering asphalt pavements, even in a region with heavy rainfall.

The ultimate amount of moisture in specimens, estimated from the curve fitting, is found to be generally positively correlated with air-void content during vapor conditioning or soaking and insensitive to the air-void content during drying. Saturation, however, is insensitive to air-void contents for specimens with 7 percent or higher air-void contents in all conditioning processes. During vapor conditioning, around 30 to 40 percent saturation can be reached by specimens with 7 to 13 percent air-void content, while specimens with 4 percent air-void content can reach a higher saturation level, around 80 percent. During the soaking conditioning, around 50 to 80 percent saturation can be reached by specimens with 7 to 13 percent air-void content, while specimens with 4 percent air-void content can reach a higher level around 80 to 90 percent. In the drying process after vapor conditioning or soaking, the asymptotic residual saturation is around 30 percent for specimens with 4 percent air-void content, but less than 15 percent for specimens with higher air-void contents. The above observations indicate that it is reasonable to specify a same saturation range (e.g., 50 to 80 percent) in a moisture sensitivity test for specimens with different air-void contents (greater than 5 percent). For specimens with air-void contents less than 5 percent, it may be more appropriate to directly specify the moisture content.

Statistical analysis reveals that air-void content has the strongest influence on the amount of moisture entering asphalt mixes, but aggregate gradation and binder type also have significant effects. Under the same conditions, mixes containing the AR-4000 binder absorb more moisture than mixes containing the PBA-6a binder. The effect of aggregate gradation differs with different conditions. To reduce the potential for moisture ingress as well as the actual quantity of moisture entering the asphalt concrete, air-void content should be strictly controlled to as low a level as practical during construction.

4.2 Effect of Construction-Induced Variation

Many potential factors during construction will affect the uniformity of the placed asphalt concrete, such as large variation in the aggregate particle size, segregation of loose material during transportation, and temperature differentiation of mixes during placement and compaction. The direct result can be large variation in the air-void content, asphalt content, and aggregate gradation in one so-called “uniform” pavement section. For example, the field investigation in Section 3.1 revealed that most pavement sections have a standard deviation of air-void contents ranging between 1 percent and 3.5 percent, as shown in Table 4.6 and Figure 4-8. During the field condition survey, it was also observed that in many cases moisture damage symptoms (e.g., potholes, pumping) typically occurred randomly at isolated spots, suggesting that variation in construction quality might be one of reasons leading to the occurrence of moisture damage. This experiment

was designed to verify this point. Specifically, the effects of variation in two variables, binder content and air-void content, are studied. These two variables are important for pavement performance and are easily affected by construction quality.

4.2.1 Experimental Design

Since the purpose of this study is to evaluate the effect of air-void content and binder content on the moisture sensitivity of asphalt concrete mixes, it is preferable to use a mix that would have good moisture resistance under laboratory testing at its optimum binder content and design air-void content. Based on the field performance data provided by Shatnawi (1995), it was recognized that a mix consisting of Aggregate B and AR-4000 binder without any antistripping additive, coded as BAN, had relatively good moisture resistance and was therefore used as the control mix in the experiment. A 19-mm nominal maximum medium dense gradation was used for all specimens. The air-void content was varied ±3 percent from the design level (7 to 8 percent) and the binder content was varied up to 1 percent less than the optimum binder content.

A fatigue-based test procedure, which was developed in this research and detailed in Chapter 5, was followed to evaluate the moisture effect on mix performance. This procedure uses beam specimens and provides response variables that are directly related to pavement performance life and are used in many mechanistic-empirical pavement design methods.

Two experiments were performed during this study, with the main difference being in the moisture conditioning procedure. The first experiment is appropriate to simulate the field condition where a large amount of moisture exists in the pavement for a short period at a mild temperature, while the second experiment is appropriate to simulate the field condition where pavements contain abundant moisture for a long period or at a high temperature, with the assumption that higher temperatures accelerated damage in the same manner as extended exposure periods. Both experiments are described below.

First Experiment

The factors included in the first experiment are as follows:

Three levels of air-void content: 4 percent, 7 percent, and 10 percent.

Two levels of binder content: optimum binder content (6 percent) and low binder content (5.5 percent).

Two preconditioning procedures for specimens: dry and wet. In the dry preconditioning, beam specimens were not conditioned with water and were stored in a 20°C room before testing. In the wet preconditioning, each beam specimen was first partially saturated under a vacuum of 16 kPa absolute pressure (635 mm-Hg vacuum) for 30 minutes, and then submerged in a 25°C water bath for 24 hours.

A full factorial design for all three factors was used and two replicates were tested at each combination of factor levels, which required a total of 24 specimens.

Second Experiment

In the second experiment, the water bath temperature in the wet preconditioning procedure was changed from 25°C to 60°C, while the other preconditioning steps remained the same as in the first experiment. Because mix materials (aggregate and binder) were depleted after the first experiment and were re-obtained from the suppliers a few months later, specimens tested in dry were refabricated and tested to eliminate the possible effect due to material variations. Compared with the first experiment, two changes were made to the second experiment, including:

The three air-void content levels were changed to 5 percent, 8 percent, and 11 percent respectively. This change was not planned in the experiment design, but was due to a frequent deviation of the air-void contents from the target values in the compaction. Because the amount of source material was limited, it was decided to use the specimens with the deviated air-void contents. This change would not affect the objectives of this study since the new air-void content levels still span the common range of field air-void contents.

Another low binder content level was added that was 1 percent lower than the optimum binder content (OBC). Deviance by 1 percent from the OBC is the approximate upper bound that the variation in the binder content may reach during construction. Addition of this factor level could provide a better picture of the effect of binder-content variation.

A full-factorial design for all three factors was used and two replicates were tested at each combination of factor levels, which required a total of 36 specimens.

For clarification, the wet preconditioning procedures in the two experiments were designated as "Wet1" and "Wet2" respectively in the later data analysis.

In both experiments, after preconditioning the specimens were tested in the four-point bending beam fatigue test under the same test conditions: 20°C test temperature, strain level controlled at 200με, and 10 Hz loading frequency.

4.2.2 Results and Analysis

The test results from both experiments are summarized in Table 4.7 and Table 4.8 respectively. The stiffness deterioration curves of all beams are plotted in Figure C-1 through Figure C-15 in Appendix C on both natural and logarithmic time scales.

4.2.2.1 General Observations

Moisture Content

The same vacuum intensity and duration, instead of the same saturation range, were specified for all the wet specimens during the presaturation procedure. The actual saturation levels of the beams, however, were approximately in the same range, generally between 60 and 85 percent, except for a few beams with small air-void contents (Figure 4-9). On the other hand, there was a good correlation between the amount of moisture absorbed and the air-void content (Figure 4-10). These observations are consistent with the findings in the previous soaking test and findings from field cores.

Initial Stiffness

The average initial stiffness at each combination of factor levels is shown in Figure 4-11 and Figure 4-12, and the ratio of initial stiffness of wet and dry specimens is shown in Figure 4-13. It can be seen that, in general, moisture reduced the initial stiffness of beams. In the first experiment, there was no clear pattern between the percentage of reduction and the air-void content or the binder content, while in the second experiment lower binder content or higher air-void content tended to increase slightly the relative reduction of initial stiffness. Compared to the specimens with 7 percent air-void content and the optimum binder content, an increase in air-void content by 3 percent or decrease in the binder content by 0.5 percent to 1 percent did not significantly reduce the initial stiffness ratio when the specimens were preconditioned by the Wet1 procedure, but reduced the ratio by about 25 percent when the specimens were preconditioned by the Wet2 procedure. All

specimens showed an initial stiffness ratio greater than 80 percent and 70 percent in the first and second experiments respectively.

Fatigue Life

The average fatigue life at each combination of factor levels is shown in Figure 4-14 and Figure 4-15, and the ratio of fatigue life of wet and dry specimens is shown in Figure 4-16. The following observations were obtained from these figures:

1. In general, fatigue life decreased with the increase of air-void content. The significance of binder changed with the air-void content, which was more significant at eight or less percent air-void content, and much less significant at 10 or more percent air-void content. For the dry specimens, there was no clear relationship pattern between fatigue life and binder content, possibly due to the small range of variation in the binder content used in the experiment.
2. The existence of moisture extended the fatigue lives of specimens tested in the first experiment. The main reason for this is possibly that the moisture effect that occurred in the first experiment was mainly the softening of the binder but not stripping. The increased specimen flexibility due to binder softening, as reflected by the lower initial stiffness, led to a lower stress level in the controlled-strain test. A general trend was that lower air-void contents led to a longer extension of fatigue life by moisture. Variation in the binder content did not have a clear impact on the fatigue life extension. In the second experiment in which wet specimens were preconditioned at 60°C, the fatigue life was almost unchanged for the specimens with optimum binder content and air-void content less than or equal to 8 percent. When the air void was increased to 11 percent or the binder content was decreased by 0.5 percent, fatigue life was reduced significantly by the moisture. In both experiments, low binder content and high air-void content was the worst combination in terms of moisture resistance.

Visual Inspection of Split Faces

When the fatigue test was finished, the condition of the broken faces of each wet specimen was inspected for the number of broken aggregates and the percentage of stripping. No clear correlation was found between the number of broken aggregates and the air-void content or the binder content. The beams preconditioned at 25°C for one day showed little stripping after the fatigue test, while the beams preconditioned at 60°C for one day showed 5 to 20 percent bare aggregates on the broken faces. No clear relationship was found between the percentage of stripping and the air-void content or the binder content.

4.2.2.2 Statistical Analysis

In this section, statistical analysis is performed to further examine the previous general observations. Specifically, the following observations are checked:

In the first experiment, the variation in air-void content and binder content did not significantly change the effect of moisture on mix performance.

In the second experiment, higher air-void contents and lower binder content significantly increased the adverse effect of moisture on the fatigue response of the mixes.

Both analysis of variance (ANOVA) and linear regression analysis are performed in each step. The ANOVA is used to identify significant factors affecting the response variable, and linear regression analysis is used to estimate the effects of different factor levels. The following linear model is used in the analysis:

$$y = \mu + \sum_{i=1}^{2} \alpha_i X_i + \sum_{j=1}^{2} \beta_j Y_j + \gamma Z + \sum_{i,j=1}^{2} (\alpha\beta)_{ij} X_i Y_j + \sum_{i=1}^{2} (\alpha\gamma)_i X_i Z + \sum_{j=1}^{2} (\beta\gamma)_j Y_j Z + \sum_{i,j=1}^{2} (\alpha\beta\gamma)_{ij} X_i Y_j Z + \varepsilon \quad \textbf{(4-16)}$$

where y is the response variable; μ is the grand mean; α_i, β_j, γ, $(\alpha\beta)_{ij}$, $(\alpha\gamma)_i$, $(\beta\gamma)_j$, and $(\alpha\beta\gamma)_{ij}$, $i, j = 1,2$, are coefficients to be estimated; X_i, Y_j, and Z are the difference of two indicator functions.

Specifically,

$X_1 = ind(5\%\text{ binder content}) - ind(6\%\text{ binder content})$

$X_2 = ind(5.5\%\text{ binder content}) - ind(6\%\text{ binder content})$

$Y_1 = ind(4\%\text{ or }5\%\text{ air voids}) - ind(7\%\text{ or }8\%\text{ air voids})$

$Y_2 = ind(10\text{ or }11\%\text{ air voids}) - ind(7\%\text{ or }8\%\text{ air voids})$

$Z = ind(\text{wet condition}) - ind(\text{dry condition})$

where $ind(\cdot)$ is an indicator function, 1 if the level of a factor is equal to the value in the parentheses, 0 otherwise. ε is a random error term, assumed to have independent normal distribution, $\varepsilon \sim N(0, \sigma^2)$. For the analysis of results from the first experiment, X_1 is removed from the model since 5 percent air-void content is not included in the experiment.

4.2.2.2.1 First Experiment

Initial Stiffness

The ANOVA table and the estimated parameters are shown in Table 4.9 and Table 4.10 respectively. The QQ-normal plot of the residuals from the model (Figure 4-17a) shows that the normal distribution assumption of the error term is not severely violated. The ANOVA shows that air-void content, binder content, and moisture all have significant effects on the initial stiffness of the beam specimens.

The estimated parameters in Table 4.10 show that fewer air voids, lower binder content, or dry condition all lead to higher initial stiffness. The effect of increasing air-void content by 3 percent is over twice the effect of moisture conditioning at 25°C for one day. For the purpose of the study, the effects of the interactions between moisture conditioning and air-void content or binder content are of interest. As can be seen, the ANOVA table shows that both interaction terms are insignificant at the 95 percent confidence level.

The moisture sensitivity of asphalt mixes is often characterized by the relative performance of a wet mix to a dry mix. To this end, the initial stiffness of the moisture-conditioned specimens is divided by the average initial stiffness of the two corresponding dry specimens, and used as the response variable. The ANOVA table based on the initial stiffness ratio (Table 4.11) shows that neither air-void content nor binder content affected significantly the initial stiffness ratio.

This analysis further verifies that when the BAN mix is conditioned for a short period in moisture at a mild temperature (25°C), the variation in the air-void content and the binder content does not significantly change the effect of moisture on the initial stiffness of the beam specimens.

Fatigue Life

The natural logarithm of the fatigue life was used as the response variable in the analysis. The ANOVA table and the estimated parameters are shown in Table 4.12 and Table 4.13 respectively. The QQ-normal plot of the residuals from the model (Figure 4-17b) shows that the normal distribution assumption of the error term is acceptable. The ANOVA shows that air-void content and moisture have significant effects on the fatigue life of the beam specimens, while the binder content is insignificant. The estimated parameters in Table 4.13 show that lower air-void content or wet condition leads to longer fatigue lives. The ANOVA table also shows that the interactions between moisture conditioning and air-void content/binder content are insignificant, indicating that when the BAN mix is conditioned for a short time in moisture at a mild temperature, the variation in air-void content and binder content does not significantly change the effect of moisture on the fatigue performance of the beam specimens. The ANOVA table based on the fatigue life ratio (FLR) is shown in Table 4.14. As can be seen, neither air-void content nor binder content significantly affects the fatigue life ratio.

This analysis shows that when the BAN mix is conditioned for a short period in moisture at a mild temperature, the variation in the air-void content and the binder content does not significantly change the effect of moisture on the fatigue life of the beam specimens.

4.2.2.2.2 Second Experiment

Initial Stiffness

The ANOVA table and the estimated parameters are shown in Table 4.15 and Table 4.16 respectively. The QQ-normal plot of the residuals from the model (Figure 4-17c) shows that the normal distribution assumption of the error term is not severely violated. The ANOVA shows that both the air-void content and moisture have significant effects on the initial stiffness of the beam specimens, while the effect of the binder content is marginally significant. The estimated parameters in Table 4.16 show that less air-void content, less binder content, or dry condition all lead to higher initial stiffness. The effect of increasing air-void content by 3 percent is over three times the effect of moisture conditioning at 60°C for one day. The ANOVA table shows that the interactions between moisture conditioning and air-void content and binder content are insignificant at the 95 percent confidence level, indicating that the moisture effect on the initial stiffness is insensitive to the variation in the air-void content or the binder content. The ANOVA table based on the initial stiffness ratio (ISR) (Table 4.17) between wet and dry specimens also shows that neither air-void content nor binder content significantly affects the initial stiffness ratio.

This analysis reaches the same conclusions as in the first experiment that the variation in the air-void content or the binder content does not significantly change the effect of moisture on the initial stiffness of the beam specimens.

Fatigue Life

The natural logarithm of the fatigue life was used as the response variable in the analysis. The ANOVA table and the estimated parameters are shown in Table 4.18 and Table 4.19 respectively. The QQ-normal plot of the residuals from the model (Figure 4-17d) shows that the normal distribution assumption of the error term is not severely violated. The ANOVA in Table 4.18 shows that air-void content, binder content, and moisture conditioning all have significant effects on the fatigue life of the beam specimens. The estimated parameters in Table 4.19 show that lower air-void content leads to longer fatigue lives and wet conditioning generally reduces the fatigue life, while the binder content effect varies with the air-void content. The ANOVA table also shows that the interaction between binder content and moisture conditioning is

significant. In the dry condition, highest fatigue lives occur at the 5.5 percent binder content, but in the wet condition, 6 percent binder content results in longer fatigue lives.

The ANOVA table based on the fatigue life ratio (Table 4.20) shows that at the 90 percent confidence level, air-void content, binder content, and their interaction all significantly affect the fatigue life ratio. The estimated parameters of the corresponding linear model (Table 4.21) show that fatigue life is greatly reduced due to the reduction of binder content by 0.5 percent or more when the air-void content of the specimens is equal to or less than 8 percent. However, when the air-void content is large (11 percent), the fatigue response of the mix with the optimum binder content tends to be similar to that of the mix with lower binder content.

This analysis shows that when the BAN mix is conditioned for a short period in moisture at a high temperature, the variation in the air-void content and the binder content significantly changes the moisture effect on the fatigue life of the beam specimens. Large air-void content or less than optimum binder content will significantly reduce the moisture resistance of a mix that has good performance in a design condition.

4.2.3 Summary and Discussion

Two major findings from the two experiments are:

1. In both moisture conditioning procedures, moisture reduces the stiffness of the hot-mix asphalt (HMA). The reduction is not significantly affected by the variation in the air-void contents or the binder content.
2. In the controlled-strain flexural beam fatigue test, when moisture resides in a mix with relatively good moisture resistance for a short period at a mild temperature, the fatigue performance of the mix at a given strain is improved instead of compromised, primarily because reduced stiffness results in a lower stress level in the controlled-strain test. The variation in the air-void content or in the binder content does not significantly change the adverse effect of moisture. However, this does not mean that fatigue life would necessarily be increased in the field because stiffness is reduced by moisture, which results in greater strains and therefore reduces fatigue life.
3. When the conditioning temperature is high, however, the fatigue performance of the mix is generally compromised by moisture, especially at a binder content 0.5 percent or more lower than the optimum binder content, an air-void content equal to or higher than 11 percent, or a combination of both conditions.

Both experiments have proved that the control mix BAN has good resistance to moisture damage at its optimum binder content and design air-void content (7 to 8 percent). Increased air-void content reduces stiffness and fatigue life. In addition, a reduction in the binder content or an increase in the air-void content can significantly further reduce the moisture resistance of the mix under repeated loading at a fixed strain. This is shown by the high temperature conditioning. This emphasizes the importance of quality control during construction.

The response variable without repeated loading (i.e., initial stiffness) does not detect the adverse effects of variation in the binder content and the air-void content on moisture resistance of the mix. This suggests that caution should be taken to use test procedures that do not include a repeated loading in the conditioning procedure for evaluating or predicting moisture damage in asphalt mixes because the test results may be inappropriate or irrelevant.

4.3 Summary

The laboratory experiment for moisture ingress and retention revealed that air-void content is by far the most important factor influencing the amount of moisture entering asphalt mixes. Binder type and

aggregate gradation also affect moisture ingress and retention, but to a much lesser extent. Another laboratory experiment, aimed at the effects of construction-induced variation, showed that a reduction in binder content or an increase in the air-void content will significantly reduce the moisture resistance of a good performance mix under repeated loading in an unfavorable environment (i.e., high temperatures).

Combining the findings from both the field and laboratory investigations, it can be seen that air-void content is a very important factor affecting moisture damage in asphalt pavements. Higher air-void contents not only allow more moisture to enter pavements, especially in areas with heavy rainfall, but also significantly reduce the fatigue resistance of mixes in wet conditions. It is necessary to strictly control air-void content during construction, preferably to a level lower than 7 percent. A good pavement drainage system is also necessary to mitigate moisture damage, even for mixes with low air-void contents.

Table 4.1. Mass of Moisture in Specimens during Vapor Conditioning (g)

Specimen ID	Binder	Gradation	Air Voids (%)	10 days	20 days	30 days	40 days	50 days	60 days	80 days	100 days	120 days	140 days	160 days
AAN-4-2	AR-4000	Medium	3.9	7.9	10.9	12.3	14.5	16.5	18.5	20.9	23.8	25.6	28.4	29.3
AAN-4-1	AR-4000	Medium	3.8	9.5	12.3	13.8	16.0	18.0	19.9	23.3	26.0	27.9	30.2	31.8
AAN-7-1	AR-4000	Medium	7.5	7.5	9.9	11.7	13.4	14.0	15.6	18.6	20.9	23.5	27.2	27.5
AAN-7-2	AR-4000	Medium	7.4	9.3	11.7	14.6	16.3	17.6	20.1	23.1	26.1	28.4	31.6	33.1
AAN-10-2	AR-4000	Medium	10.9	10.6	13.6	15.0	16.3	17.8	20.2	23.8	28.0	29.5	34.7	35.6
AAN-10-1	AR-4000	Medium	9.7	10.8	14.2	16.4	17.8	20.2	21.6	23.9	27.7	30.2	34.0	35.1
AAN-13-2	AR-4000	Medium	13.4	15.8	20.8	24.7	26.8	29.3	31.1	36.3	40.5	44.1	47.1	48.9
AAN-13-1	AR-4000	Medium	12.3	12.2	16.5	18.6	21.4	23.5	26.3	31.3	34.2	37.3	41.1	41.7
AANC-4-1	AR-4000	Coarse	4.3	8.3	11.3	12.3	14.2	15.4	17.6	19.7	22.5	24.5	26.4	27.6
AANC-4-2	AR-4000	Coarse	3.8	9.5	11.8	14.4	16.5	18.2	20.0	22.3	25.0	27.0	29.3	31.0
AANC-7-2	AR-4000	Coarse	7.5	7.9	10.8	12.5	14.0	16.2	16.5	19.5	23.5	25.1	28.1	33.6
AANC-7-1	AR-4000	Coarse	7.6	9.8	12.5	14.3	15.9	17.3	19.1	23.2	28.9	30.7	36.1	38.2
AANC-10-1	AR-4000	Coarse	9.6	10.4	13.7	16.4	18.4	20.2	23.1	27.1	32.5	36.8	40.4	41.1
AANC-10-2	AR-4000	Coarse	9.3	11.5	14.2	17.3	20.6	23.6	26.7	33.2	38.8	42.4	45.1	48.7
AANC-13-2	AR-4000	Coarse	13.5	11.2	15.0	17.7	20.3	23.3	27.0	34.7	39.3	41.5	44.6	47.2
AANC-13-1	AR-4000	Coarse	13.9	13.9	20.4	23.0	26.0	29.5	31.4	36.9	38.9	44.5	48.0	50.9
APN-4-1	PBA-6a	Medium	4.5	7.5	9.4	11.3	13.1	15.3	17.1	20.4	23.5	26.7	29.5	30.8
APN-4-2	PBA-6a	Medium	3.8	7.9	10.9	13.1	16.1	17.9	20.9	23.0	25.8	27.5	28.7	30.5
APN-7-1	PBA-6a	Medium	7.4	6.6	8.2	9.4	10.3	11.7	12.1	14.1	16.1	17.4	19.5	20.2
APN-7-2	PBA-6a	Medium	7.7	4.0	6.0	6.4	7.6	8.5	9.6	11.5	13.2	15.0	16.6	18.1
APN-10-1	PBA-6a	Medium	9.5	5.8	7.9	8.7	9.7	10.5	12.4	13.8	15.8	17.3	19.6	20.0
APN-10-2	PBA-6a	Medium	9.8	5.6	7.3	8.4	9.6	10.7	11.7	13.6	15.9	17.3	19.1	20.6
APN-13-1	PBA-6a	Medium	12.9	8.3	10.8	12.2	13.1	14.9	15.3	18.0	20.1	21.4	23.5	24.9
APN-13-2	PBA-6a	Medium	12.5	7.3	9.6	12.2	13.2	15.3	18.4	21.6	25.3	27.4	32.2	34.6
APNC-4-1	PBA-6a	Coarse	3.4	7.3	10.0	12.0	14.0	15.8	17.3	19.8	21.3	24.5	25.2	25.6
APNC-4-2	PBA-6a	Coarse	3.7	9.6	12.1	14.3	16.4	17.9	20.2	22.6	24.5	26.0	27.4	28.2
APNC-7-1	PBA-6a	Coarse	6.7	8.4	10.7	13.0	13.4	14.2	16.1	18.3	22.4	25.2	26.8	36.3
APNC-7-2	PBA-6a	Coarse	7.8	8.8	11.3	12.6	14.3	15.3	17.3	19.9	22.5	25.3	28.4	29.6
APNC-10-1	PBA-6a	Coarse	9.3	10.5	13.5	15.2	16.3	17.0	18.7	21.6	24.0	25.8	28.3	31.2
APNC-10-2	PBA-6a	Coarse	9.4	9.1	11.4	13.5	15.3	16.5	18.8	22.3	27.4	30.9	34.2	36.6
APNC-13-2	PBA-6a	Coarse	13.3	7.6	10.4	12.1	13.7	16.4	18.9	21.8	25.0	28.5	30.5	35.7
APNC-13-1	PBA-6a	Coarse	13.1	6.8	11.7	12.2	13.7	15.8	18.0	21.5	26.2	31.7	34.1	36.3

Table 4.2. Mass of Moisture in Specimens during Drying after Vapor Conditioning (g)

Specimen ID	Binder	Gradation	Air Voids (%)	0 days	1 days	2 days	3 days	5 days	7 days	9 days	13 days	17 days	30 days	44 days	58 days	86 days
AAN-4-2	AR-4000	Medium	3.9	29.3	21.3	19.3	17.8	16.2	14.8	14.3	13.1	12.2	10.4	9.0	8.7	7.7
AAN-4-1	AR-4000	Medium	3.8	31.8	23.8	21.5	20.0	18.3	17.1	16.4	15.2	14.2	12.5	11.0	10.8	9.2
AAN-7-1	AR-4000	Medium	7.5	27.5	15.8	12.6	10.5	8.2	6.5	5.9	4.6	4.0	2.5	1.9	1.6	0.8
AAN-7-2	AR-4000	Medium	7.4	33.1	21.5	18.3	15.9	12.9	11.2	10.3	8.6	7.4	5.5	4.5	3.9	3.0
AAN-10-2	AR-4000	Medium	10.9	35.6	22.0	17.5	14.9	11.6	9.5	8.5	6.8	5.7	4.5	3.8	3.6	2.8
AAN-10-1	AR-4000	Medium	9.7	35.1	23.7	19.5	16.8	13.4	11.6	10.4	8.6	7.5	6.0	5.2	4.8	4.0
AAN-13-2	AR-4000	Medium	13.4	48.9	30.3	24.6	20.3	15.5	12.6	11.2	9.1	8.1	7.0	6.6	6.4	5.6
AAN-13-1	AR-4000	Medium	12.3	41.7	27.8	22.0	18.4	13.6	11.0	9.8	7.6	6.7	5.3	4.8	4.4	3.7
AANC-4-1	AR-4000	Coarse	4.3	27.6	19.5	18.4	17.2	15.7	14.8	14.3	13.3	12.5	11.1	10.1	9.8	8.2
AANC-4-2	AR-4000	Coarse	3.8	31.0	22.5	20.7	19.3	17.7	16.6	16.2	14.9	14.2	12.6	11.6	10.8	9.6
AANC-7-2	AR-4000	Coarse	7.5	33.6	21.9	18.9	17.3	15.2	13.9	13.0	11.5	10.6	8.6	7.3	6.3	4.9
AANC-7-1	AR-4000	Coarse	7.6	38.2	26.0	22.1	20.0	17.5	15.7	14.9	13.4	12.1	9.9	8.4	7.5	5.7
AANC-10-1	AR-4000	Coarse	9.6	41.1	26.0	22.4	19.8	17.1	15.3	14.1	12.0	10.7	8.0	6.6	5.9	4.7
AANC-10-2	AR-4000	Coarse	9.3	48.7	31.6	27.4	24.8	21.7	19.6	18.2	15.8	14.0	10.5	8.1	7.0	4.6
AANC-13-2	AR-4000	Coarse	13.5	47.2	29.8	24.8	22.1	18.6	16.1	14.8	12.3	10.5	7.1	5.4	4.8	3.3
AANC-13-1	AR-4000	Coarse	13.9	50.9	32.4	27.2	23.6	19.6	16.6	15.1	11.8	9.8	6.1	5.0	4.7	3.5
APN-4-1	PBA-6a	Medium	4.5	30.8	24.9	23.5	22.3	20.8	19.7	19.2	17.9	16.9	14.9	13.4	12.4	10.8
APN-4-2	PBA-6a	Medium	3.8	30.5	24.2	22.9	21.8	20.5	19.4	18.7	17.6	16.6	14.5	13.2	12.1	10.6
APN-7-1	PBA-6a	Medium	7.4	20.2	14.4	12.5	11.2	9.4	8.2	7.8	6.7	6.1	4.8	4.1	3.5	2.8
APN-7-2	PBA-6a	Medium	7.7	18.1	11.0	9.1	7.7	5.9	4.6	4.1	2.9	2.1	0.7	0.0	0.0	0.0
APN-10-1	PBA-6a	Medium	9.5	20.0	12.7	10.5	8.8	6.7	5.4	4.7	3.4	2.6	1.4	0.9	0.7	0.1
APN-10-2	PBA-6a	Medium	9.8	20.6	12.9	10.6	8.8	6.9	5.3	4.7	3.3	2.6	1.2	0.6	0.3	0.0
APN-13-1	PBA-6a	Medium	12.9	24.9	15.2	13.3	11.4	8.5	6.7	5.9	4.3	3.6	2.8	2.2	2.0	1.4
APN-13-2	PBA-6a	Medium	12.5	34.6	22.9	19.4	16.7	13.4	11.0	9.7	7.7	6.3	3.0	1.5	0.8	0.0
APNC-4-1	PBA-6a	Coarse	3.4	25.6	19.1	18.3	17.4	16.3	15.1	14.8	13.8	13.3	11.6	10.7	10.5	9.2
APNC-4-2	PBA-6a	Coarse	3.7	28.2	21.7	20.0	19.6	17.8	16.9	16.4	15.2	14.5	13.3	12.2	11.5	10.5
APNC-7-1	PBA-6a	Coarse	6.7	36.3	26.4	24.0	22.4	20.2	18.7	17.9	16.3	14.9	12.5	10.8	9.6	7.7
APNC-7-2	PBA-6a	Coarse	7.8	29.6	20.5	18.1	16.3	14.0	12.5	11.7	10.0	8.9	6.9	5.7	5.3	3.8
APNC-10-1	PBA-6a	Coarse	9.3	31.2	21.9	19.6	17.9	16.0	14.6	13.9	12.1	11.1	9.0	7.8	7.0	5.7
APNC-10-2	PBA-6a	Coarse	9.4	36.6	25.4	23.0	21.2	18.9	17.4	16.6	14.8	13.5	11.3	9.8	9.3	7.1
APNC-13-2	PBA-6a	Coarse	13.3	35.7	24.5	20.8	18.1	14.7	12.0	10.7	8.0	5.9	3.0	2.0	1.6	1.1
APNC-13-1	PBA-6a	Coarse	13.1	36.3	24.1	19.9	17.2	13.3	10.8	9.2	6.3	4.5	1.5	0.7	0.6	0.0

Table 4.3 Mass of Moisture in Specimens during Soaking (g)

Specimen ID	Binder	Gradation	Air Voids (%)	0 days	1 days	3 days	5 days	10 days	15 days	35 days	75 days	110 days
AAN-4-2	AR-4000	Medium	3.9	9.5	14.3	17.2	19.1	21.1	22.9	26.2	29.4	32.7
AAN-4-1	AR-4000	Medium	3.8	13.0	17.8	20.6	22.3	24.3	26.7	29.8	32.1	35.6
AAN-7-1	AR-4000	Medium	7.5	14.5	24.1	28.4	31.9	36.0	40.2	48.5	54.9	61.5
AAN-7-2	AR-4000	Medium	7.4	21.5	27.6	33.1	38.4	42.6	45.4	52.2	57.0	61.8
AAN-10-2	AR-4000	Medium	10.9	36.1	41.0	47.5	51.1	55.1	59.2	65.9	71.4	79.7
AAN-10-1	AR-4000	Medium	9.7	34.7	35.5	40.3	44.4	49.2	51.9	58.4	64.4	69.4
AAN-13-2	AR-4000	Medium	13.4	52.4	55.0	62.6	68.9	73.7	78.1	87.1	95.7	104.7
AAN-13-1	AR-4000	Medium	12.3	44.2	45.2	54.3	58.0	64.3	67.8	77.5	85.5	89.6
AANC-4-1	AR-4000	Coarse	4.3	9.9	14.9	17.2	18.7	19.9	21.4	25.3	28.7	31.4
AANC-4-2	AR-4000	Coarse	3.8	11.6	16.1	18.2	19.9	20.2	22.1	24.8	27.2	30.1
AANC-7-2	AR-4000	Coarse	7.5	7.0	12.8	16.4	18.9	22.3	26.4	31.8	35.3	42.2
AANC-7-1	AR-4000	Coarse	7.6	22.5	25.0	28.2	31.7	35.3	39.1	44.7	49.5	54.8
AANC-10-1	AR-4000	Coarse	9.6	29.9	30.9	36.3	39.8	45.0	48.3	55.4	61.1	66.9
AANC-10-2	AR-4000	Coarse	9.3	28.7	30.8	35.3	38.7	43.2	46.4	52.6	58.3	63.1
AANC-13-2	AR-4000	Coarse	13.5	47.1	47.3	54.7	58.4	63.4	66.5	74.2	81.5	81.6
AANC-13-1	AR-4000	Coarse	13.9	47.2	40.0	44.5	49.6	55.4	58.7	62.2	70.2	73.6
APN-4-1	PBA-6a	Medium	4.5	11.8	15.8	16.8	18.5	19.5	20.9	24.6	27.6	31.2
APN-4-2	PBA-6a	Medium	3.8	12.1	14.4	16.4	17.6	18.9	20.8	24.8	27.5	31.2
APN-7-1	PBA-6a	Medium	7.4	14.6	18.6	21.4	24.2	27.1	31.5	37.8	42.6	48.4
APN-7-2	PBA-6a	Medium	7.7	5.3	14.3	18.8	21.9	25.6	28.5	38.2	43.0	46.0
APN-10-1	PBA-6a	Medium	9.5	22.8	25.2	29.9	33.3	37.9	41.6	50.9	59.6	68.0
APN-10-2	PBA-6a	Medium	9.8	17.3	21.3	25.2	28.5	32.5	36.6	46.4	53.7	60.6
APN-13-1	PBA-6a	Medium	12.9	29.3	50.7	57.3	62.1	66.6	71.3	80.4	91.0	93.7
APN-13-2	PBA-6a	Medium	12.5	36.0	32.8	39.8	44.5	49.7	52.2	60.3	68.2	80.2
APNC-4-1	PBA-6a	Coarse	3.4	11.4	15.2	17.2	17.5	17.8	17.9	20.5	23.3	25.4
APNC-4-2	PBA-6a	Coarse	3.7	13.0	17.2	19.4	20.0	20.1	20.3	23.8	26.1	28.5
APNC-7-1	PBA-6a	Coarse	6.7	11.2	18.7	21.3	23.9	27.1	29.5	35.1	39.2	43.9
APNC-7-2	PBA-6a	Coarse	7.8	18.7	22.1	26.1	29.4	33.1	35.3	41.7	46.4	50.3
APNC-10-1	PBA-6a	Coarse	9.3	19.8	22.4	25.8	28.6	31.5	34.4	41.2	47.5	51.8
APNC-10-2	PBA-6a	Coarse	9.4	14.4	17.8	21.1	23.2	25.8	29.8	35.4	41.2	45.5
APNC-13-2	PBA-6a	Coarse	13.3	43.7	30.2	36.3	41.2	48.3	50.6	57.2	66.7	74.4
APNC-13-1	PBA-6a	Coarse	13.1	38.8	38.8	45.2	49.0	53.8	56.4	63.9	71.9	78.8

Table 4.4. Mass of Moisture in Specimens during Drying after Soaking (g)

Specimen ID	Binder	Gradation	Air Voids (%)	0 days	1 days	2 days	3 days	5 days	7 days	9 days	13 days	17 days	30 days	44 days	61 days	80 days
AAN-4-2	AR-4000	Medium	3.9	32.7	27.8	25.1	23.3	21.8	20.6	19.6	18.6	16.8	14.7	13.2	11.9	11.3
AAN-4-1	AR-4000	Medium	3.8	35.6	28.5	26.0	24.1	22.7	21.5	20.6	19.6	18.0	15.8	14.4	13.0	12.3
AAN-7-1	AR-4000	Medium	7.5	61.5	45.6	40.9	37.3	34.3	31.7	29.5	27.0	23.7	17.7	13.9	10.3	7.5
AAN-7-2	AR-4000	Medium	7.4	61.8	46.9	39.5	36.4	33.4	31.1	28.9	26.3	23.0	17.5	13.9	10.5	8.4
AAN-10-2	AR-4000	Medium	10.9	79.7	67.6	54.0	49.2	45.0	41.3	38.2	34.5	29.7	21.5	16.5	11.9	8.4
AAN-10-1	AR-4000	Medium	9.7	69.4	56.3	46.1	42.6	38.8	35.7	33.3	30.0	26.0	19.5	15.4	12.0	9.3
AAN-13-2	AR-4000	Medium	13.4	104.7	80.3	62.4	55.4	49.0	43.6	38.9	33.5	26.9	16.2	10.5	7.6	5.2
AAN-13-1	AR-4000	Medium	12.3	89.6	63.0	53.0	48.0	43.1	38.8	35.1	30.5	25.4	16.7	11.3	6.7	4.0
AANC-4-1	AR-4000	Coarse	4.3	31.4	25.9	23.9	22.5	21.1	20.0	19.2	18.5	17.0	15.0	13.7	12.4	11.6
AANC-4-2	AR-4000	Coarse	3.8	30.1	25.1	23.4	21.6	20.4	19.5	18.5	17.9	16.5	14.7	13.3	12.2	11.8
AANC-7-2	AR-4000	Coarse	7.5	42.2	39.2	32.1	29.6	27.4	25.3	23.7	22.0	19.8	16.4	14.1	12.1	10.7
AANC-7-1	AR-4000	Coarse	7.6	54.8	41.0	33.4	30.5	28.1	25.9	23.9	22.1	19.1	14.8	12.2	10.1	8.4
AANC-10-1	AR-4000	Coarse	9.6	66.9	50.1	40.1	37.1	33.7	30.8	28.5	25.6	22.0	16.1	12.2	8.7	6.9
AANC-10-2	AR-4000	Coarse	9.3	63.1	51.0	39.7	35.0	31.8	29.1	27.0	24.2	20.9	15.4	11.9	8.4	6.7
AANC-13-2	AR-4000	Coarse	13.5	81.6	52.3	41.6	37.8	33.9	30.5	27.5	23.8	19.6	12.3	8.0	5.0	3.7
AANC-13-1	AR-4000	Coarse	13.9	73.6	64.0	40.4	34.2	29.6	25.8	22.3	18.6	13.7	6.4	2.9	1.2	0.8
APN-4-1	PBA-6a	Medium	4.5	31.2	31.4	26.4	25.1	23.7	23.1	22.3	21.4	19.8	17.5	16.1	14.8	14.1
APN-4-2	PBA-6a	Medium	3.8	31.2	31.6	26.6	25.1	24.1	23.2	22.4	21.7	20.0	17.8	16.5	15.0	14.6
APN-7-1	PBA-6a	Medium	7.4	48.4	39.2	34.3	32.0	29.7	27.8	25.8	23.8	20.6	15.8	13.0	10.5	8.7
APN-7-2	PBA-6a	Medium	7.7	46.0	38.2	31.2	28.5	26.1	24.2	22.2	20.3	17.2	12.1	9.0	6.2	4.1
APN-10-1	PBA-6a	Medium	9.5	68.0	56.3	45.3	40.3	36.9	33.7	30.9	27.7	23.4	16.3	11.8	7.8	4.6
APN-10-2	PBA-6a	Medium	9.8	60.6	51.6	40.1	36.9	33.9	31.2	28.8	26.1	22.3	15.9	11.6	7.6	5.0
APN-13-1	PBA-6a	Medium	12.9	93.7	67.3	51.3	47.7	43.5	40.1	36.4	31.8	26.1	15.5	9.3	4.3	1.8
APN-13-2	PBA-6a	Medium	12.5	80.2	72.9	56.0	49.9	45.1	41.5	38.0	33.9	28.5	18.7	12.7	7.2	2.8
APNC-4-1	PBA-6a	Coarse	3.4	25.4	21.1	20.3	19.0	18.0	17.4	16.7	16.2	14.9	13.2	12.4	11.8	11.2
APNC-4-2	PBA-6a	Coarse	3.7	28.5	23.9	22.1	20.7	19.8	19.0	18.2	17.7	16.5	14.9	14.0	13.0	12.6
APNC-7-1	PBA-6a	Coarse	6.7	43.9	36.7	31.2	28.8	26.7	24.9	23.4	21.7	19.3	15.6	13.5	11.7	10.4
APNC-7-2	PBA-6a	Coarse	7.8	50.3	35.3	31.4	28.8	26.3	24.1	21.9	19.6	16.5	11.9	9.2	6.9	5.5
APNC-10-1	PBA-6a	Coarse	9.3	51.8	38.6	34.0	31.6	29.4	27.4	25.4	23.4	20.5	16.1	13.2	10.8	9.0
APNC-10-2	PBA-6a	Coarse	9.4	45.5	34.4	31.0	28.7	26.7	25.1	23.5	21.6	19.5	16.0	13.7	11.7	10.4
APNC-13-2	PBA-6a	Coarse	13.3	74.4	64.0	51.7	48.1	43.7	39.6	35.7	30.9	24.8	13.6	6.7	2.4	1.0
APNC-13-1	PBA-6a	Coarse	13.1	78.8	57.1	50.4	46.7	42.6	38.6	34.8	30.0	24.0	12.5	5.7	0.7	0.0

Table 4.5. Wald F-tests Results from the Nonlinear Mixed Effect Model

Vapor Conditioning

	β_1		β_2	
	F-value	**p-value**	**F-value**	**p-value**
Gradation	197.77	<.0001	13.82	0.0002
Binder	170.74	<.0001	1.63	0.2032
AirVoids	108.56	<.0001	3.07	0.0280
Gradation:Binder	4.50	0.0347	1.88	0.1709
Gradation:AirVoids	56.65	<.0001	3.59	0.0141
Binder:AirVoids	35.27	<.0001	4.82	0.0027

Drying after Vapor Conditioning

	β_1		β_2		β_3	
	F-value	**p-value**	**F-value**	**p-value**	**F-value**	**p-value**
Gradation	24.1150	0.0001	18.4690	<.0001	17.1120	<.0001
Binder	5.4290	0.0310	17.7640	<.0001	19.8860	<.0001
AirVoids	48.4030	<.0001	41.1590	<.0001	33.2610	<.0001
Gradation:Binder	2.4120	0.1369	0.1310	0.7174	19.7960	<.0001
Gradation:AirVoids	9.6230	0.0004	8.8560	<.0001	7.4430	0.0001
Binder:AirVoids	5.3700	0.0075	3.6910	0.0122	0.4510	0.7164

Soaking

	β_1		β_2		β_3	
	F-value	**p-value**	**F-value**	**p-value**	**F-value**	**p-value**
Gradation	20.56	0.0002	10.64	0.00	29.13	<.0001
Binder	25.55	0.0001	64.04	<.0001	39.65	<.0001
AirVoids	155.28	<.0001	150.71	<.0001	7.21	0.0001
Gradation:Binder	2.13	0.1610	8.39	0.0042	6.62	0.0108
Gradation:AirVoids	1.85	0.1724	13.13	<.0001	3.73	0.0122
Binder:AirVoids	2.32	0.1074	23.63	<.0001	1.48	0.2209

Drying after Soaking

	β_1		β_2		β_3	
	F-value	**p-value**	**F-value**	**p-value**	**F-value**	**p-value**
Gradation	7.67	0.0122	37.80	<.0001	0.0130	0.9108
Binder	8.67	0.0083	0.04	0.8393	10.5620	0.0013
AirVoids	51.21	<.0001	229.93	<.0001	0.8930	0.4449
Gradation:Binder	0.96	0.3404	5.74	0.0172	16.3690	0.0001
Gradation:AirVoids	7.27	0.0019	2.90	0.0352	0.8330	0.4764
Binder:AirVoids	3.99	0.0233	8.76	<.0001	1.7340	0.1599

Table 4.6. Mean and Standard Deviation of Air-Void Contents at Each Field Coring Section

Section Code	Mean (%)	Standard Deviation (%)	PPRC Code	Mean (%)	Standard Deviation (%)
10N1	7.68	0.99	8N4	3.70	2.10
10U1	7.83	3.36	8N5	4.11	0.98
10U2	6.71	1.17	Q10	5.86	2.23
10U3	6.03	1.48	Q2	6.70	1.10
1U1	5.23	3.13	Q27	5.85	0.97
1U2	5.09	2.61	Q29	3.26	1.16
1U2_1	8.28	1.11	Q3	5.36	0.92
1U3	12.18	1.54	Q32	22.63	0.97
1U4	5.68	3.48	Q35	11.35	2.15
1U6	9.73	1.48	Q36	4.97	2.05
2D18	7.13	0.84	Q38	4.88	0.78
2D19	11.48	1.01	Q41	4.90	1.51
2D20	11.14	0.72	Q54	6.40	1.83
2D21	9.24	1.05	Q62	5.36	2.96
2D6_3	6.48	3.64	Q70	5.04	0.42
2N2_1	6.58	0.95	Q71	5.71	1.02
2N3	10.53	1.45	Q76	7.44	0.70
2N5	4.34	0.97	Q77	6.66	1.90
4U1	8.78	2.47	Q78	4.94	1.64
5N1	6.60	1.81	Q8	5.54	0.67
5N10	6.56	2.06	Q80	6.34	1.00
6D11	8.31	0.78	Q81	8.40	0.20
6D24	3.51	0.82	Q82	6.25	2.11
6D5	7.38	1.32	Q83	6.06	0.46
6N12/13	10.49	1.31	Q84	5.53	0.78
6N19	8.90	2.93	R11	4.03	0.81
6N20	11.75	2.15	R12	9.53	3.93
7N1	11.31	1.50	R15	6.05	1.66
7N2	9.01	1.04	R7	7.91	0.64
7N3	9.00	2.77	W5	6.31	0.47
7N3_2	5.62	2.56	W7	13.38	2.15
7N4	4.08	1.13			

Table 4.7. Summary of Results from BAN Beams Tested in the First Experiment for Construction Effects

Specimen Code	Nominal Air Voids (%)	Binder Content (%)	Condition	Actual Air Voids (%)	Saturation (%)	Absorbed Water (%)	Initial Stiffness (MPa)	Fatigue Life	Number of Broken Aggregates	Stripped Aggregates (%)
B-BAN-OM10-3	10	6.0	Dry	9.9	0.0	0.0	7,461	166,605		
B-BAN-OM7-5	10	6.0	Wet1	9.9	64.6	78.6	7,512	161,821	0	0
B-BAN-OM7-3	10	6.0	Dry	9.4	0.0	0.0	7,537	64,430		
B-BAN-OM7-4	10	6.0	Wet1	9.3	65.8	74.7	8,462	153,935	1	0
B-BAN-LM10-2A	10	5.5	Dry	9.4	0.0	0.0	9,305	166,736		
B-BAN-LM10-6A	10	5.5	Wet1	10.6	67.3	89.5	7,725	100,545	1	0
B-BAN-LM10-5A	10	5.5	Dry	11.0	0.0	0.0	9,147	129,647		
B-BAN-LM10-7B	10	5.5	Wet1	10.9	59.9	81.4	7,456	188,039	1	0
HB-BAN-OM7-8	7	6.0	Dry	6.7	0.0	0.0	10,218	212,945		
B-BAN-OM7-6A	7	6.0	Wet1	6.6	66.0	55.8	8,304	355,469	1	0
B-BAN-OM7-6B	7	6.0	Dry	6.7	0.0	0.0	10,846	321,569		
B-BAN-OM10-1	7	6.0	Wet1	6.4	62.1	49.0	9,765	303,589	1	0
B-BAN-LM4-1	7	5.5	Dry	6.6	0.0	0.0	10,706	109,571		
B-BAN-LM4-2	7	5.5	Wet1	6.3	63.5	50.1	9,008	244,507	3	5
B-BAN-LM7-1	7	5.5	Dry	7.3	0.0	0.0	10,486	178,897		
B-BAN-LM7-2	7	5.5	Wet1	7.3	73.1	68.0	9,840	184,384	2	0
B-BAN-OM4-1	4	6.0	Dry	4.0	0.0	0.0	11,933	220,265		
B-BAN-OM4-2	4	6.0	Wet1	3.6	64.2	28.7	10,029	341,320	3	0
B-BAN-OM7-1	4	6.0	Dry	4.7	0.0	0.0	10,148	153,649		
B-BAN-OM7-2	4	6.0	Wet1	4.8	67.4	39.3	8,180	319,171	1	0
B-BAN-LM4-2A	4	5.5	Dry	3.4	0.0	0.0	12,852	223,438		
B-BAN-LM4-2B	4	5.5	Wet1	3.5	49.2	22.7	11,846	386,178	1	0
B-BAN-LM4-3A	4	5.5	Dry	5.0	0.0	0.0	10,987	255,669		
B-BAN-LM4-3B	4	5.5	Wet1	4.3	46.1	26.2	11,053	241,998	1	0

Table 4.8. Summary of Results from BAN Beams Tested in the Second Experiment for Construction Effects

Specimen Code	Nominal Air Voids (%)	Binder Content (%)	Condition	Actual Air Voids (%)	Saturation (%)	Absorbed Water (%)	Initial Stiffness (MPa)	Actual Fatigue Life	Number of Broken Aggregates	Stripped Aggregates (%)
B-BAN11-1A	11	6.0	Dry	10.8	0.0	0.0	7,459	163,340		
B-BAN11-2A	11	6.0	Wet2	10.8	74.4	100.1	5,334	93,501	1	10
B-BAN11-2B	11	6.0	Dry	11.1	0.0	0.0	7,310	206,251		
B-BAN11-1B	11	6.0	Wet2	11.5	62.1	85.4	5,127	57,798	0	15
B-BANL11-5B	11	5.5	Dry	11.2	0.0	0.0	6,627	349,999		
B-BANL11-6A	11	5.5	Wet2	11.3	76.5	108.7	5,135	64,073	0	20
B-BANL11-7A	11	5.5	Dry	11.1	0.0	0.0	6,345	179,214		
B-BANL11-7B	11	5.5	Wet2	10.4	63.6	78.9	4,938	65,626	1	25
B-BANE10-5B	11	5.0	Dry	11.6	0.0	0.0	6,798	166,214		
B-BANE10-6A	11	5.0	Wet2	9.7	84.4	105.7	5,579	44,697	0	20
B-BANE10-6B	11	5.0	Dry	11.1	0.0	0.0	7,468	201,159		
B-BANE10-2B	11	5.0	Wet2	11.9	70.5	98.2	6,396	44,832	2	10
B-BAN8-1A	8	6.0	Dry	8.2	0.0	0.0	8,891	256,519		
B-BAN8-1B	8	6.0	Wet2	8.6	73.0	80.6	6,920	231,782	3	5
B-BAN8-2A	8	6.0	Dry	8.1	0.0	0.0	8,796	247,337		
B-BAN8-2B	8	6.0	Wet2	8.3	67.9	71.7	9,970	332,199	2	20
B-BANL8-5A	8	5.5	Dry	8.3	0.0	0.0	8,470	400,000		
B-BANL8-5B	8	5.5	Wet2	8.3	82.3	84.1	6,373	79,999	1	5
B-BANL8-6A	8	5.5	Dry	7.7	0.0	0.0	9,300	424,164		
B-BANL8-6B	8	5.5	Wet2	8.0	73.5	72.1	6,852	96,809	0	5
B-BANE7-1A	8	5.0	Dry	8.8	0.0	0.0	9,574	130,135		
B-BANE7-1B	8	5.0	Wet2	8.6	67.8	73.7	7,494	48,887	5	20
B-BANE7-2A	8	5.0	Dry	8.2	0.0	0.0	9,606	171,013		
B-BANE7-2B	8	5.0	Wet2	8.9	80.8	89.5	6,807	25,853	1	10

Table 4.8. Summary of Results from BAN Beams Tested in the Second Experiment for Construction Effects *(cont'd.)*

Specimen Code	Nominal Air Voids (%)	Binder Content (%)	Condition	Actual Air Voids (%)	Saturation (%)	Absorbed Water (%)	Initial Stiffness (MPa)	Actual Fatigue Life	Number of Broken Aggregates	Stripped Aggregates (%)
B-BAN5-1A	5	6.0	Dry	4.9	0.0	0.0	10,507	313,967		
B-BAN5-1B	5	6.0	Wet2	5.4	69.6	48.0	8,132	381,771	3	5
B-BAN5-2B	5	6.0	Dry	5.6	0.0	0.0	9,970	332,199		
B-BAN5-2A	5	6.0	Wet2	4.9	70.3	42.9	8,796	247,337	2	20
B-BANL5-5A	5	5.5	Dry	5.0	0.0	0.0	10,513	551,610		
B-BANL5-5B	5	5.5	Wet2	4.6	55.1	30.9	8,579	303,923	8	0
B-BANL5-6A	5	5.5	Dry	6.0	0.0	0.0	9,302	420,598		
B-BANL5-6B	5	5.5	Wet2	5.7	74.6	52.3	7,713	136,738	3	5
B-BANE4-3A	5	5.0	Dry	5.4	0.0	0.0	11,665	194,315		
B-BANE4-3B	5	5.0	Wet2	5.3	71.0	47.7	8,707	60,777	1	20
B-BANE4-4A	5	5.0	Dry	5.6	0.0	0.0	10,521	288,658		
B-BANE4-4B	5	5.0	Wet2	6.0	83.3	64.9	7,804	34,826	4	5

Table 4.9. ANOVA of Initial Stiffness in the First Experiment

Factor	Degree of Freedom	Sum of Squares	Mean Square	F-value	p-value
AV	2	32363274	16181637	20.8653	0.0001
Binder	1	4180011	4180011	5.3899	0.0358
Condition	1	6454288	6454288	8.3224	0.0120
AV:Binder	2	2005024	1002512	1.2927	0.3054
AV:Condition	2	661623	330812	0.4266	0.6610
Binder:Condition	1	18371	18371	0.0237	0.8799
Residuals	14	10857424	775530		

Table 4.10. Estimated Parameters for Initial Stiffness in the First Experiment

Coefficients	Estimated Value	Standard Error	*t* statistics	p-value
(Intercept)	10423.0	568.5	18.3357	0.0000
4% Air-void	223.4	762.7	0.2929	0.7739
10% Air-void	-2420.8	762.7	-3.1741	0.0068
5.5% Binder	282.1	719.0	0.3923	0.7007
Wet1	-1279.4	719.0	-1.7793	0.0969
4% Air-void: 5.5% Binder	1385.3	880.6	1.5730	0.1380
10% Air-void: 5.5% Binder	438.5	880.6	0.4979	0.6263
4% Air-void: Wet1	131.8	880.6	0.1496	0.8832
10% Air-void: Wet1	761.0	880.6	0.8641	0.4021
5.5% Binder:Wet1	-110.7	719.0	-0.1539	0.8799

R^2=0.808

Table 4.11. ANOVA of the Initial Stiffness Ratio in the First Experiment

Factor	Degree of Freedom	Sum of Squares	Mean Square	F-value	p-value
AV	2	0.172583	0.086291	0.5176	0.6203
Binder	1	0.044568	0.044568	0.2673	0.6236
AV:Binder	2	0.121131	0.060565	0.3633	0.7097
Residuals	6	1.000306	0.166718		

Table 4.12. ANOVA of ln(Fatigue Life) in the First Experiment

Factor	Degree of Freedom	Sum of Squares	Mean Square	F-value	p-value
AV	2	1.8717	0.9359	10.0008	0.0028
Binder	1	0.0736	0.0736	0.7867	0.3925
Condition	1	0.5572	0.5572	5.9542	0.0312
AV:Binder	2	0.5298	0.2649	2.8307	0.0984
AV:Condition	2	0.0577	0.0288	0.3083	0.7403
Binder:Condition	1	0.0677	0.0677	0.7234	0.4117
AV:Binder:Condition	2	0.1265	0.0632	0.6757	0.5272
Residuals	12	1.1229	0.0936		

Table 4.13. Estimated Parameters for ln(Fatigue Life) in the First Experiment

Coefficients	Estimated Value	Standard Error	t statistics	p-value
(Intercept)	12.4749	0.2163	57.6717	0.0000
4% Air-void	-0.3524	0.3059	-1.1519	0.2718
10% Air-void	-0.9265	0.3059	-3.0288	0.0105
5.5% Binder	-0.6254	0.3059	-2.0445	0.0635
Wet1	0.2274	0.3059	0.7435	0.4715
4% Air-void:5.5% Binder	0.8872	0.4326	2.0508	0.0628
10% Air-void:5.5% Binder	0.9754	0.4326	2.2547	0.0436
4% Air-void:Wet1	0.3571	0.4326	0.8254	0.4252
10% Air-void:Wet1	0.1935	0.4326	0.4472	0.6627
5.5% Binder:Wet1	0.189	0.4326	0.4369	0.6699
4% Air-void:5.5% Binder:Wet1	-0.5274	0.6118	-0.8621	0.4055
10% Air-void:5.5% Binder:Wet1	-0.6769	0.6118	-1.1064	0.2902

R^2=0.7452

Table 4.14. ANOVA of the Fatigue Life Ratio in the First Experiment

Factor	Degree of Freedom	Sum of Squares	Mean Square	F-value	p-value
AV	2	0.2597	0.1298	1.6134	0.2750
Binder	1	0.1179	0.1179	1.4647	0.2717
AV:Binder	2	0.3140	0.1570	1.9512	0.2224
Residuals	6	0.4828	0.0805		

Table 4.15. ANOVA of Initial Stiffness in the Second Experiment

Factor	Degree of Freedom	Sum of Squares	Mean Square	F-value	p-value
AV	2	60997415	30498708	64.3112	0.0000
Binder	2	3327696	1663848	3.5085	0.0517
Condition	1	29278921	29278921	61.7391	0.0000
AV:Binder	4	529393	132348	0.2791	0.8877
AV:Condition	2	484983	242492	0.5113	0.6082
Binder:Condition	2	734481	367241	0.7744	0.4757
AV:Binder:Condition	4	3131908	782977	1.6510	0.2051
Residuals	18	8536259	474237		

Table 4.16. Estimated Parameters for Initial Stiffness in the Second Experiment

Coefficients	Estimated Value	Standard Error	*t* statistics	p-value
(Intercept)	8843.5	486.9	18.1611	0.0000
5% Air-voids	1395.0	688.6	2.0257	0.0579
11% Air-voids	-1459.0	688.6	-2.1186	0.0483
5% Binder	746.5	688.6	1.0840	0.2927
5.5% Binder	41.5	688.6	0.0603	0.9526
Wet2	-398.5	688.6	-0.5787	0.5700
5% Air-voids: 5% Binder	108.0	973.9	0.1109	0.9129
11% Air-voids: 5% Binder	-998.0	973.9	-1.0248	0.3191
5% Air-voids: 5.5% Binder	-372.5	973.9	-0.3825	0.7066
11% Air-voids: 5.5% Binder	-940.0	973.9	-0.9652	0.3472
5% Air-voids:Wet2	-1376.0	973.9	-1.4129	0.1747
11% Air-voids:Wet2	-1755.5	973.9	-1.8026	0.0882
5% Binder:Wet2	-2041.0	973.9	-2.0957	0.0505
5.5% Binder:Wet2	-1874.0	973.9	-1.9242	0.0703
5% Air-voids: 5% Binder:Wet2	978.0	1377.3	0.7101	0.4867
11% Air-voids: 5% Binder:Wet2	3049.5	1377.3	2.2141	0.0400
5% Air-voids: 5.5% Binder:Wet2	1887.0	1377.3	1.3701	0.1875
11% Air-voids: 5.5% Binder:Wet2	2578.5	1377.3	1.8721	0.0775

R^2=0.9202

Table 4.17. ANOVA of the Initial Stiffness Ratio in the Second Experiment

Factor	Degree of Freedom	Sum of Squares	Mean Square	F-value	p-value
AV	2	0.0049	0.0024	0.2739	0.7665
Binder	2	0.0106	0.0053	0.5953	0.5717
AV:Binder	4	0.0741	0.0185	2.0801	0.1661
Residuals	9	0.0801	0.0089		

Table 4.18. ANOVA of ln(Fatigue Life) in the Second Experiment

Factor	Degree of Freedom	Sum of Squares	Mean Square	F-value	p-value
AV	2	2.7757	1.3879	17.8964	0.0001
Binder	2	5.6984	2.8492	36.7406	0.0000
Condition	1	9.2061	9.2061	118.7129	0.0000
AV:Binder	4	1.3823	0.3456	4.4562	0.0112
AV:Condition	2	0.2228	0.1114	1.4368	0.2637
Binder:Condition	2	2.4340	1.2170	15.6932	0.0001
AV:Binder:Condition	4	0.6557	0.1639	2.1138	0.1211
Residuals	18	1.3959	0.0776		

Table 4.19. Estimated Parameters for ln(Fatigue Life) in the Second Experiment

Coefficients	Estimated Value	Standard Error	*t* statistics	p-value
(Intercept)	12.4367	0.1969	63.1585	0.0000
5% Air-voids	0.2485	0.2785	0.8925	0.3839
11% Air-voids	-0.3165	0.2785	-1.1366	0.2706
5% Binder	-0.5238	0.2785	-1.8810	0.0762
5.5% Binder	0.4918	0.2785	1.7661	0.0943
Wet2	0.0968	0.2785	0.3476	0.7322
5% Air-voids: 5% Binder	0.2137	0.3938	0.5426	0.5941
11% Air-voids: 5% Binder	0.5200	0.3938	1.3205	0.2032
5% Air-voids: 5.5% Binder	-0.0921	0.3938	-0.2338	0.8178
11% Air-voids: 5.5% Binder	-0.1810	0.3938	-0.4597	0.6513
5% Air-voids:Wet2	-0.1465	0.3938	-0.3720	0.7142
11% Air-voids:Wet2	-1.0118	0.3938	-2.5691	0.0193
5% Binder:Wet2	-1.5310	0.3938	-3.8874	0.0011
5.5% Binder:Wet2	-1.6402	0.3938	-4.1648	0.0006
5% Air-voids: 5% Binder:Wet2	-0.0579	0.5570	-0.1039	0.9184
11% Air-voids: 5% Binder:Wet2	1.0387	0.5570	1.8650	0.0786
5% Air-voids: 5.5% Binder:Wet2	0.8301	0.5570	1.4904	0.1534
11% Air-voids: 5.5% Binder:Wet2	1.2039	0.5570	2.1617	0.0444

R^2=0.9413

Table 4.20. ANOVA of the Fatigue Life Ratio in the Second Experiment

Factor	Degree of Freedom	Sum of Squares	Mean Square	F-value	p-value
AV	2	0.221684	0.110842	3.80552	0.063431
Binder	2	1.302563	0.651281	22.36031	0.000322
AV:Binder	4	0.411296	0.102824	3.53024	0.053692
Residuals	9	0.26214	0.029127		

Table 4.21. Estimated Parameters for Fatigue Life Ratio in the Second Experiment

Coefficients	Estimated Value	Standard Error	*t* statistics	p-value
(Intercept)	1.1193	0.1207	9.2750	0.0000
5% Air-voids	-0.1456	0.1707	-0.8534	0.4156
11% Air-voids	-0.7099	0.1707	-4.1596	0.0024
5% Binder	-0.8711	0.1707	-5.1041	0.0006
5.5% Binder	-0.9048	0.1707	-5.3016	0.0005
5% Air-voids: 5% Binder	0.0954	0.2414	0.3953	0.7019
11% Air-voids: 5% Binder	0.7054	0.2414	2.9226	0.0170
5% Air-voids: 5.5% Binder	0.3844	0.2414	1.5927	0.1457
11% Air-voids: 5.5% Binder	0.7404	0.2414	3.0679	0.0134

R2=0.8807

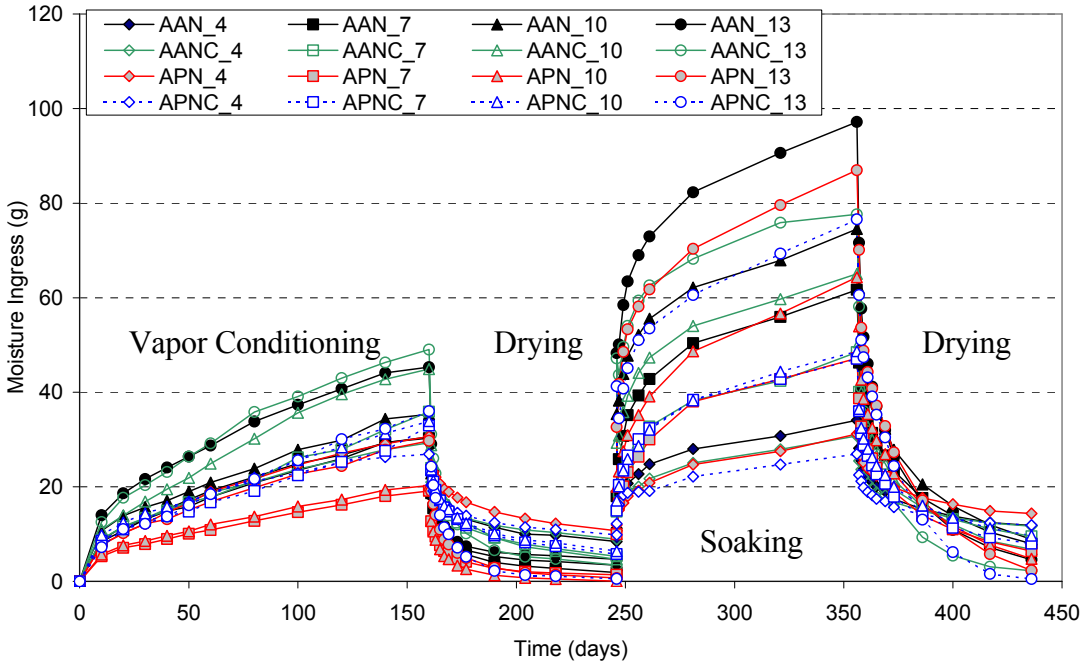

(a)

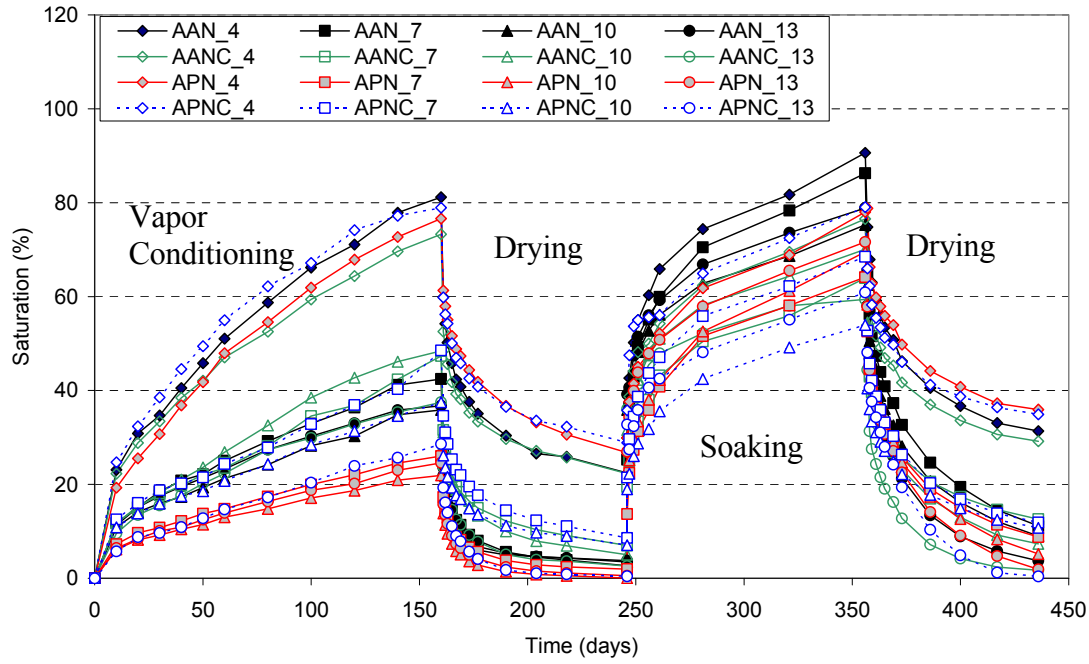

(b)

In the legend, the first letter "A" represents Aggregate A; the second letter represents binder type (A: AR-4000; P: PBA-6a); the third letter "N" represents that no additives were used; the fourth letter represents gradation type (nil, medium gradation; C, coarse gradation); and the last number represents air-void content level (4: four percent; 7: seven percent; 10: ten percent; 13: thirteen percent).

Figure 4-1. Average moisture ingress and retention process (a – moisture mass, b – saturation).

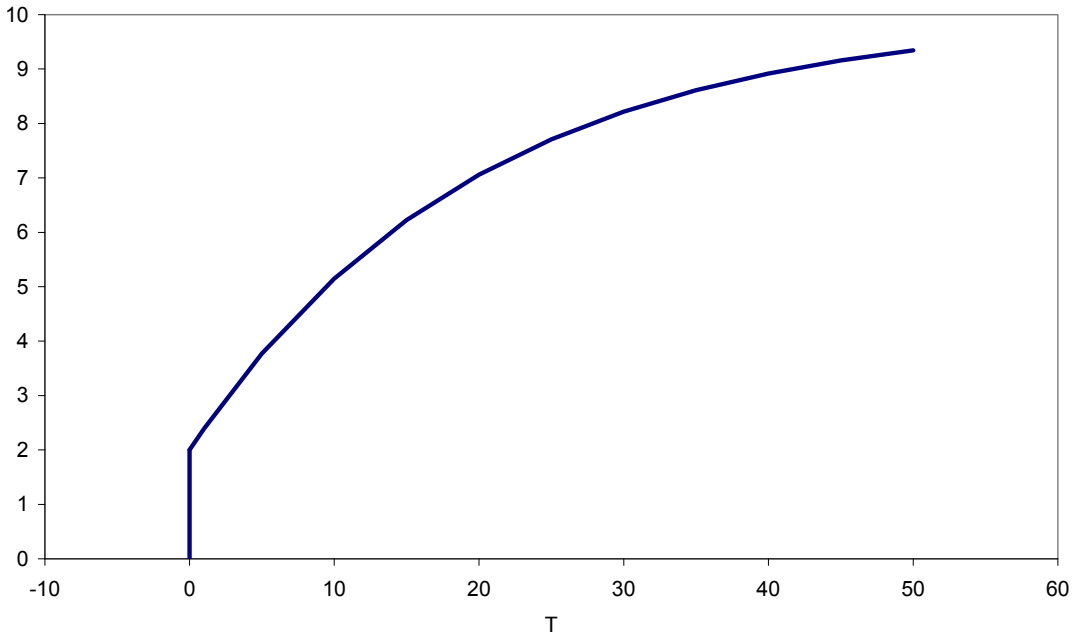

(a)

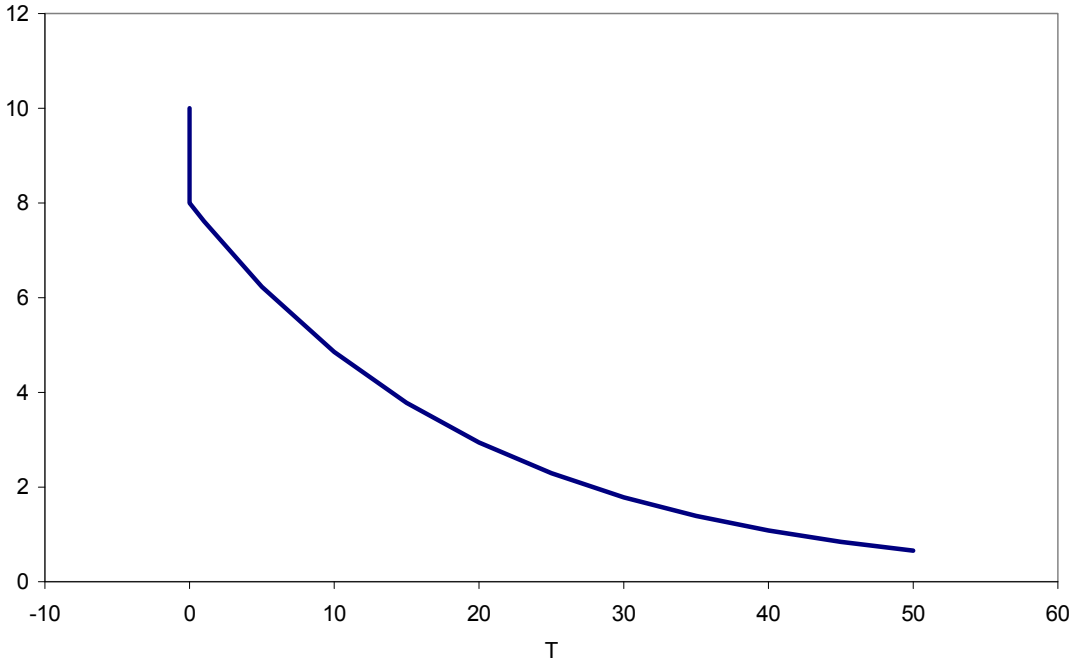

(b)

Figure 4-2. Models for moisture absorption and drying process during vapor conditioning process (a, absorption; b, drying).
(Note: y-axis represents mass of water in a specimen in grams normalized to 10 g; x-axis represents conditioning time in days.)

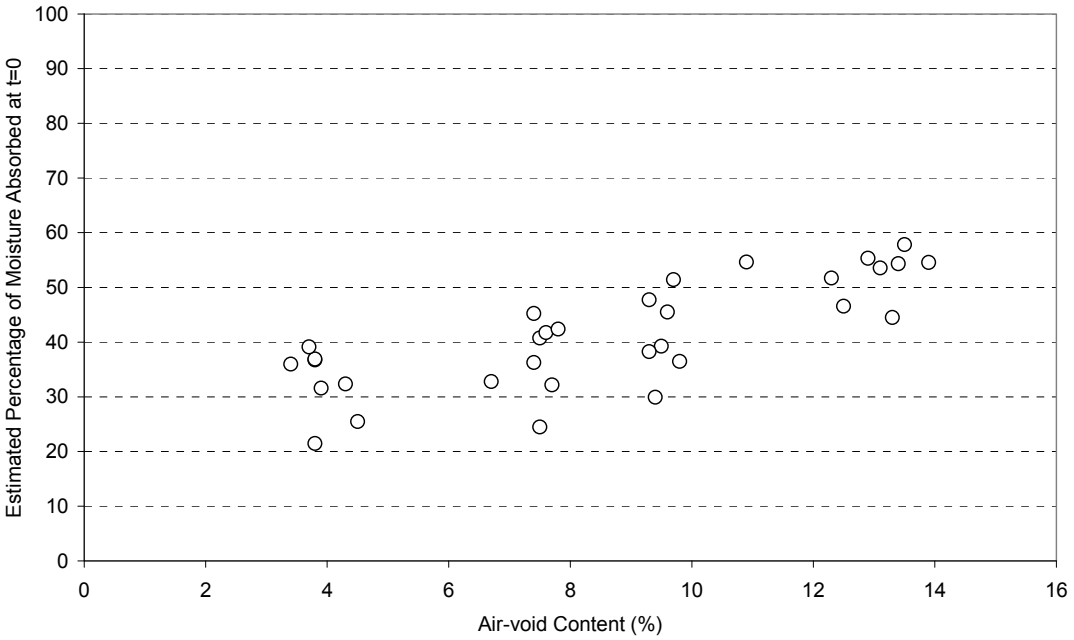

(a)

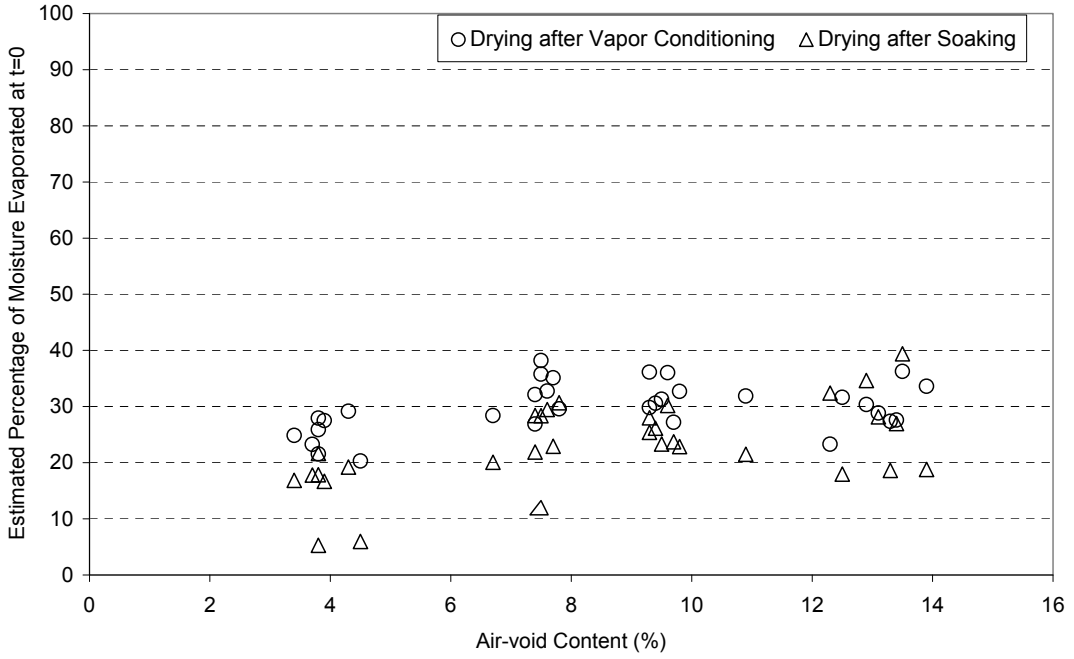

(b)

Figure 4-3. Percentage of instantaneous absorption and evaporation (a, Soaking; b, Drying).

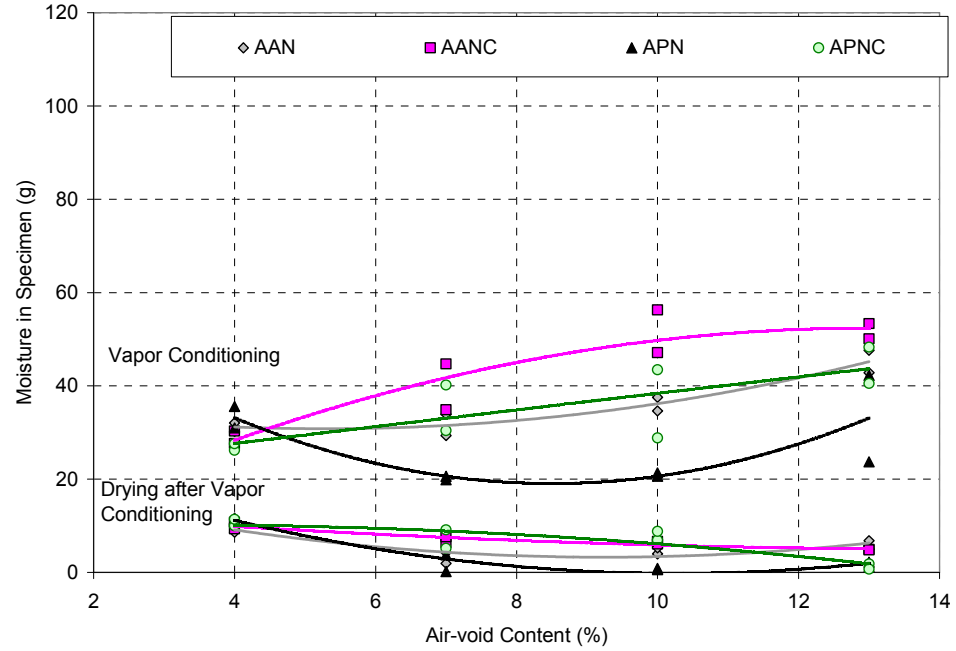

(a)

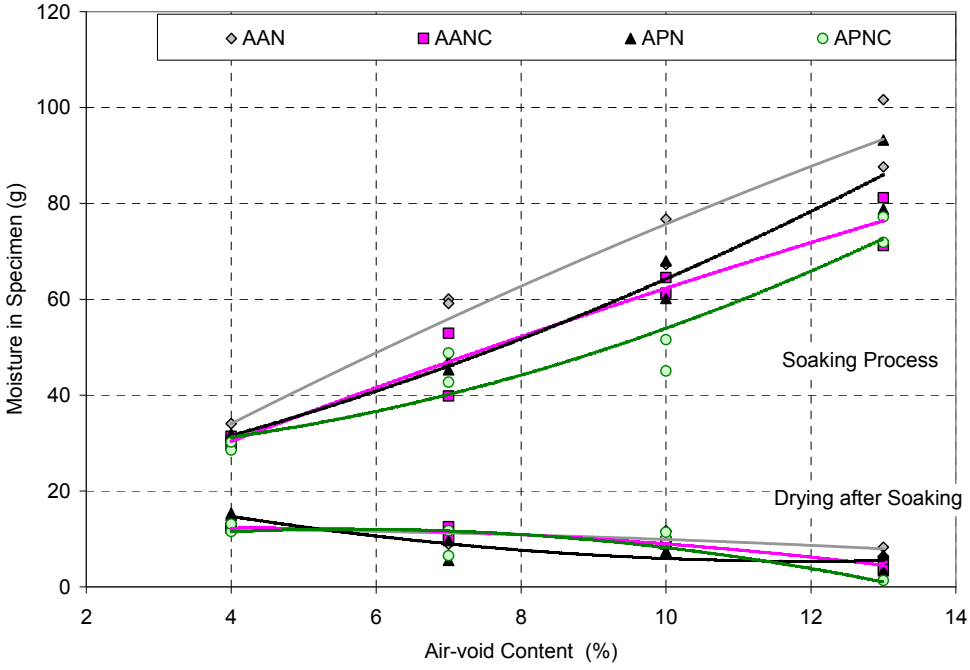

(b)

In the legend, the first letter "A" represents Aggregate A; the second letter represents binder type (A: AR-4000; P: PBA 6a); the third letter "N" represents that no additives were used; the fourth letter represents gradation type (nil, medium gradation; C, coarse gradation).

Figure 4-4. Ultimate moisture content in each process (a, Vapor Conditioning and Drying; b, Soaking and Drying).

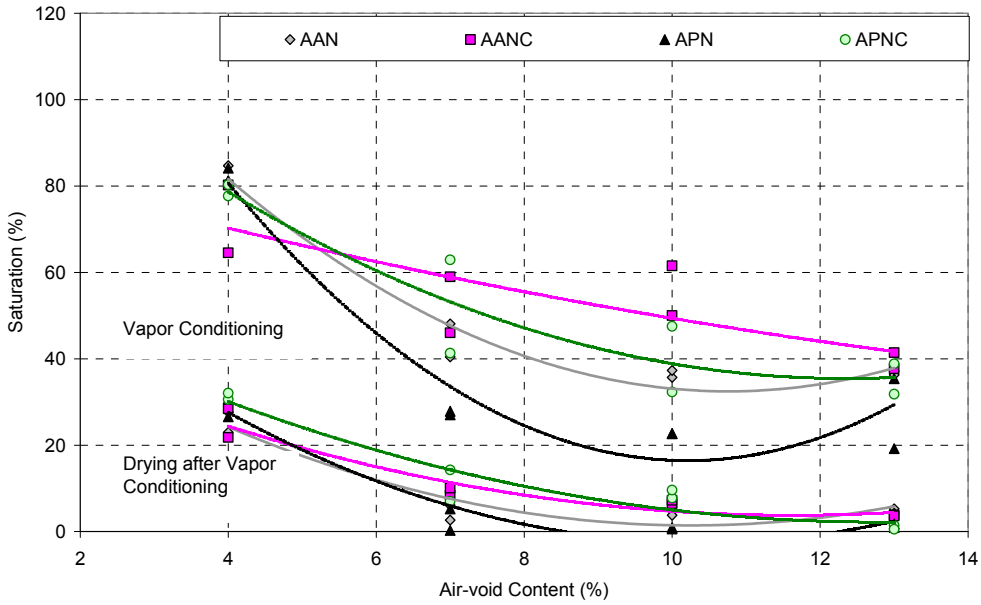

(a)

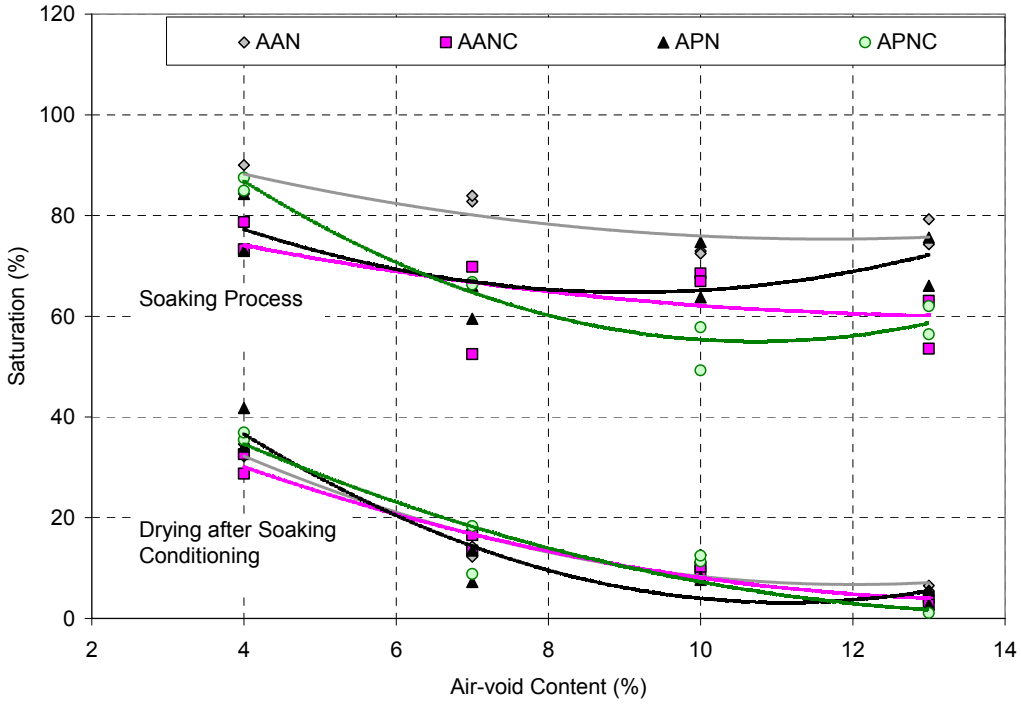

(b)

In the legend, the first letter "A" represents Aggregate A; the second letter represents binder type (A: AR-4000; P: PBA 6a); the third letter "N" represents that no additives were used; the fourth letter represents gradation type (nil, medium gradation; C, coarse gradation).

Figure 4-5. Ultimate saturation in each process (a, Vapor Conditioning and Drying; b, Soaking and Drying).

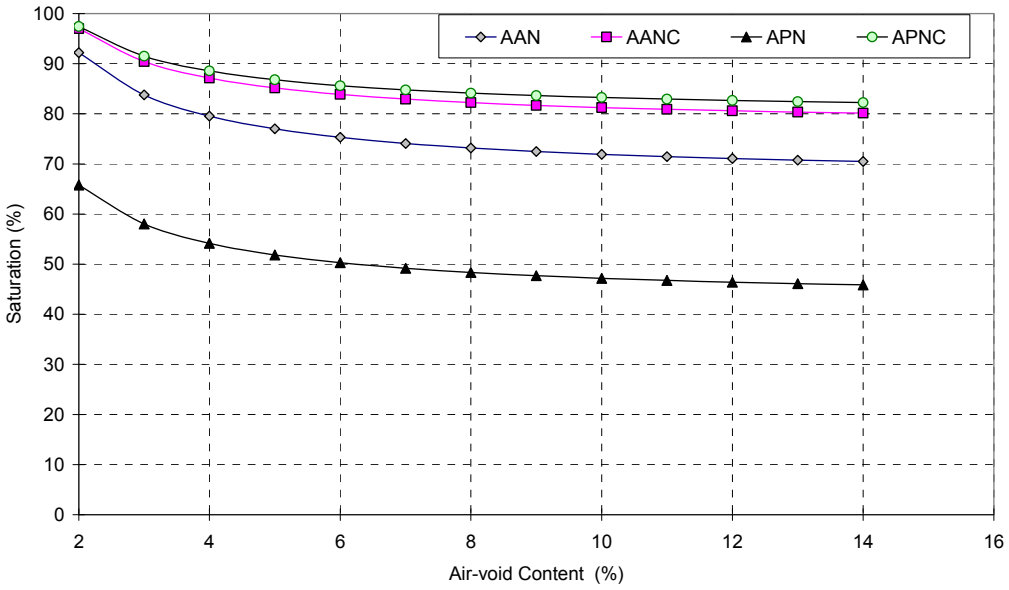

(a)

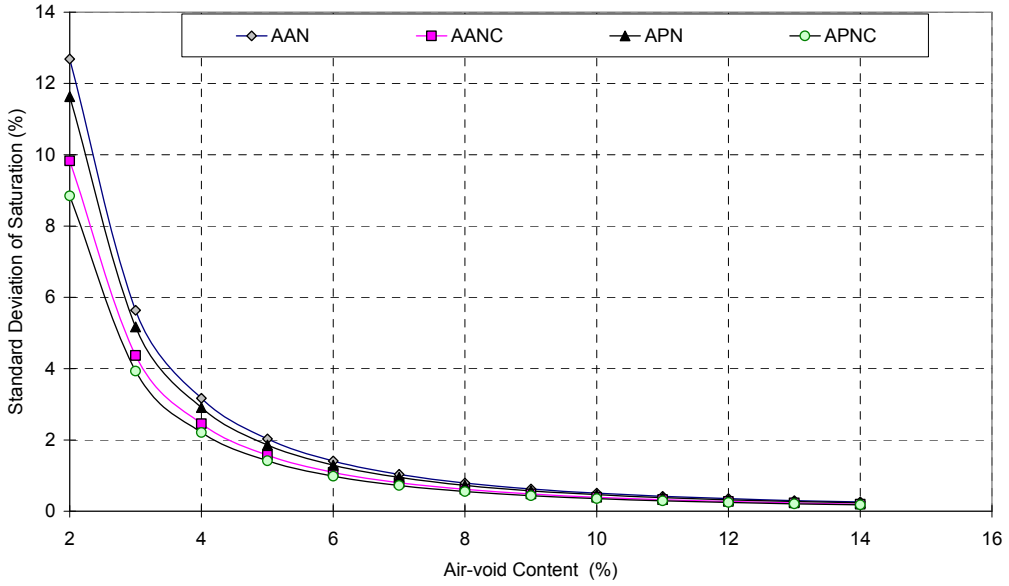

(b)

In the legend, the first letter "A" represents Aggregate A; the second letter represents binder type (A: AR-4000; P: PBA 6a); the third letter "N" represents that no additives were used; the fourth letter represents gradation type (nil, medium gradation; C, coarse gradation).

Figure 4-6. Derived saturation and its standard deviation versus air-void content (a, saturation; b, standard deviation).

```
#-----------------------------------------------------------------
#Nonlinear Mixed Effect Model
#-----------------------------Vapor, Moist-------------------------
options(contrasts=c("contr.treatment","contr.poly"))
nl.data_read.table("d:\\stripping\\Results\\soaking\\nlmedata10.txt", header=T)
nlsmall.data_nl.data
nlsmall.data$AirVoids_as.factor(nlsmall.data$AirVoids)

nlsmall.dat_groupedData(Moisture~Days|DryMass, outer=~Binder+Gradation+AirVoids, nlsmall.data,
      labels=list(x="Time",y="Absorbed Moisture"),units=list(x="(Days)",y="(g)"))
moist.uptake_function(A,B,day){A*(1-exp(B)*day))}
moist.uptake_deriv(~A*(1-exp(B)*day)),c("A","B"),function(A,B,day){})
nlsmall.nlme_nlme(Moisture~moist.uptake(A,B,Days),
data=nlsmall.dat,
fixed=list(A~(Gradation+Binder+AirVoids)^2,B~(Gradation+Binder+AirVoids)^2),
random=pdDiag(A+B~1),
start=c(25,-1,-1,0,0,0,0,0,0,0,0,0,0, -0.6,0,0,0,0,0,0,0,0,0,0,0,0),
method="ML"
)
summary(nlsmall.nlme)
anova(nlsmall.nlme)


#------------VaporDry. Moist-----------------------------
nl.data_read.table("d:\\stripping\\Results\\soaking\\nlmedata20.txt", header=T)
nlsmall.data_nl.data
nlsmall.data$AirVoids_as.factor(nlsmall.data$AirVoids)

nlsmall.dat_groupedData(Moisture~Days|AirVoida, outer=~Binder+Gradation+AirVoids, nlsmall.data,
      labels=list(x="Time",y="Absorbed Moisture"),units=list(x="(Days)",y="(g)"))
moist.uptake_function(A,B,C,day){A+B*exp(C*day)}
moist.uptake_deriv(~A+B*exp(C*day),c("A","B","C"),function(A,B,C,day){})
nlsmall.nlme_nlme(Moisture~moist.uptake(A,B,C,Days),
data=nlsmall.dat,
fixed=list(A~(Gradation+Binder+AirVoids)^2,B~(Gradation+Binder+AirVoids)^2, C~(Gradation+Binder+AirVoids)^2),
random=pdDiag(A+B+C~1),
start=c(10.227,-0.886,0.555,-7.069,-6.593,-4.124,1.485,4.669,4.579,-0.57,-1.79,
-2.495,-5.22,13.83,-3.882,-2.034,   2.243,6.991,13.039,2.793,4.988,4.866,5.011,
-2.212,-6.237,-5.065,-0.088,0.014,0.038,-0.061,-0.087,-0.119,-0.039,0.049,0.074,
0.067,-0.001,0.002,0.021),
method="ML"
)
summary(nlsmall.nlme)
anova(nlsmall.nlme)
```

Figure 4-7. S-Plus® code for nonlinear mixed effect model.

```
#------------Soak. Moisture----------------------------
nl.data_read.table("d:\\stripping\\Results\\soaking\\nlmedata30.txt", header=T)
nlsmall.data_nl.data
nlsmall.data$AirVoids_as.factor(nlsmall.data$AirVoids)

nlsmall.dat_groupedData(Moisture~Days|AirVoida, outer=~Binder+Gradation+AirVoids, nlsmall.data,
      labels=list(x="Time",y="Absorbed Moisture"),units=list(x="(Days)",y="(g)"))
moist.uptake_function(A,B,C,day){A+B*exp(C*day)}
moist.uptake_deriv(~A+B*exp(C*day),c("A","B","C"),function(A,B,C,day){})
nlsmall.nlme_nlme(Moisture~moist.uptake(A,B,C,Days),
data=nlsmall.dat,
fixed=list(A~(Gradation+Binder+AirVoids)^2,B~(Gradation+Binder+AirVoids)^2, C~(Gradation+Binder+AirVoids)^2),
random=pdDiag(A+B+C~1),
start=c(20,      3.8,  0.4,  18.9,       30.6,       47.3,       -3.3, 4.7,  10.3,       12.8,       -5.7,
-10,  -3.9, -10,  -2.1, 1.8,  -13.5,      -14.6,      -19.7,      -1.4, -2.6, -3.9, -4.4,
1.7,  -3,    -3.6, 0,     0,     0,     0,     0,     0,     0,     0,     0,     0),
method="ML",

)
summary(nlsmall.nlme)
anova(nlsmall.nlme)

#------------SoakDry. Moist----------------------------
nl.data_read.table("d:\\stripping\\Results\\soaking\\nlmedata40.txt", header=T)
nlsmall.data_nl.data
nlsmall.data$AirVoids_as.factor(nlsmall.data$AirVoids)

nlsmall.dat_groupedData(Moisture~Days|AirVoida, outer=~Binder+Gradation+AirVoids, nlsmall.data,
      labels=list(x="Time",y="Absorbed Moisture"),units=list(x="(Days)",y="(g)"))
moist.uptake_function(A,B,C,day){A+B*exp(C*day)}
moist.uptake_deriv(~A+B*exp(C*day),c("A","B","C"),function(A,B,C,day){})
nlsmall.nlme_nlme(Moisture~moist.uptake(A,B,C,Days),
data=nlsmall.dat,
fixed=list(A~(Gradation+Binder+AirVoids)^2,B~(Gradation+Binder+AirVoids)^2, C~(Gradation+Binder+AirVoids)^2),
random=A+B+C~1,
start=c(11.6,1.67, 1.44, -0.38, -1.05, -7.71, -0.25, -3.25, -2, 2.34, -3.39,      -2.68,      -4.61,      11.91,      3.87,       -1.15,
      15.53,      23.29,      40.69,      -1.18,      2.4,  9.57,       2.27,       -1.4, -6.74,      4.51,       -0.07,      0,     0.01,       -0.01,
      -0.01,      -0.03,      -0.01,      0.02,       0.01,       0.01,       0.01,       0.01,       0.03),
method="ML"
)

summary(nlsmall.nlme)
anova(nlsmall.nlme)
```

Figure 4-7. S-Plus® code for nonlinear mixed effect model *(cont'd)*.

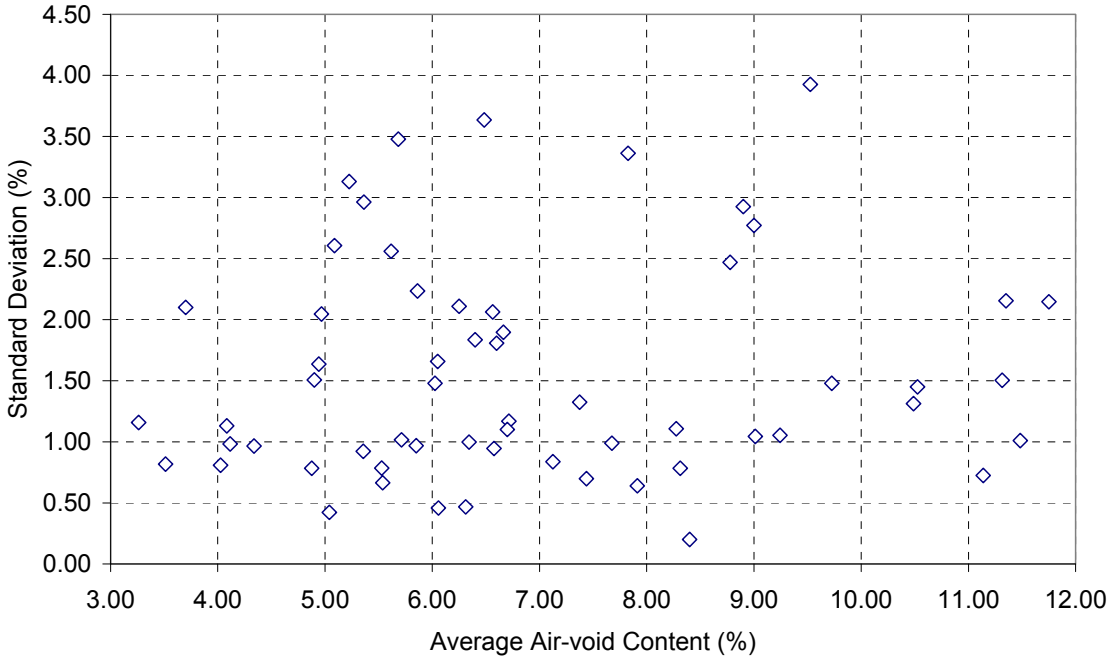

Figure 4-8. Standard deviation of in-situ air-void contents from field coring sections.

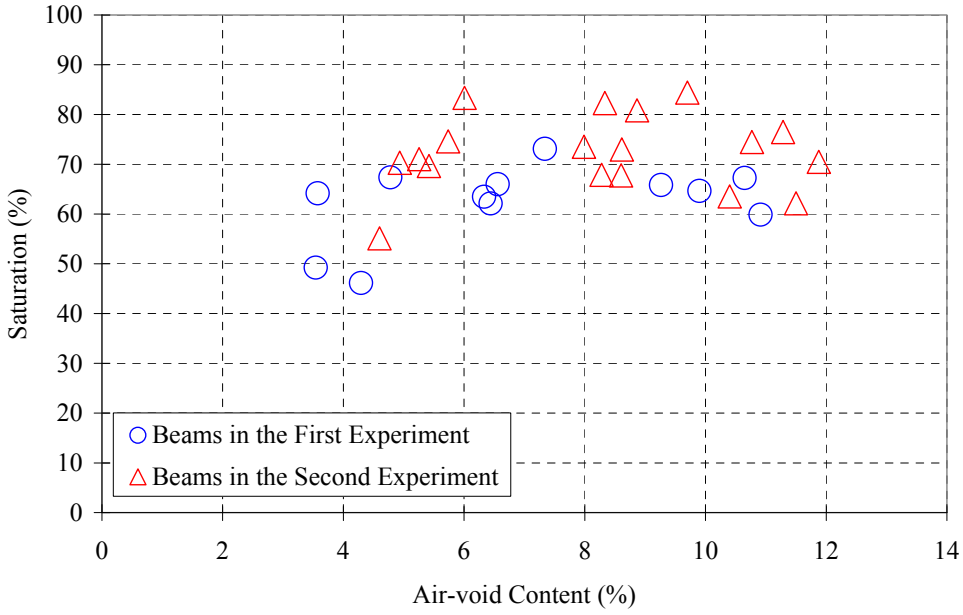

Figure 4-9. Saturation levels of beams with different air-void contents after the same vacuum saturation procedure.

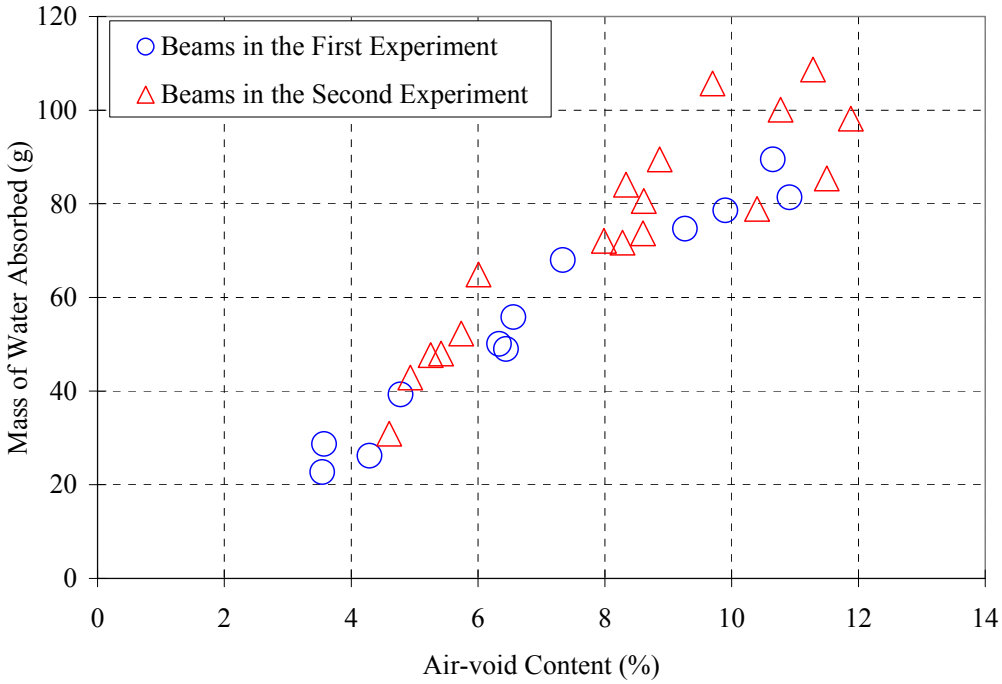

Figure 4-10. Mass of water absorbed by beams with different air-void contents after the same vacuum saturation procedure.

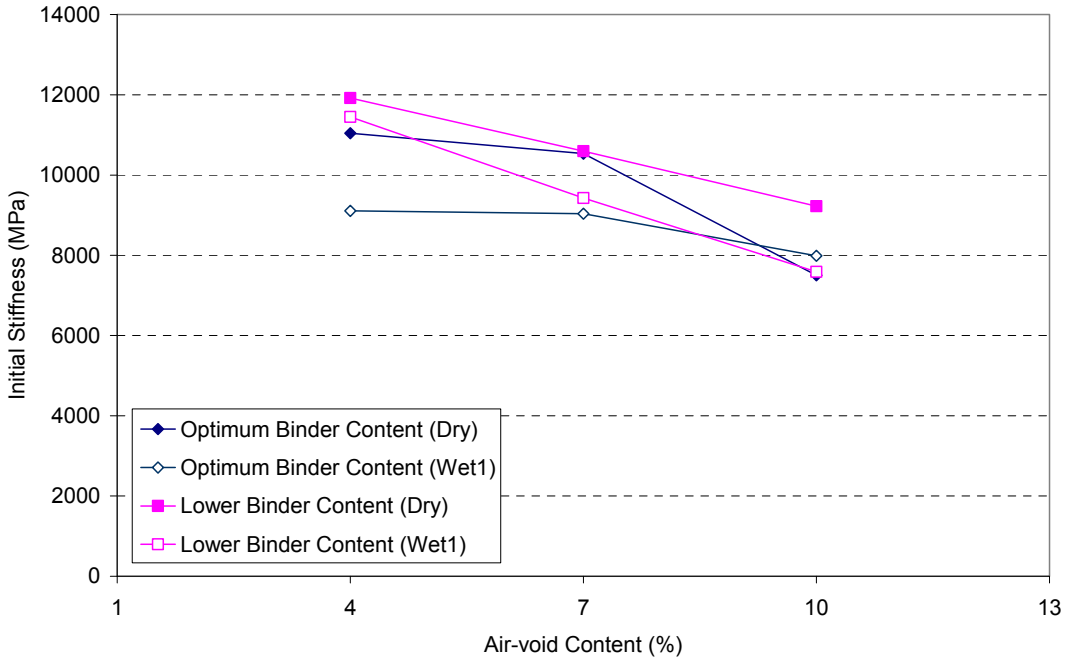

Figure 4-11. Average initial stiffness of beams in the first experiment.

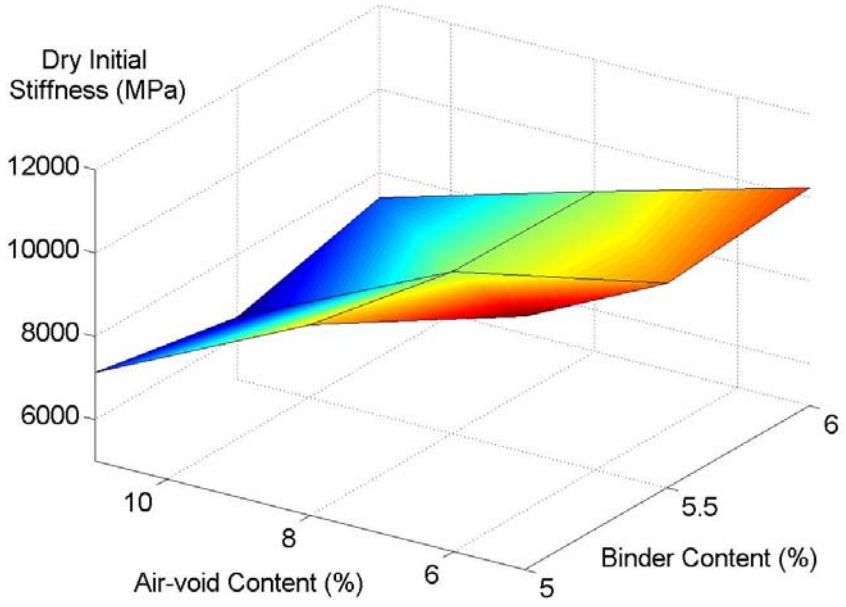

(a)

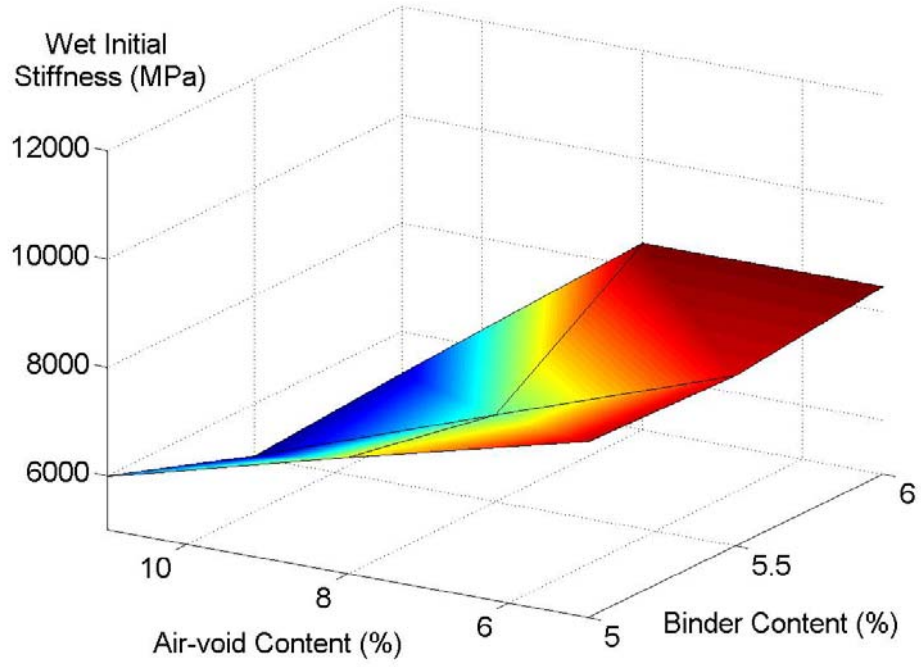

(b)

Figure 4-12. Average initial stiffness in the second experiment (a, dry beams; b, wet beams).

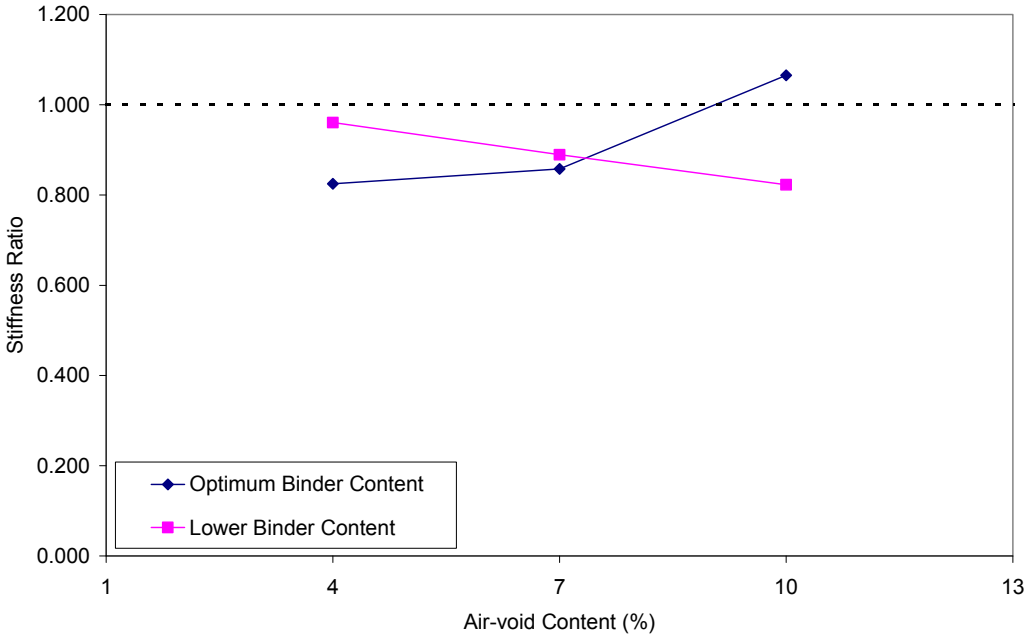

(a)

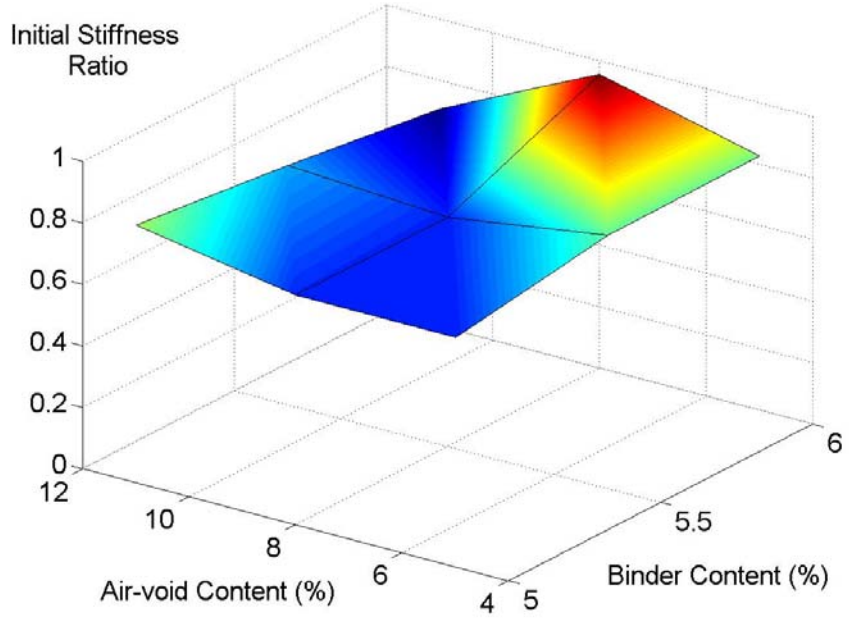

(b)

Figure 4-13. Initial stiffness ratio of beams (a, first experiment; b, second experiment).

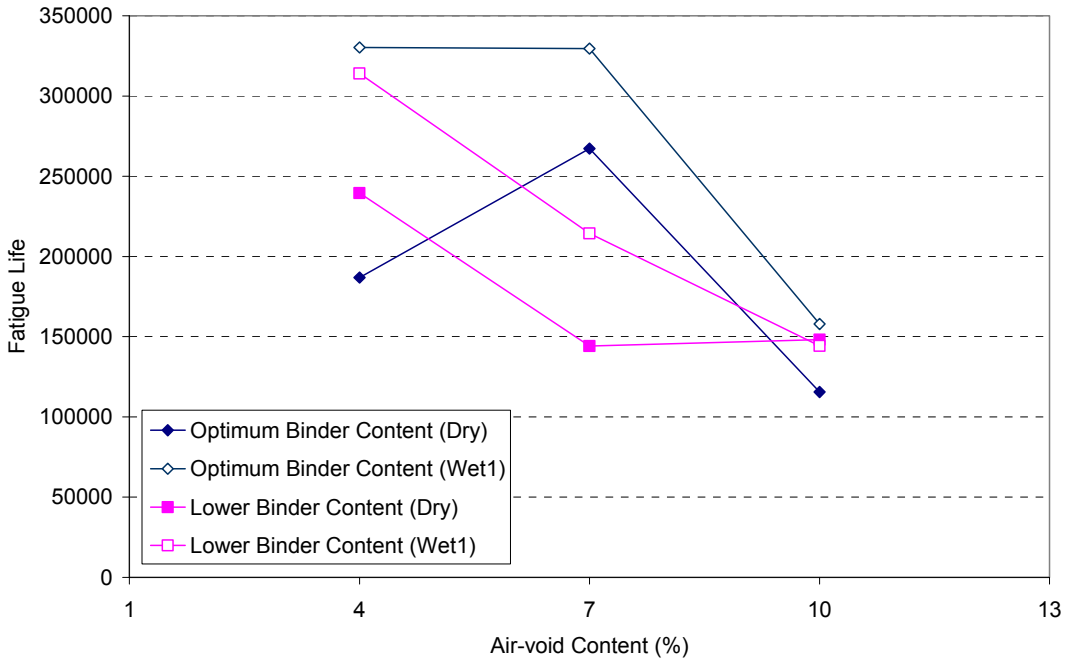

Figure 4-14. Average fatigue life of beams in the first experiment.

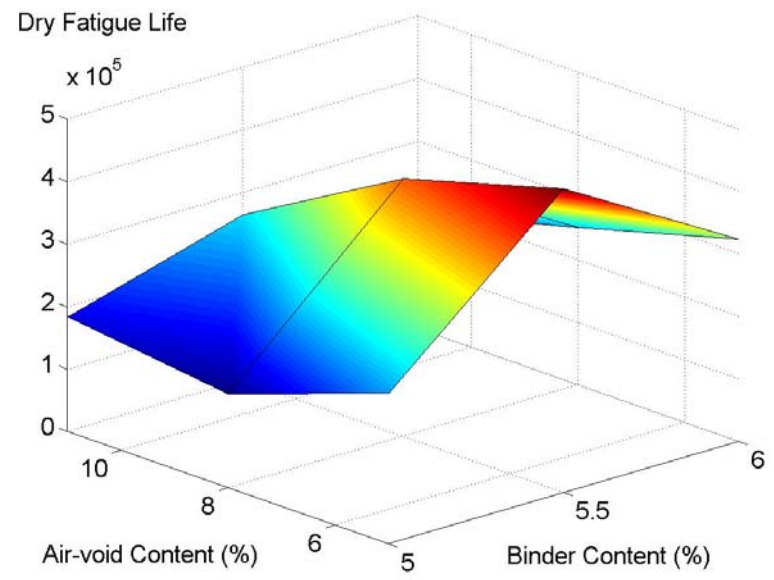

(a)

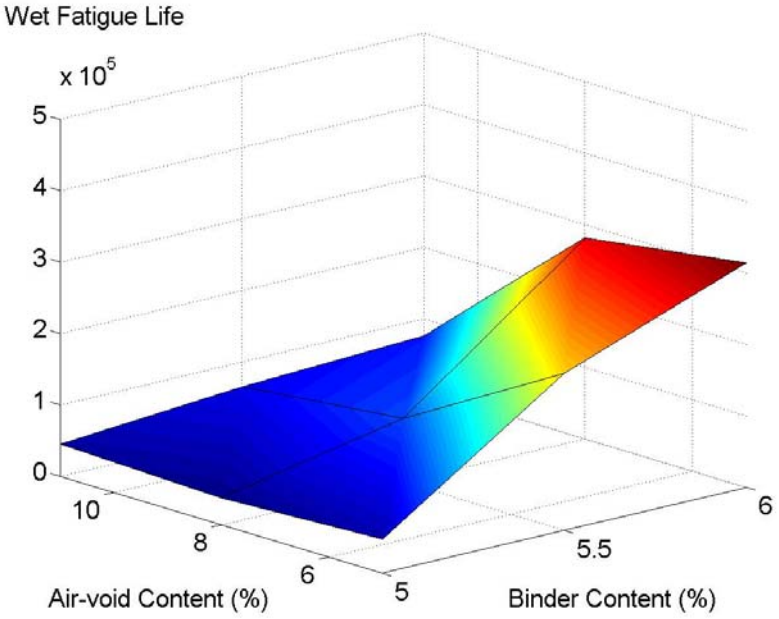

(b)

Figure 4-15. Average fatigue life in the second experiment (a, dry beams; b, wet beams).

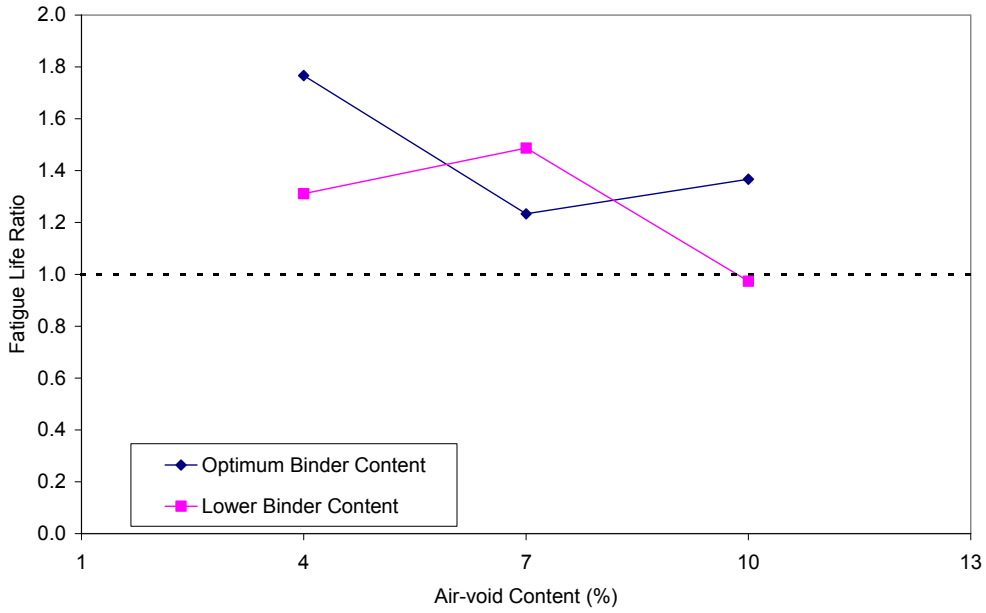

(a)

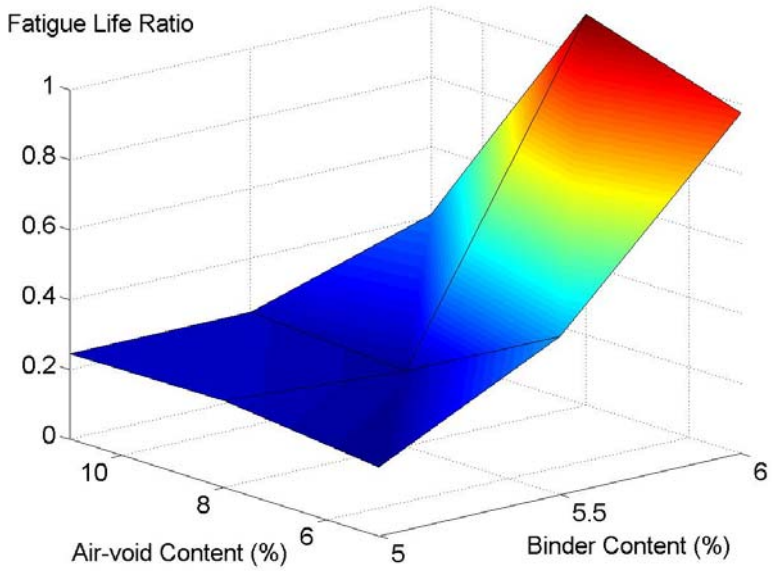

(b)

Figure 4-16. Fatigue life ratio of beams (a, first experiment; b, second experiment).

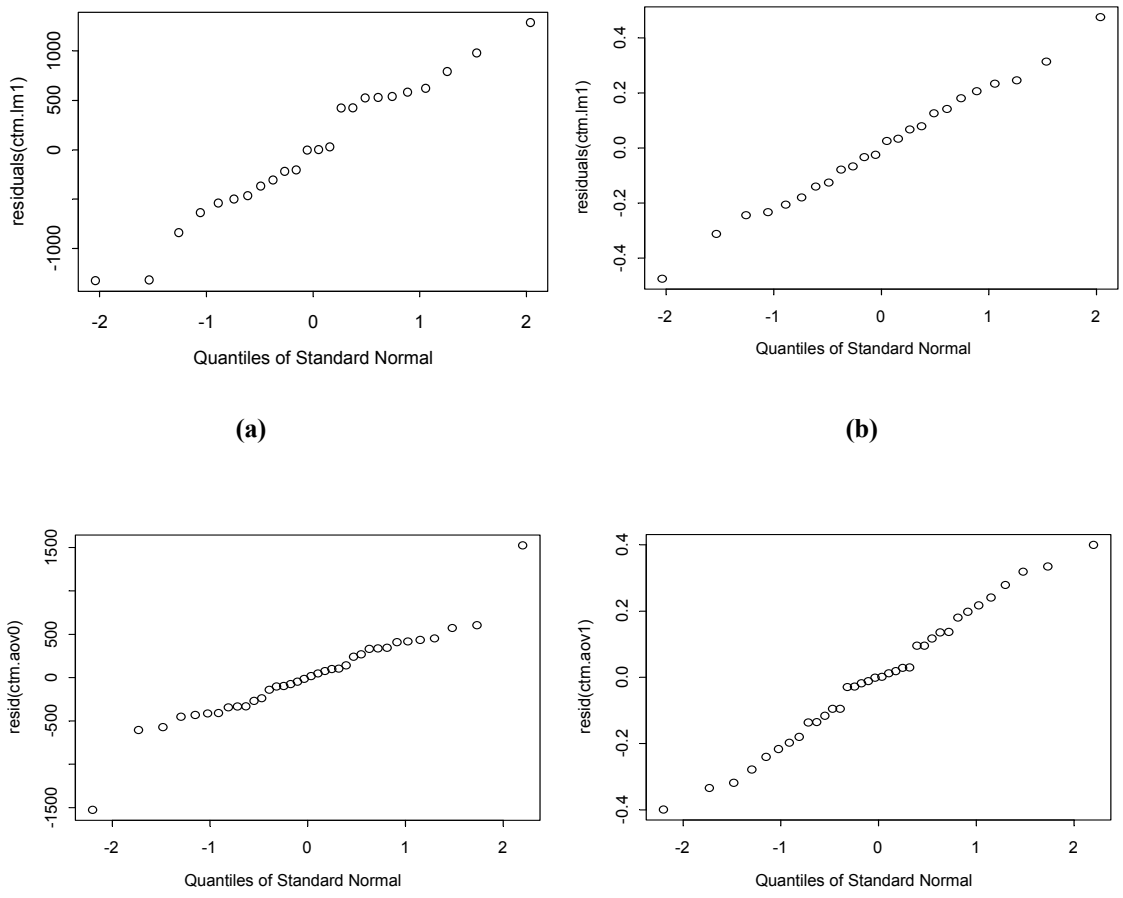

Figure 4-17. QQ-normal plot of the residuals from the linear model (a, initial stiffness in first experiment; b, fatigue life in first experiment; c, initial stiffness in second experiment; d, fatigue life in second experiment).

5.0 EVALUATION OF HAMBURG WHEEL TRACKING DEVICE TEST

The Hamburg Wheel Tracking Device (HWTD) was originally developed in the 1970s in the city of Hamburg, Germany, where the test was used as a specification requirement for pavements that were severely stressed by heavy and slow seaport trucks. The test was initially intended to measure rutting susceptibility, but later it was found to be able to measure the effects of moisture damage. The device was introduced into the United States in the early 1990s by pavement officials and engineers after a tour of European countries for technology transfer (Aschenbrener et al 1994). This initiated the research into evaluating the capability of the equipment to characterize the moisture sensitivity of asphalt mixes and to predict field performance. Compared with the tensile strength ratio (TSR) test, the HWTD applies dynamic loading in the conditioning procedure, which is believed to better simulate field conditions. Some research has been conducted to validating the effectiveness of the test and correlating the test results with field performance, and the findings seem to be promising (Aschenbrener et al 1994; Rand 2002). The scope of the research, however, is limited and specific mix compositions such as binder type have not been considered in the correlation. In order to consider the HWTD as a potential near-future substitute for the TSR test, more research is needed to verify its effectiveness on a broad range of material types and field conditions, particularly in areas such as California where the test has never been tried. This chapter is devoted to this aspect of this study, in which a common HWTD test procedure is evaluated with laboratory-fabricated specimens and cores taken from in-service asphalt pavements.

5.1 Introduction to the HWTD Test

5.1.1 Hamburg Wheel Tracking Device

The Hamburg Wheel Tracking Device (Figure 5-1) used in this study was manufactured by Precision Machine & Welding Company located in the city of Salina, Kansas. The device tests two specimens simultaneously using two reciprocating steel wheels. Each wheel has a diameter of 0.2 m and a width of 0.047 m. The weight of each wheel is fixed at 72 kg, which results in an average contact stress about 0.7 MPa on top of specimens. The wheel speed is variable, by use of an AC motor with a frequency inductor, and is set on the run screen in 5 RPM increments. The water temperature is adjustable from room temperature 5°C to 80°C, controlled to ±0.3°C. The most commonly used temperature in the City of Hamburg is 50°C. Rut depth at the specimen surface is measured by a linear variable displacement transducer (LVDT) on each wheel with a range of measurement of deformation 0 to 30 mm, ±0.01 mm. Measurements are taken along the length of the slab at 11 equally spaced points, including the center point. The machine is capable of running any number of cycles (up to 200,000) specified and ending when the number of cycles is reached or when an operator-specified amount of deformation is reached. Normally the test is run to 20,000 cycles or when 20 mm deformation is reached, whichever comes first. If one sample reaches the preset deformation, the wheel rises, and the other sample continues until the test is complete. A maximum of nine hours approximately is required for a test.

5.1.2 Specimen Preparation

A pair of samples is tested simultaneously. A sample is typically 0.26 m wide, 0.32 m long, and 0.076 m high (Figure 5-2a). For cores taken from the field that have a diameter of 0.15 m, two cores are shaved and fitted into a special mode to form one sample, as illustrated in Figure 5-2b. The specimen preparation procedure is detailed in Chapter 2. It needs to be mentioned that in other states, the HWTD specimens are typically fabricated from mixes that are aged at the compaction temperature for two hours and compacted by a linear kneading compactor. In this study, mixes were aged at 135°C for four hours and compacted by a rolling wheel compactor. It is believed that the procedure used in this study can produce specimens that simulate field conditions well.

5.1.3 Test Procedure

The test procedure selected in this study is summarized below:

1. Put specimens in the mounting trays and fill the gaps with plaster of paris slurry (water-to-plaster ratio 1:1). Allow the plaster at least one hour to set.
2. Install the trays in the testing position on the HWTD.
3. Start the computer and run the software.
4. Enter the project information and set the test parameters: water temperature (50°C), wheel pass speed (52 RPM), maximum rut depth (20 mm), and data collection interval.
5. Wait a half hour after the water temperature reaches 50°C.
6. Lower the lever arms so that the wheels rest on the specimens. Run the wheels and continue until either the required test period has elapsed or the maximum rut depth is exceeded for both specimens.

This procedure is similar to those used by most researchers/agencies (Aschenbrener et al 1994; Izzo and Tahmoressi 1999), with the exception that the water temperature is fixed at 50°C for all mixes. Some states (e.g., Colorado and Utah) suggest varying the water temperature depending on the binder grade, while other states (e.g., Texas) use a fixed temperature of 50°C. The two asphalts used in the laboratory-fabricated specimens, AR-4000 and PBA-6a, tend to grade out as PG 64-10 and PG 64-28 respectively, based on the Caltrans PG binder map (Santucci 2005). Based on the high temperature (64°C) of their PG grade, therefore, a same temperature seemed appropriate. For cores taken from the field, since most of them were from climate regions with the same designated high temperature (64°C) of the PG grade, a same test temperature was also used.

5.2 Experimental Design

In this study, the HWTD test was evaluated from both the laboratory and the field perspectives. In the laboratory evaluation, the HWTD test was performed on mixes with known relative performance and specimens prepared in the laboratory; in the field evaluation, the HWTD test was performed on cores taken from in-service pavement sections with observed performance information in terms of moisture damage.

5.2.1 Evaluation by Laboratory Specimens

The factors included in the laboratory evaluation are as follows:

Two aggregate types: A and B.

Two binder types: AR-4000 and PBA-6a.

Three additive conditions: nil, hydrated lime (1.4 percent by weight of dry aggregates), and liquid antistripping Agent A (0.75 percent by weight of asphalt).

As noted in Section 2.1, Aggregate B has better compatibility with asphalt than Aggregate A, mixes containing the PBA-6a binder have better moisture resistance than mixes containing the AR-4000 binder, and treated mixes have better moisture resistance than untreated mixes. A full factorial design for all three factors was used and two replicates were tested at each combination of factor levels, which required a total of 24 specimens. All specimens have the 19-mm nominal maximum medium dense gradation and were compacted to air-void content between 6 percent and 8 percent, a range now considered typical for newly constructed pavements in the field.

5.2.2 Evaluation by Field Cores

As noted in Section 3.2.3, eight wet cores (0.15 m in diameter) were generally taken from each of the pavement sections selected for intensive survey. Four of them, two in the wheelpath and two between the wheelpaths, were used for the HWTD test. In a few cases where wet cores were only taken from between the wheelpaths, four cores from between the wheelpaths were tested. Two cores from the same location (i.e., in the wheelpath or between the wheelpaths) were shaved and combined to form one test sample. Excluding a few sites where insufficient cores were taken due to short traffic closure windows or equipment failure, around 210 cores (105 samples) were tested for 57 pavement mixes. The air-void content of each specimen was measured before the HWTD test.

It has to be pointed out that testing on cores from in-service pavements is not a regular procedure in the HWTD test. The HWTD is intended to test laboratory-fabricated specimens or newly-placed hot mixes. Field cores have inevitably experienced certain traffic and environmental conditioning at the time of testing, so their response may be different from that of the fresh mixes. The work in this study is just a starting point for HWTD validation using the resources currently available.

5.3 Results and Analysis

The response variable in the HWTD test is the rut depth recorded at 11 points along the wheelpath on the specimen. These data were recorded automatically and saved in a Microsoft *Access* database. The rut depths at the 11 points were averaged to represent the overall rut depth on the specimen. Because the steel wheel vibrated vertically during the test, noise was introduced into the rut depth readings. This noise was reduced by taking moving averages of the readings along the time axis. In this study, the following formulae were used for taking moving averages:

$$d_{it} = 0.40d_{it} + 0.25d_{i(t+1)} + 0.15d_{i(t+2)} + 0.10d_{i(t+3)} + 0.10d_{i(t+4)} \qquad (1 \le t \le 5) \qquad \textbf{(5-1)}$$

$$\begin{aligned} d_{it} = {} & 0.05d_{i(t-5)} + 0.05d_{i(t-4)} + 0.075d_{i(t-3)} + 0.075d_{i(t-2)} + 0.15d_{i(t-1)} \\ & + 0.20d_{it} + 0.15d_{i(t+1)} + 0.075d_{i(t+2)} + 0.075d_{i(t+3)} \\ & + +0.05d_{i(t+4)} + 0.05d_{i(t+5)} \qquad (5 < t < 19995) \end{aligned} \qquad \textbf{(5-2)}$$

$$d_{it} = 0.40d_{it} + 0.25d_{i(t-1)} + 0.15d_{i(t-2)} + 0.10d_{i(t-3)} + 0.10d_{i(t-4)} \qquad (19995 \le t \le 20000) \qquad \textbf{(5-3)}$$

where d_{it} = rut depth at point i at tth wheel pass, $i = 1,2,3\cdots 11$. The coefficients for the d_{it}'s were determined by trial and error to best remove noise and retain useful information.

On a typical rut progression curve, as shown in Figure 5-3, several characteristic variables are generally defined, including creep slope, stripping slope, and stripping inflection point. The creep slope relates to rutting from plastic flow and is defined as the rut depth per wheel pass in the linear region of the rut progression curve after the postcompaction stage. The stripping slope is related to moisture damage and is defined as the rut depth per wheel pass in the linear region of the rut progression curve after the stripping inflection point. For convenience, the creep and stripping slopes are also often defined as the number of passes per unit of rut depth. The stripping inflection point is the number of wheel passes at which the slope of the rut progression curve shows an abrupt increase. It is related to the start of significant moisture damage in the mix.

Not all rut progression curves have the three characteristic variables. Some mixes will show the stripping slope immediately after the postcompaction stage, while others mixes will only show the creep slope. Specification of the test result is often defined by the rut depth. The City of Hamburg requires the rut depth at 20,000 passes to be less than 4 mm to accept a mix. However, research done in Colorado showed that this criterion was too stringent, and it was suggested that a rut depth of 10 mm after 20,000 passes or 4 mm after 10,000 passes be used instead (Aschenbrener et al 1994). The Texas Department of Transportation (TxDOT) uses 12.5 mm after 20,000 passes as the criterion for stone mastic asphalt (SMA) mixes, and limits the minimum number of passes at 12.5 mm rut depth for dense-graded hot-mix asphalt.

5.3.1 Evaluation by Laboratory Specimens

The rut progression curve of each specimen is graphed in Figure 5-4 through Figure 5-9. As can be seen, for most specimens the rut depth developed quickly in the initial few thousands of wheel passes. This is due to the postcompaction of the mixture under the steel wheel load, referred to as "bedding in" in Heavy Vehicle Simulator testing. Densification and reduction of air-void volume is the main reason of this first-stage permanent vertical deformation in the wheelpath. After this stage, the rut depth curves tended to be flat with a relatively constant slope. At this point, the further development of rut depth is mainly due to the permanent shear deformation in the asphalt concrete under and around the wheelpath. Bulging on both sides of some of the mixture specimens, evidence of shear deformation, was always observed during this stage. For some specimens, the slope of the rut progression curve changed significantly after a certain number of wheel passes.

The three characteristic variables and the rut depths at 10,000 and 20,000 wheel passes are shown in Table 5.1. For specimens whose test was terminated before reaching 20,000 passes, the rut depth at 20,000 passes was obtained by linear extrapolation. As can be seen, mixes containing the two different binders showed significantly different responses in the HWTD test. Most mixes containing the AR-4000 binder—except the untreated mix AAN—did not show moisture damage during the test, as evidenced by the fact that the stripping inflection point was larger than 20,000 passes. The rut depths at 20,000 passes were all smaller than 10 mm. On the other hand, poor results occurred in nearly all mixes containing the PBA-6a binder. The rut depths at 20,000 wheel passes were generally significantly larger than 10 mm. Based upon this result, the HWTD test showed that mixes containing the PBA-6a binder would be more susceptible to moisture damage than the mixes containing the AR-4000 binder, which is contrary to prior experience. As discussed in Chapter 2, PBA-6a binder has been used as one of the measures to reduce moisture damage in some regions of California. One possible reason for the contrary result in the HWTD test might be the low stiffness of mixes containing the PBA-6a binder. As an example, Chapter 6 shows that the flexural dynamic modulus measured on fatigue beam specimens at 20°C is about 9900 MPa and 1100 MPa for the mixes containing AR-4000 binder and PBA-6a binder, respectively. Low stiffness led to high plastic flow and deep ruts in the specimens, as shown by the significantly larger creep slope in Table 5.1. The mix along the wheelpath also became loose, falling into the wheelpath and ground by the steel wheel, and produced fines in the water. Therefore, the poor results from mixes containing PBA-6a binder are not necessarily related to moisture damage.

It is interesting to note that the PBA-6a binder showed superior rut resistance under dry conditions under both Repeated Simple Shear Testing at Constant Height, and Heavy Vehicles Simulator testing, although with a different aggregate and binder content (Pavement Research Center 1999). This is an indication that the use of the steel wheels of the HWTD for rut resistance evaluation should be approached with caution as opposed to moisture damage evaluation.

Analysis of variance (ANOVA) was performed to evaluate the capability of HWTD to distinguish aggregates and treatments with different moisture sensitivities. Two variables were used as response variables: rut depth at 10,000 passes (Rut10k), and rut depth at 20,000 passes (Rut20k). A saturated model for a $2 \times 2 \times 3$ design was selected for the analysis, as shown below:

$$d_{ijk} = \mu + \alpha_i + \beta_j + \gamma_k + (\alpha\beta)_{ij} + (\alpha\gamma)_{ik} + (\beta\gamma)_{jk} + (\alpha\beta\gamma)_{ijk} + \varepsilon_{ijk} \qquad \textbf{(5-4)}$$

where,

d_{ijk} = rut depth at 10,000 (or 20,000) passes for mix with type i aggregate, type j binder and treated with additive k;

μ = overall mean effect, α_i = main effect of aggregate i;

β_j = main effect of binder j, γ_k = main effect of treatment k;

$(\alpha\beta)_{ij}$ =effect of interaction between aggregate and binder;

$(\alpha\gamma)_{ik}$ = effect of interaction between aggregate and treatment;

$(\beta\gamma)_{jk}$ = effect of interaction between binder and treatment;

$(\alpha\beta\gamma)_{ijk}$ = effect of interaction among aggregate, binder and treatment;

ε_{ijk} = random error component.

Rut Depth at 10,000 Passes

Before examining the ANOVA table, it is worthwhile looking at some simple plots. The boxplot for the observations at each level of each factor is shown in Figure 5-10a. It appears that the variances of various groups of observations are significantly different. Plot of residuals versus fitted values from estimate of the model (5-4) further indicates that the variance of the error term increases with response variable (Figure 5-11a). This violates the assumption of constant variance in the ANOVA model. A variance-stabilizing transformation is needed to correct this violation. Power transformation is applied in this analysis, following a procedure recommended by Montgomery (1991), which is summarized below.

Suppose the transformation is a power of the original data, $y^* = y^\lambda$, and the standard deviation of y is proportional to a power of the mean of y, $\sigma_y \propto \mu^\alpha$, then the standard deviation of y^* is proportional to a power of the mean of y, say $\sigma_{y^*} \propto \mu^{\lambda+\alpha-1}$. Therefore, if $\lambda = 1-\alpha$, the variance of the transformed data y^* becomes constant. Here α is empirically estimated from the data. Since in the ith treatment combination $\sigma_{y_i} \propto \mu_i^\alpha = \theta\mu_i^\alpha$, where θ is a constant of proportionality, we may take logarithms to obtain $\log\sigma_{y_i} = \log\theta + \alpha\log\mu_i$. Therefore, a plot of $\log\sigma_{y_i}$ versus $\log\mu_i$ would be a straight line with slope α. Substitute σ_{y_i} and μ_i with the standard deviation S_i and the average $\bar{y}_{i.}$ of the ith treatment combination, α can be estimated.

Following the above procedure, a reciprocal square root transformation was applied to the rut depth at 10,000 passes. The boxplots (Figure 5-10b) show that the variances of various groups of observations are broadly constant, as also evidenced in the residual plot (Figure 5-11b). The ANOVA table based upon this transformed data is shown in Table 5.2. As can be seen, the main effect and interaction of binder type and treatment method are significant at the 95 percent confidence level, while the aggregate type is insignificant. A check of the test results showed that mixes treated with hydrated lime had smaller rut depths than mixes treated with liquid antistripping Agent A, while the latter showed smaller rut depths than the untreated mixes. This is consistent with prior knowledge.

Rut Depth at 20,000 Passes

Following the same procedure of analysis for the rut depth at 10,000 passes, a log transformation was applied to the rut depth at 20,000 passes to stabilize the variance. The boxplots and residual plots before and after the transformation are shown in Figure 5-12 and Figure 5-13 respectively. The ANOVA table based upon

this transformed data is shown in Table 5.3. As can be seen, the main effect and interaction of binder type and treatment method are significant at the 95 percent confidence level, while the aggregate type is insignificant. The same conclusions can be obtained as those based on the rut depth at 10,000 passes.

As a summary, the default test procedure performed on the laboratory fabricated specimens did not distinguish the two aggregates used in this study and showed worse results for mixes containing the PBA-6a binder, but gave a relative ranking of mixes with different treatments that was consistent with engineering experience. Moreover, the same inference can be obtained from rut depths measured at 10,000 wheel passes and 20,000 passes. Previous research has showed that water temperature has significant effects on the HWTD test results and suggested temperatures adjusted for different grades of asphalt (Aschenbrener et al 1993; Izzo et al 1999). It seems that 50°C may be too extreme for testing mixes with PBA-6a. A lower temperature may be more appropriate. In retrospect, PBA-6a asphalt is typically used in regions where the high temperature PG grade is 58 based on the software *LTPPBind.* Caltrans raised this high temperature to 64 in order to make a workable number of PG asphalts for the whole state. The selection of test temperature then should be based on the actual climate region rather than designated PG grade.

5.3.2 Evaluation by Field Cores

The HWTD test results from the field cores are summarized in Table 5.4, in which the air-void content for each sample is the average of two cores combined into that sample. The performance of each mix is shown in Table 5.5, along with other supplementary information such as binder type, traffic, and weather data. The mix performance in terms of moisture damage was determined solely based on visual inspection of dry core conditions, with the emphasis put on moisture-related distresses (e.g., stripping). The mix performance was evaluated on a scale of ordered discrete values, as shown in Table 5.6.

Although two replicates were tested for each pavement section, generally one sample was from between the wheelpaths and the other was from in the wheelpath, which might lead to different test results. A comparison of the HWTD test results from both samples were made to check this point, as is summarized in Table 5.7. In the comparison, stripping inflection points greater than 20,000 were all treated as 20,000, and nonexistent stripping slopes were all treated as zero. Table 5.7 shows that there is no significant difference between samples from in the wheelpath and between the wheelpaths based on the stripping inflection point or stripping slope, but samples from between the wheelpaths tend to have smaller rut depth than samples from in the wheelpath, as is also shown in Figure 5-14. It is believed that samples from between the wheelpaths receive much less traffic loading than samples from in the wheelpath so their conditions should be closer to those of the newly constructed mixes. Therefore, results from the samples between the wheelpaths were used for further analysis.

The relationship between mix performance rating and HWTD results are shown in Figure 5-15 through Figure 5-17 for stripping inflection point, stripping slope, and rut depth at 20,000 passes, respectively. No definite correlation is observed in these figures. In particular, all three measured parameters are broadly spread out at performance rating 2 (Fair). If the 10-mm pass-fail criterion as suggested by Colorado Department of Transportation (CDOT) is used for the rut depth after 20,000 passes, seven out of eight good mixes, 21 out of 39 fair mixes, two out of five poor mixes, and one out of five very poor mixes will pass, as shown in Figure 5-17. Similar conclusions can be obtained if 10,000 passes is used as the pass-fail criterion for the stripping inflection point, or 1 mm per 1,000 passes for the stripping slope (see Figure 5-15 and Figure 5-16). For the good mixes, the HWTD test gives satisfactory results. The only one that failed has a rut depth of 10.2 mm, which is marginal. For the fair mixes, the HWTD test gave failing ("false negative") results for about half. This is not surprising for two reasons: (1) similar observations have been noticed by other researchers (Aschenbrener et al 1994); (2) those fair mixes that failed the test are generally four to eight years old and may show unacceptable moisture damage in the late stage of their service life. For the poor or very poor mixes, most of them showed poor results in the HWTD test, but there are three mixes showing little damage in the test (i.e., "false positive" results). Examination of these three mixes revealed that they were from northern California and contained the same aggregate but different mix designs. The aggregate is of volcanic origin and

of basaltic nature. This aggregate is not used in asphalt pavements any more, mostly due to the stripping problems that have occurred. The aggregate has very good angularity, which may contribute to the small rut depths in the HWTD test, but the exact reason for their good performance in the HWTD test is still unclear.

The field mixes used for the HWTD test have different mix types, binder types, and in-situ air-void content, which might have significant effects on the test results. The data set in Table 5.4 was reduced and split to exclude the possible confounding of these factors. Table 5.5 shows that most pavement sections use dense-graded mixes while a few others use gap-graded mixes, so further analysis was concentrated on the sections containing dense-graded mixes. The air-void content of the field cores varies from 3 percent to 13 percent, but no clear correlation was found between test results and the air-void content (Figure 5-20) so no correction of test results was made for this factor. As shown in the study on laboratory specimens, binder type significantly affects the HWTD test results. To exclude its potential confounding effect, the test data was divided into two subsets – sections containing conventional binders (AR-4000, AR8000, PBA-1, and others) and sections containing polymer modified binders (PBA-6a, PBA-7).

Figure 5-18 and Figure 5-19 show the relationship between rut depth at 20,000 passes and mix performance for the dense-graded mixes containing conventional binders and polymer modified binders respectively. Among the four poor or very poor mixes that contain the conventional binders, two of them showed rut depths at 20,000 passes smaller than 10 mm. As an example, one of the very poor sections, 2D19, is on Highway 139 in Modoc County (Table 3.2). This section was severely distressed at the time of the survey and the cores taken in the wheelpath showed totally stripped aggregates (Figure 5-21a). The HWTD test performed on the cores taken between the wheelpaths, however, showed a very small rut depth at 20,000 passes and no moisture damage (Figure 5-21b). For the mixes containing the polymer-modified binders, the correlation between test results and field performance is better. If 10-mm rut depth at 20,000 passes is used as the pass-fail criterion, three good mixes all pass and four poor or very poor mixes all fail (Figure 5-19).

Based on the test data in this study, the pass-fail criterion for each of three characteristic variables (stripping inflection point, stripping slope, and rut depth at 20,000 passes) may be improved by maximizing the number of sections (with performance ratings 1 and 2) passing by the criterion and the number of sections (with performance ratings 3 and 4) failing by the criterion, that is, by achieving the following objective:

$$\max \sum [IF(P \le 2,1,0) \times IF(C \ge T,1,-1) + IF(P \le 2,0,1) \times IF(C > T,-1,1)] \quad \textbf{(5-5)}$$

where,

P = performance rating,
C = criterion to be determined,
T = test result,
$IF(Logic, v2, v3)$ = a binary selection function: if the first logic operator is true, the function takes the value $v2$, otherwise it takes the value $v3$.

The optimization was performed separately for mixes containing the conventional binders and the polymer modified binders. The solutions were not unique. From conservative considerations, the values shown in Table 5.8 were recommended for the commonly used test procedure (as described in Section 5.1).

As a summary, the common HWTD test procedure performed on field cores gives satisfactory results for mixes with good performance, but may produce false negative results for mixes with fair performance. For mixes with poor or very poor performance, the test procedure can fail most of them, but may produce false positive results in a few particular cases.

As discussed before, the weakness of the field evaluation is that samples were taken from in-service pavements instead of freshly-placed or laboratory-fabricated ones. The response of field cores in the HWTD test may be different from that of fresh mixes due to environmental and traffic conditioning. In this study, the traffic-loading effect was reduced by analyzing results of samples from between the wheelpaths, but the environmental effect (e.g., binder aging) was not considered in the analysis. Aging may improve the moisture resistance of mixes, but it is unlikely to change dramatically the moisture sensitivities of mixes (i.e., change a

moisture sensitive mix to a moisture insensitive mix). The conclusions of this field evaluation, therefore, should largely remain valid.

5.4 Summary and Discussion

This chapter attempted to evaluate the effectiveness of a default HWTD test procedure by both laboratory-fabricated specimens and field cores. It was found that the procedure can correctly identify the effect of antistripping additives, but may underestimate the performance of mixes containing soft binders at the fixed test temperature 50°C. The correlation between test results and field performance seems acceptable except that the test procedure may fail mixes that perform well in the field and, in a very few cases, give false positive results. It has to be mentioned that the above correlation is limited to testing with in-service field cores. Air-void contents and prior environmental and traffic conditioning were all uncontrollable in the field cores and inevitably increase the variability of the test results. In retrospect, making the following changes to the test procedure might improve the moisture damage results:

1. Use various water temperatures for different binder grades based on the environmental regions where the mixes are used. For mixes with low stiffness, such as those containing the PBA-6a binder, a temperature lower than 50°C may be used so that the excess plastic flow not related to moisture damage can be reduced. This approach has been suggested by some researchers and documented in some state test procedures (e.g., Colorado).
2. Run the HWTD test in dry condition when poor results are obtained from the regular test. By this approach, the confounding effects of aggregate structure, binder stiffness, and others can be minimized, and the effect of moisture can be clearly defined by a ratio or a difference of the test results under both conditions. This requires that the HWTD be capable of maintaining a high air temperature during the test, which can be achieved by adding an air-heating system and an environmental chamber to the device. The potential problem of steel wheels picking up mixes during the test may also need to be solved.

Table 5.1. HWTD Test Results on Laboratory Specimens

Specimen ID	Aggregate	Binder	Treatment	Creep Slope (mm/pass)	Stripping Inflection Point	Stripping Slope (mm/pass)	Rut Depth at 10000 Passes (mm)	Rut Depth at 20000 Passes (mm)
AAN3-1	A	AR-4000	Nil	-0.0001	9418	-0.0002	4.16	5.80
AAN2-2	A	AR-4000	Nil	-0.0002	13017	-0.0004	3.94	7.44
AAM1-2	A	AR-4000	Hydrate Lime	-0.0001	>20000	-	5.39	6.41
AAM1-1	A	AR-4000	Hydrate Lime	-0.0002	>20000	-	5.22	7.22
AALA2-2	A	AR-4000	Liquid A	-0.0002	>20000	-	5.81	7.84
AALA2-1	A	AR-4000	Liquid A	-0.0001	14232	-0.0003	3.90	5.60
BAN2-2	B	AR-4000	Nil	-0.0001	>20000	-	5.50	6.82
BAN2-1	B	AR-4000	Nil	-0.0002	>20000	-	6.59	8.85
BAM2-2	B	AR-4000	Hydrate Lime	-0.0001	>20000	-	5.21	6.56
BAM2-1	B	AR-4000	Hydrate Lime	-0.0002	>20000	-	5.82	7.32
BALA1-2	B	AR-4000	Liquid A	-0.0001	>20000	-	6.06	7.54
BALA1-1	B	AR-4000	Liquid A	-0.0001	>20000	-	5.31	6.86
APN1-2	A	PBA-6a	Nil	-0.0008	5136	-0.0024	19.06	42.77
APN1-1	A	PBA-6a	Nil	-0.0012	3836	-0.0022	20.68	41.81
APM3-1	A	PBA-6a	Hydrate Lime	-0.0003	4300	-0.0005	4.87	8.72
APM3-2	A	PBA-6a	Hydrate Lime	-0.0003	16000	-0.0005	6.07	11.61
APLA2-2	A	PBA-6a	Liquid A	-0.0006	4914	-0.0020	14.72	35.43
APLA2-1	A	PBA-6a	Liquid A	-0.0012	3162	-0.0023	20.34	43.98
BPN1-2	B	PBA-6a	Nil	-0.0008	9310	-0.0031	13.20	44.34
BPN1-1	B	PBA-6a	Nil	-0.0022	2653	-0.0034	34.42	68.42
BPM1-2	B	PBA-6a	Hydrate Lime	-0.0004	10741	-0.0010	7.96	17.07
BPM1-1	B	PBA-6a	Hydrate Lime	-0.0003	14886	-0.0006	5.83	10.39
BPLA1-2	B	PBA-6a	Liquid A	-0.0006	13684	-0.0010	8.94	17.58
BPLA1-1	B	PBA-6a	Liquid A	-0.0008	9255	-0.0019	13.24	31.69

Table 5.2. ANOVA of Transformed Rut Depth at 10,000 Passes

Factor	Degree of Freedom	Sum of Squares	Mean Square	F-value	p-value
Aggregate	1	0.00244	0.00244	1.7597	0.2094
Binder	1	0.11740	0.11740	84.8131	0.0000
Treatment	2	0.02843	0.01422	10.2700	0.0025
Aggregate:Binder	1	0.00396	0.00396	2.8591	0.1166
Aggregate:Treatment	2	0.00335	0.00168	1.2104	0.3320
Binder:Treatment	2	0.04451	0.02225	16.0764	0.0004
Aggregate:Binder: Treatment	2	0.00597	0.00298	2.1553	0.1586
Residuals	12	0.01661	0.00138		

Table 5.3. ANOVA of Transformed Rut Depth at 20,000 Passes

Factor	Degree of Freedom	Sum of Squares	Mean Square	F-value	p-value
Aggregate	1	0.01485	0.01485	0.2998	0.5941
Binder	1	10.24032	10.24032	206.6553	<0.0001
Treatment	2	2.23088	1.11544	22.5102	0.0001
Aggregate:Binder	1	0.00943	0.00943	0.1902	0.6705
Aggregate:Treatment	2	0.21656	0.10828	2.1852	0.1551
Binder:Treatment	2	2.02400	1.01200	20.4227	0.0001
Aggregate:Binder: Treatment	2	0.20727	0.10364	2.0914	0.1662
Residuals	12	0.59463	0.04955		

Table 5.4. HWTD Test Results from Field Cores

Section Code	Between the Wheelpaths					In the Wheelpath				
	Stripping Inflection Point	Stripping Slope (mm/passes)	Rut Depth at 10,000 Passes (mm)	Rut Depth at 20,000 Passes (mm)	Average Air-Void (%)	Stripping Inflection Point	Stripping Slope (mm/passes)	Rut Depth at 10,000 Passes (mm)	Rut Depth at 20,000 Passes (mm)	Average Air-Void (%)
1U1	7140	0.7	3.5	10.8	4.7	3680	1.2	10.4	22.2	1.6
1U2	3880	1.4	12.7	25.9	1.0	3660	2.1	17.9	39.0	4.5
1U2_1	>20,000	0.0	3.6	5.3	9.3	16000	0.3	3.0	5.2	6.7
1U3	7640	1.5	9.4	24.8	10.6					
Q2	5600	2.4	13.7	38.2	6.0	5900	3.8	18.1	56.5	6.2
Q3	13660	2.2	3.6	19.9	5.6	11000	1.5	5.7	20.6	6.8
2D19	>20,000	0.0	1.4	1.4	10.4					
2D20	>20,000	0.0	2.9	3.5	10.8					
2D21	>20,000	0.0	1.9	2.1	9.3	>20,000	-	1.8	2.3	9.6
2N2_1	3300	1.5	12.6	26.8	6.5					
2N3	>20,000	0.0	2.6	3.3	9.7					
2N5	12701	0.3	3.3	6.6	4.2	10820	1.0	4.9	13.6	3.8
Q10	7000	0.5	4.1	9.1	4.2	>20,000	-	3.3	3.8	8.2
Q8	11100	0.6	4.5	10.5	6.2	11800	0.5	3.6	8.4	5.9
4U1	>20,000	0.0	4.0	5.0	8.8					
Q27	12360	0.1	3.5	4.0	6.1	11020	1.8	4.0	19.7	4.7
Q29	5540	0.8	7.1	14.8	4.5	13000	0.1	2.4	3.0	2.2
Q32	13720	0.3	4.2	7.1	7.5	>20,000	-	4.0	4.9	7.2
5N1	1480	2.9	27.9	56.9	8.2					
5N10	4760	1.9	13.8	34.0	8.3	8120	0.5	4.0	9.5	5.3
Q35	18980	0.3	3.5	6.3	10.0	>20,000	-	3.1	3.8	

Table 5.4. HWTD Test Results from Field Cores *(cont'd.)*

Section Code	Between the Wheelpaths					In the Wheelpath				
	Stripping Inflection Point	Stripping Slope (mm/passes)	Rut Depth at 10,000 Passes (mm)	Rut Depth at 20,000 Passes (mm)	Average Air-Void (%)	Stripping Inflection Point	Stripping Slope (mm/passes)	Rut Depth at 10,000 Passes (mm)	Rut Depth at 20,000 Passes (mm)	Average Air-Void (%)
Q36	16100	0.5	2.9	5.6	3.8	4500	1.6	14.0	30.3	5.4
Q38	11200	0.3	2.7	5.2	5.0	4000	0.9	8.6	17.6	4.5
W5	11619	0.4	3.5	6.9	5.8	9939	0.7	6.7	13.5	6.1
W7	5802	1.5	10.1	11.7	12.1					
6D11	4281	2.1	14.2	35.2	8.4	6540	1.8	11.2	30.1	7.9
6D24	>20,000	0.0	1.7	2.2	3.7	>20,000	-	2.3	2.5	2.3
6D5	>20,000	0.0	1.6	2.0	7.3	>20,000	-	2.2	2.7	8.2
6N12/13	>20,000	0.0	2.8	3.5	10.9	>20,000	-	2.3	3.0	9.0
6N19	>20,000	0.0	2.3	3.0	9.0	>20,000	-	3.2	4.3	6.5
6N20	7160	1.4	8.9	23.3	12.8	7640	0.9	4.9	15.2	11.5
Q41	>20,000	0.0	2.0	2.3	5.5	>20,000	-	2.6	3.2	3.6
R7	16000	0.4	2.5	4.7	7.8	9200	0.7	4.5	11.2	7.4
7N1	8954	1.8	8.2	26.5	12.7	4767	1.1	8.0	19.4	9.6
7N2	>20,000	0.0	4.5	5.7	9.2	>20,000	-	1.7	2.2	8.0
7N3	15587	1.3	2.6	8.8		16670	0.8	3.3	7.7	
7N4	>20,000	0.0	2.7	5.7		>20,000	-	1.5	2.2	
8N4	8400	0.9	3.6	11.4	8.4	3300	2.0	17.9	38.4	5.7
8N5	>20,000	0.0	1.5	2.5	3.7	>20,000	-	2.4	3.2	2.7
Q54	>20,000	0.0	1.7	2.8	8.8	>20,000	-	2.4	2.7	5.7
Q62	15000	2.6	3.1	15.1	6.6	7700	1.1	4.8	15.3	3.2
Q70	6840	1.8	5.3	15.4	5.0	5780	1.0	12.0	30.5	10.1

Table 5.4. HWTD Test Results from Field Cores (cont'd.)

Section Code	Between the Wheelpaths					In the Wheelpath				
	Stripping Inflection Point	Stripping Slope (mm/passes)	Rut Depth at 10,000 Passes (mm)	Rut Depth at 20,000 Passes (mm)	Average Air-Void (%)	Stripping Inflection Point	Stripping Slope (mm/passes)	Rut Depth at 10,000 Passes (mm)	Rut Depth at 20,000 Passes (mm)	Average Air-Void (%)
Q71	12020	0.3	1.7	4.0	6.9	>20,000	-	3.6	5.9	5.6
Q76	>20,000	0.0	0.9	1.1	7.9	14000	0.2	2.2	3.7	7.6
Q77	>20,000	0.0	2.5	3.6	8.8	>20,000	-	2.6	3.4	5.5
R11	6000	1.8	11.9	30.3	3.9	6200	3.0	15.6	46.1	3.7
R12	6900	2.7	13.3	40.2	6.2					
10N1	7318	1.0	7.2	17.3	7.7	1397	1.1	10.5	22.4	7.3
10U2	2000	2.5	22.2	47.1	5.2	1000	2.4	25.8	49.8	5.9
10U3	>20,000	0.0	2.3	2.0	6.4	2769	1.6	13.6	30.5	4.6
Q78	5974	1.7	9.2	26.5	4.6	9611	1.4	4.2	16.2	3.0
Q80	>20,000	0.0	13.7	17.7	6.9	>20,000	-	15.7	30.1	5.9
Q81	6237	0.6	5.7	10.6		>20,000	-	9.1	14.8	
Q82	2400	2.7	12.2	49.4	8.4	11000	0.6	1.5	8.5	3.9
Q83	>20,000	0.0	1.9	2.4	6.2	>20,000	-	2.3	2.9	6.2
R15	>20,000	0.0	2.6	3.6	6.3	>20,000	-	2.3	3.9	4.4
Q84	9864	0.5	3.6	10.2	5.1	11222	0.7	3.0	7.3	5.7

Table 5.5. Performance and Other Supplementary Information of Pavement Sections

Section Code	Mix Performance Rating	Mix Type	Binder Type	AADTT	Annual Rainfall (mm)	Freeze-Thaw Cycle	Degree Days >30	Age (year)
1U1	Fair	DGM	PBA-1	889	1440	29	196	5
1U2	Fair	DGM	PBA-1	809	1714	17	190	5
1U2_1	Fair	DGM	PBA-1	809	1714	17	190	5
1U3	Very Poor	DGC	AR-4000	1140	1376	21	85	9
Q2	Fair	DGM	PBA-6a	919	1679	19	184	7
Q3	Fair	DGM	PBA-6a	1510	1191	20	140	7
2D19	Very Poor	DG	AR-4000	297	294	160	85	13
2D20	Poor	RAC	PBA2	297	286	162	83	13
2D21	Good	PMAC	PBA6	381	286	162	83	13
2N2_1	Very Poor	DGM	PBA-6a	6321	1200	91	215	2
2N3	Poor	DG	AR-4000	297	379	161	108	7
2N5	Fair	DG	PBA-6a	868	504	139	159	
Q10	Fair	RAC	PBA-6B	868	524	154	105	6
Q8	Fair	DGM	PBA-6B	383	391	172	114	6
4U1	Fair	RAC		8730	605	16	395	7
Q27	Fair	DGC	AR-4000	1265	848.5	21.6	264	7
Q29	Fair	DGC	AR-4000	12103	412	8	87	7
Q32	Good	DGC	AR-4000	7728	412	4	53.8	7
5N1	Poor	DG	AR-8000	3397	394	37	404	7
5N10	Fair	DG	AR-8000	350	225	33	492	16
Q35	Fair	DGC	AR-8000	2060	399	18	193	6
Q36	Fair	DGM	AR-8000	29561	446	8	206	7
Q38	Fair	DGC	AR-8000	528	406	9	88	7
W5	Good	DGM	AR-4000	2136	382	18	157	4
W7	Fair	DGM	AR-4000	295	868	15	127	3
6D11	Fair	RAC	AR-4000	1175	333	37	590	5
6D24	Fair	DGC	AR-8000	5904	290	40	454	6
6D5	Fair	DGC	AR-8000	891	159	42	558	4
6N12/13	Fair	DGC	AR-8000	6851	216	24	670	7
6N19	Fair	DGC	AR-4000	320	861	87	281	5
6N20	Fair	RAC	AR-4000	260	264	30	644	5
Q41	Good	DG	AR-4000	729	266	28	554	7
R7	Fair	DGC	AR-4000	9880	306	24	653	4
7N1	Poor	RAC	PBA-6a	1643	337	0	57	6
7N2	Fair	DG	AR-4000	18036	430	0	326	7
7N3	Fair	DG	AR-4000	1425	408	0	266	3
7N4	Fair	DG	PBA-6a	2812	460	0	273	5

Table 5.5. Performance and Other Supplementary Information of Pavement Sections *(cont'd.)*

Section Code	Mix Performance Rating	Mix Type	Binder Type	AADTT	Annual Rainfall (mm)	Freeze-Thaw Cycle	Degree Days >30	Age (year)
8N4	Very Poor	DG	PBA-6a	4378	248	39	896	5
8N5	Good	DG	AR-4000	2702	194	25	810	
Q54	Fair	DG	AR-4000	545	256	64	567	8
Q62	Fair	DGC	PBA-6a	2446	200	48	752	4
Q70	Fair	DGM	PBA-6a	589	426	134	302	6
Q71	Good	DGC	PBA-7	705	134	53	904	6
Q76	Fair	DG	PBA-6a	612	187	63	457	7
Q77	Good	DG	PBA-7	616	297	65	52	7
R11	Fair	DG	PBA-6a	185	247	119	418	7
R12	Very Poor	DGM	PBA-6a	158	454	170	83	7
10N1	Fair	DG	AR-4000	221	1120	167	8	7
10U2	Poor	RAC		11220	357	16	461	7
10U3	Fair	DG	AR-4000	6102	307	19	471	7
Q78	Fair	DGM	AR-4000	501	379	17	445	6
Q80	Fair	RAC	PBA-6a	89	1065	74	141	7
Q81	Fair	DGM	AR-4000	238	961	158	19	7
Q82	Fair	DGM	PBA-6a	1768	78	7	1543	7
Q83	Fair	DGM	PBA-6a	318	678	52	272	7
R15	Fair	DGM	PBA-6a	669	365	6	118	7
Q84	Good	DG	AR-4000	16154	353	0	152	6

Table 5.6. Mix Performance Rating Scale

Performance Rating	Condition
1 (Good)	Core is intact without any distress.
2 (Fair)	Core is debonded, but only slight stripping exists on the debonded interfaces, or core is not bebonded but shows slight amount of bare aggregate or missing fines along the core sides.
3 (Poor)	Mix is weak, with severe loss of fines and 30%-60% stripping in the cores.
4 (Very Poor)	Core is disintegrated with over 60% stripping.

Table 5.7. Comparison of HWTD Test Results on Samples from Between the Wheelpaths and in the Wheelpaths

	Stripping Inflection Point	Stripping Slope	Rut Depth at 20,000 Passes
Between wheelpaths > In wheelpath	18	18	18
Between wheelpaths = In wheelpath	14	14	-
Between wheelpaths < In wheelpath	16	16	30
Total	48	48	48

Table 5.8. Recommended Pass-Fail Criteria for HWTD Test

Characteristic Variable	Mixes Containing the Conventional Binder	Mixes Containing the Polymer Modified Binder
Stripping Inflection Point, minimum	6,000	10,000
Stripping Slope (mm/1000 passes), maximum	1.0	0.8
Rut Depth at 20,000 passes (mm), maximum	12.0	11.0

Figure 5-1. Hamburg Wheel Tracking Device.

(a)

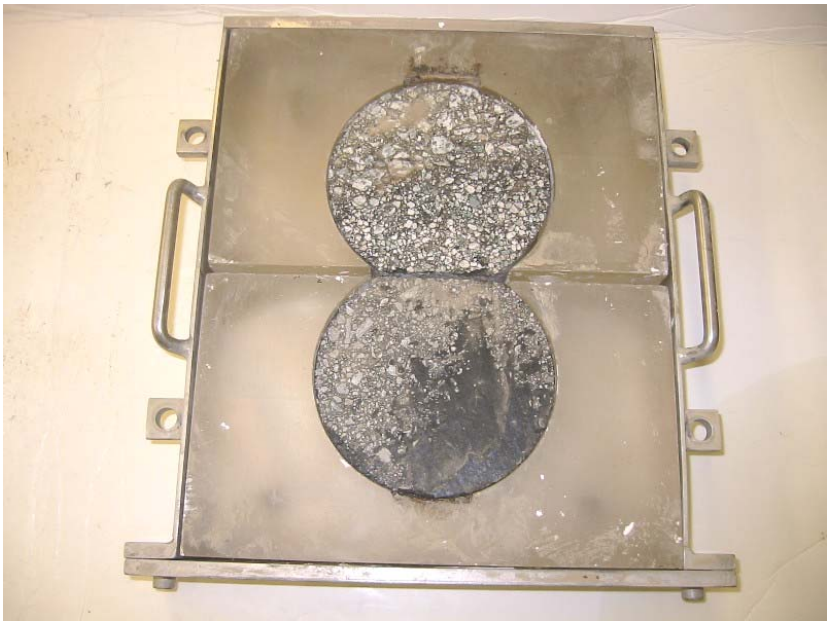

(b)

Figure 5-2. Hamburg Wheel Tracking Device test sample (a, slab sample; b, core sample).

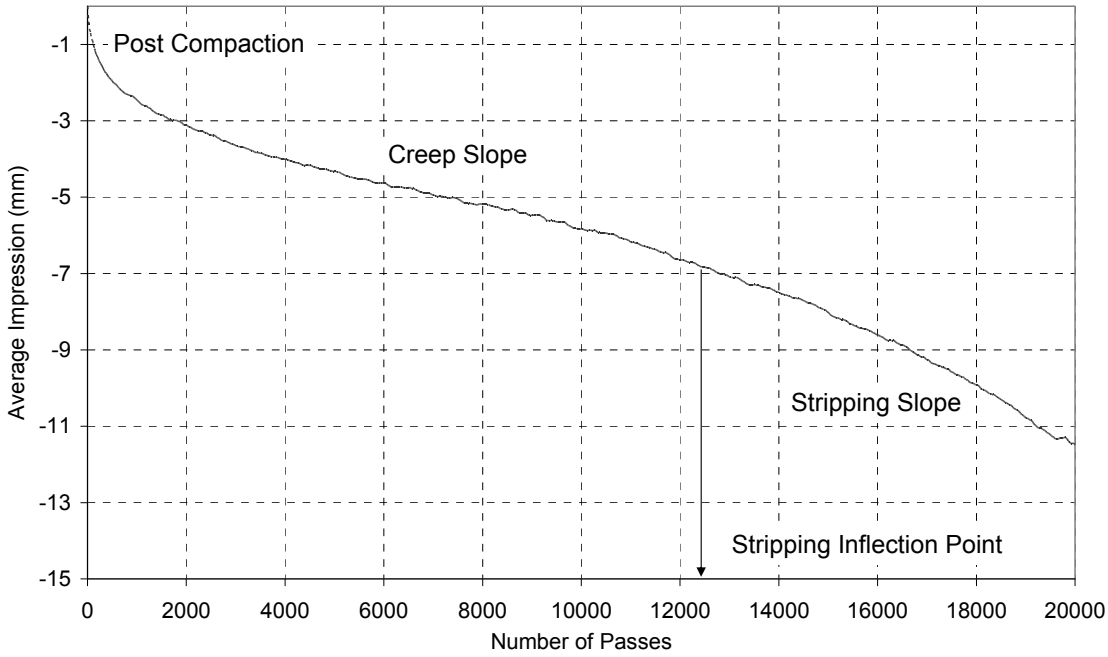

Figure 5-3. Typical HWTD test results.

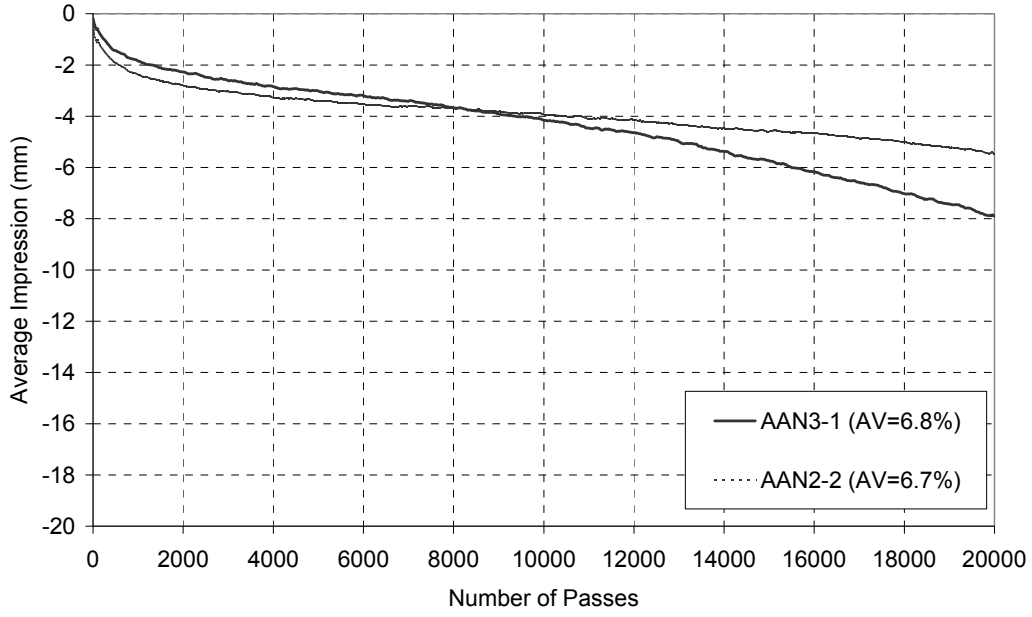

(a)

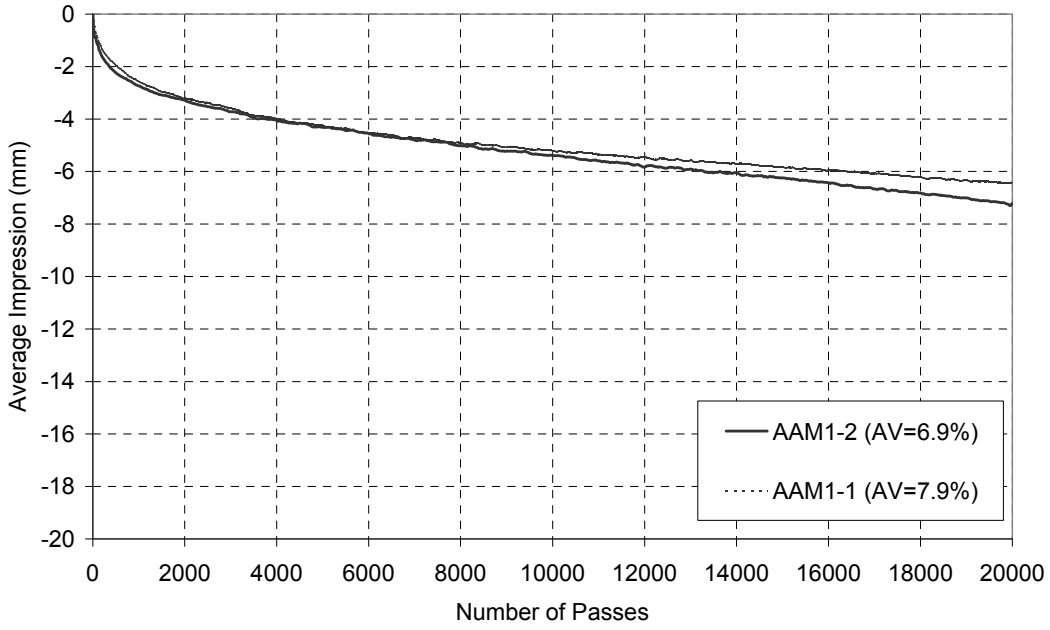

(b)

Figure 5-4. Rut progression curve (a, AAN; b, AAM).

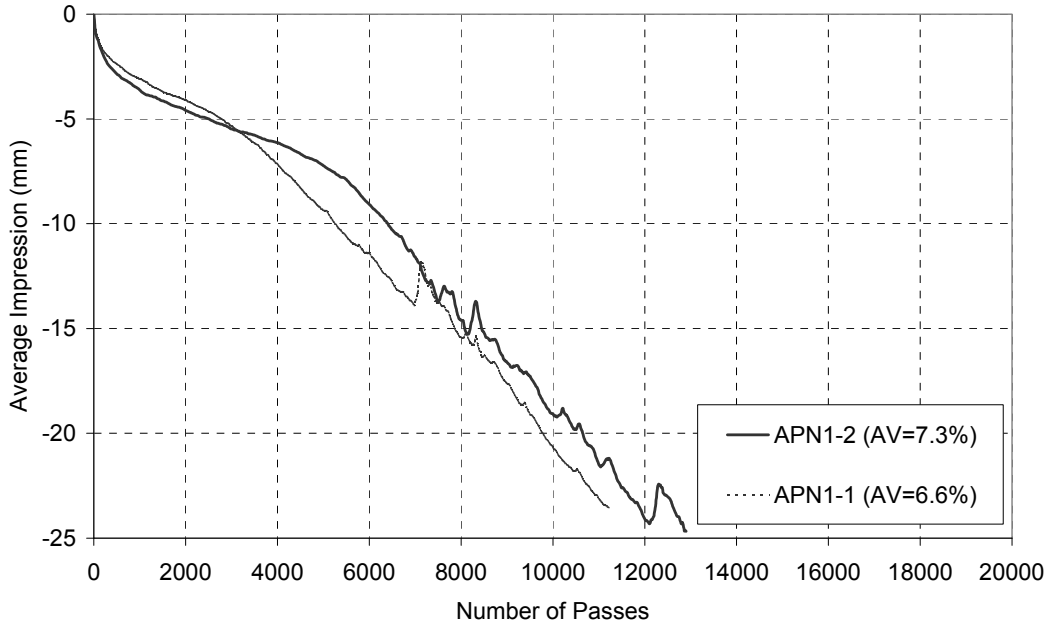

(a)

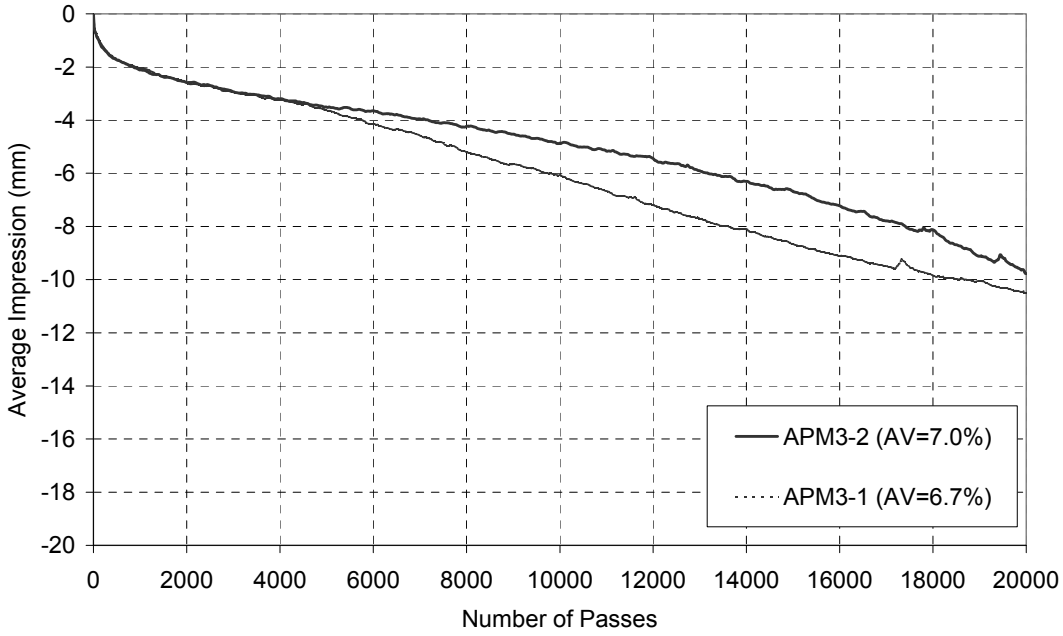

(b)

Figure 5-5. Rut progression curve (a, APN; b, APM).

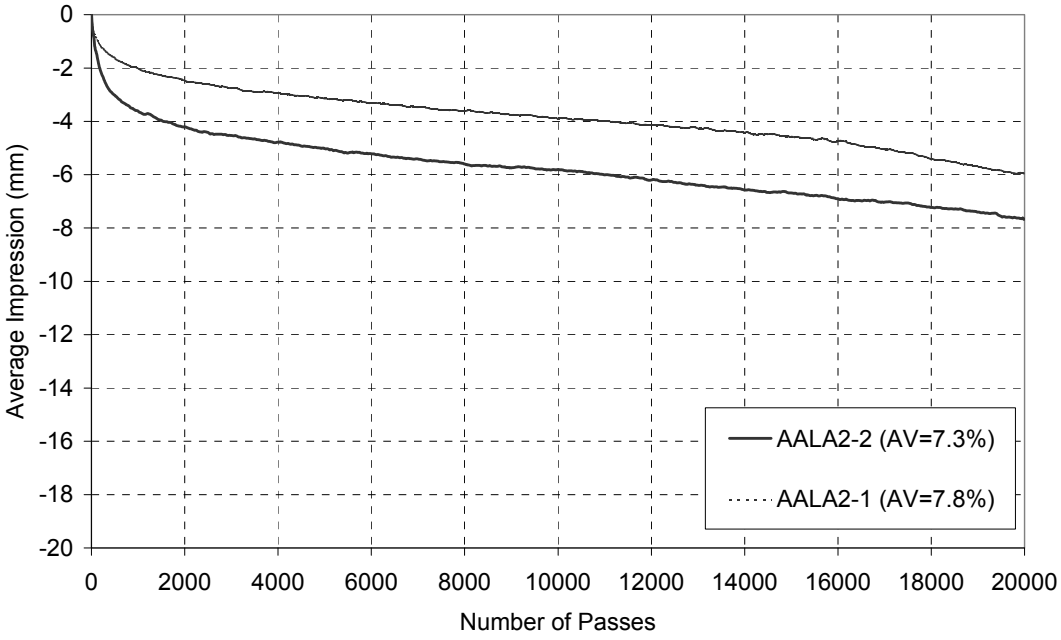

(a)

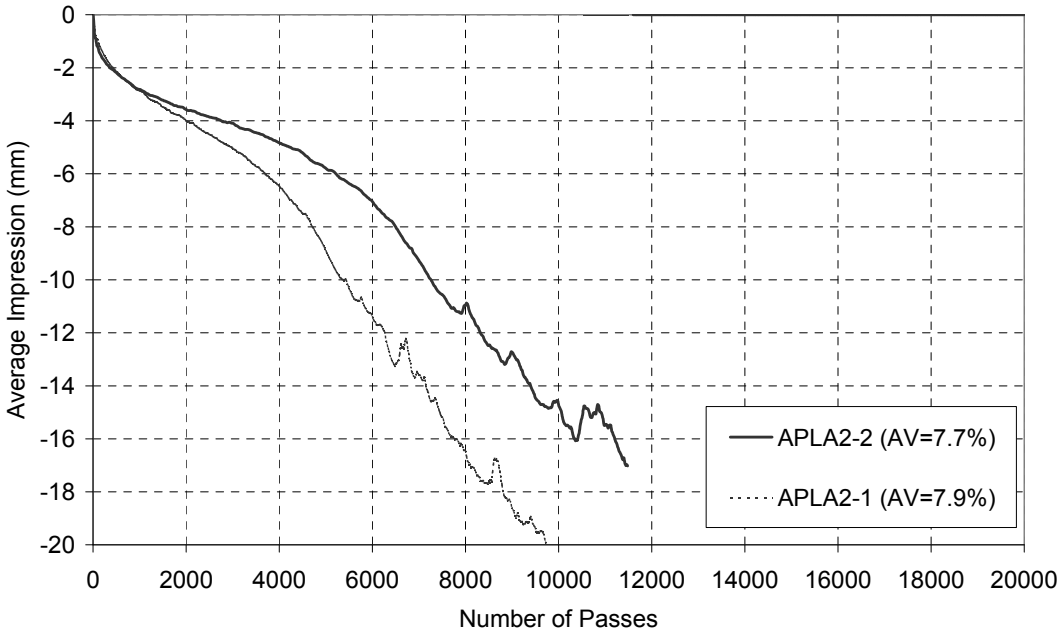

(b)

Figure 5-6. Rut progression curve (a, AALA; b, APLA).

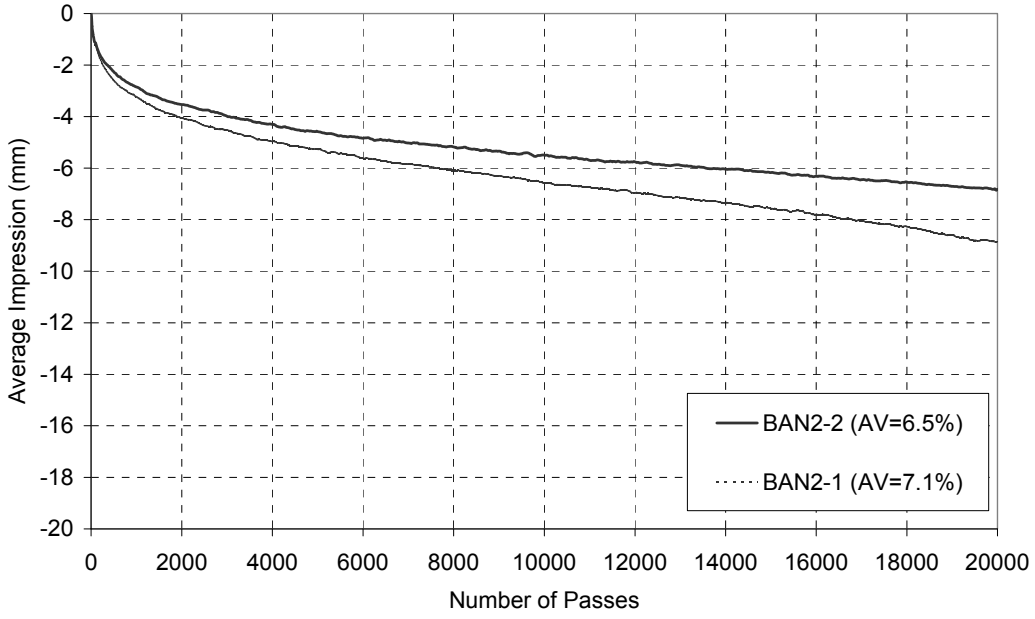

(a)

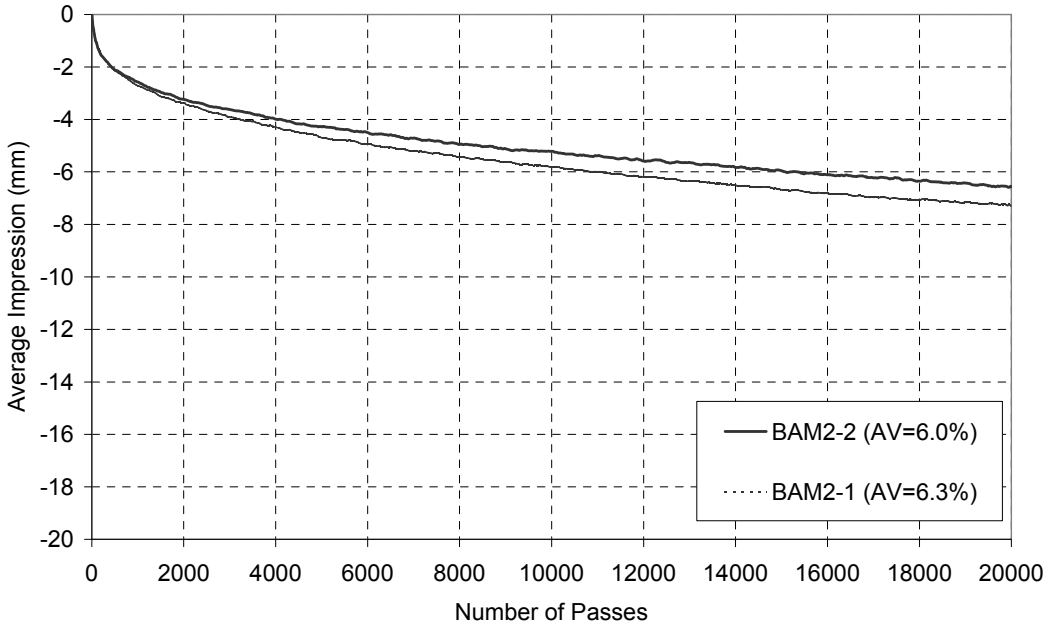

(b)

Figure 5-7. Rut progression curve (a, BAN; b, BAM).

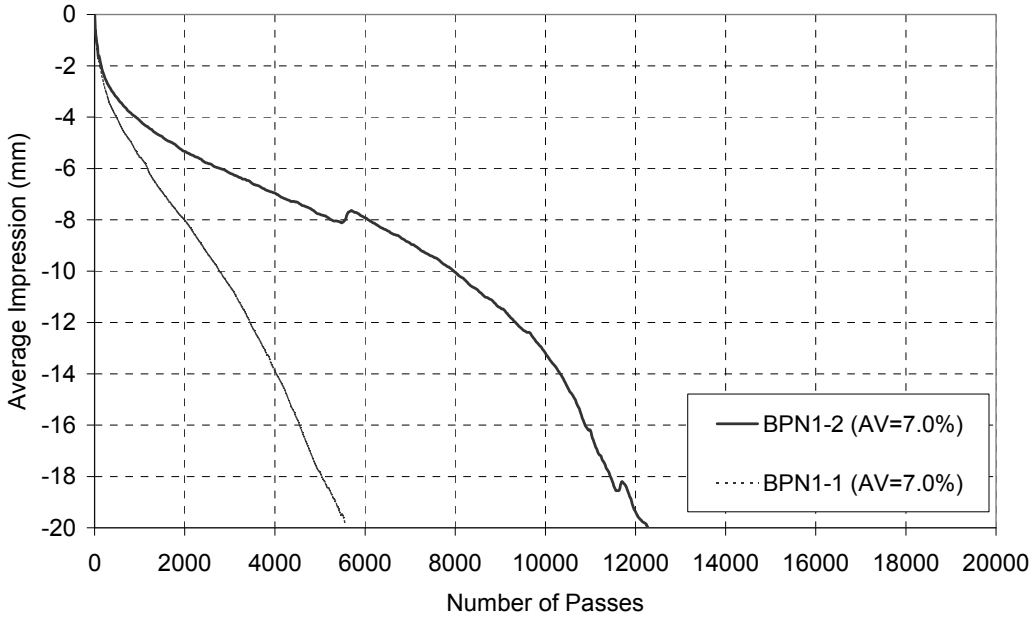

(a)

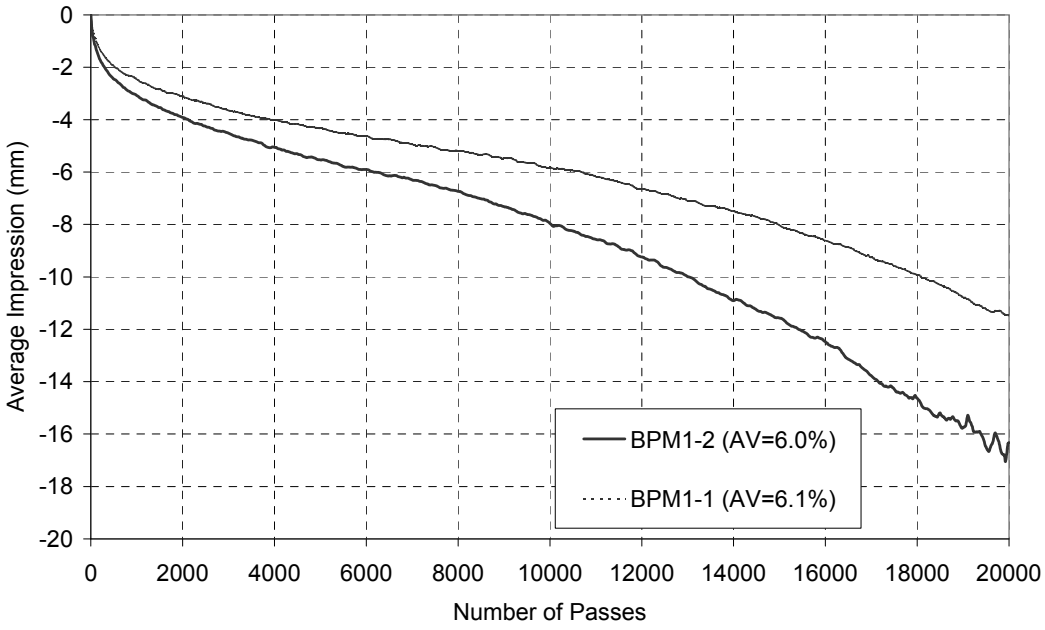

(b)

Figure 5-8. Rut progression curve (a, BPN; b, BPM).

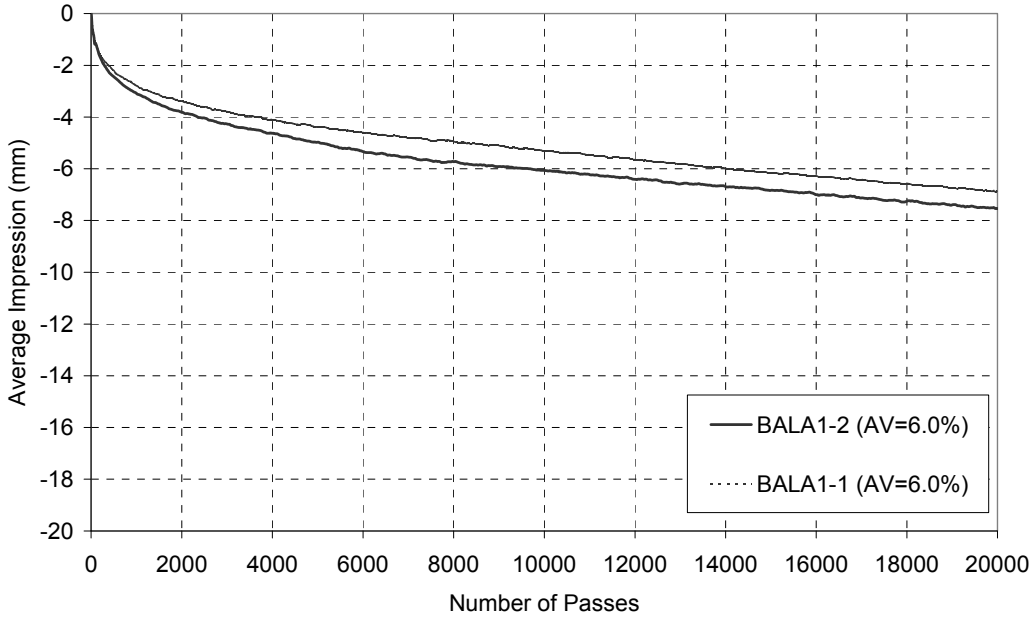

(a)

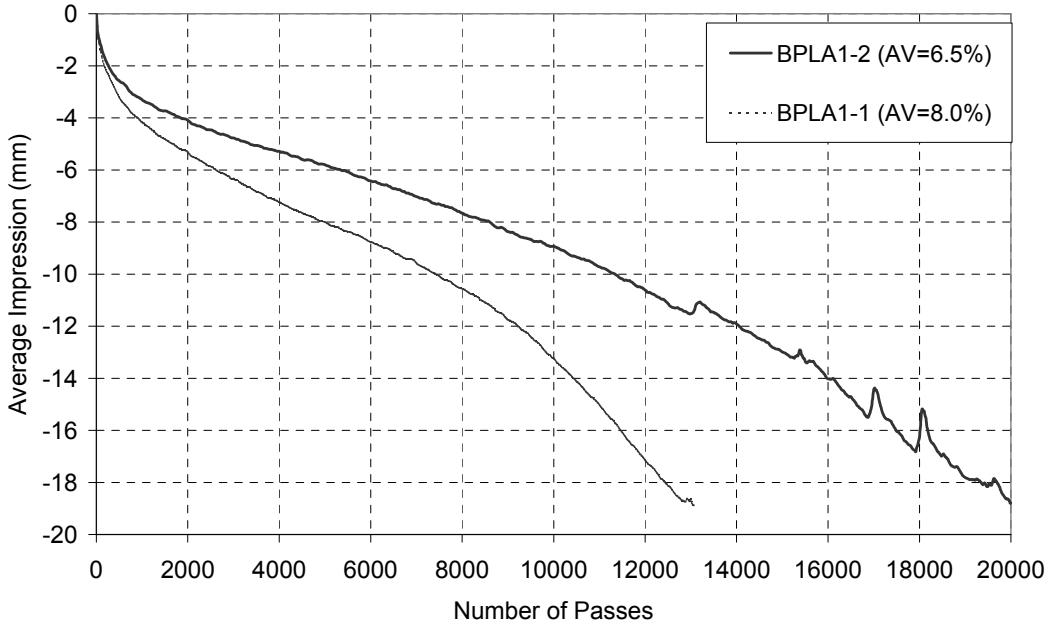

(b)

Figure 5-9. Rut progression curve (a, BALA; b, BPLA).

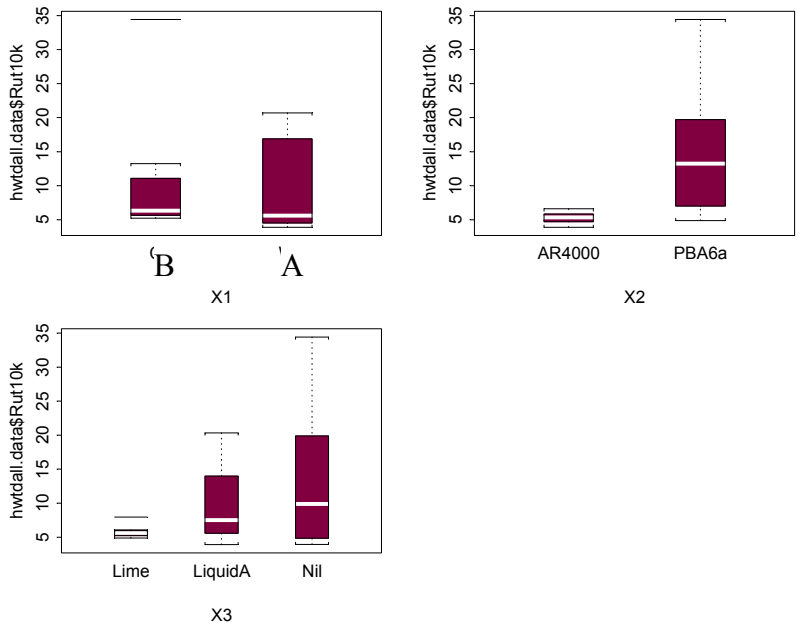

(a)

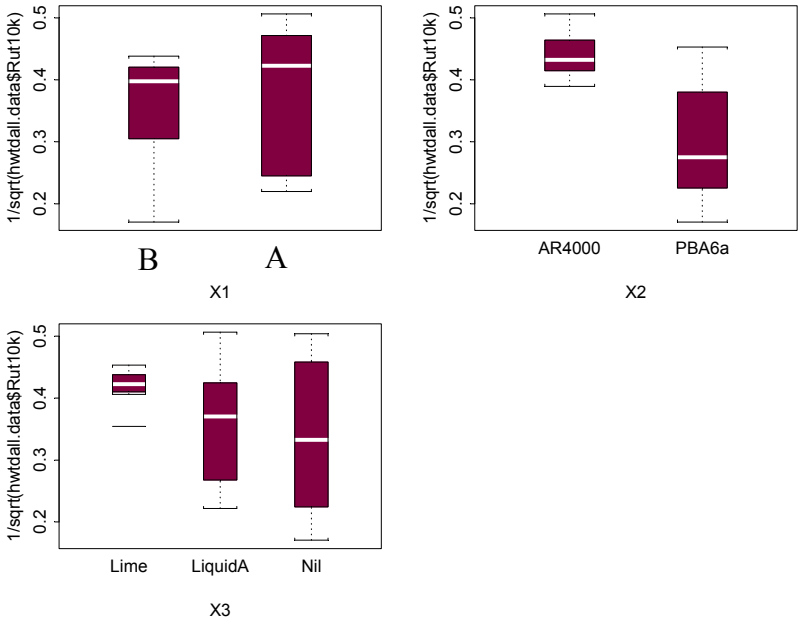

(b)

Figure 5-10. Box plots of rut depth at 10,000 passes for laboratory specimens (a, before variance-stabilizing transformation; b, after variance-stabilizing transformation).

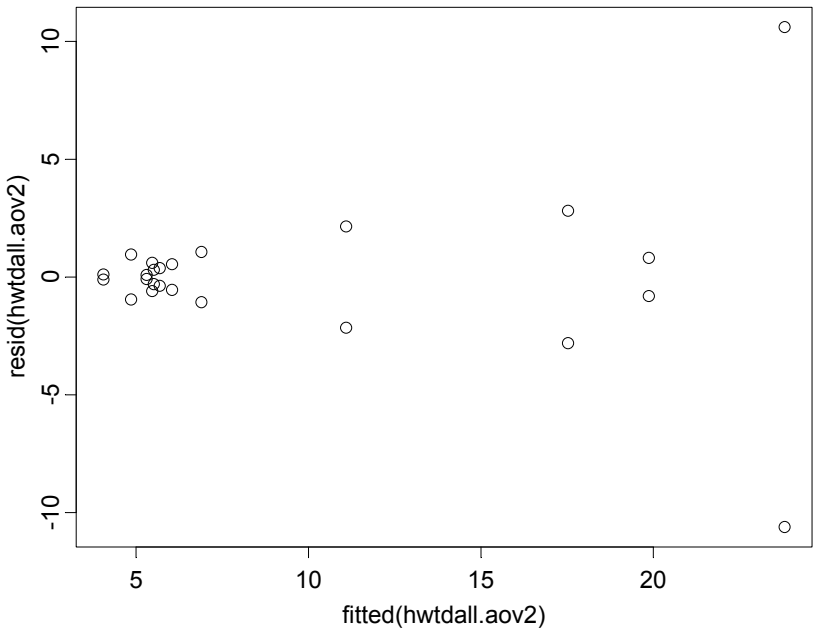

(a)

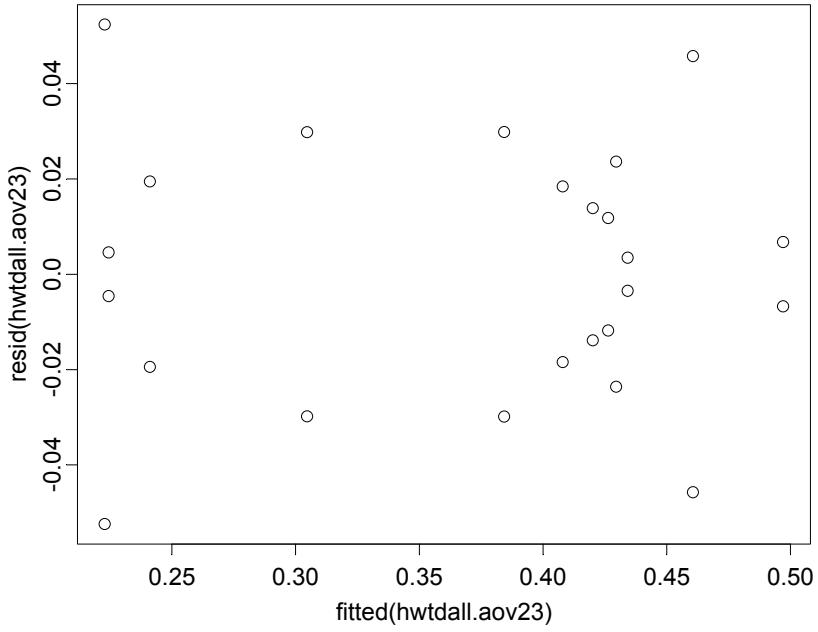

(b)

Figure 5-11. Plot of residuals versus fitted values from ANOVA model for rut depth at 10,000 passes from laboratory specimens (a, before variance-stabilizing transformation; b, after variance-stabilizing transformation).

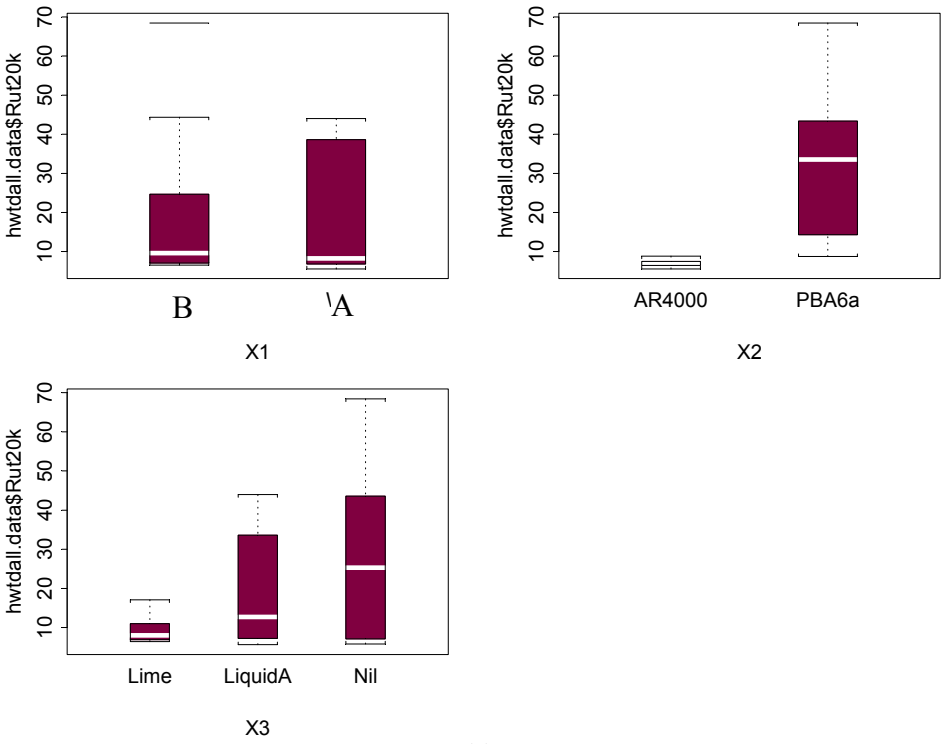

(a)

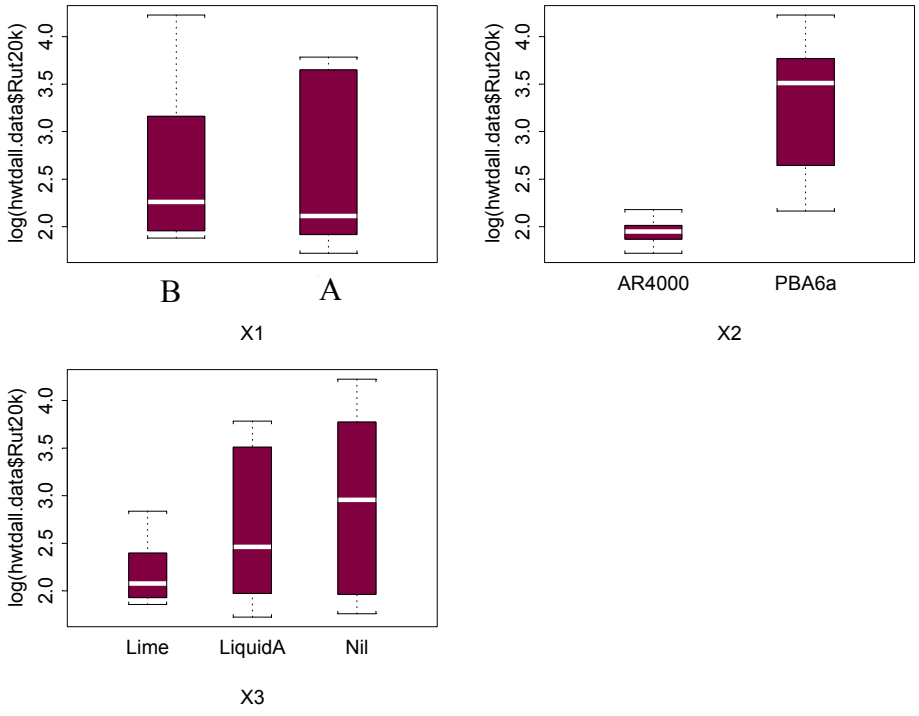

(b)

Figure 5-12. Box plots of rut depth at 20,000 passes for laboratory specimens (a, before variance-stabilizing transformation; b, after variance-stabilizing transformation).

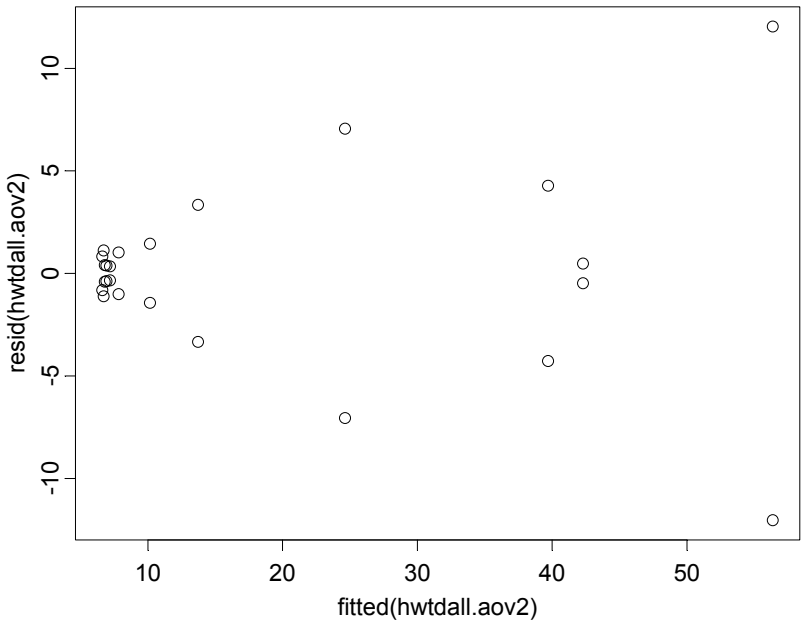

(a)

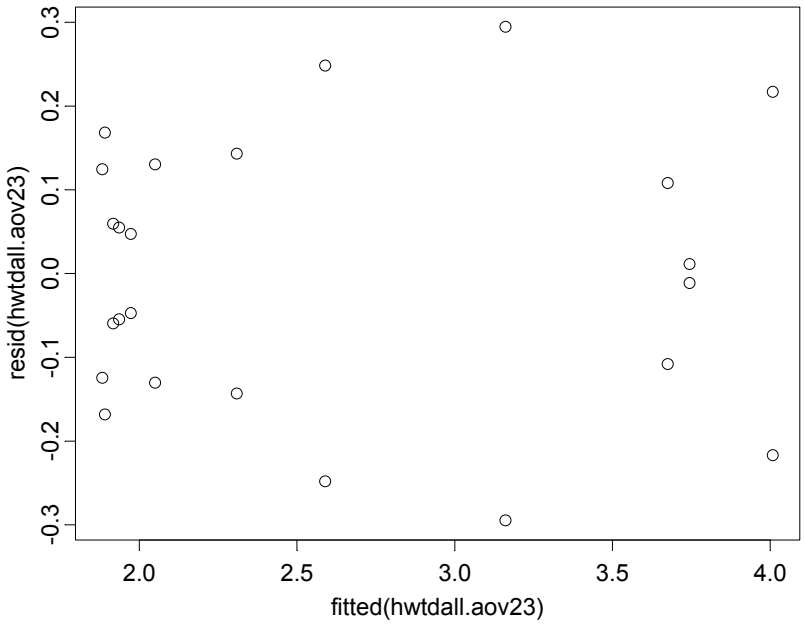

(b)

Figure 5-13. Plot of residuals versus fitted values from ANOVA model for rut depth at 20,000 passes from laboratory specimens (a, before variance-stabilizing transformation; b, after variance-stabilizing transformation).

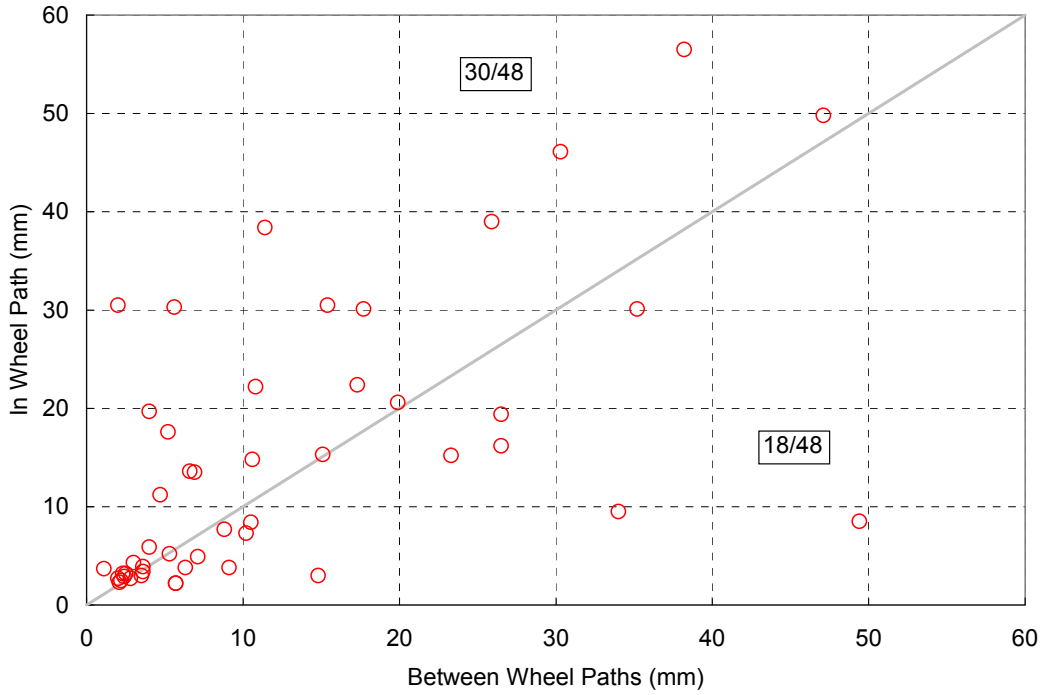

Figure 5-14. Comparison of rut depths at 20,000 passes from samples in the wheelpath and between the wheelpaths.

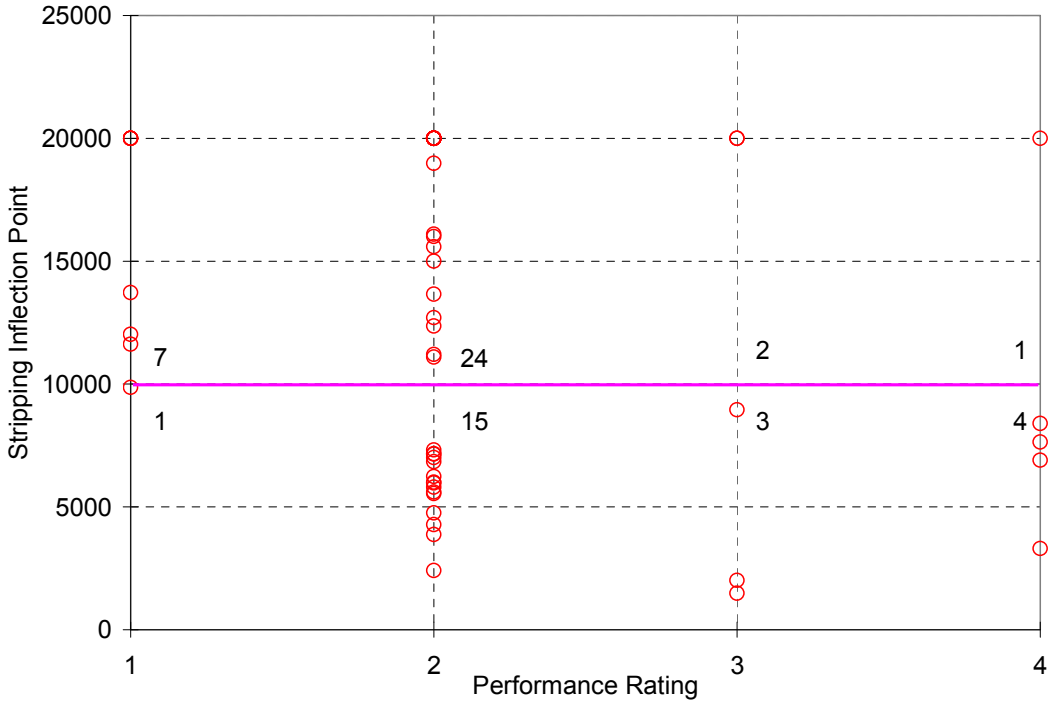

Figure 5-15. Stripping inflection point versus mix performance.

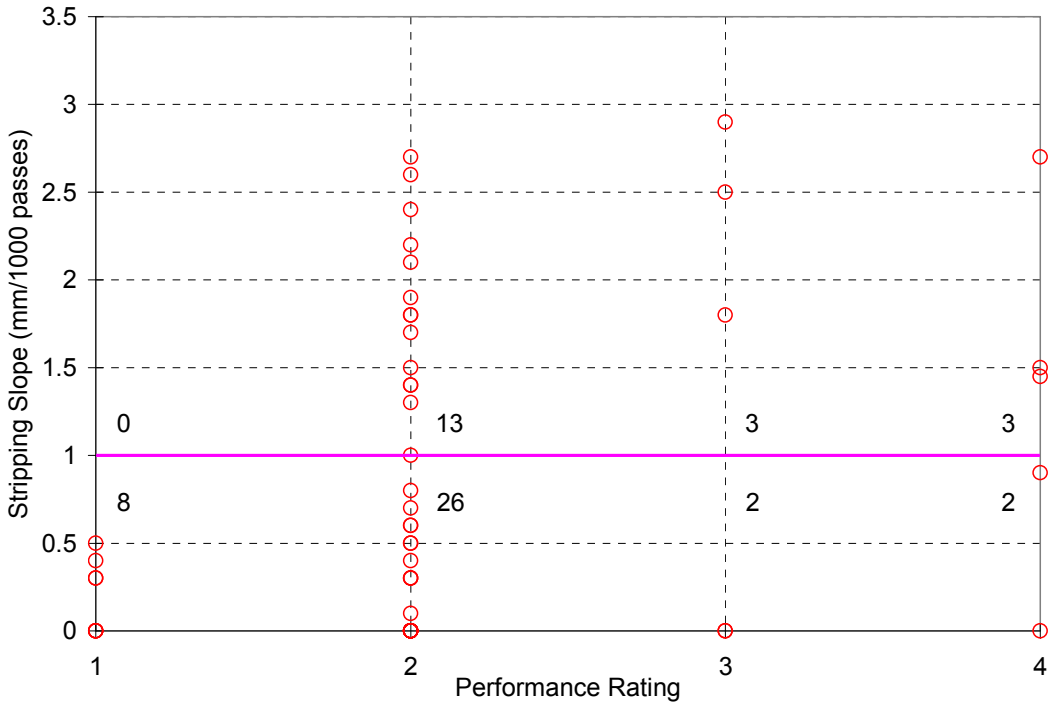

Figure 5-16. Stripping slope versus mix performance.

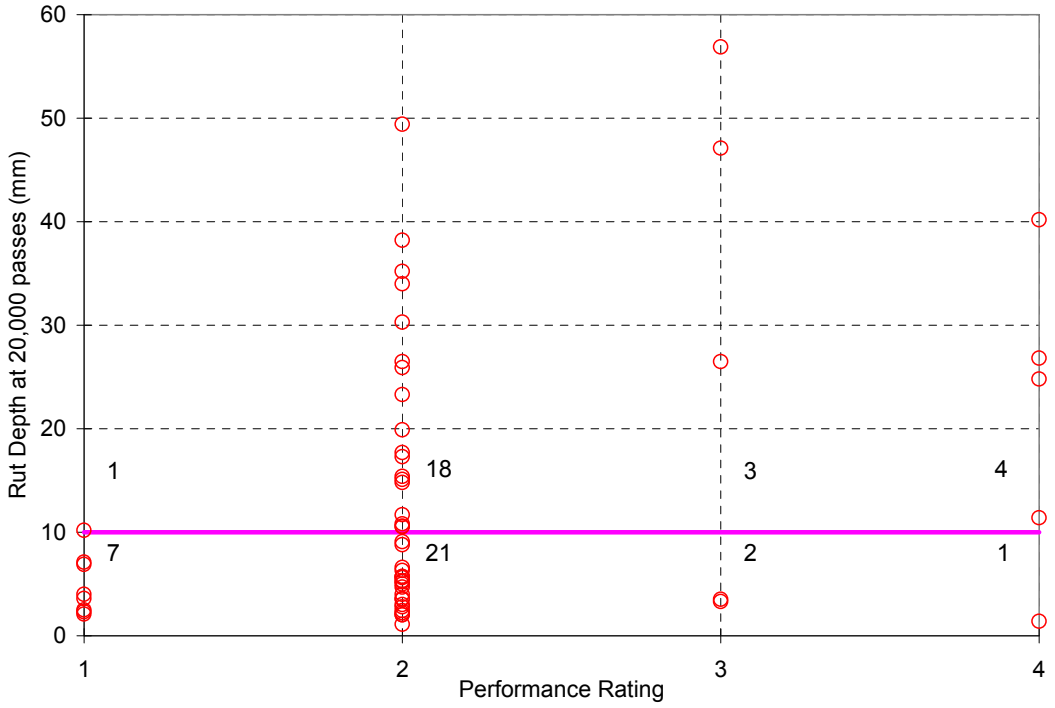

Figure 5-17. Rut depth at 20,000 passes versus mix performance.

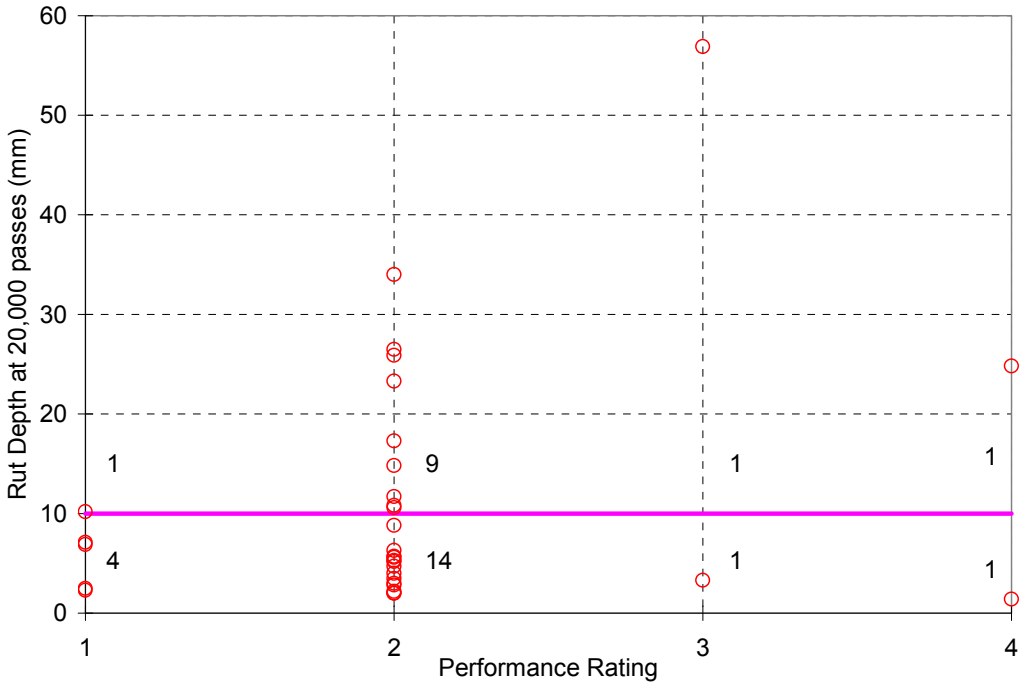

Figure 5-18. Rut depth at 20,000 passes versus mix performance for mixes with conventional binder.

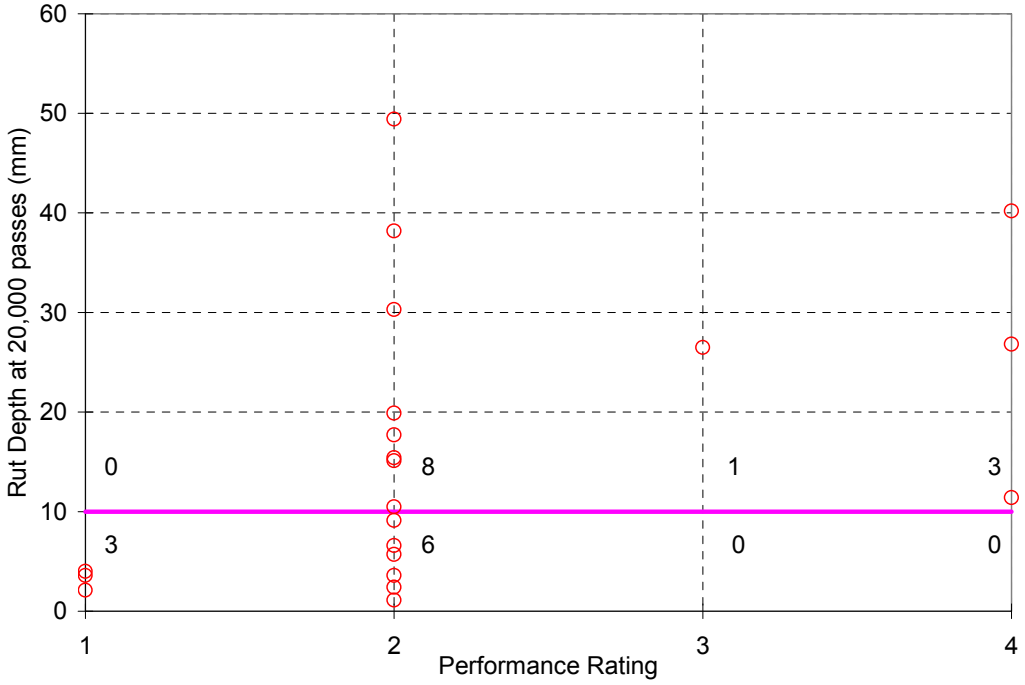

Figure 5-19. Rut depth at 20,000 passes versus mix performance for mixes with polymer modified binder.

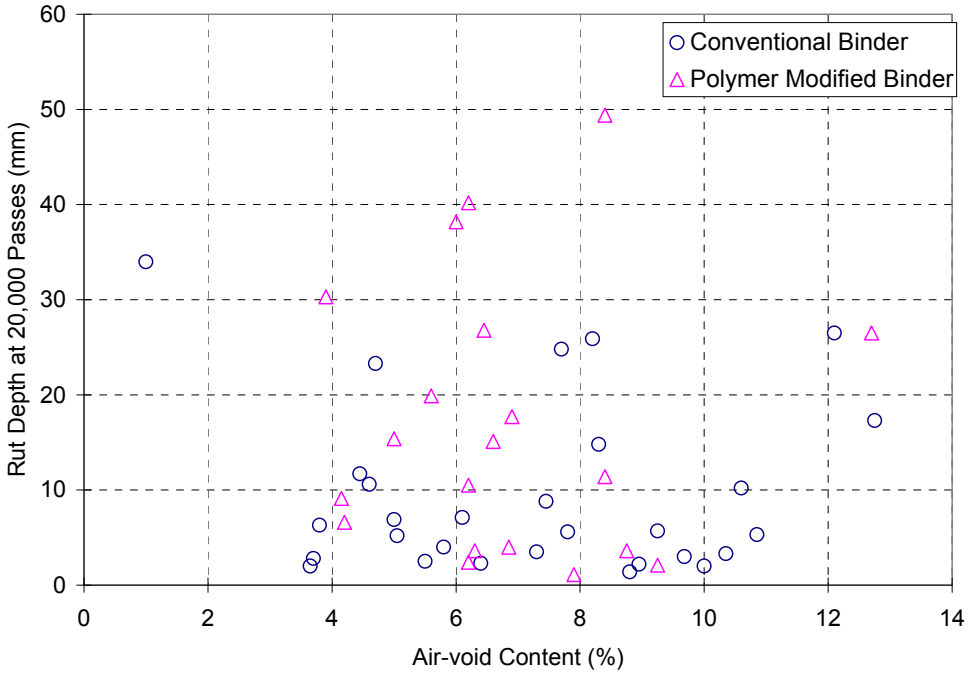

Figure 5-20. Rut depth at 20,000 passes versus air-void content.

(a)

(b)

Figure 5-21. Mix condition and HWTD test result of Section 2D19 (a, Condition of pavement and field core in the wheelpath; b, Condition of field core between the wheelpaths before and after the HWTD test).

6.0 DEVELOPMENT OF PERFORMANCE-BASED TEST PROCEDURE

As discussed in Section 1.3.2.2, most current tests, such as the HWTD, are not particularly well calibrated to field conditions and cannot be used with mechanistic-empirical design procedures. With modifications to test procedures to help improve their effectiveness, tests of this type may be useful for screening mixes. The work in this chapter addresses the need to develop a test procedure that can better simulate field conditions and can potentially be integrated into the pavement design procedure to predict pavement performance life. Pavement performance-based tests, such as the fatigue test or simple shear test, hold promise.

Most pavement design procedures include three performance indices: fatigue cracking, permanent deformation (rutting), and thermal cracking. Thermal cracking is less appropriate for studying moisture damage because it is not related to traffic loading and often occurs at very low pavement temperatures, in which moisture damage is believed to be less significant. Freeze-thaw cycle is the only low-temperature variable that has been associated with moisture damage. Tests for fatigue cracking and rutting all include dynamic loading and are both good candidates, so they were both included in the experimental design. However, due to the time constraint and the availability of test facilities, only limited number of shear tests has been performed to study the moisture effect on rutting.

This chapter concentrates on the development of the fatigue-based test procedure for evaluating the moisture sensitivity of asphalt mixes. First the test procedure is determined, including both the test parameters and preconditioning parameters. Then a comparison study is conducted to compare the results from the test procedure developed with those from both the TSR (tensile strength ratio) test and the HWTD (Hamburg wheel tracking device) test. An extension of the test procedure for use in pavement design is also discussed. The shear test results are presented and briefly discussed at the end.

6.1 Introduction to Fatigue Testing

Several test methods are available for evaluating the fatigue response of asphalt mixes, such as the uniaxial tension test, diametral test, flexural beam test, and cantilever beam test. In this study, the flexural beam fatigue test was selected, based upon the comparative study conducted in the SHRP-A-003 Project (Tayebali et al. 1994), and modified to include the moisture effect. This test is a four-point bending test in which the middle one-third of the beam is theoretically subjected to pure bending without any shear deformation.

Two loading modes are common in the test: controlled strain and controlled stress. In the controlled-strain mode, a fixed sinusoidal wave of deformation is applied to the center of the beam so strictly speaking this mode should be called “controlled-deformation” instead of “controlled-strain.” However for convention, “controlled-strain” is used for the rest of this report.. In the controlled-stress mode, a fixed sinusoidal wave of load is applied to the center of the beam. The actual loading pattern in the asphalt concrete (AC) layers of field pavements is usually somewhere between controlled strain and controlled stress, depending on thicknesses, loads, temperatures, and stiffnesses of other layers, and vary during the life of the pavement. In this study, controlled-strain mode was used because it is relatively simple to operate and it better simulates field conditions where the deformation of asphalt concrete layers is partly constrained by the underlying structures. This is closer to the case for placing thin AC overlays on old pavements, which is a major practice on current U.S. highways. For pavement design both the controlled-stress and controlled-strain modes can be used, with appropriate use of layered elastic theory to calculate tensile stresses or strains, and appropriate shift factors (Tayebali et al 1994).

The conventionally used accelerated fatigue test machine, developed by the SHRP-A-003 Project, was used for the study (Figure 6-1).

6.2 Determination of Typical Test Procedure

To evaluate the moisture sensitivity of asphalt mixes by fatigue response variables, specimens were conditioned by both moisture and repeated loading. The key issue in the development of the test procedure is how to determine an appropriate conditioning procedure. For field pavements, traffic loading and environmental factors change with time in wide ranges. Moisture damage thus develops at a varied rate under different conditions of moisture content, temperature, and traffic loading. Moisture effect on the fatigue response then should be evaluated under different loading and environmental conditions. This would require a large number of fatigue tests covering the typical loading characteristics (load magnitude, frequency) and environmental characteristics (moisture content, temperature), which is beyond the capability of the laboratory and author to achieve in a timely manner. As an alternative, in this study moisture damage was mainly evaluated in typical worst case scenarios.

The laboratory fatigue test is essentially an accelerated performance test in which the wheel loads applied on pavements in 15 to 30 years are condensed into the repeated loading applied on specimens in a few hours or days. While moisture damage is presumably partly due to traffic loading, it also develops in a non-loading condition. Whether the non-traffic-related moisture damage in the pavement can be well represented by that occurring in the short-period fatigue test is questionable. As will be shown in Section 7.0, moisture damage unrelated to loading may develop slowly over several months and will not occur in a short test period at typical fatigue test temperatures. Therefore a preconditioning process was needed before fatigue testing was performed to introduce into the specimens moisture damage unrelated to loading.

The subsequent work focused on determination of typical test parameters and an appropriate reconditioning procedure.

6.2.1 Determination of Test Parameters

As stated previously, the controlled-strain loading mode was selected for the fatigue test. Three parameters were to be determined: test temperature, strain level, and loading frequency.

6.2.1.1 Test Temperature

The common temperature range used in the flexural beam fatigue test is from 10°C to 30°C, which corresponds to the worst case where most fatigue damage occurs in the pavement. At temperatures higher than 30°C, the test is difficult to conduct and the failure mode may not be fatigue cracking, thus the temperature 20°C was chosen for the experiment. This was particularly suitable for California highways because the state's rainy season is from November to March, when the air temperature is relatively low, as is illustrated in Figure 6-2, using the San Francisco Bay Area as an example.

6.2.1.2 Strain Level

Two criteria were used to select the strain level: (1) the test should distinguish mixes with different moisture sensitivities, and (2) the test should finish in a time period of reasonable length. For typical pavement structures and mixes, the maximum tensile strain at the bottom of asphalt concrete layers is usually smaller than 400με. Thus two strain levels (200με and 400με) were initially selected as candidates and two mixes with different moisture sensitivities (AAN, Aggregate A/AR-4000 binder/without treatment; AAM, Aggregate A/AR-4000 binder/hydrated-lime treated) were tested at each strain level in both dry and wet conditions. The stiffness deterioration curves are shown in Figure 6-3.

Figure 6-3 shows that both strain levels distinguish the performance of mixes with and without hydrated lime. That is, the stiffness deterioration curve is less affected by moisture for the mix treated with hydrated lime than for the untreated mix. However, for both mixes used in the test, the stiffness deteriorated much faster at 400με than at 200με. It took less than 30 minutes to finish a fatigue test (i.e., when the stiffness

became less than 20 percent of the initial stiffness) at the higher strain level. To allow for the time for the test setup to stabilize at the beginning of the test and to let the interaction between moisture and repeated loading fully develop, it was preferable to include more repetitions in the test. Moreover, for a typical pavement structure, 400με is usually the upper limit of the actual strain level at the bottom of asphalt concrete layer containing the AR-4000 binder, while 200με is around the average value. Therefore, it was decided to choose 200με as the strain level in the test for mixes containing the AR-4000 binder. Mixes containing the PBA-6a binder have stiffness much lower than that of mixes containing the AR-4000 binder. Given the same pavement structure and wheel load, the strain in the mixes containing the PBA-6a binder would be higher than the strain in the mixes containing the AR-4000 binder. To allow for this difference, the strain level selected for mixes containing the PBA-6a binder was increased to 400με. A preliminary study showed that this change of strain level did not seem to change the effect of moisture on the fatigue response of the mixes.

6.2.1.3 Loading Frequency

A test frequency of 10 Hz, the same that is used in the conventional beam fatigue test, was selected. This corresponds to a total loading time under sinusoidal load of 0.1 second, with no rest periods. This frequency simulates in-pavement stress pulses corresponding to vehicle speeds in the 24 to 48 km/h range, and is sufficiently large to permit rapid testing while still representing the load pulses generated by rapid moving traffic (Tayebali et al. 1994).

6.2.2 Determination of Preconditioning Parameters

The primary objective of the preconditioning process is to introduce certain moisture damage in the specimen in a rapid but reasonable manner. Three parameters were determined for the preconditioning process: moisture content (or saturation level), conditioning temperature, and conditioning duration. Moisture content is the ratio of moisture mass in a mix to the dry mix mass, while saturation level is the percentage of air voids that are filled with water. A sensitivity study was first performed to identify the relative importance of these parameters. The determination of each parameter is subsequently discussed.

6.2.2.1 Sensitivity Study

6.2.2.1.1 Experimental Design

Two levels were chosen for each conditioning parameter, as follows:

Moisture Content: low and high. For the low moisture content, each beam was partially saturated under a 250 mm-Hg vacuum for three minutes, which typically corresponds to 20 to 30 percent saturation. For the high moisture content, each beam was partially saturated under a 635 mm-Hg vacuum for 30 minutes, which typically corresponds to 50 to 70 percent saturation.

Conditioning Temperature: 25°C and 60°C.

Conditioning Duration: one day and ten days. The ten-day duration was selected as the upper limit of the time that can be tolerated for the laboratory testing.

The flexural beam fatigue test was performed on four mixes using the previously determined test parameters and eight combinations of the above conditioning parameters. The four mixes consist of AR-4000 binder and the following aggregates and additives:

Aggregate: A or B

Treatment: nil or hydrated lime.

One specimen was tested at each factor level combination. Thus, the experiment was a 2^5 factorial design with a single replicate. To normalize the test results, two additional beams for each mix were tested without moisture conditioning (i.e., in dry condition). Therefore, a total of 40 beams were tested for the sensitivity study. All beams had the 19-mm nominal maximum medium dense gradation and were compacted to the air-void content range of 6.5 to 8.5 percent.

6.2.2.1.2 Results and Analysis

The test results of the experiment are summarized in Table 6.1, in which the initial stiffness is defined as the flexural complex modulus measured at 50 repetitions and the fatigue life is defined as the number of repetitions to 50 percent reduction of the initial stiffness. The number of broken aggregates and percentage of stripping on the cracked faces of each specimen were also recorded in the table. To isolate the moisture effect, the results of each wet beam were normalized by the average results of the two dry beams for each mix, as shown in Table 6.2. The stiffness deterioration curves of all beams are plotted in Figure 6-4 through Figure 6-7, on both natural and logarithmic time (repetition) scales.

6.2.2.1.2.1 General Observations

Moisture Content

As described in the experimental design, fixed vacuum intensity and duration, instead of a predetermined saturation range, were specified separately for specimens with low and high moisture contents. It turned out that specimens subjected to a 635 mm-Hg vacuum for 30 minutes generally had saturation levels 30 to 40 percent higher than specimens subjected to a 250 mm-Hg vacuum for three minutes.

Initial Stiffness

The initial stiffness ratio of each wet beam was generally less than one (Table 6.2), indicating that moisture always changes mix properties once it gets into the mix. The effect of conditioning temperature was most significant. Changing the conditioning temperature from 25°C to 60°C would reduce the stiffness ratio by 10 percent more. On the other hand, moisture content level did not seem to affect the amount of the reduction. Low moisture content had a reduction effect similar to high moisture content. The ranking of the four mixes based on the average initial stiffness ratio is AAN < BAN < AAM < BAM.

Fatigue Life

The fatigue life result is more complex than the initial stiffness result. A large portion of the specimens had a fatigue life ratio greater than one, which means that the fatigue life of the mix was extended due to moisture. This phenomenon was more significant when a specimen was preconditioned at the low temperature (25°C) than at the high temperature (60°C). The effect of additives was also very significant. Adding the hydrated lime would change the average fatigue life ratio from the lowest (70 percent) to the highest (130 percent). On the other hand, moisture content level did not seem to affect fatigue life. Low moisture content resulted in a similar change of fatigue life to high moisture content. The ranking of the four mixes based on the average fatigue life is AAN < BAN < AAM < BAM, which is consistent with the rank based on the initial stiffness ratio.

Visual Inspection of Cracked Faces

No clear relationship was found between the number of broken aggregates and different factor levels. In all cases, mixes treated with hydrated lime showed slight stripping or none. On the other hand, mixes without treatment showed stripping varying from 5 percent to 40 percent: 5 to 10 percent for specimens preconditioned at the low temperature (25°C) and 20 to 40 percent for specimens preconditioned at the high temperature (60°C). The ranking of stripping severity of the four mixes is generally consistent with the ranking based on the initial stiffness ratio or fatigue life ratio.

6.2.2.1.2.2 Statistical Analysis

In this section, statistical analysis is performed to verify the previous general observations. Initial stiffness ratio and fatigue life ratio are used separately as the response variables. The following linear model is used to fit the test data:

$$y = \mu + \sum_{i=1}^{5} \beta_i X_i + \sum_{j,k=1,k>j}^{5} \beta_{jk} X_{jk} + \varepsilon \qquad \textbf{(6-1)}$$

where, y is the initial stiffness ratio or fatigue life ratio; μ is the grand mean; β_i and β_{jk} are the parameters to be estimated; X_i is the difference of two indicator functions.

Specifically,

$X_1 = ind(aggregate\ \mathrm{B}) - ind(aggregate\ \mathrm{A})$

$X_2 = ind(No\ Treatment) - ind(Hydrated\ Lime)$

$X_3 = ind(Low\ Moisture) - ind(High\ Moisture)$

$X_4 = ind(25C) - ind(60C)$

$X_5 = ind(1\ day) - ind(10\ days)$

where, $ind(\cdot)$ is an indicator function, 1 if the level of a factor is equal to the value in the parentheses, 0 otherwise. For example, $ind(aggregate\ \mathrm{B}) = 1$ if the data used was from the specimen containing aggregate B, 0 otherwise. X_{jk} is the product of X_j and X_k, $X_{jk} = X_j X_k$. ε is a random error term, assumed to have independent normal distribution, $\varepsilon \sim N(0, \sigma^2)$.

Third or higher order interaction terms are not included in the model due to their insignificance from a preliminary analysis.

Initial Stiffness

Initial stiffness ratio being the response variable, the estimation results and the corresponding ANOVA are shown in Table 6.3 and Table 6.4 respectively. The QQ-normal plot of the residuals shows that the normal distribution assumption of the error term is not severely violated (Figure 6-8a). The ANOVA results show that aggregate type, treatment, conditioning temperature, and conditioning period all have significant effects on the initial stiffness ratio of the beam specimens. Moreover, the interactions between treatment and moisture content, conditioning temperature, or conditioning period is also significant. The estimated parameters in Table 6.3 show that the reduction of stiffness due to moisture is less for mixes containing Aggregate B than mixes containing Aggregate A, and less for mixes treated with lime than mixes without treatment. Lower conditioning temperature or shorter conditioning period both lead to less of a

reduction in stiffness. Among all the factors, the effect of conditioning temperature is most significant. When the conditioning temperature is raised from 25°C to 60°C, average stiffness is further reduced by 12 percent. The second most important factor is treatment. Mixes treated with hydrated lime have 9 percent less reduction in stiffness than mixes without treatment. On the other hand, moisture content is insignificant in affecting the initial stiffness. The significance of the three interaction terms indicates that mixes treated with hydrated lime are significantly less sensitive to the variation in moisture-conditioning parameters (moisture content, conditioning temperature, and conditioning duration) than untreated mixes.

Fatigue Life

Fatigue life ratio being the response variable, the estimation results and the ANOVA are shown in Table 6.5 and Table 6.6 respectively. The QQ-normal plot of the residuals shows that the normal distribution assumption of the error term is not severely violated (Figure 6-8b). The ANOVA results show that aggregate type, treatment, and conditioning temperature have significant effects on the fatigue life ratio of the beam specimens. Moreover, the second order interactions among these three factors are also significant. Interestingly, neither "Condition" nor "Period" is significant at the 95 percent confidence level, suggesting moisture effect on fatigue response is not sensitive to moisture content or conditioning duration. The estimated parameters in Table 6.5 show that the intercept term is close to one, indicating the grand average fatigue life of all the specimens tested is not changed by moisture. The average fatigue life of mixes containing Aggregate A is reduced by about 25 percent due to moisture, while the average fatigue life of mixes containing Aggregate B is increased by about 25 percent. The average fatigue life of untreated mixes is reduced by about 30 percent due to moisture, while mixes treated with hydrated lime increase fatigue life by about 30 percent. Moreover, the average fatigue life of mixes preconditioned at 25°C is increased by about 21 percent, and that of the mixes preconditioned at 60°C is reduced by about 21 percent. The significance of the interaction between aggregate and treatment indicates that the performance improvement due to hydrated lime is more significant in mixes containing Aggregate A than mixes containing Aggregate B. This is because Aggregate B has better compatibility with asphalt than Aggregate A. The significance of the interaction between aggregate and temperature indicates that the performance difference between mixes containing Aggregate B and mixes containing Aggregate A is more significant at low temperature (25°C) than at high temperature (60°C). This is because mixes containing Aggregate B are less affected by moisture at 25°C than at 60°C, while mixes containing Aggregate A are significantly affected by moisture at both temperatures. The significance of the interaction between treatment and temperature suggests that the moisture resistance of mixes containing hydrated lime is less affected by temperature than that of untreated mixes.

6.2.2.1.3 Summary of Sensitivity Study

The following summarizes the findings obtained from the sensitivity study:

1. The ranking of the four mixes is consistent when evaluated by initial stiffness, fatigue life, or surface stripping percentage.
2. The introduction of moisture into a mix always changes the mix properties, as was verified by the consistent reduction in in initial stiffness. However, it does not always jeopardize the mix performance (i.e., fatigue resistance), especially for mixes with good moisture resistance conditioned for a short period at a mild temperature. When the conditioning temperature is high, however, the fatigue performance of the mix is generally reduced by moisture, especially for untreated mixes.
3. Among the three conditioning parameters, the conditioning temperature has the most important effect on the moisture resistance of asphalt mixes. High temperature significantly

promotes moisture damage in mixes, especially in untreated mixes. On the other hand, moisture content level does not significantly affect the extent of moisture damage, while the conditioning duration has an intermediate effect.

4. In the eight moisture conditioning scenarios, mixes with hydrated lime are less sensitive to different conditions than untreated mixes, no matter whether dynamic loading is applied or not.

6.2.2.2 Selection of Moisture Content

The sensitivity study revealed that fatigue response is not very sensitive to moisture content. Specifying a saturation level of 30 percent or 60 percent tended to make no significant difference in the fatigue test results. To be consistent with other test methods and to take into consideration that at higher moisture contents pore pressure is more likely to occur than at lower moisture contents, it is preferable to run the test at high moisture contents.

The moisture content of specimens in the laboratory should be consistent with the actual level in pavements. That is, the moisture content specified for specimens should not exceed the maximum moisture content that would occur in the pavement. There are few data in the literature regarding the in-situ moisture content in asphalt concrete, but the dry cores taken in the field investigation and the moisture ingress and retention experiment results, as discussed in Chapter 3 and Chapter 4, provided valuable information for estimating the maximum in-situ moisture content.

For the laboratory test, it is assumed that the maximum field moisture content can be estimated from the amount of moisture entering specimens that are submerged in water. The laboratory soaking test in Chapter 4 showed that the asymptotic moisture content is proportional to the air-void content, but the asymptotic saturation does not change significantly with the air voids. For specimens soaked in a 25°C water bath, the ultimate saturation is generally between 50 percent and 80 percent.

As introduced in Section 3.2.3, four dry cores were generally taken from each of the 63 pavement sections selected for intensive survey. The moisture content and air-void content of each dry core were all measured in the laboratory. It was seen in Chapter 3 that moisture content of asphalt mixes in the field is proportional to the air-void content. On the other hand, the saturation level, as shown in Figure 6-9, has no clear correlation with the air-void content. These findings are consistent with the laboratory soaking results. Moreover, most field cores have a saturation level less than 60 percent, with a few others less than 80 percent, even though some were taken during the rainy season of a wet year.

Based on the above findings, it seems to be appropriate to specify a saturation level of about 50 to 80 percent as the high moisture level in the specimens.

6.2.2.3 Vacuum Level and Duration

The laboratory soaking test showed that it took several months for a specimen to reach a saturation of 60 percent (Chapter 4). A vacuum had to be applied to accelerate the moisture intrusion. For specimens with similar air-void contents, it makes little difference whether to specify a uniform saturation level or to use a fixed vacuum level and duration during the vacuum saturation process. The latter approach was adopted in the experiment since the test is easier to perform.

Special equipment was developed to saturate the beam specimens under vacuum, as illustrated in Figure 6-10. The beam specimen was put into a casket made of acrylic plexiglass with a perforated aluminum sheet at the bottom. The casket was then filled with water and slid into a cylindrical vacuum chamber. Vacuum was applied to the chamber to force air out of the specimen.

The relationship between saturation and vacuum level and duration was explored by saturating a set of beams (with 7±0.3 percent air voids) at different vacuum level and duration combinations (Appendix D). The results showed that a 30 minute application of a 635 mm-Hg vacuum resulted in a saturation of about 60 percent, which is appropriate for the saturation range required for the fatigue test. A separate study revealed that the application of a 635 mm-Hg vacuum for 30 minutes did not significantly affect the mix strength (Appendix E), which eliminated the concern that such a high vacuum might introduce confounding damage to specimens.

6.2.2.4 Selection of Conditioning Period

The sensitivity study showed that fatigue response is insensitive to the length of conditioning period (one day versus ten days). To keep the test duration short, it was decided to condition specimens for one day.

6.2.2.5 Selection of Conditioning Temperature

Preconditioning temperature has significant effect on test results and needs to be selected carefully. Initially 25°C was selected because it is more common in the pavements. However, most mixes conditioned at this temperature for one day showed a fatigue life extended by moisture rather than one reduced by it, as was revealed in both the study on the effects of construction-induced variation (Section 4.2) and the previous sensitivity study. In another long-term study (Chapter 6), it was found that moisture has a time effect and that fatigue life is usually reduced by moisture after long-term conditioning at a mild temperature. Field surveys revealed that moisture exists in pavements for a long period, therefore the one-day conditioning at 25°C tends to be insufficient to introduce the amount of moisture damage that will occur in the field. On the other hand, the long-term moisture effect can be better simulated by a one-day conditioning at high temperatures, as illustrated in Figure 6-11. In this figure, the test data for one-day conditioning is from the sensitivity study while the data for four-month conditioning is from a long-term study, as detailed in Chapter 6. The figure shows that for a mix with good moisture resistance (AAM) the time effect of moisture is not significant, but for a mix sensitive to moisture (AAN), four-month moisture conditioning significantly reduces both initial stiffness and fatigue life, and this reduction can be well approximated by that after one day conditioning at 60°C. Therefore, it was decided to choose 60°C as the preconditioning temperature.

The following preconditioning procedure was determined: saturate the specimen at 635 mm-Hg vacuum for 30 minutes, place it in a 60°C water bath for 24 hours, cool the specimen to 20°C and wrap it with Parafilm M®, a moisture-resistant, thermoplastic flexible plastic sheet so it retains its internal moisture (Figure 6-12). Moisture loss during the fatigue test can be controlled within one gram by Parafilm.

6.3 Comparison of Results from Different Tests

The test procedure determined in the previous section is compared with two common tests, the TSR (tensile strength ratio) test and the HWTD (Hamburg Wheel Tracking Device) test. For the TSR test, the procedure specified in the Caltrans version CTM 371-03 was followed using the equipment shown in Figure 6-13. CTM 371-03 made a few modifications to the conventional TSR test to reduce the variability of test results, including increasing the number of replicates from three to six, narrowing the allowable air-void content range to between 6.5 percent and 7.5 percent, and narrowing the allowable saturation range to between 70 percent and 80 percent. The HWTD test was detailed in Chapter 4.

6.3.1 Experimental Design

Eight mixes with different moisture sensitivities were involved, consisting of two aggregates (A and B), two binders (AR-4000 and PBA-6a), and two additives (nil and hydrated lime). All mixes had the 19-mm nominal maximum medium dense gradation and were compacted to air-void contents between 6.5 percent and 8.5 percent for the beam and slab specimens.

For each mix in the fatigue-based test, two beams were tested in dry condition and two beams were tested after being conditioned by moisture at 60°C for one day. As part of the initial experimental design, two more beams were also tested after being conditioned by moisture at 25°C for one day. Therefore, a total of 48 beams were included, but one third of the experiment had already been conducted in the sensitivity study. In the TSR test, 12 specimens were tested for each mix, six in dry and six in wet as specified in the CTM 371-03, so a total of 96 specimens were tested. For the HWTD test, results from all eight mixes were presented in Chapter 5, so no more specimens were tested.

6.3.2 Results and Analysis

The fatigue-based test results are summarized in Table 6.7, and the stiffness deterioration curve of each specimen is plotted in Appendix F. The fatigue lives of specimens containing the PBA-6a binder were the results of extrapolation of the stiffness deterioration curves because the corresponding tests were generally terminated after three million repetitions to keep the test duration reasonably short. The TSR test results are shown in Appendix G. The HWTD test results are given in Table 5.1. For comparison, the results of all three tests are summarized in Table 6.8.

The fatigue responses of mixes containing two different binders are quite distinct. Mixes containing the AR-4000 binder showed a continuous decrease of stiffness until the specimen cracked. Mixes containing the PBA-6a binder initially showed a quick reduction of stiffness, but the stiffness deterioration became trivial after about one million repetitions so it would take a long time to reach a 50 percent reduction in stiffness. The fatigue test was therefore terminated at three million repetitions (about three and a half days). The fatigue lives (repetitions to 50 percent reduction of initial stiffness) for the PBA-6a mixes are all very large based on extrapolation. Some are larger than one billion, which is practically impossible. Considering the uncertainty introduced by the extrapolation, the fatigue lives shown in Table 6.7 for the PBA-6a mixes may be quite unrealistic. Therefore, no inference was made based on these data. A direct examination of the stiffness deterioration curves (Figure F-5 through Figure F-8) revealed that except for mix APN, moisture showed little influence on the stiffness deterioration process of the PBA-6a mixes, no matter what the preconditioning temperature was. For the mix APN, moisture shifted downward the stiffness deterioration curves, and to a larger extent when the preconditioning temperature was 60°C. For the AR-4000 mixes preconditioned at 60°C, the fatigue life ratios (FLR) shown in Table 6.8 indicate that the fatigue lives of the two untreated mixes (AAN and BAN) were all reduced by moisture, with BAN less affected than AAN. On the other hand, the fatigue lives of the two treated mixes (AAM and BAM) were all extended by moisture. Based upon the fatigue response, the relative ranking of the mixes is as follows: mixes containing the PBA-6a binder are less affected by moisture than mixes containing the AR-4000 binder; mixes containing Aggregate B are less affected by moisture than mixes containing Aggregate A; mixes treated with hydrated lime are less affected by moisture than untreated mixes.

As found in the sensitivity study, the 60°C preconditioning temperature reduces the initial stiffness for mixes containing the AR-4000 binder (Table 6.8) more than the 25°C preconditioning.The initial stiffness ratios (ISR) after the preconditioning at 60°C (Table 6.8) correspond to a 2^3 experimental design with a single replicate and can be analyzed by Daniel's half normal plot (Montgomery 1991). In this plot, the effects that are negligible are normally distributed and will tend to fall along a straight line in the lower left corner, whereas significant effects will not lie along the straight line. The Daniel's half normal plot of the ISR after preconditioning at 60°C is shown in Figure 6-14a. It can be seen that the effect of aggregate, binder, and

treatment, and that of the interaction between aggregate and treatment all tend to be significant. A check of the ISR values reveals the following results: (1) mixes containing Aggregate B have higher ISR than mixes containing Aggregate A; (2) mixes containing the PBA-6a binder have higher ISR than mixes containing the AR-4000 binder; (3) mixes treated with hydrated lime have higher TSR than untreated mixes; (4) hydrated lime improves ISR more in mixes containing Aggregate A than in mixes containing Aggregate B.

The Daniel's half normal plots of the tensile strength ratio (TSR) from the CTM 371-03 test and the rut depth at 20,000 passes from the HWTD test are shown in Figure 6-14b and Figure 6-14c respectively. For TSR, it can be seen that the effect of aggregate, binder, and treatment, and that of the interaction between aggregate and treatment all tend to be significant. A check of the TSR values reveals the same rankings as those based on the ISR after preconditioning at 60°C. For the HWTD test results, it can be seen that binder type, treatment, and their interaction are significant in affecting the rut depth, whereas the aggregate type is insignificant, which has been known from the ANOVA on a larger data set in Chapter 4.

In summary, the test procedure determined in Section 6.2 distinguishes mixes with different moisture sensitivities, and gives a ranking of mixes consistent with prior field experience. The TSR test results are consistent with the fatigue-based test results and the field experience, while the HWTD test does not distinguish mixes containing different aggregates and gives contrary results for mixes containing different binders.

6.3.3 Discussion

For mixes treated with hydrated lime, it was found that fatigue life is increased instead of decreased by moisture even for the specimens that have been preconditioned at 60°C. Several reasons may contribute to this result. First, the increased specimen flexibility due to moisture, as reflected by the lower initial stiffness, leads to a lower stress level in the controlled-strain test. Second, since the fatigue life is defined as the number of repetitions to *50 percent reduction of the initial stiffness*, a lower initial stiffness also leads to a lower final stiffness as the stopping point of the test, which corresponds to more repetitions. Third, during the preconditioning, hydrated lime may further react with asphalt and aggregate and form a stronger bond among the mix components. Whether the extension of fatigue life due to moisture can occur in the field is unknown. For the same mix in the pavement, a lower stiffness will lead to higher stress and strain levels under the same wheel load, which may counteract the beneficial effect of moisture. Caution should be taken before extending the laboratory results to the field.

The test procedure developed in Section 6.2 evaluates the moisture effect on the fatigue response of mixes under a typical condition. Its usage is mainly for evaluating the relative performance of different materials, but not for predicting performance life. To achieve the latter objective, fatigue response at the typical spectra of conditioning and test parameters should be evaluated, and extensive field performance data need to be collected for test result calibration, which is out of the scope of this research. The idea of incorporating the moisture effect in pavement design, however, is simply illustrated in the next section.

6.4 Incorporation of Moisture Effect in Pavement Design

The use of a performance-based test to evaluate moisture effect enables us to explicitly incorporate moisture effect into pavement design, which is impossible in the traditional test case. This section provides a simple example showing the possible application of the performance-based test results.

Pavement fatigue life can be expressed by a function of maximum tensile strain and initial mix stiffness (Monismith et al. 1985):

$$N_f = \alpha(1/\varepsilon_t)^{\beta} (1/S_{mix})^{\gamma} \quad \textbf{(6-2)}$$

where, ε_t = tensile strain; S_{mix} = initial stiffness; N_f = fatigue life; α, β, γ = experimentally determined parameters.

The existence of moisture will affect all the variables and parameters on the right side of the equation (6-2), and so also influence the fatigue life. Pavements in the field will experience variational environmental conditions, including different moisture contents and temperatures. It is assumed that the pavement condition can be represented by "dry" and "wet" statuses, and the different fatigue responses in these two statuses can be characterized by the laboratory fatigue test in dry and wet conditions respectively. Moreover, fatigue damage is assumed to be cumulative and can be calculated by the linear-sum-of-cycle-ratios, or Miner's Law (1945):

$$\sum_{i=1}^{n} \frac{n_i}{N_i} = 1, \qquad n = 2 \tag{6-3}$$

where, n_i = number of actual traffic load applications in condition i; N_i = number of allowable traffic load applications in condition i, calculated by Equation (6-2).

The two assumptions remain to be validated by field data, but they are used here for the purpose of illustration. For a particular pavement structure, fatigue life then can be calculated from the fatigue responses in two conditions and the percentages of load repetitions in two conditions. Specifically, we have

$$n_1 + n_2 = N \tag{6-4}$$

$$\frac{n_1}{N} = r_1 = 1 - r_2 \tag{6-5}$$

where, N = number of actual allowable traffic load applications; r_1, r_2 = percentage of traffic load applications when the pavement is in condition "dry" or "wet", which can be estimated from traffic and weather data.

The actual fatigue life, N, then can be solved from Equations (6-2) through (6-5), as below:

$$N = N_1 N_2 / (r_1 N_2 + r_2 N_1) \tag{6-6}$$

As an example, we consider a typical pavement structure consisting of three layers: 0.15-m asphalt concrete, 0.30-m aggregate base, and subgrade. The Possion's ratio is assumed to be 0.35, 0.40, and 0.45 for the three layers respectively, and the modulus of elasticity is assumed to be 240 MPa and 40 MPa for the aggregate base and subgrade respectively. Each of two mixes is used for the asphalt concrete layer: AAN (aggregate A/AR-4000 binder/no treatment) and AAM (aggregate A/AR-4000 binder/hydrated lime). Their initial stiffness and fatigue life at different strain levels in both dry and wet conditions were measured by the flexural beam fatigue test, as summarized in Table 6.9 with the fatigue life-versus-strain curves plotted in Figure 6-15. The parameters for Equation (6-2) are estimated by linear regression and shown in Table 6.10. The average initial stiffness of each mix is input into the linear layered-elastic program *ELSYM5* to calculate the maximum principal strain at the bottom of the asphalt concrete layer. With this strain and the initial stiffness, the fatigue life of each mix in each condition is obtained from Equation (6-2). Suppose the pavement structure is in an environment where the percentage of traffic load applications when the pavement is in "dry" condition is 60 percent, its fatigue life in that environment is then estimated by Equation (6-6), and shown in Table 6.11. It can be seen from Table 6.11 that when only the dry condition is considered, which is the current design practice, the number of allowable traffic load applications of the untreated mix (AAN) is around nine million, over twice as large as that of the treated mix (AAM). When both dry and wet conditions are considered, however, the number of actual allowable traffic load applications of the treated mix is over twice as large as that of the untreated mix.

Although others factors affecting fatigue life in the field, such as temperature variation, traffic wandering, and crack propagation, have not been considered in the analysis, the example above clearly shows the significant effect of moisture on the key parameter (fatigue life) in pavement design. A pavement design procedure that explicitly includes the moisture effect should make it superior to most current design practices, which vaguely include the moisture effect in a general shift factor.

6.5 Exploratory Study of Moisture Effect on Permanent Deformation

It is expected that the disruption of adhesion between aggregates and asphalt will reduce the resistance of asphalt mixes to permanent deformation (rutting). In the field investigation described in Chapter 3, excess irregular rutting was observed on pavements with severe moisture damage in the mixes. This section tries to use the test procedure for permanent deformation to evaluate moisture effect on pavement performance.

6.5.1 Experimental Design

The repeated shear test at constant height (RSST-CH) was selected in this study to evaluate the rutting resistance of asphalt mixes, following the procedure described in AASHTO 320-03. During the test, a 69 ± 5 kPa repeated haversine shear stress was applied to the specimen for 0.1 s followed by a 0.6-s rest period, while the specimen height was maintained constant by applying sufficient axial stress, and the specimen temperature was maintained at 50 ± 0.5°C. The test was continued until five percent shear strain or 50,000 cycles was reached, whichever came first.

Due to constraints on time and testing facilities, only a small number of mixes were included in the experiment. These mixes consisted of two aggregates (A and B), two binders (PBA-6a and AR-4000), and two additives (liquid A and hydrated lime). In total, six mixes were tested: AAN, AAM, AALA, APN, BAN, and BPN. (The meaning of mix designation is described in Section 2.2.4.)

Cylindrical specimens (152.4 mm ϕ × 50.8 mm), fabricated in the laboratory following the procedures described in Chapter 2, were used in the test. Both dry and wet specimens were tested for each mix, with two repetitions. Therefore, a total of 24 specimens were included in the test.

To introduce the moisture effect, wet specimens were conditioned before testing, following this procedure:

1. Put the specimen on a perforated spacer in a vacuum chamber, fill the chamber with water to a level about one inch higher than the specimen upper surface, and apply a 635 mm-Hg vacuum for 30 minutes.
2. Condition the specimen in a water bath at 25°C for 24 hours.
3. Take the specimen out of the water bath and use rags to bring it to surface dry condition.
4. Use epoxy to bond the specimen to two platens, and wrap the specimen with two layers of parafilm to ensure moisture is fully retained.
5. Before testing, the specimen was left in an oven at 50°C for at least two hours to bring the specimen temperature to the target test value.

The vacuum saturation procedure in Step 1 typically resulted in a saturation level of around 80 percent for specimens with 7 to 8 percent air-void content, which is consistent with beam specimens used in the fatigue test. The reason to choose a mild preconditioning temperature (25°C) is that the RSST-CH was performed at a high temperature (50°C), at which it was expected that moisture damage would further develop during the test. It is the moisture damage developed under the combination of high temperatures and repeated loading that is more critical in the field and is of more interest in this study.

6.5.2 Test Results

The test results are summarized in Table 6.12 and plotted in Figure 6-16. It can be seen that four of the six mixes showed higher resistance to permanent deformation when moisture was introduced, while two other mixes, BPN (aggregate B/PBA-6a/no additive) and AAM (aggregate A/AR-4000/hydrate lime), had larger permanent deformation when tested in wet. There is no fundamental mechanism to explain the inconsistent effect of moisture. It is likely that for most mixes moisture damage has not sufficiently developed during the maximum ten-hour test duration. On the other hand, moisture filled up most air voids so that the shear modulus of specimens increased, resulting in smaller shear strains. To overcome the positive effect of moisture, a harsher preconditioning procedure is needed, such as at a higher conditioning temperature.

6.6 Summary

This chapter focused on the development of the fatigue-based test procedure for evaluating moisture sensitivity of asphalt mixes. A typical test procedure was determined for comparative evaluation of different mixes, which is a controlled-strain flexural beam fatigue test performed at 20°C, 10 Hz, and 200με on specimens presaturated under a 635 mm-Hg vacuum for 30 minutes and preconditioned at 60°C for one day. An extension of the test procedure for use in pavement design was also discussed. The major findings of this chapter are summarized as follows:

1. Conditioning temperature significantly affects the moisture resistance of asphalt mixes. High temperature significantly promotes moisture damage in mixes, especially in untreated mixes. On the other hand, moisture content and conditioning duration have less effect on the extent of moisture damage in the fatigue test.
2. The typical fatigue beam test procedure determined in Section 6.2 can distinguish mixes with different moisture sensitivities and give a ranking of mixes consistent with prior field experience. The TSR test results are consistent with the fatigue-based test results and the field experience, while the HWTD test results are not consistent with respect to aggregate type and binder type.
3. For mixes treated with hydrated lime, fatigue life is increased instead of decreased by moisture even if the specimens were preconditioned at 60°C. Several reasons may contribute to this result, as discussed in Section 6.3.3.
4. The fatigue-based test procedure can be applied in pavement design to explicitly include the moisture effect. However, a thorough study of the fatigue response at the typical spectra of conditioning and test parameters should be conducted, and extensive field performance data need to be collected for test result calibration before this procedure can be implemented.
5. To sufficiently account for the moisture effect on the rutting resistance of asphalt mixes in the RSST-CH test, specimens need to be preconditioned with moisture in a harsh environment, such as at high temperatures.

Table 6.1. Summary of Fatigue Test Results for Sensitivity Study

Specimen ID	Agg.	Additive	Air Voids (%)	Cond.	Temp. (°C)	Period (Days)	Absorbed Moisture (g)	Sat. (%)	Initial Stiffness (MPa)	Fatigue Life	# of Broken Agg.	Stripping (%)
B-AAN-32A	A	Nil	7.5	Dry	-	-	0.0	0.0	10,109	237,780	2	0
B-AAN-36B	A	Nil	7.3	Dry	-	-	0.0	0.0	9,661	263,569	3	0
B-AAN-34B	A	Nil	7.0	Low	25	1	24.1	28.9	8,645	148,577	1	10
B-AAN-31A	A	Nil	7.4	Low	25	10	31.6	35.8	8,174	134,287	3	10
B-AAN-40A	A	Nil	7.3	Low	60	1	29.8	33.3	7,228	39,686	2	5
B-AAN-35A	A	Nil	7.6	Low	60	10	21.8	22.7	6,121	33,027	0	20
B-AAN-34A	A	Nil	6.5	High	25	1	49.7	63.3	9,246	107,924	1	10
B-AAN-32B	A	Nil	7.0	High	25	10	65.1	78.4	7,156	89,089	1	10
B-AAN-36A	A	Nil	7.0	High	60	1	56.9	66.7	6,524	68,828	2	20
B-AAN-31B	A	Nil	6.7	High	60	10	70.9	88.4	5,220	8,557	0	40
B-AAM-34B	A	Lime	7.2	Dry	-	-	0.0	0.0	10,338	164,169	0	0
B-AAM-40A	A	Lime	6.6	Dry	-	-	0.0	0.0	11,411	115,358	5	0
B-AAM-38B	A	Lime	6.7	Low	25	1	38.2	47.6	9,195	148,746	2	0
B-AAM-36B	A	Lime	7.3	Low	25	10	55.0	61.4	8,766	104,436	2	0
B-AAM-33A	A	Lime	7.6	Low	60	1	51.4	51.5	8,139	179,130	5	0
B-AAM-36A	A	Lime	6.9	Low	60	10	50.1	58.4	8,516	120,415	1	0
B-AAM-35B	A	Lime	7.2	High	25	1	74.1	82.0	9,348	130,853	6	0
B-AAM-38A	A	Lime	7.2	High	25	10	78.4	89.9	9,056	229,308	4	0
B-AAM-40B	A	Lime	7.1	High	60	1	70.0	78.5	9,163	251,336	4	0
B-AAM-34A	A	Lime	6.6	High	60	10	68.3	79.5	9,149	203,671	5	0
B-BAN7-22B	B	Nil	8.2	Dry	-	-	0.0	0.0	8,516	271,860	3	0
B-BAN7-25B	B	Nil	7.6	Dry	-	-	0.0	0.0	8,500	233,745	3	0
B-BAN7-24B	B	Nil	8.5	Low	25	1	44.7	41.7	7,819	299,689	2	0
B-BAN7-23A	B	Nil	8.3	Low	25	10	43.0	40.6	7,350	624,237	4	5

Table 6.1. Summary of Fatigue Test Results for Sensitivity Study *(cont'd)*

Specimen ID	Agg.	Additive	Air Voids (%)	Cond.	Temp. (°C)	Period (Days)	Absorbed Moisture (g)	Sat. (%)	Initial Stiffness (MPa)	Fatigue Life	# of Broken Agg.	Stripping (%)
B-BAN7-26A	B	Nil	8.3	Low	60	1	42.3	39.7	6,886	306,355	1	20
B-BAN7-22A	B	Nil	8.2	Low	60	10	41.5	40.0	5,794	70,086	2	20
B-BAN7-27B	B	Nil	8.3	High	25	1	65.1	71.4	7,703	334,571	3	5
B-BAN7-25A	B	Nil	8.0	High	25	10	79.1	78.3	6,849	497,043	1	10
B-BAN7-24A	B	Nil	8.5	High	60	1	80.7	71.7	6,385	100,628	2	10
B-BAN7-21B	B	Nil	8.3	High	60	10	77.2	75.9	5,352	36,963	2	40
B-BAM7-11A	B	Lime	7.8	Dry	-	-	0.0	0.0	8,870	200,961	3	0
B-BAM7-12A	B	Lime	8.5	Dry	-	-	0.0	0.0	9,185	325,236	2	0
B-BAM7-11B	B	Lime	8.2	Low	25	1	25.6	24.9	8,396	488,373	3	0
B-BAM7-12B	B	Lime	8.5	Low	25	10	31.3	28.3	9,041	451,866	2	5
B-BAM7-23A	B	Lime	7.9	Low	60	1	25.5	25.6	7,478	369,010	2	0
B-BAM7-23B	B	Lime	7.9	Low	60	10	28.5	28.5	6,999	312,365	2	0
B-BAM7-13B	B	Lime	8.0	High	25	1	61.5	58.5	8,058	428,422	2	0
B-BAM7-10A	B	Lime	8.5	High	25	10	58.6	56.3	8,530	298,374	2	5
B-BAM7-15A	B	Lime	8.5	High	60	1	62.3	58.8	7,988	441,031	0	5
B-BAM7-14A	B	Lime	7.9	High	60	10	59.3	60.2	7,616	158,612	1	10

Table 6.2. Normalized Fatigue Test Results for Sensitivity Study

Specimen ID	Aggregate	Treatment	Air-Void Content (%)	Condition	Temperature (°C)	Period (Days)	Initial Stiffness Ratio	Fatigue Life Ratio
B-AAN-34B	A	Nil	7.0	Low	25	1	0.87	0.59
B-AAN-31A	A	Nil	7.4	Low	25	10	0.83	0.54
B-AAN-40A	A	Nil	7.3	Low	60	1	0.73	0.16
B-AAN-35A	A	Nil	7.6	Low	60	10	0.62	0.13
B-AAN-34A	A	Nil	6.5	High	25	1	0.94	0.43
B-AAN-32B	A	Nil	7.0	High	25	10	0.72	0.36
B-AAN-36A	A	Nil	7.0	High	60	1	0.66	0.27
B-AAN-31B	A	Nil	6.7	High	60	10	0.53	0.03
B-AAM-38B	A	Lime	6.7	Low	25	1	0.85	1.06
B-AAM-36B	A	Lime	7.3	Low	25	10	0.81	0.75
B-AAM-33A	A	Lime	7.6	Low	60	1	0.75	1.28
B-AAM-36A	A	Lime	6.9	Low	60	10	0.78	0.86
B-AAM-35B	A	Lime	7.2	High	25	1	0.86	0.94
B-AAM-38A	A	Lime	7.2	High	25	10	0.83	1.64
B-AAM-40B	A	Lime	7.1	High	60	1	0.84	1.80
B-AAM-34A	A	Lime	6.6	High	60	10	0.84	1.46
B-BAN7-24B	B	Nil	8.5	Low	25	1	0.92	1.19
B-BAN7-23A	B	Nil	8.3	Low	25	10	0.86	2.47
B-BAN7-26A	B	Nil	8.3	Low	60	1	0.81	1.21
B-BAN7-22A	B	Nil	8.2	Low	60	10	0.68	0.28
B-BAN7-27B	B	Nil	8.3	High	25	1	0.91	1.32
B-BAN7-25A	B	Nil	8.0	High	25	10	0.80	1.97

Table 6.2. Normalized Fatigue Test Results for Sensitivity Study *(cont'd.)*

Specimen ID	Aggregate	Treatment	Air-Void Content (%)	Condition	Temperature (°C)	Period (Days)	Initial Stiffness Ratio	Fatigue Life Ratio
B-BAN7-24A	B	Nil	8.5	High	60	1	0.75	0.40
B-BAN7-21B	B	Nil	8.3	High	60	10	0.63	0.15
B-BAM7-11B	B	Lime	8.2	Low	25	1	0.93	1.86
B-BAM7-12B	B	Lime	8.5	Low	25	10	1.00	1.72
B-BAM7-23A	B	Lime	7.9	Low	60	1	0.83	1.40
B-BAM7-23B	B	Lime	7.9	Low	60	10	0.78	1.19
B-BAM7-13B	B	Lime	8.0	High	25	1	0.89	1.63
B-BAM7-10A	B	Lime	8.5	High	25	10	0.94	1.13
B-BAM7-15A	B	Lime	8.5	High	60	1	0.88	1.68
B-BAM7-14A	B	Lime	7.9	High	60	10	0.84	0.60

Table 6.3 Estimated Parameters for Initial Stiffness Ratio

Coefficients		Estimated Value	*t* statistics	p-value
Intercept	μ	0.8097	104.5643	0.0000
Aggregate	β_1	0.0309	3.9953	0.0010
Treatment	β_2	0.0434	5.6096	0.0000
Condition	β_3	-0.0059	-0.7668	0.4544
Temperature	β_4	0.0628	8.1117	0.0000
Period	β_5	0.0291	3.7532	0.0017
Aggregate:Treatment	β_{12}	0.0022	0.2825	0.7812
Aggregate:Condition	β_{13}	-0.0047	-0.6054	0.5534
Aggregate:Temperature	β_{14}	0.0028	0.3632	0.7212
Aggregate:Period	β_{15}	-0.0047	-0.6054	0.5534
Treatment:Condition	β_{23}	0.0178	2.3003	0.0352
Treatment:Temperature	β_{24}	-0.0272	-3.511	0.0029
Treatment:Period	β_{25}	-0.0284	-3.6725	0.0021
Condition:Temperature	β_{34}	-0.0053	-0.6861	0.5025
Condition:Period	β_{35}	0.0084	1.0896	0.2920
Temperature:Period	β_{45}	-0.0053	-0.6861	0.5025

R^2=0.910

Table 6.4 NOVA of Initial Stiffness Ratio

Factor	Degree of Freedom	Sum of Squares	Mean Square	F-value	p-value
Aggregate	1	0.0306	0.0306	15.9625	0.0010
Treatment	1	0.0604	0.0604	31.4674	0.0000
Condition	1	0.0011	0.0011	0.5880	0.4544
Temperature	1	0.1263	0.1263	65.7997	0.0000
Period	1	0.0270	0.0270	14.0863	0.0017
Aggregate:Treatment	1	0.0002	0.0002	0.0798	0.7812
Aggregate:Condition	1	0.0007	0.0007	0.3665	0.5534
Aggregate:Temperature	1	0.0003	0.0003	0.1319	0.7212
Aggregate:Period	1	0.0007	0.0007	0.3665	0.5534
Treatment:Condition	1	0.0102	0.0102	5.2915	0.0352
Treatment:Temperature	1	0.0237	0.0237	12.3274	0.0029
Treatment:Period	1	0.0259	0.0259	13.4870	0.0021
Condition:Temperature	1	0.0009	0.0009	0.4707	0.5025
Condition:Period	1	0.0023	0.0023	1.1873	0.2920
Temperature:Period	1	0.0009	0.0009	0.4707	0.5025
Residuals	16	0.0307	0.0019		

Table 6.5 Estimated Parameters for Fatigue Life Ratio

Coefficients		Estimated Value	*t* statistics	p-value
Intercept	μ	1.0156	17.0465	0.0000
Aggregate	β_1	0.2469	4.1436	0.0008
Treatment	β_2	0.2969	4.9828	0.0001
Condition	β_3	-0.0275	-0.4616	0.6506
Temperature	β_4	0.2094	3.5142	0.0029
Period	β_5	0.0606	1.0175	0.3240
Aggregate:Treatment	β_{12}	-0.1581	-2.6540	0.0173
Aggregate:Condition	β_{13}	-0.1250	-2.0980	0.0521
Aggregate:Temperature	β_{14}	0.1894	3.1785	0.0058
Aggregate:Period	β_{15}	0.0131	0.2203	0.8284
Treatment:Condition	β_{23}	0.0750	1.2588	0.2262
Treatment:Temperature	β_{24}	-0.1806	-3.0317	0.0079
Treatment:Period	β_{25}	0.0831	1.3952	0.1820
Condition:Temperature	β_{34}	-0.0200	-0.3357	0.7415
Condition:Period	β_{35}	0.0100	0.1678	0.8688
Temperature:Period	β_{45}	-0.1581	-2.6540	0.0173

R^2=0.859

Table 6.6 ANOVA of Fatigue Life Ratio.

Factor	Degree of Freedom	Sum of Squares	Mean Square	F-value	p-value
Aggregate	1	1.9503	1.9503	17.1695	0.0008
Treatment	1	2.8203	2.8203	24.8286	0.0001
Condition	1	0.0242	0.0242	0.2130	0.6506
Temperature	1	1.4028	1.4028	12.3496	0.0029
Period	1	0.1176	0.1176	1.0354	0.3240
Aggregate:Treatment	1	0.8001	0.8001	7.0438	0.0173
Aggregate:Condition	1	0.5000	0.5000	4.4017	0.0521
Aggregate:Temperature	1	1.1476	1.1476	10.1030	0.0058
Aggregate:Period	1	0.0055	0.0055	0.0485	0.8284
Treatment:Condition	1	0.1800	0.1800	1.5846	0.2262
Treatment:Temperature	1	1.0440	1.0440	9.1910	0.0079
Treatment:Period	1	0.2211	0.2211	1.9466	0.1820
Condition:Temperature	1	0.0128	0.0128	0.1127	0.7415
Condition:Period	1	0.0032	0.0032	0.0282	0.8688
Temperature:Period	1	0.8001	0.8001	7.0438	0.0173
Residuals	16	1.8175	0.1136		

Table 6.7 Fatigue-Based Test Results for the Comparative Study

Specimen ID	Agg.	Binder	Treatment	Air Voids (%)	Pre. Temp. (□C)	Initial Stiffness (MPa)	Fatigue Life
B-AAN7-32A	A	AR-4000	Nil	7.5	-	10,109	237,780
B-AAN7-36B	A	AR-4000	Nil	7.2	-	9,661	263,569
B-AAN7-34A	A	AR-4000	Nil	6.5	25	9,246	107,924
B-AAN7-14A	A	AR-4000	Nil	7.0	25	8,120	41,387
B-AAN7-36A	A	AR-4000	Nil	7.0	60	6,524	68,828
B-AAN7-30A	A	AR-4000	Nil	7.8	60	5,933	71,655
B-AAM7-34B	A	AR-4000	Lime	7.2	-	10,338	164,169
B-AAM7-40A	A	AR-4000	Lime	6.6	-	11,411	115,358
B-AAM7-35B	A	AR-4000	Lime	7.2	25	9,348	130,853
B-AAM7-8B	A	AR-4000	Lime	6.5	25	10,335	316,789
B-AAM7-40B	A	AR-4000	Lime	7.1	60	9,163	251,336
B-AAM7-28A	A	AR-4000	Lime	7.9	60	8,937	342,974
B-BAN7-22B	B	AR-4000	Nil	8.2	-	8,516	271,860
B-BAN7-25B	B	AR-4000	Nil	7.6	-	8,500	233,745
B-BAN7-27B	B	AR-4000	Nil	8.3	25	7,703	334,571
B-BAN7-2	B	AR-4000	Nil	7.7	25	8,180	329,979
B-BAN8-1B	B	AR-4000	Nil	8.0	60	6,920	231,782
B-BAN7-24A	B	AR-4000	Nil	8.5	60	6,385	100,628
B-BAM7-11A	B	AR-4000	Lime	7.8	-	8,870	200,961
B-BAM7-12A	B	AR-4000	Lime	8.6	-	9,185	325,236
B-BAM7-13B	B	AR-4000	Lime	8.0	25	8,058	428,422
B-BAM7-11B	B	AR-4000	Lime	8.1	25	8,396	488,373
B-BAM7-15A	B	AR-4000	Lime	8.6	60	7,988	441,031
B-BAM7-23A	B	AR-4000	Lime	7.9	60	7,478	369,010

Table 6.7 Fatigue-Based Test Results for the Comparative Study *(cont'd.)*

Specimen ID	Agg.	Binder	Treatment	Air Voids (%)	Pre. Temp. (□C)	Initial Stiffness (MPa)	Fatigue Life[a]
B-APN7-2A	A	PBA-6a	Nil	7.7	-	994	96,436,283
B-APN7-4B	A	PBA-6a	Nil	6.3	-	1,220	5,047,837
B-APN7-1B	A	PBA-6a	Nil	6.3	25	773	125,374,680
B-APN7-3A	A	PBA-6a	Nil	7.7	25	1,103	14,185,657
B-APN7-4A	A	PBA-6a	Nil	6.9	60	926	16,465,919
B-APN7-2B	A	PBA-6a	Nil	7.6	60	775	65,191,529
B-APM7-2A	A	PBA-6a	Lime	7.8	-	1,181	2,278,575,900
B-APM7-4A	A	PBA-6a	Lime	6.6	-	1,016	15,021,183,464
B-APM7-4B	A	PBA-6a	Lime	7.0	25	1,029	4,472,431,944
B-APM7-2B	A	PBA-6a	Lime	7.3	25	1,159	34,095,361,462
B-APM7-6A	A	PBA-6a	Lime	6.7	60	1,299	625,402,656
B-APM7-6B	A	PBA-6a	Lime	6.8	60	1,253	1,499,510,666
B-BPN7-1A	B	PBA-6a	Nil	6.6	-	834	88,782,770
B-BPN7-2B	B	PBA-6a	Nil	7.6	-	852	49,438,851
B-BPN7-2A	B	PBA-6a	Nil	6.5	25	768	147,687,049
B-BPN7-3A	B	PBA-6a	Nil	7.7	25	819	71,545,693
B-BPN7-1B	B	PBA-6a	Nil	7.0	60	857	28,095,251
B-BPN7-3B	B	PBA-6a	Nil	7.5	60	935	29,456,133
B-BPM7-2A	B	PBA-6a	Lime	6.7	-	971	929,207,166
B-BPM7-3B	B	PBA-6a	Lime	6.8	-	913	115,308,131,495
B-BPM7-2B	B	PBA-6a	Lime	6.3	25	950	52,419,247,658
B-BPM7-4A	B	PBA-6a	Lime	7.7	25	963	96,011,695,494
B-BPM7-3A	B	PBA-6a	Lime	6.9	60	953	420,219,363
B-BPM7-4B	B	PBA-6a	Lime	8.0	60	1,033	6,577,936,291

[a]Fatigue lives of specimens containing PBA-6a binder were all calculated from extrapolated stiffness deterioration curves.

Table 6.8 Comparison of Normalized Fatigue Test Results with TSR and HWTD Test Results

Mix Type[a]	Preconditioning Temperature 25°C		Preconditioning Temperature 60°C		Tensile Strength Ratio (%)	Rut Depth after 20,000 Passes (mm)
	ISR	FLR	ISR	FLR		
AAN	0.88	0.30	0.63	0.28	29	6.62
AAM	0.91	1.60	0.83	2.13	85	6.82
BAN	0.93	1.31	0.78	0.66	52	7.84
BAM	0.91	1.74	0.86	1.54	91	6.94
APN	0.85	-	0.77	-	47	42.3
APM	1.00	-	1.16	-	86	10.17
BPN	0.94	-	1.06	-	85	56.40
BPM	1.02	-	1.05	-	100	13.73

[a]First letter represents aggregate (A or B); second letter represents binder (A – AR-4000, P – PBA-6a); third letter represents treatment (N – nil, M – hydrated lime).

Table 6.9 Fatigue Responses at Different Strain Levels

Mix	Specimen ID	Air Voids (%)	Preconditioning Status	Strain Level (micron)	Initial Stiffness (MPa)	Fatigue Life
AAN	B-AAN7-30A	7.8	Wet at 60°C	200	5,933	71,655
AAN	B-AAN7-36A	7.0	Wet at 60°C	200	6,524	68,828
AAN	B-AAN7-26A	6.0	Wet at 60°C	300	7,458	9,097
AAN	B-AAN7-40B	7.7	Wet at 60°C	300	6,031	6,452
AAN	B-AAN7-26B	6.3	Wet at 60°C	400	7,166	3,066
AAN	B-AAN7-33A	7.8	Wet at 60°C	400	5,117	2,094
AAN	B-AAN7-32A	7.5	Dry	200	10,109	237,780
AAN	B-AAN7-36B	7.2	Dry	200	9,661	263,569
AAN	B-AAN7-35B	7.9	Dry	300	9,759	38,263
AAN	B-AAN7-39B	7.1	Dry	300	10,083	45,396
AAN	B-AAN7-25A	7.4	Dry	400	11,396	23,953
AAN	B-AAN7-22B	6.5	Dry	400	10,830	18,901
AAM	B-AAM7-28A	7.9	Wet at 60°C	200	8,937	342,974
AAM	B-AAM7-40B	7.1	Wet at 60°C	200	9,163	251,336
AAM	B-AAM7-26A	7.1	Wet at 60°C	300	9,415	67,499
AAM	B-AAM7-39B	8.2	Wet at 60°C	300	9,394	37,601
AAM	B-AAM7-26B	6.8	Wet at 60°C	400	6,976	3,066
AAM	B-AAM7-28B	7.8	Wet at 60°C	400	9,202	28,174
AAM	B-AAM7-34B	7.2	Dry	200	10,338	164,169
AAM	B-AAM7-40A	6.6	Dry	200	11,411	115,358
AAM	B-AAM7-29B	6.6	Dry	300	11,049	31,166
AAM	B-AAM7-39A	8.1	Dry	300	9,191	44,712
AAM	B-AAM7-25A	7.2	Dry	400	11,888	7,581
AAM	B-AAM7-37B	6.9	Dry	400	11,044	8,643

Table 6.10 Estimated Parameters for Fatigue Functions under Different Conditions

Mix	Condition	$\ln(\alpha)$	β	γ	R-square
AAN	Wet at 60°C	30.5112	-4.8197	0.6974	0.984
AAN	Dry	-4.8065	-4.3020	4.3498	0.992
AAM	Wet at 60°C	-23.5527	-3.9530	6.2532	0.957
AAM	Dry	57.0914	-3.8708	-2.6613	0.997

Table 6.11 Calculation of Fatigue Life with Moisture Effect Included

Mix	Condition	Initial Stiffness (MPa)	Maximum Principal Strain in AC Layer (micron)	Fatigue Life in one Condition	Percentage of Traffic in Each Condition	Field Fatigue in Composite Conditions
AAN	Dry	10,306	91	8,725,382	60%	1,518,423
	Wet2	6,372	123	678,181	40%	
AAM	Dry	10,820	88	3,400,084	60%	3,444,300
	Wet2	8,848	100	3,512,825	40%	

Table 6.12 RSST-CH Test Results

Mix Type	Specimen ID	Air-void Content (%)	Condition	Saturation (%)	Cycles to 5% Permanent Strain	Permanent Strain at 4000 Cycles
APN	C-APN7-8A	7.6	DRY	0	1,820	0.064
APN	C-APN7-11A	7.3	DRY	0	1,390	0.072
APN	C-APN7-9B	7.6	WET	76	3,375	0.053
APN	C-APN7-10A	7.9	WET	79	3,903	0.051
BPN	C-BPN7-10B	8.3	DRY	0	883	0.085
BPN	C-BPN7-9B	6.4	DRY	0	7,011	0.044
BPN	C-BPN7-8B	8.1	WET	80	368	0.120
BPN	C-BPN7-9A	8.4	WET	71	2,393	0.058
AAN	C-AAN-OM7-10	8.4	DRY	0	7,722	0.040
AAN	C-AAN-OM7-18	8.2	DRY	0	18,450	0.022
AAN	C-AAN-OM7-11	8.3	WET	73	35,874	0.023
AAN	C-AAN-OM7-12	6.7	WET	90	>50,000	0.020
BAN	C-BAN-OM7-9	7.4	DRY	0	712	0.091
BAN	C-BAN-OM7-12	7.0	DRY	0	9,300	0.037
BAN	C-BAN-OM7-10	6.9	WET	88	1,237	0.080
BAN	C-BAN-OM7-11	7.6	WET	84	11,496	0.034
AAM	C-AAM-OM7-1	6.8	DRY	0	>44205	0.024
AAM	C-AAM-OM7-2	7.6	DRY	0	>50,000	0.018
AAM	C-AAM-OM7-21	7.8	WET	68	27,667	0.025
AAM	C-AAM-OM7-8	7.9	WET	63	7,266	0.040
AALA	C-AALA-OM7-11	7.3	DRY	0	9,571	0.037
AALA	C-AALA-OM7-4	7.6	DRY	0	4,129	0.049
AALA	C-AALA-OM7-5	7.3	WET	84	>50,000	0.020
AALA	C-AALA-OM7-7	8.0	WET	77	>10,000	0.032

Figure 6-1. Flexural beam fatigue testing machine.

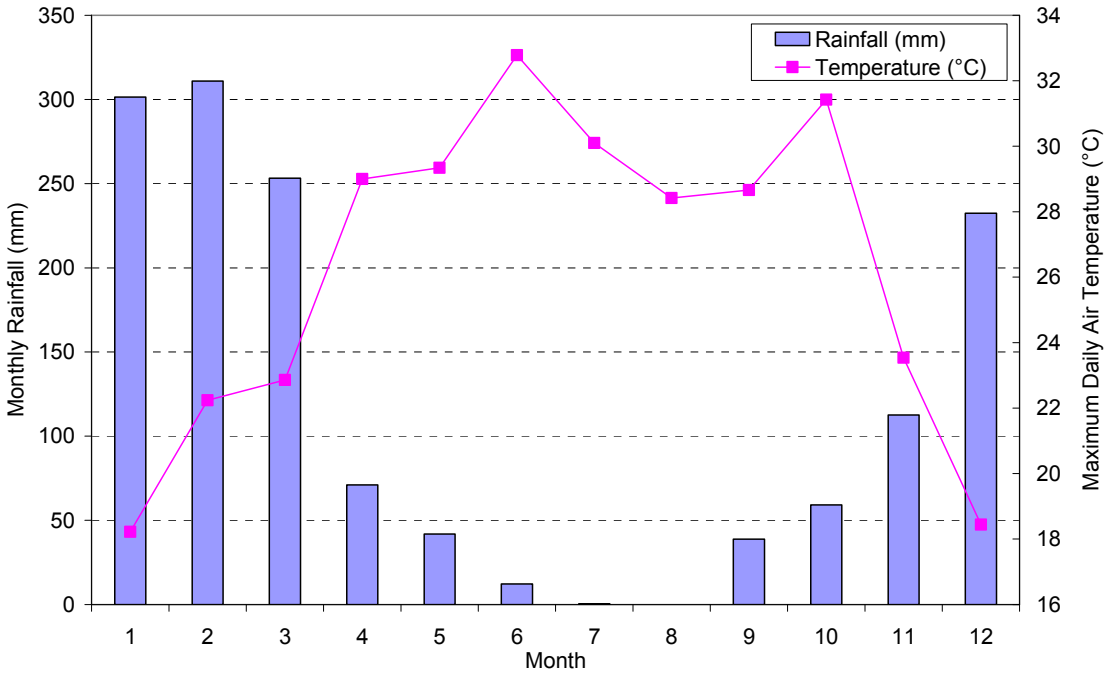

Figure 6-2. Monthly rainfall and maximum daily air temperature in the San Francisco Bay Area.

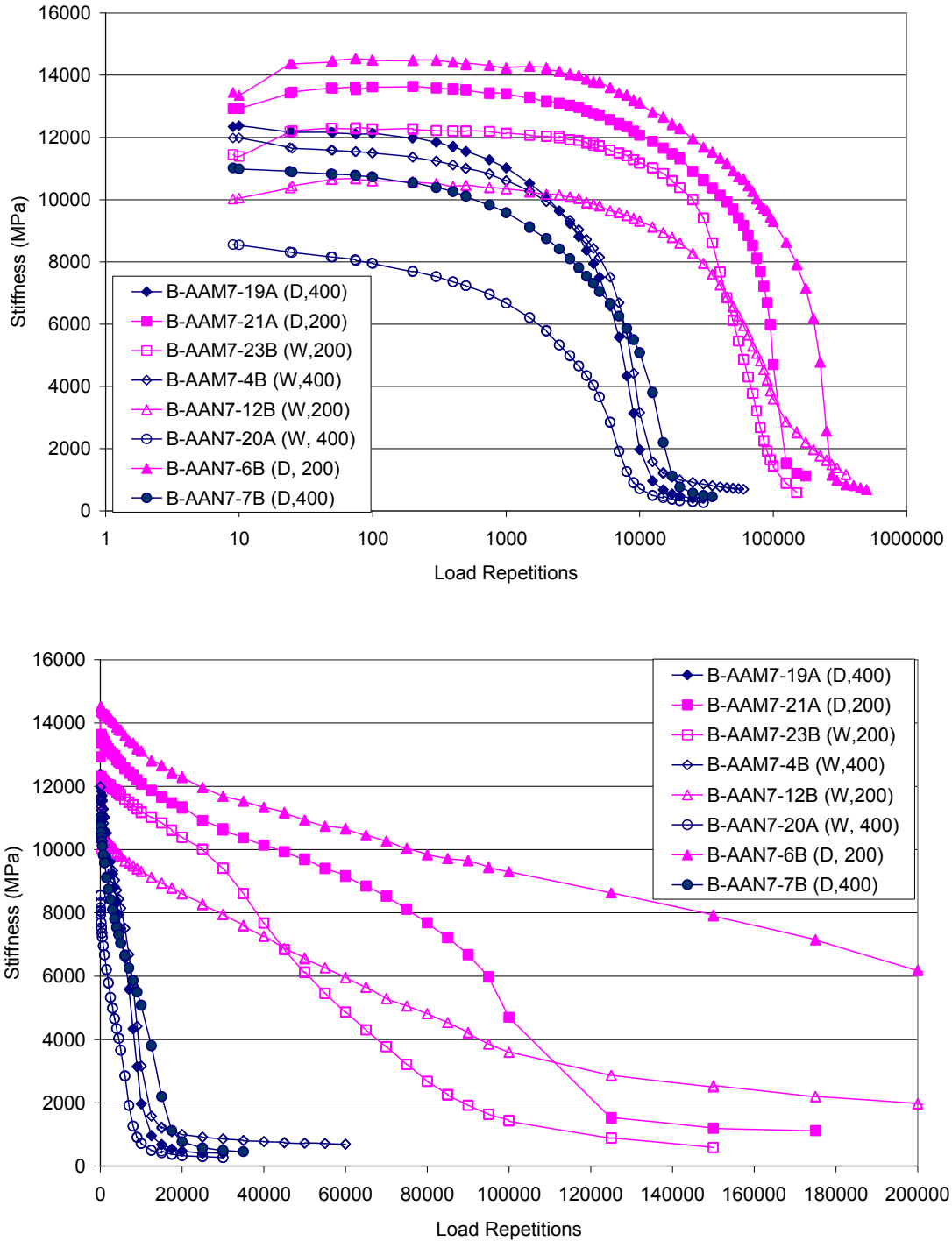

Figure 6-3. Stiffness deterioration curves of mixes used to determine the strain level.

(The first letter in the parentheses of the legend represents condition: W, Wet; D, Dry; the number in parenthesis is strain level.)

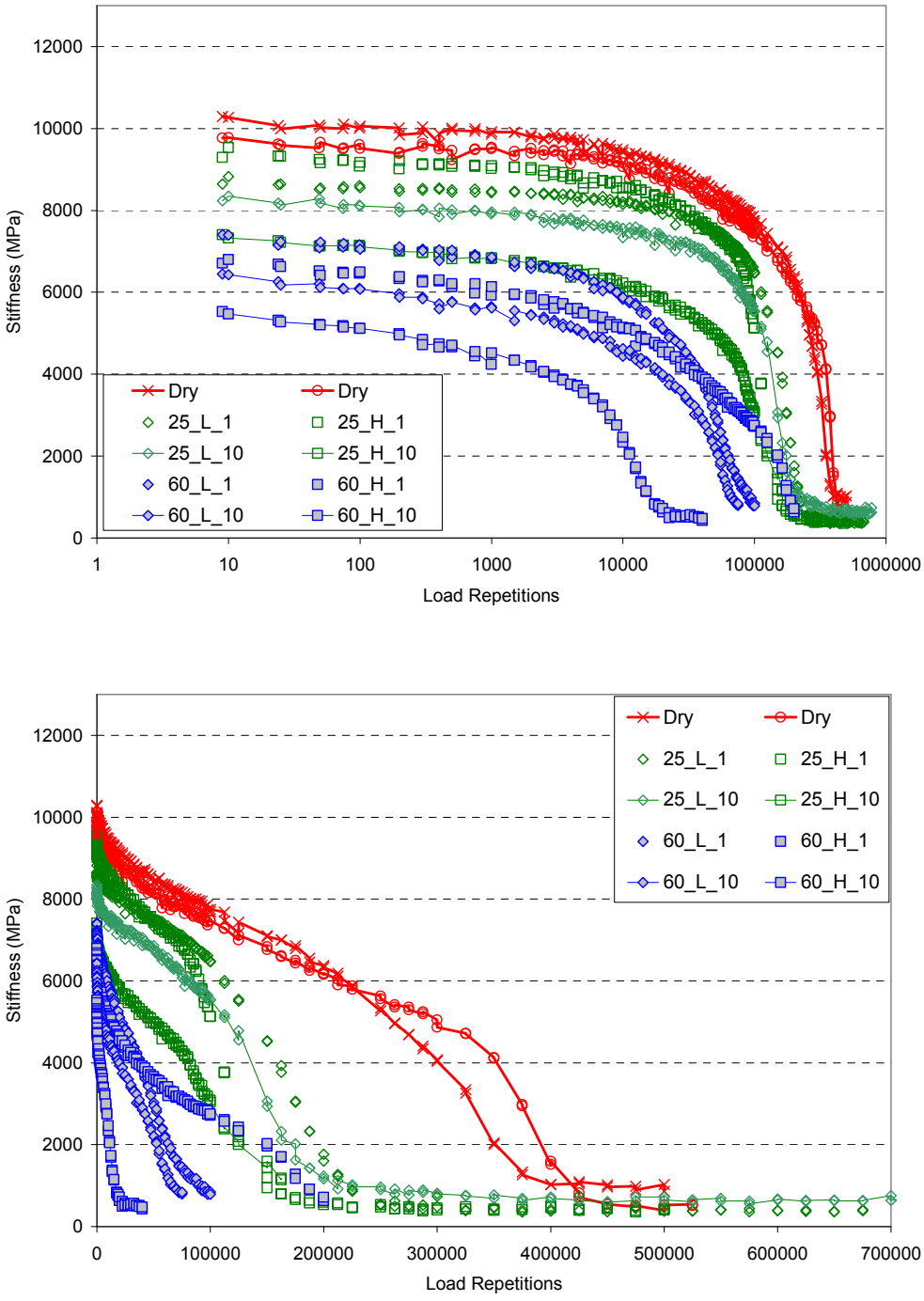

Figure 6-4. Stiffness deterioration curves of AAN.

(The first component in the parentheses of the legend represents preconditioning temperature: 25 - 25°C, 60 – 60°C; the second component represents moisture content: L –low, H – high; the third component represents condition duration: 1 – 1 day, 10 – 10 days.).

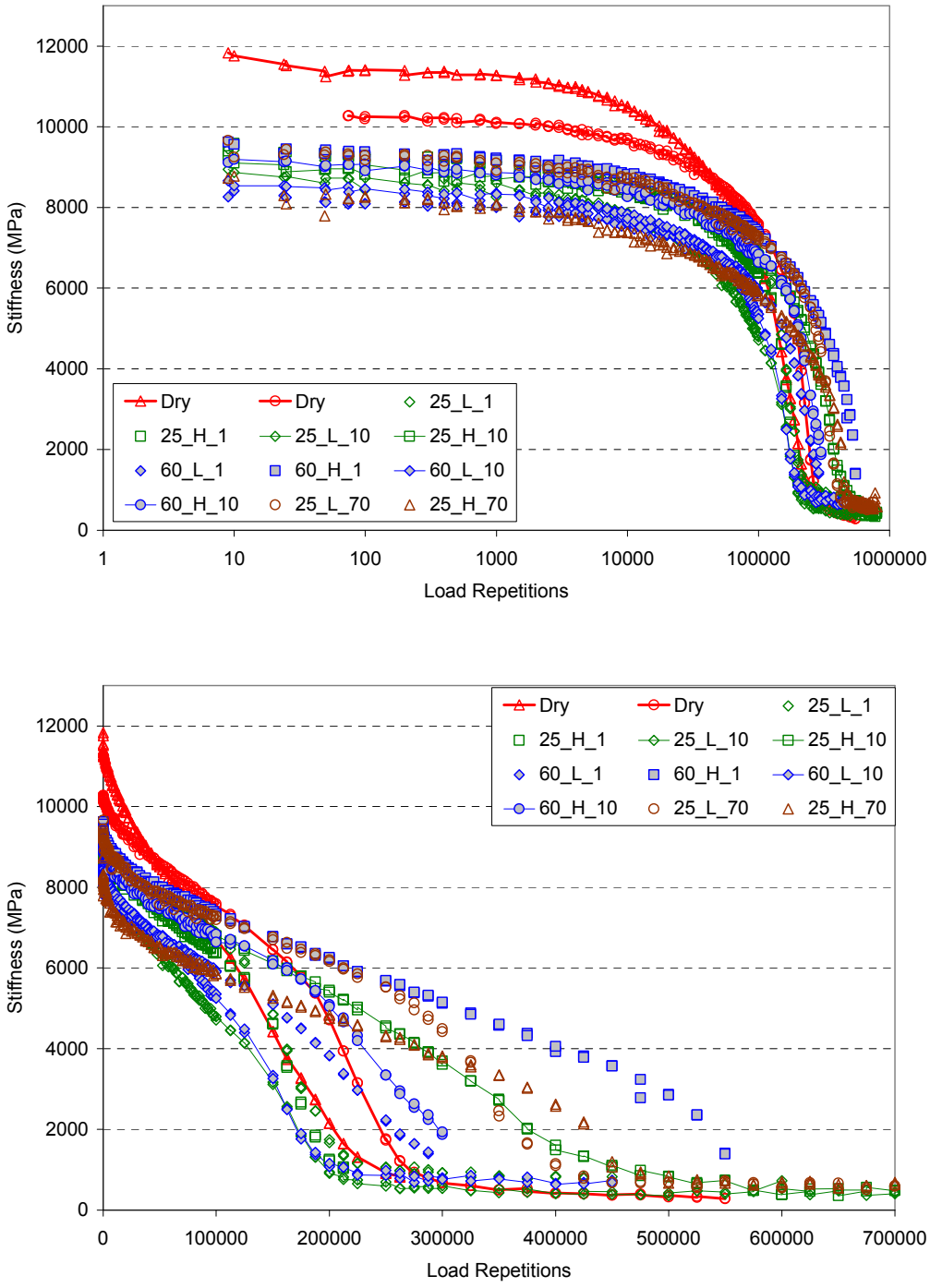

Figure 6-5. Stiffness deterioration curves of AAM.

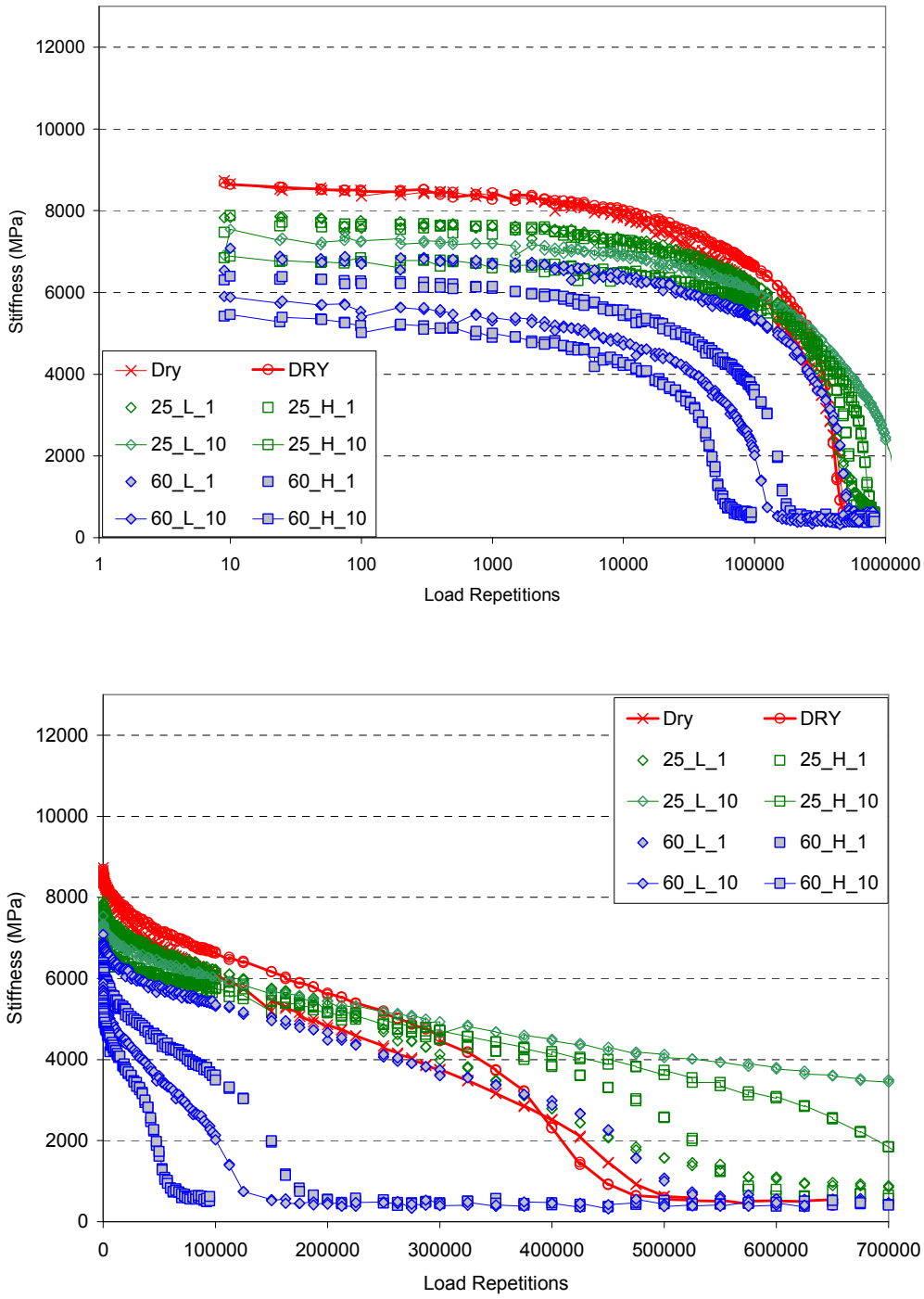

Figure 6-6. Stiffness deterioration curves of BAN.

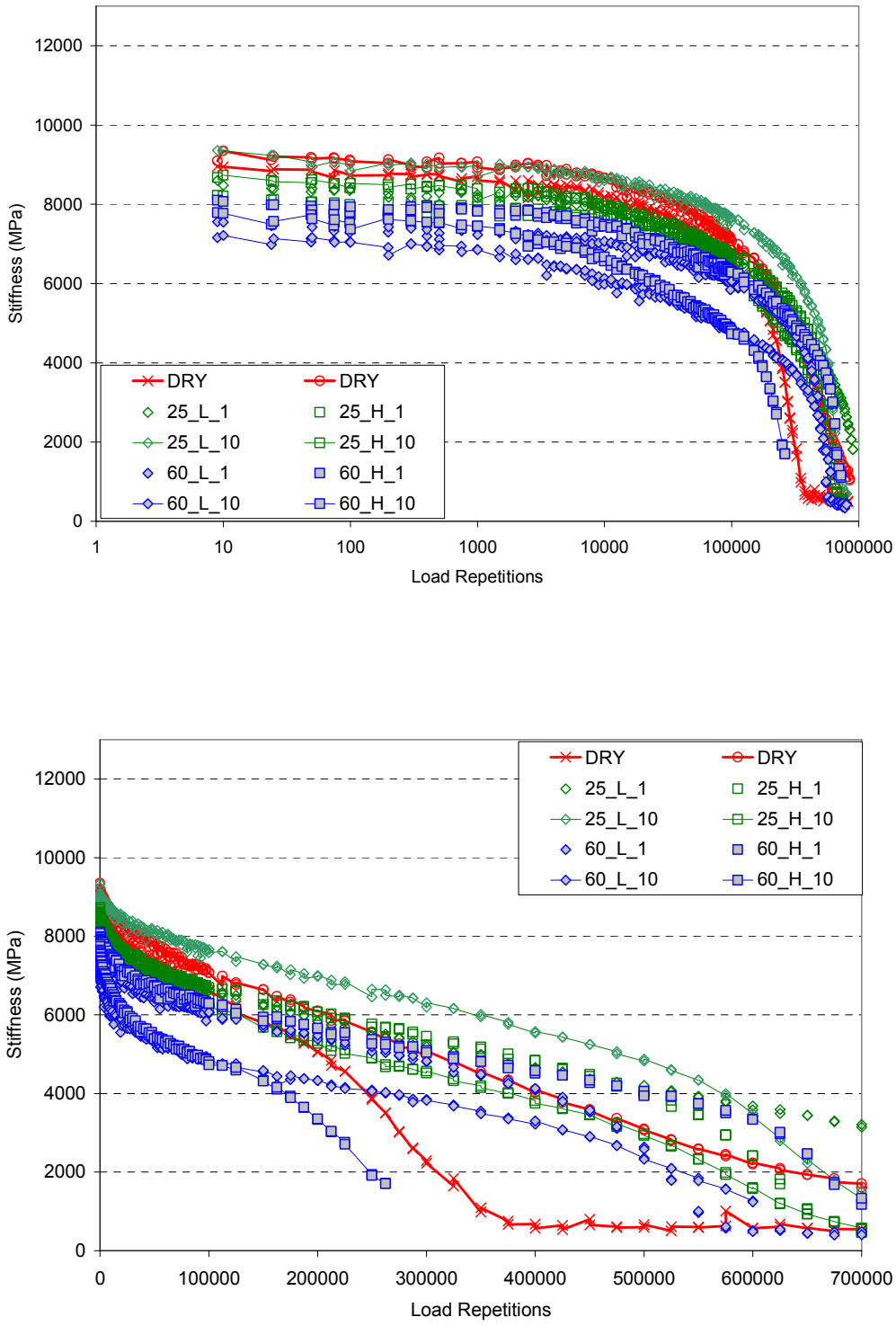

Figure 6-7. Stiffness deterioration curves of BAM.

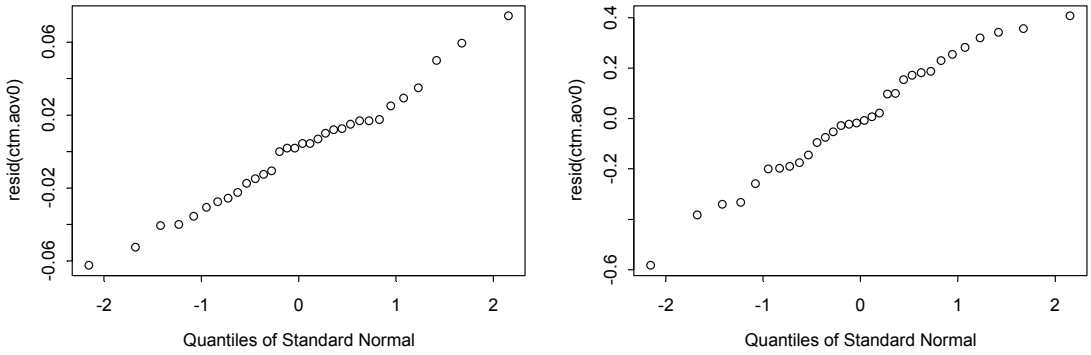

(a) (b)

Figure 6-8. QQ-normal plots of residuals (a. – Initial Stiffness Ratio, b – Fatigue Life Ratio).

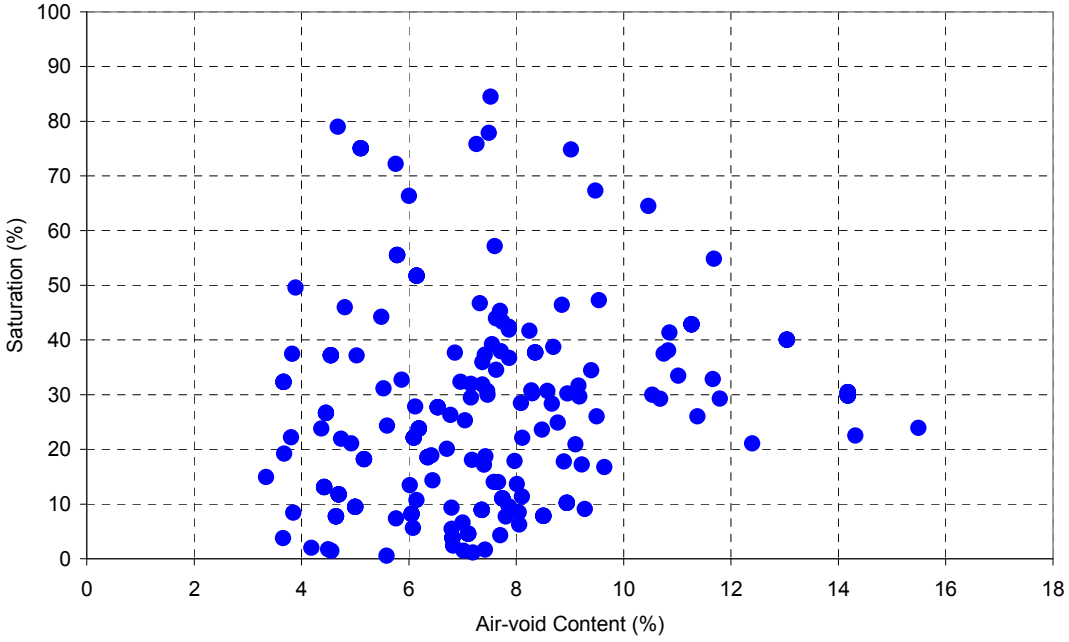

Figure 6-9. In-situ saturation versus air-void content measured from dry cores.

Figure 6-10. Apparatus for saturating specimens by vacuum.

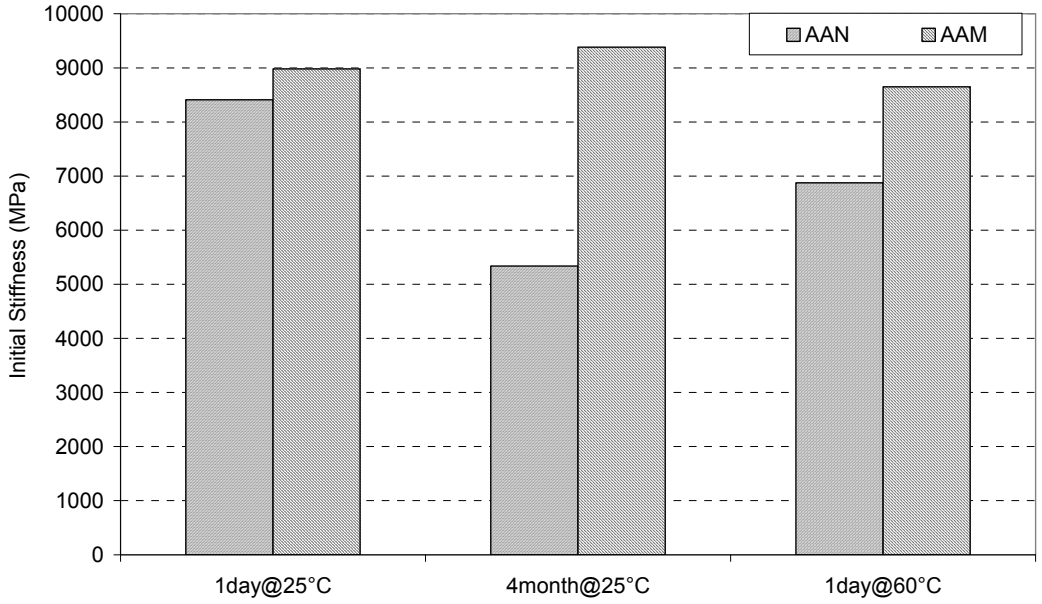

(a)

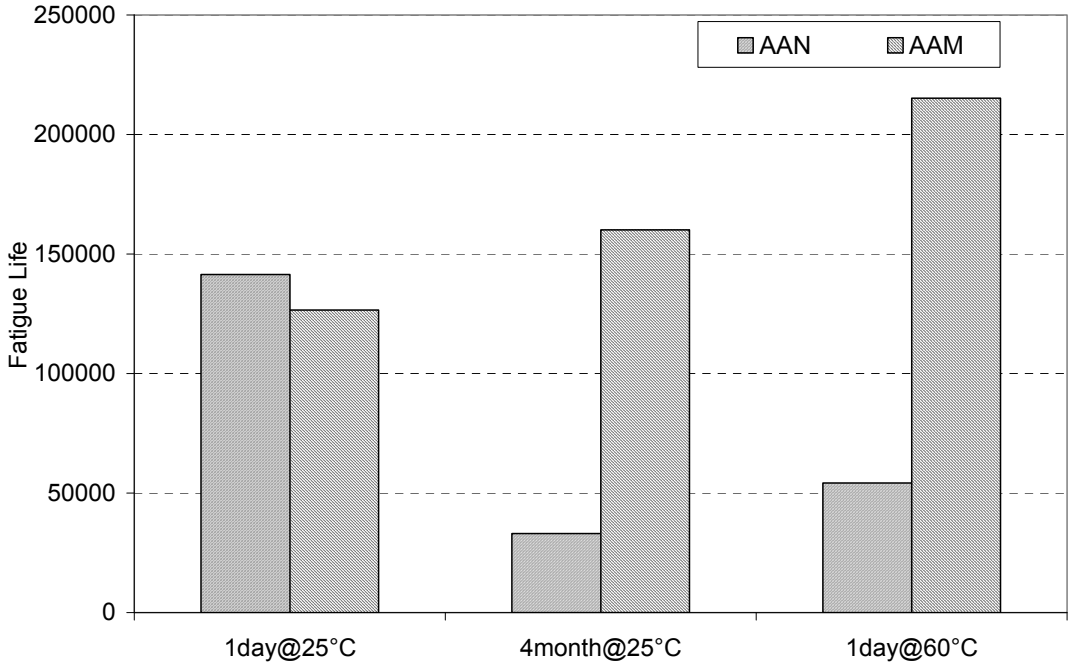

(b)

Figure 6-11. Comparison of fatigue test results after different conditioning procedures (a- initial stiffness, b – fatigue life).

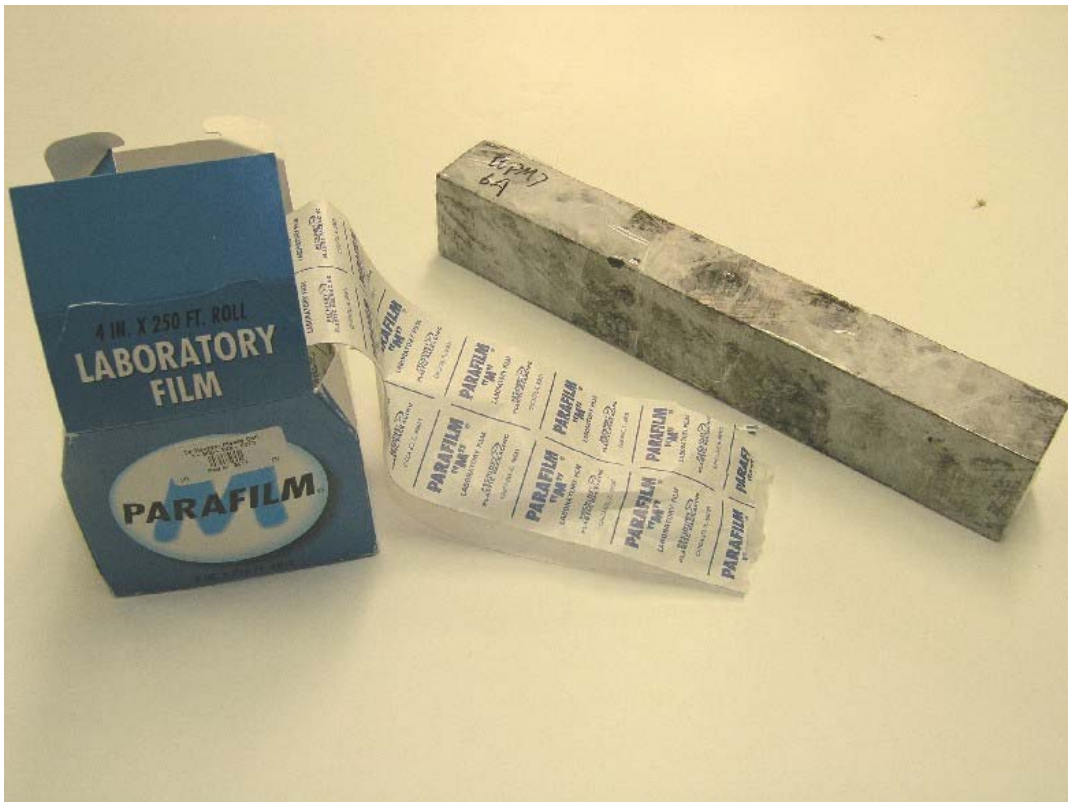

Figure 6-12. Fatigue beam specimen wrapped with Parafilm.

(a)

(b)

Figure 6-13. Equipment used for the TSR test (a – Southwark Tate-Emery hydraulic testing machine, b –Gilson MS-35 Lottman breaking head).

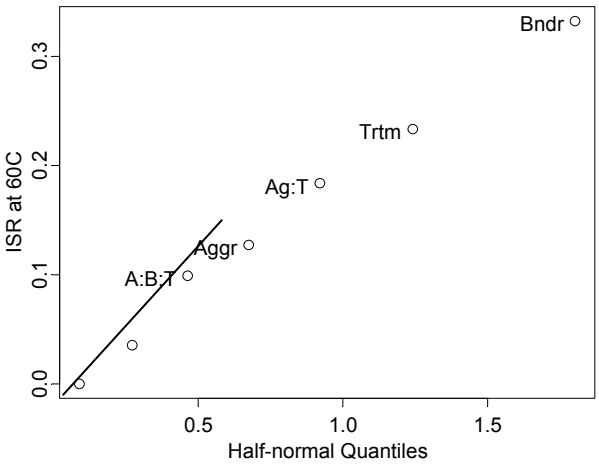

(a)

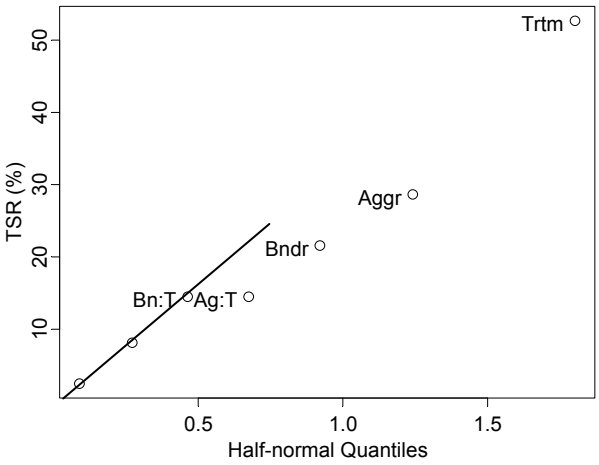

(b)

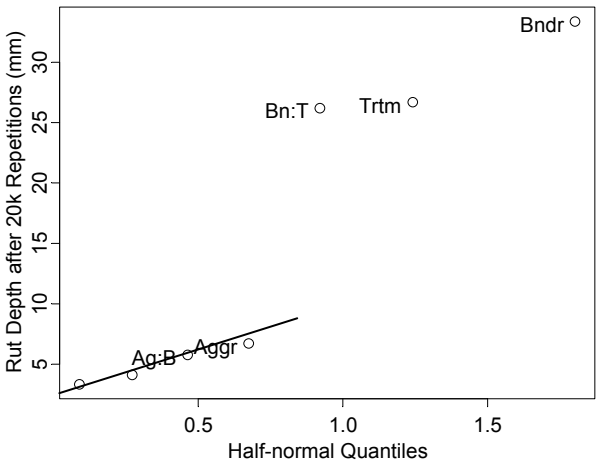

(c)

Figure 6-14. Daniel's half normal plot (a – ISR after preconditioning at 60°C, b – TSR, c – Rut Depth at 20,000 passes).

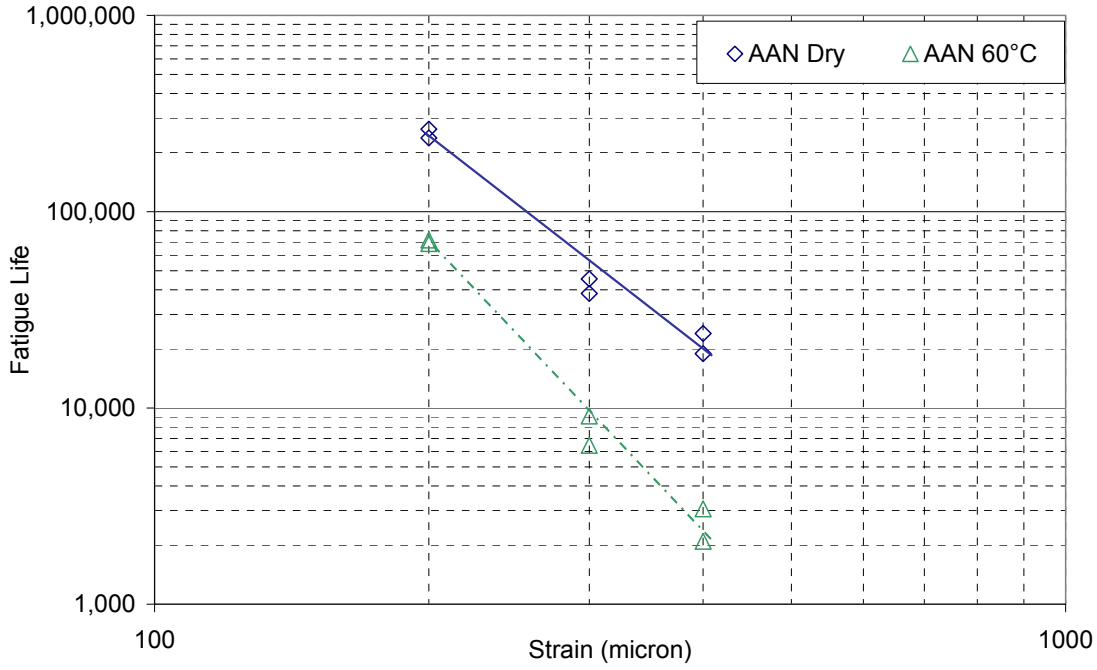

(a)

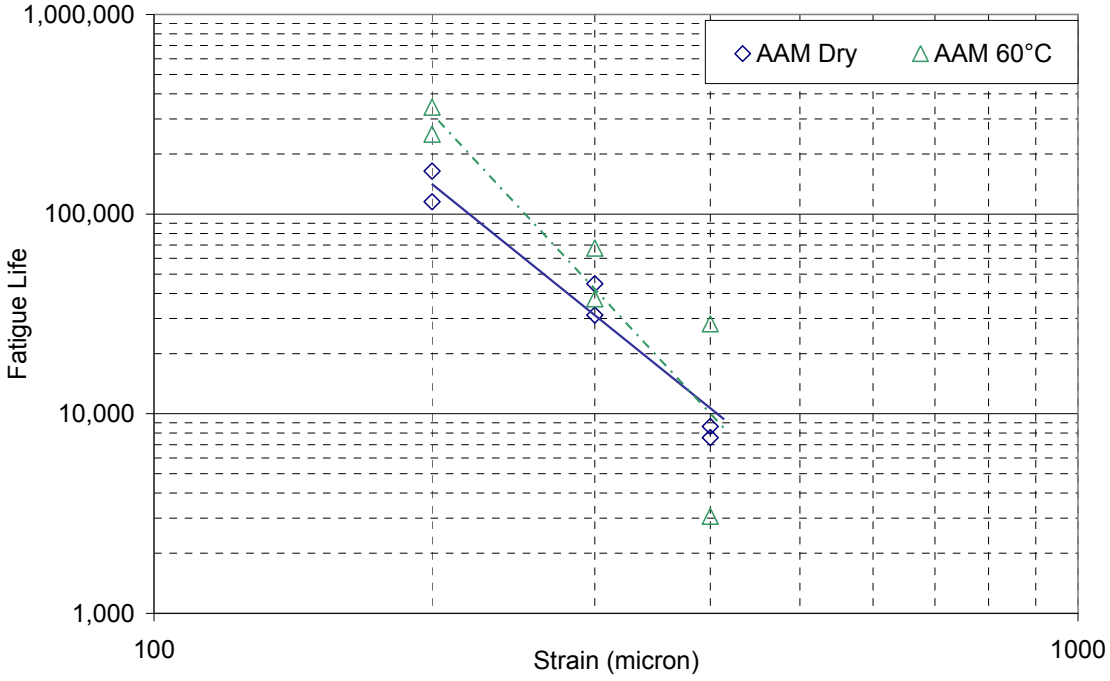

(b)

Figure 6-15. Fatigue life versus strain level (a – AAN, b – AAM).

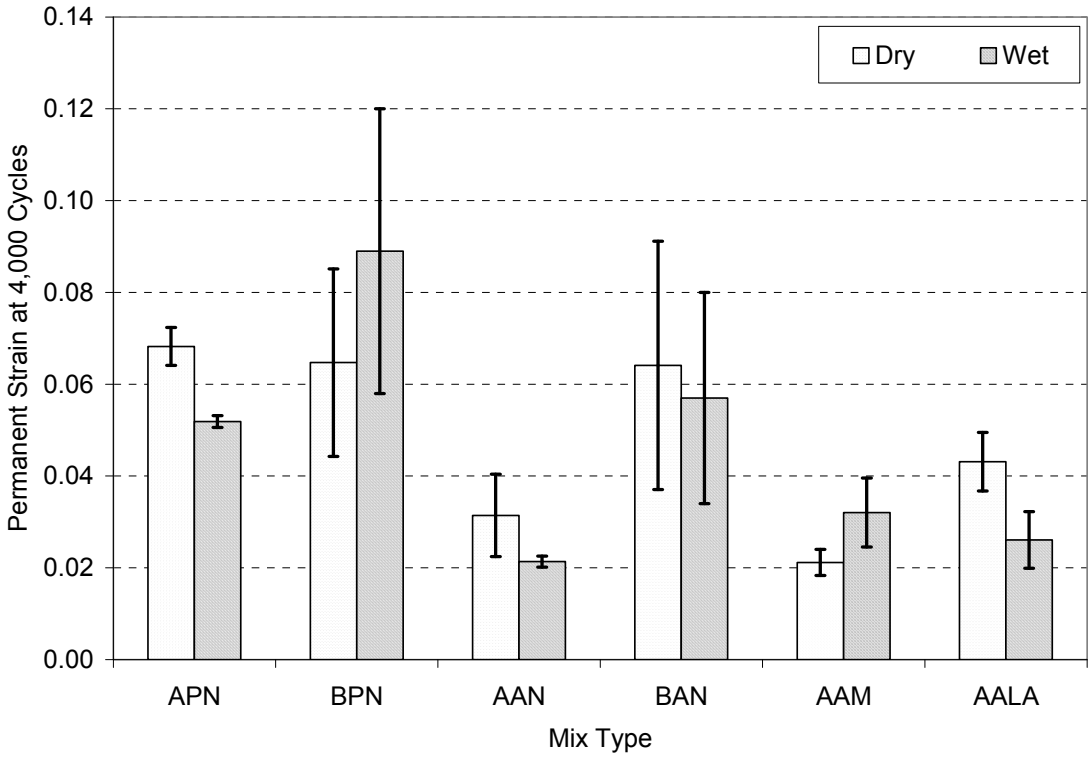

Figure 6-16. RSST-CH test results.

7.0 LONG-TERM EFFECTIVENESS OF ADDITIVES

This chapter focuses on the long-term effectiveness of antistripping additives under prolonged moisture conditioning situation. Also studied here are the evolution of moisture effect with time and the equivalency of different conditioning procedures.

7.1 Experimental Design

Two test methods were used to examine the long-term effectiveness of antistripping additives: the indirect tensile strength ratio (TSR) test and the flexural beam fatigue test. The TSR test examines the strength loss of asphalt mixes due to moisture, whereas the flexural beam fatigue test examines the effect of moisture on the fatigue response of asphalt mixes.

The control mix used in the experiment consists of Aggregate A and the AR-4000 binder, using the 19-mm nominal maximum medium dense gradation. Both hydrated lime and two liquid antistripping agents (A and B) are included as antistripping additives.

7.1.1 Indirect Tensile Strength Ratio (TSR) Test

Hveem specimens 101 mm in diameter and 63.5 mm in height were used in this test. The specimens were compacted to an air-void content targeted at 6.5 percent by a kneading compactor.

The factors included in the experiment were as follows:

Three antistripping additive cases: nil, hydrated lime, and liquid antistripping Agent A. Hydrated lime was added to dampened aggregates at a ratio of 1.4 percent (by dry mass of aggregate), while the liquid antistripping Agent A was added to asphalt at a ratio of 0.75 percent (by mass of asphalt).

Four conditioning periods: zero, four, eight, and twelve months. The period "zero months" means that specimens were tested immediately after moisture was introduced by vacuum.

Three conditioning procedures: *Dry*, *25C*, and *CTM371*. *Dry* means that dry specimens were stored in a room at a controlled temperature 20°C until testing. *25C* means the specimens were first submerged in water under a vacuum of 50 kPa absolute pressure (381 mm-Hg vacuum pressure) for three minutes and stored in a humid room at 25°C and 100 percent relative humidity (RH) until testing. *CTM371* means that after the conditioning procedure as used in *25C*, the specimens were further conditioned following the procedure in the CTM 371 test, that is, a freeze-thaw cycle of 16 hours at -18°C and then 24 hours at 60°C.

The partially saturated specimens were wrapped with a plastic film and sealed in ziplock bags before they were stored in the humid room. Before the strength testing, all specimens were placed in a 25°C water bath for two hours to reach the target test temperature. The indirect tensile strength (ITS) was measured with a Gilson MS-35 breaking head at a loading rate of 50 mm per minute on a Southwark Tate-Emery testing machine.

A 3×4×3 full factorial experiment was designed and three replicates were tested at each combination of factor levels. Therefore, a total of 108 Hveem specimens were used in the experiment.

Multiple response variables were recorded during the test, including the maximum load at failure, the extent of stripping by visual inspection, and the number of broken aggregates on the split faces. The extent of stripping was evaluated visually on an ordered categorical scale: None (no stripping), L (less than 10 percent

stripping), LM (10 to 20 percent stripping), M (20 to 40 percent stripping), MH (40 to 60 percent stripping), and H (more than 60 percent stripping).

7.1.2 Flexural Beam Fatigue Test

The same factor levels as in the TSR test were included in the flexural beam fatigue test with two exceptions: the *CTM371* conditioning procedure was not included; another liquid antistripping agent (liquid B) was added. Moreover, two replicates were tested at each factor level combination. Therefore, a total of 64 beam specimens were used in this test. All beams had the 19-mm nominal maximum medium dense gradation and were compacted to an air-void content between 6 percent and 8 percent.

The beams tested in wet condition were first saturated under a vacuum of 16 kPa absolute pressure (635 mm-Hg vacuum pressure) for 30 minutes, then wrapped in a plastic bag and left in the same humid room as the Hveem specimens. Before testing, the specimens were placed in a 20°C temperature chamber for at least two hours to reach the target test temperature.

The stiffness deterioration process was recorded during the test. Moreover, the extent of stripping and the number of broken aggregates on the split faces were also observed after the test. The extent of stripping was estimated visually on a percentage scale.

7.2 Results and Analysis

7.2.1 TSR Test

Results of the TSR test are summarized in Table 7.1. The air-void content and saturation level of each specimen are plotted in Figure 7-1, which shows that both variables were well controlled in a narrow range, so their effects on the test results should not be significant, as verified later in the statistical analysis.

7.2.1.1 General Observations

7.2.1.1.1 Indirect Tensile Strength

The average ITS at each factor level combination is shown in Figure 7-2, and the tensile strength ratio after different conditioning procedures is shown in Figure 7-3 and Figure 7-4. The following observations are obtained from these graphs:

1. The presence of moisture consistently reduced the ITS of all three mixes.
2. Both hydrated lime and liquid antistripping Agent A improved the moisture resistance of the control mix (AAN). The ITS of the mix treated with hydrated lime (AAM) was least affected by moisture, while the ITS of the control mix (AAN) was most reduced by moisture. The effect of moisture on the mix treated with the liquid antistripping Agent A (AALA) was between that of AAN and AAM.
3. For a conditioning period as long as one year, both the hydrated lime and the liquid antistripping Agent A were still effective in improving the moisture resistance of the control mix. The effectiveness of the hydrated lime did not seem to change with the conditioning time, while the effectiveness of the liquid antistripping Agent A seemed to slightly decrease with time.
4. For the dry specimens of all three mixes, the ITS increased with the storage time. This can be attributed to binder aging and/or chemical reaction in the mix.

5. In addition to improving the ITS of wet specimens, hydrated lime also increased the ITS of dry specimens. On the other hand, the addition of the liquid antistripping agent did not significantly affect the ITS of dry specimens.
6. In general, the ITS of wet specimens decreased as the length of the conditioning period increased. The reduction of strength, however, was not linear with time. The ITS was reduced most significantly for all mixes after the first four months' conditioning, then decreased at a much slower rate for the control mix (AAN), fluctuated slightly for the mix treated with the liquid antistripping Agent A (AALA), and increased for the mix treated with hydrated lime (AAM). The fluctuation or increase of the ITS at the later stage might be a result of binder aging in the wet specimens.
7. The additional long-term moisture conditioning at the room temperature did not significantly affect the ITS of the specimens conditioned with the *CTM371* procedure before the strength test. Moreover, the additional *CTM371* conditioning procedure did not significantly affect the ITS of the specimens after long-term moisture conditioning. In terms of the tensile strength ratio (TSR), there is fairly good equivalency between the two conditioning procedures: *CTM371* and long-term moisture conditioning at room temperature. Cores obtained from the field revealed that moisture generally exists in the asphalt pavements all year around, so the long-term moisture conditioning is a more realistic approximation to the field conditions experienced by asphalt pavements. From this perspective, the equivalency between the *CTM371* procedure and the long-term moisture conditioning provided support for using the *CTM371* conditioning procedure in the laboratory to evaluate the moisture sensitivity of asphalt mixes.

7.2.1.1.2 Visual Inspection of Split Faces

After the test, the condition of the split faces of each specimen was examined to determine the extent of stripping. Although the mix containing liquid antistripping Agent A showed higher strength than the control mix, visual inspection of the split faces revealed that stripping was almost as severe in the mix treated with the liquid antistripping Agent A after the *CTM371* conditioning procedure and the long-term moisture conditioning as in the control mix. On the other hand, very little stripping was observed in the mix treated with hydrated lime, even after one-year moisture conditioning and the *CTM371* procedure. To facilitate analysis, the extent of stripping was converted to a numerical scale by the following rule: None→ 0, L → 2, LM → 3, M → 4, MH → 5, H → 6. The average extent of stripping of each mix after different conditioning periods (Figure 7-5) revealed the same phenomenon as above.

The average number of broken aggregates of each mix after different conditioning periods is shown in Figure 7-6. The general trend is similar to that of the indirect tensile strength. That is, dry specimens had more aggregates broken than moisture-conditioned specimens; the mix treated with hydrated lime (AAM) showed more broken aggregates than the mix treated with liquid antistripping Agent A (AALA), while the latter had more aggregates broken than the control mix (AAN). Moreover, these relative rankings changed little with the length of the conditioning period. Because more broken aggregates on the split faces reflect higher binder bonding strength, there is a positive correlation between the strength of the specimens and the number of broken aggregates. The number of broken aggregates can be used as a supplementary index of the moisture resistance of asphalt mixes.

7.2.1.2 Statistical Analysis

In this section, statistical analysis was performed to further verify the general observations. Specifically, the following observations were checked:

The antistripping additives were effective after 4-, 8-, and 12-month moisture conditioning.

There was no significant difference between the indirect tensile strengths of wet specimens conditioned for 4 months and 12 months.

After 4-month moisture conditioning, there was no significant difference between the indirect tensile strengths of wet specimens conditioned by *25C* and by *25C* plus *CTM371*.

The statistical analysis consisted of the following two steps:

Analysis with all the data to check the long-term effectiveness of additives.

Analysis with the data obtained from moisture-conditioned specimens after four months to check the second and third observations.

Both analysis of variance (ANOVA) or analysis of covariance (ANCOVA) and linear regression analysis were performed in each step. The ANOVA/ANCOVA was used to identify significant factors affecting the response variable, and the linear regression analysis was used to estimate the contrast of different factor levels and to test hypotheses. The following linear model was used in the analysis:

$$\begin{aligned} y = \mu &+ \sum_{i=1}^{2} \alpha_i X_i + \sum_{j=1}^{2} \beta_j Y_j + \sum_{k=1}^{3} \gamma_k Z_k + \sum_{i=1}^{2}\sum_{j=1}^{2} (\alpha\beta)_{ij} X_i Y_j \\ &+ \sum_{i=1}^{2}\sum_{k=1}^{3} (\alpha\gamma)_{ik} X_i Z_k + \sum_{j=1}^{2}\sum_{k=1}^{3} (\beta\gamma)_{jk} Y_j Z_k \\ &+ \sum_{i=1}^{2}\sum_{j=1}^{2}\sum_{k=1}^{3} (\alpha\beta\gamma)_{ijk} X_i Y_j Z_k + \theta(x - \bar{x}) + \varepsilon \end{aligned} \qquad \textbf{(7-1)}$$

where y is the response variable; μ is the grand mean; α_i, β_j, γ_k, $(\alpha\beta)_{ij}$, $(\alpha\gamma)_{ik}$, $(\beta\gamma)_{jk}$, $(\alpha\beta\gamma)_{ijk}$, θ, $i, j = 1,2$, $k = 1,2,3,$ are coefficients to be estimated; X_i, Y_j, Z_k are the difference of two indicator functions.

Specifically,

$X_1 = ind(\text{AALA}) - ind(\text{AAN})$, $X_2 = ind(\text{AAM}) - ind(\text{AAN})$

$Y_1 = ind(25\text{C}) - ind(\text{Dry})$, $Y_2 = ind(\text{CTM371}) - ind(\text{Dry})$

$Z_1 = ind(4\text{month Period}) - ind(0\text{month Period})$

$Z_2 = ind(8\text{month Period}) - ind(0\text{month Period})$

$Z_3 = ind(12\text{month Period}) - ind(0\text{month Period})$

where, $ind(\cdot)$ is an indicator function, 1 if the level of a factor is equal to the value in the parentheses, 0 otherwise. x is the air-void content; $\bar{x}$ is the average air-void content. ε is a random error term, assumed to have independent normal distribution, $\varepsilon \sim N(0, \sigma^2)$.

The interaction between the air-void content and other factors were not included in the model because the air-void content of specimens was controlled in a narrow range (6 to 8 percent) in the experiment design.

7.2.1.2.1 Indirect Tensile Strength (ITS)

The ANCOVA table (Table 7.3) shows that the main effects and interactions of all factors are significant at the 95 percent confidence level except that of air-void content. The insignificance of air-void content was expected since it had been controlled in a narrow range.

Based upon the above results, the linear model including the third-order interaction terms was estimated (Table 7.4) in which the reference factor level combination is the control mix AAN at zero period in dry condition. The QQ-normal plot of the residuals (Figure 7-8a) indicates that the normal distribution assumption of the error term is not severely violated. The results in Table 7.4 are discussed below.

The p-values for the main effects of additives (*AALA* and *AAM*), and the interactions between additives and periods (*Period4*, *Period8*, and *Period12*) are all greater than 0.05, indicating that at the 95 percent confidence level, neither liquid antistripping Agent A nor hydrated lime significantly affected the indirect tensile strength (ITS) of the control mix in dry condition across the whole year.

The p-value for the moisture conditioning procedure *25C* is larger than 0.05, indicating that moisture did not significantly reduce the ITS of the control mix when it had been in the mix for only a short period (less than one day). The p-values for the interactions between *25C* and conditioning periods (*Period4*, *Period8*, and *Period12*), however, are all smaller than 0.05, indicating that the long-term (equal to or longer than four months) moisture conditioning at 25°C significantly affected the ITS of the control mix. The estimates of these interactions are all negative and decrease with time, indicating that longer conditioning period led to lower ITS of the control mix. The p-values for the interactions between AALA or AAM and *25C* are all greater than 0.05, indicating that neither the liquid antistripping Agent A nor the hydrated lime significantly affected the ITS of the control mix when moisture had been in the mix for only a short period.

The p-value for *CTM371* is less than 0.05, indicating that the freeze-thaw cycle conditioning significantly reduced the ITS of the control mix. The p-values for the interactions between *CTM371* and conditioning periods are greater than 0.05 for *Period4* and *Period8*, but less than 0.05 for *Period12*, indicating that the adverse effect of the freeze-thaw cycle did not change significantly unless there were 12 months of conditioning. The p-values for the interactions between *CTM371* and additives are all less than 0.05. The positive estimates mean that both the liquid antistripping Agent A and the hydrated lime significantly alleviated the adverse effect of moisture on ITS of the control mix when it was conditioned by the freeze-thaw cycle.

The p-values for the main effects of periods (*Period4*, *Period8*, and *Period12*) are greater than 0.05 except that of *Period12*. The estimated value of the effect of *Period* is positive, meaning the ITS of the control mix increased after one year. This is possibly due to the aging of the asphalt, which would increase the stiffness of the binder.

The p-values for the third-order interactions among *AALA*, *25C*, and conditioning periods are greater than 0.10 for *Period4* and less than 0.10 for *Period8* and *Period12*. The positive estimates indicate that liquid antistripping Agent A is marginally effective in reducing the moisture effect on the ITS of the control mix after long-term moisture conditioning at 25°C. The p-values for the third-order interactions among *AAM*, *25C*, and conditioning periods are greater than 0.05 for *Period4* and less than 0.05 for *Period8* and *Period12*. The positive estimates indicate that the hydrated lime is significantly effective in reducing the moisture effect on the ITS of the control mix after long-term moisture conditioning at 25°C. The relative values of the estimates show that hydrated lime is more effective than liquid antistripping Agent A at any period.

The p-values for the third-order interactions among additives (*AALA*, *AAM*), *CTM371*, and conditioning periods are generally greater than 0.05, indicating that hydrated lime and liquid antistripping Agent A remained effective in reducing the moisture effect on the ITS of the control mix after long-term moisture conditioning at 25°C plus the freeze-thaw cycle.

7.2.1.2.2 ITS of Specimens after Different Moisture Conditioning Procedures

In this subsection, the ITS results of wet specimens with and without the *CTM371* conditioning procedure are statistically compared. The ITS data from specimens after four or more months of moisture conditioning are used in the analysis. Figure 7-2 shows that the additional *CTM371* conditioning procedure did not dramatically reduce the ITS of specimens after four or more months of moisture conditioning at 25°C.

The analysis of covariance (ANCOVA) table (Table 7.5) shows that both conditioning procedure and conditioning period are significant in affecting ITS. The third-order interaction is insignificant. Therefore, the linear model was estimated without the third-order interaction terms. Here the reference factor level combination in the model is the control mix AAN conditioned at 25°C for four months.

Results of the linear regression analysis are shown in Table 7.6. The QQ-normal plot of the residuals (Figure 7-8b) shows that the normal distribution assumption of the error term is not severely violated. The estimated parameter for *CTM371* is -268 kN with a p-value of 0.0043, and the p-values for the interactions between *CTM371* and periods are all greater than 0.05. This indicates that for the control mix AAN, the additional freeze-thaw cycle further reduced the ITS of the mix. The p-value for the interaction between *AALA* and *CTM371* is greater than 0.05, indicating that for the mix containing the liquid antistripping Agent A, the additional freeze-thaw cycle did not further reduce the ITS. On the other hand, the p-value for the interaction between *AAM* and *CTM371* is less than 0.05, suggesting that for the mix containing hydrated lime, the additional freeze-thaw cycle significantly affected ITS. The average reduction in ITS during the 4th month and 12th month due to the additional freeze-thaw cycle, however, is only about 13 percent, -3 percent, and 5 percent of the initial ITS in dry condition for AAN, AALA, and AAM respectively. Negative value indicates that the ITS was increased due to the additional freeze-thaw cycle.

The p-values for *Period8* and *Period12* are all greater than 0.05, indicating that for the control mix, additional conditioning after four months did not significantly affect the ITS. The p-values for the interactions between *AALA* and periods are all greater than 0.05, indicating that for the mix containing the liquid antistripping Agent A, additional conditioning after four months did not significantly affect the ITS either. On the other hand, the p-values for the interactions between *AAM* and periods are all less than 0.05, indicating that for the mix containing hydrated lime, additional conditioning after four months significantly affected ITS. The estimated parameters showed that the ITS of AAM increased with time, possibly due to the continuing chemical reaction between hydrated lime, aggregate, and asphalt in the mix when moisture existed. The average increase is about 9 percent after one year. Therefore, the additional 8-month moisture conditioning did not further significantly reduce the ITS of the wet AAN or AALA specimens, and increased the ITS of the wet AAM specimens.

As a summary, this analysis further verifies that both antistripping agents are effective in the long term to improve the moisture resistance of a mix conditioned in an unfavorable environment. The effectiveness of hydrated lime is more significant than that of liquid antistripping Agent A. The detrimental effect of moisture on mix strength predominantly occurs in the first four months, and after four-month moisture conditioning, additional freeze-thaw cycle conditioning generally does not further reduce the mix strength.

7.2.2 Flexural Beam Fatigue Test

The flexural beam fatigue test results are summarized in Table 7.2 and illustrated graphically in Figure 7-10 through Figure 7-15. The stiffness deterioration curve of each specimen is shown in Appendix H.

7.2.2.1 General Observations

7.2.2.1.1 Air-Void Content and Saturation Level

Figure 7-9 shows the air-void content and saturation level of each specimen. The air-void contents fall in the range of 6 to 8 percent, as specified in the experimental design. Moisture was introduced into specimens by fixed vacuum intensity and vacuum duration. As can be seen in the figure, the distribution of saturation level is not the same for different mixes. Specimens containing the liquid antistripping agents had a saturation level between 70 percent and 80 percent, with a few exceptions. Specimens containing the hydrated lime had a wider range of saturation level, between 50 percent and 90 percent. Specimens without treatment had similar

saturation levels to other specimens in the first month, but much higher values in the late stage. The increase in saturation level was due to the continuous uptake of moisture in the conditioning period. Because specimens were conditioned in the humid room, they could absorb moisture vapor abundant in the surrounding air. The significantly higher saturation level in the untreated mixes indicates either they had a different air-void structure that is more permeable to moisture or the untreated mastic (mix of binder and fines) had a potential to hold more moisture. The saturation levels for untreated mixes that are greater than 100 percent in Figure 7-9 indicate that, additional moisture was absorbed into the mastic in addition to filling of all air-voids (100 percent saturation). The different saturation levels may affect the fatigue test results, but they can be treated as an intrinsic property of the mixes and, therefore, are not included as an independent variable in the statistical analysis.

7.2.2.1.2 Initial Stiffness

The following observations about the effect of moisture on initial flexural stiffness can be made from Figure 7-10 and Figure 7-11:

1. Moisture reduced the initial stiffness of all four mixes.
2. When moisture was initially introduced into the specimens for a short period, the percentage of reduction in initial stiffness was small among the treated and untreated mixes, between 10 and 20 percent. After four or more months of conditioning, the percentage of reduction of stiffness for the untreated mix increased significantly, to 40 percent, whereas for the untreated mixes with hydrated lime or liquid antistripping agents initial stiffness was reduced much less. No further reduction of stiffness with conditioning time was observed after four months for any of the mixes
3. Specimens containing hydrated lime showed the highest initial stiffness in both dry and wet conditions. Mixes containing either liquid antistripping agent showed initial stiffness in dry condition similar to the untreated mix, but higher stiffness in wet condition than the untreated mix.
4. The aging effect on initial stiffness was not significant in both dry and wet conditions.
5. Based upon the measurements of initial stiffness, it was found that both hydrated lime and liquid antistripping agents were effective in improving the moisture resistance of HMA, with hydrated lime being more effective than both liquid antistripping agents.

7.2.2.1.3 Fatigue Life

The following observations can be made about the effect of moisture on fatigue life from Figure 7-12 and Figure 7-13:

1. Moisture may reduce or extend fatigue life. When moisture was initially introduced into specimens for a short period, the fatigue life of mixes containing additives was extended, while that of the untreated mixes was reduced.
2. After four months' conditioning, moisture reduced fatigue life in mixes containing liquid antistripping agents, reduced it slightly further in untreated mixes, and did not effect it in the mix containing hydrated lime. After one year conditioning, the benefit of liquid antistripping Agent B had almost disappeared in terms of fatigue life, while the benefit of liquid antistripping Agent A and hydrated lime was almost unchanged. Both hydrated lime and liquid antistripping Agent A showed good long-term effectiveness while liquid antistripping Agent B was effective for only a short period.

7.2.2.1.4 Visual Inspection of Split Faces

The condition of the fractured faces of each specimen was inspected after the fatigue test, in which the percentage of stripped aggregates and the number of broken aggregates were recorded, as shown in Figure 7-14 and Figure 7-15 respectively.

The untreated mix showed a much larger extent of stripping than the mixes with additives. For all mixes, the extent of stripping tended to increase with the conditioning period. These observations are consistent with the results from the TSR test.

The observations on the number of broken aggregates were also similar to those from the TSR test. That is, dry specimens had more aggregates broken on the fracture faces than moisture-conditioned specimens. For the moisture-conditioned specimens, treated mixes showed more broken aggregates than the untreated mix, with the mix treated with hydrated lime showing the most broken aggregates and the mix treated with liquid antistripping Agent B showing the least broken aggregates. The number of broken aggregates did not change with the length of conditioning period.

Based upon visual inspection, the ranking of the four mixes in terms of their moisture resistance is AAM > AALA >AALB > AAN, which is consistent with the TSR test results.

7.2.2.2 Statistical Analysis

In this section, statistical analysis is performed to verify the general observations. The initial stiffness and fatigue life are used as the response variables in the analysis following three procedures shown below:

1. Perform analysis of variance (ANOVA) or analysis of covariance (ANCOVA) to identify significant factors affecting the response variable.
2. Perform linear regression analysis to estimate the contrasts of different factor levels and to test hypotheses. The linear model was selected based upon the results from the ANOVA (or ANCOVA).
3. Normalize the results from the conditioned specimens by the results from the dry specimens, and perform linear regression analysis to examine the effects of different factor levels on moisture sensitivity in terms of relative performance.

A linear model similar to that in Equation (7-1) is used in Procedure 2. Procedure 2 and Procedure 3 analyze the test results from two different aspects, the absolute value and relative value, to give a complete picture of the moisture effect.

7.2.2.2.1 Initial stiffness

The ANCOVA table (Table 7.7) shows that the main effects and second-order interactions of all factors are significant at the 95 percent confidence level. The effect of the covariate, air-void content, is also significant. The third-order interaction among mix, period, and condition, however, is insignificant.

Based upon the above results, the linear model in Procedure 2 was estimated without the third-order interaction term (Table 7.8). The QQ-normal plot of the residuals, as shown in Figure 7-16(a), indicates that the normal distribution assumption of the error term is not severely violated.

The estimates of the effects of the three additives indicate that compared to the untreated mix (AAN), liquid antistripping Agent A significantly reduced initial stiffness and hydrated lime significantly increased initial stiffness, whereas liquid antistripping Agent B had no significant effect on initial stiffness. The estimates of the effects of periods are insignificant for *Period 8* and *Period 12*, indicating that generally the initial stiffness did not change with the length of period, but significant for *Period4* with a negative value. The

reduction in initial stiffness after four months possibly resulted from a setup change in the test equipment instead of a change in the mix properties. The interactions between additives and periods are all insignificant except those between Liquid A and the three periods, suggesting that the relative effectiveness of hydrated lime and liquid antistripping Agent B did not change with time, while the relative effectiveness of liquid antistripping Agent A increased after four months. A check of the original data revealed that the increase in the relative effectiveness of liquid antistripping stripping Agent A resulted from the reduction of initial stiffness of the untreated mix with time instead of the actual increase of the initial stiffness of the treated mix. The estimate of the effect of moisture is negative and significant, indicating that moisture significantly reduced the initial stiffness. The effect of air-void content is also significant with a negative value, indicating that higher air-void contents resulted in lower initial stiffness.

The interactions between additives and condition are all significant with positive values, indicating that the improvement in initial stiffness due to additives was significantly higher for moisture-conditioned specimens than for dry specimens.

The interactions between periods and condition are all significant with negative values, indicating that the reduction in initial stiffness after four months was significantly higher for moisture-conditioned specimens than for dry specimens. Combining the previous estimates of the effects of period, it can be concluded that the initial stiffness of dry specimens did not change significantly with time, while the initial stiffness of wet specimens decreased with length of conditioning period, mainly in the first four months.

Moisture sensitivity of HMA is often characterized by the relative performance of a wet mix to a dry mix. To this end, the initial stiffness of the moisture-conditioned specimens was divided by the average initial stiffness of the two corresponding dry specimens, and used as the response variable in the Procedure 3 analysis.

The ANCOVA table (Table 7.9) shows that air-void content and the main effect and interaction of mix type and conditioning period are all significant in affecting the initial stiffness ratio at a 95 percent confidence level. Based upon the above results, the linear model in Procedure 2 was estimated without the third-order interaction term (Table 7.10). The QQ-normal plot of the residuals, as shown in Figure 7-16(c). indicates that the normal distribution assumption of the error term is not severely violated. The results show that the p-values for the mixes *AALA* and *AAM* are all greater than 0.20, indicating that initially (after "Zero Month" conditioning) there was no significant difference in stiffness ratio between the untreated mix and the mixes treated with liquid antistripping Agent A or hydrated lime. The interactions of these two additives and the three periods, however, are all significant with positive values. This means that after four-months of moisture conditioning, the initial stiffness ratios of mixes containing the hydrated lime or the liquid antistripping Agent A was significantly higher than that of the untreated mix. On the other hand, the p-value is less than 0.05 for mix *AALB* but greater than 0.05 for the interactions between *AALB* and periods, indicating that liquid antistripping Agent B improved the initial stiffness ratio at the beginning, but no further improvement was realized afterwards. The estimates for the three periods are nearly the same (around -0.24) and are all significant. The negative estimates mean that the effect of the moisture developed with time, while the similar values indicate that the time effect diminished after four months. The multiple comparisons by the Tukey method (Table 7.11) verified the latter point.

7.2.2.2.2 Fatigue Life

The natural logarithm of fatigue life was used as the response variable in the analysis. The ANCOVA results (Table 7.12) show that the main effects and second-order interactions, except that between mix type and conditioning period, of all factors are significant at the 95 percent confidence level. The covariate air-void content is insignificant. Moreover, the third-order interaction among mix, period, and condition is insignificant.

The linear model in Procedure 2 was estimated without the third-order interaction term and the air-void content (Table 7.13). The QQ-normal plot of the residuals, as shown in Figure 7-16 (b) indicates that the normal distribution assumption of the error term is not severely violated. The p-values for the three mixes

(*AALA*, *AALB*, *AAM*) are all greater than 0.05, indicating that at the 95 percent confidence level, the three additives did not significantly change the fatigue life of the HMA mix when the specimens were dry. The conditioning period *Period4* is significant with a negative estimate, indicating that the fatigue test conducted four months later gave significantly lower results for the dry specimens than the results obtained at the beginning of the test. This result is abnormal because four-month storage of the dry specimens should not have changed the mix properties significantly. It is very likely that some changes in the set-up of the test equipment caused the difference. The p-value for the factor *Condition* is less than 0.05, indicating that for the untreated mix moisture significantly shortened its fatigue life. The p-values for the interactions between mix and period are all greater than 0.05, meaning that the difference in fatigue response between the treated mixes and the untreated mix did not change with time. The interactions between the three mixes (*AALA*, *AALB*, *AAM*) and the factor *Condition* are all significant with positive estimates, meaning that the fatigue response of the mixes treated with additives was significantly less affected by moisture than that of the untreated mix. Based upon the estimated values, the relative ranking of the three additives is AAM > AALA > AALB. The interactions between *Period8* and *Condition*, and between *Period12* and *Condition* are significant with negative estimates, indicating that long-term conditioning of specimens by moisture would further reduce their fatigue performance. In other words, moisture has a time effect.

Fatigue life ratio (FLR), calculated by normalizing the fatigue lives of the moisture-conditioned specimens by the average fatigue life of the two corresponding dry specimens, was used as the response variable in the Procedure 3 analysis. The ANCOVA table (Table 7.14) shows that only mix type had significant effect on fatigue life ratio. The linear model in Procedure 2 was estimated without the air-void content and second-order interaction terms (Table 7.15). The QQ-normal plot of the residuals (d) indicates that the normal distribution assumption of the error term is not severely violated. The results show that the p-values for the mixes *AALA* and *AAM* are smaller than 0.05, indicating that both liquid antistripping Agent A and hydrated lime can significantly reduce the adverse effect of moisture on the fatigue response. On the other hand, the p-value for the mix *AALB* is larger than 0.05, indicating that the liquid antistripping Agent B is not significantly effective in improving the moisture resistance of the mix used in this experiment in terms of fatigue response. The estimates for the two periods (*Period8* and *Period12*) are all negative with a p-value less than 0.05, meaning that long-term conditioning of specimens by moisture would further reduce their fatigue performance, especially after eight months.

7.3 Summary

The following conclusions are obtained from the research:

1. Both hydrated lime and liquid antistripping agents can improve the moisture resistance of the control mix used in the experiment. Mix properties—including indirect tensile strength, flexural stiffness, and fatigue life—were least affected by moisture in the mix treated with hydrated lime (AAM), most affected by moisture in the untreated mix (AAN), and moderately affected by moisture in the mixes treated with liquid antistripping agents (AALA, AALB). Different liquid antistripping agents have different effectiveness. Liquid antistripping agents do not significantly change the mix properties in dry condition. Hydrated lime does not significantly change the indirect tensile strength or fatigue response, but significantly increases the flexural stiffness in dry condition.
2. For a conditioning period as long as one year, both hydrated lime and liquid antistripping agents are effective in improving the moisture resistance of asphalt mixes. The effectiveness of hydrated lime does not decrease, but instead in some cases increases with the conditioning time, while the effectiveness of the liquid antistripping agents generally does not change with time.
3. There is good equivalency between the two conditioning procedures: CTM 371 and long-term moisture conditioning at a room temperature. This equivalency provides support for

using the CTM 371 conditioning procedure in the laboratory to test the moisture sensitivity of asphalt mixes.

4. Moisture damage develops with time on a nonlinear scale. At a mild temperature (25°C), the damage evolves significantly in the first four months then levels off. For the untreated mix, moisture damage develops slowly after four months, but for treated mixes moisture damage tends to stop developing after four months.
5. When moisture exists in the mix for a short period, neither indirect tensile strength nor flexural initial stiffness can discriminate between mixes with and without treatments. However, fatigue life can show sufficiently the difference between untreated and treated mixes. It is more discriminative to use the fatigue life ratio as the index of moisture sensitivity.
6. Moisture may reduce or extend the fatigue life of asphalt mixes. For moisture-sensitive mixes, fatigue life is reduced whenever moisture exists in the mixes. For moisture-insensitive mixes the fatigue life may be extended by moisture. Mixes treated with hydrated lime have longer fatigue lives in wet condition after any length of moisture conditioning. Mixes treated with liquid antistripping agents, however, have longer fatigue lives in wet condition after a short period of conditioning, but shorter fatigue lives after a long period of conditioning.
7. Both the visual inspection of stripping and examination of the number of broken aggregates on the split faces can be used as supplementary indices of the moisture resistance of asphalt mixes.

Table 7.1 Results from the Indirect Tensile Strength Ratio (TSR) Test

Cond. Time (Month)	Specimen ID	Test Cond.	Height (mm)	Dry Mass (g)	Mass in Water (g)	SSD Mass (g)	Air-Void (%)	Mass in Water after Cond. (g)	SSD Mass after Cond. (g)	Saturation (%)	Height before Testing (mm)	Indirect Tensile Strength (kPa)	Stripping	Number of Broken Aggregates
0	AAN39	Dry	63.6	1218.1	716.6	1222.1	6.6				63.6	1770.4	NO	9
	AAN36	Dry	63.5	1216.5	719.5	1222.3	6.2				63.5	1541.1	NO	11
	AAN51	Dry	63.3	1218.2	725.9	1224.9	5.4				63.3	1672.3	NO	14
	AAN63	25°C	63.1	1217.6	718.0	1223.8	6.7	736.9	1240.0	66.1	63.5	1268.7	NO	7
	AAN46	25°C	63.0	1217.7	720.8	1222.2	5.9	734.5	1236.7	64.5	63.8	1658.6	NO	5
	AAN53	25°C	63.0	1216.6	714.7	1221.2	6.9	730.2	1234.1	50.0	63.2	1597.8	NO	4
	AAN50	CTM371	63.0	1216.5	723.1	1221.1	5.3	729.5	1234.3	67.1	63.7	716.6	M	4
	AAN35	CTM371	63.8	1217.2	723.6	1225.1	5.9	729.1	1235.1	60.2	64.0	436.8	M	2
	AAN62	CTM371	63.2	1218.5	716.6	1223.8	6.9	730.3	1236.2	50.6	64.2	507.5	M	1
4	AAN31	Dry	63.3	1217.2	719.5	1223.0	6.3				63.3	1567.9	NO	12
	AAN34	Dry	63.6	1218.1	717.6	1221.9	6.4				63.6	1581.4	NO	10
	AAN40	Dry	63.4	1216.3	718.1	1220.6	6.2				63.4	1560.8	NO	14
	AAN52	25°C	64.3	1218.6	718.1	1224.1	6.7	732.8	1235.0	48.6	63.7	472.1	M	4
	AAN67	25°C	63.2	1216.8	722.0	1222.4	5.8	734.4	1235.9	66.3	63.6	728.2	M	4
	AAN66	25°C	62.8	1216.6	719.5	1220.1	5.8	729.4	1231.6	51.6	63.5	635.0	M	4
	AAN55	CTM371	62.9	1216.0	713.3	1219.5	6.9	729.6	1235.3	55.3	63.7	487.4	M	4
	AAN60	CTM371	63.1	1217.9	719.1	1222.6	6.3	734.9	1240.9	73.1	63.9	216.4	M	9
	AAN37	CTM371	63.4	1217.6	716.4	1221.5	6.6	733.1	1238.9	64.2	63.9	197.9	M	6

Table 7.1 Results from the Indirect Tensile Strength Ratio (TSR) Test *(cont'd.)*

Cond. Time (Month)	Specimen ID	Test Cond.	Height (mm)	Dry Mass (g)	Mass in Water (g)	SSD Mass (g)	Air-Void (%)	Mass in Water after Cond. (g)	SSD Mass after Cond. (g)	Saturation (%)	Height before Testing (mm)	Indirect Tensile Strength (kPa)	Stripping	Number of Broken Aggregates
8	AAN44	Dry	63.7	1215.8	719.2	1222.2	6.3				63.7	1518.8	NO	13
	AAN32	Dry	63.2	1216.2	716.4	1221.8	6.7				63.2	1533.9	NO	7
	AAN54	Dry	62.9	1219.8	724.4	1224.9	5.5				62.9	1888.0	NO	10
	AAN38	25°C	63.8	1214.4	717.3	1219.1	6.2	728.6	1232.3	57.5	64.1	638.2	MH	7
	AAN59	25°C	63.0	1218.3	720.2	1222.5	6.0	731.7	1237.2	62.7	63.7	486.6	MH	4
	AAN61	25°C	63.1	1217.6	723.6	1224.1	5.7	737.3	1239.4	76.2	63.8	441.8	M	7
	AAN48	CTM371	62.9	1218.7	723.0	1224.6	5.8	738.0	1240.1	73.1	63.6	416.4	H	1
	AAN42	CTM371	63.5	1218.0	720.0	1222.9	6.1	732.0	1236.5	60.0	63.9	412.5	H	3
	AAN58	CTM371	62.9	1216.9	718.9	1220.7	6.0	730.2	1233.3	54.4	63.8	425.6	H	6
12	AAN65	Dry	62.9	1216.8	718.0	1220.1	6.1				62.9	1979.5	NO	10
	AAN45	Dry	63.5	1216.9	716.3	1220.9	6.5				63.5	1904.9	NO	12
	AAN57	Dry	62.9	1217.5	719.4	1221.2	6.0				62.9	2078.1	NO	15
	AAN56	25°C	63.1	1216.7	717.9	1220.3	6.1	728.9	1233.0	52.8	63.5	499.3	H	3
	AAN41	25°C	64.3	1216.3	718.9	1226.8	7.2	735.6	1244.0	75.9	64.2	507.0	M	12
	AAN33	25°C	63.6	1217.4	718.9	1222.2	6.3	734.2	1239.3	69.6	64.0	464.7	H	7
	AAN43	CTM371	63.6	1217.7	719.3	1222.5	6.2	733.0	1237.7	64.0	63.9	250.0	H	7
	AAN47	CTM371	62.9	1217.5	716.6	1221.6	6.6	731.5	1237.9	61.6	63.6	305.8	H	3
	AAN64	CTM371	63.3	1214.9	722.1	1220.6	5.5	733.4	1234.3	70.2	63.9	264.3	H	4

Table 7.1 Results from the Indirect Tensile Strength Ratio (TSR) Test *(cont'd.)*

Cond. Time (Month)	Specimen ID	Test Cond.	Height (mm)	Dry Mass (g)	Mass in Water (g)	SSD Mass (g)	Air-Void (%)	Mass in Water after Cond. (g)	SSD Mass after Cond. (g)	Saturation (%)	Height before Testing (mm)	Indirect Tensile Strength (kPa)	Stripping	Number of Broken Aggregates
0	AAM42	Dry	62.7	1203.4	711.0	1208.1	6.3				62.7	1737.1	NO	8
	AAM52	Dry	62.6	1203.4	710.5	1207.6	6.3				62.6	1823.5	NO	9
	AAM65	Dry	62.8	1202.5	707.6	1206.5	6.7				62.8	1890.1	NO	12
	AAM45	25°C	62.6	1204.7	711.8	1208.5	6.1	721.8	1219.0	47.2	62.9	2028.8	NO	3
	AAM33	25°C	64.1	1205.7	707.0	1211.6	7.5	721.6	1227.3	57.1	64.5	1412.5	NO	2
	AAM38	25°C	62.6	1205.7	714.2	1210.4	5.9	724.8	1221.5	53.7	63.1	2138.3	NO	2
	AAM53	CTM371	63.0	1203.2	705.3	1206.7	7.1	721.5	1220.0	47.2	63.4	1578.8	NO	5
	AAM66	CTM371	62.7	1203.0	711.3	1206.5	5.9	720.5	1220.8	60.4	63.1	1733.5	L	3
	AAM54	CTM371	62.7	1203.5	709.4	1207.6	6.5	723.1	1223.0	60.4	63.2	1568.6	L	5
4	AAM31	Dry	63.0	1203.8	707.8	1208.1	6.8				63.0	1793.1	NO	11
	AAM48	Dry	62.7	1202.9	712.3	1207.8	6.0				62.7	1804.0	NO	7
	AAM46	Dry	62.8	1205.6	710.8	1209.3	6.4				62.8	1703.7	NO	11
	AAM60	25°C	62.8	1203.3	707.7	1207.4	6.8	722.8	1222.5	56.7	63.3	1392.6	L	12
	AAM57	25°C	62.7	1202.5	710.7	1206.7	6.1	725.3	1221.5	62.4	63.1	1552.4	NO	15
	AAM40	25°C	62.9	1206.4	713.9	1211.5	6.1	727.3	1225.0	60.9	63.2	1339.2	NO	13
	AAM34	CTM371	63.1	1204.4	708.3	1208.5	6.8	720.3	1221.3	49.8	63.4	1662.0	L	10
	AAM47	CTM371	62.7	1201.3	710.8	1206.4	6.2	723.6	1218.0	54.7	63.1	1448.8	NO	11
	AAM58	CTM371	62.7	1202.8	710.9	1206.7	6.1	722.6	1217.5	48.8	63.0	1394.9	L	10

Table 7.1 Results from the Indirect Tensile Strength Ratio (TSR) Test *(cont'd.)*

Cond. Time (Month)	Specimen ID	Test Cond.	Height (mm)	Dry Mass (g)	Mass in Water (g)	SSD Mass (g)	Air-Void (%)	Mass in Water after Cond. (g)	SSD Mass after Cond. (g)	Saturation (%)	Height before Testing (mm)	Indirect Tensile Strength (kPa)	Stripping	Number of Broken Aggregates
8	AAM44	Dry	62.9	1204.9	711.1	1209.4	6.4				62.9	1921.9	NO	7
	AAM62	Dry	62.7	1204.8	710.0	1209.0	6.5				62.7	1750.8	NO	11
	AAM64	Dry	62.8	1202.0	710.5	1207.5	6.4				62.8	1996.8	NO	5
	AAM51	25°C	62.7	1201.8	708.2	1205.8	6.5	720.2	1218.4	51.4	63.1	1711.7	NO	8
	AAM43	25°C	62.4	1203.8	716.9	1209.8	5.4	727.8	1221.6	66.3	62.9	1786.6	NO	12
	AAM63	25°C	62.9	1202.9	708.8	1208.0	6.7	723.5	1222.4	58.2	63.5	1532.3	L	13
	AAM59	CTM371	62.8	1197.5	706.4	1202.7	6.6	719.9	1216.9	59.3	63.0	1596.9	L	12
	AAM37	CTM371	62.7	1203.4	709.2	1207.7	6.5	721.9	1219.2	48.5	63.1	1936.8	NO	10
	AAM39	CTM371	62.6	1206.0	711.8	1210.5	6.4	723.8	1223.6	55.3	63.1	2048.8	NO	12
12	AAM35	Dry	62.9	1208.0	714.9	1213.2	6.1				62.9	1833.5	NO	8
	AAM61	Dry	62.9	1202.8	714.2	1209.6	6.0				62.9	2088.3	NO	8
	AAM49	Dry	62.6	1201.9	710.8	1206.3	6.1				62.6	2223.3	NO	14
	AAM32	25°C	63.1	1205.5	709.7	1210.1	6.7	724.9	1226.6	62.6	63.4	1831.7	NO	12
	AAM36	25°C	62.9	1205.2	708.6	1209.3	6.8	721.3	1222.5	50.7	63.3	2130.5	NO	12
	AAM50	25°C	62.6	1201.9	707.8	1206.8	6.8	722.6	1221.4	57.9	63.3	1909.2	NO	20
	AAM55	CTM371	62.9	1203.5	712.4	1209.3	6.2	726.0	1223.1	63.3	63.1	1618.1	L	11
	AAM41	CTM371	62.9	1204.8	714.4	1209.8	5.8	725.2	1220.0	52.5	63.2	1884.4	NO	11
	AAM56	CTM371	62.8	1203.2	710.5	1207.7	6.3	724.5	1222.0	59.9	63.2	2050.7	NO	9

Table 7.1 Results from the Indirect Tensile Strength Ratio (TSR) Test *(cont'd.)*

Cond. Time (Month)	Specimen ID	Test Cond.	Height (mm)	Dry Mass (g)	Mass in Water (g)	SSD Mass (g)	Air-Void (%)	Mass in Water after Cond. (g)	SSD Mass after Cond. (g)	Saturation (%)	Height before Testing (mm)	Indirect Tensile Strength (kPa)	Stripping	Number of Broken Aggregates
0	AAL21	Dry	63.2	1229.5	729.2	1234.3	6.5				63.2	1498.3	NO	8
	AAL37	Dry	62.7	1230.1	728.7	1234.4	6.6				62.7	1950.6	NO	7
	AAL39	Dry	63.0	1226.6	723.6	1229.9	7.0				63.0	1874.9	NO	11
	AAL40	25°C	63.1	1228.0	727.0	1233.0	6.8	742.1	1246.9	54.7	63.8	1459.2	NO	4
	AAL9	25°C	63.1	1225.3	722.3	1228.1	7.0	736.1	1243.4	51.2	63.3	1768.0	NO	3
	AAL15	25°C	62.9	1227.5	728.6	1233.7	6.7	739.3	1245.1	52.0	63.5	1684.4	NO	7
	AAL29	CTM371	63.4	1228.3	726.6	1234.0	7.1	741.5	1246.2	50.0	64.1	967.2	LM	6
	AAL5	CTM371	63.4	1229.1	730.1	1232.8	6.1	739.5	1246.0	54.8	63.6	1041.1	L	3
	AAL17	CTM371	63.0	1228.9	724.1	1233.0	7.3	740.2	1246.4	47.2	63.8	1141.7	L	2
4	AAL4	Dry	63.3	1229.8	725.2	1235.9	7.5				63.3	1611.4	NO	10
	AAL43	Dry	63.8	1228.4	721.4	1231.8	7.6				63.8	1668.6	NO	5
	AAL34	Dry	63.2	1229.9	721.7	1238.1	8.6				63.2	1478.3	NO	11
	AAL14	25°C	62.8	1229.0	728.3	1234.7	6.8	740.3	1245.3	47.2	63.8	968.2	M	8
	AAL27	25°C	62.8	1228.3	728.9	1234.0	6.6	740.5	1248.0	58.8	63.7	869.5	M	11
	AAL12	25°C	63.2	1228.1	727.2	1234.6	7.1	740.8	1248.7	57.4	64.2	749.2	M	9
	AAL28	CTM371	63.1	1227.4	721.9	1232.7	7.7	735.6	1245.0	44.5	64.1	913.9	M	6
	AAL36	CTM371	63.1	1229.4	729.6	1233.6	6.4	740.5	1246.4	53.1	63.8	578.5	M	8
	AAL38	CTM371	62.9	1228.1	724.7	1231.9	7.0	739.0	1244.8	46.8	64.1	642.7	M	9

Table 7.1 Results from the Indirect Tensile Strength Ratio (TSR) Test *(cont'd.)*

Cond. Time (Month)	Specimen ID	Test Cond.	Height (mm)	Dry Mass (g)	Mass in Water (g)	SSD Mass (g)	Air-Void (%)	Mass in Water after Cond. (g)	SSD Mass after Cond. (g)	Saturation (%)	Height before Testing (mm)	Indirect Tensile Strength (kPa)	Stripping	Number of Broken Aggregates
8	AAL31	Dry	63.4	1228.2	729.9	1233.7	6.4				63.4	1626.6	NO	10
	AAL33	Dry	62.9	1227.1	729.6	1234.2	6.6				62.9	1474.6	NO	20
	AAL16	Dry	62.9	1227.5	722.1	1230.7	7.3				62.9	2017.7	NO	15
	AAL10	25°C	63.1	1229.0	728.8	1232.9	6.4	737.8	1244.1	46.8	63.9	1196.3	H	2
	AAL13	25°C	63.0	1228.1	725.6	1233.2	7.1	737.8	1244.7	46.0	63.9	1061.3	H	6
	AAL7	25°C	63.7	1229.2	728.9	1234.5	6.7	738.3	1247.0	52.8	64.0	874.6	MH	10
	AAL41	CTM371	63.1	1227.6	721.4	1230.7	7.5	736.1	1243.1	40.8	63.8	1179.1	MH	6
	AAL32	CTM371	63.2	1229.0	729.1	1235.0	6.7	742.3	1249.2	59.3	63.7	820.6	M	4
	AAL20	CTM371	63.5	1228.5	724.2	1231.2	7.0	736.9	1243.9	43.6	63.8	1111.0	H	4
12	AAL35	Dry	63.3	1226.4	726.3	1231.3	6.8				63.3	1915.1	NO	10
	AAL42	Dry	62.9	1222.4	721.0	1226.5	7.2				62.9	1883.8	NO	20
	AAL19	Dry	63.5	1226.9	730.1	1231.7	6.1				63.5	2062.7	NO	13
	AAL8	25°C	63.9	1228.0	727.2	1232.9	6.8	741.4	1247.8	57.8	63.5	785.4	M	6
	AAL22	25°C	63.3	1227.9	728.5	1233.3	6.6	743.0	1246.9	56.9	63.9	1042.8	H	9
	AAL23	25°C	63.5	1227.6	724.9	1231.2	6.9	739.0	1244.7	48.9	63.9	921.5	M	7
	AAL11	CTM371	63.1	1229.0	729.1	1232.8	6.3	742.8	1248.2	60.3	63.7	967.6	H	6
	AAL6	CTM371	63.1	1228.3	729.6	1233.5	6.4	741.3	1244.8	51.0	63.7	617.9	H	8
	AAL26	CTM371	63.6	1228.4	727.8	1235.4	7.1	741.0	1248.0	54.5	64.2	875.9	H	13

Table 7.2 Results of the Flexural Beam Fatigue Test

Specimen ID	Air-Void (%)	Conditioning Period (month)	Condition	Saturation (%)	Strain Level	Test Temperature (°C)	Initial Stiffness (kPa)	Fatigue Life	Stripping (%)	Broken Aggregates
B-AALA-OM7-10B	7.3	0	Dry	0.0	0.000206	19.7	9,367	141,756	0	4
B-AALA-OM7-16A	7.3	0	Dry	0.0	0.000206	19.7	8,918	122,728	0	5
B-AALA-OM7-11B	7.2	0	Wet	77.9	0.000211	19.7	7,314	109,282	0	2
B-AALA-OM7-15A	8.0	0	Wet	75.8	0.000209	19.7	7,005	197,193	0	0
B-AALA-OM7-11A	7.6	4	Dry	0.0	0.000213	19.1	8,841	98,882	0	5
B-AALA-OM7-2A	6.4	4	Dry	0.0	0.000206	19.6	9,801	53,713	0	5
B-AALA-OM7-14A	7.6	4	Wet	73.2	0.000217	19.3	7,138	60,580	5	3
B-AALA-OM7-6B	6.9	4	Wet	76.3	0.00022	19.0	7,447	77,015	10	3
B-AALA-OM7-3A	6.7	8	Dry	0.0	0.000214	19.4	10,359	71,883	0	6
B-AALA-OM7-8B	7.9	8	Dry	0.0	0.000209	19.7	10,492	118,808	0	4
B-AALA-OM7-5A	6.8	8	Wet	72.0	0.000209	19.3	7,861	69,015	5	2
B-AALA-OM7-6A	7.1	8	Wet	69.7	0.000213	19.5	8,076	100,000	15	3
B-AALA-OM7-7A	7.2	12	Dry	0.0	0.000209	19.6	10,756	79,950	0	3
B-AALA-OM7-8A	7.2	12	Dry	0.0	0.000208	19.7	9,499	116,257	0	4
B-AALA-OM7-7B	7.2	12	Wet	74.6	0.000206	19.5	8,032	51,582	10	1
B-AALA-OM7-9B	7.4	12	Wet	73.4	0.000208	19.6	7,249	142,895	20	0

Table 7.2: Results of the Flexural Beam Fatigue Test *(cont'd.)*

Specimen ID	Air-Void (%)	Conditioning Period (month)	Condition	Saturation (%)	Strain Level	Test Temperature (°C)	Initial Stiffness (kPa)	Fatigue Life	Stripping (%)	Broken Aggregates
B-AALB-OM7-10B	7.9	0	Dry	0.0	0.000208	19.8	10,144	102,716	0	3
B-AALB-OM7-17A	8.1	0	Dry	0.0	0.000212	19.4	9,256	177,705	0	3
B-AALB-OM7-10A	8.1	0	Wet	75.1	0.000211	19.4	8,399	268,993	0	4
B-AALB-OM7-13A	7.1	0	Wet	71.8	0.000212	19.7	9,125	98,279	0	3
B-AALB-OM7-12A	6.5	4	Dry	0.0	0.000213	19.3	9,533	79,635	0	4
B-AALB-OM7-20A	8.0	4	Dry	0.0	0.000212	19.2	10,036	126,152	0	5
B-AALB-OM7-3B	6.6	4	Wet	66.5	0.000218	19.2	7,355	19,999	0	3
B-AALB-OM7-2B	8.0	4	Wet	58.9	0.000213	18.9	6,826	64,074	0	0
B-AALB-OM7-12B	7.4	8	Dry	0.0	0.000209	19.5	10,285	88,571	0	4
B-AALB-OM7-8B	8.0	8	Dry	0.0	0.000207	19.4	10,758	105,941	0	3
B-AALB-OM7-16A	7.3	8	Wet	68.6	0.000214	19.4	7,175	41,767	5	4
B-AALB-OM7-9A	7.9	8	Wet	67.7	0.000214	19.5	7,320	77,500	5	2
B-AALB-OM7-14A	6.7	12	Dry	0.0	0.000207	19.5	10,764	128,884	0	4
B-AALB-OM7-15A	7.7	12	Dry	0.0	0.000206	19.5	10,008	199,005	0	4
B-AALB-OM7-19B	7.7	12	Wet	56.7	0.000212	19.7	7,939	49,106	10	4
B-AALB-OM7-3A	6.9	12	Wet	65.7	0.000212	19.6	8,042	27,500	5	2

Table 7.2: Results of the Flexural Beam Fatigue Test *(cont'd.)*

Specimen ID	Air-Void (%)	Conditioning Period (month)	Condition	Saturation (%)	Strain Level	Test Temperature (°C)	Initial Stiffness (kPa)	Fatigue Life	Stripping (%)	Broken Aggregates
B-AAM-OM7-12B	7.8	0	Dry	0.0	0.000204	19.8	12,269	175,667	0	4
B-AAM-OM7-8A	6.5	0	Dry	0.0	0.000205	20.0	12,143	266,082	0	2
B-AAM-OM7-11A	7.8	0	Wet	62.3	0.000206	20.1	11,065	300,705	0	4
B-AAM-OM7-8B	6.5	0	Wet	51.0	0.000207	20.1	10,335	316,789	0	6
B-AAM-OM7-11B	7.5	4	Dry	0.0	0.000218	19.1	11,631	83,642	0	4
B-AAM-OM7-1A	6.4	4	Dry	0.0	0.000212	19.3	11,733	135,757	0	5
B-AAM-OM7-12A	7.4	4	Wet	56.7	0.000216	19.2	8,613	220,431	0	3
B-AAM-OM7-1B	6.3	4	Wet	48.8	0.000219	19.2	10,157	99,739	0	5
B-AAM-OM7-21B	7.8	8	Dry	0.0	0.000209	19.1	11,444	170,389	0	3
B-AAM-OM7-2B	6.0	8	Dry	0.0	0.000208	19.5	12,594	140,572	0	3
B-AAM-OM7-22A	7.9	8	Wet	70.6	0.000212	19.5	8,925	114,585	5	4
B-AAM-OM7-3B	6.0	8	Wet	40.1	0.000212	19.3	10,508	205,424	10	6
B-AAM-OM7-4A	7.4	12	Dry	0.0	0.000208	19.6	11,945	174,861	0	4
B-AAM-OM7-6A	7.0	12	Dry	0.0	0.000207	19.5	11,891	276,275	0	3
B-AAM-OM7-5B	7.4	12	Wet	73.5	0.000207	19.6	10,252	405,692	5	4
B-AAM-OM7-6B	7.0	12	Wet	77.5	0.000209	19.6	10,001	190,539	5	4

Table 7.2: Results of the Flexural Beam Fatigue Test *(cont'd.)*

Specimen ID	Air-Void (%)	Conditioning Period (month)	Condition	Saturation (%)	Strain Level	Test Temperature (°C)	Initial Stiffness (kPa)	Fatigue Life	Stripping (%)	Broken Aggregates
B-AAN-OM7-19A	6.8	0	Dry	0	0.000208	20.7	9,640	151,189	0	1
B-AAN-OM7-19B	7.2	0	Dry	0.0	0.000206	19.6	9,674	156,941	0	2
B-AAN-OM7-11B*	6.7	0	Wet	49.2	0.000209	20.0	8,163	119,938	10	2
B-AAN-OM7-14A	7.0	0	Wet	88.6	0.000213	19.9	8,120	41,387	20	4
B-AAN-OM7-13B	7.6	4	Dry	0.0	0.000213	19.4	8,997	75,232	0	3
B-AAN-OM7-9B	6.7	4	Dry	0.0	0.000214	19.3	8,894	58,360	0	0
B-AAN-OM7-13A	7.8	4	Wet	78.3	0.000225	19.2	5,365	20,891	20	0
B-AAN-OM7-22B	6.5	4	Wet	73.6	0.000224	19.0	5,309	45,220	30	0
B-AAN-OM7-15B	7.0	8	Dry	0.0	0.000211	19.4	10,115	205,424	0	3
B-AAN-OM7-16B	7.1	8	Dry	0.0	0.00021	19.4	9,693	184,689	0	3
B-AAN-OM7-18A	7.0	8	Wet	68.3	0.000218	19.4	5,641	31,754	35	2
B-AAN-OM7-33AS	7.0	8	Wet	73.0	0.000214	19.6	6,120	21,279	40	4
B-AAN-OM7-17A	7.5	12	Dry	0.0	0.00021	19.7	10,059	272,621	0	2
B-AAN-OM7-18B	6.6	12	Dry	0.0	0.00021	19.6	9,721	158,959	0	3
B-AAN-OM7-17B	7.7	12	Wet	102.5	0.000215	19.5	5,368	28,299	30	1
B-AAN-OM7-33BS	6.7	12	Wet	101.3	0.000212	19.6	6,232	39,999	40	0

Table 7.3 Aalysis of Covariance of Indirect Tensile Strength from the TSR Test

Factor	Degree of Freedom	Sum of Squares	F-value	p-value
Mix	2	12147912	238.4115	0.0000
Condition	2	11853196	232.6275	0.0000
Period	3	1700448	22.2483	0.0000
AirVoid	1	2057	0.0807	0.7771
Mix:Condition	4	4250906	41.7135	0.0000
Mix:Period	6	815977	5.3380	0.0001
Condition:Period	6	1958911	12.8150	0.0000
Mix:Condition:Period	12	667127	2.1821	0.0217
Residuals	71	1808851		

Table 7.4 Estimated Parameters of Linear Model for Indirect Tensile Strength from the TSR Test

Coefficients	Estimated Value	Standard Error	*t* statistics	p-value
(Intercept)	2025.3	266.8	7.5903	0.0000
AALA	151.3	132.9	1.1386	0.2587
AAM	177.6	131.2	1.3539	0.1801
25C	-126.9	131.5	-0.9647	0.3380
CTM371	-1109.6	130.3	-8.5139	0.0000
Period4	-77.2	130.7	-0.5910	0.5564
Period8	-8.4	130.4	-0.0642	0.9490
Period12	334.2	130.4	2.5623	0.0125
AirVoid	-60.0	41.3	-1.4538	0.1504
AALA:25C	-2.5	184.7	-0.0135	0.9892
AAM:25C	173.9	184.9	0.9402	0.3503
AALA:CTM371	393.0	184.4	2.1310	0.0366
AAM:CTM371	923.7	184.4	5.0105	0.0000
AALA:Period4	-39.3	188.6	-0.2082	0.8357
AAM:Period4	25.3	184.6	0.1368	0.8915
AALA:Period8	-55.9	184.3	-0.3035	0.7624
AAM:Period8	81.3	184.4	0.4410	0.6606
AALA:Period12	-155.0	184.4	-0.8404	0.4035
AAM:Period12	-124.8	185.5	-0.6728	0.5033
25C:Period4	-843.4	186.2	-4.5306	0.0000
CTM371:Period4	-141.8	184.8	-0.7674	0.4454
25C:Period8	-1009.8	186.2	-5.4246	0.0000
CTM371:Period8	-131.1	184.4	-0.7108	0.4795
25C:Period12	-1350.3	184.4	-7.3244	0.0000
CTM371:Period12	-610.5	184.3	-3.3120	0.0015
AALA:25C:Period4	185.0	261.7	0.7068	0.4820
AAM:25C:Period4	453.5	261.5	1.7346	0.0872
AALA:CTM371:Period4	-68.0	266.4	-0.2552	0.7993
AAM:CTM371:Period4	60.7	261.3	0.2324	0.8169
AALA:25C:Period8	475.0	261.4	1.8173	0.0734
AAM:25C:Period8	735.9	261.0	2.8193	0.0062
AALA:CTM371:Period8	196.3	261.0	0.7521	0.4545
AAM:CTM371:Period8	292.0	260.7	1.1200	0.2665
AALA:25C:Period12	446.4	260.7	1.7125	0.0912
AAM:25C:Period12	1254.1	262.4	4.7792	0.0000
AALA:CTM371:Period12	187.7	260.7	0.7199	0.4740
AAM:CTM371:Period12	601.1	260.7	2.3063	0.0240

R^2=0.9486

Table 7.5 Analysis of Covariance of ITS After Four and More Months Moisture Conditioning

Factor	Degree of Freedom	Sum of Squares	F-value	p-value
Mix	2	15037256	343.7880	0.0000
Condition	1	89874	4.1095	0.0503
Period	2	360864	8.2502	0.0012
AirVoid	1	42502	1.9434	0.1721
Mix:Condition	2	166877	3.8152	0.0317
Mix:Period	4	438788	5.0159	0.0027
Condition:Period	2	64167	1.4670	0.2444
Mix:Condition:Period	4	36169	0.4135	0.7977
Residuals	35	765448		

Table 7.6 Estimated parameters for ITS After Four and More Months Moisture Conditioning

Coefficients	Estimated Value	Standard Error	*t* statistics	p-value
(Intercept)	353.0	363.8	0.9705	0.3378
AALA	247.9	100.3	2.4702	0.0180
AAM	875.7	95.7	9.1545	0.0000
CTM371	-268.0	88.5	-3.0294	0.0043
Period8	-49.1	97.9	-0.5015	0.6188
Period12	-80.3	97.1	-0.8272	0.4132
AirVoid	37.3	57.3	0.6521	0.5182
AALA:CTM371	122.4	95.7	1.2781	0.2088
AAM:CTM371	266.3	95.9	2.7772	0.0084
AALA:Period8	226.4	118.8	1.9063	0.0640
AAM:Period8	275.5	119.1	2.3135	0.0261
AALA:Period12	163.9	117.7	1.3926	0.1716
AAM:Period12	509.1	117.2	4.3418	0.0001
CTM371:Period8	154.8	95.6	1.6195	0.1134
CTM371:Period12	14.5	102.9	0.1410	0.8886

R^2=0.9529

Table 7.7 Analysis of Covariance for Initial Stiffness from the Fatigue Test

Factor	Degree of Freedom	Sum of Squares	F-value	p-value
Mix	3	81133520	144.4624	0.0000
Period	3	6162636	10.9729	0.0000
Condition	1	96980642	518.0371	0.0000
AirVoid	1	2770940	14.8014	0.0006
Mix:Period	9	5292688	3.1413	0.0083
Mix:Condition	3	4128710	7.3514	0.0007
Period:Condition	3	5329647	9.4897	0.0001
Mix:Period:Condition	9	2381978	1.4137	0.2249
Residuals	31	5803445		

Table 7.8 Estimated Parameters of Linear Model for Initial Stiffness from the Fatigue Test

Coefficients	Estimated Value	Standard Error	*t* statistics	p-value
(Intercept)	12393.2	856.4	14.4712	0.0000
AALA	-1122.5	362.0	-3.1008	0.0035
AALB	145.0	373.2	0.3885	0.6997
AAM	1961.5	358.6	5.4699	0.0000
Period4	-1115.9	358.2	-3.1155	0.0034
Period8	-200.9	357.9	-0.5612	0.5778
Period12	-409.7	357.9	-1.1448	0.2591
Condition	-2355.0	299.3	-7.8680	0.0000
AirVoid	-334.5	116.8	-2.8651	0.0066
AALA:Period4	1729.8	456.9	3.7859	0.0005
AALB:Period4	713.6	460.8	1.5488	0.1293
AAM:Period4	679.6	455.8	1.4912	0.1438
AALA:Period8	1910.8	455.1	4.1989	0.0001
AALB:Period8	576.9	453.3	1.2726	0.2105
AAM:Period8	313.0	454.0	0.6896	0.4944
AALA:Period12	1653.4	454.8	3.6358	0.0008
AALB:Period12	760.6	460.8	1.6508	0.1066
AAM:Period12	573.3	452.7	1.2664	0.2127
AALA:Condition	1099.8	320.0	3.4364	0.0014
AALB:Condition	958.9	320.0	2.9967	0.0047
AAM:Condition	1335.1	319.9	4.1739	0.0002
Period4:Condition	-1133.7	320.1	-3.5414	0.0010
Period8:Condition	-1545.4	319.9	-4.8304	0.0000
Period12:Condition	-1155.2	320.4	-3.6060	0.0009

R^2=0.9610

Table 7.9 Analysis of Covariance for Initial Stiffness Ratio from the Fatigue Test

Factor	Degree of Freedom	Sum of Squares	F-value	p-value
Mix	3	0.1346	32.2794	0.0000
Period	3	0.0960	23.0067	0.0000
AirVoid	1	0.0247	17.7411	0.0008
Mix:Period	9	0.0474	3.7886	0.0113
Residuals	15	0.0209		

Table 7.10 Estimated Parameters of Linear Model for Initial Stiffness Ratio from the Fatigue Test

Coefficients	Estimated Value	Standard Error	*t* statistics	p-value
(Intercept)	1.1208	0.0970	11.5501	0.0000
AALA	-0.0279	0.0388	-0.7180	0.4838
AALB	0.0926	0.0388	2.3847	0.0307
AAM	0.0488	0.0376	1.2959	0.2146
Period4	-0.2330	0.0376	-6.2031	0.0000
Period8	-0.2421	0.0374	-6.4791	0.0000
Period12	-0.2414	0.0376	-6.4129	0.0000
AirVoid	-0.0408	0.0137	-2.9739	0.0095
AALA:Period4	0.2173	0.0536	4.0555	0.0010
AALB:Period4	0.0414	0.0535	0.7738	0.4511
AAM:Period4	0.1459	0.0535	2.7268	0.0156
AALA:Period8	0.1977	0.0539	3.6698	0.0023
AALB:Period8	0.0269	0.0528	0.5092	0.6180
AAM:Period8	0.1643	0.0530	3.0973	0.0074
AALA:Period12	0.1995	0.0536	3.7225	0.0020
AALB:Period12	0.0949	0.0536	1.7713	0.0968
AAM:Period12	0.2150	0.0530	4.0600	0.0010

R^2=0.9355

Table 7.11 Simultaneous Confidence Intervals for Contrasts of Initial Stiffness Ratio after Different Conditioning Periods, by the Tukey Method

Contrast	Estimated Value	Standard Error	Lower Bound	Upper Bound
Period 0 - Period 4	0.1320	0.0188	0.0777	0.1860
Period 0 - Period 8	0.1450	0.0188	0.0907	0.1990
Period 0 - Period 12	0.1140	0.0187	0.0602	0.1680
Period 4 - Period 8	0.0131	0.0186	-0.0407	0.0668
Period 4 - Period 12	-0.0178	0.0187	-0.0717	0.0361
Period 8 - Period 12	-0.0309	0.0187	-0.0848	0.0231

Table 7.12 Analysis of Covariance for ln(Fatigue Life) from the Fatigue Test

Factor	Degree of Freedom	Sum of Squares	F-value	p-value
Mix	3	8.4472	17.5628	0.0000
Period	3	5.2013	10.8141	0.0001
Condition	1	3.5186	21.9466	0.0001
AirVoid	1	0.3796	2.3678	0.1340
Mix:Period	9	0.5419	0.3756	0.9380
Mix:Condition	3	5.9235	12.3157	0.0000
Period:Condition	3	1.3967	2.9038	0.0504
Mix:Period:Condition	9	1.7329	1.2010	0.3294
Residuals	31	4.9701		

Table 7.13 Estimated Parameters of Linear Model for ln(Fatigue Life) from the Fatigue Test

Coefficients	Estimated Value	Standard Error	*t* statistics	p-value
(Intercept)	12.0095	0.2472	48.5792	0.0000
AALA	-0.3614	0.3260	-1.1084	0.2741
AALB	0.0353	0.3260	0.1082	0.9144
AAM	0.1207	0.3260	0.3701	0.7132
Period4	-0.6618	0.3260	-2.0299	0.0489
Period8	-0.0653	0.3260	-0.2003	0.8423
Period12	0.1612	0.3260	0.4945	0.6236
Condition	-0.9113	0.2728	-3.3409	0.0018
AALA:Period4	0.1574	0.4124	0.3817	0.7047
AALB:Period4	-0.0694	0.4124	-0.1683	0.8672
AAM:Period4	0.1163	0.4124	0.2819	0.7794
AALA:Period8	-0.0813	0.4124	-0.1972	0.8446
AALB:Period8	-0.3102	0.4124	-0.7521	0.4563
AAM:Period8	-0.1354	0.4124	-0.3284	0.7443
AALA:Period12	-0.2059	0.4124	-0.4994	0.6202
AALB:Period12	-0.4396	0.4124	-1.0659	0.2927
AAM:Period12	0.1750	0.4124	0.4244	0.6735
AALA:Condition	1.3017	0.2916	4.4639	0.0001
AALB:Condition	0.6346	0.2916	2.1762	0.0354
AAM:Condition	1.5749	0.2916	5.4009	0.0000
Period4:Condition	-0.3496	0.2916	-1.1987	0.2375
Period8:Condition	-0.6318	0.2916	-2.1668	0.0361
Period12:Condition	-0.7604	0.2916	-2.6076	0.0127

R^2=0.7829

Table 7.14 Analysis of Covariance for Fatigue Life Ratio from the Fatigue Test

Factor	Degree of Freedom	Sum of Squares	F-value	p-value
Mix	3	4.2645	7.5079	0.0027
Period	3	0.9698	1.7073	0.2082
AirVoid	1	0.2965	1.5660	0.2299
Mix:Period	9	0.8765	0.5144	0.8423
Residuals	15	2.8400		

Table 7.15 Estimated Parameters of Linear Model for Fatigue Life Ratio from the Fatigue Test

Coefficients	Estimated Value	Standard Error	*t* statistics	p-value
(Intercept)	0.6117	0.1874	3.2641	0.0032
AALA	0.6563	0.2003	3.2764	0.0031
AALB	0.3131	0.2003	1.563	0.1306
AAM	0.9738	0.2003	4.8612	0.0001
Period4	-0.2814	0.2003	-1.4045	0.1725
Period8	-0.4313	0.2003	-2.1532	0.0411
Period12	-0.4213	0.2003	-2.1031	0.0457

R^2=0.5660

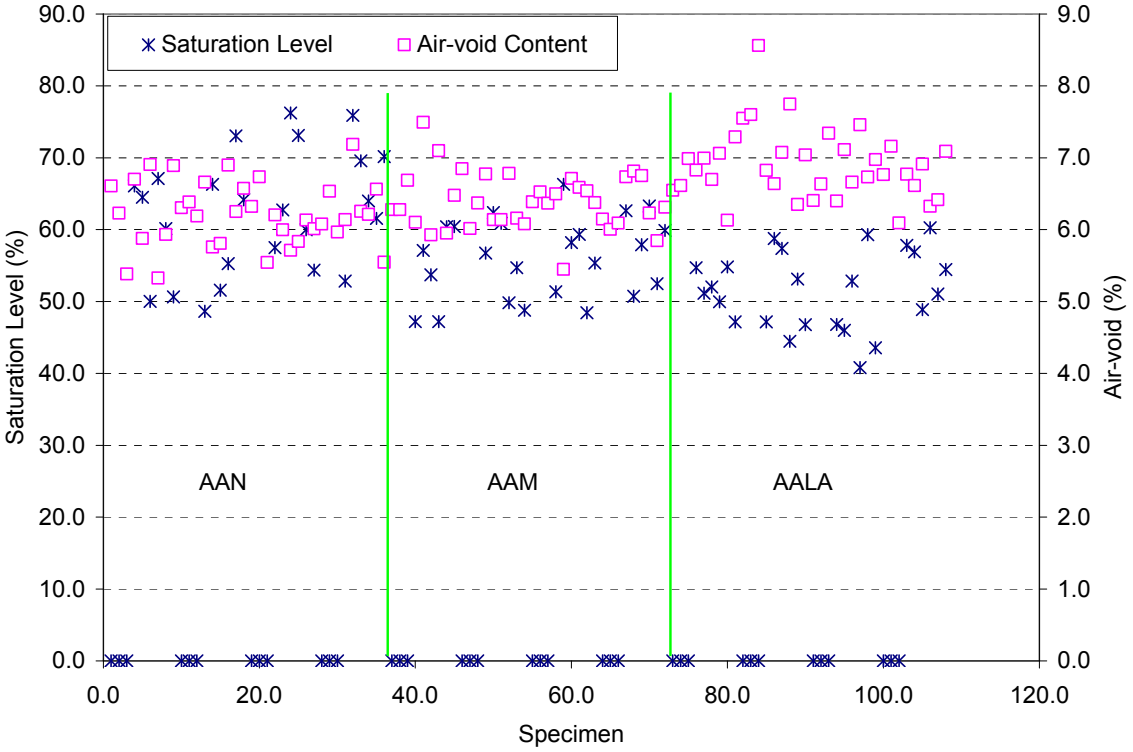

Figure 7-1. Saturation levels and air-void contents of all Hveem specimens.

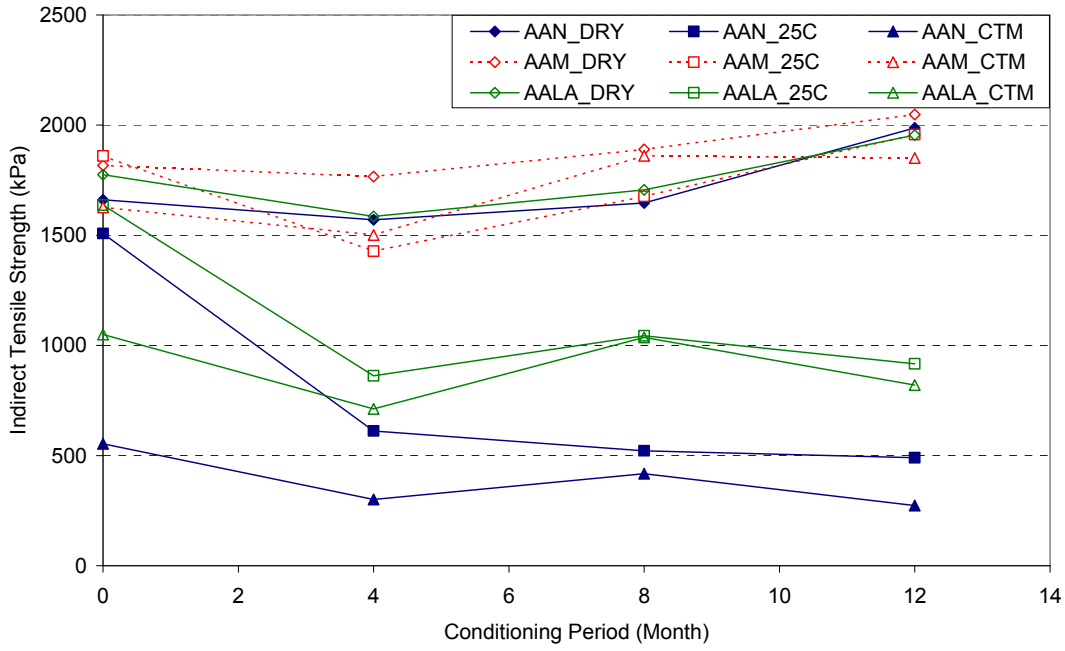

Figure 7-2. Average indirect tensile strength of each mix after different conditioning periods.

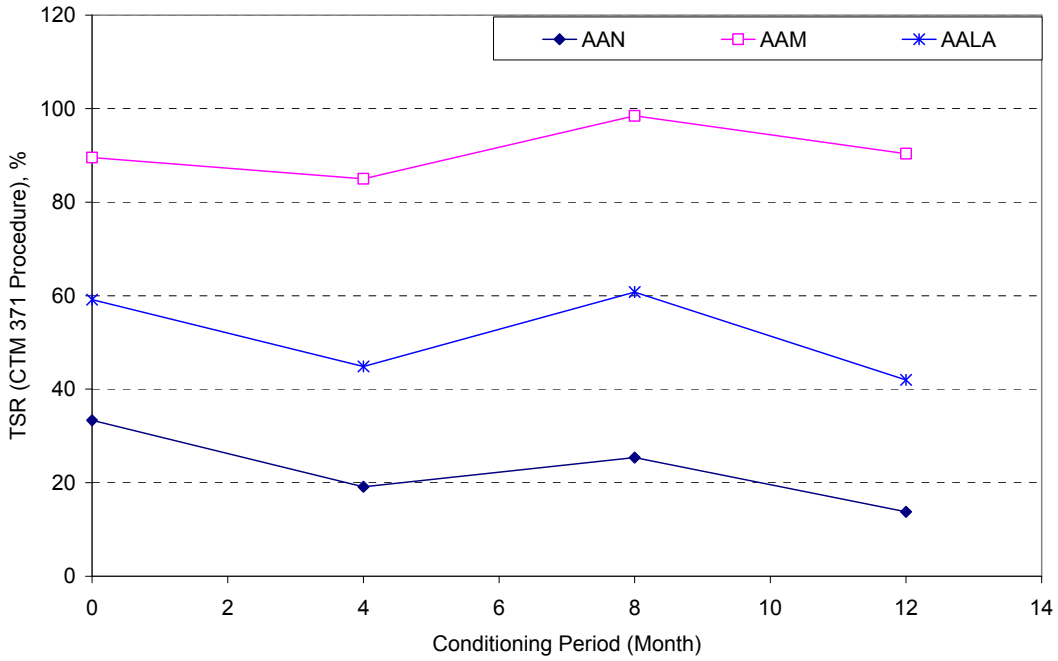

Figure 7-3. Tensile strength ratio (TSR) of each mix after different conditioning periods by the 25°C plus CTM 371 conditioning procedure.

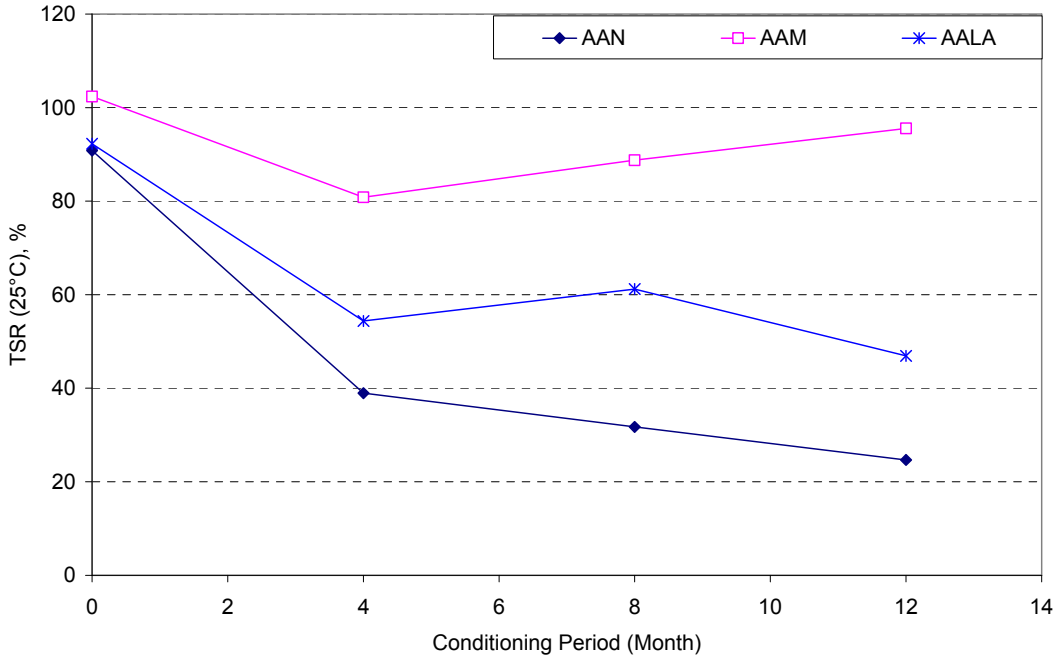

Figure 7-4. Tensile strength ratio (TSR) of each mix after different conditioning periods at 25°C.

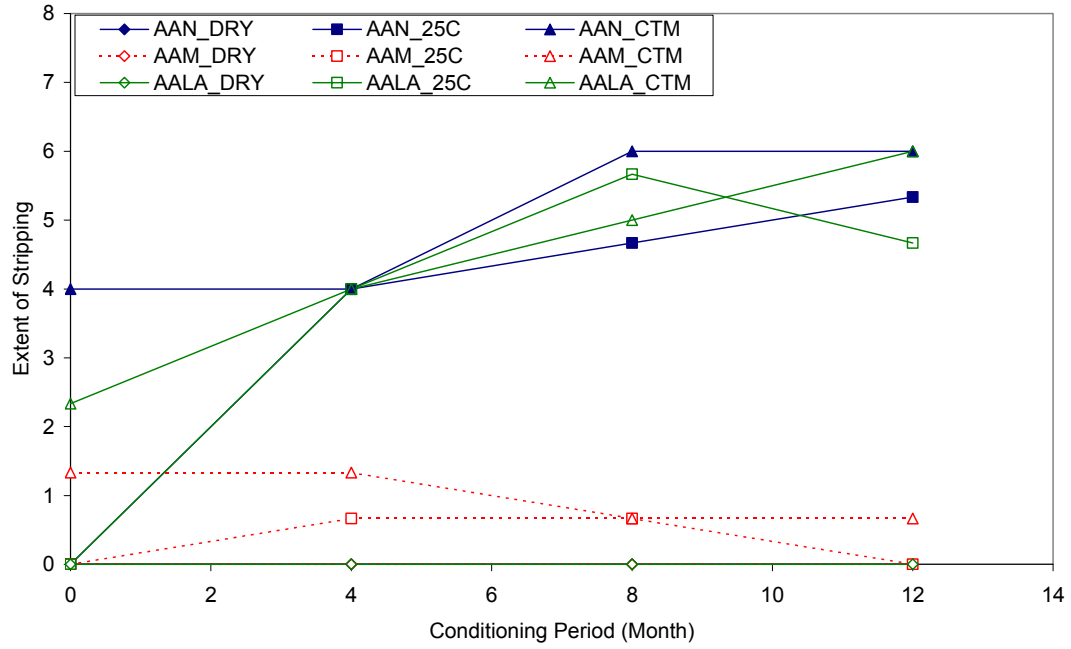

Figure 7-5. Average extent of stripping of each mix after different conditioning periods.

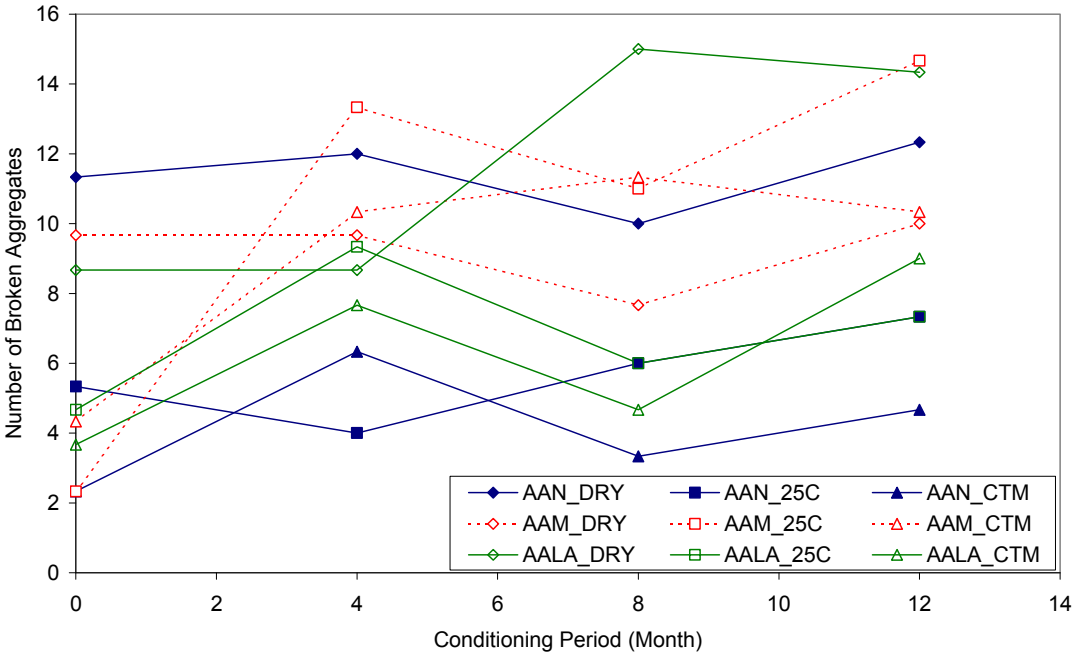

Figure 7-6. Average number of broken aggregates of each mix after different conditioning periods.

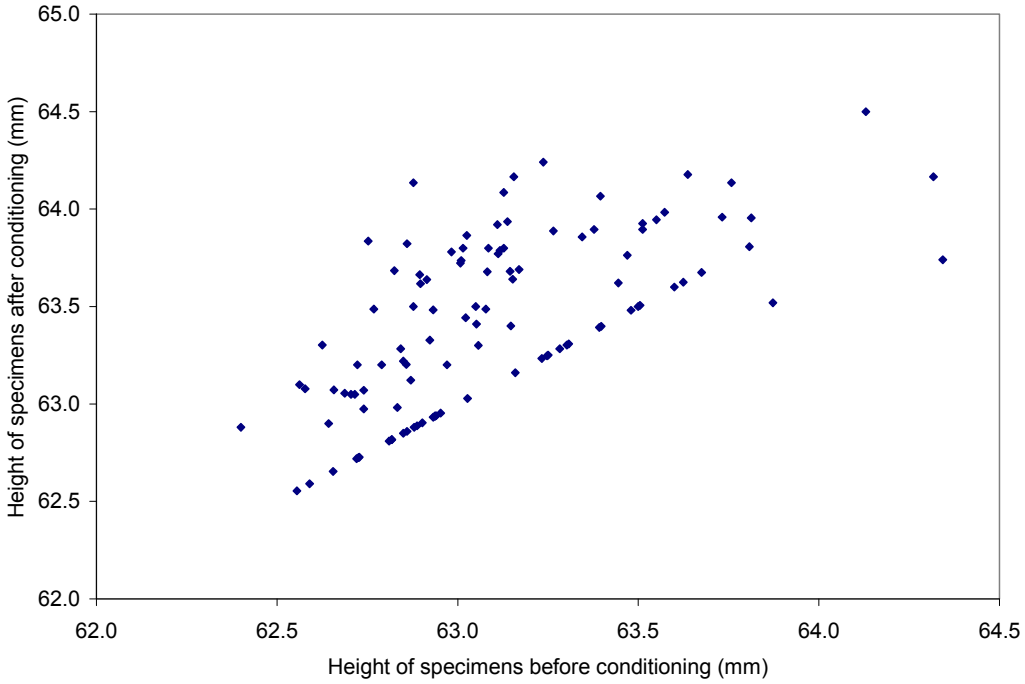

Figure 7-7. Height of specimens before and after moisture conditioning.

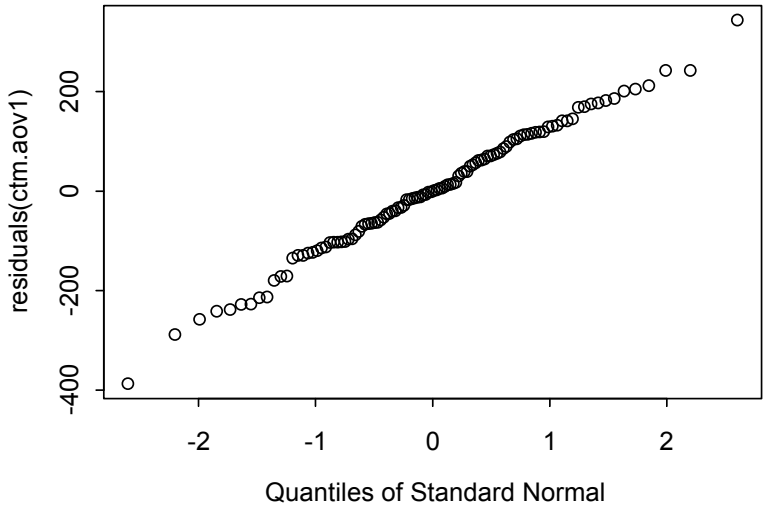

(a)

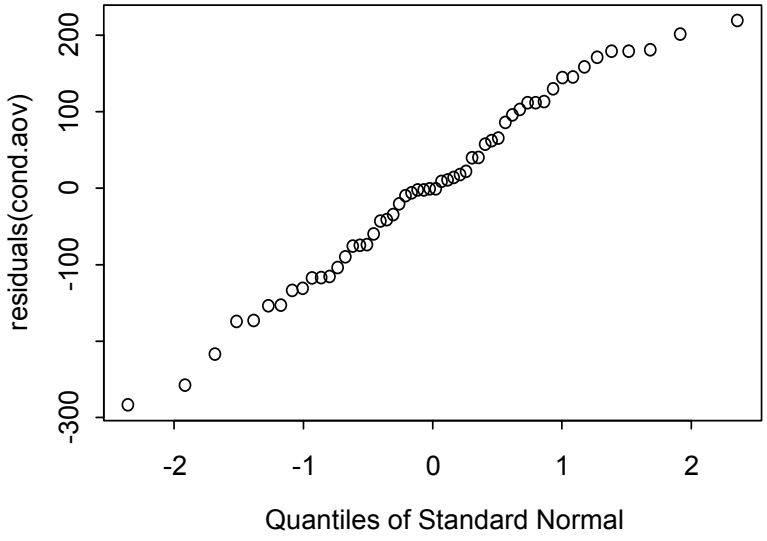

(b)

Figure 7-8. QQ-normal plot of the residuals from the linear model for indirect tensile strength (a – all specimens, b – wet specimens).

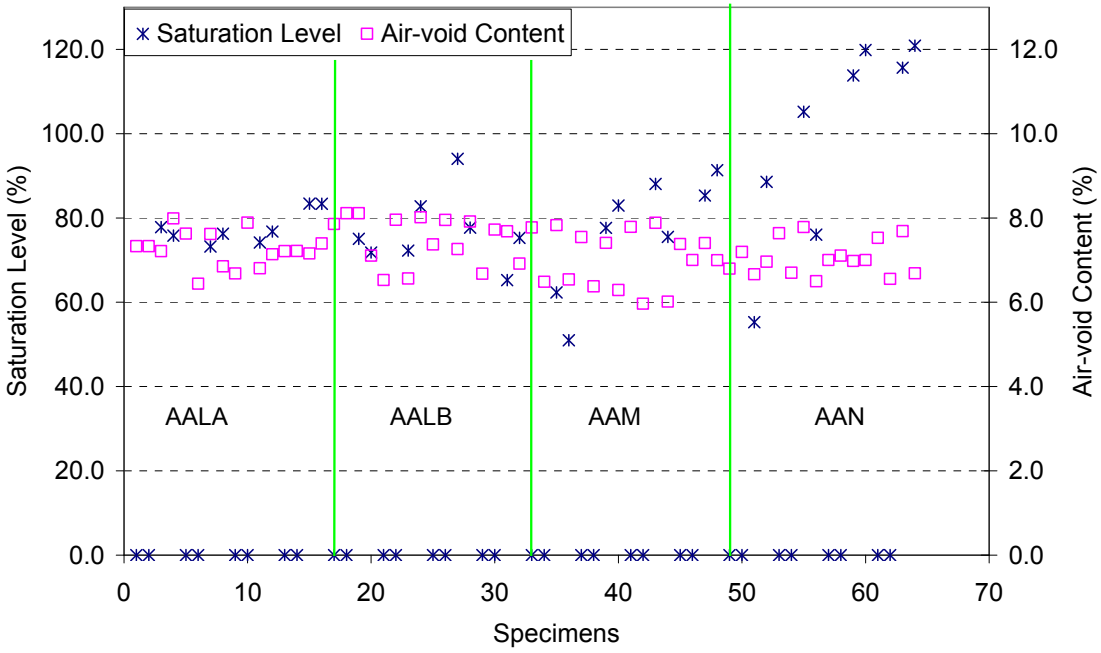

Figure 7-9. Saturation levels and air-void contents of all beam specimens.

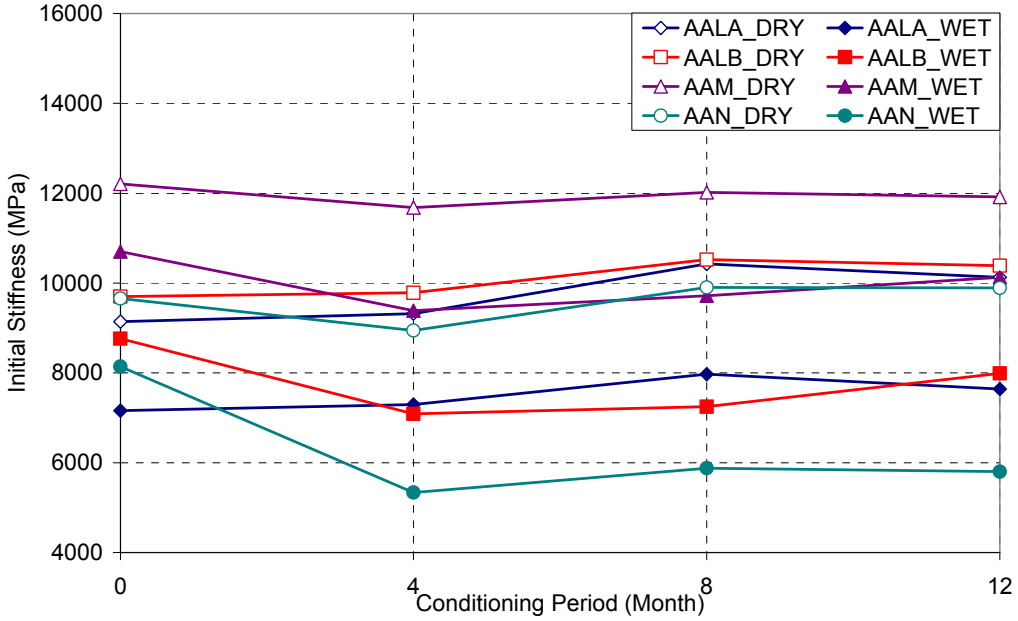

Figure 7-10. Average initial stiffness of each mix after different conditioning periods.

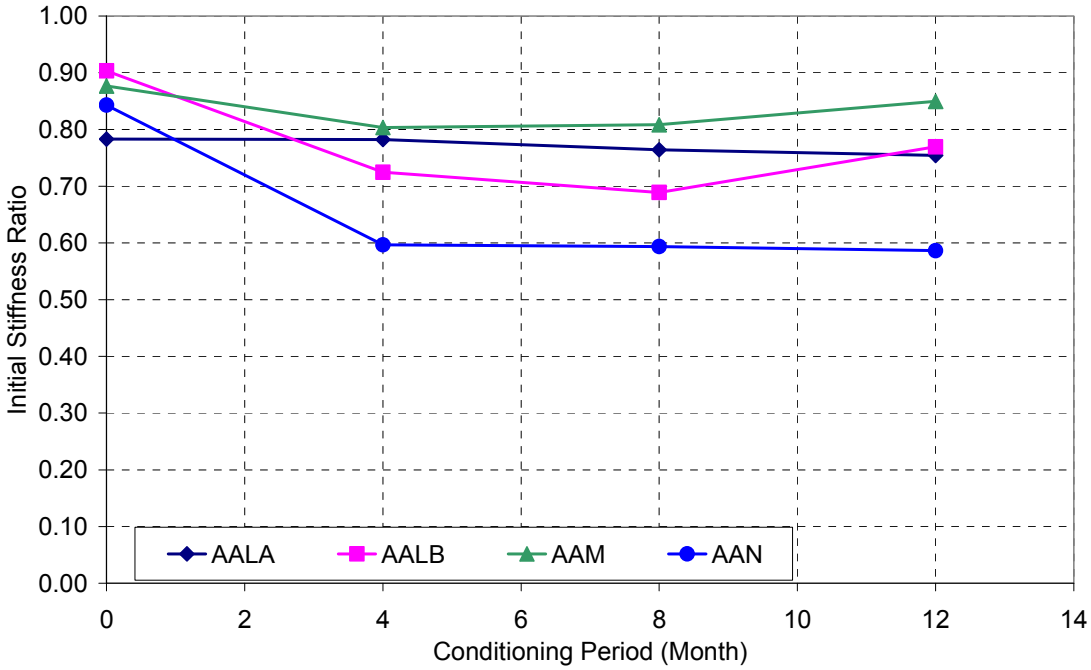

Figure 7-11. Initial stiffness ratio of each mix after different conditioning periods.

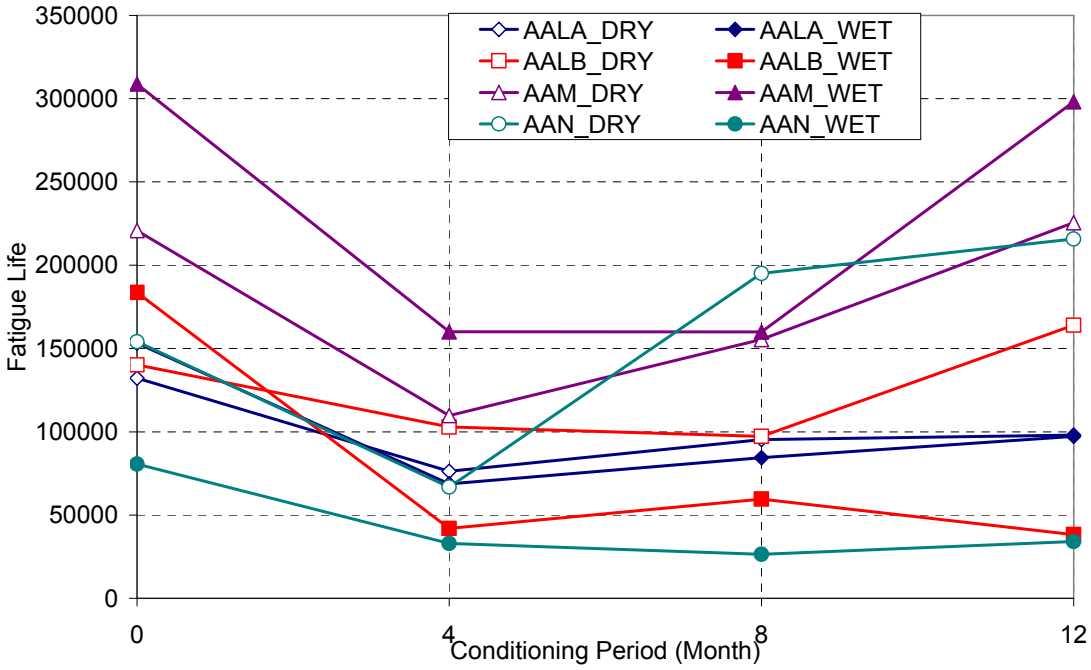

Figure 7-12. Average fatigue life of each mix after different conditioning periods.

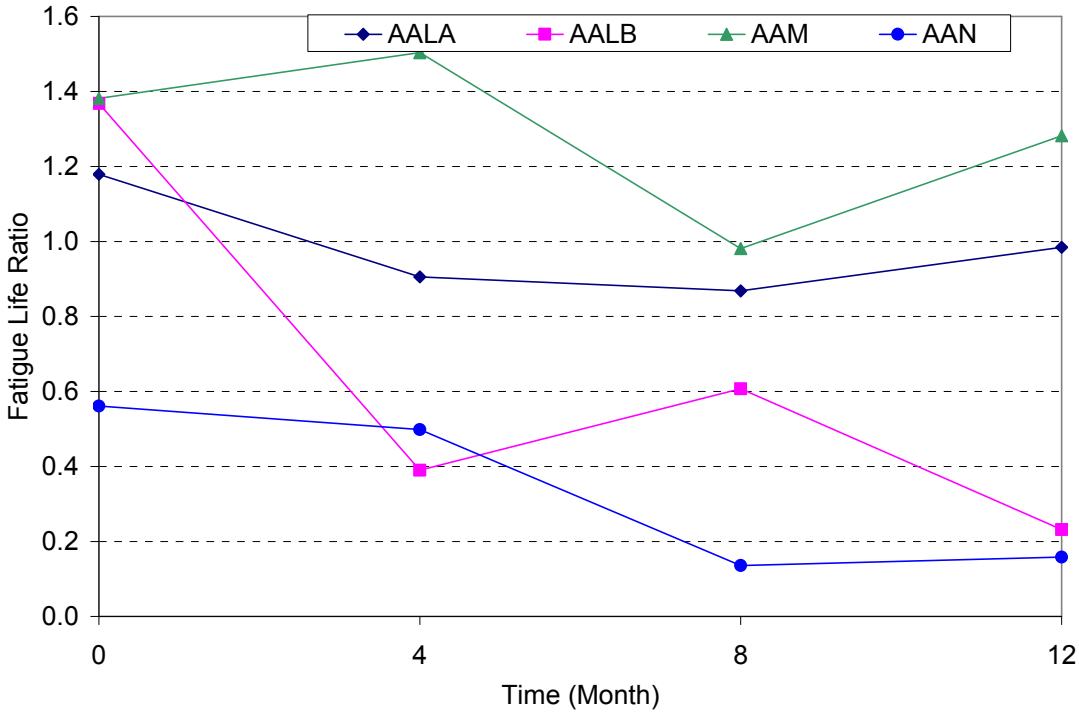

Figure 7-13. Fatigue life ratio of each mix after different conditioning periods.

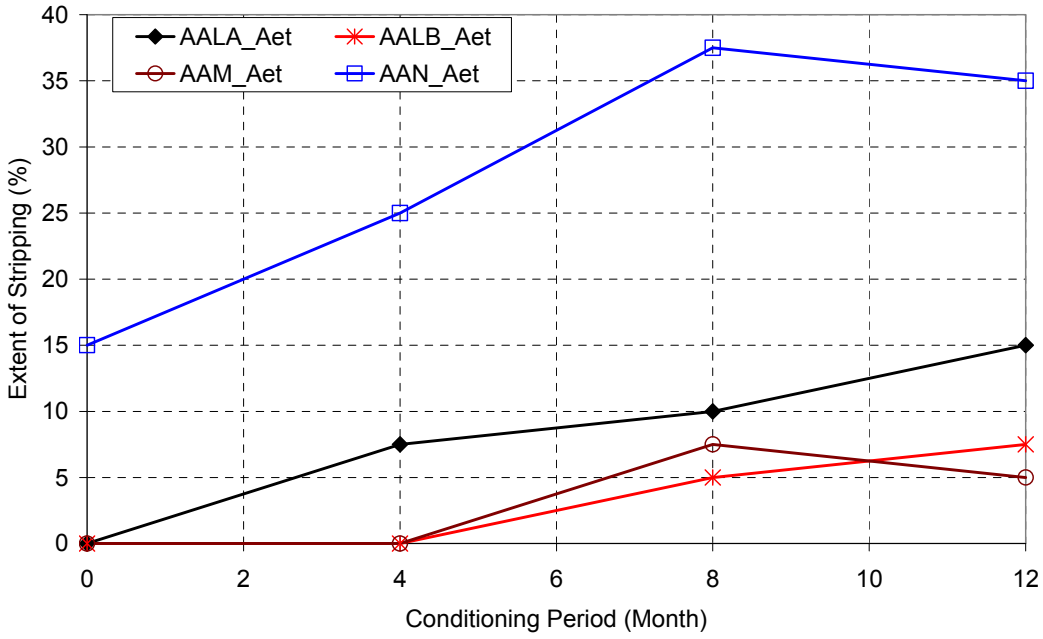

Figure 7-14. Average extent of stripping of each mix in the flexural beam fatigue test after different conditioning periods.

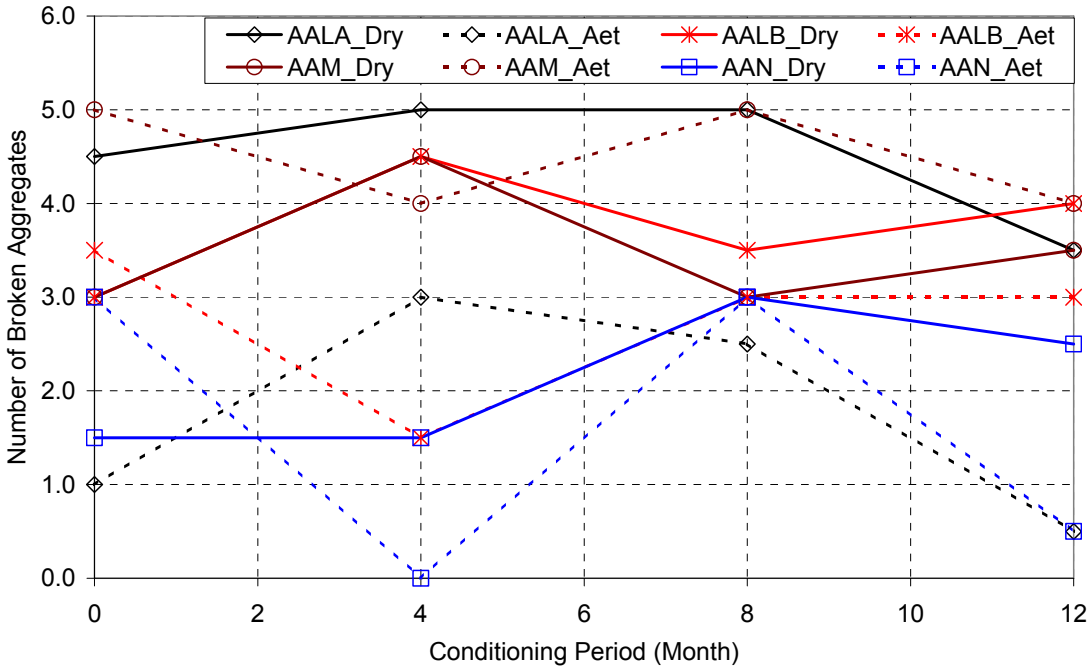

Figure 7-15. Average number of broken aggregates of each mix in the flexural beam fatigue test after different conditioning periods.

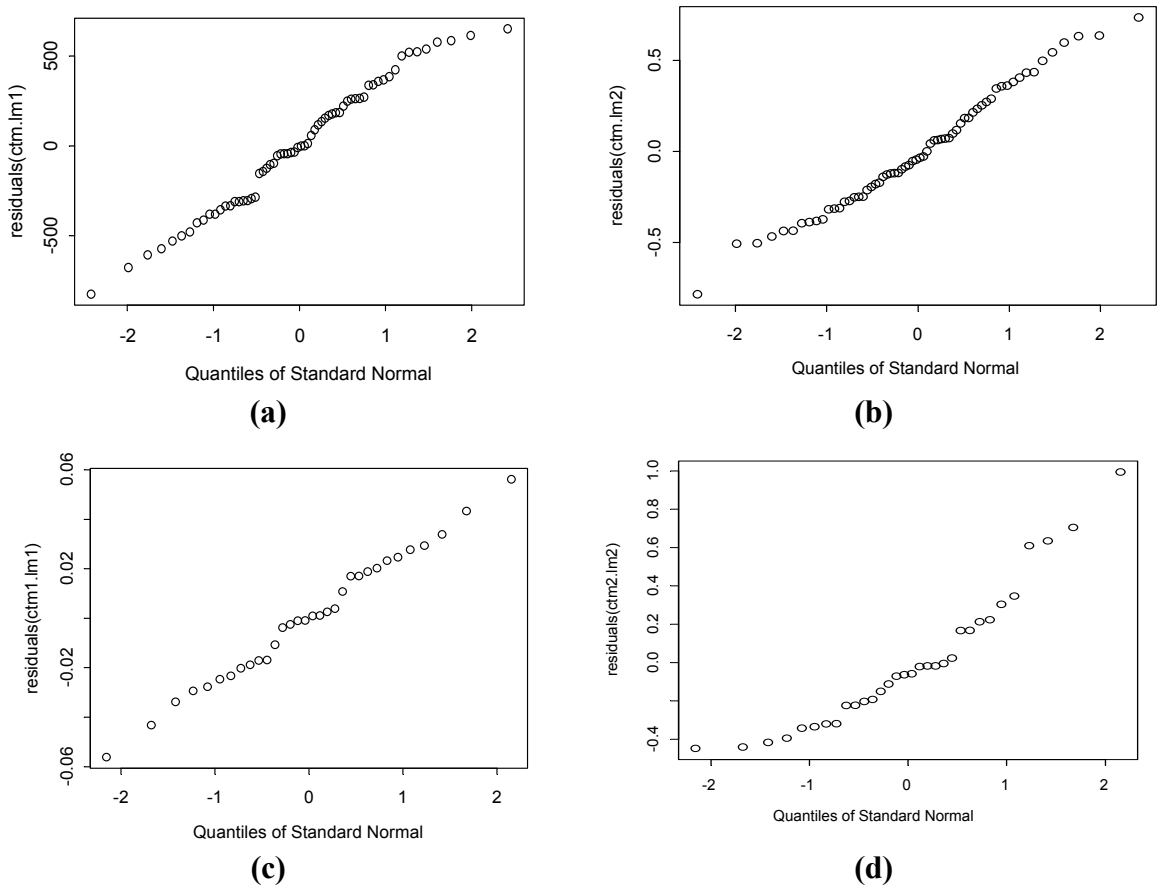

Figure 7-16. Normal probability plots of the residuals from the linear model (a. initial stiffness, b. ln(fatigue life), c. initial stiffness ratio, d. fatigue life ratio).

8.0 SUMMARY

This research investigated the factors contributing to moisture damage in asphalt mixes using field and laboratory data; evaluated the effectiveness of the Hamburg Wheel Tracking Device (HWTD) test for predicting mix performance in terms of moisture damage; compared various conditioning procedures for use with the HWTD, California Method CTM 371, and the flexural beam fatigue test; evaluated the effect of moisture on rutting resistance, flexural stiffness, and fatigue responses and developed a typical fatigue-based test procedure; and evaluated the effectiveness of antistripping additives. Conclusions are presented in Chapters 3, 4, 5, 6, and 7 for these studies and a summary of these conclusions is contained in this chapter. Recommendations resulting from the research are also provided. This chapter concludes with recommendations for future research.

8.1 Conclusions and Recommendations

Overall conclusions and recommendations from both the field and laboratory investigations of moisture damage in asphalt mixes are as follows:

1. Severe moisture damage exists in some asphalt pavements in California. About 10 percent of pavements with previously unknown performance in the survey list showed appreciable moisture damage. Although the incomplete random sampling used in this study does not necessarily reflect the statewide extent of moisture damage, it does suggest that moisture damage should not be neglected in asphalt pavements.
2. Substantial knowledge has been gained in terms of the effects of a variety of factors on the occurrence and severity of moisture damage in asphalt pavements. Air-void content, pavement structure (whether or not underlying portland cement concrete or cement-treated base exists), cumulative rainfall, mix type (dense-graded asphalt concrete or gap-graded rubberized asphalt concrete), use of additives, and pavement age (an indicator of long-term exposure to the climate conditions) have high significance as revealed by statistical analysis. High air-void contents not only allow more moisture to enter pavements, but also significantly reduce the fatigue resistance of mixes in wet conditions. Dry cores revealed that a substantial amount of moisture exists in many pavements even several months after rain, and the amount of moisture present in cores is positively correlated to the air-void content. The air-void content of conventional dense-graded asphalt mixes in California highways cored from about 50 sites ranges from 2 percent to 14 percent with a mean around 7 percent, indicating that better control of compaction during construction to reduce both the mean and variance of air-void content in pavements is necessary to reduce the risk of moisture damage. Reduction of the binder content also significantly reduces the moisture resistance of asphalt mixes under repeated loading in terms of fatigue performance.
3. Based on a limited number of samples, RAC-G mixes did not show an apparent advantage in improving moisture resistance as compared to dense-graded mixes with conventional asphalt binders. Severe stripping has been observed in a few pavement sections using the RAC-G mixes. Higher air-void contents in a number of these mixes compared to the air-void contents of QC/QA dense-graded mixes may be one of the reasons leading to this observed moisture damage.
4. Increased annual rainfall and pavement age also increase the probability of moisture damage.
5. Occurrence of repeated loading (whether or not in the wheelpath) had a marginally significant effect on moisture damage but cumulative truck traffic did not appear to be a significant factor. This suggests that simulation of repeated traffic loading should be a factor

in assessing moisture damage in the laboratory; however, its existence and not the total number of repetitions is the significant test parameter.

6. The HWTD test procedure used in this study can correctly identify the effect of antistripping additives but may underestimate the performance of mixes containing soft binders at the fixed test temperature 50°C. The correlation between laboratory test results and field performance seems acceptable except that the test procedure may fail mixes that perform well in the field and, in a very few cases, give false positive results. Improvement of the prediction accuracy of the HWTD test may be obtained by the following two changes to the test procedure. First, use a test temperature that is appropriate to the environment where the mix is placed. It is better to determine the temperature based on the seven-day high air temperature rather than on a designated high-temperature performance grade (PG) of asphalt binders; the selection criteria proposed in the Colorado DOT Laboratory Procedure 5112 can be followed. Second, run the test in dry condition when poor results are obtained from the regular wet test. Using this approach, the confounding effects of aggregate structure, binder stiffness, and other potential factors can be minimized, and the effect of moisture can be clearly identified.

7. Fatigue-based test results (i.e., fatigue life) can distinguish mixes with different moisture sensitivities and give the ranking of mixes consistent with field experience. The initial stiffness measured in the fatigue beam test, however, is not as discriminative as fatigue life. The indirect tensile strength ratio (TSR) test results are consistent with fatigue test results and field experience, while the HWTD test results are not with respect to aggregate type and binder type.

8. Moisture has a complex influence on the fatigue response of asphalt mixes in the controlled-strain flexural beam fatigue test, extending or reducing fatigue life, depending on the conditioning procedure. Conditioning temperature significantly affects the moisture resistance of asphalt mixes. High temperature significantly increases moisture damage in mixes, especially in untreated mixes. On the other hand, moisture content and conditioning duration have less effect on the extent of moisture damage in the fatigue test.

9. A typical performance-based test procedure has been determined for comparative evaluation of different mixes. The procedure is a controlled-strain flexural beam fatigue test performed at 20°C, 10 Hz, and 200με on specimens presaturated under a 635 mm-Hg vacuum for 30 minutes and preconditioned at 60°C for one day. Although the variance of results is relatively high, this procedure can distinguish mixes with different moisture sensitivities and give a ranking of mixes consistent with prior engineering experience.

10. The fatigue-based test procedure could be applied in pavement design to explicitly include the moisture effect. However, a thorough study of the fatigue response at the typical spectra of conditioning and test parameters should be conducted, and extensive field performance data need to be collected for test result calibration before this procedure can actually be applied.

11. Preliminary evaluation of the moisture effect on the rutting resistance of asphalt mixes by the RSST-CH test did not produce the expected results. In some cases, the existence of moisture reduced the permanent shear strain. It is possible that the preconditioning procedure used in this study is insufficient. A harsher conditioning procedure, such as use of high temperatures, is needed to better simulate field conditions.

12. Both hydrated lime and liquid antistripping agents can improve the moisture resistance of asphalt mixes, as evidenced by both field and laboratory data. Mix properties, including indirect tensile strength, flexural stiffness, and fatigue life, are least affected by moisture for mixes treated with hydrated lime and moderately affected by moisture for mixes treated with liquid antistripping agents. Different liquid antistripping agents have different effectiveness.

Liquid antistripping agents do not significantly change mix properties in dry condition. Hydrated lime does not significantly change the indirect tensile strength or fatigue response, but significantly increases the flexural stiffness in dry condition.

13. For a conditioning period as long as one year, both hydrated lime and liquid antistripping agents are effective in improving the moisture resistance of asphalt mixes. The effectiveness of hydrated lime does not decrease, but instead in some cases increases with conditioning time, while the effectiveness of the liquid antistripping agents generally does not change with time.
14. There is good equivalency between the two conditioning procedures: a short-term freeze-thaw cycle and long-term moisture conditioning at 25°C.
15. Moisture damage develops with time on a nonlinear scale. At a mild temperature, damage evolves significantly in the first four months, then levels off.
16. When moisture exists in the mix for a short period, neither indirect tensile strength nor the flexural initial stiffness can discriminate between mixes with and without treatments. However, fatigue life can show sufficiently the difference between untreated and treated mixes. It is more discriminative to use the fatigue life ratio as the index of moisture sensitivity if very short conditioning periods are used.

8.2 Future Research

Due to the limitations of time and resources, several aspects of this research have not been fully explored and remain as future work:

1. The aggregate effects on moisture damage have not been considered in the field investigation, primarily due to the lack of information on aggregate chemical compositions and properties. The literature and laboratory tests conducted in this study showed that aggregates have an important influence on moisture damage. The statistical analysis in the field investigation included the aggregate effects in the error term, which essentially inflated the variance of the error term and reduced the power of hypothesis testing. For a better analysis, it is necessary to quantify the aggregate property and include it in the statistical model. In such an analysis, aggregate cannot be treated as a class variable, and a key question will be how to characterize aggregate type. Although there is some consensus on mineral types of aggregate expected to have better performance, there are many contradictions in the literature, and the extent to which problems associated with aggregate type can be overcome by construction compaction and mix design were not definitively defined in this study. Some insight was gained by examining the performance for two aggregates used in later laboratory testing: many other factors such as compaction and environmental conditions may well complicate aggregate effects. Mineral composition-based tests (e.g., petrographic analysis) or thermodynamics-based tests (e.g., surface energy measurement) may be used to characterize aggregate properties related to moisture damage.
2. The HWTD test procedure needs further improvement and standardization. Its effectiveness after the suggested changes to the default test procedure should be further verified by laboratory-fabricated specimens and corresponding mix performance in the field.
3. The fatigue-based test procedure needs to be expanded to incorporate different test conditions and environmental conditions, and further calibrated. Modifications to the test procedure may also be necessary.
4. Further research is needed to evaluate the moisture effect on permanent deformation of asphalt mixes by the simple shear test and to explore the potential of using simple shear test-

based procedure to predict pavement performance in terms of moisture damage. The conditioning procedure to incorporate the moisture effect in the simple shear test needs to be improved.

5. The collection of field performance data and related project data needs to be continued in a systematic and standard approach. Since a variety of asphalt mixes are used in the field and the number of factors affecting moisture damage is large, it is necessary to have a large and complete database for adequate statistical analysis and calibration of laboratory test results for different mixes. From a long-term point of view, pavement performance needs to be evaluated regularly by a standard procedure to assure the proper identification of moisture damage. In addition, recommendations need to be provided for highway construction and management agencies to make sure relevant project data are properly archived and readily available, because in this study it turned out to be very difficult to pull out historical project data from agency offices, especially for pavements with an age greater than five years.
6. Test sections may be necessary to further evaluate the long-term effectiveness of antistripping additives.

9.0 REFERENCES

1. Anderson, D. A., Dukatz, E. L., and Petersen, J. C. (1982). "The Effect of Antistrip Additives on the Properties of Asphalt Cement." *Proceedings Association of Asphalt Paving technologists Technical Sessions*, Kansas City, Missouri.
2. Allen, W. L., and Terrel, R. L. (1994). "Field Validation of the Environmental Conditioning System." *Strategic Highway Research Program*, Report No. SHRP-A-396, National Research Council, Washington, D.C.
3. Aria, E. H., Amini, J., and Saradjian, M.R. (2003). "Back propagation neural network for classification of IRS-1D satellite images." Joint Workshop of *High Resolution Mapping from Space*, Tehran University, Iran.
4. Aschenbrener, T., Terrel, R. L., and Zamora, R. A. (1994). "Comparison of the Hamburg Wheel Tracking Device and the Environmental Conditioning System to Pavements of Known Stripping Performance." Report No. CDOT-DTD-R-94-1, Colorado Department of Transportation, Denver.
5. American Association of State Highway and Transportation Officials (AASHTO). (1995). *AASHTO Provisional Standards*. March Edition, Washington D. C., American Association of State Highway and Transportation Officials.
6. Balghunaim, F. A. (1991). "Improving Adhesion Characteristics of Bituminous Mixes by Washing Dust-Contaminated Coarse Aggregates." *Transportation Research Record* 1323, 134–142.
7. Benefield, L. D., and Parker, F. (1988). "Microbial Degradation as a Factor Contributing to Stripping of Asphalt Pavements." IR-88-02, Highway Research Center, Auburn University, Auburn, Alabama.
8. Benefield, L. D., and Parker, F. (1989). "Effect of Microbial Degradation on Bond Between Asphaltic Concrete Layers." IR-89-03, Highway Research Center, Auburn University, Auburn, Alabama.
9. Bejarano, M. O., Harvey, J. T., Ali, A., Mahama, D., Hung, D., and Preedonant, P. (2003). "Performance of Drained and Undrained Flexible Pavement Structures in Accelerated Loading under Wet Conditions—Summary Report Goal 5 Partnered Pavement Performance Program." Draft report no. UCPRC-RR-2003-04 prepared for the California Department of Transportation, Pavement Research Center, Institute of Transportation Studies, University of California, Berkeley, 20–22.
10. Berger, E., Monismith, C. L., Kwong, J., and Nodes, J. (2003). "Summary Report: Breakout Session 2—Testing and Treatments." *Moisture Sensitivity of Asphalt Pavements, A National Seminar*, Transportation Research Board Miscellaneous Report, Transportation Research Board, Washington D. C., 293–301.
11. Breslin, P., Frunzi, N., Napoleon, E., and Ormsby, T. (1999). "Getting to Know ArcView GIS." ESRI Press, Redlands, California.
12. Busching, H.W., Burati, J.L., Jr., and Amirkanian,S.N. (1986). "An Investigation of Stripping in Asphalt Concrete in South Carolina." Report No. FHWA-SC-86-02. Clemson University.
13. California Department of Transportation. (2004). Standard Specifications. Sacramento, California.
14. Cheng, D., Little, D. N., Lytton, R. L., and Holtse, J. C. (2002). "Use of Surface Free Energy Properties of Asphalt-Aggregate System to Predict Damage Potential." Presented at Annual Meeting of the Association of Asphalt Paving Technologists.
15. Choubane, B., Page, G.C., and Musselman, J.A. (1998). "Investigation of Water Permeability of Coarse Graded Superpave Pavements." *Journal of the Association of Asphalt Paving Technologists*, Volume 67, pp. 255–276.

16. Collins, R., Johnson, A., Wu, Y., and Lai, J. (1997). "Evaluation of moisture susceptibility of compacted asphalt mixture by asphalt pavement analyzer." *Compendium of Papers at 76th Annual Meeting*, Transportation Research Board, Washington D. C.

17. Cooley, L. A., Jr., Prowell, B. D., Hainin, M. R., Buchanan, M. S., Harrington, J. (2002). "Bulk Specific Gravity Round-Robin Using the Corelok Vacuum Sealing Device." NCAT Report 02-11, National Center for Asphalt Technology, Auburn University, Auburn, Alabama.

18. Corelok® Operator's Guide. (2001). Version 10, Instrotek Incorporated, Raleigh, NC.

19. Cranfield, J., and Magnusson, E. (2003). "Canadian Consumer's Willingness-To-Pay for Pesticide Free Food Products: An Ordered Probit Analysis." *International Food and Agribusiness Management Review*, Vol. 6, Number 4, 13–30.

20. Davidian, M. and Giltinam, D. M. (2003). "Nonlinear Models for Repeated Measurement Data: An Overview and Update." *Journal of Agricultural, Biological, and Environmental Statistics*, Volume 8, Number 4, 387–419.

21. Dunning, R. L. (1987). "Water Sensitivity of Asphalt Concrete." Prepared Personal Discussion.

22. Epps, J., Berger, E., and Anagnos, J. N. (2003). "Treatments." *Moisture Sensitivity of Asphalt Pavements, A National Seminar.* Transportation Research Board Miscellaneous Report, Transportation Research Board, Washington D. C., 117–186.

23. Estrella, A. (1998). "A New Measure of Fit for Equations with Dichotomous Dependent Variables." *Journal of Business and Economic Statistics*. 16, 198–205.

24. Fromm, H. J. (1974). "The Mechanisms of Asphalt Stripping from Aggregate Surfaces." *Proceedings of the Association of Asphalt Paving Technologists*, Vol. 43, 191–219.

25. Greene, W. (2000). "Econometric Analysis." Fourth Edition, Prentice Hall International, Inc., New York, N.Y.

26. Huang, W., and Qian, Z. D. (2001). "Theory and Methodology of Advanced Asphalt Pavement Design." Science Publishing House, Beijing, China.

27. Harvey, J. T. (1991). "Asphalt Concrete Specimen Preparation Protocol: SHRP Asphalt Project A—003A." Version 3.0, SHRP Technical Memorandum TM-UCB-A-003A-91-2. University of California, Berkeley.

28. Harvey, J., Tsai, B., Long, F., and Hung, D. (1999). "CAL/APT Program—Asphalt Treated Permeable Base (ATPB)." Report number UCPRC-RR-1999-05 prepared for the California Department of Transportation, Pavement Research Center, Institute of Transportation Studies, University of California, Berkeley.

29. Hicks, R. G., Santucci, L., and Aschenbrener, T. (2003). "Introduction and Seminar Objectives." *Moisture Sensitivity of Asphalt Pavements, A National Seminar*, Transportation Research Board Miscellaneous Report, Transportation Research Board, Washington D. C., 3–36.

30. Izzo, R. P., and Tahmoressi, M. (1999). "Use of the Hamburg Wheel-Tracking Device for Evaluating Moisture Susceptibility of Hot-Mix Asphalt." *Transportation Research Record: Journal of the Transportation Research Board, No. 1681*, TRB, National Research Council, Washington, D. C. 76–85.

31. Kandhal, P. S., Lynn, C. Y., and Parker, F. (1998). "Test for Plastic Fines in Aggregates Related to Stripping in Asphalt Paving Mixtures." *Journal of the Association of Asphalt Paving Technologists*, Vol. 67.

32. Kandahl, P. S., and Rickards, I. J. (2001). "Premature Failure of Asphalt Overlays from Stripping: Case Histories." NCAT Report 01-01, National Center for Asphalt Technology, Auburn University, Auburn, Alabama.

33. Kennedy, T. W., and Ping, W. V. (1991). "Comparison Study of Moisture Damage Test Methods for Evaluating Antistripping Treatments in Asphalt Mixtures." *Transportation Research Record 1323*, Transportation Research Board, Washington, D. C.

34. Kiggundu, B. M., Bagampadde U., and Mukunya, J. S. (2002). "Exploratory Stripping Studies on Bituminous Mixtures in Uganda." *Moisture Damage Symposium*, Western Research Institute, Laramie, Wyoming.

35. Kiggundu, B. M., and Roberts, F. L. (1988). "Stripping in HMA Mixtures: State-of-the-art and Critical Review of Test Methods." *NCAT Report No. 88-2*, National Center for Asphalt Technology, Auburn University, Auburn, Alabama.

36. Larson, G., and Dempsey, B. (2003). "EICM Software. Enhanced Integrated Climatic Model Version 3.0 (EICM)." University of Illinois, Urbana, Illinois.

37. Lea, J., Harvey, J. T. (2004). "Data Mining of the Caltrans Pavement Management System (PMS) Database." Draft report number UCPRC-RR-2002-04 prepared for the California Department of Transportation, Pavement Research Center, University of California, Berkeley.

38. Lottman, R. P. (1982). "Predicting Moisture-induced Damage to Asphaltic Concrete: Field Evaluation." National Cooperative Highway Research Program Report 246, Transportation Research Board, National Research Council, Washington, D.C.

39. Lu, Q., Harvey, J. T., Lea, J., Quinley, R., Redo, D., and Avis, J. (2002). "Truck Traffic Analysis using Weigh-In-Motion (WIM) Data in California." Report no. UCPRC-RR-2002-01 prepared by the Pavement Research Center, Institute of Transportation Studies, University of California, Berkeley.

40. Lytton, R. L. (2002). "Mechanics and Measurement of Moisture Damage." *Moisture Damage Symposium*, Western Research Institute, Laramie, Wyoming.

41. Madanat, S., Mishalani, R., and Ibrahim, W. (1995). "Estimation of Infrastructure Transition Probabilities from Condition Rating Data." *Journal of Infrastructure Systems*, 120–125.

42. McGennis, R. B., Kennedy, T. W., and Machemehl, R. B. (1984). "Stripping and Moisture Damage in Asphalt Mixtures." Center for Transportation Research, Bureau of Engineering Research, University of Texas at Austin.

43. Majidzadeh, K., and Brovold, F. N. (1968). "State of the Art: Effect of Water on Bitumen-Aggregate Mixtures." Special Report 98, Highway Research Board.

44. Mathews, D. J. (1958). "Adhesion in Bituminous Road Materials: A Survey of Present Knowledge." *Journal of the Institute of Petroleum*, 44(420), 423-432.

45. Mack, C. (1964). *Bituminous Materials*. Vol. 1, Interscience Publishers, New York, N.Y.

46. Miner, M. A. (1945). "Cumulative Damage in Fatigue." *Transactions*, American Society of Mechanical Engineers, Vol. 67, A159-A164.

47. Monismith, C. L., Epps, J. A., and Finn, F. N. (1985). "Improved Asphalt Mix Design." *Proceedings of the Association of Asphalt Paving Technologists*, Vol. 54.

48. Montgomery, D. C. (1991). "Design and Analysis of Experiments." Third Edition, John Wiley & Sons, New York, NY.

49. Nguyen, T., Byrd, E., Bentz, D., and Seiler, J. (1996). "Development of a Method for Measuring Water-Stripping Resistance of Asphalt/Siliceous Aggregate Mixtures." IDEA Program, Transportation Research Board, National Research Council, Washington, D.C.

50. Ntekim, A. (2001). "Effects of Moisture on Asphalt-Rubber Mixtures Using SUPERPAVE." Dissertation, Polytechnic University, New York.

51. Parker, F., Jr. (1987). “Stripping of Asphalt Concrete-Physical Testing.” Final Report no. 930-111, Alabama Highway Department, Alabama.

52. Parr, W. K. (1958). “Field Observations of the Behavior of Bituminous Pavements as Influenced by Moisture.” *Symposium on Effect of Water on Bituminous Paving Mixtures*, ASTM Special Technical Publication No. 240, 3–16.

53. Pan, C., and White, T. D. (1999). “Conditions for Stripping Using Accelerated Testing.” Final Report, FHWA/IN/JTRP-97/13, Joint Transportation Research Program, Purdue University.

54. Pavement Research Center. (1999). “Mix Design and Analysis and Structural Section Design for Full Depth Pavement for Interstate Route 710.” Technical Memorandum no. UCPRC-TM-1999-02 prepared for the Long Life Pavement Task Force. Pavement Research Center, CAL/APT Program, Institute of Transportation Studies, University of California, Berkeley, California.

55. Pavement Systems LLC. (2004). Climate Database for Integrated Model (CDIM), Version 1.0. Bethesda, MD. Software program prepared for the University of California Pavement Research Center, funded by the California Department of Transportation.

56. Peek, M. S., Russek-Cohen, E., Wait, D. A., and Forseth, I. N. (2002). “Physiological Response Curve Analysis Using Nonlinear Mixed Models.” *Oecologia*, 132, 175–180.

57. Petersen, J.C., Plancher, H., Ensley, E. K., Venable, R. L., and Miyake. (1982). “Chemistry of Asphalt Aggregate Interaction: Relationship with Pavement Moisture-Damage Test.” *Transportation Research Record 843*, Transportation Research Board, Washington, D.C., 95–104.

58. Pindyck, R. S., Rubinfeld, D. L., Hall, B. H., and Schmukler, S. L. (1997). “TSP Handbook to Accompany Econometric Models and Economic Forecasts by Pindyck and Rubenfeld.” Fourth edition, McGraw-Hill/Irwin.

59. Plancher, H., Dorrence, S. M., and Petersen, J. C. (1977). “Identification of Chemical Types in Asphalt Strongly Adsorbed at The Asphalt—Aggregate Interface and Their Relative Displacement by Water.” *Proceedings of the Association of Asphalt Paving Technologists*, Vol. 46, 151-175.

60. Ramamurti, K., and Jayaprakash, G. P. (1987). “Bacteria and Asphalt Stripping.” Report no. FHWA-KS-87/1, Kansas Department of Transportation, Kansas.

61. Rand, D. A. (2002). “HMA Moisture Sensitivity: Past, Present & Future, TxDOT Experiences.” *Moisture Damage Symposium*, Western Research Institute, Laramie, Wyoming.

62. Robertson, R. E. (1991). “Chemical Properties of Asphalts and Their Relationship to Pavement Performance.” SHRP-A/UWP-91-510, Strategic Highway Research Program, National Research Council, Washington, D.C.

63. Santucci, L. (2005). “Performance Graded (PG) Asphalts in California.” Technical Transfer Program, No. 6. Institute of Transportation Studies, University of California, Berkeley, California.

64. Santucci, L. (2002). “Moisture Sensitivity of Asphalt Pavements.” Technical Transfer Program, Institute of Transportation Studies, University of California, Berkeley, California.

65. Schmidt, R. J., and Graf, P. E. (1972). “The Effect of Water on the Resilient Modulus of Asphalt-treated Mixes.” *Proceedings of the Association of Asphalt Paving Technologists*, Vol. 41, 118–162.

66. Scott, J. A. N. (1978). “Adhesion and Disbonding Mechanisms of Asphalt Used in Highway Construction and Maintenance.” *Proceedings of the Association of Asphalt Paving Technologists*, Vol. 47, 19–48.

67. Sha, Q. L. (1999). *Asphalt Pavement on Semi-Rigid Roadbase for High-Class Highways.* People’s Communication Publication House, China.

68. Sha, Q. L. (2001). Observation and Prevention of Premature Failures of Asphalt Pavements on Freeways. People’s Communication Publication House, China.

69. Shackley, S. (2002). “What Is XRF (X-Ray Fluorescence Spectrometry)?” Berkeley Archaeological XRF Laboratory, University of California, Berkeley.

70. Shatnawi, S. R. (1995). “Premature AC Pavement Distress - District 2 Investigation (Final Report).” Report Number FHWA/CA/TL-92-07, Office of Materials Engineering and Testing Services, California Department of Transportation, Sacramento, California.

71. Shomglin, K. (2003). Personal communications on mineral compositions of aggregates.

72. American Society for Testing and Materials. (1996). “Standard Practice for Effect of Water on Bituminous-Coated Aggregate Using Boiling Water, ASTM D 3635.” American Society for Testing and Materials, Philadelphia.

73. State of California, Business, Transportation and Housing Agency, Department of Transportation. (1999). Standard Specifications, Section 39, California Department of Transportation, Sacramento, California.

74. Stuart, K. D. (1990). “Moisture Damage in Asphalt Mixtures—A State-of-the-Art Report.” Report no. FHWA-RD-90-019, U.S. Department of Transportation, Federal Highway Administration.

75. Tandon, V., Vemuri, N., Nazarian, S., and Tahmoressi, M. (1997). “A Comprehensive Evaluation of Environmental Conditioning System.” *Proceedings of the Association of Asphalt Paving Technologists*, Vol. 66, 187–210.

76. Tarrer, A. R. (1986). “Stripping of Asphalt Concrete: Chemical Testing.” Alabama Highway Research, HPR 105B, Alabama.

77. Tarrer, A. R., and Wagh, V. (1991). “The Effect of the Physical and Chemical Characteristics of the Aggregate on Bonding.” *SHRP-A/UIR-91-507, Strategic Highway Research Program*, National Research Council, Washington, D.C.

78. Tayebali, A. A., Deacon, J. A., Coplantz, J. S., Harvey, J. T., and Monismith, C. L. (1994). “Fatigue Response of Asphalt-Aggregate Mixes.” SHRP-A-404, Asphalt Research Program, Institute of Transportation Studies, University of California, Berkeley.

79. Terrel, R. L., and Al-Swailmi, S. H. (1994). “Water Sensitivity of Asphalt-Aggregate Mixes: Test Selection.” *SHRP A-403, Strategic Highway Research Program*, National Research Council, Washington, D.C.

80. Tsai, B., John, T. H., and Monismith, C. L. (2005). “Characterization of Mix Fatigue Damage Process Using Three-Stage Weibull Equation and Tree-Based Model.” *Compendium Papers of CD-ROM at 84th Annual Meeting*, Transportation Research Board, Washington D. C.

81. Tunnicliff, D. G., and Root, R. E. (1995). “Use of Antistripping Additives in Asphalt Concrete Mixtures: Field Evaluation.” NCHRP Report 373, Transportation Research Board, National Research Council.

82. Tunnicliff, D. G., and Root, R. E. (1982). “Antistripping Additives in Asphalt Concrete-State-Of-The-Art 1981.” *Proceedings Association of Asphalt Paving Technologists Technical Sessions*, Kansas City, Missouri.

83. Williams, T. M., and Miknis, F. P. (1998). “Use of Environmental SEM to Study Asphalt – Water Interactions.” *Journal of Materials in Civil Engineering*, Vol. 10, No. 2, 121–124.

84. Yoon, H. H. (1987). “Interface Phenomenon and Surfactants in Asphalt Paving Materials.’’ Dissertation, Auburn University, Auburn, Alabama.

APPENDIX A: DETERMINATION OF METHYLENE BLUE ADSORPTION OF MINERAL AGGREGATE FILLERS AND FINES (OHIO DOT 1995)

1. Scope

This supplement covers the procedure for measuring the amount of potentially harmful fine material (including clay and organic material) present in an aggregate.

2. Equipment

This test shall be performed in a Level 2 laboratory, containing the following additional equipment:

amber colored burette, mounted on a titration stand, with sufficient capacity to completely perform the test

3 suitable glass beakers or flasks

magnetic mixer with stir bar

balance, sensitive to 0.01 gram, of sufficient capacity to perform the test

250 mm glass rod with an 8 mm diameter

laboratory timer or stop watch

75 μm (No. 200) sieve and pan

1000 ml volumetric flask

Whatman No. 2 filter paper

3. Reagents

a. Methylene Blue, reagent grade, dated and stored for no more than 4 months in a brown bottle wrapped with foil in a dark cabinet, at lab temperature

b. distilled or deionized water at lab temperature

4. Procedure

This test shall be performed on a sample(s) of material passing the 75 μm (No. 200) sieve, taken from the washed gradation of a 2000 g sample of the individual or combined materials (as required). The washed sample is dried to a constant weight and mixed thoroughly. Three separate samples of 10 g (±0.05 g) each are taken. Each of these samples is combined with 30 g of distilled water in a beaker by stirring with the magnetic stirrer until thoroughly wet and dispersed.

One gram of Methylene Blue is dissolved in enough distilled water to make up a 200 ml solution, with each 1 ml of solution containing 5 mg of Methylene Blue. This Methylene Blue solution is titrated stepwise in 0.5 ml aliquots from the burette into the beakers containing the fine aggregate solution, while continually stirring the fine aggregate solution, keeping the fine aggregate in suspension. After each addition of the Methylene Blue solution, stirring is continued for 1 minute. After this time, a small drop of the aggregate suspension is removed and placed on the filter paper with the glass rod. Successive additions of the Methylene Blue solution are repeated until the end point is reached.

Initially, a well defined circle of Methylene Blue-stained dust is formed and is surrounded with an outer ring or corona of clear water. The end point is reached when a permanent light blue coloration or "halo" is observed in this ring of clear water. When the initial end point is reached, stirring is continued for five minutes and the test repeated to ascertain the permanent endpoint. Small additions of Methylene Blue solution are continued until the 5 minute permanent end point is reached. The number of milligrams of Methylene Blue is calculated by multiplying the number of milliliters of Methylene Blue (MB) by 5 mg/ml (ml MB × 5 mg/ml = mg MB).

The Methylene Blue Value (MBV) is reported as milligrams of Methylene Blue solution per gram of fine aggregate (e.g. MBV = 55 mg/10g or 5.5 mg/g). Multiple tests should be reported separately.

5. Notes

a. Certain clays will give poor results with this test. If so, soak the 75 μm (No. 200) sieve material in the distilled water at 90°C for three hours while stirring. Allow to cool to lab temperature before proceeding with titration.

b. With experience, the person performing the test can reach the end point quicker by skipping early aliquots.

APPENDIX B: GENERAL CONDITION SURVEY FORM FOR INVESTIGATION OF MOISTURE DAMAGE IN ASPHALT PAVEMENTS

Moisture Sensitivity (MS) ID flowchart, Version 15 Jul 04
Prepared by J Harvey, C Monismith, Q Lu
Caltrans/Industry Moisture Sensitivity Committee (chairs: M. Cook, J. St. Martin)
MSID subcommittee (Subcommittee 1, chairs: N. Hosseinzadeh, R. Smith/B. Milar)
Table to be filled out starting at top. Easiest questions and data are at top, get more difficult as move down. All data will often not be available.

MS Factor	Start at Top in Left Hand Column and Work Down through the Relevant Observed Distresses, answer yes or no to questions
Location	
District, County, Route, Postmile, Direction, EA(optional)	*Fill in:* County: Route: kilo-post (or PM): Direction: Lane: District: EA:
Date	*Fill in (day/month/year):*
Performance Observation	*Visit the site in question and observe the distresses present. If unsure of distresses, best to consult pavement management condition survey guide*
1. Which distress(es) are present on the area to be evaluated for water damage?	**Measure and enter below the extent in lane-meters of each distress and which lanes and directions it is in** Raveling Stripping Delamination Cracking Rutting Bleeding
Drainage Observations	*Visit the site in question and observe the drainage during a rainfall event, or consult with local maintenance forces to obtain this information.*
2. Is water flowing over the pavement	Yes No
3. Is water ponding on the pavement	Yes No
4. What is the transverse slope?	Fill in
5. Is the location in a cut or fill, or if in a flat area is it on grade or embankment	Cut Fill On grade Embankment
6. What is the condition of the edge drain system	No system Working Blocked
7. What is the condition of the drainage ditches during rain	No ditches Draining Ponding

Core and/or Material Observation	*Take Cores (dry) and/or Trench. Check cores or material for the following and if answer is Yes note layer in core for each question (for example note whether chip seal present at surface or between layers 2 and 3):*
8. Mix type (if identifiable) and thickness of each layer (number the layers top to bottom); indicate plant source and plant type if available for each layer (if information not available leave blank)	Fill In
9. Water present in mix	Yes No Layer(s):
10. Bare aggregates in mix	Yes No Layer(s):
11. Bare aggregates in broken face of core	Yes No Layer(s):
12. Lack of bonding between lifts	(if there is no delamination or cracking distress, skip this question) Yes No Layer(s):
13. Cracks at surface extend directly down through other AC layers	Yes No Layer(s):
14. Open graded material below surface	Yes No Layer(s):
15. Chip seal or slurry seal present	Yes No Layer(s):
16. SAMI or fabric present	Yes No Layer(s):

17. Material weak (can be broken by hand)	Yes No Layer(s):
Construction	*Make Field Observations at site in question*
18. Segregation present (you see only coarse aggregates in certain locations)	(if there is no delamination or cracking distress, skip this question) Yes No
19. Distress is only along longitudinal joint (take cores and check air-voids at joints)	Yes No
	Check construction data (repeat for all layers for which data available, additional pages for other layers available attached to this form)
20. Layer number for construction data	Layer:
21. Compaction specification type (nuc gauge = without QC/QA)	QC/QA Nuclear Gauge Method
22. Air-void Content or Density Relative to LTMD (Mean and Standard Deviation)	Fill-in
23. Dust content (passing 0.075 mm sieve) greater than in job mix formula	Yes No
24. Binder content lower than in job mix formula	Yes No
25. Admixtures used (lime, liquid anti-strip, etc.)	Yes No if yes, which
Mix Design	*Check mix design records (repeat for all layers for which data available, additional pages for other layers available attached to this form)*
26. Layer number for construction data	Layer:
27. Binder grade	Fill In
28. Note aggregate sources (SMARA # if in California), gradation	Fill In
	Information at Optimum Bitumen Content (Caltrans Hveem mix design assumed, if other than Hveem, appropriate questions will be provided)

29. Mix Design Optimum Bitumen Content (OBC) by mass of aggregate	Fill In
30. Final Recommended Binder Content Range by mass of aggregate	Fill In
31. Air-void Content at OBC	Fill In
32. Hveem stability at OBC	Fill In
33. Flushing observed at next binder content above OBC	Yes No
Truck Traffic Index	*Note presence of heavy trucks or note approximate Traffic Index (and number of years in TI)*
34. What is the Caltrans Traffic Index (note whether 5, 10, 20 year TI); provide ESALs per year if TI not available	Fill In
35. Year of TI calculation; or year of ESAL count if non-Caltrans section	Fill In
Climate Region	*Note Climate Region factors*
36. What is the nearest town (will be used to find nearest weather station)	Fill In
37. What is the elevation (ft or m)	Fill In
38. Approximate number of snow days per year	Fill In
39. Are studded tires typically used in this area	Yes No

Additional Sheet for Distress Evaluation:

#	**Distress Type**	**Observed?**	**Severity**	**Description**
1	No visual distress	YES NO		Set to Yes when no distress was visually observed
2	Segregation present	YES NO	Slight Medium Severe	Segregation is the separation of coarse aggregates from fines
3	Distress along longitudinal joints	YES NO	Slight Medium Severe	Set to Yes when distress is mainly along the longitudinal joints
4	Patching	YES NO	Slight Medium Severe	Set to Yes when patching exists within the sample section
5	Potholes	YES NO	Slight Medium Severe	Potholes are a result of the loss of alligatored pavement. They may form in bowl-shaped hole, but usually are irregular due to the adjacent alligatored pavement.
6	Pumping	YES NO	Slight Medium Severe	Pumping is the ejection of water and base material fines through the longitudinal joints, transverse joints, cracks, or pavement edge.
7	Raveling	YES NO	Slight Medium Severe	Raveling is caused by the action of traffic on a weak surface.
8	Light or Fine Raveling	YES NO	Slight Medium Severe	Fine Raveling is the wearing away of the pavement surface, resulting in a extremely roughened surface texture. This rough surface texture is due to the wearing away of fine aggregate and asphalt binder.
9	Coarse Raveling	YES NO	Slight Medium Severe	Coarse Raveling is the wearing away of the pavement surface, resulting in an extremely roughened surface texture. The rough surface texture is due to the dislodging of coarse aggregate and loss of asphalt binder

#	Distress Type	Observed?	Severity	Description
10	Rutting	YES NO	Slight Medium Severe	Rutting is a longitudinal surface depression in the wheelpath caused by the consolidation or lateral movement of roadbed material under heavy loads.
11	Shoving	YES NO	Slight Medium Severe	Shoving is localized displacement or bulging of pavement material in the direction of loading pressure.
12	Stripping	YES NO	Slight Medium Severe	Stripping is the loss of asphalt film from the aggregate surface due to the action of water.
13	Bleeding	YES NO	Slight Medium Severe	Bleeding is a film of free asphalt on the surface of the pavement that creates a shiny, reflective surface.
14	Delamination	YES NO	Slight Medium Severe	Delamination is loss of bond between different layers of lifts, which is sometimes evidenced by the relative slippage of one layer to the adjacent layer.
15	Alligator A	YES NO	<1/4" >1/4" CLOSED	Alligator A is a load-related distress characterized by a single longitudinal crack in the wheelpath. Severity of Alligator A observed within the sampled..
16	Alligator B	YES NO	<1/4" >1/4" CLOSED	Alligator B is load-related distress characterized by interconnected or interlaced cracks in the wheelpath, forming a series of small polygons, generally less than 1 foot on each side. Severity of Alligator B observed within the sampled.
17	Alligator C	YES NO	<1/4" >1/4" CLOSED	Alligator C is load-related distress characterized by interconnected or interlaced cracks *outside* the wheelpath, forming a series of small polygons, generally less than 1 foot on each side.

#	Distress Type	Observed?	Severity	Description
18	Longitudinal Cracking	YES NO	<1/4" >1/4"	Longitudinal Cracks are non-load associated single cracks approximately parallel to the centerline. Overall crack width represented by either < ¼" or > ¼".
19	Longitudinal Cracking Extent	1 2 3		1 represents crack length < 100 feet, 2 represents crack length is between 100 feet and 200 feet, 3 represents crack length > 200 feet
20	Transverse Cracking	YES NO	<1/4" >1/4"	Transverse Cracks are non-load associated cracks that appear approximately at right angles to the centerline. Overall crack width represented by either < ¼" or > ¼".
21	Transverse Cracking Extent			Number of cracks per 30 meters.
22	Reflective Cracking	YES NO	<1/4" >1/4"	Set to Yes when reflective cracks exist within the sample section. Overall crack width represented by either < ¼" or > ¼".
23	Reflective Cracking Extent	1 2 3		1 represents slight, 2 represents medium, 3 represents severe.
24	Potential site for coring			Please write down the direction, postmile, and lane number where cores are needed.
25	Other Comments:			

APPENDIX C: STIFFNESS DETERIORATION CURVES OF BEAM SPECIMENS IN THE STUDY OF EFFECTS OF CONSTRUCTION-INDUCED VARIATIONS ON MOISTURE SENSITIVITY

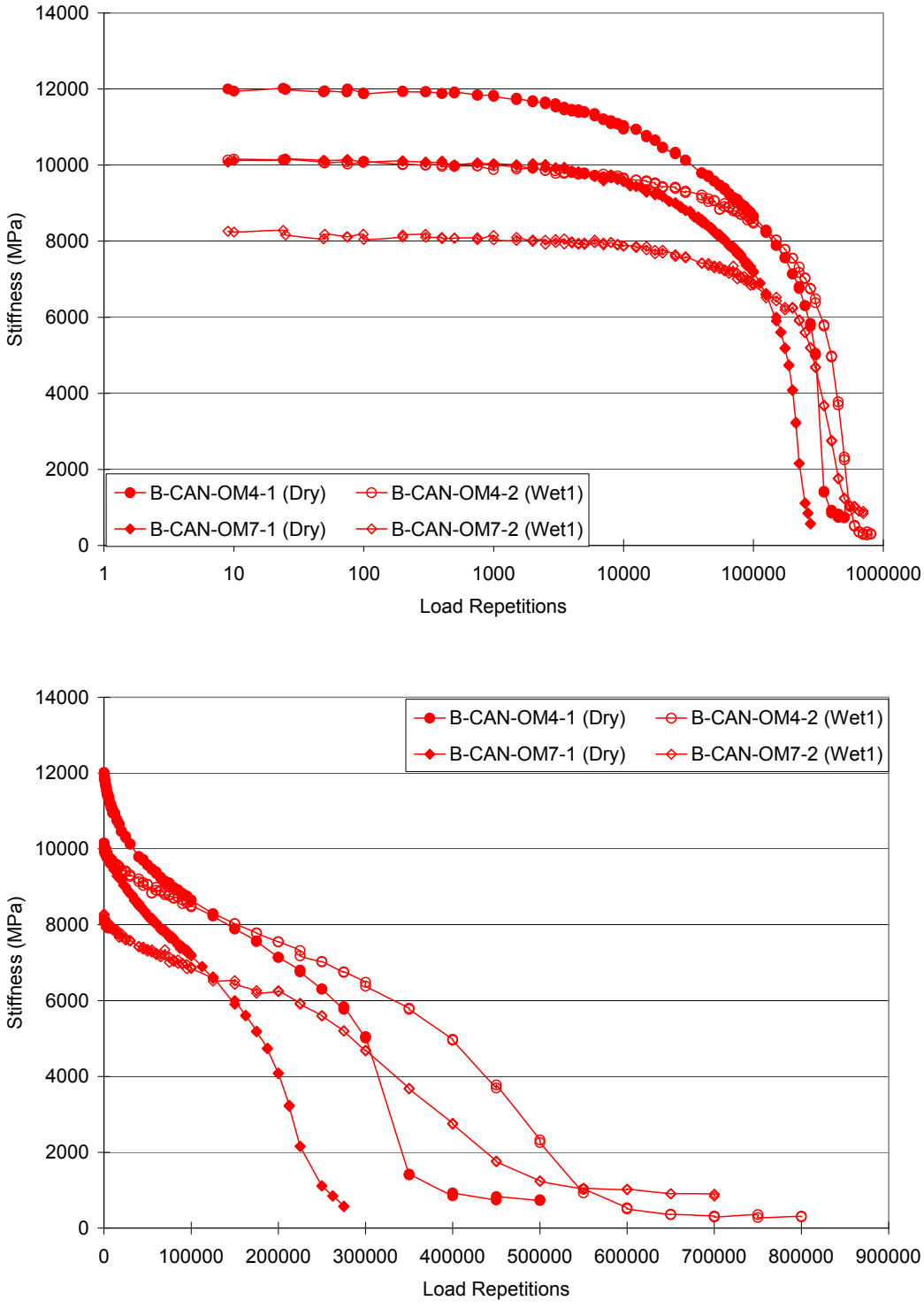

Figure C-1. Stiffness deterioration curves of BAN at 6.0 percent binder content with 4 percent air-void content.

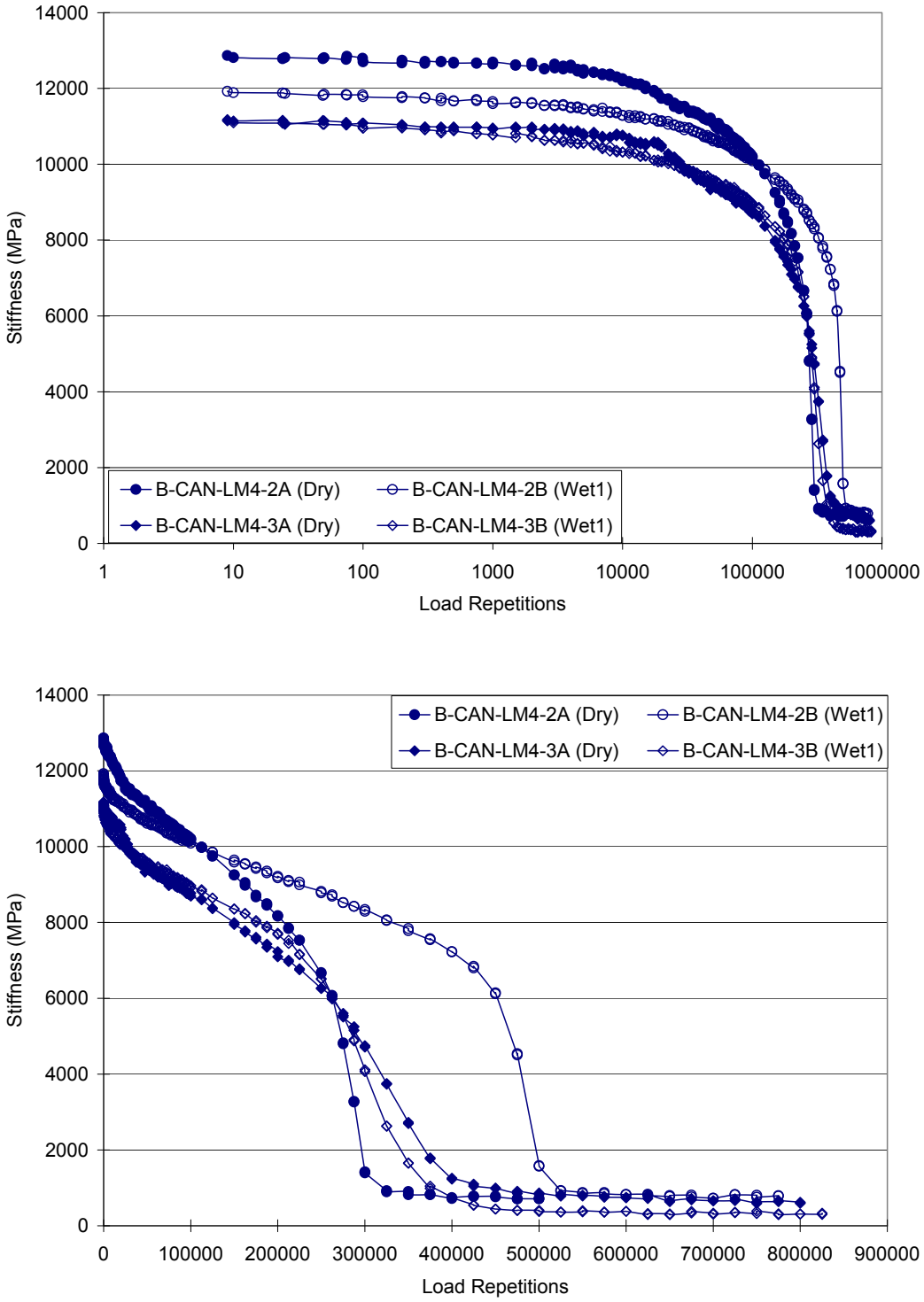

Figure C-2. Stiffness deterioration curves of BAN at 5.5 percent binder content with 4 percent air-void content.

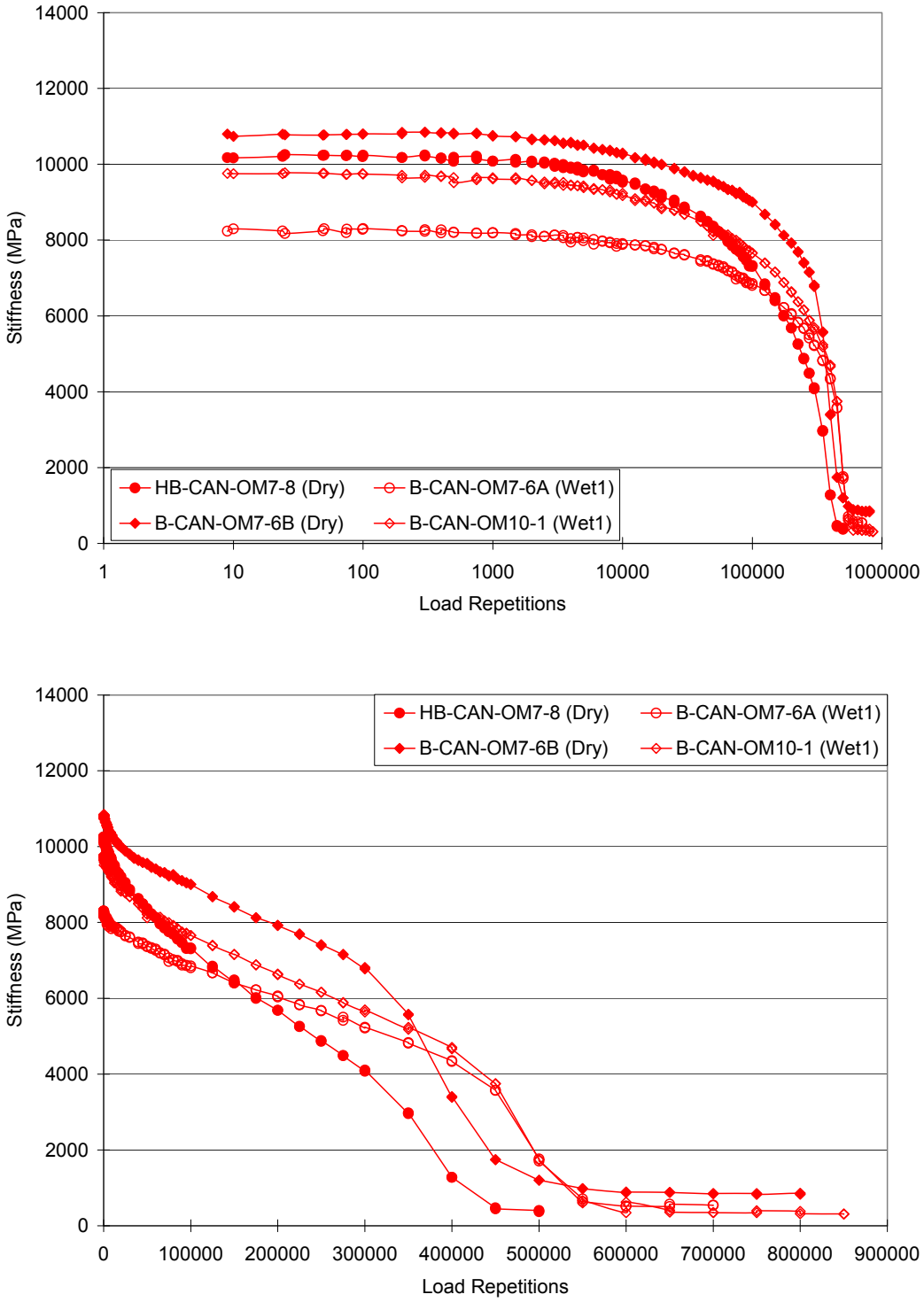

Figure C-3. Stiffness deterioration curves of BAN at 6.0 percent binder content with 7 percent air-void content.

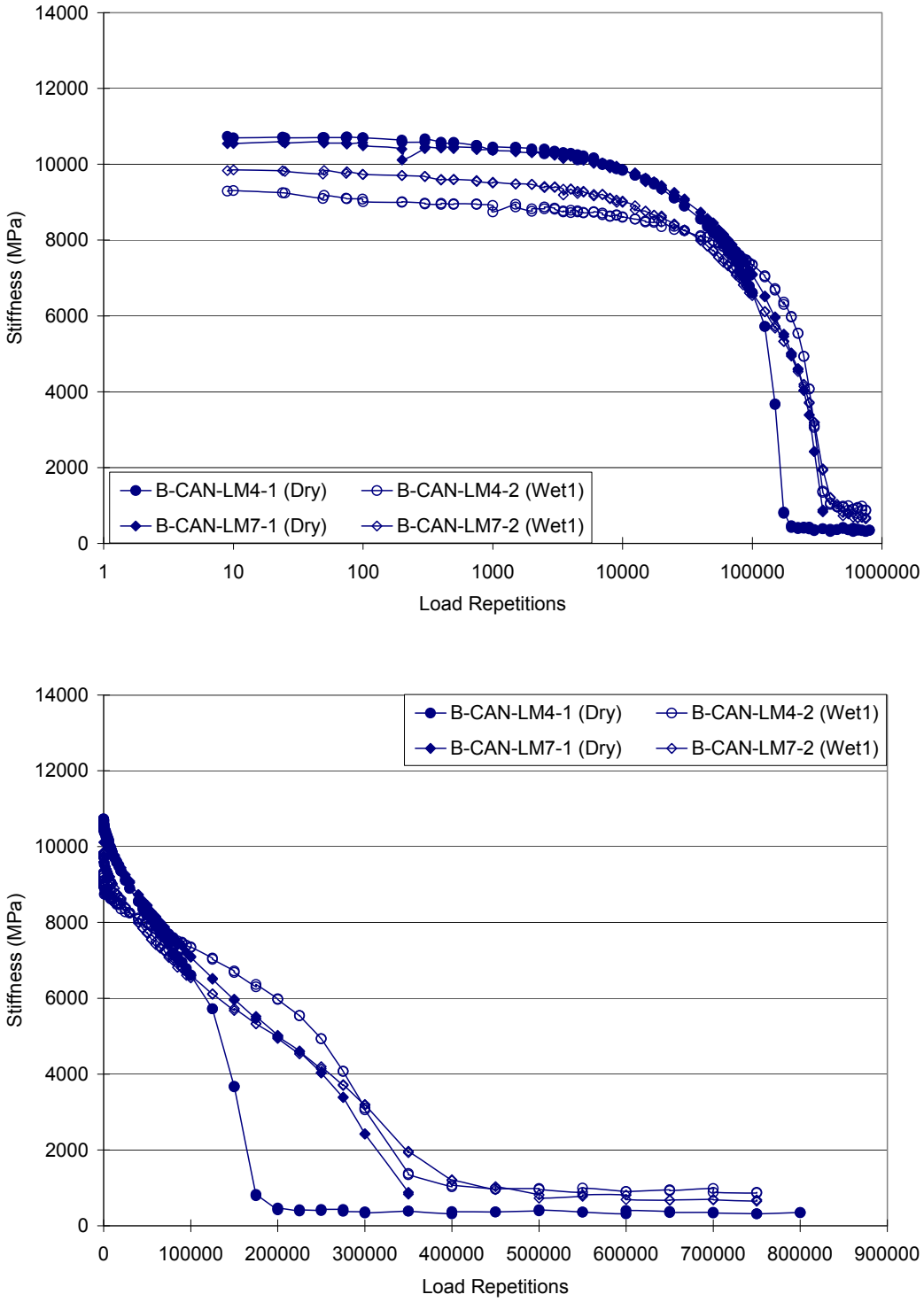

Figure C-4. Stiffness deterioration curves of BAN at 5.5 percent binder content with 7 percent air-void content.

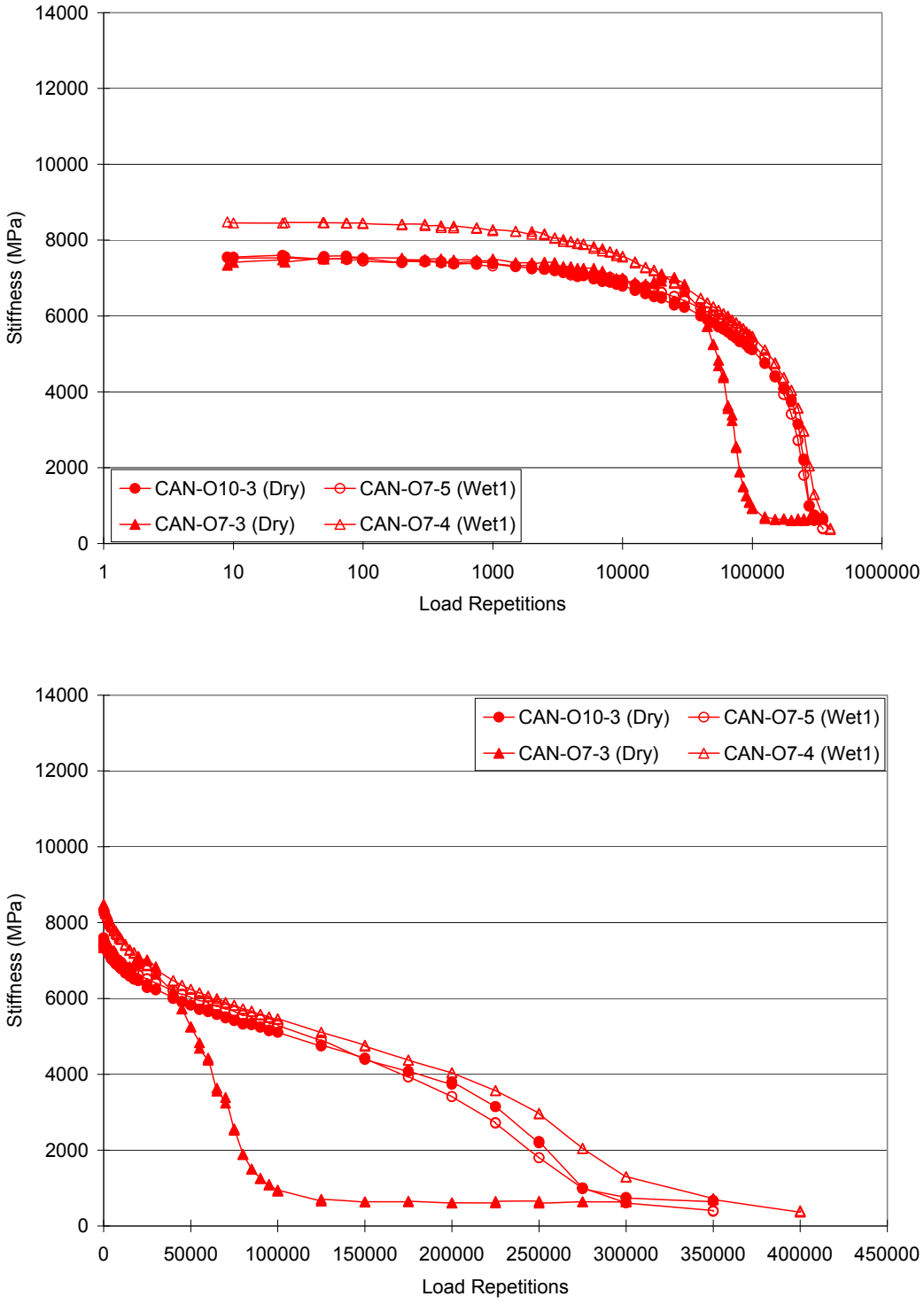

Figure C-5. Stiffness deterioration curves of BAN at 6.0 percent binder content with 10 percent air-void content.

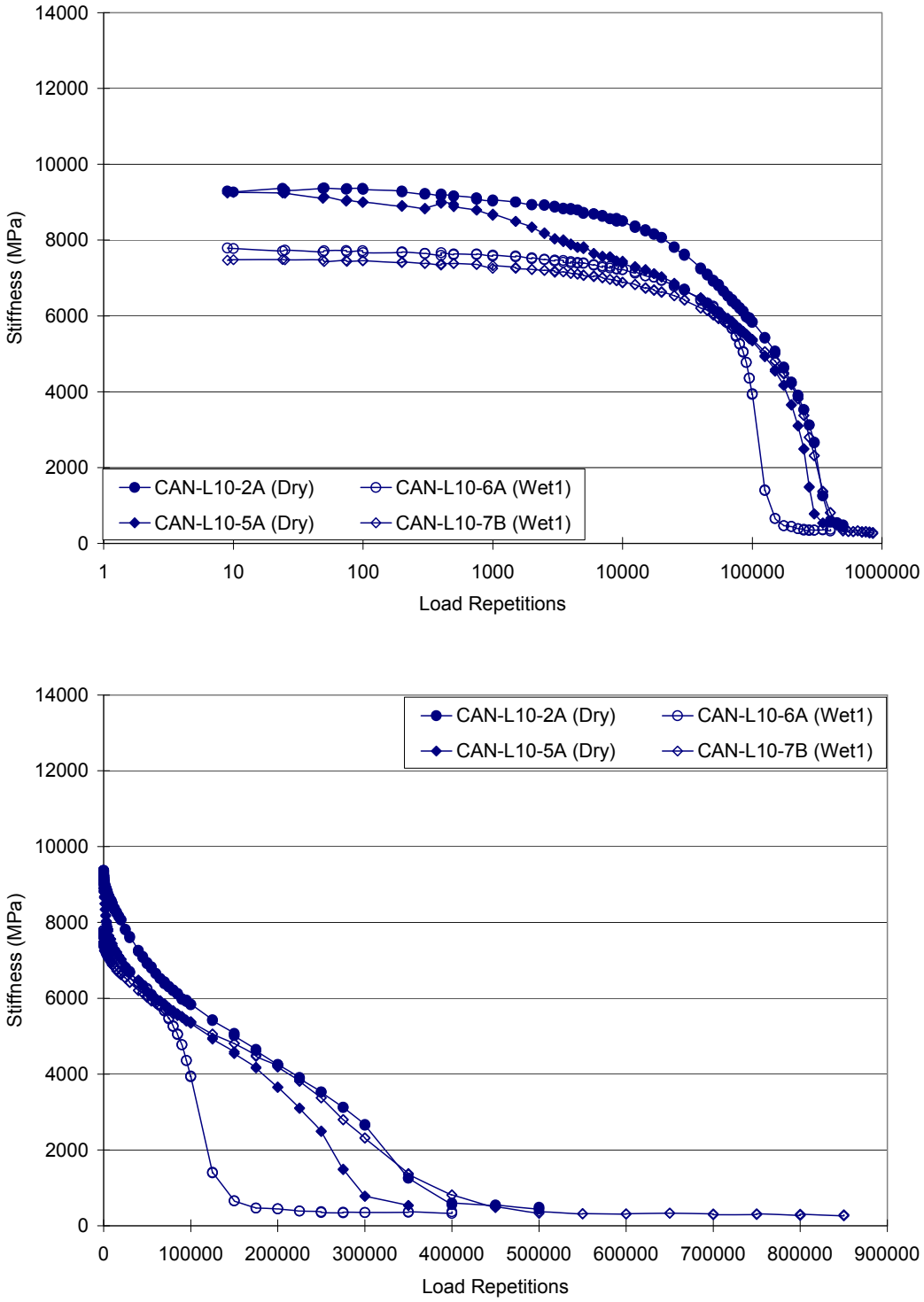

Figure C-6. Stiffness deterioration curves of BAN at 5.5 percent binder content with 10 percent air-void content.

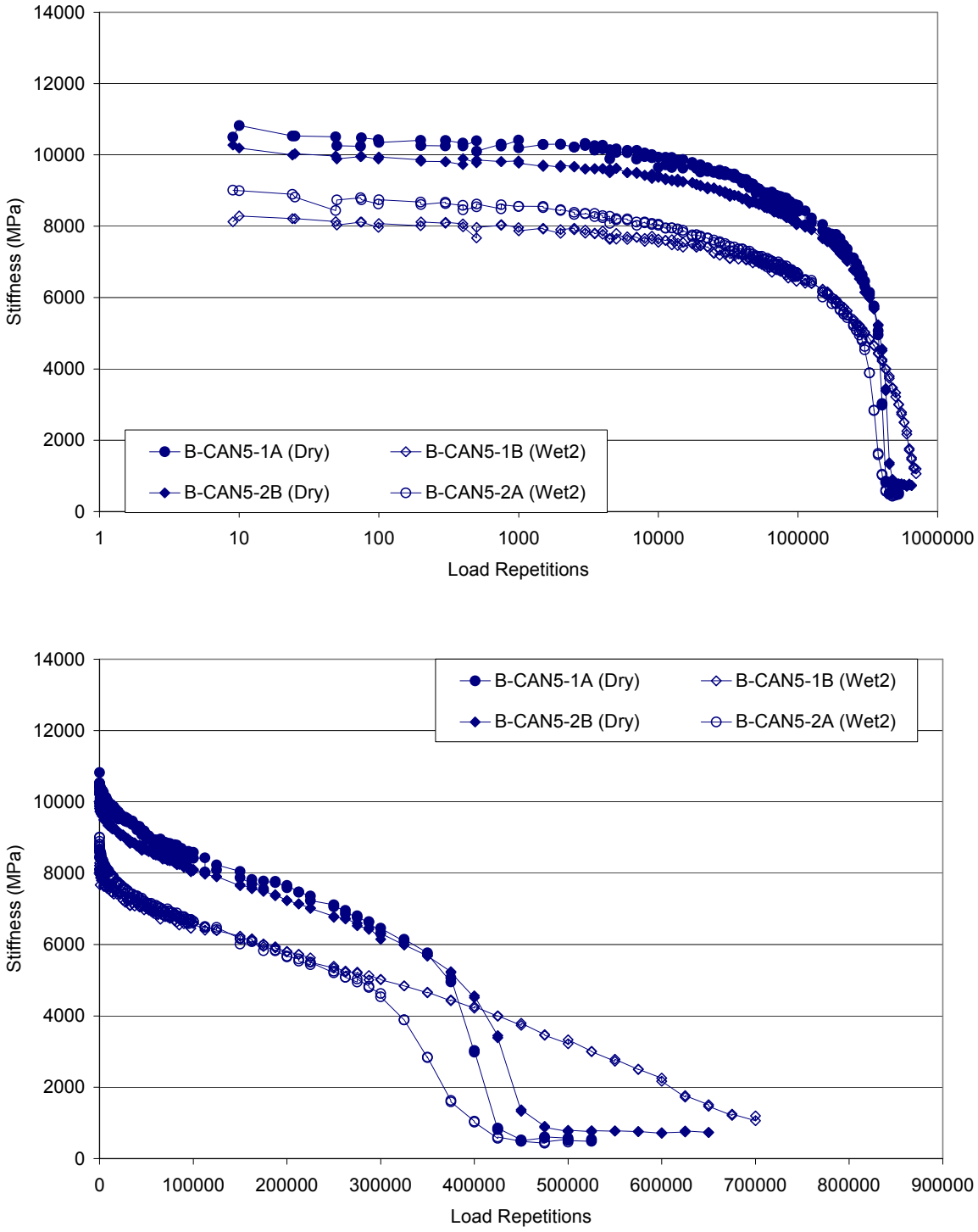

Figure C-7. Stiffness deterioration curves of BAN at 6.0 percent binder content with 5 percent air-void content.

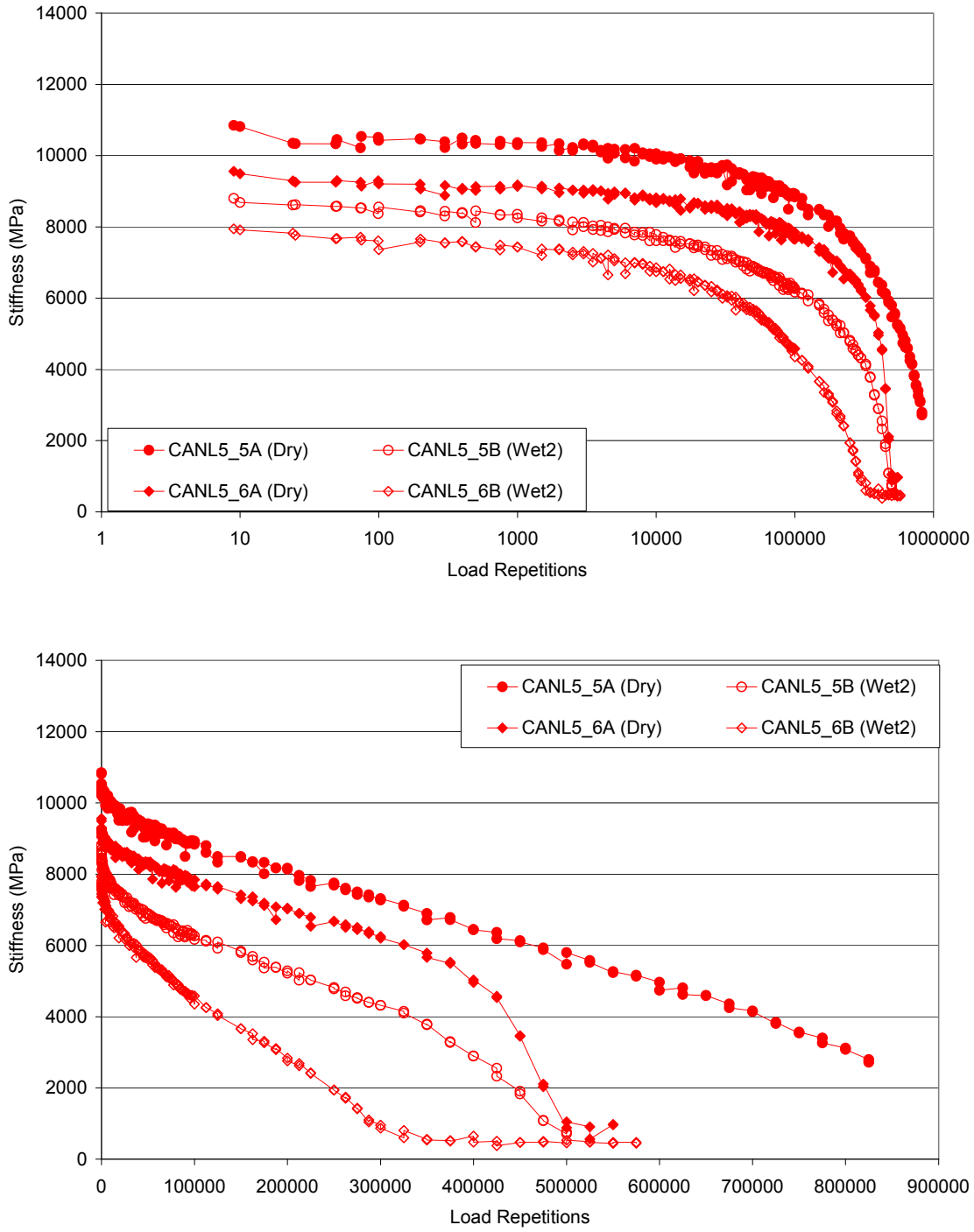

Figure C-8. Stiffness deterioration curves of BAN at 5.5 percent binder content with 5 percent air-void content.

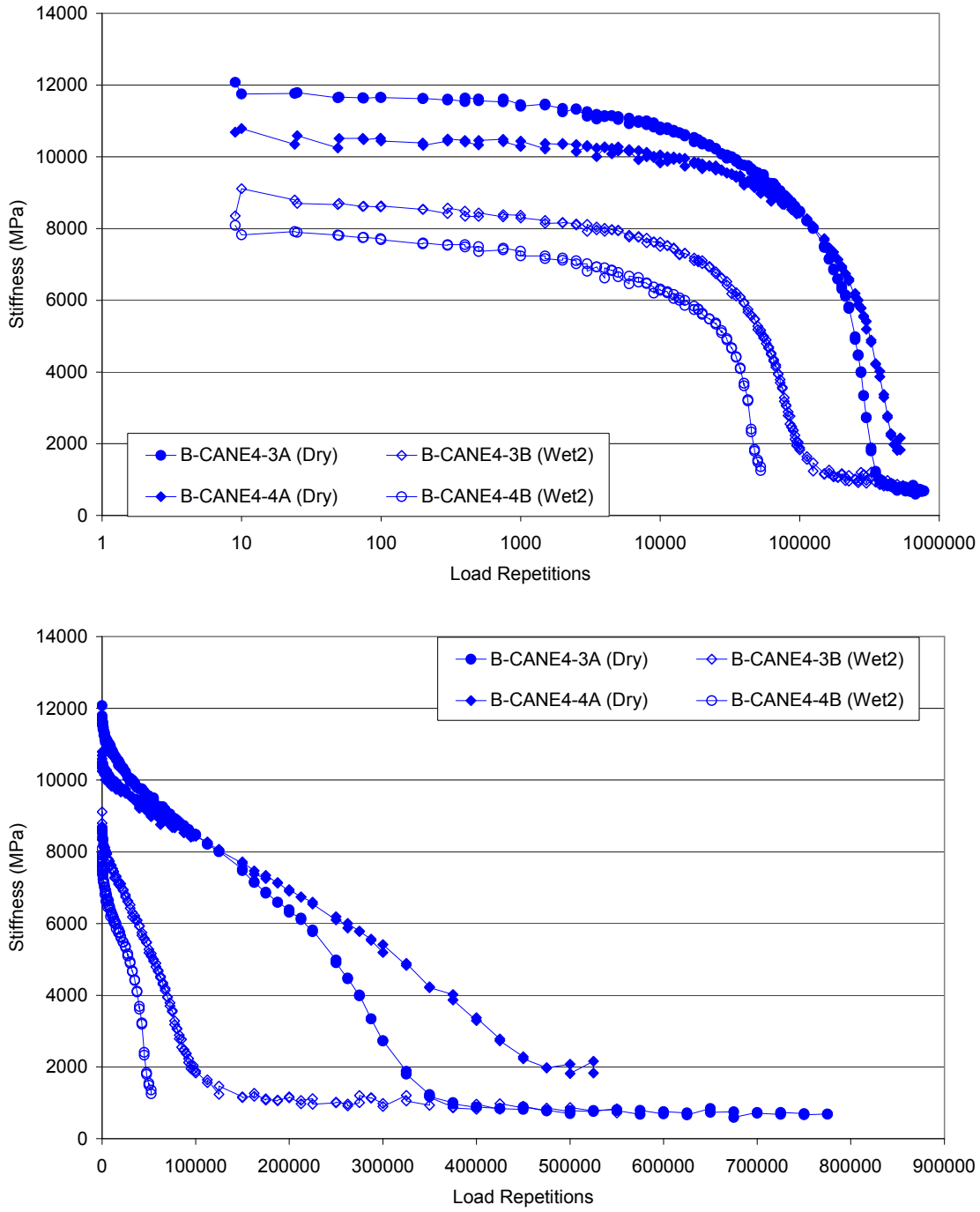

Figure C-9. Stiffness deterioration curves of BAN at 5.0 percent binder content with 5 percent air-void content.

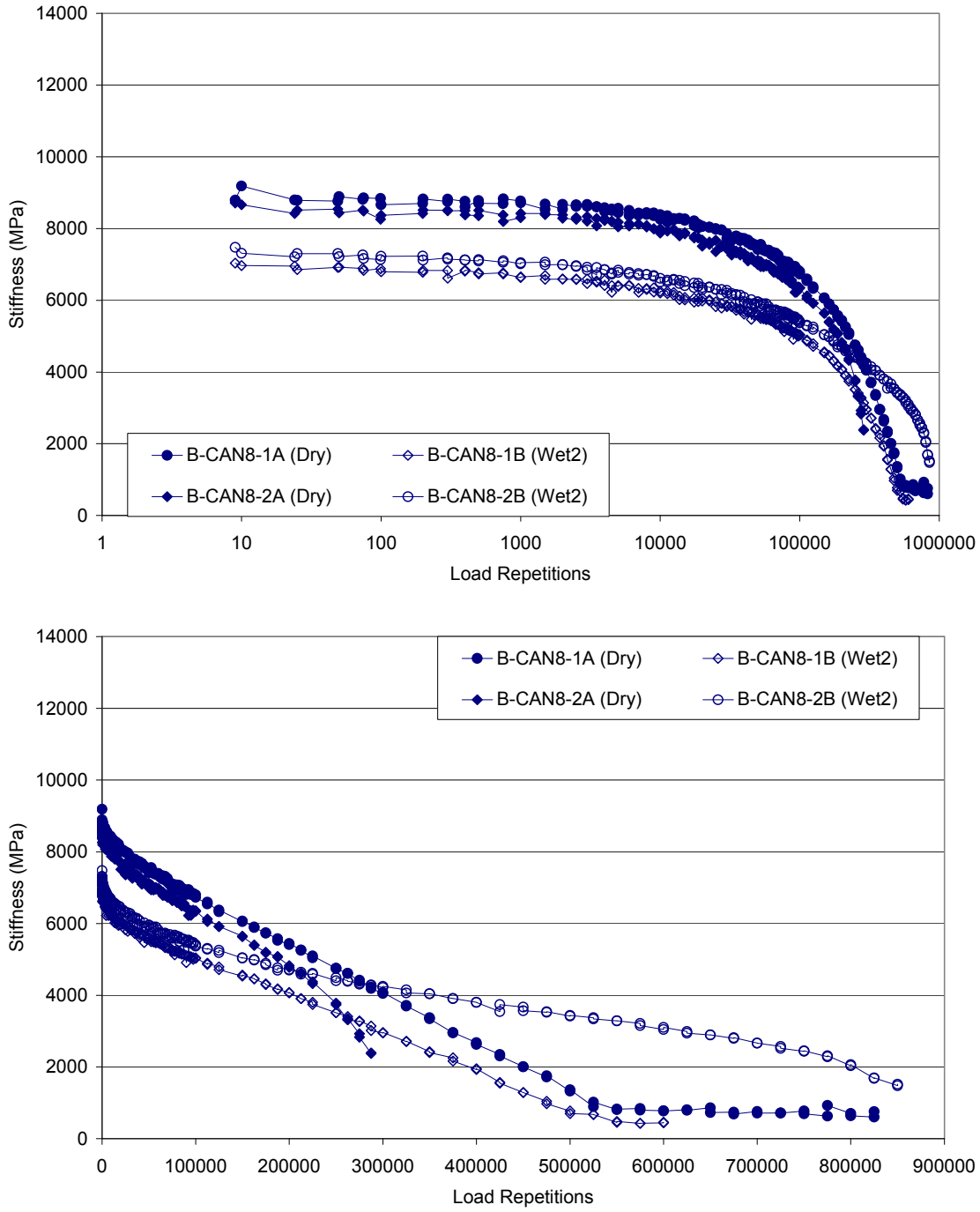

Figure C-10. Stiffness deterioration curves of BAN at 6.0 percent binder content with 8 percent air-void content.

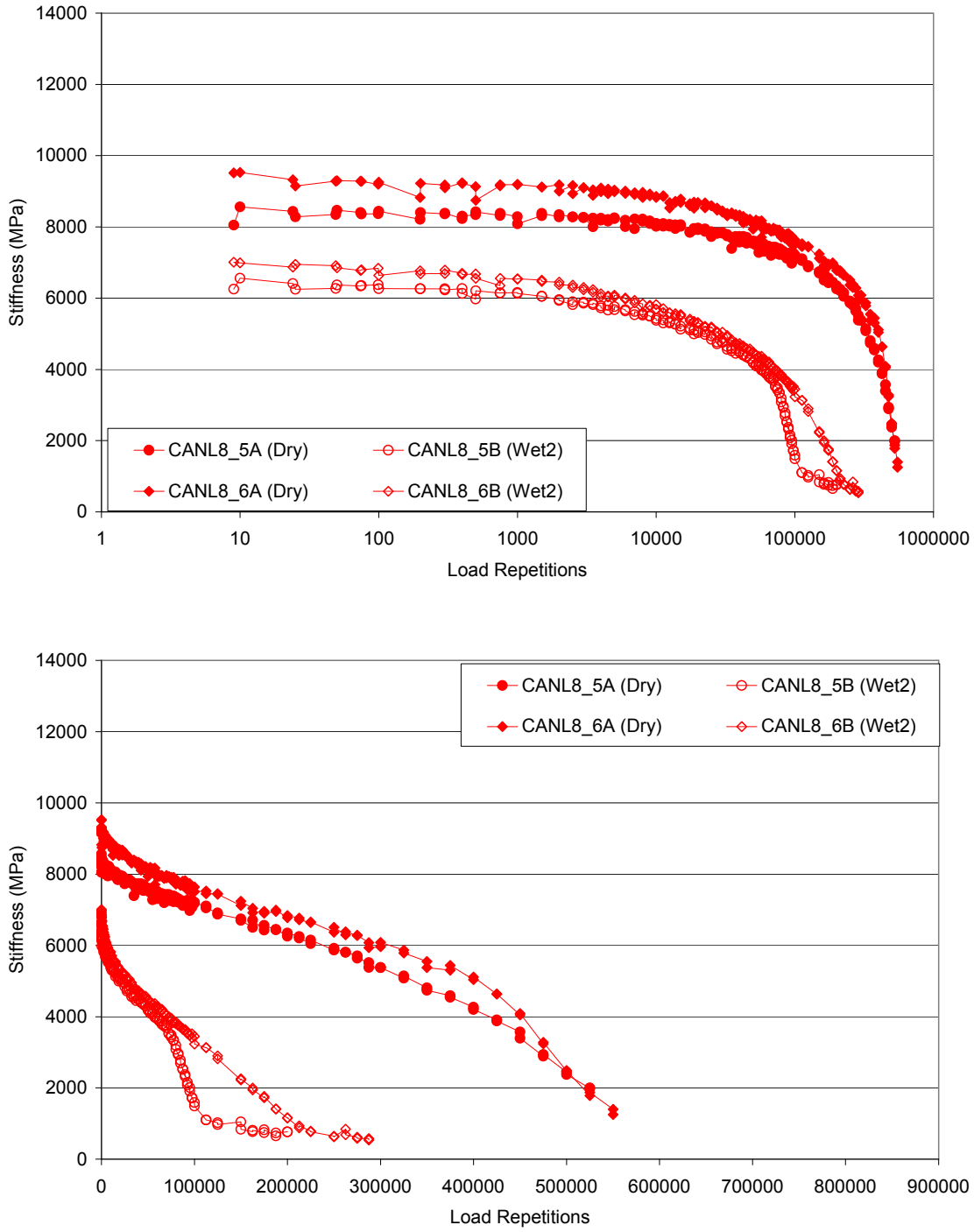

Figure C-11. Stiffness deterioration curves of BAN at 5.5 percent binder content with 8 percent air-void content.

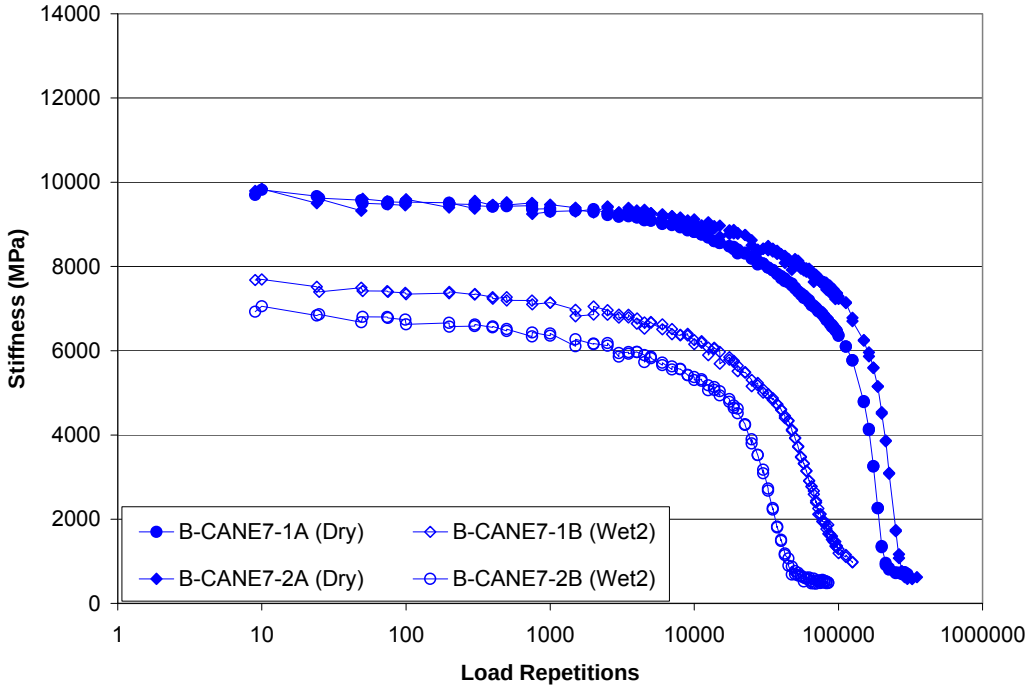

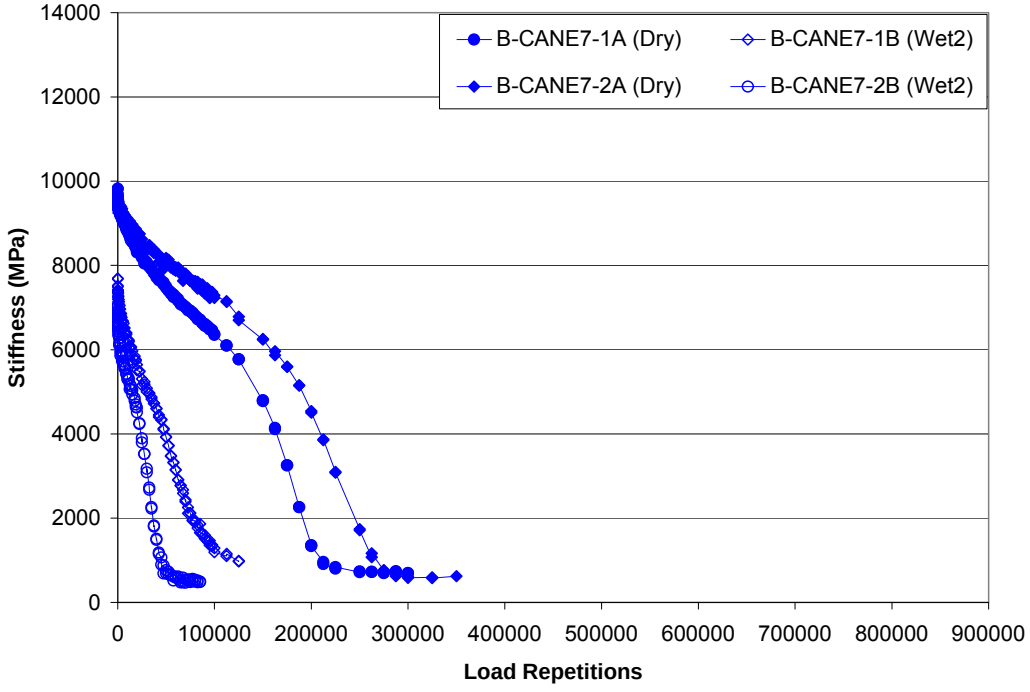

Figure C-12. Stiffness deterioration curves of BAN at 5.0 percent binder content with 8 percent air-void content.

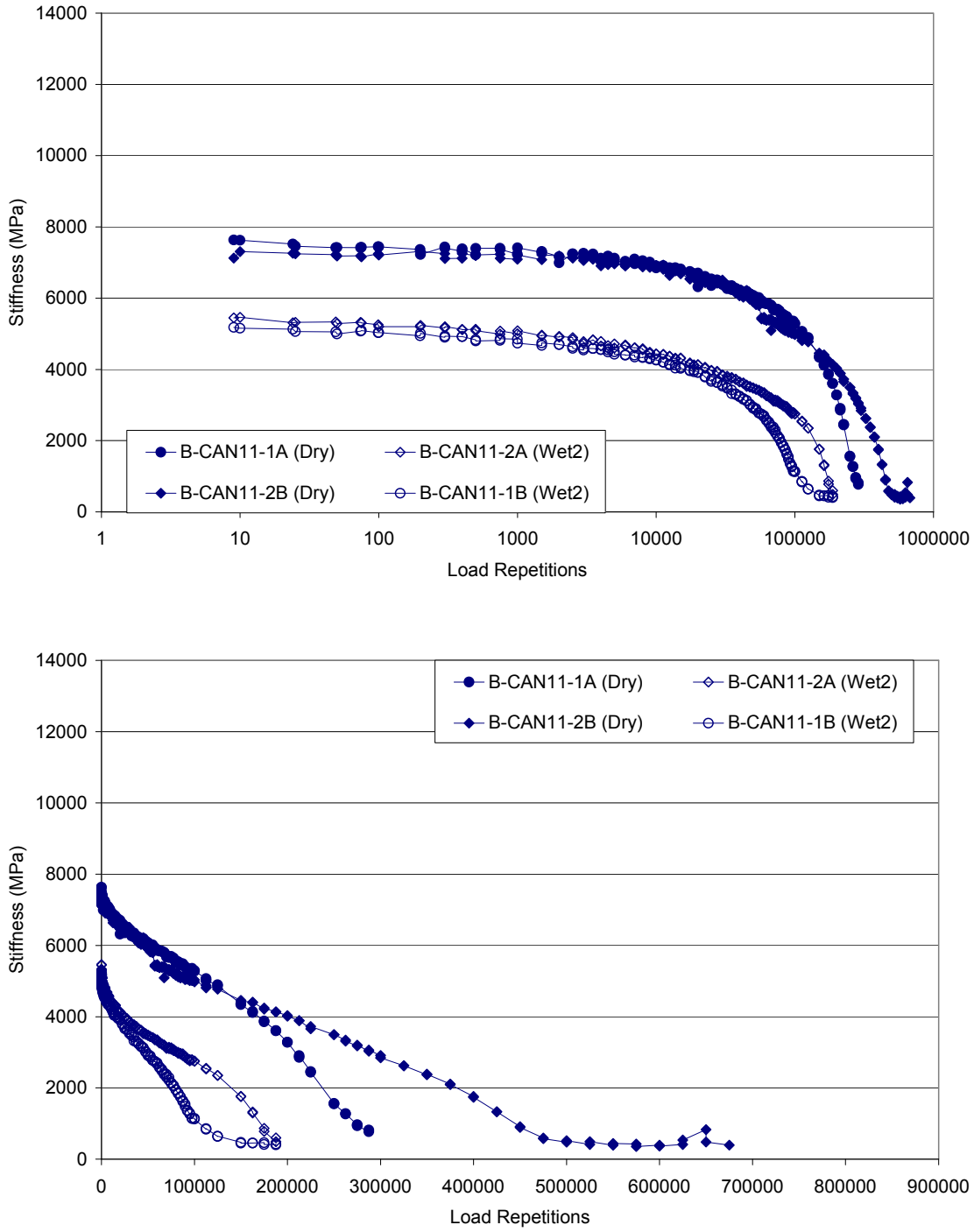

Figure C-13. Stiffness deterioration curves of BAN at 6.0 percent binder content with 11 percent air-void content.

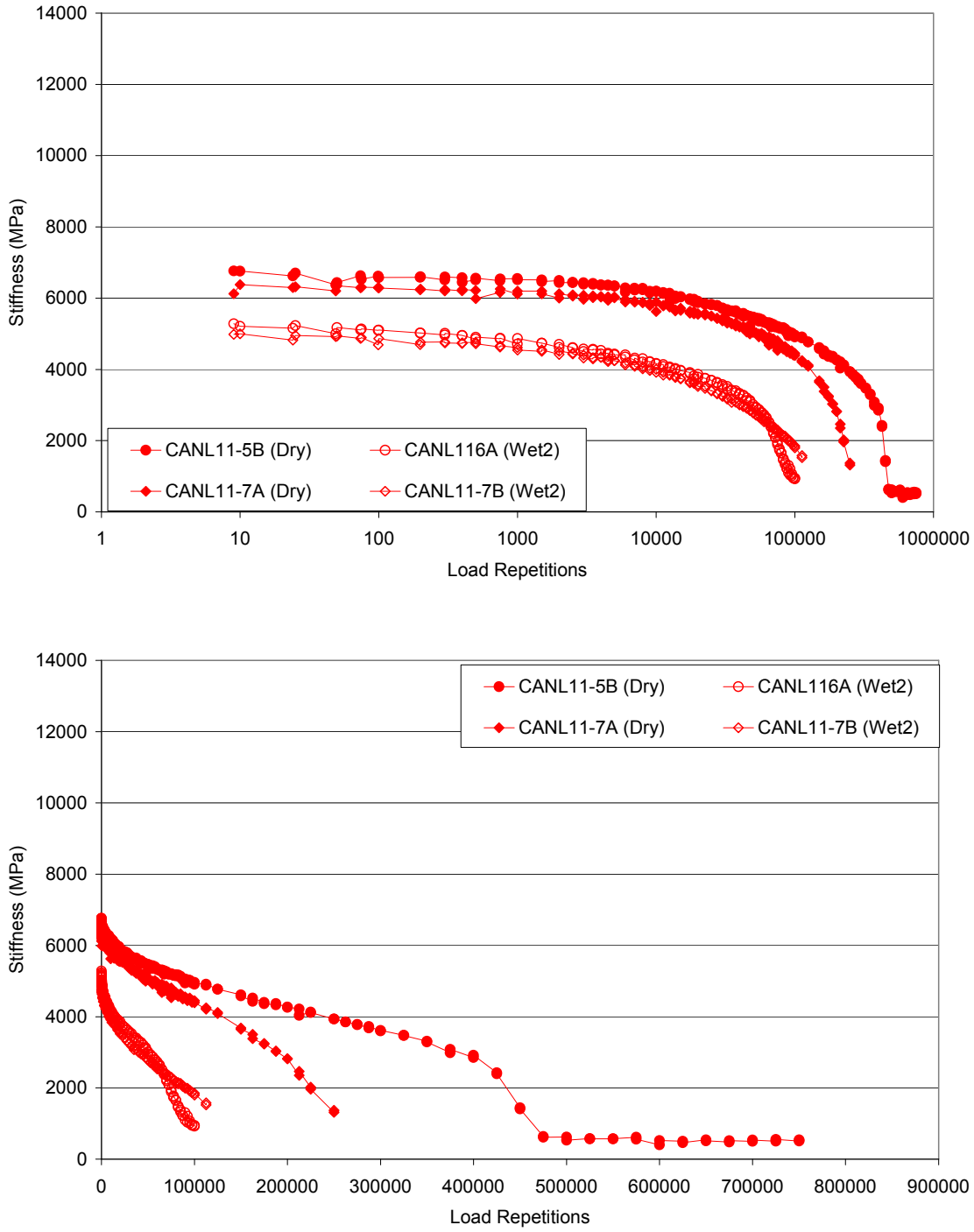

Figure C-14. Stiffness deterioration curves of BAN at 5.5 percent binder content with 11 percent air-void content.

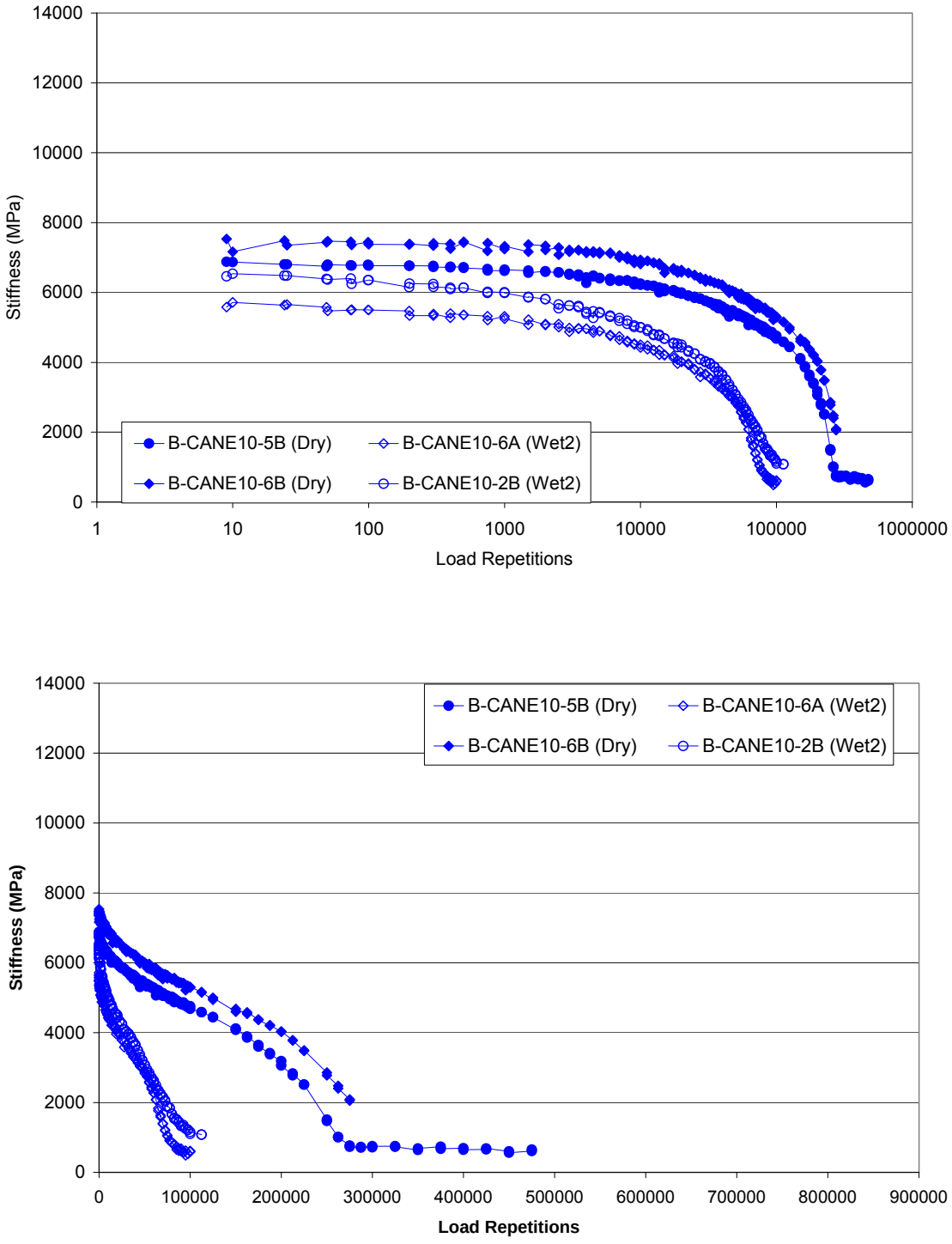

Figure C-15. Stiffness deterioration curves of BAN at 5.0 percent binder content with 11 percent air-void content.

APPENDIX D: ACCELERATED SATURATION PROCESS OF BEAM SPECIMENS

The saturation level in the specimens is affected by both the intensity and duration of the applied vacuum. To determine the appropriate vacuum level and duration for the fatigue beam specimen to reach 50 percent to 80 percent saturation levels, 15 beams with air-void contents between 6 percent and 8 percent were saturated at different vacuum levels and durations, as shown in Table D-1. Each beam was submerged in water up to 30 minutes under partial vacuum and the saturation levels were measured at 1, 3, 10, and 30 minutes.

The saturation level in the specimen was calculated by Equation (4-3) in Chapter 4. The mass of moisture in the specimen (W_t) was calculated by Equation (4-1). Concern was raised that when W_t was measured in air some water might drip off the specimen during the drying and weighing operation, affecting the accuracy of measurement. As an alternative, the specimen might be weighed underwater after vacuum saturation. In this way, W_t was calculated by Equation (4-2). In this test, W_t was measured both in air and in water in a random order on each specimen. It was found that both methods give quite similar results, as shown in Figure D-1. The saturation level obtained by weighing in water is slightly larger than that obtained by weighing in air, indicating that some internal water did drip off specimens during the drying and weighing operation, but the relative difference (1.1 percent) is small enough to be ignored. Therefore, either method can be used to determine the saturation level. Because weighing in air is quicker than weighing in water, it was used in the subsequent test.

The test results are summarized in Table D-2 and plotted in Figure D-2. It can be seen that the saturation level was affected more by the vacuum intensity than by the vacuum duration. For all specimens tested, the satuation level reached a high value after only one minute of soaking under partial vacuum. After one minute, only slight gains in saturation level were observed. Generally, the saturation level increased with the increase of vacuum intensity. The specimens tested can reach a saturation of 60 percent after the application of a 635 mm-Hg vacuum for 30 minutes.

Table D-1. Experimental Design for Determination of Vacuum Level and Duration

Vacuum Level (mm-Hg)	Vacuum Duration (minutes)			
	1	3	10	30
250	X X X[1]			
381	X X X			
500	X X X			
572	X X X			
635	X X X			

[1]Each "X" represents one beam specimen.

Table D-2. Saturation Levels at Different Vacuum Levels and Durations

Vacuum Level (mm-Hg)	Air-Void Content (%)	Saturation Duration			
		1 minute	3 minutes	10 minutes	30 minutes
250	7.0	24.3	24.8	26.7	27.9
	7.0	33.8	38.2	40.0	40.1
	7.3	36.4	38.0	39.3	40.5
381	6.7	49.2	49.3	50.6	52.1
	7.7	41.7	44.5	45.6	46.5
	7.1	43.4	46.1	47.0	48.2
500	7.2	54.0	55.2	55.4	54.3
	7.2	57.0	58.9	58.8	59.1
	7.2	54.3	54.8	54.1	56.2
572	6.7	48.4	51.9	50.6	51.6
	7.7	62.1	63.2	63.6	64.7
	7.1	48.6	50.7	51.0	51.1
635	7.2	54.7	56.5	57.1	58.1
	7.2	58.3	58.5	59.3	59.8
	7.2	54.8	54.1	55.2	55.4

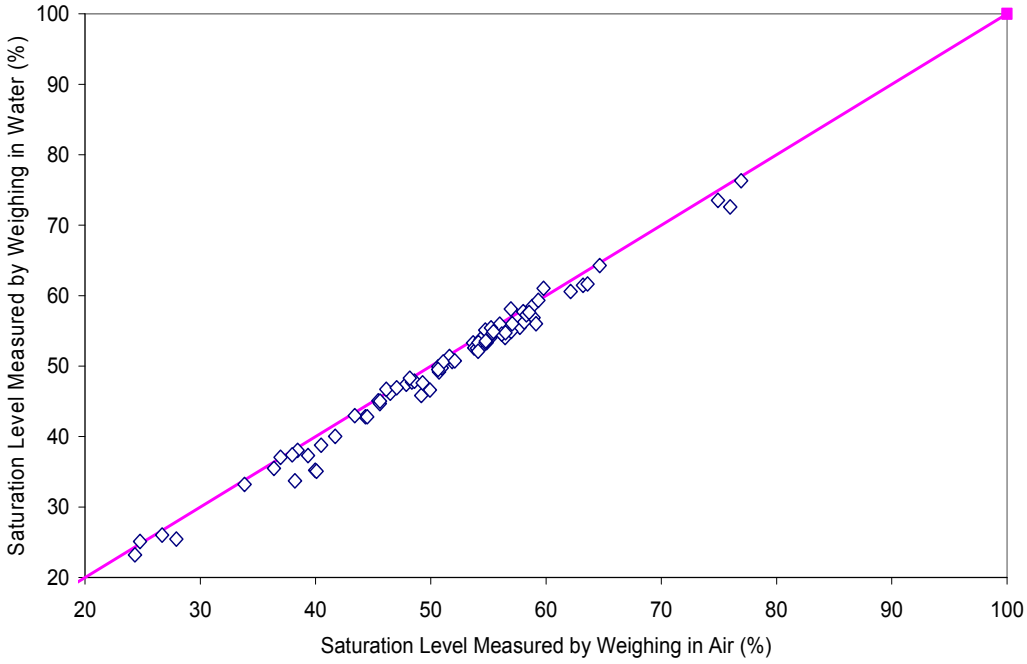

Figure D-1. Comparison of saturation levels measured by two methods.

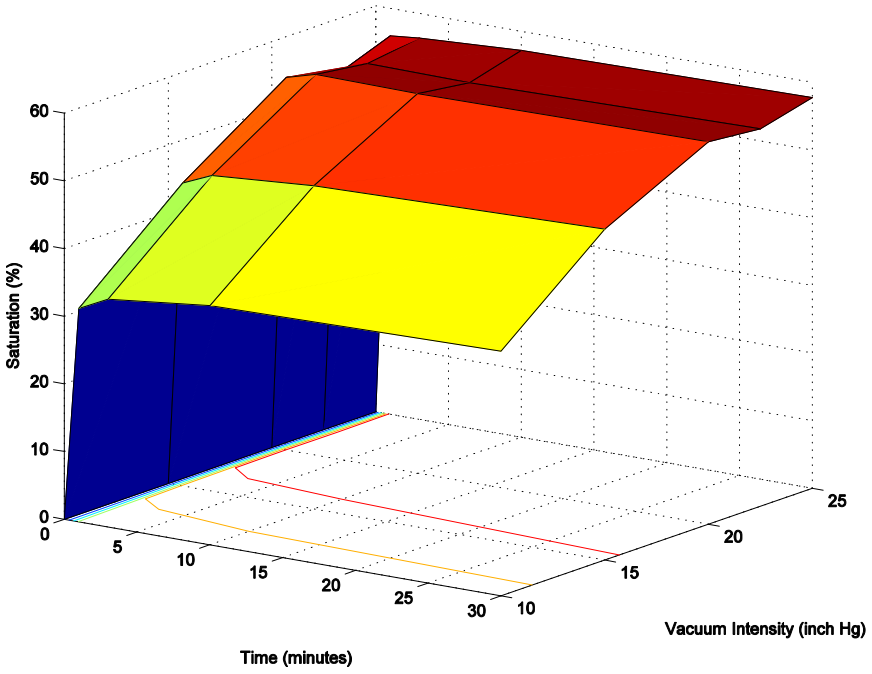

Figure D-2. Saturation levels at different vacuum intensities and durations.

APPENDIX E: VACUUM EFFECT ON MIX STRENGTH

Introduction

In a test to evaluate the moisture sensitivity of asphalt mixes, a vacuum is often used to accelerate the moisture intrusion into specimens. Depending on the air-void content and internal void structure of a specimen, the partial vacuum applied ranges between 250 mm-Hg and 660 mm-Hg. However, there was a concern in the pavement community that a high vacuum pressure such as 635 mm-Hg would disturb the structure of the specimen and reduce its strength, so that the effect of the subsequent moisture conditioning would be confounded. This concern needed to be cleared before applying the high vacuum in moisture sensitivity tests. In this study, a factorial experiment was conducted to evaluate the effect of vacuum on the mix properties.

Experimental Design

The indirect tensile strength of Hveem specimen is selected as the dependent variable for evaluation. The specimens were compacted by a kneading compactor to a size of 101 mm in diameter and 63.5 mm in height. Air-void content was measured following the procedure specified in AASHTO T166 method A. Each specimen was left in a 25°C water bath for two hours for temperature stabilization, and then tested for its indirect tensile strength at a loading rate of 50 mm/minute.

A full factorial experiment is designed to include four factors: aggregate, binder, additive and vacuum. Each factor has two levels, as shown below:

Aggregate: A and B

Binder: A (AR-4000) and P (PBA-6a)

Additive: N (nil) and M (hydrated lime)

Vacuum: 0 (no vacuum applied), and 1 (635 mm-Hg vacuum applied for 30 minutes)

Two replicates were tested at each combination of the factor levels. Therefore, a total of 32 specimens were tested. The air-void content of these specimens varies between 4.1% and 7.1%. The specimens were chosen in such a way that each pair of vacuumed and un-vacuumed specimens of the same mix have similar air-void content. The sequence of testing on all the specimens was randomized to avoid bias introduced by some block effect.

Test Result

The results are shown in Table E- 1 and plotted in Figure E-1. Figure E-1 shows that the effect of vacuum is not very significant. A full linear model includes both the main effects and all order interaction terms was first fitted, but it turned out that all interaction terms were insignificant at a 95% confidence level. Therefore, the following linear model including only the main effect terms was used:

$$y_i = \mu + \beta_1 I_A(W)_i + \beta_2 I_B(P)_i + \beta_3 I_{AD}(N)_i + \beta_4 I_V(V)_i + \beta_5 AV_i + \varepsilon_i \qquad \textbf{(E-1)}$$

where, y_i = observed indirect tensile strength of *i*th specimen,

μ = intercept term, $\beta_1,\ldots,\beta_5$ = parameters to be estimated,

$I_A(W)_i$ = indicator function for aggregate type, equal to 1 if *i*th specimen contains aggregate A, 0 otherwise,

$I_B(P)_i$ = indicator function for binder type, equal to 1 if *i*th specimen contains PBA-6a binder, 0 otherwise,

$I_{AD}(N)_i$ = indicator function for additive type, equal to 1 if *i*th specimen has no additive, 0 otherwise,

$I_V(V)_i$ = indicator function for vacuum application, equal to 1 if *i*th specimen is conditioned by vacuum, 0 otherwise,

AV_i = air-void content of *i*th specimen, ε_i = random error term, assumed to have independent normal distribution.

The least-squares estimates and corresponding t statistics and p-values are shown in Table E-2. As can be seen, aggregate type and binder type have significant effects on the indirect tensile strength (ITS) of the Hveem specimens, while additive type, vacuum application, and air void have insignificant effects. This indicates that the application of a vacuum to accelerate the water intrusion does not significantly affect specimen strength.

Conclusions

This study shows that a vacuum of 635 mm-Hg applied for 30 minutes does not reduce the strength of asphalt concrete specimens, or the effect is within the range of the variation inherent in the test results.

Table E- 1 Test Results for the Study of Vacuum Effects

Mix Type	ID	Aggregate	Binder	Additive	Vacuum	Air Voids (%)	Height (mm)	Strength (kPa)
AAN	74	A	A	N	0	5.6	62.73	2554.8
AAN	75	A	A	N	0	6.2	63.06	2497.4
AAN	72	A	A	N	1	7.0	63.16	1862.2
AAN	80	A	A	N	1	5.6	62.62	2158.8
AAM	7	A	A	M	0	6.1	63.39	2497.2
AAM	11	A	A	M	0	6.3	63.33	2482.1
AAM	8	A	A	M	1	6.1	63.37	2344.1
AAM	12	A	A	M	1	6.3	63.20	2416.7
APN	38	A	P	N	0	7.1	63.28	325.9
APN	34	A	P	N	0	7.1	63.28	290.7
APN	36	A	P	N	1	6.5	63.33	378.5
APN	37	A	P	N	1	7.1	63.21	321.9
APM	14	A	P	M	0	6.2	62.95	456.1
APM	16	A	P	M	0	6.1	62.78	417.3
APM	5	A	P	M	1	5.9	62.73	431.0
APM	15	A	P	M	1	6.3	62.88	421.1
BAN	7a	B	A	N	0	6.2	62.80	1375.8
BAN	8a	B	A	N	0	5.5	62.93	1399.6
BAN	1a	B	A	N	1	6.4	63.00	1526.3
BAN	15a	B	A	N	1	5.5	63.35	1671.8
BAM	1	B	A	M	0	4.2	62.93	1948.9
BAM	71	B	A	M	0	6.2	62.82	1721.3
BAM	2	B	A	M	1	4.1	62.75	1918.8
BAM	75	B	A	M	1	6.1	62.68	1716.5
BPN	30	B	P	N	0	6.1	62.70	280.1
BPN	23	B	P	N	0	6.1	62.92	310.1
BPN	28	B	P	N	1	6.1	63.10	247.4
BPN	24	B	P	N	1	6.2	62.38	303.8
BPM	23	B	P	M	0	6.3	62.82	337.2
BPM	30	B	P	M	0	5.9	62.82	328.3
BPM	27	B	P	M	1	6.3	62.69	337.9
BPM	31	B	P	M	1	6.3	62.85	372.5

Table E-2 Statistical Analysis Results

Coefficients	Estimated Value	Standard Error	*t* statistics	p-value
Intercept, μ	1745.753	462.935	3.771	0.0008
Aggregate, β_1	212.708	42.673	4.985	0.0000
Binder, β_2	-805.208	42.885	-18.776	0.0000
Additive, β_3	-66.215	40.476	-1.636	0.1139
Vacuum, β_4	-23.046	38.272	-0.602	0.5523
Air-void Content, β_5	-93.395	75.709	-1.234	0.2284

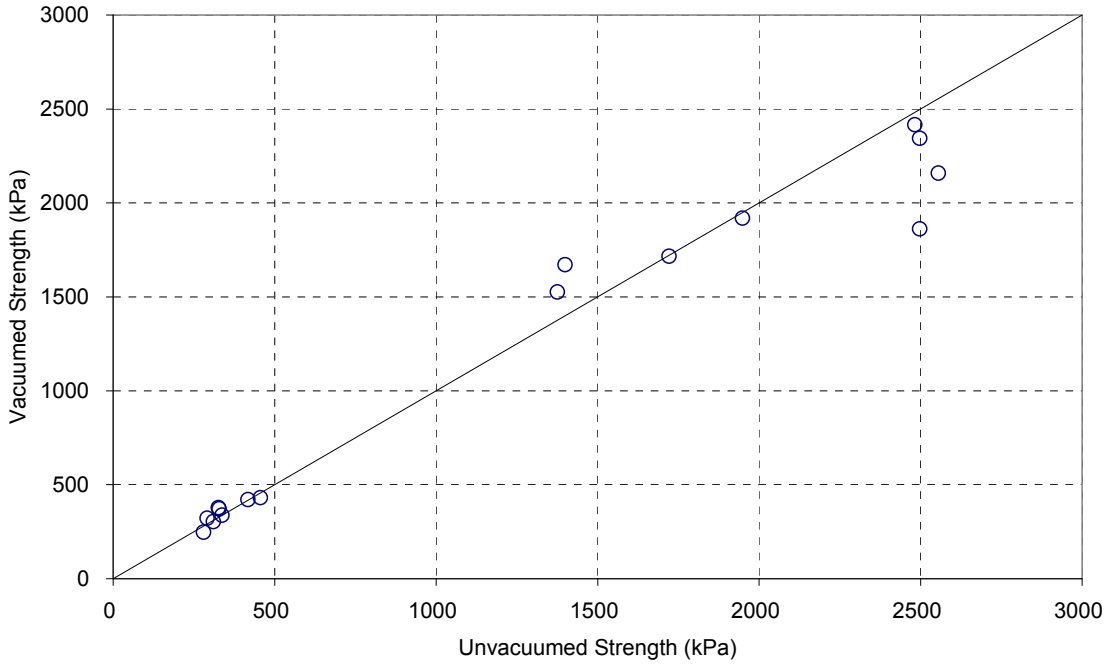

Figure E-1. Comparison of the indirect tensile strength of specimens with and without vacuum application.

APPENDIX F: STIFFNESS DETERIORATION CURVES OF FATIGUE-BASED TESTS FOR THE COMPARATIVE STUDY

Note: In the legends of all figures, "WET1" represents preconditioning at 25°C for one day while "WET2" represents preconditioning at 60°C for one day.

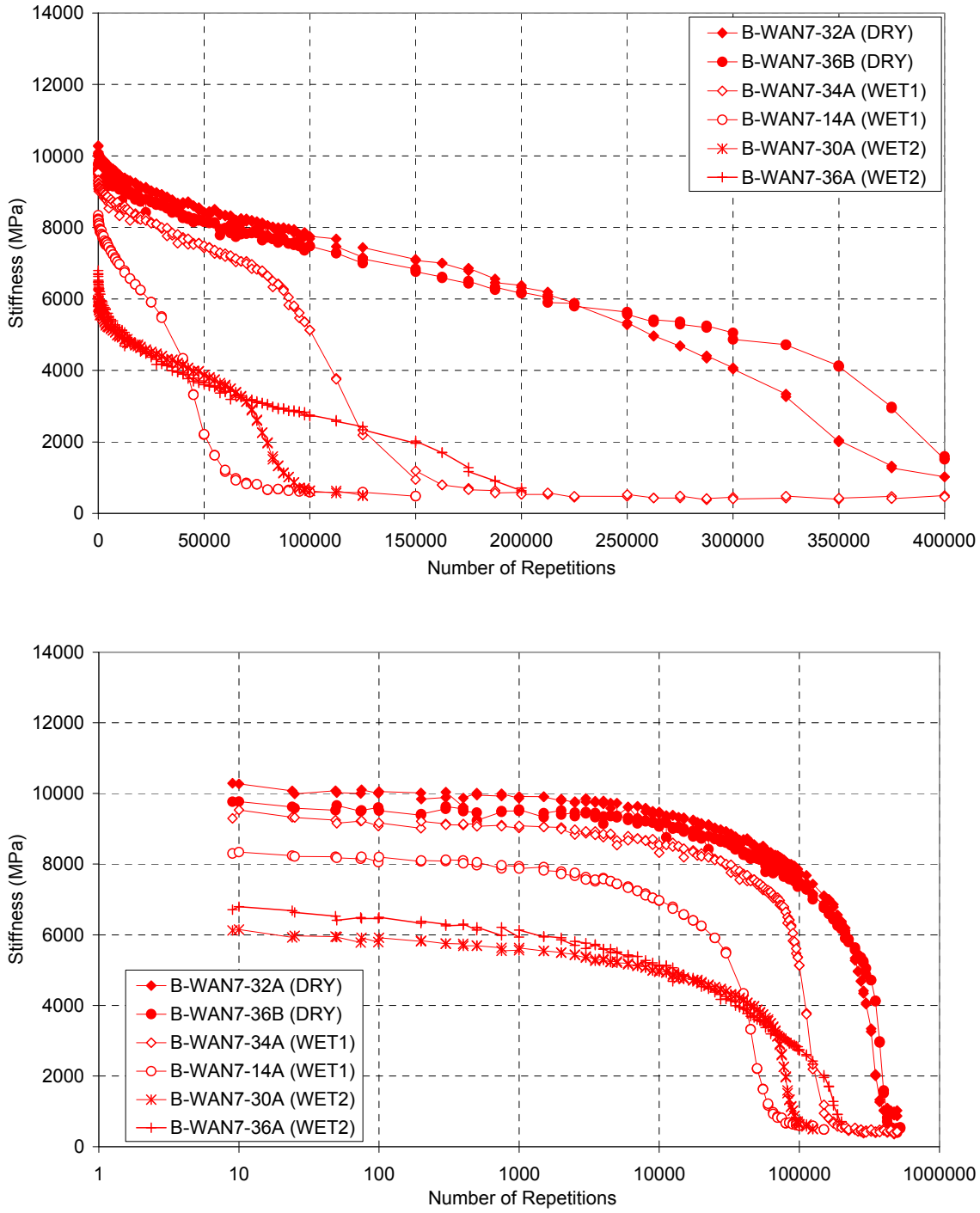

Figure F-1. Stiffness deterioration curves of AAN.

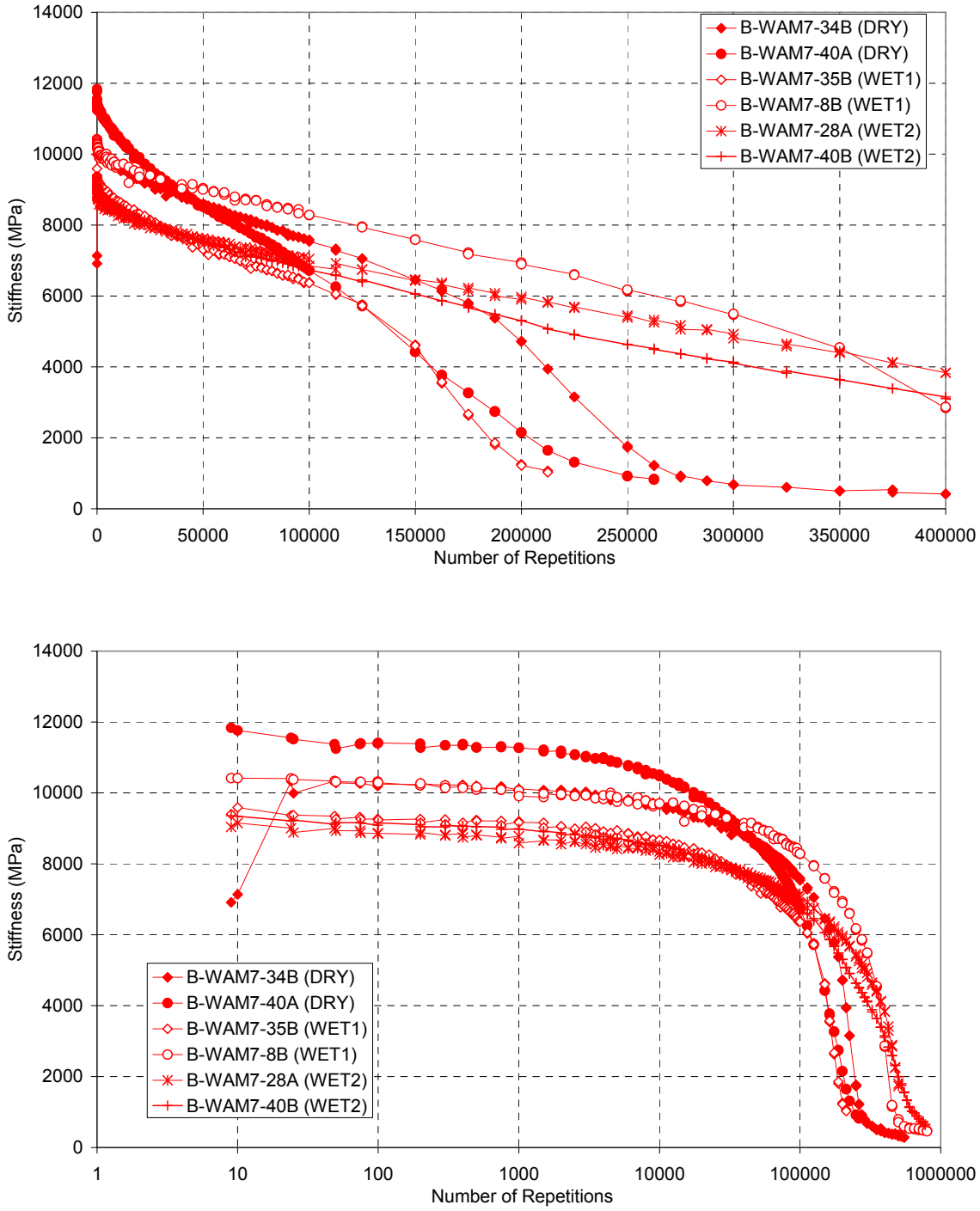

Figure F-2. Stiffness deterioration curves of AAM.

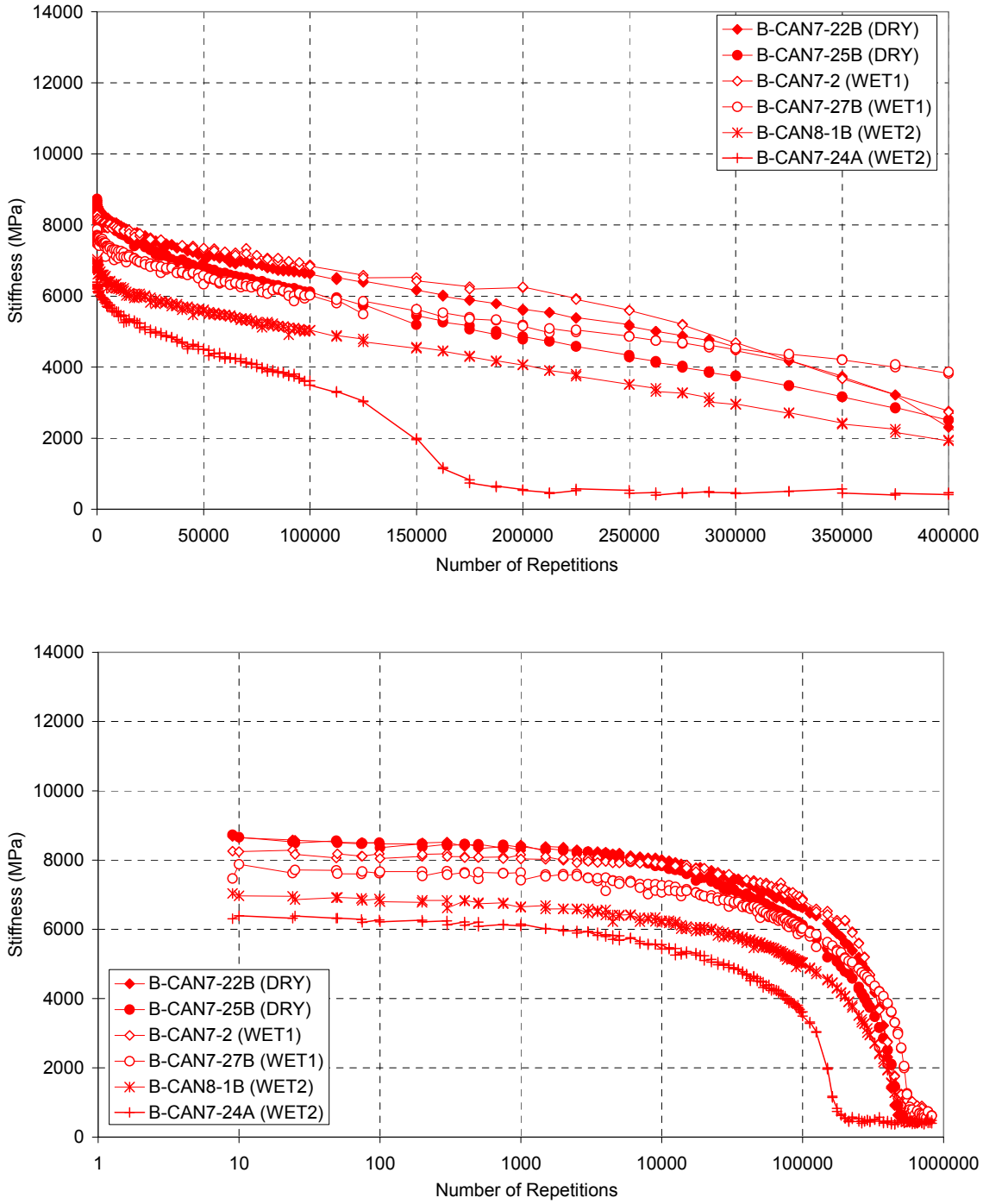

Figure F-3. Stiffness deterioration curves of BAN.

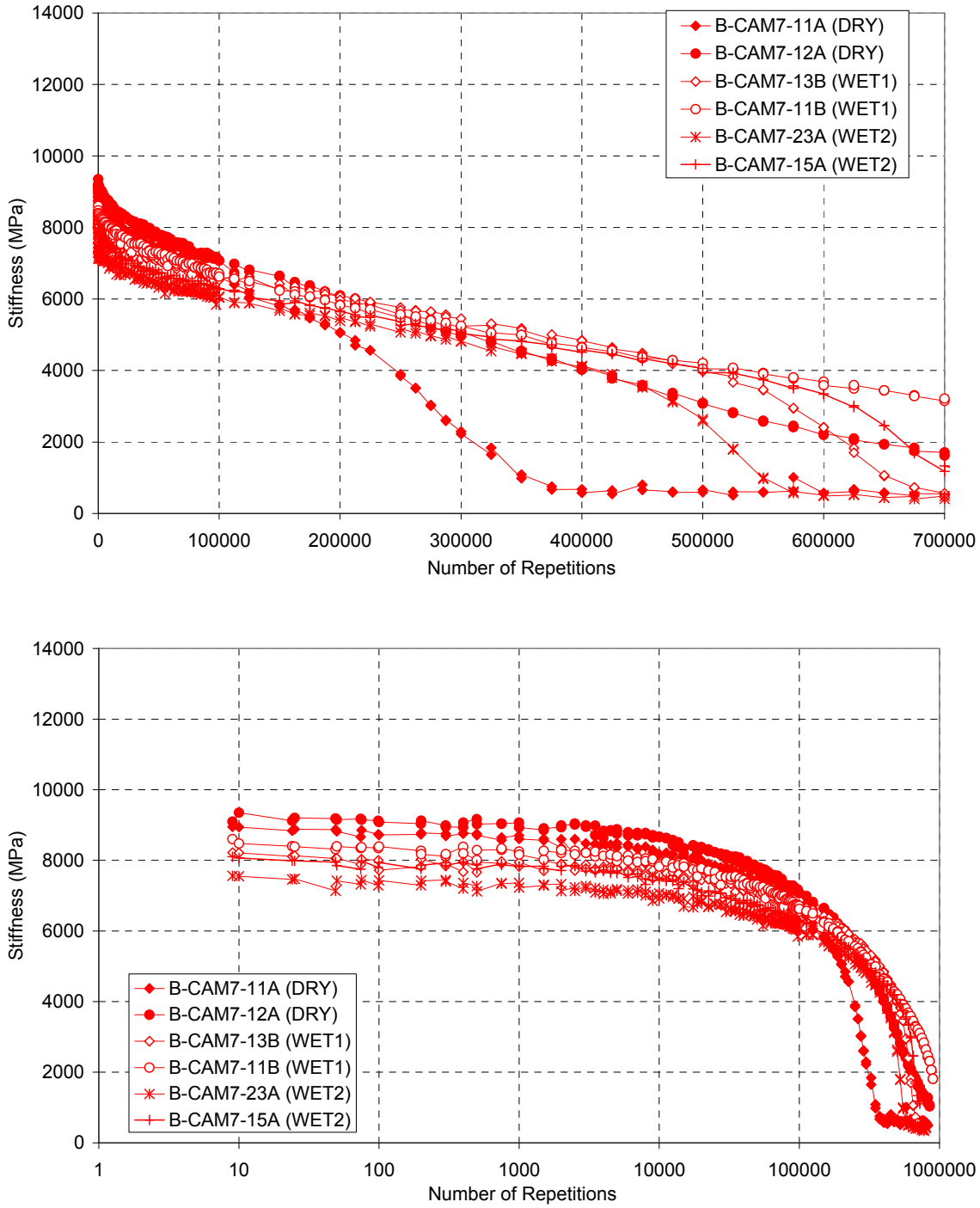

Figure F-4. Stiffness deterioration curves of BAM.

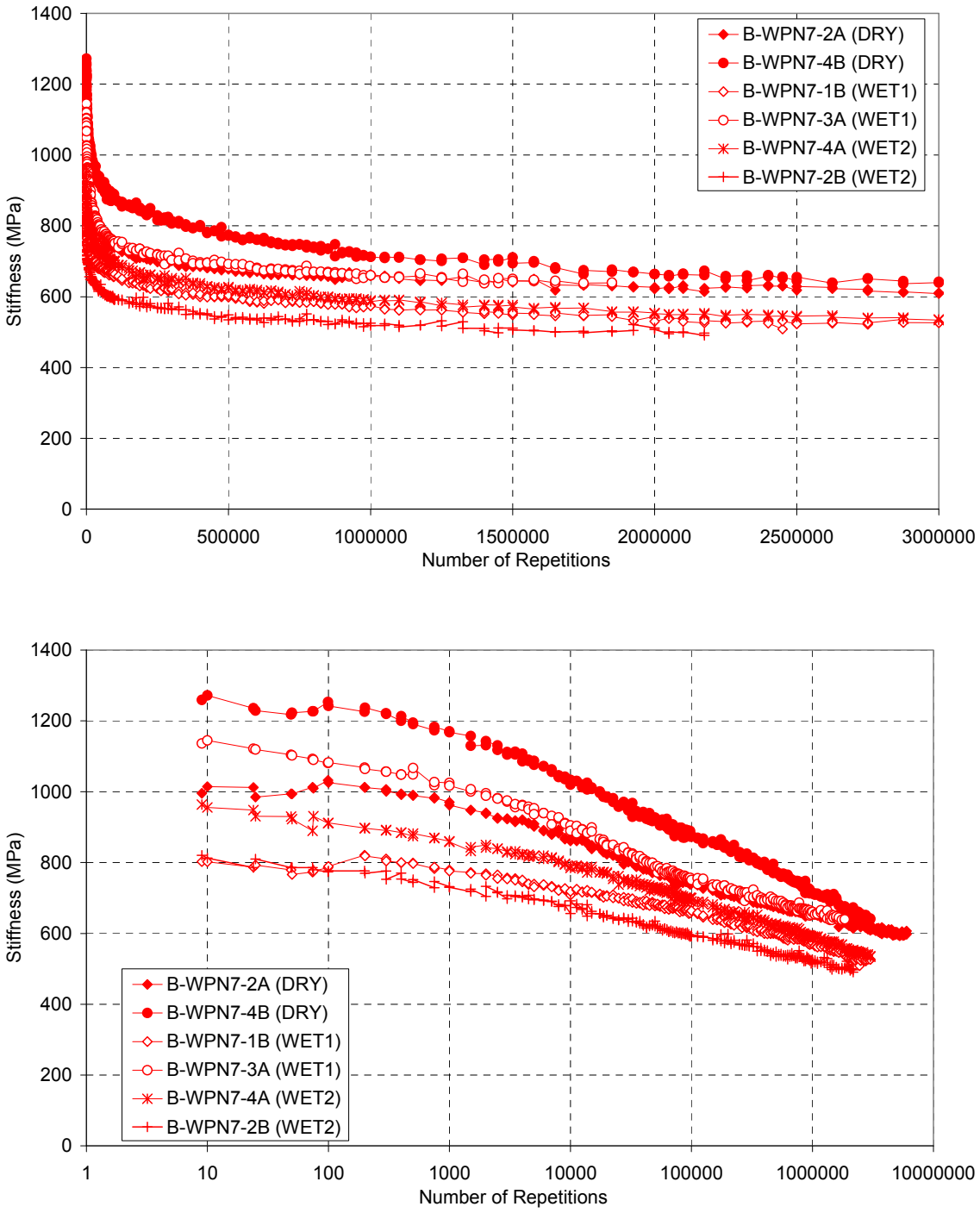

Figure F-5. Stiffness deterioration curves of APN.

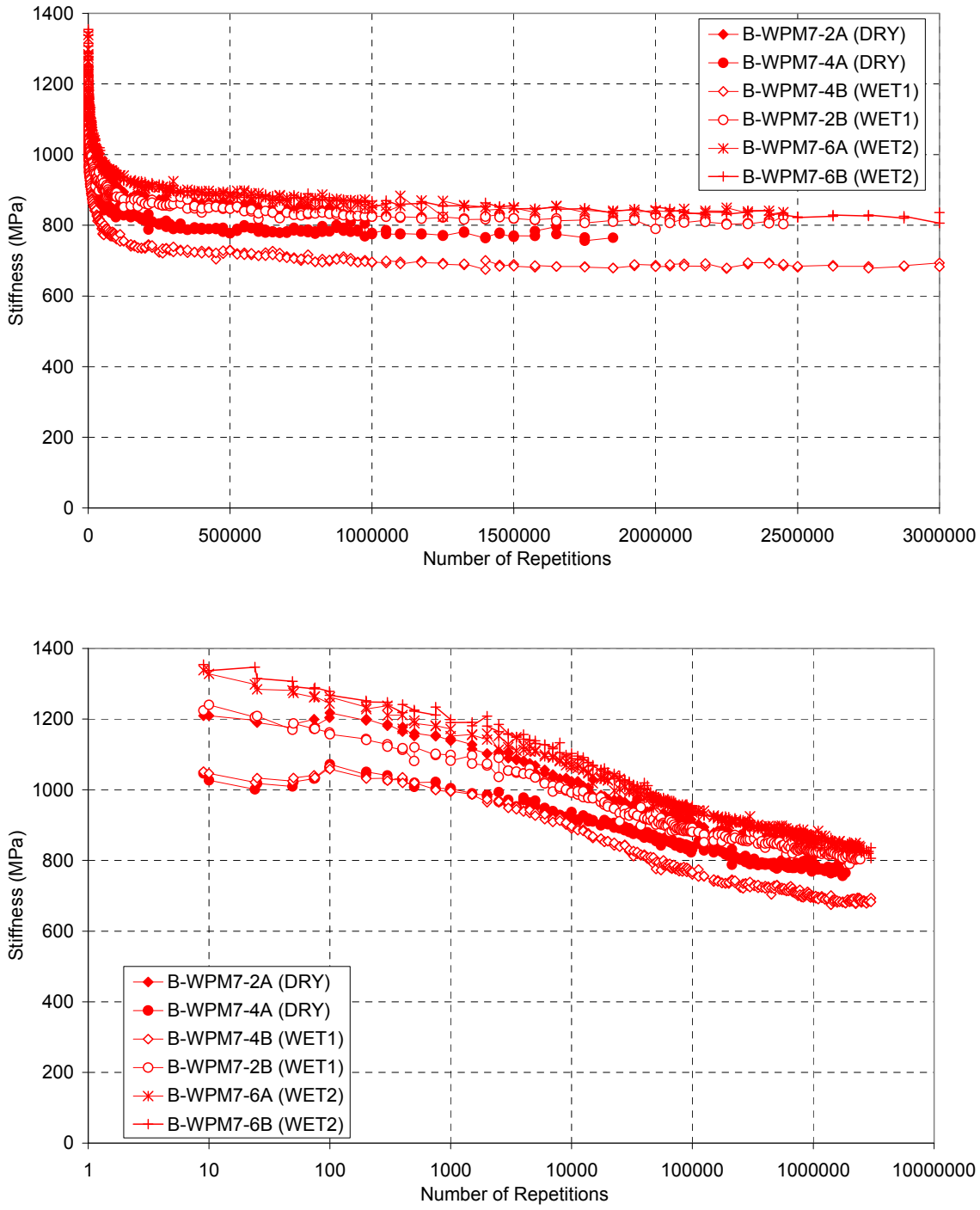

Figure F-6. Stiffness deterioration curves of APM.

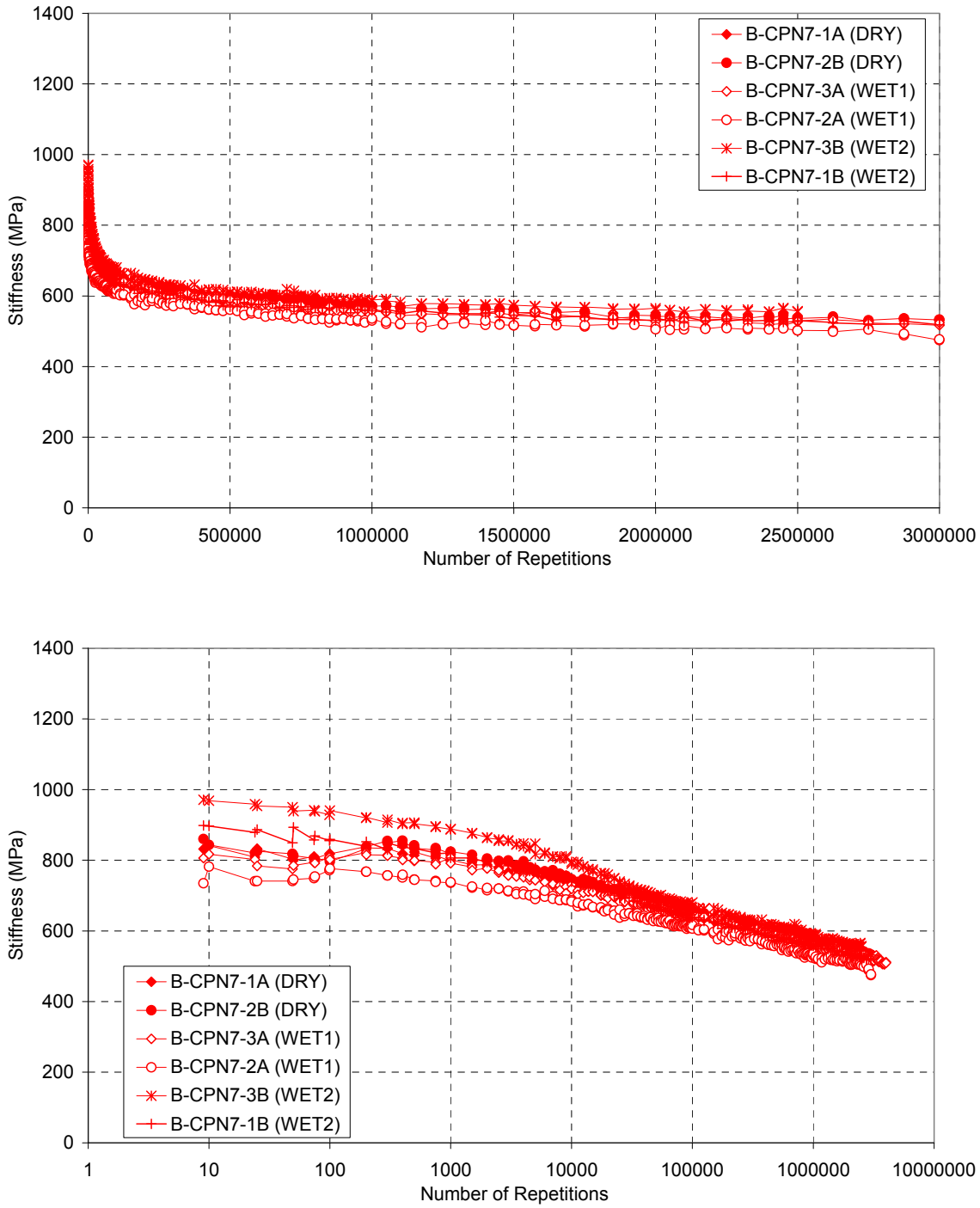

Figure F-7. Stiffness deterioration curves of BPN.

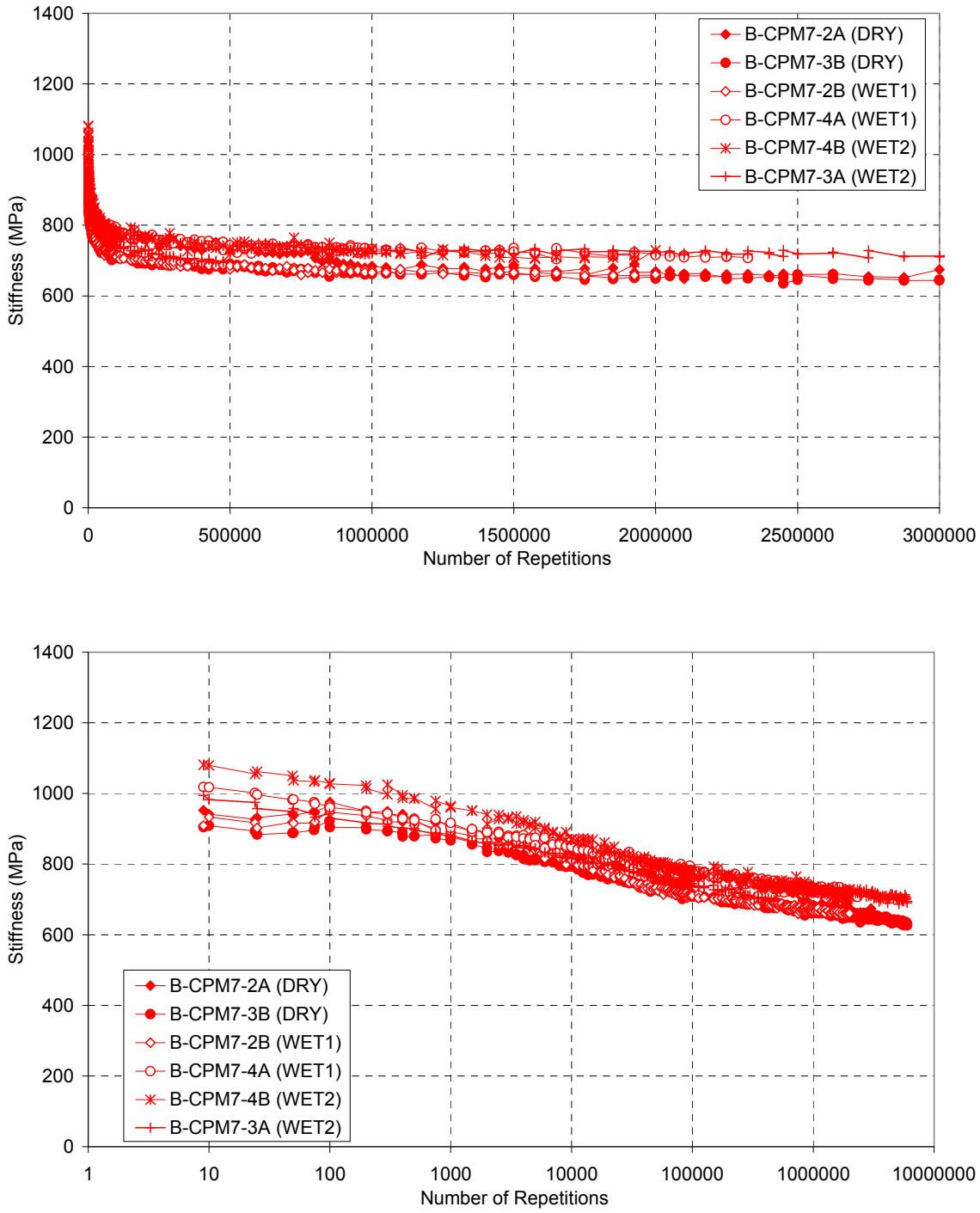

Figure F-8. Stiffness deterioration curves of BPM.

APPENDIX G: TSR TEST RESULTS FOR THE COMPARATIVE STUDY

Table G-1 TSR Results for Mix AAN (Aggregate A/AR-4000 Binder/No Additive)

Aggregate W				Mix: 3/4" Nominal maximum aggregate size, Medium dense gradation, Shell AR 4000 Binder, 5% binder content									
Additive: None				Dosage %: 0									
Date Tested: 10/23/2003				Tester: Qing Lu									
Sample ID		**WAN14**	**WAN10**	**WAN9**	**WAN5**	**WAN13**	**WAN1**	**WAN4**	**WAN6**	**WAN12**	**WAN7**	**WAN3**	**WAN8**
Diameter, mm	D	101.6	101.6	101.6	101.6	101.6	101.6	101.6	101.6	101.6	101.6	101.6	101.6
Thickness, mm	t	63.55	63.56	63.56	63.60	63.60	63.68	63.55	63.65	63.65	63.62	63.63	63.48
Dry Mass in Air, g	A	1218.2	1218.3	1217.9	1219.1	1218.4	1215.8	1218.2	1218.9	1215.8	1218	1216.8	1219.2
S.S.D. Mass, g	B	1223.1	1223.7	1222.1	1224.7	1222.5	1224.3	1223.1	1224.6	1221.3	1223.3	1223.4	1223.4
Mass in Water, g	C	717.6	718.3	716.4	717	715.7	719.3	717.6	717.9	714.2	716.4	717.2	718.2
Volume (B-C), cc	E	505.5	505.4	505.7	507.7	506.8	505	505.5	506.7	507.1	506.9	506.2	505.2
Bulk Sp. Gr. (A/E)	F	2.410	2.411	2.408	2.401	2.404	2.408	2.410	2.406	2.398	2.403	2.404	2.413
Max Sp. Gr.	G	2.5802	2.5802	2.5802	2.5802	2.5802	2.5802	2.5802	2.5802	2.5802	2.5802	2.5802	2.5802
% Air Voids [100(G-F)/G]	H	6.6	6.6	6.7	6.9	6.8	6.7	6.6	6.8	7.1	6.9	6.8	6.5
Volume Air Voids (H*E/100), cc	I	33.37	33.23	33.68	35.22	34.59	33.80	33.37	34.29	35.90	34.84	34.61	32.68
Load (Dry), N	P	14678.4	16902.4	16724.5	14678.4	15834.9	15568						
Saturation													
Absolute Pressure: Hg @ Manometer								15	15	15	15	15	15
Absolute Pressure: Hg @ Pump								15	15	15	15	15	15
Time, Minutes								3+1	3	3	3	3	3
Moisture Conditioned, One Freeze Thaw Cycle													
S.S.D. Mass, g	B'							1242.8	1246.2	1244.1	1246.0	1241.3	1245.3
Mass in Water, g	C'							731.0	737.7	736.1	736.6	732.2	737.0
Volume (B'-C'), cc	E'							511.8	508.5	508.0	509.4	509.1	508.3
Volume Absorbed Water (B'-A), cc	J'							24.6	27.3	28.3	28.0	24.5	26.1
% Saturation (100*J'/I)	S'							73.7	79.6	78.8	80.4	70.8	79.9
% Swell [100(E'-E)/E]	W'							1.2	0.4	0.2	0.5	0.6	0.6
Thickness, mm	t'							64.3	64.7	64.2	64.2	64.3	64.0
Load (Wet), N	P'							5070.7	4092.2	4892.8	4448.0	4425.8	4803.8
Dry Strength (2000*P/π*t*D), kPa	S_{td}	1447.3	1666.3	1648.8	1446.2	1560.1	1531.9						
Wet Strength (2000*P'/π*t'*D), kPa	S_{tw}							494.1	396.6	477.8	434.2	431.3	470.0
Visual Moisture Damage (Yes/No)								M	M	M	M	M	M
Aggregate Break Damage (Number of particles)								5	5	3	2	4	5
Soft Aggregate (Number of particles)													

Initial Tensile Strength Values

	Dry (S_{td})[1]	Wet (S_{tw})[1]
1	1447.3	**494.1**
2	**1666.3**	**396.6**
3	1648.8	477.8
4	**1446.2**	434.2
5	1560.1	431.3
6	1531.9	470.0

Final Tensile Strength Values

Dry (S_{td})[2]	Wet (S_{tw})[2]
1447.3	477.8
1648.8	434.2
1560.1	431.3
1531.9	470.0
1547.0 S_1	453.3 S_2

Conversions:
PSI to kPa, Multiply psi by 6.895
lb_f to N, Multiply lb_f by 4.448

Tensile Strength Ratio S_2/S_1*100= **29** %

Table G-2 TSR Results for Mix AAM (Aggregate A/AR-4000 Binder/Hydrated Lime)

Aggregate W				Mix: 3/4" Nominal maximum aggregate size, Medium dense gradation, Shell AR 4000 Binder, 5% binder content										
Additive: Hydrated lime				Dosage %:1.4 by dry mass of aggregate										
Date Tested: 11/10/2003				Tester: Qing Lu										
Sample ID		**WAM3**	**WAM4**	**WAM17**	**WAM19**	**WAM20**	**WAM23**	**WAM24**	**WAM1**	**WAM26**	**WAM18**	**WAM21**	**WAM22**	**WAM25**
Diameter, mm	D	101.6	101.6	101.6	101.6	101.6	101.6	102.6	101.6	102.6	101.6	101.6	101.6	101.6
Thickness, mm	t	63.56	63.43	63.09	63.22	62.70	62.82	63.12	63.43	62.99	62.68	62.91	62.77	63.18
Dry Mass in Air, g	A	1209	1208.7	1204.3	1203.3	1204.3	1205	1205.3	1210.2	1204.9	1205.6	1204.6	1204.7	1204.7
S.S.D. Mass, g	B	1214.1	1212.9	1209.9	1209.8	1209	1210.2	1210.1	1214	1210	1210.7	1210.7	1209.5	1209.4
Mass in Water, g	C	711.2	712.5	708.3	709.6	709.7	711.5	706.6	712.6	708.2	707	711.7	710.2	707.7
Volume (B-C), cc	E	502.9	500.4	501.6	500.2	499.3	498.7	503.5	501.4	501.8	503.7	499	499.3	501.7
Bulk Sp. Gr. (A/E)	F	2.404	2.415	2.401	2.406	2.412	2.416	2.394	2.414	2.401	2.393	2.414	2.413	2.401
Max Sp. Gr.	G	2.5830	2.5830	2.5830	2.5830	2.5830	2.5830	2.5830	2.5830	2.5830	2.5830	2.5830	2.5830	2.5830
% Air Voids [100(G-F)/G]	H	6.9	6.5	7.0	6.9	6.6	6.5	7.3	6.6	7.0	7.3	6.5	6.6	7.0
Volume Air Voids (H*E/100), cc	I	34.84	32.46	35.36	34.35	33.06	32.19	36.87	32.88	35.33	36.96	32.64	32.90	35.30
Load (Dry), N	P		17124.8	15123.2	16457.6	16857.92	16279.68	16457.6						
Saturation														
Absolute Pressure: Hg @ Manometer									15	15/20	15/20	15/20	20	20
Absolute Pressure: Hg @ Pump									15	15/20	15/20	15/20	20	20
Time, Minutes									3	3/1	3/1	5/1	3	3
Moisture Conditioned, One Freeze Thaw Cycle														
S.S.D. Mass, g	B'								1234.8	1230.5	1231.6	1229.1	1228.4	1232.7
Mass in Water, g	C'								729.8	726.6	728.0	727.6	729.2	729.9
Volume (B'-C'), cc	E'								505.0	503.9	503.6	501.5	499.2	502.8
Volume Absorbed Water (B'-A), cc	J'								24.6	25.6	26.0	24.5	23.7	28.0
% Saturation (100*J'/I)	S'								74.8	72.5	70.4	75.1	72.0	79.3
% Swell [100(E'-E)/E]	W'								0.7	0.4	0.0	0.5	0.0	0.2
Thickness, mm	t'								63.8	63.4	63.1	63.3	63.2	63.3
Load (Wet), N	P'								13788.8	14989.8	13321.8	14500.5	14233.6	13922.2
Dry Strength (2000*P/π*t*D), kPa	S_{td}	0.0	1691.7	1502.1	1631.3	1684.8	1623.9	1617.9						
Wet Strength (2000*P'/π*t'*D), kPa	S_{tw}								1354.1	1467.7	1323.1	1435.8	1411.7	1377.7
Visual Moisture Damage (Yes/No)									N	N	N	N	N	N
Aggregate Break Damage (Number of particles)									7	6	5	6	4	6
Soft Aggregate (Number of particles)														

Initial Tensile Strength Values

	Dry (S_{td})[1]	Wet (S_{tw})[1]
1	**1691.7**	1354.1
2	**1502.1**	**1323.1**
3	1631.3	1435.8
4	1684.8	1411.7
5	1623.9	1377.7
6	1617.9	**0.0**

Tensile Strength Ratio S_2/S_1*100=

Final Tensile Strength Values

Dry (S_{td})[2]	Wet (S_{tw})[2]
1631.3	1354.1
1684.8	1435.8
1623.9	1411.7
1617.9	1377.7
1639.5 S_1	1394.8 S_2

85 %

Conversions:
PSI to kPa, Multiply psi by 6.895
lb_f to N, Multiply lb_f by 4.448

Table G-3 TSR Results for Mix APN (Aggregate A/PBA-6a Binder/No Additive)

Aggregate W				Mix: 3/4" Nominal maximum aggregate size, Medium dense gradation, Valero PBA-6a Binder, 5% binder content									
Additive: None				Dosage %: 0									
Date Tested:				Tester: Qing Lu									
Sample ID		**WPN22**	**WPN25**	**WPN27**	**WPN29**	**WPN30**	**WPN32**	**WPN23**	**WPN26**	**WPN28**	**WPN31**	**WPN33**	**WPN35**
Diameter, mm	D	101.6	101.6	101.6	101.6	101.6	101.6	101.6	101.6	101.6	101.6	101.6	101.6
Thickness, mm	t	63.035	62.9875	63.2875	63.175	63.2125	63.2425	63.0	63.295	63.4	63.3525	63.1425	63.425
Dry Mass in Air, g	A	1208.8	1208.1	1214	1213.4	1213.8	1214.1	1208.0	1214.2	1212.3	1214	1213	1209.8
S.S.D. Mass, g	B	1213.8	1213.8	1217.8	1217.3	1218.6	1217.9	1213.0	1217.6	1218.9	1218.2	1216.9	1213.6
Mass in Water, g	C	709.8	711.4	714.8	715	713.3	714.2	708.9	714.6	716.2	714.0	713.9	709.7
Volume (B-C), cc	E	504	502.4	503	502.3	505.3	503.7	504.1	503	502.7	504.2	503	503.9
Bulk Sp. Gr. (A/E)	F	2.398	2.405	2.414	2.416	2.402	2.410	2.396	2.414	2.412	2.408	2.412	2.401
Max Sp. Gr.	G	2.5916	2.5916	2.5916	2.5916	2.5916	2.5916	2.5916	2.5916	2.5916	2.5916	2.5916	2.5916
% Air Voids [100(G-F)/G]	H	7.5	7.2	6.9	6.8	7.3	7.0	7.5	6.9	6.9	7.1	6.9	7.4
Volume Air Voids (H*E/100), cc	I	37.57	36.24	34.56	34.10	36.94	35.22	37.98	34.49	34.92	35.76	34.95	37.08
Load (Dry), N	P	3158.08	3158.08	3380.48	3158.08	3336	3513.92						
Saturation													
Absolute Pressure: Hg @ Manometer								20/25	23	23	23	23	23
Absolute Pressure: Hg @ Pump								20/25	23	23	23	23	23
Time, Minutes								4/1	2	2	2	2	2
Moisture Conditioned, One Freeze Thaw Cycle													
S.S.D. Mass, g	B'							1236.4	1239.1	1240.0	1241.0	1241.0	1237.1
Mass in Water, g	C'							732.0	736.7	736.6	736.3	737.0	734.0
Volume (B'-C'), cc	E'							504.4	502.4	503.4	504.7	504.0	503.1
Volume Absorbed Water (B'-A), cc	J'							28.4	24.9	27.7	27.0	28.0	27.3
% Saturation (100*J'/I)	S'							74.8	72.2	79.3	75.5	80.1	73.6
% Swell [100(E'-E)/E]	W'							0.1	-0.1	0.1	0.1	0.2	-0.2
Thickness, mm	t'							63.6	63.6	63.7	63.7	63.6	63.8
Load (Wet), N	P'							1556.8	1512.3	1601.3	1512.3	1734.7	1556.8
Dry Strength (2000*P/π*t*D), kPa	S_{td}	313.9	314.2	334.7	313.2	330.7	348.2						
Wet Strength (2000*P'/π*t'*D), kPa	S_{tw}							153.3	149.0	157.5	148.7	170.9	153.0
Visual Moisture Damage (Yes/No)								M	H	M	M	M	M
Aggregate Break Damage (Number of particles)								2	1	3	1	2	2
Soft Aggregate (Number of particles)													

Initial Tensile Strength Values

	Dry (S_{td})[1]	Wet (S_{tw})[1]
1	313.9	153.3
2	314.2	149.0
3	334.7	157.5
4	**313.2**	**148.7**
5	330.7	**170.9**
6	**348.2**	153.0

Tensile Strength Ratio S_2/S_1*100=

Final Tensile Strength Values

	Dry (S_{td})[2]	Wet (S_{tw})[2]
	313.9	153.3
	314.2	149.0
	334.7	157.5
	330.7	153.0
	323.4 S_1	153.2 S_2

47 %

Conversions:
PSI to kPa, Multiply psi by 6.895
lb_f to N, Multiply lb_f by 4.448

Table G-4 TSR Results for Mix APM (Aggregate A/PBA-6a Binder / Hydrated Lime)

Aggregate W				Mix: 3/4" Nominal maximum aggregate size, Medium dense gradation, Valero PBA-6a, 5% binder content									
Additive: Hydrated lime				Dosage %:1.4 by dry mass of aggregate									
Date Tested:				Tester: Qing Lu									
Sample ID		**WPM13**	**WPM18**	**WPM20**	**WPM22**	**WPM24**	**WPM28**	**WPM11**	**WPM12**	**WPM17**	**WPM19**	**WPM21**	**WPM23**
Diameter, mm	D	101.6	101.6	101.6	101.6	101.6	101.6	101.6	101.6	101.6	101.6	101.6	101.6
Thickness, mm	t	62.955	62.7275	62.7775	62.9425	62.845	63.12	62.8025	62.785	62.9125	62.92	62.775	62.8375
Dry Mass in Air, g	A	1203.3	1205.8	1204	1203	1201.3	1203.6	1210.1	1209.5	1202.8	1201.7	1203.3	1204.9
S.S.D. Mass, g	B	1207.9	1210.3	1207.9	1207.7	1205.6	1208.2	1217.3	1215.9	1207.8	1206.3	1207.2	1210.2
Mass in Water, g	C	709.9	711.2	710.0	706.8	707.2	708.9	716.7	716.0	709.4	709.0	706.3	710.4
Volume (B-C), cc	E	498	499.1	497.9	500.9	498.4	499.3	500.6	499.9	498.4	497.3	500.9	499.8
Bulk Sp. Gr. (A/E)	F	2.416	2.416	2.418	2.402	2.410	2.411	2.417	2.419	2.413	2.416	2.402	2.411
Max Sp. Gr.	G	2.5875	2.5875	2.5875	2.5875	2.5875	2.5875	2.5875	2.5875	2.5875	2.5875	2.5875	2.5875
% Air Voids [100(G-F)/G]	H	6.6	6.6	6.5	7.2	6.8	6.8	6.6	6.5	6.7	6.6	7.2	6.8
Volume Air Voids (H*E/100), cc	I	32.96	33.09	32.59	35.97	34.13	34.14	32.93	32.46	33.55	32.87	35.86	34.14
Load (Dry), N	P	4314.56	3869.76	4714.88	4003.2	4047.68	4225.6						
Saturation													
Absolute Pressure: Hg @ Manometer								23/25	25	25	25	25	25
Absolute Pressure: Hg @ Pump								23/25	25	25	25	25	25
Time, Minutes								2/6	2	3	3	3	3
Moisture Conditioned, One Freeze Thaw Cycle													
S.S.D. Mass, g	B'							1233.5	1232.3	1227.4	1227.6	1232.1	1230.3
Mass in Water, g	C'							731.7	734.7	727.4	728.7	729.8	730.8
Volume (B'-C'), cc	E'							501.8	497.6	500.0	498.9	502.3	499.5
Volume Absorbed Water (B'-A), cc	J'							23.4	22.8	24.6	25.9	28.8	25.4
% Saturation (100*J'/I)	S'							71.1	70.2	73.3	78.8	80.3	74.4
% Swell [100(E'-E)/E]	W'							0.2	-0.5	0.3	0.3	0.3	-0.1
Thickness, mm	t'							63.0	62.9075	63.1	63.1	63.1	63.2
Load (Wet), N	P'							3558.4	3914.24	3558.4	3469.4	3558.4	3558.4
Dry Strength (2000*P/π*t*D), kPa	S_{td}	429.4	386.6	470.6	398.5	403.6	419.5						
Wet Strength (2000*P'/π*t'*D), kPa	S_{tw}							353.7	389.9	353.1	344.6	353.2	352.8
Visual Moisture Damage (Yes/No)								L	L	L	L	L	L
Aggregate Break Damage (Number of particles)								7	3	7	5	5	3
Soft Aggregate (Number of particles)													

Initial Tensile Strength Values

	Dry $(S_{td})^1$	Wet $(S_{tw})^1$
1	429.4	353.7
2	**386.6**	353.1
3	**470.6**	**344.6**
4	398.5	353.2
5	403.6	352.8
6	419.5	**389.9**

Tensile Strength Ratio S_2/S_1*100= **86** %

Final Tensile Strength Values

Dry $(S_{td})^2$	Wet $(S_{tw})^2$
429.4	353.7
398.5	353.1
403.6	353.2
419.5	352.8
412.8 S_1	353.2 S_2

Conversions:
PSI to kPa, Multiply psi by 6.895
lb_f to N, Multiply lb_f by 4.448

Table G-5 TSR Results for Mix BAN (Aggregate B/AR-4000 Binder/No Additive)

Aggregate C		Mix: 3/4" Nominal maximum aggregate size, Medium dense gradation, Shell AR 4000 Binder, 6% binder content												
Additive: None		Dosage %: 0												
Date Tested: 11/17/2003		Tester: Qing Lu												
Sample ID		**CAN1**	**CAN4**	**CAN10**	**CAN18**	**CAN23**	**CAN26**	**CAN28**	**CAN3**	**CAN7**	**CAN30**	**CAN20**	**CAN21**	**CAN25**
Diameter, mm	D	101.6	101.6	101.6	101.6	101.6	101.6	102.6	101.6	101.6	102.6	101.6	101.6	101.6
Thickness, mm	t	63.54	63.55	63.56	63.11	62.65	62.69	62.69	63.66	63.57	62.68	62.86	62.73	63.17
Dry Mass in Air, g	A	1155.3	1157.7	1156.8	1144.1	1138	1138	1137.9	1157.7	1158.7	1138.3	1144.4	1136.6	1138.8
S.S.D. Mass, g	B	1161.4	1162.7	1163.6	1151	1145.1	1145.2	1145.5	1163.1	1162.8	1144.2	1150.4	1142.4	1147.5
Mass in Water, g	C	659.6	661.2	662.9	655.2	652.2	648.3	650.6	660.9	660.8	651.9	654.9	646.5	652.5
Volume (B-C), cc	E	501.8	501.5	500.7	495.8	492.9	496.9	494.9	502.2	502	492.3	495.5	495.9	495
Bulk Sp. Gr. (A/E)	F	2.302	2.308	2.310	2.308	2.309	2.290	2.299	2.305	2.308	2.312	2.310	2.292	2.301
Max Sp. Gr.	G	2.4600	2.4600	2.4600	2.4600	2.4600	2.4600	2.4600	2.4600	2.4600	2.4600	2.4600	2.4600	2.4600
% Air Voids [100(G-F)/G]	H	6.4	6.2	6.1	6.2	6.1	6.9	6.5	6.3	6.2	6.0	6.1	6.8	6.5
Volume Air Voids (H*E/100), cc	I	32.17	30.89	30.46	30.72	30.30	34.30	32.34	31.59	30.98	29.58	30.30	33.87	32.07
Load (Dry), N	P	13788.8	13566.4	14278.08		13344	14678.4	12676.8						
Saturation														
Absolute Pressure: Hg @ Manometer									15/20	20	20	20	20	20
Absolute Pressure: Hg @ Pump									15/20	20	20	20	20	20
Time, Minutes									3/3	3	3	3	5	3
Moisture Conditioned, One Freeze Thaw Cycle														
S.S.D. Mass, g	B'								1180.0	1182.7	1159.7	1166.6	1161.2	1163.4
Mass in Water, g	C'								674.7	677.4	666.6	670.2	662.8	666.2
Volume (B'-C'), cc	E'								505.3	505.3	493.1	496.4	498.4	497.2
Volume Absorbed Water (B'-A), cc	J'								22.3	24.0	21.4	22.2	24.6	24.6
% Saturation (100*J'/I)	S'								70.6	77.5	72.4	73.3	72.6	76.7
% Swell [100(E'-E)/E]	W'								0.6	0.7	0.2	0.2	0.5	0.4
Thickness, mm	t'								64.0	63.9	63.3	63.3	63.1	63.5
Load (Wet), N	P'								6494.1	7606.1	8006.4	7339.2	7339.2	5649.0
Dry Strength (2000*P/p*t*D), kPa	S_{td}	1359.9	1337.8	1407.6	0.0	1334.7	1467.1	1254.8						
Wet Strength (2000*P'/p*t'*D), kPa	S_{tw}								636.1	745.6	785.2	727.0	728.3	557.1
Visual Moisture Damage (Yes/No)									M	M	M	M	M	M
Aggregate Break Damage (Number of particles)									4	2	4	2	2	1
Soft Aggregate (Number of particles)														

Initial Tensile Strength Values

	Dry $(S_{td})^1$	Wet $(S_{tw})^1$
1	1359.9	636.1
2	1337.8	745.6
3	1407.6	727.0
4	1334.7	728.3
5	**1467.1**	**557.1**
6	**1254.8**	**785.2**

Tensile Strength Ratio S_2/S_1*100=

Final Tensile Strength Values

	Dry $(S_{td})^2$	Wet $(S_{tw})^2$
	1359.9	636.1
	1337.8	745.6
	1407.6	727.0
	1334.7	728.3
	1360.0 S_1	709.3 S_2

52 %

Conversions:
PSI to kPa, Multiply psi by 6.895
lb_f to N, Multiply lb_f by 4.448

Table G-6 TSR Results for Mix BAM (Aggregate B/AR-4000 Binder/Hydrated Lime)

Aggregate C				Mix: 3/4" Nominal maximum aggregate size, Medium dense gradation, Shell AR 4000 Binder, 6% binder content									
Additive: Hydrated lime				Dosage %: 1.4% by dry mass of aggregate									
Date Tested: 11/17/2003				Tester: Qing Lu									
Sample ID		**CAM7**	**CAM8**	**CAM17**	**CAM20**	**CAM26**	**CAM28**	**CAM9**	**CAM19**	**CAM21**	**CAM22**	**CAM25**	**CAM31**
Diameter, mm	D	101.6	101.6	101.6	101.6	101.6	101.6	101.6	101.6	101.6	101.6	101.6	101.6
Thickness, mm	t	62.80	62.55	62.78	62.85	62.36	62.30	62.88	62.55	62.93	62.78	62.78	62.595
Dry Mass in Air, g	A	1125.8	1124.3	1134.7	1135.7	1126.8	1129.6	1122.4	1135	1129.1	1130.7	1126.3	1125.6
S.S.D. Mass, g	B	1127.7	1132.6	1141.2	1142.1	1131.7	1133.3	1130.3	1140.4	1136.2	1134.2	1137.2	1132.5
Mass in Water, g	C	640.5	641.2	647.8	651.5	643.4	644.4	645.1	648.6	645.3	645.4	647	645.1
Volume (B-C), cc	E	487.2	491.4	493.4	490.6	488.3	488.9	485.2	491.8	490.9	488.8	490.2	487.4
Bulk Sp. Gr. (A/E)	F	2.311	2.288	2.300	2.315	2.308	2.310	2.313	2.308	2.300	2.313	2.298	2.309
Max Sp. Gr.	G	2.4620	2.4620	2.4620	2.4620	2.4620	2.4620	2.4620	2.4620	2.4620	2.4620	2.4620	2.4620
% Air Voids [100(G-F)/G]	H	6.1	7.1	6.6	6.0	6.3	6.2	6.0	6.3	6.6	6.0	6.7	6.2
Volume Air Voids (H*E/100), cc	I	29.93	34.74	32.51	29.31	30.62	30.09	29.31	30.79	32.29	29.54	32.73	30.21
Load (Dry), N	P	11965.12	13432.96	14166.88	15167.68	14456	14633.92						
Saturation													
Absolute Pressure: Hg @ Manometer								20	20/25	20/25	20	20	20
Absolute Pressure: Hg @ Pump								20	20/25	20/25	20	20	20
Time, Minutes								3	3/2	3/2	3	3	3
Moisture Conditioned, One Freeze Thaw Cycle													
S.S.D. Mass, g	B'							1145.5	1156.7	1153.7	1151.5	1151.3	1147.1
Mass in Water, g	C'							658.0	666.7	662.9	661.6	660.8	658.9
Volume (B'-C'), cc	E'							487.5	490.0	490.8	489.9	490.5	488.2
Volume Absorbed Water (B'-A), cc	J'							23.1	21.7	24.6	20.8	25.0	21.5
% Saturation (100*J'/I)	S'							78.8	70.5	76.2	70.4	76.4	71.2
% Swell [100(E'-E)/E]	W'							0.5	-0.4	0.0	0.2	0.1	0.2
Thickness, mm	t'							63.0	62.6	63.1	63.3	63.7	63.0
Load (Wet), N	P'							13922.2	12454.4	13566.4	13121.6	10986.6	12854.7
Dry Strength (2000*P/π*t*D), kPa	S_{td}	1193.9	1345.7	1414.1	1512.3	1452.6	1471.9						
Wet Strength (2000*P'/π*t'*D), kPa	S_{tw}							1385.4	1246.3	1348.0	1299.0	1080.4	1279.2
Visual Moisture Damage (Yes/No)								L	L	L	L	L	L
Aggregate Break Damage (Number of particles)								3	2	1	1	1	1
Soft Aggregate (Number of particles)													

Initial Tensile Strength Values

	Dry $(S_{td})^1$	Wet $(S_{tw})^1$
1	**1193.9**	**1385.4**
2	1345.7	1246.3
3	1414.1	1348.0
4	**1512.3**	1299.0
5	1452.6	**1080.4**
6	1471.9	1279.2
	Tensile Strength Ratio S_2/S_1*100=	

Final Tensile Strength Values

	Dry $(S_{td})^2$	Wet $(S_{tw})^2$
	1345.7	1246.3
	1414.1	1348.0
	1452.6	1299.0
	1471.9	1279.2
	1421.1 S_1	1293.1 S_2
	91 %	

Conversions:
PSI to kPa, Multiply psi by 6.895
lb_f to N, Multiply lb_f by 4.448

Table G-7 TSR Results for Mix BPN (Aggregate B/PBA-6a Binder/No Additive)

Aggregate C				Mix: 3/4" Nominal maximum aggregate size, Medium dense gradation, Valero PBA-6a, 6% binder content									
Additive: None				Dosage %: 0									
Date Tested:				Tester: Qing Lu									
Sample ID		**CPN14**	**CPN18**	**CPN19**	**CPN21**	**CPN22**	**CPN27**	**CPN11**	**CPN13**	**CPN15**	**CPN16**	**CPN20**	**CPN26**
Diameter, mm	D	101.6	101.6	101.6	101.6	101.6	101.6	101.6	101.6	101.6	101.6	101.6	101.6
Thickness, mm	t	62.6975	62.7125	62.815	62.89	62.955	62.89	62.8075	62.98	62.7975	63.0125	62.99	63.0625
Dry Mass in Air, g	A	1128	1131.1	1125.4	1132.6	1126.6	1125.9	1135	1128.8	1128.2	1130.1	1128.7	1130.6
S.S.D. Mass, g	B	1132.8	1135.1	1130.8	1137.1	1131.6	1131.6	1141.2	1134.1	1134.1	1135.8	1134.7	1137.5
Mass in Water, g	C	640.1	641.4	637	643.4	638.1	641.1	646.4	638.8	640.9	638.8	642.4	644.2
Volume (B-C), cc	E	492.7	493.7	493.8	493.7	493.5	490.5	494.8	495.3	493.2	497	492.3	493.3
Bulk Sp. Gr. (A/E)	F	2.289	2.291	2.279	2.294	2.283	2.295	2.294	2.279	2.288	2.274	2.293	2.292
Max Sp. Gr.	G	2.4577	2.4577	2.4577	2.4577	2.4577	2.4577	2.4577	2.4577	2.4577	2.4577	2.4577	2.4577
% Air Voids [100(G-F)/G]	H	6.8	6.8	7.3	6.7	7.1	6.6	6.7	7.3	6.9	7.5	6.7	6.7
Volume Air Voids (H*E/100), cc	I	33.73	33.47	35.89	32.86	35.10	32.39	32.99	36.01	34.15	37.18	33.05	33.28
Load (Dry), N	P	3024.64	2802.24	2624.32	3113.6	2891.2	2846.72						
Saturation													
Absolute Pressure: Hg @ Manometer								20/25	20/25	25	24	24	25
Absolute Pressure: Hg @ Pump								20/25	20/25	25	24	24	25
Time, Minutes								3/1	1.5/1.5	2	2	2	15
Moisture Conditioned, One Freeze Thaw Cycle													
S.S.D. Mass, g	B'							1161.1	1155.3	1154.6	1158.6	1154.5	1154.4
Mass in Water, g	C'							665.2	660.8	660.7	661.1	662.8	663.4
Volume (B'-C'), cc	E'							495.9	494.5	493.9	497.5	491.7	491.0
Volume Absorbed Water (B'-A), cc	J'							26.1	26.5	26.4	28.5	25.8	23.8
% Saturation (100*J'/I)	S'							79.1	73.6	77.3	76.7	78.1	71.5
% Swell [100(E'-E)/E]	W'							0.2	-0.2	0.1	0.1	-0.1	-0.5
Thickness, mm	t'							62.9	63.2	63.0	63.1	63.2	63.0
Load (Wet), N	P'							2579.8	2357.4	2579.8	2179.5	2401.9	2802.2
Dry Strength (2000*P/π*t*D), kPa	S_{td}	302.3	280.0	261.8	310.2	287.8	283.6						
Wet Strength (2000*P'/π*t'*D), kPa	S_{tw}							257.1	233.9	256.7	216.6	238.2	278.7
Visual Moisture Damage (Yes/No)								M	M	M	M	M	M
Aggregate Break Damage (Number of particles)		4	3	3	5	3	3	2	2	3	1	0	0
Soft Aggregate (Number of particles)													

Initial Tensile Strength Values

	Dry (S_{td})[1]	Wet (S_{tw})[1]
1	302.3	257.1
2	280.0	233.9
3	**261.8**	**216.6**
4	287.8	238.2
5	283.6	**278.7**
6	**310.2**	256.7

Tensile Strength Ratio S_2/S_1*100= **85** %

Final Tensile Strength Values

	Dry (S_{td})[2]	Wet (S_{tw})[2]
	302.3	257.1
	280.0	233.9
	287.8	238.2
	283.6	256.7
	288.4 S_1	246.5 S_2

Conversions:
PSI to kPa, Multiply psi by 6.895
lb_f to N, Multiply lb_f by 4.448

Table G-8 TSR Results for Mix BPM (Aggregate B/PBA-6a Binder/Hydrated Lime)

Aggregate C				Mix: 3/4" Nominal maximum aggregate size, Medium dense gradation, Valero PBA-6a binder, 6% binder content									
Additive: Hydrated lime				Dosage %: 1.4% by dry mass of aggregate									
Date Tested:				Tester: Qing Lu									
Sample ID		**CPM16**	**CPM18**	**CPM20**	**CPM28**	**CPM29**	**CPM34**	**CPM15**	**CPM17**	**CPM19**	**CPM21**	**CPM22**	**CPM25**
Diameter, mm	D	101.6	101.6	101.6	101.6	101.6	101.6	101.6	101.6	101.6	101.6	101.6	101.6
Thickness, mm	t	62.6725	62.705	62.615	62.525	62.89	62.4325	62.5675	62.485	62.825	62.56	62.3925	62.875
Dry Mass in Air, g	A	1123.6	1124.7	1123.4	1114.8	1117.5	1114.3	1115.9	1117.7	1121.9	1119	1116.6	1122.1
S.S.D. Mass, g	B	1131.3	1134.2	1131.9	1124.2	1125.8	1125	1123.7	1123.9	1131.6	1126.9	1123.3	1129.9
Mass in Water, g	C	639.2	644.9	642.1	634.2	636.5	636.6	638.5	637.1	642.8	638.7	634.8	639.9
Volume (B-C), cc	E	492.1	489.3	489.8	490	489.3	488.4	485.2	486.8	488.8	488.2	488.5	490
Bulk Sp. Gr. (A/E)	F	2.283	2.299	2.294	2.275	2.284	2.282	2.300	2.296	2.295	2.292	2.286	2.290
Max Sp. Gr.	G	2.4591	2.4591	2.4591	2.4591	2.4591	2.4591	2.4591	2.4591	2.4591	2.4591	2.4591	2.4591
% Air Voids [100(G-F)/G]	H	7.1	6.5	6.7	7.5	7.1	7.2	6.5	6.6	6.7	6.8	7.0	6.9
Volume Air Voids (H*E/100), cc	I	35.18	31.94	32.97	36.66	34.87	35.27	31.42	32.28	32.58	33.16	34.43	33.69
Load (Dry), N	P	2980.16	3113.6	3380.48	3113.6	2891.2	3158.08						
Saturation													
Absolute Pressure: Hg @ Manometer								24	24	24	24	24	24
Absolute Pressure: Hg @ Pump								24	24	24	24	24	24
Time, Minutes								3	3	3	3	3	3
Moisture Conditioned, One Freeze Thaw Cycle													
S.S.D. Mass, g	B'							1141.0	1143.2	1147.2	1143.4	1143.8	1146.0
Mass in Water, g	C'							656.8	654.9	658.7	656.1	656.9	658.6
Volume (B'-C'), cc	E'							484.2	488.3	488.5	487.3	486.9	487.4
Volume Absorbed Water (B'-A), cc	J'							25.1	25.5	25.3	24.4	27.2	23.9
% Saturation (100*J'/I)	S'							79.9	79.0	77.7	73.6	79.0	70.9
% Swell [100(E'-E)/E]	W'							-0.2	0.3	-0.1	-0.2	-0.3	-0.5
Thickness, mm	t'							62.8	63.1	62.9	62.4	62.7	63.0
Load (Wet), N	P'							3158.1	2624.3	2980.2	3647.4	3158.1	3113.6
Dry Strength (2000*P/π*t*D), kPa	S_{td}	298.0	311.1	338.3	312.0	288.1	317.0						
Wet Strength (2000*P'/π*t'*D), kPa	S_{tw}							315.0	260.8	296.7	366.2	315.7	309.8
Visual Moisture Damage (Yes/No)								L	L	L	L	N	L
Aggregate Break Damage (Number of particles)		2	4	4	1	1	3	1	7	3	0	0	3
Soft Aggregate (Number of particles)													

Initial Tensile Strength Values

	Dry $(S_{td})^1$	Wet $(S_{tw})^1$
1	298.0	315.0
2	311.1	**260.8**
3	**338.3**	296.7
4	312.0	**366.2**
5	**288.1**	315.7
6	317.0	309.8

Tensile Strength Ratio S_2/S_1*100= **100** %

Final Tensile Strength Values

	Dry $(S_{td})^2$	Wet $(S_{tw})^2$
	298.0	315.0
	311.1	296.7
	312.0	315.7
	317.0	309.8
	309.5 S_1	309.3 S_2

Conversions:
PSI to kPa, Multiply psi by 6.895
lb_f to N, Multiply lb_f by 4.448

APPENDIX H: STIFFNESS DETERIORATION CURVES OF BEAM SPECIMENS IN THE STUDY OF LONG-TERM EFFECTIVENESS OF ANTISTRIPPING ADDITIVES

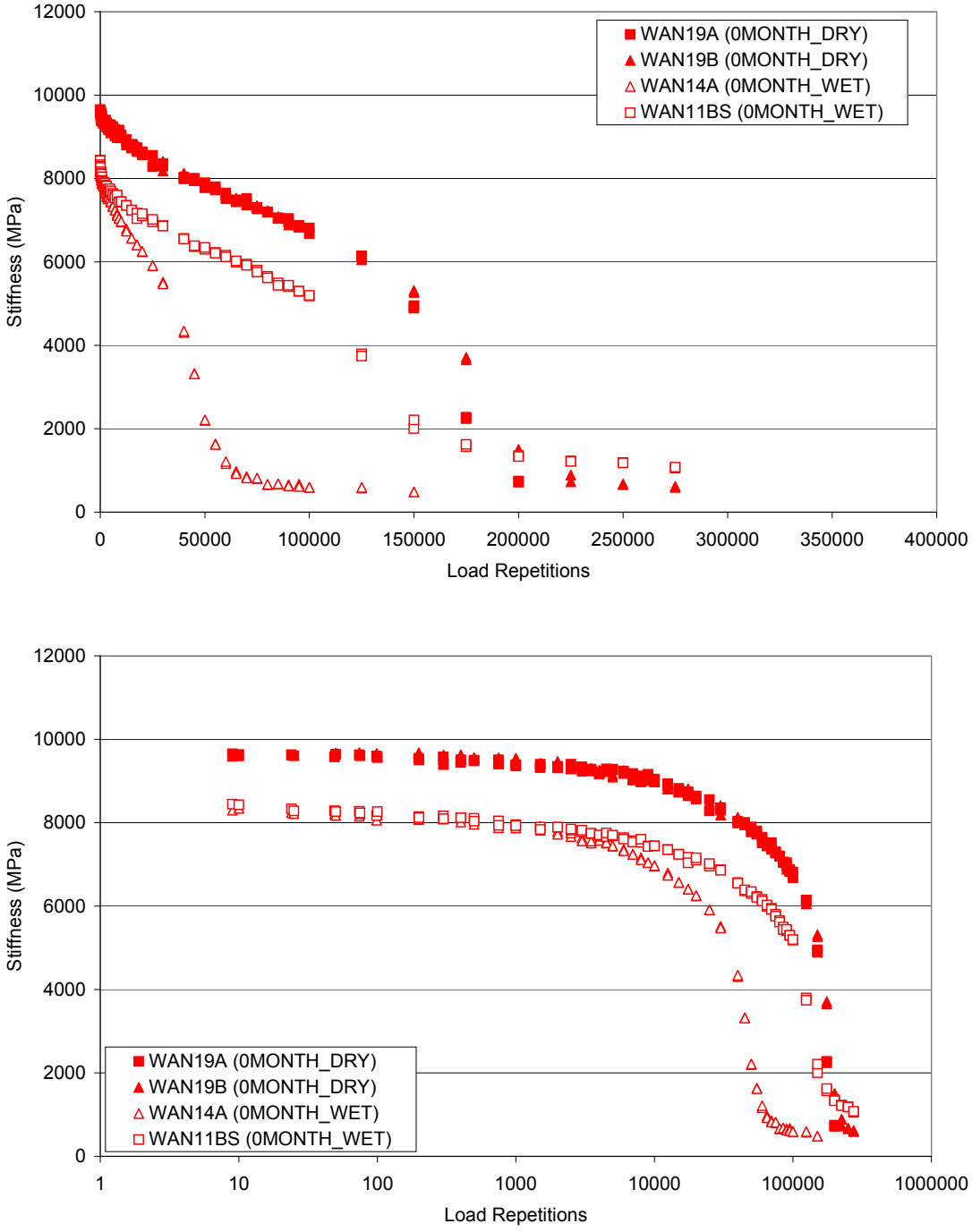

Figure H-1. Stiffness deterioration curves of mix AAN after zero-month conditioning.

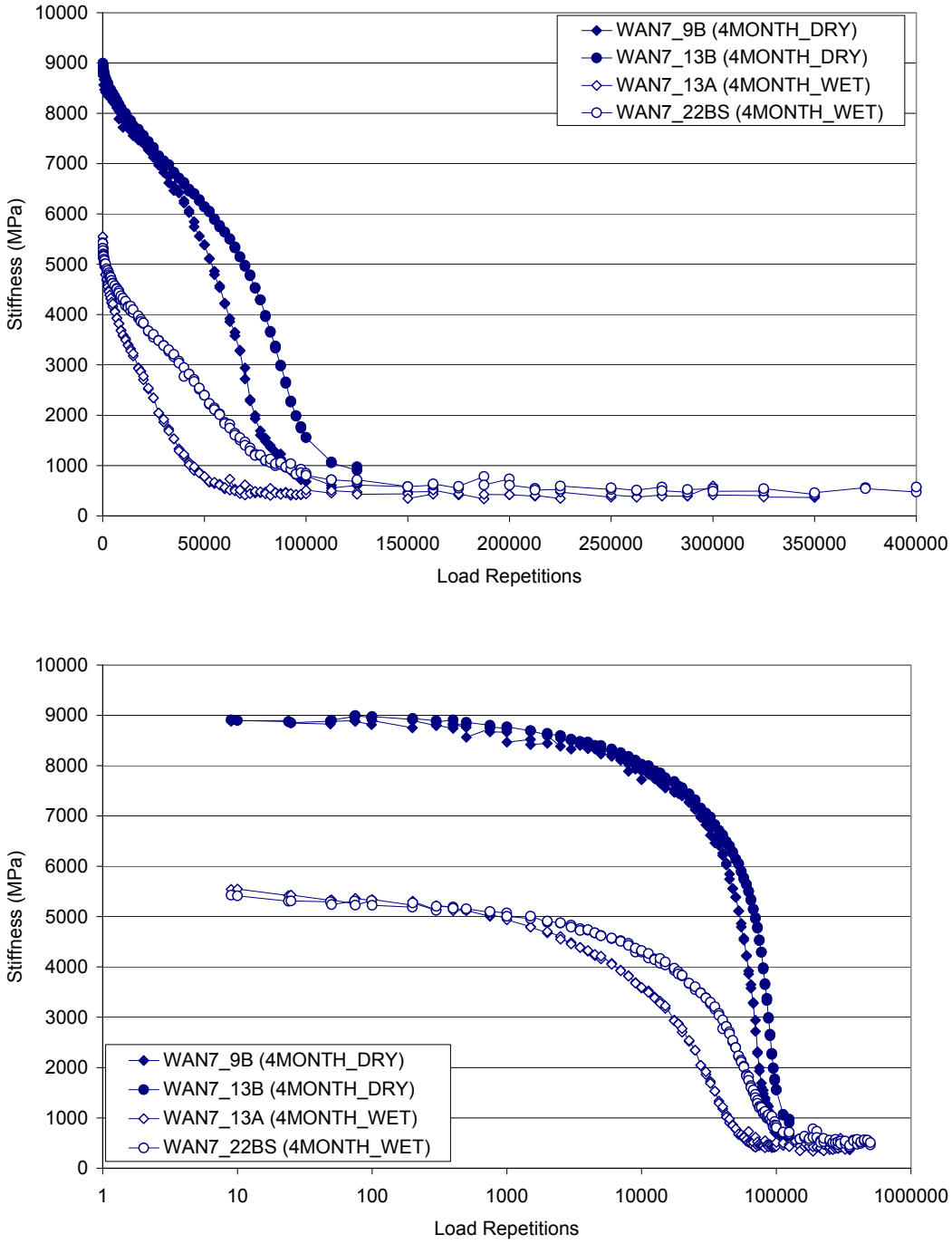

Figure H-2. Stiffness deterioration curves of mix AAN after four-month conditioning.

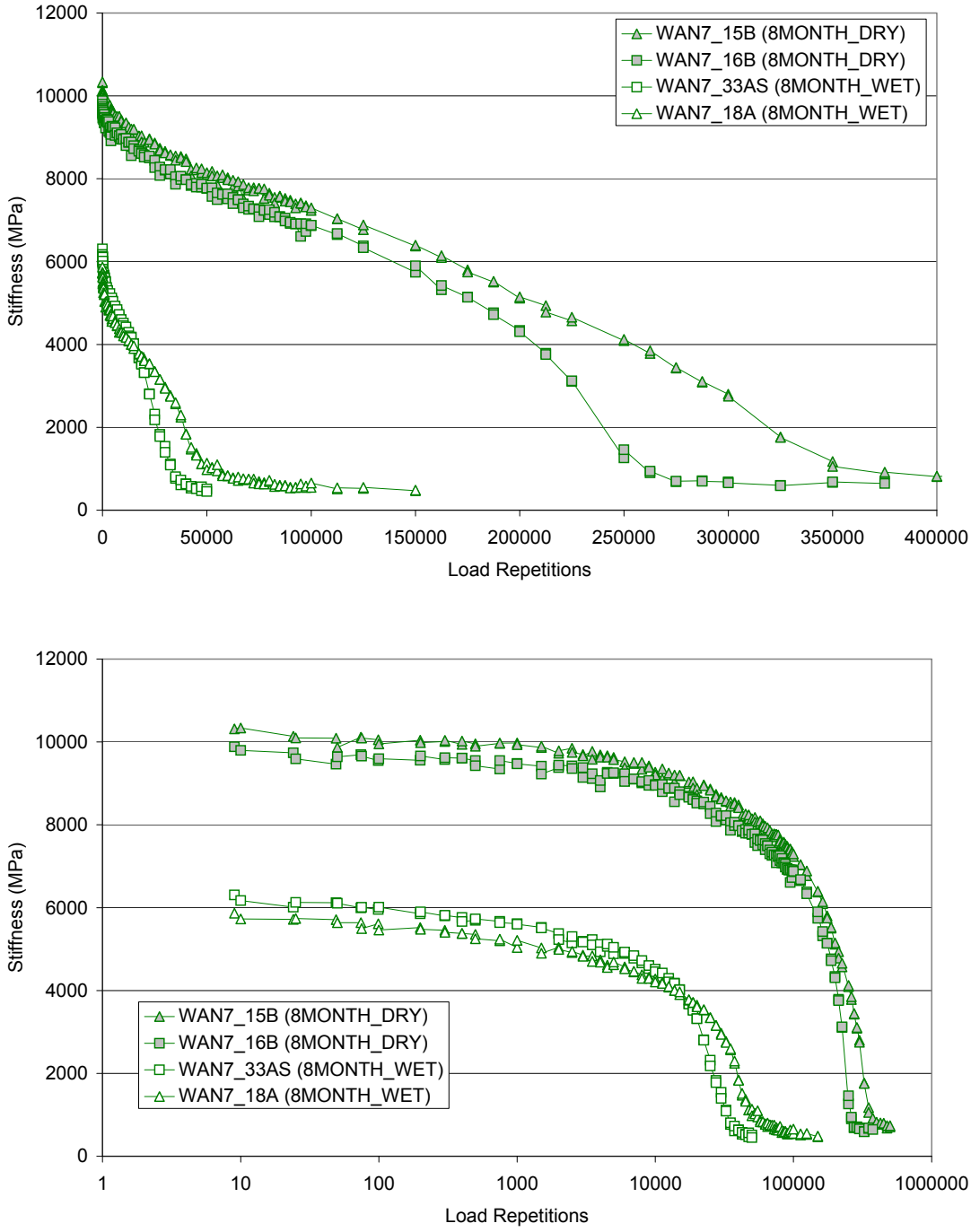

Figure H-3. Stiffness deterioration curves of mix AAN after eight-month conditioning.

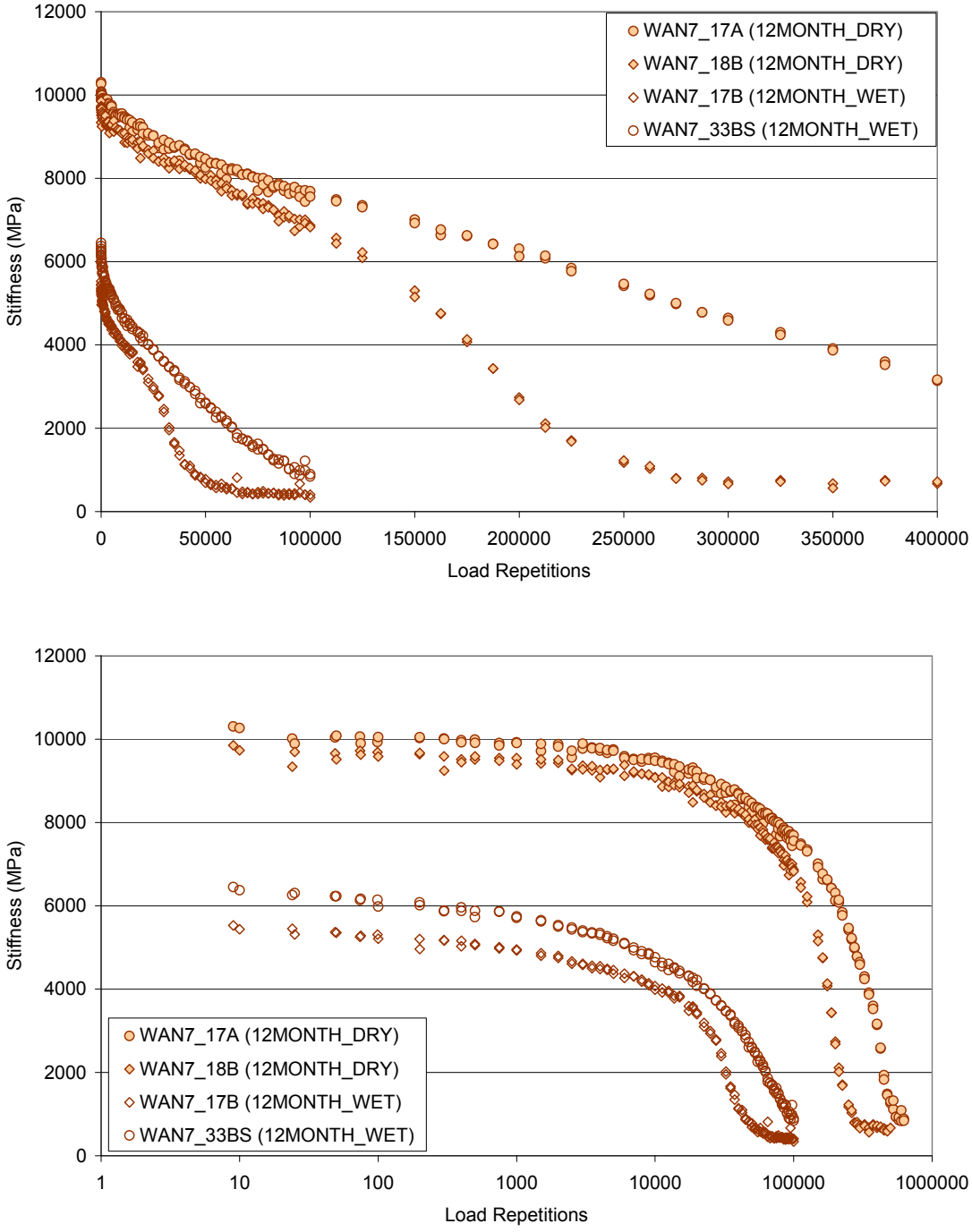

Figure H-4. Stiffness deterioration curves of mix AAN after twelve-month conditioning.

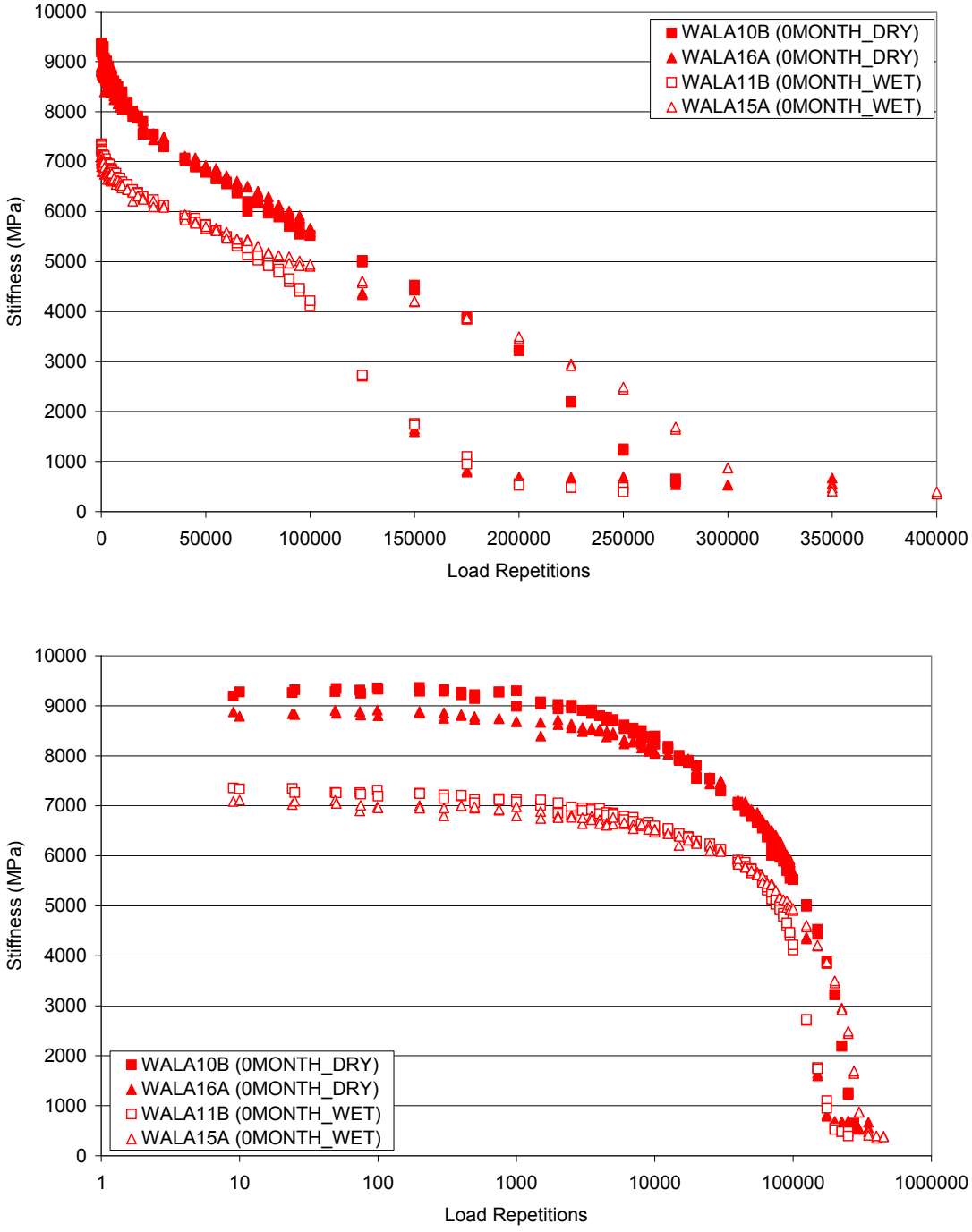

Figure H-5. Stiffness deterioration curves of mix AALA after zero-month conditioning.

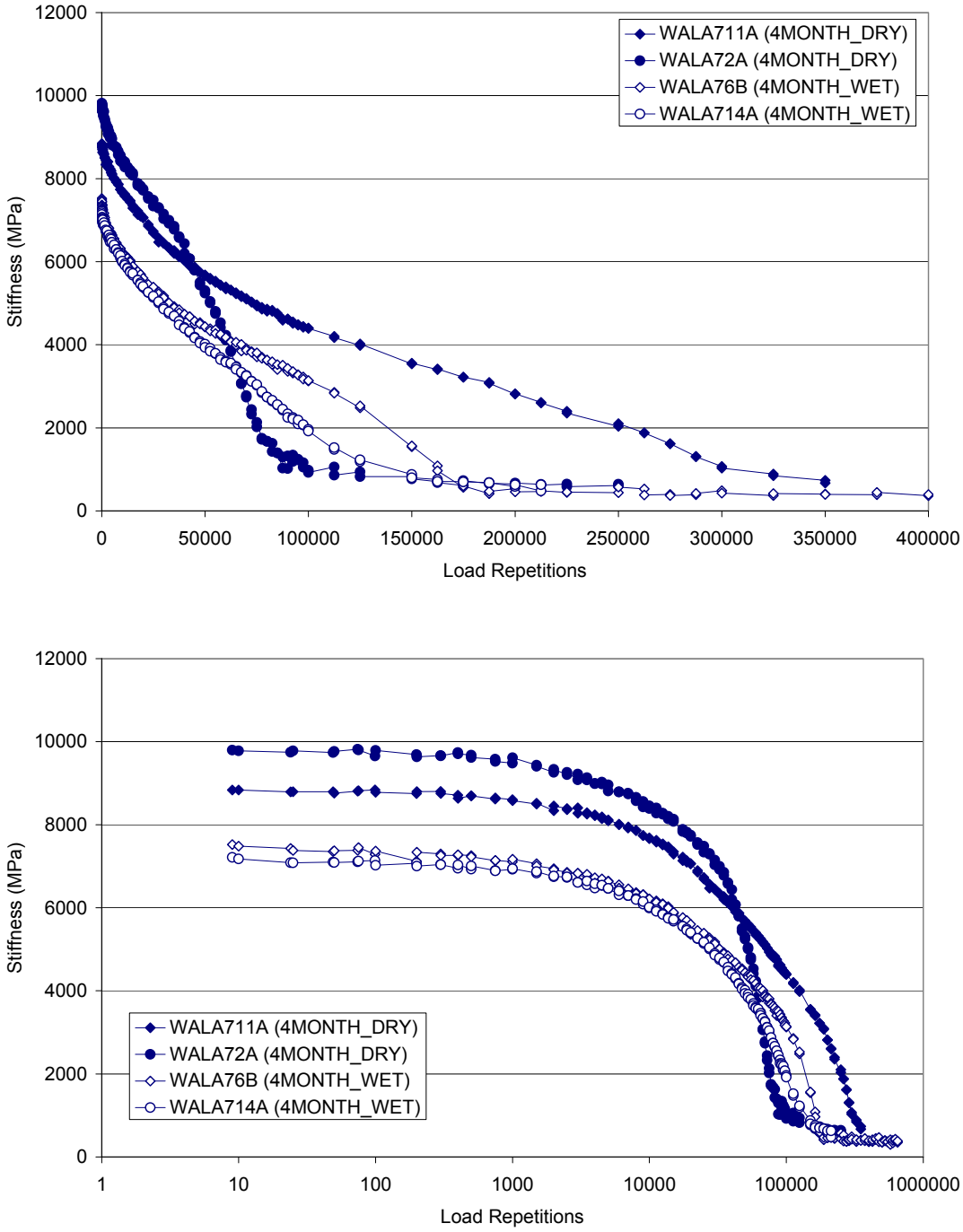

Figure H-6. Stiffness deterioration curves of mix AALA after four-month conditioning.

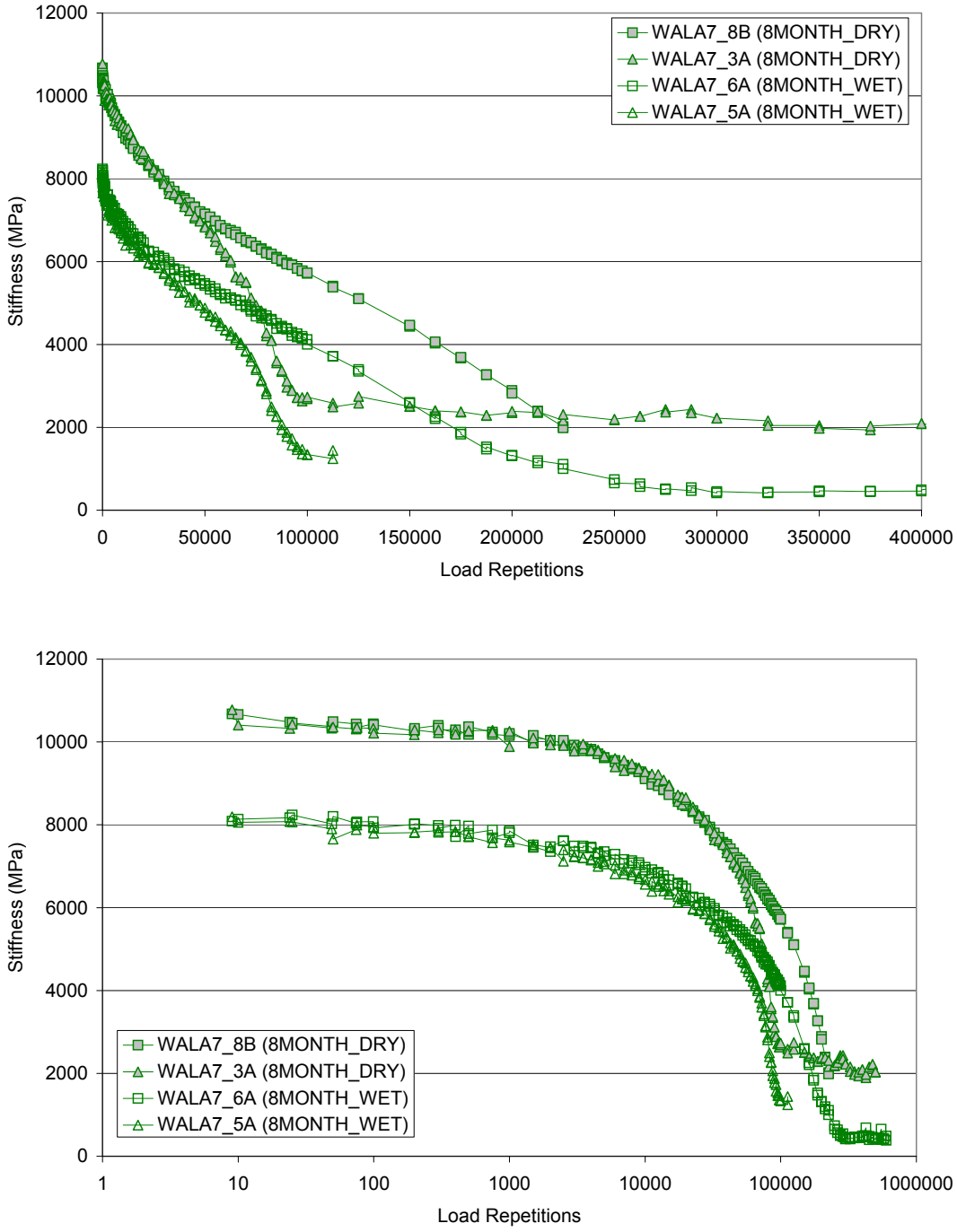

Figure H-7. Stiffness deterioration curves of mix AALA after eight-month conditioning.

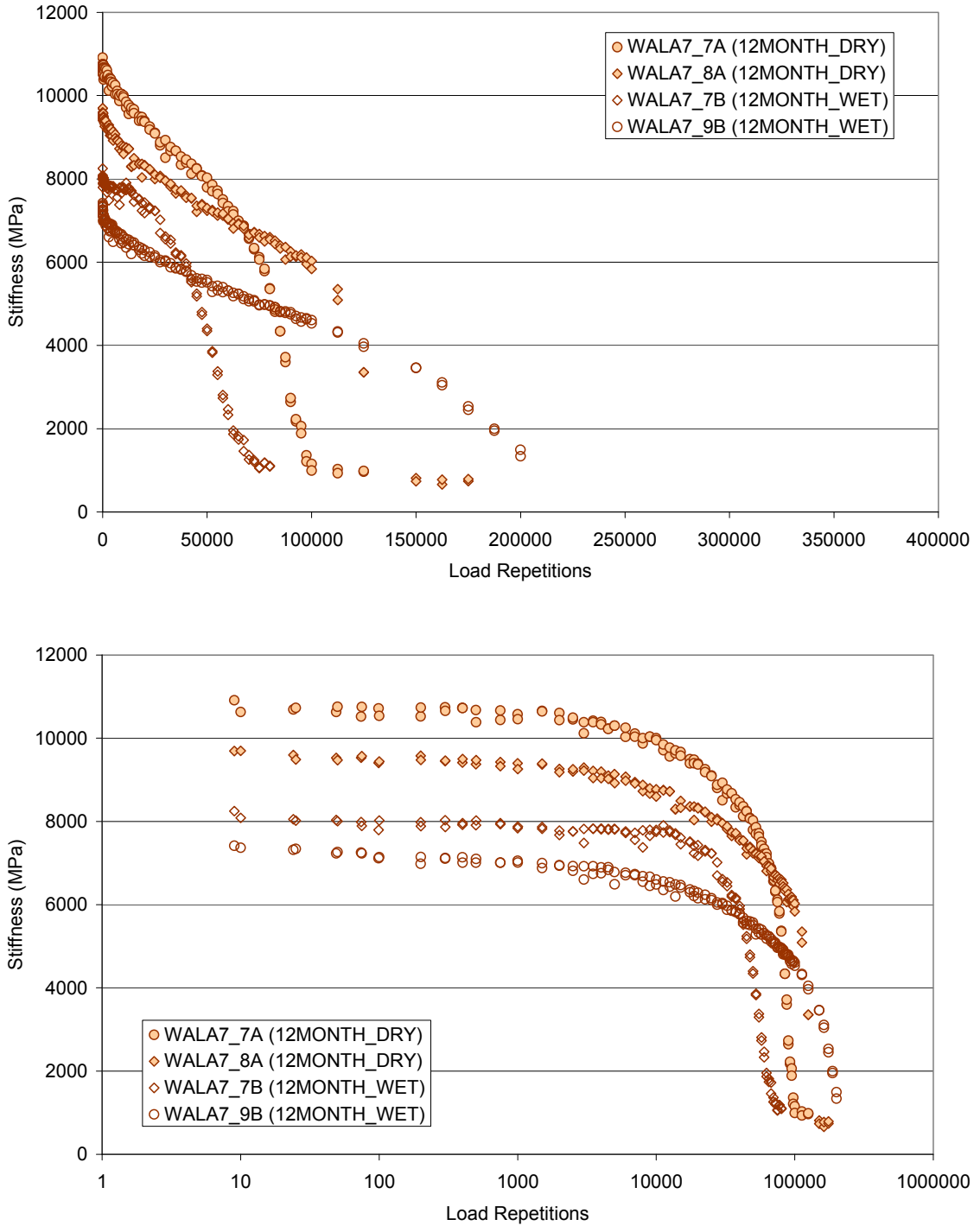

Figure H-8. Stiffness deterioration curves of mix AALA after twelve-month conditioning.

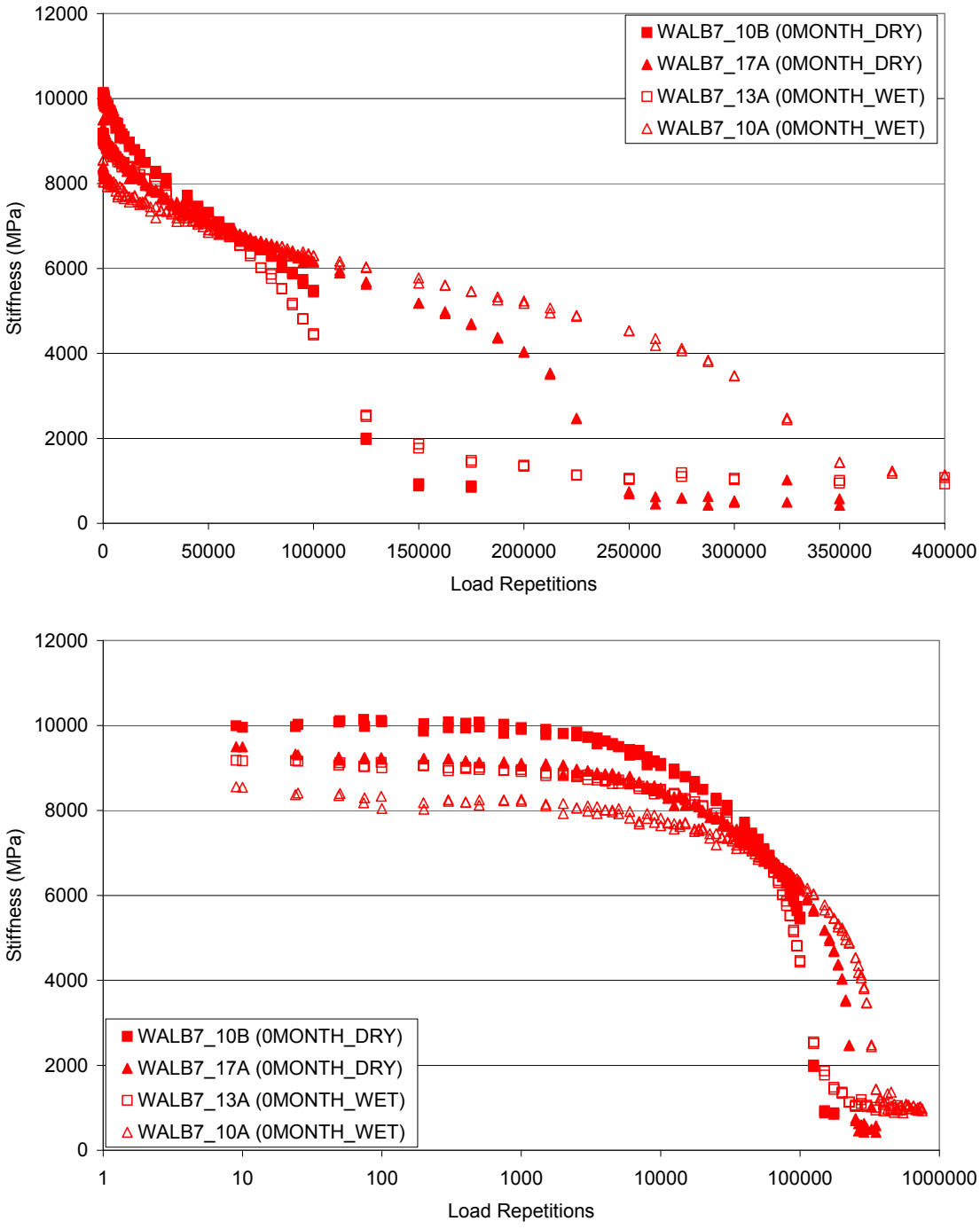

Figure H-9. Stiffness deterioration curves of mix AALB after zero-month conditioning.

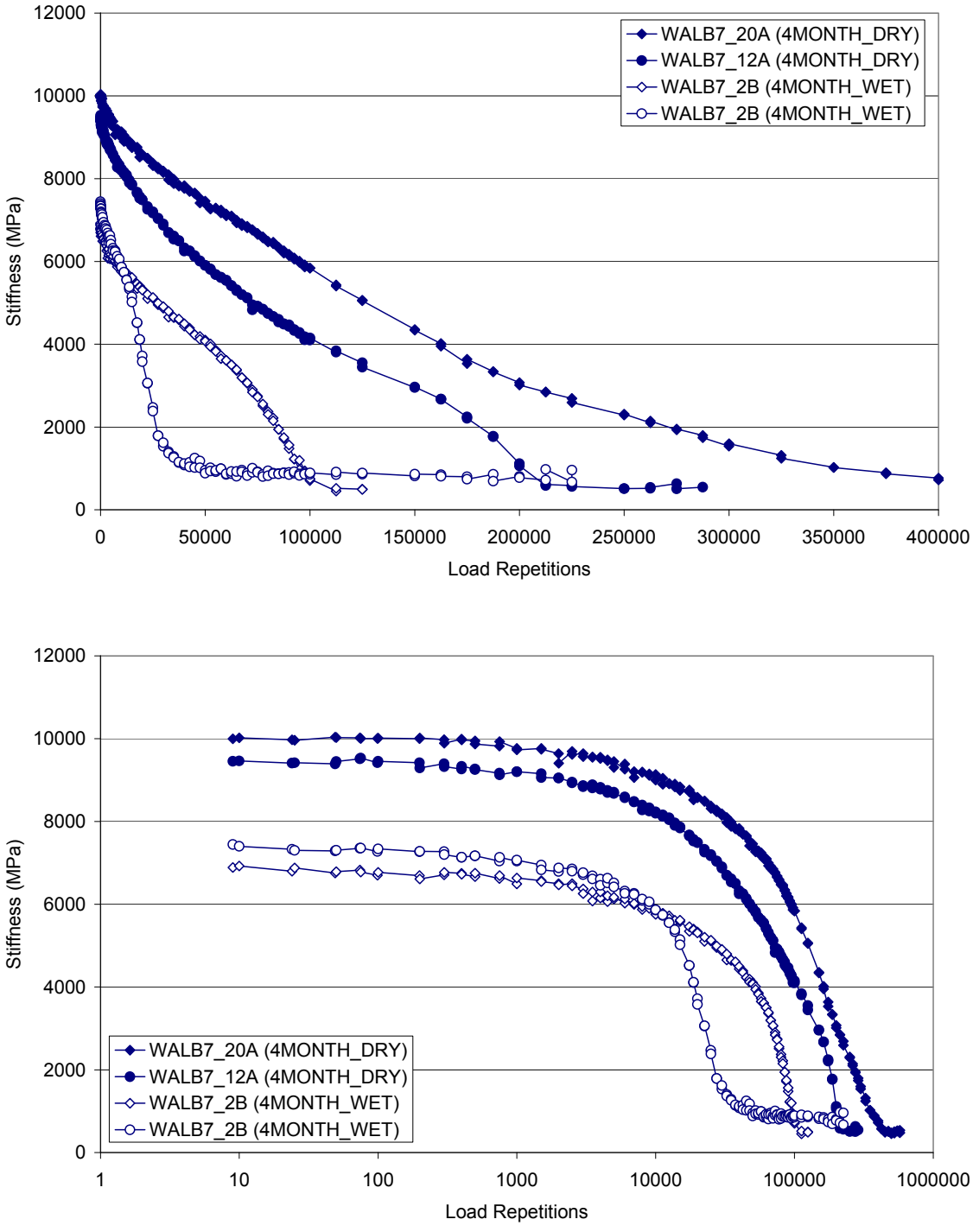

Figure H-10. Stiffness deterioration curves of mix AALB after four-month conditioning.

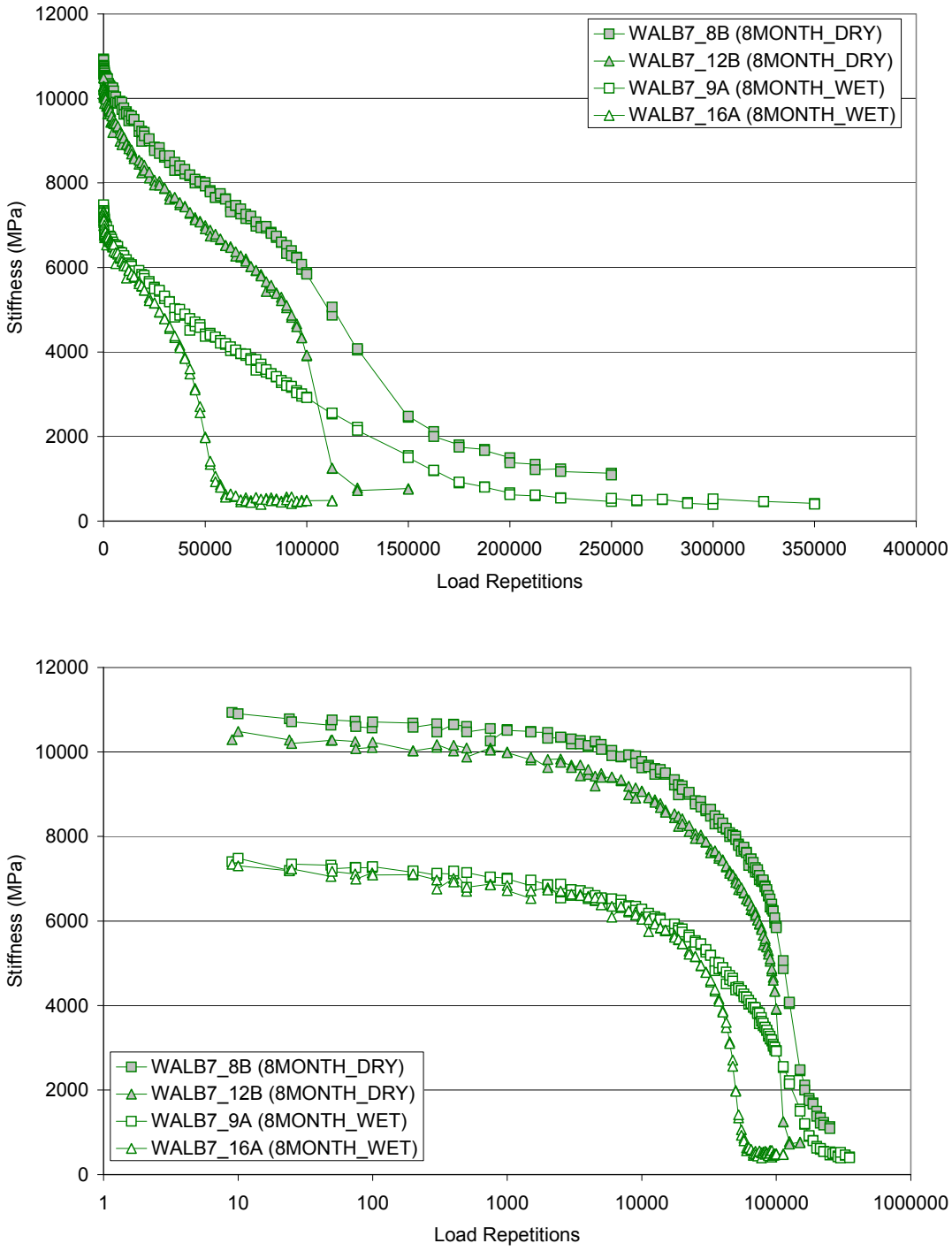

Figure H-11. Stiffness deterioration curves of mix AALB after eight-month conditioning.

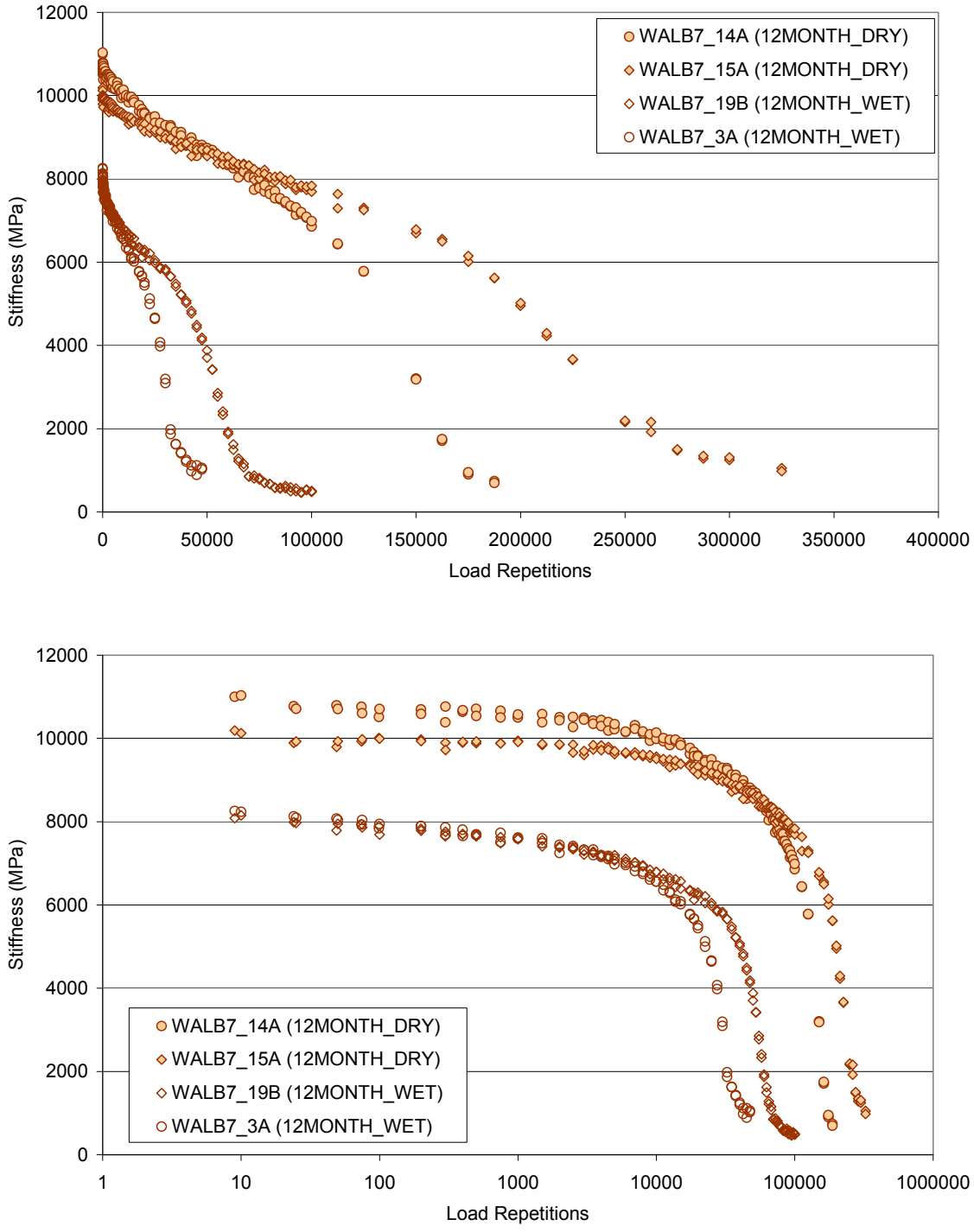

Figure H-12. Stiffness deterioration curves of mix AALB after twelve-month conditioning.

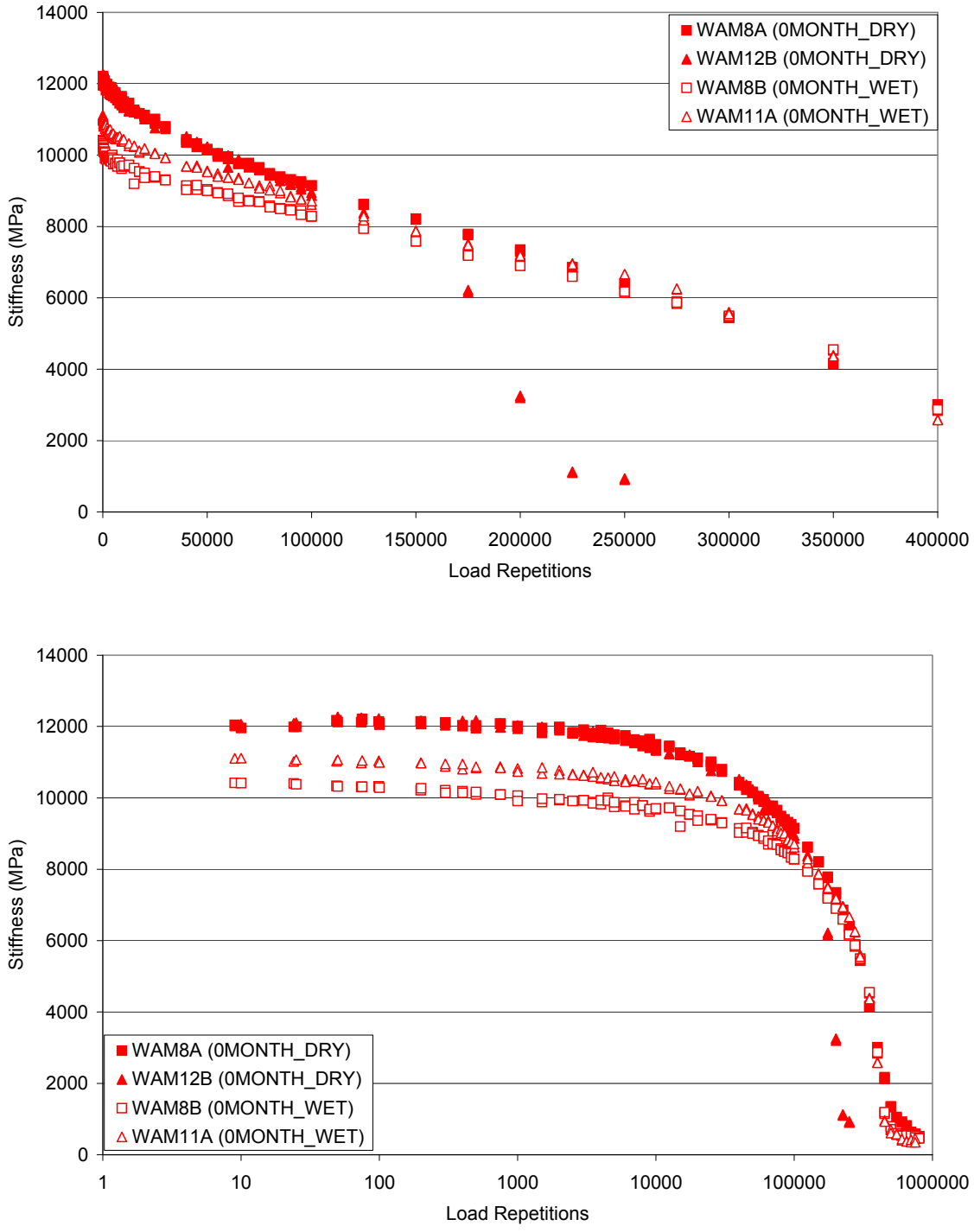

Figure H-13. Stiffness deterioration curves of mix AAM after zero-month conditioning.

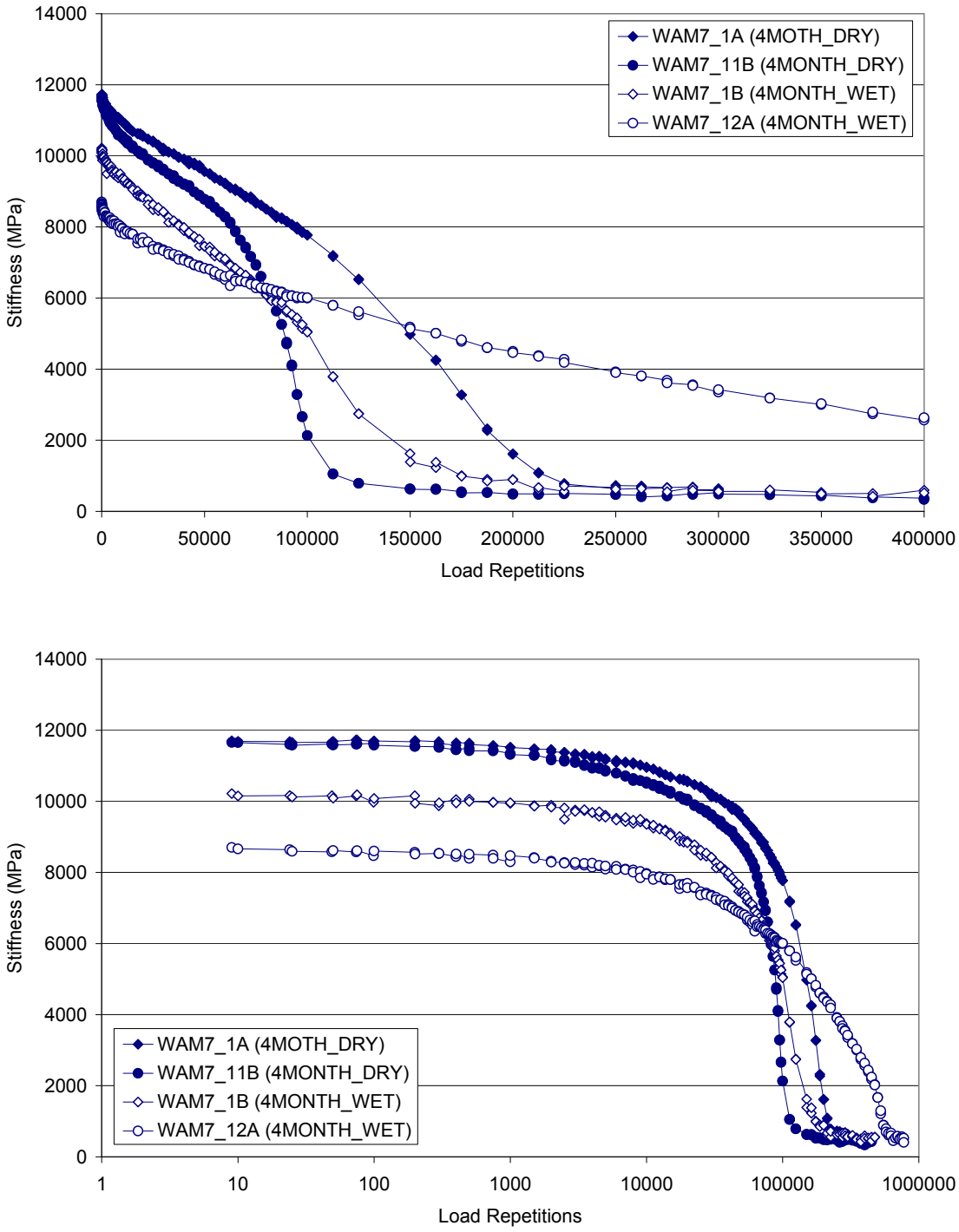

Figure H-14. Stiffness deterioration curves of mix AAM after four-month conditioning.

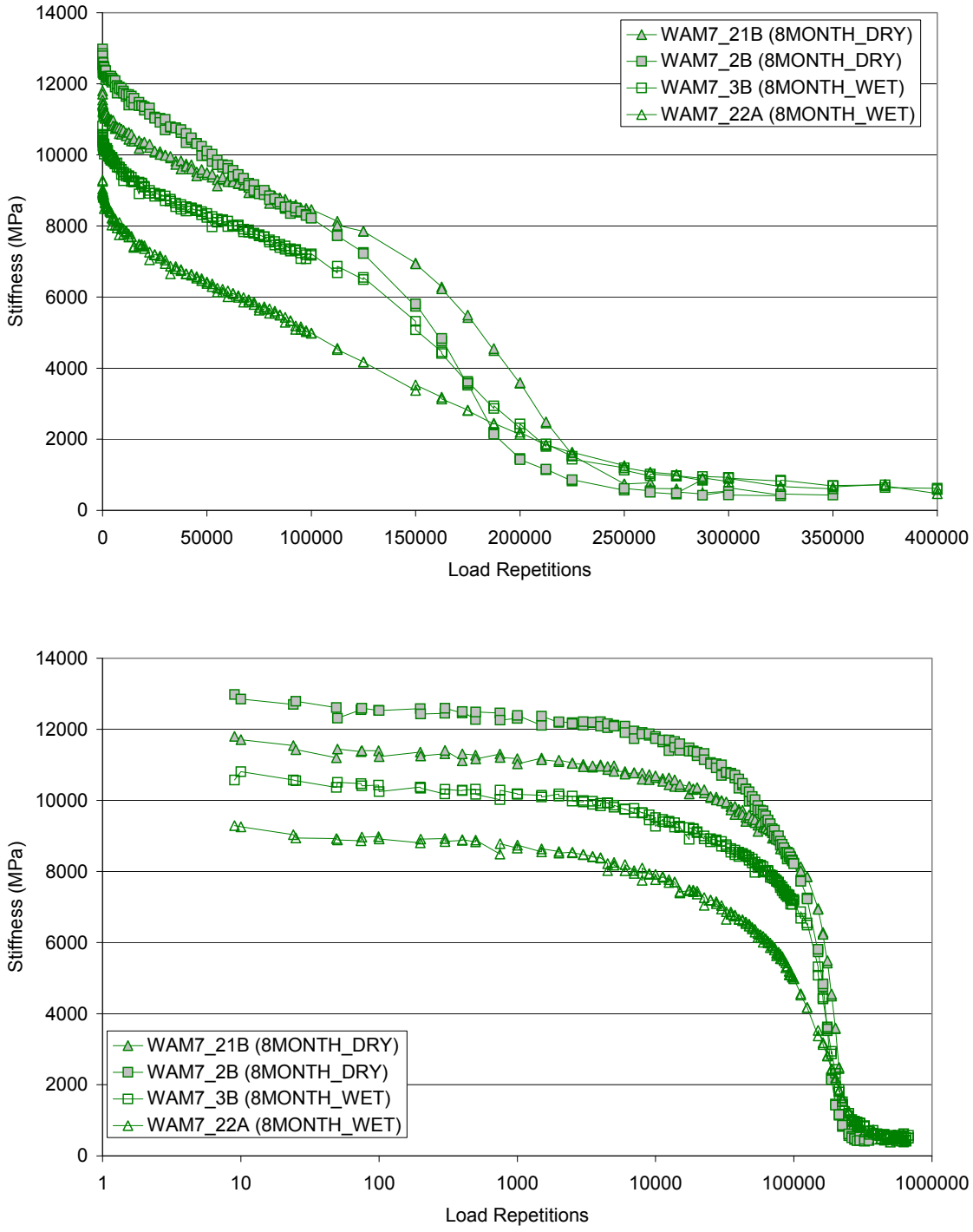

Figure H-15. Stiffness deterioration curves of mix AAM after eight-month conditioning.

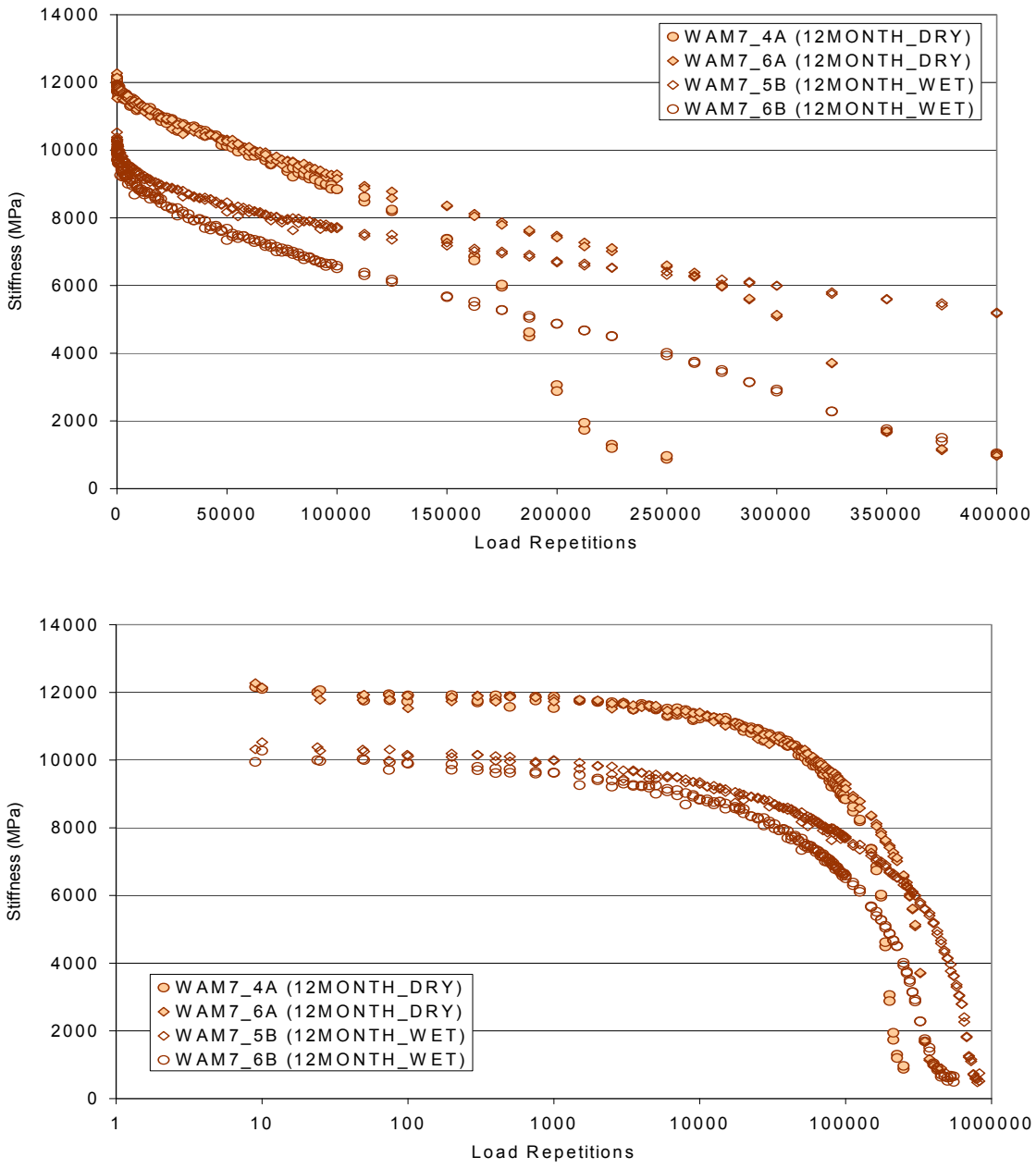

Figure H-16. Stiffness deterioration curves of mix AAM after twelve-month conditioning.

TERMS AND ABBREVIATIONS USED IN THE TEXT

aggregate base (AB)
annual average daily traffic (AADT)
annual average daily truck traffic (AADTT)
artificial neural network (ANN)
asphalt-treated permeable base (ATPB) material
cement-treated base (CTB)
dense-graded asphalt concrete (DGAC)
Dynamic shear rheometer (DSR) test (AASHTO TP5)
environmental conditioning system (ECS)
Enhanced Integrated Climatic Model (EICM) software
environmental scanning electron microscope (ESEM)
fatigue life ratio (FLR)
gap-graded asphalt rubber mixes (RAC-G)
indirect tensile strength ratio (TSR)
Heavy Vehicle Simulator (HVS)
Hamburg wheel tracking device (HWTD)
hot mix asphalt (HMA)
indirect tensile strength (ITS)
linear variable displacement transducer (LVDT)
maximum likelihood estimation (MLE)
nominal maximum aggregate size (NMAS)
optimum binder content (OBC)
Pavement Management System (PMS)
pavement reinforcement fabric (PRF)
polymer modified asphalt concrete (PMAC)
portland cement concrete (PCC)
relative humidity (RH)
repeated shear test at constant height (RSST-CH)
Rolling Thin Film Oven (RTFO)
rubberized asphalt concrete (RAC)
sand equivalent (SE) Weigh-In-Motion (WIM)
stress absorption membrane interlayer (SAMI)
Texas Department of Transportation (TxDOT)
Traffic Index (TI)